

MODERN TOPICS IN RELATIVISTIC SPIN DYNAMICS AND
MAGNETISM

by

Andrew James Steinmetz

Copyright © Andrew James Steinmetz 2023

A Dissertation Submitted to the Faculty of the
DEPARTMENT OF PHYSICS

In Partial Fulfillment of the Requirements
For the Degree of

DOCTOR OF PHILOSOPHY
WITH A MAJOR IN PHYSICS

In the Graduate College

THE UNIVERSITY OF ARIZONA
2023

THE UNIVERSITY OF ARIZONA
GRADUATE COLLEGE

As members of the Dissertation Committee, we certify that we have read the dissertation prepared by Andrew James Steinmetz, titled *Modern topics in relativistic spin dynamics and magnetism* and recommend that it be accepted as fulfilling the dissertation requirement for the Degree of Doctor of Philosophy.

Date:

John Rutherford

Date:

Shufang Su

Date:

Sean Fleming

Date:

Stefan Meinel

Date:

Date:

Final approval and acceptance of this dissertation is contingent upon the candidate's submission of the final copies of the dissertation to the Graduate College.

I hereby certify that I have read this dissertation prepared under my direction and recommend that it be accepted as fulfilling the dissertation requirement.

Date:

Dissertation Director: Johann Rafelski

STATEMENT BY AUTHOR

This dissertation has been submitted in partial fulfillment of requirements for an advanced degree at the University of Arizona and is deposited in the University Library to be made available to borrowers under rules of the Library.

Brief quotations from this dissertation are allowable without special permission, provided that accurate acknowledgment of source is made. Requests for permission for extended quotation from or reproduction of this manuscript in whole or in part may be granted by the head of the major department or the Dean of the Graduate College when in his or her judgment the proposed use of the material is in the interests of scholarship. In all other instances, however, permission must be obtained from the author.

SIGNED: Andrew James Steinmetz

ACKNOWLEDGEMENTS

In my long journey to obtain my PhD, I have benefited from the immense support and friendship of many people in my life. To them I am incredibly grateful.

I first would like to thank Dr. Johann Rafelski who as my PhD advisor guided me on my physics journey towards ever increasing heights of knowledge, understanding, and most importantly a humble awareness of our ignorance towards much of the universe's inner workings. I dearly hope we continue to chip away at those mysteries together.

I also would like to thank Victoria Grossack for hosting many students including myself at her and Dr. Rafelski's lovely home. I promise future gluten-free pies which I am now bound to by the publication of this dissertation.

To my fellow research collaborators, fellow students, and dear friends I also thank for our wonderful time spent together (in alphabetical order): Stefan Evens, Martin Formanek, Christopher Grayson, Will Price, Cheng Tao Yang. I look forward to many more years and publications together.

To friends, to family, and to all who have shown me kindness. Good health and long life to all.

TABLE OF CONTENTS

LIST OF FIGURES	9
LIST OF TABLES	12
ABSTRACT	13
PUBLICATIONS AND AUTHOR CONTRIBUTIONS	14
CHAPTER 1 The importance of spin	17
1.1 Quantum magnetic dipoles and wave equations	18
1.1.1 Anomalous magnetic moment	22
1.1.2 Dirac and Dirac-Pauli equations	23
1.2 Klein-Gordon-Pauli equation	27
1.2.1 Features of the KGP Lagrangian	29
1.2.2 The special case of $g = 2$	31
1.3 A few words on cosmology	34
CHAPTER 2 Dynamics of charged particles with arbitrary magnetic moment	38
2.1 Homogeneous magnetic fields	39
2.2 Hydrogen-like atoms	44
2.2.1 Non-relativistic Coulomb problem energies	49
2.2.2 g-Lamb Shift between 2S and 2P orbitals	50
2.2.3 g-Fine structure effects within P orbitals	52
2.3 Particles in strong electromagnetic fields	53
2.3.1 Strong homogeneous magnetic fields	54
2.3.2 High-Z hydrogen-like atoms	56
2.4 Combination of mass and magnetic moment	62
2.5 Classical relativistic spin dynamics	66
2.5.1 Covariant magnetic potential and modified Lorentz force	67
2.5.2 Equivalency of Gilbertian and Ampèrian Stern-Gerlach forces	69

TABLE OF CONTENTS – *Continued*

CHAPTER 3	Dynamic neutrino flavor mixing through transition moments	72
3.1	Electromagnetic characteristics of neutrinos	72
3.2	Neutrino flavor mixing and electromagnetic fields	74
3.2.1	Effective Majorana neutrino Lagrangian	75
3.2.2	Chiral properties of the relativistic Pauli dipole	78
3.3	Electromagnetic-flavor mixing for two generations	79
3.3.1	Separating electromagnetic-mass mixing into two rotations . .	81
3.3.2	Effective electromagnetic-mass eigenvalues	84
3.4	Strong field (degenerate mass) and weak field limits	86
CHAPTER 4	Matter-antimatter origin of cosmic magnetism	88
4.1	Short survey of magnetism in the universe	88
4.2	Electron-positron abundance	90
4.3	Theory of thermal matter-antimatter plasmas	92
4.3.1	Eigenstatess of magnetic moment in cosmology	94
4.3.2	Magnetized fermion partition function	96
4.3.3	Boltzmann approach to electron-positron plasma	100
4.3.4	Non-relativistic limit of the magnetized partition function .	104
4.3.5	Electron-positron chemical potential	105
4.4	Relativistic paramagnetism of electron-positron gas	107
4.4.1	Evolution of electron-positron magnetization	109
4.4.2	Dependency on g-factor	111
4.4.3	Magnetization per lepton	113
4.5	Polarization potential and ferromagnetism	115
4.5.1	Hypothesis of ferromagnetic self-magnetization	116
4.5.2	Matter inhomogeneities in the cosmic plasma	118
CHAPTER 5	Outlook and key results	120
CHAPTER 6	Future research efforts	123
6.1	Klein-Gordon-Pauli extensions to non-Abelian fields	123
6.2	Electromagnetic forced neutrino CP violation	126
6.2.1	Jarlskog invariant	127
6.2.2	Toy model: CP violation amplification	129
6.2.3	Electric dipole moments and CP symmetry	130
6.3	Spin in 5D Kaluza-Klein theory	133

TABLE OF CONTENTS – *Continued*

REFERENCES	135
APPENDIX A Magnetic dipole moment in relativistic quantum mechanics .	150
APPENDIX B Strong fields and neutral particle magnetic moment dynamics	160
APPENDIX C Relativistic dynamics of point magnetic moment	165
APPENDIX D Dynamic fermion flavor mixing through transition dipole moments	172
APPENDIX E A Short Survey of Matter-Antimatter Evolution in the Primordial Universe	180
APPENDIX F Matter-antimatter origin of cosmic magnetism	206

LIST OF FIGURES

<p>1.1 A schematic of the universe's evolution since the Big Bang. The region of interest studied in this dissertation is emphasized (in the highlighted box) to contain a dense nearly charge neutral matter-antimatter plasma.</p> <p>2.2 The $n = 0$, $s = 1/2$ ground state for a KGP electron given by Eq. (2.16) with $g/2 - 1 = \alpha/2\pi$ in a homogeneous magnetic field. We consider the particle with no z-direction momentum. The particle state (solid red) and antiparticle (dashed red) are presented.</p> <p>2.3 The $n = 0$, $s = 1/2$ ground state for a DP electron given by Eq. (2.19b) with $g/2 - 1 = \alpha/2\pi$ in a homogeneous magnetic field. We consider the particle with no z-direction momentum. The particle state (solid red) and antiparticle (dashed red) are presented.</p> <p>2.4 The KGP $1S_{1/2}$ (lower red curves) and $2P_{1/2}$ (upper green curves) energy levels for g-factor values $g = \{1.8, 1.9977, 2.0023, 2.2\}$ are shown for large Z hydrogen-like atoms. The curves for the Dirac $g=2$ case for (lower dashed blue) $1S_{1/2}$ and (upper dashed blue) $2P_{1/2}$ are also presented.</p> <p>2.5 The KGP $1S_{1/2}$ and $2P_{1/2}$ states are plotted for hydrogen-like energies for $220 > Z > 0$. The spread of lines corresponds to a spread of g-factor values: $4 > g > 0$. Integer multiples of $Z = 137/2$ are marked with vertical dashed lines. The separation between any two adjacent curves is $g_i - g_{i+1} = 0.05$. The unique curve which dives towards and stops at the boundary $E = 0$ is the Dirac $g = 2$ ground state.</p> <p>2.6 A close up of the KGP $1S_{1/2}$ and $2P_{1/2}$ states between $2.0625 > g > 1.9375$. The separation between any two adjacent curves is $g_i - g_{i+1} = 0.003125$. The value $Z = 137$ is marked with a vertical dashed line.</p> <p>2.7 Energy level curves are plotted for total angular momentum quantum number $j = 1/2, 3/2$ with the relativistic principle quantum number $n_r = 0$. The separation between any two adjacent curves is $g_i - g_{i+1} = 0.2$. Dashed vertical lines indicate integer multiples of $Z = 137/2$.</p>	<p>35</p> <p>56</p> <p>57</p> <p>58</p> <p>59</p> <p>60</p> <p>61</p>
--	---

LIST OF FIGURES – *Continued*

2.8	The $n = 0, s = 1/2$ ground state for a IKGP proton given by Eq. (2.68) with $g = 5.58$ in a homogeneous magnetic field. The magnetic minimum is well visible for particles with larger anomalous moment such as proton. We consider the particle with no z -direction momentum. The particle state (solid red) and antiparticle (dashed red) are presented. The magnetic field scale is $B'_S = (m_p^2/m_e^2)B_S$	65
4.1	Qualitative plot of the primordial magnetic field strength over cosmic time. All figures are printed in temporal sequence in the expanding universe beginning with high temperatures (and early times) on the left and lower temperatures (and later times) on the right.	90
4.2	Number density of electron e^- and positron e^+ to baryon ratio n_{e^\pm}/n_B as a function of photon temperature in the universe. See text for further details. In this work we measure temperature in units of energy (keV) thus we set the Boltzmann constant to $k_B = 1$. Figure courtesy of Cheng Tao Yang.	91
4.3	Organizational schematic of matter-antimatter (σ) and polarization (s) states with respect to the sign of the non-relativistic magnetic dipole energy U_{Mag} obtainable from Eq. (4.4).	93
4.4	The chemical potential over temperature μ/T is plotted as a function of temperature with differing values of spin potential η and magnetic scale b_0	106
4.5	The magnetization \mathfrak{M} , with $g = 2$, of the primordial e^+e^- plasma is plotted as a function of temperature. Figure made in collaboration with Cheng Tao Yang.	110
4.6	The magnetization \mathfrak{M} as a function of g -factor plotted for several temperatures with magnetic scale $b_0 = 10^{-3}$ and polarization fugacity $\xi = 1$	112
4.7	The magnetic moment per lepton $ \vec{m} _z$ along the field axis as a function of temperature. Figure made in collaboration with Cheng Tao Yang.	114
4.8	The spin potential η and chemical potential μ are plotted under the assumption of self-magnetization through a nonzero spin polarization in bulk of the plasma. Figure made in collaboration with Cheng Tao Yang.	117

LIST OF FIGURES – *Continued*

LIST OF TABLES

1.1	The g -factor of various particles found in Tiesinga et al. (2021); Workman et al. (2022).	22
4.1	Organizational schematic of matter-antimatter (σ) and polarization (s) states with respect to the chemical μ and polarization η potentials as seen in Eq. (4.32). Companion to Table 4.3.	101
6.1	Time (T), parity (P) and PT symmetries of electric \mathbf{E} , magnetic \mathbf{B} , spin \mathbf{s} three-vectors and the inner products which describe the dipole Hamiltonian terms.	131

ABSTRACT

Magnetism is a rich subject touching all aspects of physics. My goal with this dissertation is to explore spin and magnetic dipole moments in *relativistic* mechanics from both a quantum and classical perspective. We emphasize the special case of gyromagnetic ratio $g = 2$ and its relationship to the algebraic spin structure of the wave equations of motion.

In relativistic quantum mechanics, we investigate generalizations of the Dirac equation for arbitrary magnetic dipole moments for fermions. We analyze the homogeneous magnetic field case and the Coulomb problem for hydrogen-like atoms with emphasis on the role of the anomalous magnetic moment (AMM). We explore alternative approaches which combine mass and the magnetic moment. Extensions to include both electromagnetic and quantum chromodynamic (QCD) dipole moments are considered. Classically, we propose a relativistic covariant model of the Stern-Gerlach force via the introduction of a magnetic four-potential. This model modifies the covariant torque equations and unites the Ampèreian and Gilbertian models for magnetic dipole moments.

We further study (transition) magnetic dipoles in Majorana neutrinos specifically analyzing the relationship between flavor mixing and electromagnetic fields. We demonstrate this explicitly in the 2-flavor model and develop electromagnetic flavor mixing into a dynamical mass basis with an electromagnetic rotation matrix.

An interesting application of these theoretical developments is to study primordial magnetization in the early universe during the hot dense electron-positron plasma epoch. We propose a model of magnetic thermal matter-antimatter plasmas. We analyze the paramagnetic characteristics of electron-positron plasma when exposed to an external primordial field. We determine the magnitude of a small polarization asymmetry is sufficient to generate field strengths in agreement with those measured today in deep intergalactic space.

Publications and author contributions

In the course of satisfying the University of Arizona Department of Physics's requirements for a Ph.D. doctoral dissertation, I prepared the following publications which are reprinted in full in the appendices. These articles are not ordered chronologically, but in the contextual order of presentation in this document. My contribution to each work is described under each item.

- Appendix A - “Magnetic dipole moment in relativistic quantum mechanics” by [Steinmetz, Formanek, and Rafelski \(2019\)](#) is a study and comparison of DP and KGP wave equations for homogeneous magnetic fields and hydrogen-like atoms. I performed all computation, writing, and figure making in preparation of the first draft and approved the final draft before submission. I acknowledge the help and consultation of Martin Formanek (MF) and Johann Rafelski (JR) in research, writing and editing.
- Appendix B - “Strong fields and neutral particle magnetic moment dynamics” by [Formanek, Evans, Rafelski, Steinmetz, and Yang \(2018\)](#) is an overview of our research group’s efforts in studying neutral particle dynamics in electromagnetic fields. I wrote Section 2.1 in collaboration with MF. I consulted and helped lead author MF and co-authors Stefan Evans (SE) and Cheng Tao Yang (CTY) in editing and revising the overall manuscript.
- Appendix C - “Relativistic dynamics of point magnetic moment” by [Rafelski, Formanek, and Steinmetz \(2018\)](#) introduces a new covariant formulation of classical spin dynamics and unifies Gilbertian and Ampèrian dipoles. I wrote Section 3 in collaboration with JR and MF and aided in the computation in Section 5.1. I otherwise consulted in the research, writing, and editing process of this publication.
- Appendix D - “Dynamic fermion flavor mixing through transition dipole moments” by [Rafelski, Steinmetz, and Yang \(2023c\)](#) is a study of Majorana neu-

trino flavor mixing in electromagnetic fields and proposes a novel dynamical EM-mass basis for propagating neutrinos. The article was written originally via invitation of JR by Gerhard Buchalla, Dieter Lüst and Zhi-Zhong Xing as a memorial chapter in a book dedicated to Harald Fritzsch. I performed all computation and writing in preparation of the first draft and approved the final draft before submission. I acknowledge the help and consultation of JR and CTY in research, writing and editing.

- Appendix E - “A Short Survey of Matter-Antimatter Evolution in the Primordial Universe” by [Rafelski, Birrell, Steinmetz, and Yang \(2023a\)](#) is a 50 page long review with many novel results describing the role of antimatter in the early universe. I supervised (in collaboration with CTY) the document creation, combining the writing contributions of all authors (including myself, Jeremiah Birrell (JB), CTY, and JR) into one coherent presentation. I also coordinated with all authors in formatting and editing the technical figures in this review by JB, CTY, and JR.
- Appendix F - “Matter-antimatter origin of cosmic magnetism” by [Steinmetz, Yang, and Rafelski \(2023\)](#) proposes a model of para-magnetization driven by the large matter-antimatter (electron-positron) content of the early universe. I carried out all writing in preparation of the first draft and approved the final draft before submission. Computation and figure making was done in collaboration with CTY who contributed key results and five technical figures. I acknowledge the help and consultation of CTY and JR in research, writing and editing.

This is not a total catalogue of my research efforts, but lists the works that form the foundation of Chapter 2, Chapter 3 and Chapter 4 of this dissertation. Where noted, these chapters also contain sections of complete yet unpublished work. Chapter 6 contains brief discussions of still-in-progress research efforts to be completed after submission of this dissertation.

I was also co-author on the following publications which are not used extensively in this dissertation and are not reprinted as appendices. They are listed in chronological

order below. In these three works I consulted with MF, CTY and JR in research and editing making content clarifying contributions to these manuscripts:

- “Classical neutral point particle in linearly polarized EM plane wave field” by [Formanek, Steinmetz, and Rafelski \(2019\)](#) explores the dynamical equations presented in Appendix C for neutral particles with magnetic moment.
- “Radiation reaction friction: Resistive material medium” by [Formanek, Steinmetz, and Rafelski \(2020\)](#) introduces a novel model of relativistic covariant friction within a medium.
- “Motion of classical charged particles with magnetic moment in external plane-wave electromagnetic fields” by [Formanek, Steinmetz, and Rafelski \(2021b\)](#) is a followup to the above 2019 work and Appendix C for charged particles with magnetic moment.
- “Decomposition of Fermi gas into zero and finite temperature distributions with examples” by [Yang, Formanek, Steinmetz, and Rafelski \(2023\)](#) is a mathematical methods paper detailing a novel analytic form of the finite temperature behavior of the Fermi-Dirac distribution function. The cold magnetized gas is analyzed as an example.

CHAPTER 1

The importance of spin

All fundamental particles known in physics have a non-zero quantized spin angular momentum with the exception of the Higgs boson which is a scalar with spin-0. All other confirmed elementary particles (such as electrons, quarks, photons, etc...) have values of either spin-1/2 or spin-1. Particles with even values of spin are known as bosons while half-integer particles with spin are called fermions. Composite particles (such as atomic nuclei) can exhibit more exotic spin values and fundamental particles with higher spins such as spin-3/2 or spin-2 graviton are commonly predicted in beyond-standard-model (BSM) physics.

In the realm of the Poincaré group of spacetime symmetry (rotations, boosts and translations) transformations, each particle can be uniquely labeled by two distinct Casimir invariants: mass and spin. These two operators commute with all generators of the Poincaré group and act as labels which represent a particle. Therefore in a relativistic context, particle mass and spin are of fundamental importance on equal footing.

If a particle is electrically charged, then by virtue of its spin it will have a magnetic dipole moment. Most neutral particles with spin, though not all, will also have magnetic dipoles though for more complex reasons. Therefore the magnetic behavior of particle is an important window into probing one of the most fundamental properties in physics. As quantum mechanics is not well described in terms of forces or accelerations (except in the context of Ehrenfest-style equations), there is no simple operator description of torque and spin-forces despite having played a key role in the development of quantum mechanics. For a short historical overview of spin and its relationship to angular momentum, see [Ohanian \(1986\)](#).

This introduction serves to motivate the fundamental concepts of spin, magnetic moment and electromagnetism which have played a crucial role in the history physics

and will be explored in the subsequent research chapters. Magnetic (and electric) dipoles, anomalous magnetic moments (AMM), and the Dirac and Dirac-Pauli wave equations which describe spin-1/2 fermions are covered in Section 1.1. The Klein-Gordon-Pauli equation is introduced in Section 1.2. Lastly, Section 1.3 covers topics in Λ CDM cosmology which are particular relevance to Chapter 4. This chapter will also serve to establish notation and mathematical conventions. SI units will be used unless otherwise stated.

1.1 Quantum magnetic dipoles and wave equations

In classical theory, when charges rotate or circulate in some manner, a magnetic field is produced characterized by the magnetic dipole moment of the system. An Ampèrean loop of wire with a current is the quintessential example. This concept can be transplanted into quantum theory for spinning particles where the natural size of the magnetic moment of a particle (in this context a charged lepton) is given by the magneton value

$$\mu_\ell \equiv \frac{e\hbar}{2m_\ell} \quad (1.1)$$

where the lepton (denoted by ℓ) has charge e and mass m_ℓ .

A quick word on notation: Euclidean three-vectors and matrices will be denoted by boldface font. If indices are specifically printed, they will be done so using Latin indices such as s_i . Inner products of three-vectors will be noted via $\mathbf{a} \cdot \mathbf{b} = a_i b_i$ using Einstein summation notation where repeated indices are summed over. For electrons, Eq. (1.1) is referred to as the Bohr magneton μ_B . The non-relativistic spin operator \mathbf{S} for a spin-1/2 particle is defined as

$$\mathbf{S} = \frac{\hbar}{2}\boldsymbol{\sigma} = \frac{\hbar}{2}(\sigma_1, \sigma_2, \sigma_3)^T, \quad (1.2)$$

where $\boldsymbol{\sigma}$ is the three-vector comprised of the familiar 2×2 Pauli matrices which act upon two-component spinors $\chi = (\chi_1, \chi_2)^T$. Spinor indices will be suppressed

or noted with Latin indices. The algebra defined by the commutators of the Pauli matrices serves as a representation of $SU(2)$ group structure

$$\{\sigma_i, \sigma_j\} = 2\delta_{ij}, \quad [\sigma_i, \sigma_j] = 2i\varepsilon_{ijk}\sigma_k, \quad (1.3)$$

where ε_{ijk} is the totally antisymmetric Levi-Civita symbol and δ_{ij} is the Kronecker delta.

The relativistic theory of spin-1/2 fermions however necessitates a four-component spinor $\psi = (\psi_1, \psi_2, \psi_3, \psi_4)^T$ which as Dirac famously noted accommodates the required degrees of freedom for particles and antiparticles as well as both spin up (\uparrow) and spin down (\downarrow) eigenstates. The Hamiltonian density (in the Dirac representation) for the magnetic dipole moment interaction is given by

$$\mathcal{H}_{\text{int}} = \frac{e\hbar}{2m_\ell} \psi^\dagger \begin{pmatrix} -\boldsymbol{\sigma} \cdot \mathbf{B} & i\boldsymbol{\sigma} \cdot \mathbf{E}/c \\ -i\boldsymbol{\sigma} \cdot \mathbf{E}/c & \boldsymbol{\sigma} \cdot \mathbf{B} \end{pmatrix} \psi, \quad (1.4)$$

where ψ^\dagger is the complex conjugate transpose of the ψ spinor. The electric \mathbf{E} and magnetic \mathbf{B} fields are defined in terms of the scalar potential V and vector potential \mathbf{A} in the usual way.

$$\mathbf{E} = -\nabla V - \frac{\partial \mathbf{A}}{\partial t}, \quad \mathbf{B} = \nabla \times \mathbf{A}. \quad (1.5)$$

In the non-relativistic limit for particle states, the lower (antiparticle) components of ψ are suppressed by $|\mathbf{p}|/mc$. We can approximate the particle states in terms of two-component spinors χ to first order as

$$\psi \approx \left(\chi, \frac{\boldsymbol{\sigma} \cdot \boldsymbol{\pi}}{2m_\ell c} \chi \right)^T, \quad \boldsymbol{\pi} = \mathbf{p} - e\mathbf{A}. \quad (1.6)$$

A more rigorous method of obtaining non-relativistic Hamiltonian can be found in [Foldy and Wouthuysen \(1950\)](#). The operator $\boldsymbol{\pi}$ is the kinetic momentum operator written in terms of canonical momentum \mathbf{p} and vector potential \mathbf{A} . Making use

of the identity

$$\sigma_i \sigma_j = \delta_{ij} + i \varepsilon_{ijk} \sigma_k , \quad (1.7)$$

we insert Eq. (1.6) into Eq. (1.4) yielding to order $\mathcal{O}(1/m^3)$

$$\mathcal{H}_{\text{int}} \approx -\chi^\dagger \left(\frac{e\hbar}{2m_\ell} \boldsymbol{\sigma} \cdot \mathbf{B} + \frac{ie\hbar}{4m_\ell^2 c^2} [(\boldsymbol{\sigma} \cdot \mathbf{E}), (\boldsymbol{\sigma} \cdot \boldsymbol{\pi})] \right) \chi \quad (1.8)$$

$$\mathcal{H}_{\text{int}} \approx -\chi^\dagger \left(\frac{e\hbar}{2m_\ell} \boldsymbol{\sigma} \cdot \mathbf{B} + \frac{e\hbar^2}{4m_\ell^2 c^2} \nabla \cdot \mathbf{E} + \frac{e\hbar}{4m_\ell^2 c^2} \boldsymbol{\sigma} \cdot (\mathbf{E} \times \boldsymbol{\pi} - \boldsymbol{\pi} \times \mathbf{E}) \right) \chi . \quad (1.9)$$

Keeping only up to first order, the dipole interaction Eq. (1.4) reduces to

$$\mathcal{H}_{\text{int}} \approx -\frac{e\hbar}{2m_\ell} \chi^\dagger \boldsymbol{\sigma} \cdot \mathbf{B} \chi , \quad (1.10)$$

which is the expected non-relativistic quantum dipole term. The second and third terms in Eq. (1.9) can be interpreted as a Darwin term $\sim \nabla \cdot \mathbf{E}$ sensitive to charge density and spin orbit coupling $\sim \boldsymbol{\sigma} \cdot (\mathbf{E} \times \mathbf{p})$. We will return to relativistic notation and concepts in Section 1.1.2.

The magnetic moment operator $\boldsymbol{\mu}$, as suggested by Eq. (1.10) is defined in terms of the Pauli matrices as

$$\boldsymbol{\mu} = g \left(\frac{e\hbar}{2m_\ell} \right) \frac{\boldsymbol{\sigma}}{2} = g\mu_\ell \frac{\boldsymbol{\sigma}}{2} , \quad \mu \equiv \frac{g}{2}\mu_\ell , \quad (1.11)$$

where μ is the ‘total magneton’ value representing the full magnetic moment. The parameter g in Eq. (1.11) is the gyromagnetic ratio (or g -factor) of the particle. The ‘natural’ value is $g = 2$. While this prediction is normally attributed to the Dirac equation, it justified from the construction of the kinetic energy operator in the Schrödinger-Pauli equation; see Section 1.2.2 and [Sakurai \(1967\)](#).

In non-relativistic quantum mechanics, the time-dependant Schrödinger-Pauli

(SP) equation (with Hamiltonian H_{SP}) for a charged particle is given by

$$H_{\text{SP}}\chi = \left(\frac{1}{2m_\ell} \boldsymbol{\pi}^2 - \boldsymbol{\mu} \cdot \mathbf{B} + eV \right) \chi = i\hbar \frac{\partial}{\partial t} \chi, \quad \boldsymbol{\pi} = \mathbf{p} - e\mathbf{A}, \quad (1.12)$$

where χ is again a two-component spinor. It is well known that Eq. (1.12) is obtainable from the Dirac equation (see Section 1.1.2) in the non-relativistic limit.

Before moving on, we will verify that the SP Eq. (1.12) contains within it an expression of the Stern-Gerlach force which was used to first provide evidence of the quantization of angular momentum (Gerlach and Stern, 1922). To accomplish this, we will work in the Heisenberg representation where operators obey the following equation of motion

$$i\hbar \frac{d\mathbf{O}}{dt} = [\mathbf{O}, H] + i\hbar \frac{\partial \mathbf{O}}{\partial t}, \quad (1.13)$$

To obtain a ‘force’ in quantum mechanics we need to find the time derivative of the kinematic momentum operator $\boldsymbol{\pi}$ which is given by

$$\frac{d\boldsymbol{\pi}}{dt} = -\frac{i}{\hbar} [\boldsymbol{\pi}, H_{\text{SP}}] + \frac{\partial \boldsymbol{\pi}}{\partial t} = -\frac{i}{\hbar} \left[\boldsymbol{\pi}, \frac{(\boldsymbol{\sigma} \cdot \boldsymbol{\pi})^2}{2m} + eV \right] + \frac{\partial \boldsymbol{\pi}}{\partial t}, \quad (1.14)$$

$$\frac{\partial \boldsymbol{\pi}}{\partial t} = -\frac{\partial e\mathbf{A}}{\partial t}, \quad [\pi_i, \pi_j] = ie\hbar\varepsilon_{ijk}B_k, \quad [\pi_i, B_j] = -i\hbar\nabla_i B_j. \quad (1.15)$$

After some derivation and making use of the identities in Eq. (1.15), we arrive at the quantum analog of the Lorentz force for particles with spin

$$\frac{d\boldsymbol{\pi}}{dt} = e\mathbf{E} + \frac{e}{2m}(\boldsymbol{\pi} \times \mathbf{B} - \mathbf{B} \times \boldsymbol{\pi}) + \frac{e\hbar}{2m}\sigma_i \nabla B_i.$$

(1.16)

The last term in the expression is the Stern-Gerlach force which is sensitive to inhomogeneous magnetic fields. We also note this equation is suggestive of the ‘Ampérian’ dipole force which is in the direction of the gradient ∇ rather than the ‘Gilbertian’ type of dipole force which is in the direction of the field \mathbf{B} ; see Section 2.5. Eq. (1.16) can be connected to our classical understanding by taking the expectation value and casting it as an Ehrenfest-style theorem (Ehrenfest, 1927).

particle	category	<i>g</i> -factor
electron	elementary	-2.002 319 304 362 56(35)
muon	elementary	-2.002 331 8418(13)
tau	elementary	-2.036(34)
neutron	composite	-3.826 085 45(90)
proton	composite	5.585 694 6893(16)
deuteron	composite	0.857 438 2338(22)
triton	composite	5.957 924 931(12)

Table 1.1: The *g*-factor of various particles found in Tiesinga et al. (2021); Workman et al. (2022).

1.1.1 Anomalous magnetic moment

In nature there is no particle with exactly $g = 2$. As seen in Table 1.1, composite particles often deviate from $g = 2$ greatly as the *g*-factor of a composite particle is related to its internal composition. In the case of the neutron and proton, the internal quarks themselves are responsible in a nontrivial fashion (Chang et al., 2015). The comparison between three listed isotopes of hydrogen also displays how magnetic moments can ‘cancel out’ or add together: While the deuterium nucleus value of g is suppressed by the extra neutron, the two neutrons in the tritium nucleus balance one another returning the ratio into one manifestly similar to the proton. This reasoning however only works as a heuristic and non-perturbative Lattice QCD computations (Detmold et al., 2019) are needed to obtain the magnetic moments of hadrons with great accuracy.

When $g \neq 2$ (which is true for all physical particles with magnetic moment; composite of otherwise) the anomalous magnetic moment (AMM) can be defined via

$$a \equiv \frac{g}{2} - 1, \quad a \frac{e\hbar}{2m_\ell} \rightarrow \delta\mu \equiv \mu - \mu_\ell, \quad (1.17)$$

where a is the anomaly parameter. We also introduce $\delta\mu$ as the anomalous magneton which will be helpful in our proposal to connect mass and magnetic moment in Section 2.4 and Section 3.1.

The anomalous magnetic moment of a particle can arise from a variety of physical

sources with the most famous being the one-loop vacuum polarization contribution to the electron first computed by [Schwinger \(1951\)](#). In that work, the first correction to g is given by

$$a_e = \frac{\alpha}{2\pi}, \quad \alpha \equiv \frac{1}{4\pi\varepsilon_0} \frac{e^2}{\hbar c}, \quad (1.18)$$

where α is the fine structure constant with an approximate value of $1/137$. The measurement of the electron's g -factor is among the most precise measurements in all of physics ([Tiesinga et al., 2021](#)) and rapid advancements in the measurement of the muon's anomalous magnetic moment are occurring to this day ([Aguillard et al., 2023](#)). This makes the study of magnetic moment, and spin, an exciting area of physical research as new developments continue today.

1.1.2 Dirac and Dirac-Pauli equations

While it is always beneficial to be well-appraised of non-relativistic mechanics, nature is intrinsically relativistic and therefore this dissertation must be as well. The relativistic generalization of Eq. (1.12) is the Dirac equation given by

$$(\gamma_\alpha (i\hbar\partial^\alpha - eA^\alpha) - m_\ell c) \psi = 0, \quad (1.19)$$

$$\pi^\alpha = i\hbar\tilde{\nabla}^\alpha = i\hbar\partial^\alpha - eA^\alpha. \quad (1.20)$$

The wave function ψ in Eq. (1.19) is understood to be a four-component spinor and $\tilde{\nabla}^\alpha$ in Eq. (1.20) is the covariant derivative. π^α is the four-vector version of the kinetic momentum versus the four-momentum $p^\alpha = i\hbar\partial^\alpha$. Four-vectors and tensors in this work will be denoted by Greek indices. Inner products of four-vectors will be noted by $a \cdot b = a^\alpha \eta_{\alpha\beta} b^\beta = a^\alpha b_\alpha$ again following Einstein notation. The four-derivative ∂^α and four-potential A^α are defined as

$$\partial^\alpha = \left(\frac{1}{c} \frac{\partial}{\partial t}, -\boldsymbol{\nabla} \right), \quad A^\alpha = \left(\frac{V}{c}, \boldsymbol{A} \right). \quad (1.21)$$

We have written the Dirac equation here in the covariant form where γ^α are the gamma matrices which obey the anticommuting Clifford algebra

$$\{\gamma_\alpha, \gamma_\beta\} = \gamma_\alpha \gamma_\beta + \gamma_\beta \gamma_\alpha = 2\eta_{\alpha\beta}, \quad (1.22)$$

$$\eta_{\alpha\beta} = \text{diag}(+1, -1, -1, -1), \quad (1.23)$$

where $\eta_{\alpha\beta}$ is the flat spacetime Minkowski metric tensor defined with a positive time metric signature. The metric tensor is also responsible for raising and lowering covariant and contravariant indices e.g. $a_\alpha = \eta_{\alpha\beta} a^\beta$. As γ^α are also spinor matrices, the commutator in Eq. (1.22) carries implicit spinor indices which here computes to the 4×4 identity matrix $\mathbb{1}_4$ (which is suppressed). We also introduce the ‘fifth’ gamma matrix γ^5 which anticommutes with γ^α and the following standard conventions following [Itzykson and Zuber \(1980\)](#)

$$\boldsymbol{\alpha} = \gamma^0 \boldsymbol{\gamma}, \quad \boldsymbol{\Sigma} = \gamma^5 \boldsymbol{\alpha}, \quad \gamma^5 = i\gamma^0 \gamma^1 \gamma^2 \gamma^3, \quad \gamma_5^2 = 1. \quad (1.24)$$

As mentioned before, Eq. (1.19) predicts $g=2$ which is a standard calculation in many textbooks. The most straight-forward manner to generalize the Dirac equation allowing for an anomalous magnetic moment is to add a Pauli term proportional to the anomalous parameter a . While in most texts, the anomaly is given in terms of $g-2$ or a , we wish to keep our equations generalized to fermions of any given charge e and magnetic moment μ .

Therefore we make use of the substitution in Eq. (1.17) and write the Dirac-Pauli (DP) equation as

$$\left(\gamma_\alpha (i\hbar \partial^\alpha - eA^\alpha) - m_e c - \delta\mu \frac{1}{2c} \sigma_{\alpha\beta} F^{\alpha\beta} \right) \psi = 0, \quad (1.25)$$

where the antisymmetric spin tensor $\sigma_{\alpha\beta}$ is defined in terms of the commutator of the gamma matrices

$$\sigma_{\alpha\beta} = \frac{i}{2} [\gamma_\alpha, \gamma_\beta] = \frac{i}{2} (\gamma_\alpha \gamma_\beta - \gamma_\beta \gamma_\alpha). \quad (1.26)$$

Exact solutions to the DP equation are relatively scarce due to the complicating nature of the anomalous term. The most extensively studied solutions are those with high symmetries or constant external fields (Thaller, 2013). When the anomalous part $\delta\mu$ is zero, the Dirac equation is recovered. $F^{\alpha\beta}$ is the standard antisymmetric electromagnetic field tensor defined by

$$F^{\alpha\beta} = \partial^\alpha A^\beta - \partial^\beta A^\alpha = \begin{pmatrix} 0 & -E_1/c & -E_2/c & -E_3/c \\ E_1/c & 0 & -B_3 & B_2 \\ E_2/c & B_3 & 0 & -B_1 \\ E_3/c & -B_2 & B_1 & 0 \end{pmatrix}. \quad (1.27)$$

The electromagnetic field tensor can also be defined in terms of the commutators of the covariant derivative Eq. (1.20) as

$$[\tilde{\nabla}^\alpha, \tilde{\nabla}^\beta] = \frac{ie}{\hbar} F^{\alpha\beta}. \quad (1.28)$$

It is also useful to define the Hodge dual of the electromagnetic field tensor

$$F_{\alpha\beta}^* = \frac{1}{2} \varepsilon_{\alpha\beta\mu\nu} F^{\mu\nu} = \begin{pmatrix} 0 & -B_1 & -B_2 & -B_3 \\ B_1 & 0 & -E_3/c & E_2/c \\ B_2 & E_3/c & 0 & -E_1/c \\ B_3 & -E_2/c & E_1/c & 0 \end{pmatrix}, \quad (1.29)$$

where we use the four-dimensional fully antisymmetric Levi-Civita pseudo-tensor $\varepsilon_{\alpha\beta\mu\nu}$ with the $\varepsilon_{0123} = +1$ convention. The contracted portion $\sigma_{\alpha\beta} F^{\alpha\beta}$ in the Pauli term in Eq. (1.25) can be further expressed as

$$\frac{1}{2} \sigma_{\alpha\beta} F^{\alpha\beta} = i\boldsymbol{\alpha} \cdot \mathbf{E}/c - \boldsymbol{\Sigma} \cdot \mathbf{B} = i\gamma^0 \boldsymbol{\gamma} \cdot \mathbf{E}/c - \gamma^5 \gamma^0 \boldsymbol{\gamma} \cdot \mathbf{B}, \quad (1.30)$$

which captures that relativistic magnetic moments should be sensitive to electric as well as magnetic fields as required by Lorentz transformations of the \mathbf{E} and \mathbf{B} fields. We note that Eq. (1.30) is the matrix which appears in Eq. (1.4) specifically in the

Dirac representation of $\boldsymbol{\alpha}$ and $\boldsymbol{\Sigma}$. This should be unsurprising if one considers how the non-relativistic dipole form must generalize under Lorentz boosts which mix electric and magnetic fields.

The DP equation can be obtained from perturbative QED as an effective field theory for leptons due to vacuum polarization; see standard texts Itzykson and Zuber (1980); Schwartz (2014). However, if a particle's anomalous magnetic moment is not sourced by perturbative QFT, then the Pauli term introduced in Eq. (1.25) must be added by hand *ad hoc* or obtained via non-perturbative means such as Lattice calculations (Aoyama et al., 2020). This is the case for the hadronic contribution to anomalous magnetic moment of leptons as well as any composite particle such as the proton or neutron whose moment is determined by internal structure (Hewett et al., 2012; Green et al., 2015).

Therefore we can describe the AMM as an added Lagrangian interaction term

$$\mathcal{L}_{\text{DP,AMM}} = -\bar{\psi} \left(\delta\mu \frac{1}{2} \sigma_{\alpha\beta} F^{\alpha\beta} \right) \psi, \quad (1.31)$$

where $\bar{\psi} = \psi^\dagger \gamma^0$ is the Dirac adjoint. While the focus of this dissertation is not on quantum field theory (QFT), it is valuable to note that the Pauli Lagrangian term in Eq. (1.31) is considered 5-dimensional as the ψ fields have natural units of $[\text{length}]^{-3/2}$ as determined from the Dirac Lagrangian

$$\mathcal{L}_D/c = \bar{\psi} \left(i\hbar\gamma_\alpha \tilde{\nabla}^\alpha - m_\ell c \right) \psi, \quad \mathcal{L}_{\text{DP}} = \mathcal{L}_D + \mathcal{L}_{\text{DP,AMM}}. \quad (1.32)$$

To demonstrate, we note that the electromagnetic field tensor has natural units of $F^{\alpha\beta} \sim [\text{length}]^{-2}$. Therefore the product $\psi \sigma_{\alpha\beta} F^{\alpha\beta} \psi$ has natural units of $[\text{length}]^{-5}$ and the coefficient of Eq. (1.31) (given by $\delta\mu$) has to compensate with $\delta\mu \sim [\text{length}]^1$. This makes the DP Lagrangian unsuitable for renormalization which is an essential feature required for well-behaved QFTs. While this does not stop us using DP as an effective QFT with some natural cutoff scale responsible for the anomalous moment, it does reduce the usefulness of the equation as a general description of quantum dipole moments.

As such, there is no reason to expect non-perturbative sources of magnetic moment to strictly adhere to the DP form. An example of this would be the hadronic contribution to the lepton AMM. Additionally, the DP equation has the physically inelegant consequence of splitting the spin dynamics of fermions into (a) natural $g=2$ behavior (see Section 1.2.2) encompassed by the spinor structure of the Dirac equation and (b) the anomalous behavior contained in the Pauli term.

1.2 Klein-Gordon-Pauli equation

While the DP equation is more commonly used, there exists an alternative wave equation which describes the magnetic behavior of fermions called the Klein-Gordon-Pauli (KGP) equation. This equation was first introduced by Fock (1937) and found usefulness in the quantum electrodynamics (Feynman, 1951) and in studying weak interactions (Feynman and Gell-Mann, 1958) due to the ease of describing chiral states.

The KGP equation is generally considered to be the ‘square’ of the Dirac equation as unlike the Dirac or DP equations, it is a second order equation wave equation for the four-component spinor Ψ

$$\left((i\hbar\partial^\alpha - eA^\alpha)^2 - m_\ell^2c^2 - g\mu_\ell m_\ell \frac{1}{2}\sigma_{\alpha\beta}F^{\alpha\beta} \right) \Psi = 0. \quad (1.33)$$

In the above we printed both only the magnetic moment term; some remarks about electric dipole moments (EDM) and CP violation can be found in Section 6.2.3. The initial benefit of the KGP formulation is that the wave equation fully commutes with γ^5 making eigen-functions explicitly good chiral states. This equation is physically distinct from the DP and Dirac equations and only share solutions when $g=2$ which is seen if one tries to naively square the DP Eq. (1.25).

Eq. (1.33) is mathematically similar to the Klein-Gordon equation which describes charged scalar particles. In the same manner as scalar-QED, the squared covariant derivative contains a $e^2 A^2$ term which in QFT results in the presence of a 4-vertex seagull interaction (Schwartz, 2014) at tree-level.

It is important to emphasize that the KGP Eq. (1.33) and DP Eq. (1.25) are distinct wave equations which do not share solutions except when $g=2$ whereas both reduce to the Dirac Eq. (1.19); a detail that has occasionally gone missed in the literature. We will clarify on the relationship between the KGP and Dirac equations here by rewriting the Dirac equation in Eq. (1.19) as

$$\mathcal{D}_\pm = i\hbar\gamma_\alpha \tilde{\nabla}^\alpha \pm m_\ell c, \quad \mathcal{D}_-\psi = 0, \quad (1.34)$$

with a ‘Dirac operator’ \mathcal{D}_\pm defined in terms of positive and negative mass. This operator has the following properties

$$\mathcal{D}_- = -\gamma^5 \mathcal{D}_+ \gamma^5, \quad [\mathcal{D}_+, \mathcal{D}_-] = 0. \quad (1.35)$$

Ignoring the proportionality factor of $\sqrt{\hbar/m_\ell c}$ which accommodate the units of ψ versus Ψ , we can complete the square of the Dirac equation via the substitution $\psi \rightarrow \mathcal{D}_+ \Psi$

$$\mathcal{D}_-\psi \rightarrow \mathcal{D}_- \mathcal{D}_+ \Psi, \quad \mathcal{D}_+ \mathcal{D}_- \Psi = \left(-\hbar^2 \tilde{\nabla}^2 - m_\ell^2 c^2 - e\hbar \frac{1}{2} \sigma_{\alpha\beta} F^{\alpha\beta} \right) \Psi = 0. \quad (1.36)$$

This procedure yields the KGP equation for $g=2$. This algebraic ‘square root’ will be elaborated on further in Section 1.2.2.

For $g \neq 2$ the relationship between the DP and KGP equation becomes more complicated. Instead of a clean algebraic separation, the substitution between ψ and Ψ requires an infinite series expansion resulting from the non-local inverse substitution

$$\Psi \rightarrow \frac{1}{\mathcal{D}_+} \psi = \frac{1}{m_\ell c} \left(1 - \frac{\hbar}{m_\ell c} i\gamma_\alpha \tilde{\nabla}^\alpha - \frac{\hbar^2}{m_\ell^2 c^2} (\gamma_\alpha \tilde{\nabla}^\alpha)^2 + \dots \right) \psi. \quad (1.37)$$

The expansion in Eq. (1.37) is considered non-local because it requires an infinite number of initial conditions to determine.

While this procedure ‘square roots’ the KGP equation ($\sqrt{\text{KGP}}$), the resulting AMM Pauli Lagrangian Eq. (1.31) picks up an infinite number of derivative and field

terms which makes the theory rather unpalatable.

$$\mathcal{L}_{\sqrt{\text{KGP}}} = \mathcal{L}_D + \mathcal{L}_{\sqrt{\text{KGP}}, \text{AMM}}, \quad (1.38)$$

$$\mathcal{L}_{\sqrt{\text{KGP}}, \text{AMM}} = -\bar{\psi} \left(\delta\mu \frac{1}{2} \sigma_{\alpha\beta} F^{\alpha\beta} \left(1 - \frac{\hbar}{m_\ell c} i\gamma_\alpha \tilde{\nabla}^\alpha - \frac{\hbar^2}{m_\ell^2 c^2} (\gamma_\alpha \tilde{\nabla}^\alpha)^2 + \dots \right) \right) \psi. \quad (1.39)$$

We note each term in Eq. (1.39) is preceded by powers of the reduced Compton wavelength $\lambda_C \equiv \hbar/m_\ell c$ therefore the $\sqrt{\text{KGP}}$ model still might be of interest to study assuming the physical system that admits a reasonable cutoff.

While the first term present in Eq. (1.39) is indeed the correct $\mathcal{L}_{DP, \text{AMM}}$ term, the resulting non-local behavior ultimately breaks the unitarity of the theory making it unsuitable as a fundamental particle theory (Veltman, 1998). While the above is suggestive that there exists no unitary transform between the KGP and DP wave equations, we do not claim it as an absolute proof. If a generalized description of $g=2$ magnetic moment theories exists and makes a good fundamental quantum field theory, then likely non-minimal electromagnetic terms are required to maintain both renormalization and unitarity.

1.2.1 Features of the KGP Lagrangian

Before continuing to specific physical problems, we consider how current conversation functions in the KGP formulation of fermions and how it might differ from the Dirac current $\mathcal{J}_D^\mu \propto -i\bar{\psi}\gamma^\mu\psi$. The KGP equation can be obtained from a Lagrangian not dissimilar to the Klein-Gordon Lagrangian (Delgado-Acosta et al., 2011) and has the expression

$$\mathcal{L}_{\text{KGP}}/c^2 = \left(i\hbar \tilde{\nabla}^\mu \right)^\dagger \bar{\Psi} h_{\mu\nu} \left(i\hbar \tilde{\nabla}^\mu \right) \Psi - m^2 c^2 \bar{\Psi} \Psi, \quad h_{\mu\nu} = \eta_{\mu\nu} - i\frac{g}{2} \sigma_{\mu\nu}. \quad (1.40)$$

The matrix $h_{\mu\nu}$ acts an ‘effective’ metric which has been modified to account for the presence of an AMM. We note that the field Ψ must have units [length] $^{-1}$ such that the Lagrangian density itself has natural units of [length] $^{-4}$.

In comparison to the DP AMM Lagrangian Eq. (1.31), the KGP magnetic moment Lagrangian obtained from Eq. (1.40) is

$$\mathcal{L}_{\text{KGP,MM}}/c^2 = -\bar{\Psi} \left(\frac{g}{2} \mu_\ell m_\ell \sigma_{\alpha\beta} F^{\alpha\beta} \right) \Psi. \quad (1.41)$$

While they are mathematically similar both being ‘Pauli terms’, there are some important differences. Here the combination of fields Ψ and $F^{\alpha\beta}$ have natural units $[\text{length}]^{-4}$ and the coupling coefficient $\mu m_\ell \propto g$ is manifestly dimensionless. This means the KGP Lagrangian is at first inspection renormalizable which is an improvement over the DP Lagrangian (Rafelski et al., 2023b). Literature however suggests that the KGP Lagrangian requires additional fermion self-interactions $\mathcal{L}_{\text{int}} \sim \mathcal{O}(\bar{\Psi}\Psi)^2$ to be fully renormalizable (unless $g = 0, \pm 2$) which are not forbidden at tree-level (Angeles-Martinez and Napsuciale, 2012; Vaquera-Araujo et al., 2013).

The conserved current obtained from Eq. (1.40) can be expressed as

$$\mathcal{J}^\mu = -\frac{1}{c^2} \frac{\partial \mathcal{L}}{\partial e A_\mu} \equiv \mathcal{J}_{\text{Conv}}^\mu + \mathcal{J}_{\text{Mag}}^\mu, \quad (1.42)$$

$$\mathcal{J}^\mu = \bar{\Psi} \left(i\hbar \tilde{\nabla}^\mu \right) \Psi + \left(i\hbar \tilde{\nabla}^\mu \right)^\dagger \bar{\Psi} \Psi + i\frac{g}{2} \bar{\Psi} \sigma^{\mu\nu} \left(i\hbar \tilde{\nabla}_\nu \right) \Psi + i\frac{g}{2} \left(i\hbar \tilde{\nabla}_\nu \right)^\dagger \bar{\Psi} \sigma^{\nu\mu} \Psi. \quad (1.43)$$

The conserved current Eq. (1.42) can be interpreted as the sum of a convection current $\mathcal{J}_{\text{Conv}}$ and magnetization current \mathcal{J}_{Mag} .

$$\mathcal{J}_{\text{Conv}}^\mu = \bar{\Psi} \left(i\hbar \tilde{\nabla}^\mu \right) \Psi + \left(i\hbar \tilde{\nabla}^\mu \right)^\dagger \bar{\Psi} \Psi, \quad (1.44)$$

$$\mathcal{J}_{\text{Mag}}^\mu = \frac{g}{2} \hbar \partial_\nu \left(\bar{\Psi} \sigma^{\nu\mu} \Psi \right). \quad (1.45)$$

This is nearly identical to the Gordon Decomposition of the Dirac current \mathcal{J}_D^μ , with the exception that the magnetization current is proportional to g -factor.

The covariant derivative happens to simplify as $\tilde{\nabla} \rightarrow \partial$ in Eq. (1.45) such that the current is a divergence of the spin density $\bar{\Psi} \sigma_{\mu\nu} \Psi$. Because of the antisymmetry of $\sigma_{\mu\nu}$ the spin tensor, the magnetization current is conserved independently of the

the charge current. That both are independently conserved indicates conservation in both charge (e) and magnetic moment (μ).

1.2.2 The special case of $g = 2$

There is a strong predilection in nature towards $g = 2$ which can be explained by the requirements of kinetic operator in quantum mechanics. Rather than taking the non-relativistic limit of the Dirac equation, $g=2$ can also be derived as a consequence of replacing the definition of the inner product for vectors which accounts for spinor structure via an argument attributed to R. P. Feynman; see footnote in Chap. 3.2 of [Sakurai \(1967\)](#).

The Schrödinger equation can be extended into the Schrödinger-Pauli Eq. (1.12) via the replacement

$$\boldsymbol{\pi}^2 \rightarrow (\boldsymbol{\sigma} \cdot \boldsymbol{\pi})^2 = \pi_i \sigma_i \sigma_j \pi_j. \quad (1.46)$$

We note that because the 2×2 Pauli matrices σ_i all anticommute, we can write down the relation

$$(\boldsymbol{\sigma} \cdot \mathbf{a})(\boldsymbol{\sigma} \cdot \mathbf{b}) = \mathbf{a} \cdot \mathbf{b} + i\boldsymbol{\sigma} \cdot (\mathbf{a} \times \mathbf{b}). \quad (1.47)$$

The non-relativistic kinetic energy (KE) Hamiltonian from Eq. (1.12) then reads as

$$H_{\text{SP,KE}} = \frac{1}{2m} (\boldsymbol{\sigma} \cdot \boldsymbol{\pi})^2 = \frac{1}{2m} \boldsymbol{\pi}^2 + i\boldsymbol{\sigma} \cdot (\boldsymbol{\pi} \times \boldsymbol{\pi}) = \frac{1}{2m} \boldsymbol{\pi}^2 - \frac{e\hbar}{2m} \boldsymbol{\sigma} \cdot \mathbf{B}. \quad (1.48)$$

As the kinetic momentum operator $\boldsymbol{\pi}$ does not self-commute, its cross product is non-zero resulting in a magnetic moment term with magneton size $\mu_\ell = e\hbar/2m_\ell$ and $g=2$. Therefore, we see there is conceptual value in replacing the inner dot product with a more intricate algebraic structure; in this case: $\delta_{ij} \rightarrow \sigma_i \sigma_j$.

The natural gyromagnetic ratio then appears to arise from the $SU(2)$ Lie algebra representation that the Pauli matrices describe and electromagnetic minimal coupling. The natural scale of the magnetic moment can be interpreted as originating from

group symmetry requirements on charged particles.

An almost identical argument that g -factor arises from spin-structure and electromagnetic coupling can be made for the relativistic case as well. First we consider the quantum analog to the energy-momentum relation

$$\eta_{\alpha\beta} p^\alpha p^\beta \Phi = m^2 c^2 \Phi. \quad (1.49)$$

Eq. (1.49) as written evaluates to the Klein-Gordon equation on scalar field Φ where the four-momentum is written in the position basis $p^\alpha \rightarrow i\hbar\partial^\alpha$. Much like the non-relativistic example, we can introduce spin by replacing the momentum inner product with one sensitive to a Clifford algebra (Weinberg, 2005). Rather than the Pauli matrices, the relativistic replacement utilizes the gamma matrices yielding

$$\eta_{\alpha\beta} \rightarrow \gamma_\alpha \gamma_\beta, \quad \gamma_\alpha \gamma_\beta p^\alpha p^\beta \Psi = m^2 c^2 \Psi. \quad (1.50)$$

Here Ψ is understood to be a four-component spinor unlike in Eq. (1.49). The corresponding 4×4 matrix contraction identity analog to Eq. (1.47) is then

$$\gamma_\alpha \gamma_\beta a^\alpha b^\beta = \eta_{\alpha\beta} a^\alpha b^\beta - i\sigma_{\alpha\beta} a^\alpha b^\beta. \quad (1.51)$$

In both the relativistic and non-relativistic cases, the distinction between spin-1/2 and spinless particles is only made apparent in the kinematics in the presence of electromagnetic fields. For minimal coupling $\pi^\alpha = p^\alpha - eA^\alpha$ we take advantage of the fact that any tensor product of vectors can be decomposed as a sum of commuting (symmetric) and anticommuting (antisymmetric) parts

$$\pi^\alpha \pi^\beta = \frac{1}{2} \{ \pi^\alpha, \pi^\beta \} + \frac{1}{2} [\pi^\alpha, \pi^\beta], \quad \gamma^\alpha \gamma^\beta = \frac{1}{2} \{ \gamma^\alpha, \gamma^\beta \} + \frac{1}{2} [\gamma^\alpha, \gamma^\beta]. \quad (1.52)$$

From the above and Eq. (1.50) and Eq. (1.28) we obtain

$$\gamma_\alpha \gamma_\beta \pi^\alpha \pi^\beta \Psi = \left(\eta_{\alpha\beta} \pi^\alpha \pi^\beta - \frac{e\hbar}{2} \sigma_{\alpha\beta} F^{\alpha\beta} \right) \Psi = m^2 c^2 \Psi. \quad (1.53)$$

Eq. (1.53) is the square of the Dirac equation with precisely $g = 2$ but in a different sense than the argument established in Eq. (1.36). Rather than squaring the Dirac equation, from this perspective, we are enlarging the structure of the energy-momentum relation. The spin-1 Proca equations and spin-3/2 Rarita-Schwinger equations can also be justified via this line of reasoning with different replacements for the field and inner-product definition.

How $g \neq 2$ AMM ‘breaks’ the inner product substitution is seen more explicitly when we write the effective metric tensor $h_{\mu\nu}$ from Eq. (1.40) as

$$h_{\mu\nu} = \frac{1}{2}\{\gamma_\mu, \gamma_\nu\} + \frac{1}{2}(1+a)[\gamma_\mu, \gamma_\nu] = \gamma_\mu \gamma_\nu + \frac{a}{2}[\gamma_\mu, \gamma_\nu]. \quad (1.54)$$

The anomalous part in Eq. (1.54) is inconveniently unable to be packaged as the elementary tensor product of two four-vectors like in Eq. (1.50). The same issue occurs with any anomalous EDM introduction as well. We suggest that more elaborate algebraic structures might accommodate such terms more naturally though we leave that to future work.

Furthermore, compelling arguments can be made that all elementary particles of any spin must have a natural gyromagnetic factor of $g=2$, though a competing idea is Belinfante’s conjecture of $g=1/s$. To paraphrase the arguments by [Ferrara, Porrati, and Telepidi \(1992\)](#), $g=2$ is likely the natural scale for particles of any spin because:

1. The W boson, as the only known higher spin charged elementary particle, has at tree level $g=2$ via a Proca-like equation.
2. The relativistic TBMT torque equation is the same for any classical spin value and is most simple when the anomalous moment is zero.
3. For arbitrary spin, $g = 2$ facilitates finite Compton scattering cross sections without additional physical requirements.
4. For charged interacting particles with arbitrary spin, open bosonic and supersymmetric string theory predicts $g=2$.

We would like to add the additional argument that rotating charged black holes described by the Kerr-Newman metric also have a magnetic dipole moment with fixed $g=2$ character ([Carter, 1968](#)). This illustrates that in some sense the spin of a

black hole is ‘particle-like’ and dissimilar to the orbital Ampèrean motion of matter which has an orbital g -factor of $g_L = 1$; see Section 2.1.

While the above provide a nice justification for why particles should tend to this specific g -factor, the reality is no particle has exactly $g = 2$ with all of them displaying some form of anomaly. The charged leptons come the closest to the natural value, but famously have vacuum polarization contributions (Schwinger, 1951) from QED, non-perturbative hadronic contributions (Jegerlehner, 2017), and potentially BSM interactions (Knecht, 2004) contributing to their anomalous magnetic dipole moment.

While the perturbative approach has proven to be exceedingly successful for the charged leptons, it is not appropriate for particles whose moments are dramatically different from $g = 2$ or if the origin of the anomaly comes from internal structure such as the hadrons whose moments are determined by non-perturbative QCD (Pacetti et al., 2015) and not weakly coupled $\alpha \sim 1/137 \ll 1$ EM vacuum structure.

1.3 A few words on cosmology

This section introduces some necessary concepts which will be useful in describing the magnetization of the electron-positron primordial plasma in Chapter 4. We operate under the Λ Cold Dark Matter (Λ CDM) model of cosmology where the contemporary universe is approximately 69% dark energy, 26% dark matter, 5% baryons, and < 1% photons and neutrinos in energy density (Davis and Lineweaver, 2004; Aghanim et al., 2020). The standard picture of the universe’s evolution is outlined in Figure 1.1.

The Friedmann-Lemaître-Robertson-Walker (FLRW) line element and metric (Weinberg, 1972) in spherical coordinates is

$$ds^2 = dt^2 - a^2(t) \left[\frac{dr^2}{1 - kr^2} + r^2 d\theta^2 + r^2 \sin \theta^2 d\phi^2 \right], \quad (1.55)$$

$$g_{\alpha\beta} = \begin{pmatrix} 1 & 0 & 0 & 0 \\ 0 & -\frac{a^2(t)}{1 - kr^2} & 0 & 0 \\ 0 & 0 & -a^2(t)r^2 & 0 \\ 0 & 0 & 0 & -a^2(t)r^2 \sin \theta^2 \end{pmatrix}. \quad (1.56)$$

The Gaussian curvature k informs the spatial shape of the universe with the following possibilities: infinite flat Euclidean ($k = 0$), finite spherical but unbounded ($k = +1$), or infinite hyperbolic saddle-shaped ($k = -1$). Observation indicates our universe is flat or nearly so.

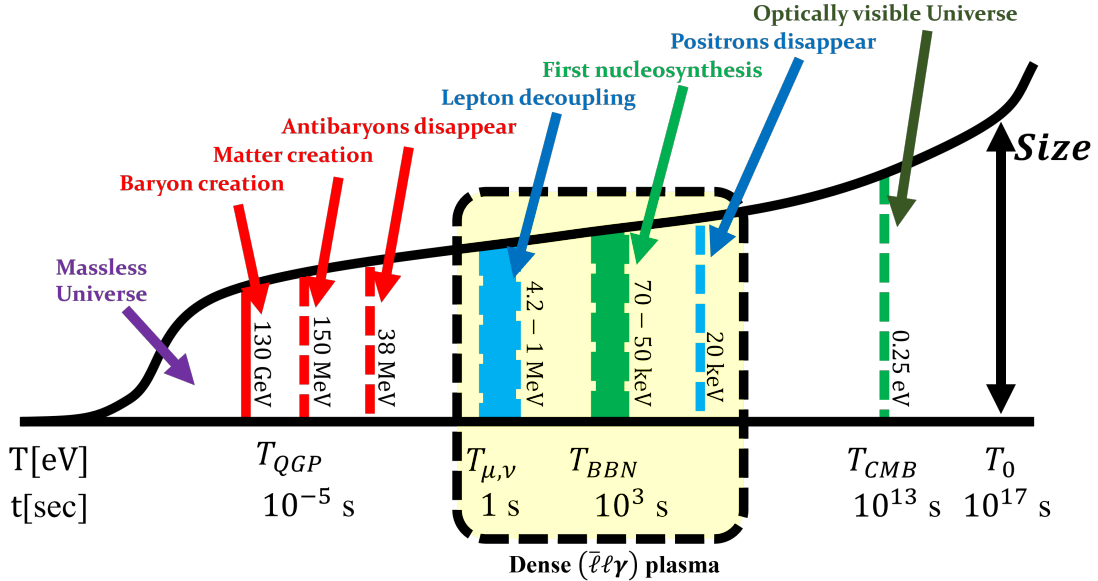


Figure 1.1: A schematic of the universe's evolution since the Big Bang. The region of interest studied in this dissertation is emphasized (in the highlighted box) to contain a dense nearly charge neutral matter-antimatter plasma.

The scale factor $a(t)$ denotes the change of proper distances $L(t)$ over time as

$$L(t) = L_0 \frac{a_0}{a(t)} \rightarrow L(z) = L_0(1+z), \quad (1.57)$$

where z is the redshift and L_0 the comoving length. In an expanding (or contracting) universe which is both homogeneous and isotropic, this implies volumes change with $V(t) = V_0/a^3(t)$ where $V_0 = L_0^3$ is the comoving Cartesian volume. The evolutionary expansion of the universe is then traditionally defined in terms of the Hubble

parameter $H(t)$ following the conventions in Weinberg (1972)

$$H(t)^2 \equiv \left(\frac{\dot{a}}{a}\right)^2 = \frac{8\pi G_N}{3} \rho_{\text{total}}, \quad \rho_{\text{total}}(t) = \rho_\Lambda + \rho_{\text{DM}}(t) + \rho_{\text{Baryons}}(t) + \dots \quad (1.58)$$

$$\frac{\ddot{a}}{a} = -qH^2, \quad q \equiv -\frac{a\ddot{a}}{\dot{a}^2}, \quad \dot{H} = -H^2(1+q). \quad (1.59)$$

where G_N is the Newtonian constant of gravitation. Eq. (1.58) and Eq. (1.59) are also known as the Friedmann equations. The total density ρ_{total} is the sum of all contributions from any form of matter, radiation or field. This includes but is not limited to: dark energy (Λ), dark matter (DM), baryons (B), leptons (ℓ, ν) and photons (γ). Depending on the age of the universe, the relative importance of each group changes as each dilutes different under expansion with dark energy infamously remaining constant in density and accelerating the universe today.

The parameter q is the cosmic deceleration parameter where for historical reasons expansion is slowing down for $q > 0$. before the discovery of dark energy. The early universe was radiation dominated with $q = 1$, subsequently matter dominated with $q = 1/2$, and the contemporary universe is undergoing a transition from matter to dark energy dominated whereas the deceleration settles on the asymptotic value of $q = -1$; see Rafelski and Birrell (2014).

We can consider the expansion to be an adiabatic process (Abdalla et al., 2022) which results in a smooth shifting of the relevant dynamical quantities. As the universe undergoes isotropic expansion, the temperature decreases as

$$T(t) = T_0 \frac{a_0}{a(t)} \rightarrow T(z) = T_0(1+z), \quad (1.60)$$

where z is the redshift. The entropy within a comoving volume is kept constant until gravitational collapse effects become relevant. The comoving temperature T_0 is given by the present CMB temperature $T_0 = 2.7 \text{ K} \simeq 2.3 \times 10^{-4} \text{ eV}$ (Aghanim et al., 2020), with contemporary scale factor $a_0 = 1$.

As the universe expands, redshift reduces the momenta of particles lowering their

contribution to the energy content of the universe. This cosmic redshift is written as

$$p_i(t) = p_{i,0} \frac{a_0}{a(t)} . \quad (1.61)$$

Momentum (and the energy of massless particles $E = pc$) scales with the same factor as temperature. The energy of massive free particles in the universe however scales differently based on their momentum (and thus temperature).

When hot and relativistic, particle energy scales inversely like radiation. As the particles transition to non-relativistic (NR) momenta, their energies scale with the inverse square of the scale factor

$$E(t) = E_0 \frac{a_0}{a(t)} \xrightarrow{\text{NR}} E_0 \frac{a_0^2}{a(t)^2} . \quad (1.62)$$

This occurs because of the functional dependence of energy on momentum in the relativistic $E \sim p$ versus non-relativistic $E \sim p^2$ cases.

CHAPTER 2

Dynamics of charged particles with arbitrary magnetic moment

In Section 1.1, we addressed two different models of introducing anomalous magnetic moment in QM:

- (a) the Dirac-Pauli (DP) first order equation which is the Dirac equation where g -factor is precisely fixed to the $g=2$, with the addition of an incremental Pauli term; and
- (b) the Klein-Gordon-Pauli (KGP) second order equation which “squares” the Dirac equation and thereafter allows the magnetic moment μ to vary independently of charge and mass, unlike Dirac theory.

These two approaches coincide when the anomaly a vanishes. However, all particles that have magnetic moments differ from the Dirac value $g = 2$, either due to their composite nature, or, for point particles, due to the quantum vacuum fluctuation effect.

We find that even a small magnetic anomaly has a large effect in the limit of strong fields generated by massive magnetar stars (Kaspi and Beloborodov, 2017). Therefore it is not clear that the tacit assumption of $g = 2$ in the case of strong fields (Rafelski et al., 1978; Greiner et al., 2012a; Rafelski et al., 2017) is prudent (Evans and Rafelski, 2018). This argument is especially applicable to tightly bound composite particles such as protons and neutrons where the large anomalous magnetic moment can be taken as an external prescribed parameter unrelated to the elementary quantum vacuum fluctuations. It is then of particular interest to study the dynamical behavior of these particles in fields of magnetar strength. This interest carries over to the environment of strong fields created in focus of ultra-intense laser pulses and the associated particle production processes (Dunne, 2014; Hegelich et al., 2014). We

consider also precision spectroscopic experiments and recognize consequences even in the weak coupling limit.

This chapter reviews our work done in exploring relativistic dynamics with arbitrary magnetic dipoles in both a quantum mechanical and classical context. Section 2.1 and Section 2.2 and covers analytic solutions for the Klein-Gordon-Pauli (KGP) equation in the presence of homogeneous magnetic fields and the Coulomb problem for hydrogen-like atoms. Comparisons with the Dirac-Pauli (DP) and Dirac solutions are made and novel consequences for strong fields are discussed in Section 2.3. Section 2.4 explores extensions to KGP which combine mass and magnetic moment into a dynamical mass which is sensitive to electromagnetic fields. This work is primarily based on [Steinmetz et al. \(2019\)](#).

Relativistic classical spin dynamics is discussed in Section 2.5 and is based on our work in [Rafelski et al. \(2018\)](#). We propose in Section 2.5.1 a covariant form of magnetic dipole potential which modifies the Lorentz force, extends the Thomas-Bargmann-Michel-Telegdi (TMBT) equation, and reproduces the Stern-Gerlach force in the non-relativistic limit. Section 2.5.2 demonstrates that this magnetic potential also serves to unify both the Ampèrian and Gilbertian pictures of dipole moments.

2.1 Homogeneous magnetic fields

The case of the homogeneous magnetic field, sometimes referred to as the Landau problem, provides a stepping stone in which to examine the consequences of quantum spin dynamics in a concrete analytical fashion. We present here an abbreviated analysis and the full treatment of this solution in terms of Ladder operators can be found in [Steinmetz et al. \(2019\)](#) while alternative approaches are shown in texts such as [Itzykson and Zuber \(1980\)](#). We take a constant magnetic field in the z -direction to be

$$\mathbf{B} = (0, 0, B). \quad (2.1)$$

For our choice of gauge, there are two common options: (a) the Landau \mathbf{A}_L gauge and (b) the symmetric \mathbf{A}_S gauge

$$\mathbf{A}_L = B(0, x, 0), \quad \mathbf{A}_S = \frac{B}{2}(-y, x, 0). \quad (2.2)$$

As the system has a manifest rotational symmetry perpendicular to the direction of the homogeneous field, we will choose the symmetric gauge \mathbf{A}_S which preserves this symmetry explicitly.

Before we examine relativistic wave equations, it will be helpful to first consider the non-relativistic Schrödinger-Pauli case as the KGP-Landau problem can be written as equivalent to the Schrödinger-Pauli Hamiltonian. We consider energy eigenstates of an electron with m_e described by Eq. (1.12) under Eq. (2.1) as

$$\chi \rightarrow \chi_E \exp\left(-\frac{iEt}{\hbar}\right), \quad \left(\frac{1}{2m_e}\boldsymbol{\pi}^2 - \boldsymbol{\mu} \cdot \mathbf{B}\right)\chi_E = E\chi_E, \quad (2.3)$$

where μ is the magnitude of the magnetic moment as defined in Eq. (1.11). Eq. (2.3) can be further rewritten using angular momentum \mathbf{L} and the symmetric gauge Eq. (2.2) as

$$\left(\frac{1}{2m_e}\mathbf{p}^2 + \frac{e^2B^2}{8m_e}(x^2 + y^2) - \frac{eB}{2m_e}L_3 - \mu B\sigma_3\right)\chi_E = E\chi_E, \quad (2.4)$$

$$\mathbf{L} = \mathbf{r} \times \mathbf{p}, \quad L_i = \varepsilon_{ijk}x_j p_k. \quad (2.5)$$

The above can be broken into a set of three mutually commuting Hamiltonian operators:

- (a) Free particle Hamiltonian (Free)
- (b) Quantum harmonic oscillator (HO)
- (c) Zeeman interaction (ZI)

given by

$$(a) \quad H_{\text{Free}} = \frac{p_3^2}{2m}, \quad (2.6)$$

$$(b) \quad H_{\text{HO}} = \frac{1}{2m_e} (p_1^2 + p_2^2) + \frac{1}{2} m_e \omega^2 (x^2 + y^2), \quad (2.7)$$

$$(c) \quad H_{\text{ZI}} = -\mu_B B \frac{L_3}{\hbar} - \mu_B \sigma_3, \quad (2.8)$$

which forms the total Hamiltonian

$$H_{\text{total}} = H_{\text{Free}} + H_{\text{HO}} + H_{\text{Mag.}}. \quad (2.9)$$

The cyclotron frequency appears in Eq. (2.7) as $2\omega = \omega_C = eB/m_e$. We note that the Zeeman Eq. (2.8) is usually expressed as

$$H_{\text{ZI}} = -\frac{e}{2m} (g_L \mathbf{L} + g_S \mathbf{S}) \cdot \mathbf{B}, \quad g_L = 1, \quad (2.10)$$

with \mathbf{S} defined in Eq. (1.2). We see explicitly that the orbital gyromagnetic ratio g_L which is a coefficient to the angular momentum operator \mathbf{L} is unity unlike for spin. We refer back to our comment about black hole rotation in Section 1.2.2 as spin-like rather than orbital-like in terms of its magnetic behavior. As all the above Hamiltonian operators are mutually commuting, the energy eigenvalue of the total Hamiltonian is the sum of the individual energy eigenvalues. Our remaining goal will be to convert the KGP eigenvalue equation into the above three non-relativistic Hamiltonian operators.

We now return to the KGP equation and write expand Eq. (1.33) for the Landau problem with energy eigenstates Ψ_E yielding

$$\left(\frac{E^2}{c^2} - m_e^2 c^2 - \mathbf{p}^2 - \frac{1}{4} e^2 B^2 (x^2 + y^2) + e B L_3 + 2\mu m_e B \sigma_3 \right) \Psi_E = 0. \quad (2.11)$$

We introduce the substitutions

$$E \rightarrow m'c^2, \quad \frac{E^2 - m_e^2 c^4}{2E} \rightarrow E', \quad (2.12)$$

and recast KGP Eq. (2.11) into a Schrödinger-style Hamiltonian equation

$$\left(\frac{1}{2m'} \mathbf{p}^2 + \frac{e^2 B^2}{8m'} (x^2 + y^2) - \frac{eB}{2m'} L_3 - \mu \left(\frac{m_e}{m'} \right) B \sigma_3 \right) \Psi_E = E' \Psi_E, \quad (2.13)$$

which matches the non-relativistic Hamiltonian presented in Eq. (2.9).

The energy eigenvalues of Eq. (2.9) are given by

$$E'_{n,s}(p_3, B) = \frac{p_3^2}{2m'} + \frac{e\hbar B}{m'} \left(n + \frac{1}{2} \right) - \mu B \left(\frac{m_e}{m'} \right) s, \quad (2.14)$$

where $n \in 1, 2, 3 \dots$ is the Landau orbital quantum number and $s \in \pm 1$ is the spin quantum number. The physical relativistic energies can be obtained by undoing the substitutions in Eq. (2.12) yielding from Eq. (2.14)

$$E_{n,s}^2(p_3, B) = m_e^2 c^4 + p_3^2 c^2 + 2e\hbar c^2 B \left(n + \frac{1}{2} \right) - 2\mu B m_e c^2 s, \quad (2.15)$$

$$E_{n,s} = \pm \sqrt{m_e^2 c^4 + p_3^2 c^2 + 2e\hbar c^2 B \left(n + \frac{1}{2} \right) - 2\mu B m_e c^2 s}. \quad (2.16)$$

This expression for the relativistic Landau levels is the same as found by Weisskopf (1936) for the Dirac equation setting $g=2$ in Eq. (2.16). The Landau orbital part and spin portions can be combined when the magnetic moment is expressed in terms of e/m , but the form in Eq. (2.16) keeps it generalized for the case of neutral particles.

Restricting ourselves to the positive energy spectrum, the non-relativistic reduction of Eq. (2.16) can be carried out in powers of $1/m$ in the large mass limit yielding

$$\begin{aligned} E_{n,s}|_{\text{NR}} &= m_e c^2 + \frac{p_3^2}{2m_e} + \mu_B B \left(2n + 1 - \frac{g}{2}s \right) - \frac{p_3^4}{8m_e^3 c^2} \\ &\quad - \frac{p_3^2}{2m_e} \frac{\mu_B B}{m_e c^2} \left(2n + 1 - \frac{g}{2}s \right) - \frac{\mu_B^2 B^2}{2m_e c^2} \left(2n + 1 - \frac{g}{2}s \right)^2 + \mathcal{O}(1/m_e^5), \end{aligned} \quad (2.17)$$

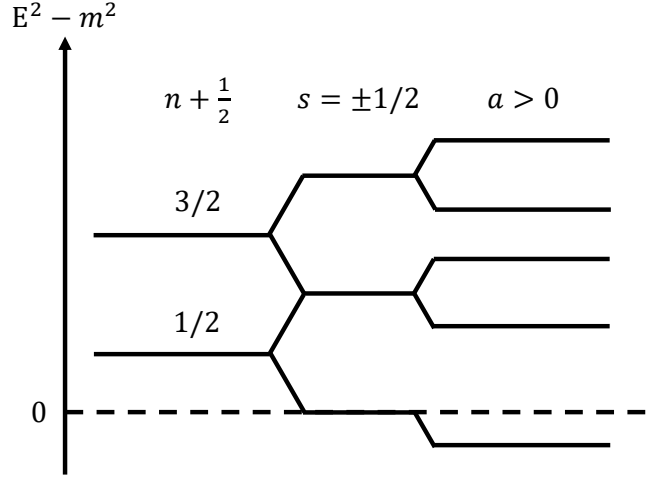


Figure 2.1: Diagram organizing the KGP-Landau levels for particles with zero z-component momentum. The Landau levels n and spin s serve to split levels while the anomaly a controls the degeneracy among levels.

which contains the expected terms such as the non-relativistic kinetic energy in the z-direction, the first relativistic correction to kinetic energy, the Landau energies, and cross terms that behave like modifications to the mass of the particle.

The KGP-Landau levels above the ground state lose their (accidental) degeneracy for $g \neq 2$. This is shown schematically in Figure 2.1. The anomaly also causes the ground state to be pushed downward, such that $E^2 < m^2$; if the anomaly and the magnetic field are large enough, states above the ground state are also pushed below the rest mass energy of the particle.

However, we recognize a periodicity considering the energy as a function of g . We recall that in Eq. (2.16) $n = 0, 1, 2, \dots$. As g varies, each time $gs/2$ crosses an integer value, for a different value of n the energy eigenvalue E repeat as a function of changing g . All possible values of energy E are reached (at fixed m and p_3^2) for $-2 \leq g \leq 2$. Moreover, while for almost all $g \neq 2$ the degeneracy is completely broken, this periodicity implies that energy degeneracy is restored for values [Evans \(2022\)](#); [Evans and Rafelski \(2022\)](#)

$$g_k/2 = 1 + k, \quad \lambda'_L = \lambda_L - ks, \quad \lambda_L = n + \frac{1}{2} - s, \quad (2.18)$$

where $k = 0, \pm 1, \pm 2, \dots$. The Landau levels Eq. (2.15) contain an infinite number of degenerate levels bounded from below. Certain states change the sign of the magnetic energy and their total energies become unphysical in the limit that $g_k B$ becomes large; for even k there are $k/2$ such states and for odd k there are $(k+1)/2$.

It is useful to compare the KGP solution to the the Landau levels for the DP equation which we obtained by [Tsai and Yildiz \(1971\)](#). The DP-Landua energy eigenstates are given by

$$E_{n,s}^2(p_3, B)|_{\text{DP}} = \left(\sqrt{m_e^2 c^4 + 2e\hbar c^2 B \left(n + \frac{1}{2} - s \right)} - \frac{eB\hbar}{2m_e}(g-2)s \right)^2 + p_3^2 c^2, \quad (2.19a)$$

$$E_{n,s}|_{\text{DP}} = \pm \sqrt{\left(\sqrt{m_e^2 c^4 + 2e\hbar c^2 B \left(n + \frac{1}{2} - s \right)} - \frac{eB\hbar}{2m_e}(g-2)s \right)^2 + p_3^2 c^2}, \quad (2.19b)$$

which in our opinion fails Dirac's principle of mathematical beauty when compared to the KGP result Eq. (2.16). Both Eqs. (2.16) and (2.19b) have the correct non-relativistic reduction at the lowest order though, the latter obscures the physical interpretation.

The most egregious issue with the DP-Landau levels is that, in a perturbative expansion, it includes cross terms between the $g=2$ magnetic moment and anomalous terms in $a = (g-2)/2$; thus the result does not depend on the particle magnetic moment alone; there is a functional dependence on the magnetic anomaly a . The presence of these cross terms implies that above first order the results cannot be given in terms of the full magnetic moment alone. In comparison, for the KGP-Landau levels Eq. (2.19b), the entire effect of magnetic moment is contained in a single term.

2.2 Hydrogen-like atoms

The Coulomb problem, or sometimes referred to as the Kepler problem, provides us an important application of any quantum theory to explore. As the hydrogen-like atoms are the the most well understood atomic system in physics, any non-minimal

behavior especially for high- Z systems can lead to consequences for the resulting spectral lines. We take the Coulomb potential to be

$$eV_C \equiv eA^0 = \frac{Z\alpha\hbar c}{r} , \quad \mathbf{A} = 0 . \quad (2.20)$$

The KGP-Coulomb problem with arbitrary magnetic moment can be solved analytically and we will briefly sketch out the solution and its consequences.

For energy states $\Psi = e^{-iEt/\hbar}\Psi_E$ the KGP equation yields the following differential equation

$$\left(\frac{E^2 - m^2c^4}{\hbar^2c^2} + \frac{Z^2\alpha^2}{r^2} + \frac{2E}{\hbar c} \frac{Z\alpha}{r} + \frac{1}{r} \frac{\partial \mathbf{L}^2}{\partial r^2} r - \frac{\mathbf{L}^2/\hbar^2}{r^2} - \frac{g}{2} Z\alpha \frac{i\boldsymbol{\alpha} \cdot \hat{\mathbf{r}}}{r^2} \right) \Psi_E = 0 . \quad (2.21)$$

We recast the squared angular momentum operator \mathbf{L}^2 with the Dirac spin-alignment operator

$$\mathcal{K} = \gamma^0 \left(1 + \boldsymbol{\Sigma} \cdot \frac{\mathbf{L}}{\hbar} \right) , \quad \mathbf{L}^2/\hbar^2 = \mathcal{K} (\mathcal{K} - \gamma^0) . \quad (2.22)$$

The operator \mathcal{K} commutes with $\boldsymbol{\alpha} \cdot \hat{\mathbf{r}}$ and its eigenvalues are given as either positive or negative integers $\kappa = \pm(j + 1/2)$ where j is the total angular momentum quantum number. By grouping all terms proportional to $1/r^2$, we see the effective angular momentum eigenvalues take on non-integer values which in the limit of classical mechanics corresponds to orbits which do not close. The non-integer eigenvalues depends explicitly on g -factor.

The difficulty of this equation is that the effective angular momentum operator is non-diagonal in spinor space due to the presence of $\boldsymbol{\alpha} \cdot \hat{\mathbf{r}}$ which mixes upper and lower components. The effective radial potential within Eq. (2.21) is then

$$V_{\text{eff}} = -\frac{2E}{\hbar c} \frac{Z\alpha}{r} - \frac{Z^2\alpha^2}{r^2} + \frac{g}{2} Z\alpha \frac{i\boldsymbol{\alpha} \cdot \hat{\mathbf{r}}}{r^2} .$$

(2.23)

We emphasize that the distinguishing characteristic which separates the KGP solutions (and Dirac for $g = 2$) from the Klein-Gordon solutions is the last term in the

effective potential Eq. (2.23). This is the dipole-charge interaction term which exists only because of the relativistic expression for the magnetic dipole and is entirely absent non-relativistically.

Following the procedure of [Martin and Glauber \(1958\)](#), we introduce the operator

$$\mathfrak{L} = -\gamma^0 \mathcal{K} - \frac{g}{2} Z \alpha (i\boldsymbol{\alpha} \cdot \hat{\mathbf{r}}) , \quad (2.24)$$

but with the novel modification that g -factor directly appears in the second term. This operator is also sometimes referred to as the Temple operator, therefore we will refer to it as the g -Temple operator. This operator then commutes with the spin-alignment operator \mathcal{K} and has eigenvalues

$$\Lambda = \pm \sqrt{\kappa^2 - \frac{g^2}{4} Z^2 \alpha^2} , \quad (2.25)$$

where the absolute values are denoted as $\lambda = |\Lambda|$. The angular momentum contributions to Eq. (2.21) can then be replaced by

$$\mathcal{K}(\mathcal{K} - \gamma^0) - Z^2 \alpha^2 - \frac{g}{2} Z \alpha (i\boldsymbol{\alpha} \cdot \hat{\mathbf{r}}) = \mathfrak{L}(\mathfrak{L} + 1) + \left(\frac{g^2}{4} - 1 \right) Z^2 \alpha^2 . \quad (2.26)$$

If the g -factor is taken to be $g=2$, then the differential Eq. (2.21) reverts to the one discussed in [Martin and Glauber \(1958\)](#). The coefficient $g^2/4 - 1$ will be commonly seen to precede new more complicated terms, which conveniently vanish for $|g| = 2$ demonstrating that as function of g there is a “cusp” ([Rafelski et al., 2023b](#)) for $|g| = 2$. This will become especially evident when we discuss strongly bound systems which behave very differently for $|g| < 2$ versus $|g| > 2$.

We omit further derivation which can be found in [Steinmetz et al. \(2019\)](#). We

find the resulting energy levels of the KGP-Coulomb equation to be

$$E_{\pm\lambda}^{n_r,j} = mc^2 \left[1 + \frac{Z^2\alpha^2}{(n_r + 1/2 + \nu)^2} \right]^{-1/2}, \quad (2.27)$$

$$\nu = \sqrt{(\lambda \pm 1/2)^2 + \left(\frac{g^2}{4} - 1 \right) Z^2\alpha^2}, \quad \lambda = \sqrt{(j + 1/2)^2 - \frac{g^2}{4} Z^2\alpha^2}. \quad (2.28)$$

where n_r is the node quantum number which takes on the values $n_r = 0, 1, 2, \dots$. Eq. (2.27) is the same “Sommerfeld-style” expression for energy that we can obtain from the Dirac or KG equations. The difference between them arises from the expression of the relativistic angular momentum which depends on g -factor for the KGP equation. The KGP eigenvalues Eq. (2.27) for arbitrary spin were obtained by [Niederle and Nikitin \(2006\)](#) using a tensor approach.

In the limit that $g \rightarrow 2$ for the Dirac case the expressions for λ and ν reduce to

$$\lim_{g \rightarrow 2} \lambda = \sqrt{(j + 1/2)^2 - Z^2\alpha^2}, \quad (2.29a)$$

$$\lim_{g \rightarrow 2} \nu_{\pm\lambda} = \lambda \pm 1/2. \quad (2.29b)$$

This procedure requires taking the root of perfect squares; therefore, the sign information is lost in Eq. (2.29a). As long as $Z^2\alpha^2 < 3/4$ we can drop the absolute value notation as ν is always positive. The energy is then given by

$$E_{\pm\lambda}^{n_r,j} = mc^2 \left[1 + \frac{Z^2\alpha^2}{\left(n_r \begin{smallmatrix} +1 \\ +0 \end{smallmatrix} + \sqrt{(j + 1/2)^2 - Z^2\alpha^2} \right)^2} \right]^{-1/2}. \quad (2.30)$$

The $\begin{smallmatrix} +1 \\ +0 \end{smallmatrix}$ notation is read as the upper value corresponding to the $+\lambda$ states and the lower value corresponding to the $-\lambda$ states.

The ground state energy (with: $n_r = 0$, $\Lambda < 0$, $j = 1/2$) is therefore

$$E_{-\lambda(j=1/2)}^{0,1/2} = mc^2 \sqrt{1 - Z^2\alpha^2}, \quad (2.31)$$

as expected for the Dirac-Coulomb ground state. Eq. (2.30) reproduces the Dirac-

Coulomb energies and also contains a degeneracy between states of opposite λ sign, same j quantum number and node quantum numbers offset by one

$$E_{-\lambda}^{n_r+1,j} = E_{+\lambda}^{n_r,j}, \quad (2.32)$$

which corresponds to the degeneracy between $2S_{1/2}$ and $2P_{1/2}$ states. There is no degeneracy for the $E_{-\lambda}^{0,j}$ states.

In the limit that $g \rightarrow 0$, which is the KG case, the expressions are given by

$$\lim_{g \rightarrow 0} \lambda = j + 1/2, \quad (2.33a)$$

$$\lim_{g \rightarrow 0} \nu_{\pm\lambda} = \sqrt{(j_{+0}^{+1})^2 - Z^2\alpha^2}, \quad (2.33b)$$

which reproduces the correct expressions for the energy levels for the Klein-Gordon case

$$E_{\pm\lambda}^{n_r,j} = mc^2 \left[1 + \frac{Z^2\alpha^2}{\left(n_r + 1/2 + \sqrt{(j_{+0}^{+1})^2 - Z^2\alpha^2} \right)^2} \right]^{-1/2}, \quad (2.34)$$

except that in this limit we are still considering the total angular moment quantum number j rather than orbital momentum quantum number ℓ . It is interesting to note that the KG-Coulomb problem's energy formula contains $\ell + 1/2$, which matches identically to our half-integer j values; therefore, this artifact of spin, untethered and invisible by the lack of magnetic moment, does not alter the energies of the states. The degeneracy in energy levels are given by

$$E_{-\lambda}^{n_r,j+1} = E_{+\lambda}^{n_r,j}, \quad (2.35)$$

with levels of opposite λ sign, same node quantum number and shifted j values by one. In a similar fashion to the Dirac case, here we have no degeneracy for $E_{-\lambda}^{n_r,1/2}$ states.

2.2.1 Non-relativistic Coulomb problem energies

The first regime of interest to understand the effect of variable g in the KGP-Coulomb problem is the non-relativistic limit characterized by the weak binding of low-Z atoms. We now will convert from n_r , j and $\pm\lambda$ to the familiar quantum numbers of n , j and ℓ allowing for easy comparison with the hydrogen spectrum in standard notation. We start by expanding Eq. (2.27) in powers of $Z\alpha$ to compare to the known hydrogen spectrum.

To order $\mathcal{O}(Z^4\alpha^4)$ the energy levels are given by

$$\frac{E_{\pm\lambda}^{n_r,j}}{mc^2} = 1 - \frac{1}{2} \frac{Z^2\alpha^2}{(n_r + 1/2 + (\nu_{\pm\lambda})|_{Z=0})^2} + \frac{(\nu_{\pm\lambda})'|_{Z=0} Z^3\alpha^3}{(n_r + 1/2 + (\nu_{\pm\lambda})|_{Z=0})^3} \\ + \frac{1}{2} \frac{(3/4 - 3(\nu_{\pm\lambda})|_{Z=0}^2)Z^4\alpha^4}{(n_r + 1/2 + (\nu_{\pm\lambda})|_{Z=0})^4} + \frac{1}{2} \frac{(\nu_{\pm\lambda})''|_{Z=0} Z^4\alpha^4}{(n_r + 1/2 + (\nu_{\pm\lambda})|_{Z=0})^3} + \mathcal{O}(Z^6\alpha^6), \quad (2.36)$$

where primed $\nu_{\pm\lambda}$ indicate derivatives with respect to $Z\alpha$. These derivatives evaluate to

$$(\nu_{\pm\lambda})|_{Z=0} = j + 1/2 \pm 1/2, \quad (2.37) \\ (\nu_{\pm\lambda})'|_{Z=0} = 0, \\ (\nu_{\pm\lambda})''|_{Z=0} = \frac{(g^2/4 - 1)}{j + 1/2 \pm 1/2} - \frac{g^2/4}{j + 1/2}.$$

Eq. (2.36) then simplifies to

$$\frac{E_{\pm\lambda}^{n_r,j}}{mc^2} = 1 - \frac{1}{2} \frac{Z^2\alpha^2}{\left(n_r + j_{+1/2}^{+3/2}\right)^2} + \frac{3}{8} \frac{Z^4\alpha^4}{\left(n_r + j_{+1/2}^{+3/2}\right)^4} \\ + \frac{1}{2} \left(\frac{(g^2/4 - 1)}{j_{+0}^{+1}} - \frac{g^2/4}{j + 1/2} \right) \frac{Z^4\alpha^4}{\left(n_r + j_{+1/2}^{+3/2}\right)^3} + \mathcal{O}(Z^6\alpha^6). \quad (2.38)$$

In the non relativistic limit, the node quantum number corresponds to the principle quantum number via $n_r = n' - j - 1/2$ with $n' = 1, 2, 3 \dots$ Using Eq. (2.38) and Eq. (2.24) we see that in the non relativistic limit $+\lambda$ corresponds to $\kappa > 0$ or anti-aligned spin-angular momentum with $j = \ell - 1/2$ and $\ell \geq 1$. Conversely $-\lambda$

corresponds to $\kappa < 0$ or aligned spin-angular momentum with $j = \ell + 1/2$.

With all this input we arrive at

$$\frac{E_{\kappa>0}^{n,j}}{mc^2} = 1 - \frac{1}{2} \frac{Z^2 \alpha^2}{(n'_{+0}^{+1})^2} + \frac{3}{8} \frac{Z^4 \alpha^4}{(n'_{+0}^{+1})^4} + \frac{1}{2} \frac{(g^2/4 - 1)}{j_{+0}^{+1}} \frac{Z^4 \alpha^4}{(n'_{+0}^{+1})^3} - \frac{1}{2} \frac{g^2/4}{j + 1/2} \frac{Z^4 \alpha^4}{(n'_{+0}^{+1})^3} + \mathcal{O}(Z^6 \alpha^6). \quad (2.39)$$

Lastly we recast, for the $\kappa > 0$ states, the principle quantum number as $n' + 1 \rightarrow n$ with $n \geq 2$ and we simply relabel $n' \rightarrow n$ for $\kappa < 0$ states. This allows Eq. (2.39) to be completely written in terms of n , j , and ℓ as

$$\frac{E_{\ell}^{n,j}}{mc^2} = 1 - \frac{1}{2} \frac{Z^2 \alpha^2}{n^2} + \frac{3}{8} \frac{Z^4 \alpha^4}{n^4} + \frac{1}{2} \frac{(g^2/4 - 1)}{\ell + 1/2} \frac{Z^4 \alpha^4}{n^3} - \frac{1}{2} \frac{g^2/4}{j + 1/2} \frac{Z^4 \alpha^4}{n^3} + \mathcal{O}(Z^6 \alpha^6), \quad (2.40)$$

where it is understood that $n - \ell \geq 1$, this condition allows us to write what was previously described in Eq. (2.39) as two distinct spectra now as a single energy spectra. In the limit $g \rightarrow 2$ or $g \rightarrow 0$ the correct expansion to order $Z^4 \alpha^4$ of the Dirac or KG energies are obtained. In the following we explore some consequences of our principal non-relativistic result, Eq. (2.40).

2.2.2 g-Lamb Shift between 2S and 2P orbitals

The breaking of degeneracy in Eq. (2.40) between states of differing ℓ orbital quantum number, but the same total angular momentum j and principle quantum number n is responsible for the Lamb shift due to anomalous magnetic moment. The only term in Eq. (2.40) (up to order $Z^4 \alpha^4$) that breaks the degeneracy between the $E_{\ell=j+1/2}^{n,j}$ and $E_{\ell=j-1/2}^{n,j}$ states for $n \geq 2$ is the fourth term. This is unsurprising as it depends exclusively on quantum number ℓ and n . The lowest order Lamb shift due to anomalous

magnetic moment is then

$$\frac{\Delta E_{\text{gLamb}}^{n,j}}{mc^2} = E_{\ell=j-1/2}^{n,j} - E_{\ell=j+1/2}^{n,j} = (g^2/8 - 1/2) \left(\frac{1}{j} - \frac{1}{j+1} \right) \frac{Z^4 \alpha^4}{n^3}. \quad (2.41)$$

For the $2S_{1/2}$ and $2P_{1/2}$ states Eq. (2.41) reduces to

$$\frac{\Delta E_{\text{gLamb}}^{2S_{1/2}-2P_{1/2}}}{mc^2} = (g^2/8 - 1/2) \frac{Z^4 \alpha^4}{6} = (a + a^2/2) \frac{Z^4 \alpha^4}{6}. \quad (2.42)$$

Our result in Eq. (2.41) and Eq. (2.42) is sensitive to $g^2/8 - 1/2 = a + a^2/2$. Traditionally the Lamb shift due to an anomalous lepton magnetic moment is obtained perturbatively (Itzykson and Zuber, 1980) by considering the DP equation which is sensitive to $g/2 - 1 = a$ the shift takes on the expression at lowest order

$$\frac{\Delta E_{\text{gLamb,DP}}^{2S_{1/2}-2P_{1/2}}}{mc^2} = \left(\frac{g-2}{2} \right) \frac{Z^4 \alpha^4}{6} = a \frac{Z^4 \alpha^4}{6}. \quad (2.43)$$

It is of experimental interest to resolve this discrepancy between the first order DP equation and the second order fermion formulation KGP. We recall the present day values

$$a_e = 1159.65218091(26) \times 10^{-6} \simeq \frac{\alpha}{2\pi}, \quad (2.44a)$$

$$a_\mu - a_e = 6.2687(6) \times 10^{-6}. \quad (2.44b)$$

The largest contribution to the anomalous moment for charged leptons is, as indicated the lowest order QED Schwinger result $a = \alpha/2\pi$. For the KGP approach, the anomalous g -factor mixes contributions of different powers of fine structure α . Precision values for the fundamental constants are taken from Tiesinga et al. (2021). For the $2S_{1/2} - 2P_{1/2}$ states, the shift is

$$\frac{\Delta E_{\text{gLamb}}^{2S_{1/2}-2P_{1/2}}}{mc^2} = \frac{Z^4 \alpha^5}{12\pi} + \frac{Z^4 \alpha^6}{48\pi^2}. \quad (2.45)$$

The scale of the discrepancy between KGP and DP for the hydrogen atom is then

$$\begin{aligned}\Delta E_{\text{gLamb,KGP}}^{2S_{1/2}-2P_{1/2}} - \Delta E_{\text{gLamb,DP}}^{2S_{1/2}-2P_{1/2}} &= \frac{\alpha^6 mc^2}{48\pi^2} \\ &= 1.62881214 \times 10^{-10} \text{ eV} = 39.3845030 \text{ kHz ,}\end{aligned}\quad (2.46)$$

without taking into account the standard corrections such as reduced mass, recoil, radiative, or finite nuclear size; for more information on those corrections please refer to Jentschura and Pachucki (1996); Eides et al. (2001); Tiesinga et al. (2021). It is to be understood that the corrections presented here are illustrative of the effect magnetic moment has on the spectroscopic levels, but that further work is required to compare these to experiment: for example we look here on behavior of point particles only.

While the discrepancy is small for the hydrogen system, it is ≈ 40 kHz and will be visible in this or next generation's spectroscopic experiments. The discrepancy is also non-negligible for hydrogen-like exotics such as proton-antiproton because the proton g -factor is much larger

$$g_p = 5.585694702(17) , \quad a_p = 1.792847351(9) . \quad (2.47)$$

The discrepancy for the proton-antiproton system is

$$\Delta E_{\text{gLamb,KGP}}^{2S_{1/2}-2P_{1/2}} - \Delta E_{\text{gLamb,DP}}^{2S_{1/2}-2P_{1/2}} = 0.71268151 \text{ eV} . \quad (2.48)$$

2.2.3 g-Fine structure effects within P orbitals

The fifth term in Eq. (2.40), which depends on j and n , will shift the levels due to an anomalous moment, but does not contribute to the Lamb shift. Rather this expression, which contains the spin-orbit $\vec{L} \cdot \vec{S}$ coupling, is responsible for the fine structure splittings. From Eq. (2.40) the fine structure splitting is given by

$$\frac{\Delta E_{\text{gFS}}^{n,\ell}}{mc^2} = E_\ell^{n,j=\ell+1/2} - E_\ell^{n,j=\ell-1/2} = (g^2/8) \left(\frac{1}{\ell} - \frac{1}{\ell+1} \right) \frac{Z^4 \alpha^4}{n^3} . \quad (2.49)$$

The splitting between the $2P_{3/2}$ and $2P_{1/2}$ states is therefore

$$\frac{\Delta E_{\text{gFS}}^{2P_{3/2}-2P_{1/2}}}{mc^2} = \left(g^2/8\right) \frac{Z^4\alpha^4}{16} = \left(1/2 + a + a^2/2\right) \frac{Z^4\alpha^4}{16}. \quad (2.50)$$

In comparison the fine structure dependence on g -factor in the DP equation is given as

$$\frac{\Delta E_{\text{gFS,DP}}^{2P_{3/2}-2P_{1/2}}}{mc^2} = \left(\frac{g-1}{2}\right) \frac{Z^4\alpha^4}{16} = (1/2 + a) \frac{Z^4\alpha^4}{16}. \quad (2.51)$$

Just as in the case of the Lamb shift, we find that the KGP and DP equations disagree for fine structure splitting. For the hydrogen atom this discrepancy is

$$\begin{aligned} \Delta E_{\text{gFS,KGP}}^{2P_{3/2}-2P_{1/2}} - \Delta E_{\text{gFS,DP}}^{2P_{3/2}-2P_{1/2}} &= \frac{\alpha^6 mc^2}{128\pi^2} \\ &= 6.10804553 \times 10^{-11} \text{ eV} = 14.7691885 \text{ kHz}, \end{aligned} \quad (2.52)$$

and for proton-antiproton, the fine structure splitting discrepancy is

$$\Delta E_{\text{gFS,KGP}}^{2P_{3/2}-2P_{1/2}} - \Delta E_{\text{gFS,DP}}^{2P_{3/2}-2P_{1/2}} = 0.26725557 \text{ eV}. \quad (2.53)$$

For fine structure of the muonic-hydrogen system, the KGP-DP discrepancy is

$$\Delta E_{\text{gFS,KGP}}^{2S_{1/2}-2P_{1/2}} - \Delta E_{\text{gFS,DP}}^{2S_{1/2}-2P_{1/2}} = 1.272774 \times 10^{-8} \text{ eV} \quad (2.54)$$

We can make a general observation that non minimal magnetic coupling, such as we have studied in the DP and KGP cases, enlarge energy level splittings. The above shows that these discrepancies will remain when calculating within more realistic finite nuclear size context.

2.3 Particles in strong electromagnetic fields

Care must be taken when interpreting the results presented in strong electromagnetic fields; see [Gonoskov et al. \(2022\)](#); [Fedotov et al. \(2023\)](#). Strong fields are produced in

heavy-ion collisions forming quark-gluon-plasma which have electromagnetic properties (Grayson et al., 2022). For physical electrons the AMM interaction is the result of vacuum fluctuations whose strength also depends on the strength of the field. For example in the large magnetic field limit a QED computation shows that the ground state is instead of Eq. (2.16) given by Jancovici (1969)

$$E_0 \approx mc^2 + \frac{\alpha}{4\pi} mc^2 \ln^2 \left(\frac{2e\hbar B}{m^2 c^3} \right), \quad (2.55)$$

which even for enormous magnetic fields does not deviate significantly from the rest mass-energy of the electron. Further the AMM radiative corrections approach zero for higher Landau levels (Ferrer et al., 2015; Hackebill, 2022). Therefore the AMM in the case of electrons does not have a significant effect in highly magnetized environments such as those found in astrophysics (magnetars).

The situation is different for composite particles such as the proton, neutron and light nuclei whose anomalous magnetic moments are dominated by their internal structure and not by vacuum fluctuations. In this situation we expect that the AMM interaction in high magnetic fields remains significant. Therefore, asking whether the DP or KGP equations better describes the dynamics of composite hadrons and atomic nuclei in presence of magnetar strength fields is a relevant question despite the standard choice in literature being the DP equation (Broderick et al., 2000). The same question can be asked for certain exotic hydrogen-like atoms where the constituent particles have anomalous moments which can be characterized as an external parameter.

2.3.1 Strong homogeneous magnetic fields

The magnetic moment anomaly can flip the sign of the magnetic energy for the least excited states causing the gap between particle and antiparticle states to decrease with magnetic field strength. Setting $p_z = 0$ in Eq. (2.15), we show in Figure 2.2 that the energy of the lowest KGP Landau eigenstate $n = 0, s = 1/2$ reaches zero where

the gap between particle and antiparticle states vanishes for the field

$$B_{\text{crit}}^e = \frac{B_S^e}{a_e} \simeq 861 B_S^e = 3.8006 \times 10^{16} \text{ G} , \quad (2.56\text{a})$$

$$B_{\text{crit}}^p = \frac{B_S^p}{a_p} \simeq \frac{1}{1.79} B_S^p = 8.3138 \times 10^{19} \text{ G} , \quad (2.56\text{b})$$

where B_S is the so-called Schwinger critical field ([Schwinger, 1951](#)).

$$B_S^e \equiv \frac{m_e^2 c^2}{e \hbar} = \frac{m_e c^2}{2 \mu_B} = 4.4141 \times 10^{13} \text{ G} , \quad (2.57\text{a})$$

$$B_S^p \equiv \frac{m_p^2 c^2}{e \hbar} = \frac{m_p c^2}{2 \mu_N} = 1.4882 \times 10^{20} \text{ G} . \quad (2.57\text{b})$$

The numerical results are evaluated for the anomalous moment of the electron and proton, given by Eq. (2.44a) and Eq. (2.47). At the critical field strength B_{crit} the Hamiltonian loses self-adjointness and the KGP loses its predictive properties. The Schwinger critical field Eq. (2.57a) denotes the boundary when electrodynamics is expected to behave in an intrinsically nonlinear fashion, and the equivalent electric field configurations become unstable ([Labun and Rafelski, 2009](#)). However, it is also possible that the vacuum is stabilized by such strong magnetic fields ([Evans and Rafelski, 2018](#)).

The critical magnetic fields as shown in Eq. (2.56a) appear in discussion of magnetars ([Kaspi and Beloborodov, 2017](#)). The magnetar field is expected to be more than 100-fold that of the Schwinger critical magnetic field which is on the same order of magnitude as B_{crit} for an electron. While the critical field for a proton exceeds that of a magnetar, the dynamics of protons (and neutrons) in such fields is nevertheless significantly modified. A correct description of magnetic moment therefore has relevant consequences to astrophysics.

Figure 2.3 shows analogous reduction in particle/antiparticle energy gap for the DP equation. In this case the vanishing point happens at a larger magnetic field strength. This time the solutions continue past this point, but require allowing the states to cross into the opposite continua which we consider nonphysical. We are not satisfied with either model's behavior though the KGP description is preferable.

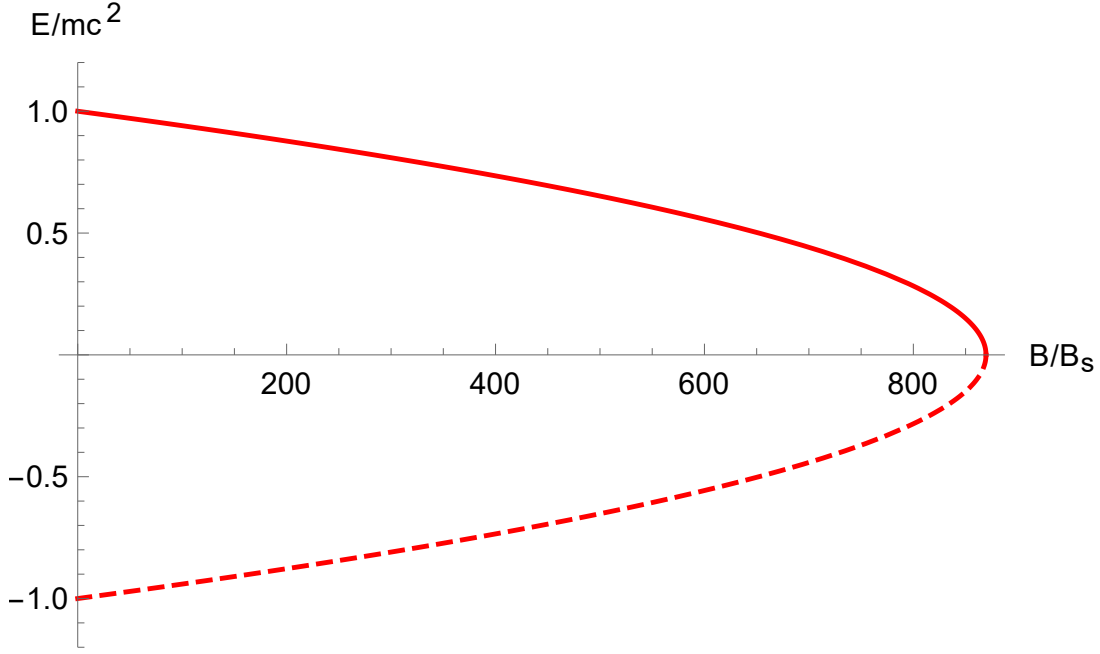


Figure 2.2: The $n = 0$, $s = 1/2$ ground state for a KGP electron given by Eq. (2.16) with $g/2 - 1 = \alpha/2\pi$ in a homogeneous magnetic field. We consider the particle with no z -direction momentum. The particle state (solid red) and antiparticle (dashed red) are presented.

However, it is undesirable that both KGP and DP solutions loose physical meaning and vacuum stability in strong magnetic fields.

2.3.2 High-Z hydrogen-like atoms

For the case of $g = 2$ hydrogen-like systems with large Z nuclei, there is extensive background related to the long study of the solutions of the Dirac equation (Rafelski et al., 1978; Greiner et al., 2012a; Rafelski et al., 2017). For $g \neq 2$ and $1/r$ singular potential we refer back to the exact expression for the KGP energy levels in Eq. (2.27). In the situation of critical electric fields, states lose self-adjointness for large Z in both the Dirac $g=2$ case (Gesztesy et al., 1985) and for KGP $g \neq 2$. Thaller (2013) notes that the DP-Coulomb solutions retain self-adjointness via ‘diving’ states. For KGP $|g| < 2$, states vanish similar to Dirac energy levels for the $1/r$ singular potential, but if $|g| > 2$ there is merging of particle to particle states (and antiparticle to antiparticle)

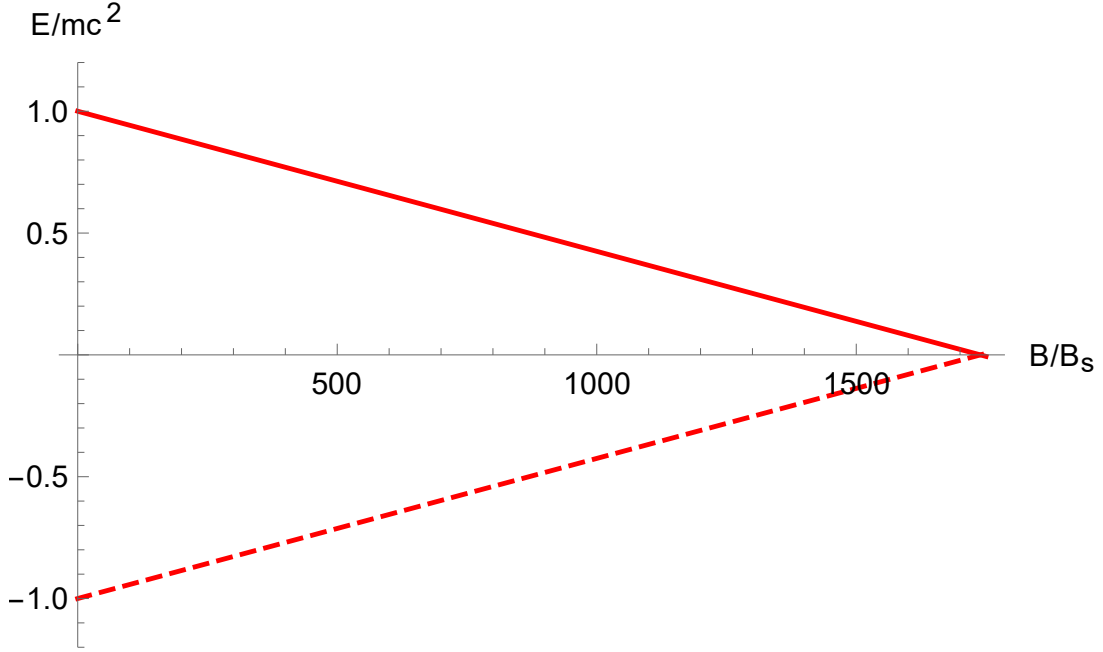


Figure 2.3: The $n = 0$, $s = 1/2$ ground state for a DP electron given by Eq. (2.19b) with $g/2 - 1 = \alpha/2\pi$ in a homogeneous magnetic field. We consider the particle with no z -direction momentum. The particle state (solid red) and antiparticle (dashed red) are presented.

for states of the same total angular momentum quantum number j , but opposite spin orientations.

This merging state behavior can be seen in Figure 2.4, which shows the meeting of the $1S_{1/2}$ and $2P_{1/2}$ states when $|g| > 2$. For $|g| < 2$ there is no state merging, but the solution is discontinuous in the sense that even for $1S_{1/2}$ we see a maximum allowed value of Z at a finite energy. This is reminiscent of the Dirac $g=2$ behavior we are familiar with for the $2P_{1/2}$ state (see upper dashed blue line in Figure 2.4) and many other $g=2$ eigenstates. We know from study of numerical solutions of the Dirac equation that the regularization of the Coulomb potential by a finite nuclear size removes this singular behavior. It remains to be seen how this exactly works in the context of the KGP equation allowing for the magnetic anomaly.

Thaller (2013) presented numerically computed DP equation energy levels for large Z hydrogen like atoms. These numerical solutions involve crossings in energy

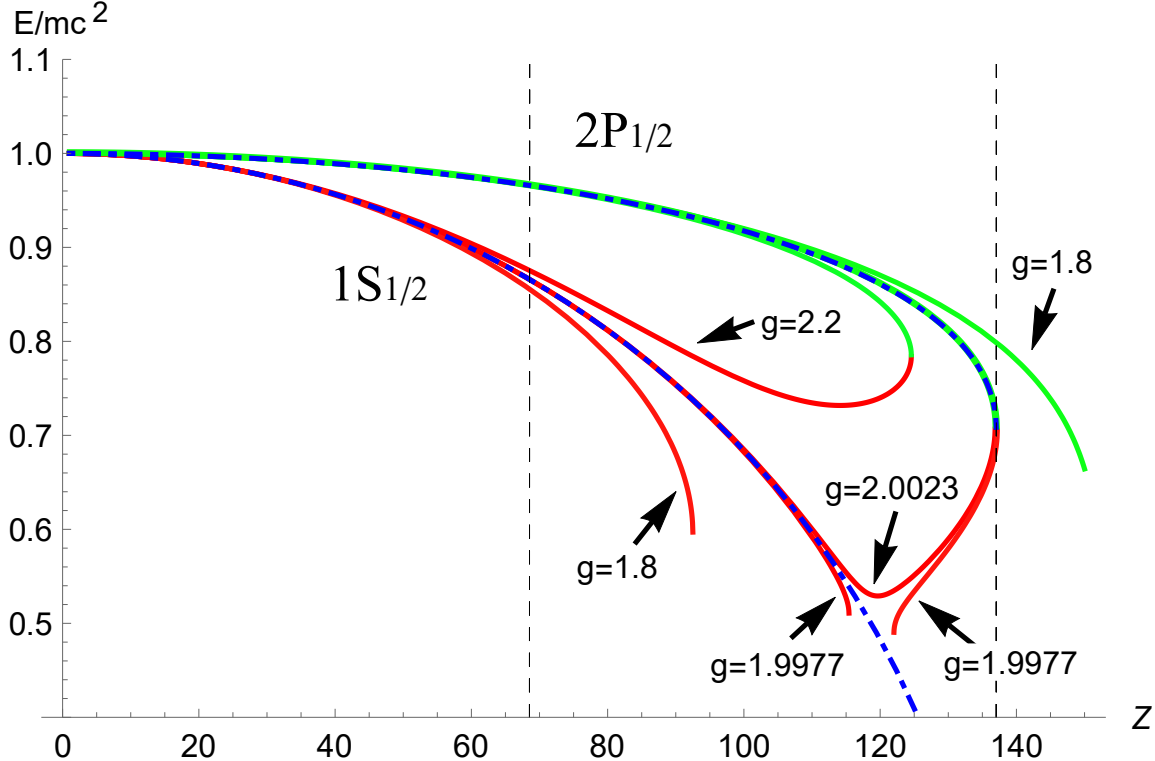


Figure 2.4: The KGP $1S_{1/2}$ (lower red curves) and $2P_{1/2}$ (upper green curves) energy levels for g -factor values $g = \{1.8, 1.9977, 2.0023, 2.2\}$ are shown for large Z hydrogen-like atoms. The curves for the Dirac $g = 2$ case for (lower dashed blue) $1S_{1/2}$ and (upper dashed blue) $2P_{1/2}$ are also presented.

levels between states with the same total angular quantum number j , but differing spin orientations such as $1S_{1/2}$ and $2P_{1/2}$; these states also have the behavior of diving into the antiparticle lower continuum even for $1/r$ -potential. These features are not present for the KGP-Coulomb solution. However, there is a similarity between the numerical solutions of the DP equation and our analytical KGP solutions, because for $|g| > 2$ the merging states as described above correspond to the crossing states in the DP solution.

The DP equation also allows for the so-called ‘super-positronium’ states as described by Barut and Kraus (1975, 1976). Such states represent resonances due to the magnetic interaction that reside incredibly close to the center of the atom i.e $\sqrt{\langle r^2 \rangle} \approx a\alpha\hbar/mc$, but this feature is absent from the KGP formation of the Coulomb

problem as all KGP-Coulomb wave functions which can be normalized can be successfully matched to their Dirac ($g=2$) companions.

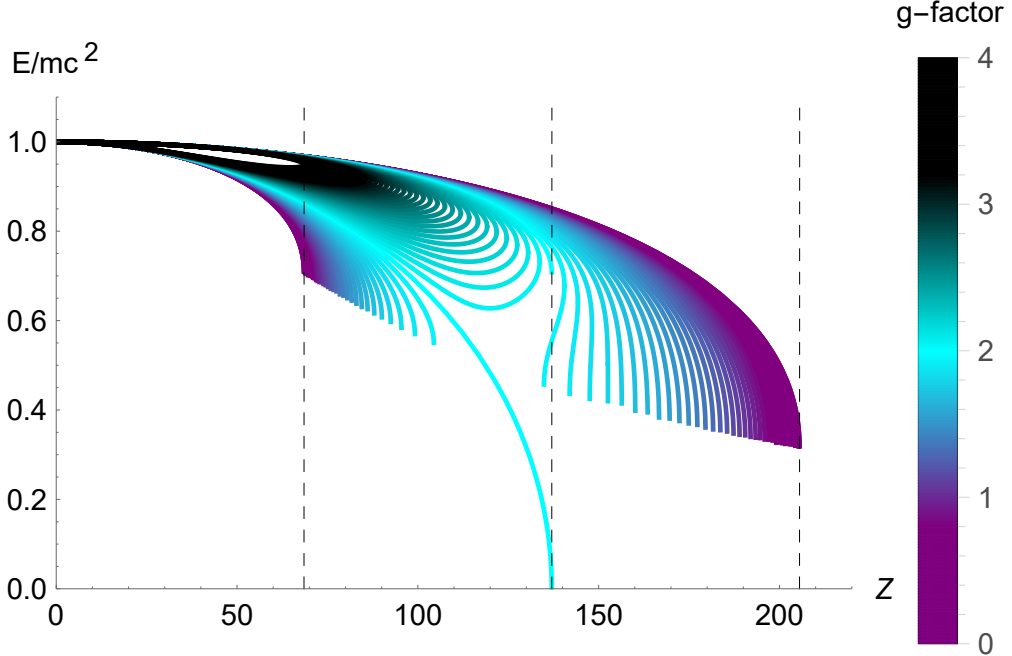


Figure 2.5: The KGP $1S_{1/2}$ and $2P_{1/2}$ states are plotted for hydrogen-like energies $220 > Z > 0$. The spread of lines corresponds to a spread of g -factor values: $4 > g > 0$. Integer multiples of $Z = 137/2$ are marked with vertical dashed lines. The separation between any two adjacent curves is $|g_i - g_{i+1}| = 0.05$. The unique curve which dives towards and stops at the boundary $E = 0$ is the Dirac $g = 2$ ground state.

Because analytical solutions of the DP-Coulomb problem are not available, unlike our results for KGP, it is hard to pinpoint precisely the origin of the diving and crossing state behavior. However, we can hypothesize that the problems arise due to the pathological structure of DP equation where the magnetic anomaly rather than full magnetic moment appears. On the other hand KGP framework for large Z shows interesting and well-behaved analytical behavior.

We further can explore the g -dependency on the $1S_{1/2}$ and $2P_{1/2}$ states by plotting a spectrum of g -factor values as is done in Figure 2.5. Purple regions are where $g \rightarrow 0$

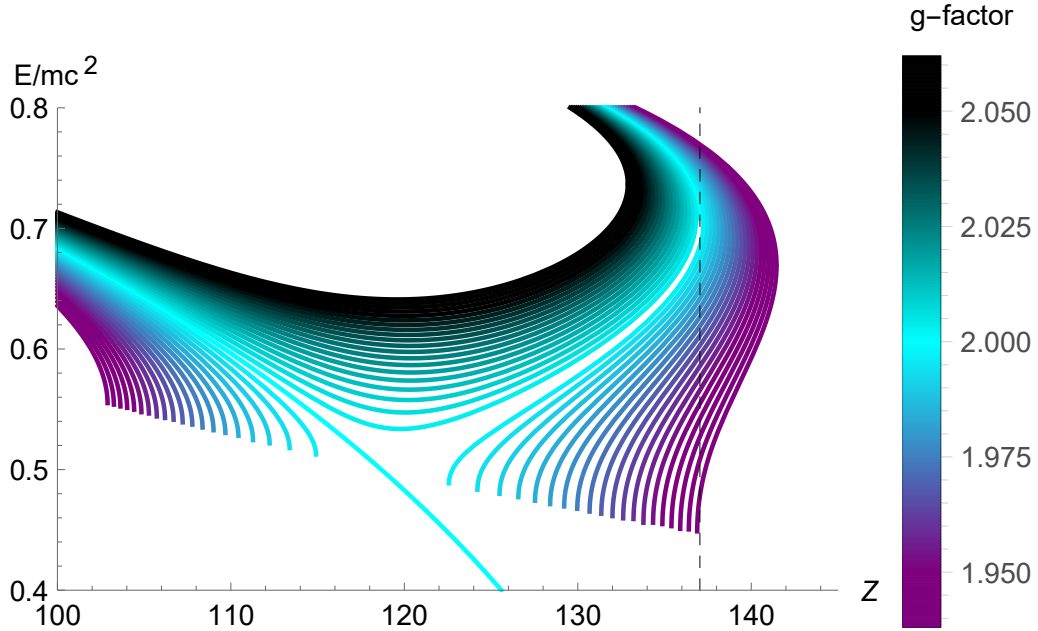


Figure 2.6: A close up of the KGP $1S_{1/2}$ and $2P_{1/2}$ states between $2.0625 > g > 1.9375$. The separation between any two adjacent curves is $|g_i - g_{i+1}| = 0.003125$. The value $Z = 137$ is marked with a vertical dashed line.

and the energies resembles the familiar Klein-Gordon case. As $g \rightarrow 0$, small changes in g -factor only lead to modest changes in the energies for large Z systems. The black curves represent where $g \rightarrow 4$. A unique feature of $g > 2$ fermions is that after a certain point, certain states become *less* bound with increasing Z . These rising curves represent spin anti-aligned $-\lambda$ levels which become nonphysical (e.g the slope becomes vertical) and merge with their spin aligned $+\lambda$ counterparts precisely where those states also become nonphysical.

The cyan curves in Figure 2.5 are where $g \approx 2$ and the states resemble the Dirac case. At exactly $g = 2$ there is a unique behavior where the $1S_{1/2}$ state dashes downward and terminates at $Z = 1/\alpha$. This path is unique and does not occur for any $g \neq 2$. Additionally, the $g = 2$ state does not smoothly connect with the $g \approx 2$ solutions for large Z hydrogen-like atoms. This is more visible in Figure 2.6 (note

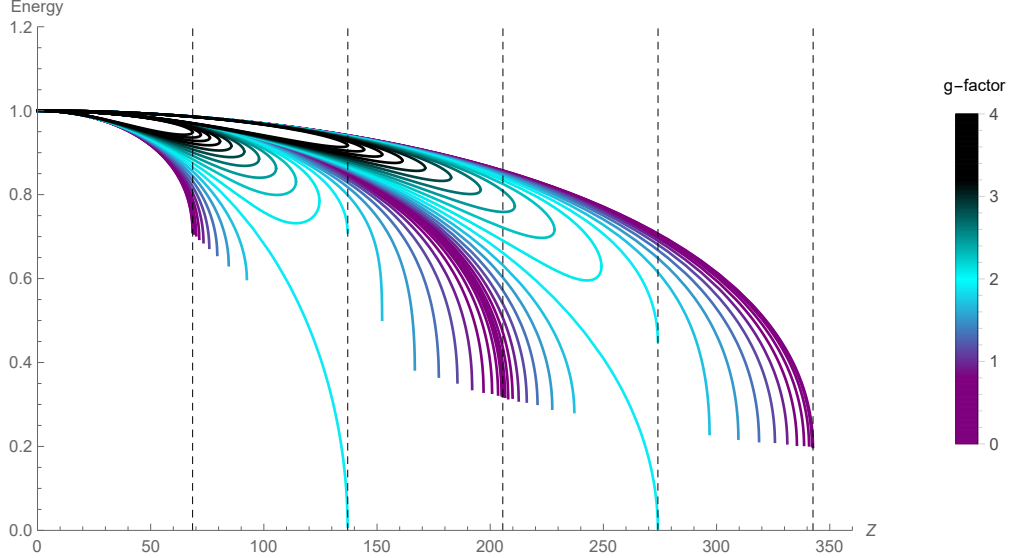


Figure 2.7: Energy level curves are plotted for total angular momentum quantum number $j = 1/2, 3/2$ with the relativistic principle quantum number $n_r = 0$. The separation between any two adjacent curves is $|g_i - g_{i+1}| = 0.2$. Dashed vertical lines indicate integer multiples of $Z = 137/2$.

the same purple-cyan-black color scheme is used but for different g -factor values) which plots a variety of g -factor values near $g \approx 2$. More specifically, small changes in g -factor lead to large deviations in the energies which is represented by the lack of dense lines near $g=2$ indicating the “cusp-like” nature of the Dirac case for very small anomalies.

The pattern of merging states with the same angular momentum first discussed in Figure 2.4 repeats itself for higher values of j total angular momentum. We show this explicitly in Figure 2.7 where mergers between $j = 1/2$ states occur in the left lobe while mergers between $j = 3/2$ states occur in the right lobe for $g > 2$.

2.4 Combination of mass and magnetic moment

While we have thus far focused on the DP and KGP models for magnetic dipole moments, the non-uniqueness of spin dynamics allows us to invent further non-linear EM models which all in the non-relativistic limit yield the non-relativistic QM magnetic dipole Hamiltonian. One such extension to quantum spin dynamics is to note the close relationship mass and magnetic moment share in the KGP formalism which we describe below.

Neutral particle electromagnetic interactions are of interest [Bruce and Diaz-Valdes \(2020\)](#); [Bruce \(2021b,a\)](#) allowing for a variety of model-building. The ‘Landau’ energies for neutral particles (*i.e.* neutron with mass m_N) in Eq. (2.16) simplifies to

$$E_{n,s}|_{e=0} \rightarrow E_s(\mathbf{p}, B) = \sqrt{m_N^2 c^4 + \mathbf{p}^2 c^2 - 2\mu B m_N c^2 s} , \quad (2.58)$$

which is just the free particle motion with a magnetic dipole energy. We note the correspondence between the quantized Landau orbitals and continuous transverse momentum $\mathbf{p}^2 = p_3^2 + p_T^2$. We can define an ‘effective’ polarization mass given by

$$\tilde{m}_s^2(B) = m^2 c^4 - 2\mu B m c^2 s . \quad (2.59)$$

This effective polarization mass (which also is easily defined for charged particles) will find use when we consider cosmic thermodynamics and plasmas in Chapter 4.

Inspired by Eq. (2.59), we can write a unified dipole-mass as

$$\tilde{m}(\mathbf{E}, \mathbf{B}) = m + \mu \frac{\sigma_{\alpha\beta} F^{\alpha\beta}}{2c^2} , \quad (2.60)$$

which satisfies the wave equation

$$((i\hbar\partial_\mu - eA_\mu)^2 - \tilde{m}^2(\mathbf{E}, \mathbf{B})c^2) \Psi = 0 , \quad (2.61)$$

$$\left((i\hbar\partial_\mu - eA_\mu)^2 - \left(mc + \mu \frac{\sigma^{\alpha\beta} F_{\alpha\beta}}{2c} \right)^2 \right) \Psi = 0 . \quad (2.62)$$

This modified KGP formulation then requires spin sensitive mass and an explicit electromagnetic component to the charged lepton mass. The dynamical mass concept introduced here is the driving motivation behind Chapter 3 and our work in [Steinmetz et al. \(2023\)](#) in the context of dynamic neutrino flavor mixing. As informed by classical mechanics, charged particles should be understood to derive at least some of their mass from the mass-energy of their electromagnetic fields. Eq. (2.64) results in higher order vertex diagrams coupling fermions to photons.

We note that Eq. (2.60) suggests that there may be some perturbative connection between particle mass and magnetic moment and note that this relationship would only manifest in strong fields where non-minimal coupled electromagnetism may be large. To this end we propose the following as a possible ansatz

$$\tilde{m}(\mathbf{E}, \mathbf{B}) = m \exp\left(\frac{\mu}{m} \frac{\sigma_{\alpha\beta} F^{\alpha\beta}}{2c^2}\right), \quad (2.63)$$

which for weak fields $F \rightarrow 0$ reduces to the prior form Eq. (2.60). We will not explore Eq. (2.63) further in this work.

The approach in Eq. (2.60) is superficially similar to the model proposed by [Frenkel \(1926\)](#) in classical mechanics by giving the particle a spin dependent mass of the form $m \sim \Sigma_{\mu\nu} F^{\mu\nu}$ where $\Sigma_{\mu\nu}$ is the covariant generalization of the classical magnetic and electric dipole; a more detailed exploration can be found in [Formanek \(2020\)](#). Eq. (2.62) is however distinct in that the mass is allowed off-diagonal components in spinor space (a subspace which doesn't exist classically). The dipole-mass Eq. (2.60) is off-diagonal in spinor space in the Dirac representation and no longer commutes like a scalar.

Eq. (2.60) also differs from the regular KGP equation by the presence of an additional quadratic interaction which we can evaluate using Eq. (1.30) in the Dirac

representation as

$$\delta V = -\frac{\mu^2}{4} (\gamma_\alpha \gamma_\beta F^{\alpha\beta})^2 = \mu^2 \begin{pmatrix} i\boldsymbol{\sigma} \cdot \mathbf{E}/c & -\boldsymbol{\sigma} \cdot \mathbf{B} \\ -\boldsymbol{\sigma} \cdot \mathbf{B} & i\boldsymbol{\sigma} \cdot \mathbf{E}/c \end{pmatrix} \begin{pmatrix} i\boldsymbol{\sigma} \cdot \mathbf{E}/c & -\boldsymbol{\sigma} \cdot \mathbf{B} \\ -\boldsymbol{\sigma} \cdot \mathbf{B} & i\boldsymbol{\sigma} \cdot \mathbf{E}/c \end{pmatrix}, \quad (2.64)$$

$$\delta V = \mu^2 \begin{pmatrix} \mathbf{B}^2 - \mathbf{E}/c^2 & -i\mathbf{E} \cdot \mathbf{B} \\ -i\mathbf{E} \cdot \mathbf{B} & \mathbf{B}^2 - \mathbf{E}/c^2 \end{pmatrix} = 2\mu^2 \begin{pmatrix} \mathcal{S} & -i\mathcal{P} \\ -i\mathcal{P} & \mathcal{S} \end{pmatrix}. \quad (2.65)$$

We define the invariants of the electromagnetic field tensor $F^{\alpha\beta}$ in Eq. (2.65) letting us write the above more compactly as

$$\mathcal{S} = \frac{1}{2}(\mathbf{B}^2 - \mathbf{E}^2/c^2), \quad \mathcal{P} = \mathbf{E} \cdot \mathbf{B}/c, \quad \delta V = 2\mu^2 (\mathcal{S} - i\gamma^5 \mathcal{P}). \quad (2.66)$$

We note that $\sigma_{\alpha\beta} F^{\alpha\beta}/2$ can also be written in terms of its four eigenvalues

$$\lambda_1 = +\mathcal{S} + i\mathcal{P}, \quad \lambda_2 = +\mathcal{S} - i\mathcal{P}, \quad \lambda_3 = -\mathcal{S} + i\mathcal{P}, \quad \lambda_4 = -\mathcal{S} - i\mathcal{P}. \quad (2.67)$$

This represents simply only one possible non-linear extension to electromagnetism in relativistic quantum mechanics of which there are a family of extensions ([Foldy, 1952](#)).

For the homogeneous magnetic field Eq. (2.62) can be solved in much the same way as the KGP equation in Section 2.1. One obtains energy eigenvalues by noting the simple shift that occurs in the mass of $m^2 \rightarrow m^2 + \mu^2 B^2$ quadratic in the magnetic field. Quadratic (spin independent) contributions are often referred to as scalar polarization ([Holstein and Scherer, 2014](#)). The resulting energy levels are

$$E_{n,s}(\mathbf{B}) = \sqrt{m_e^2 c^4 + \mu^2 B^2 + p_3^2 c^2 + 2e\hbar c^2 B \left(n + \frac{1}{2}\right) - 2\mu B m_e c^2 s} \quad (2.68)$$

Interestingly in ultra-high magnetic fields ($B \gg B_S$), Eq. (2.68) approximates

$$E \approx \mu B. \quad (2.69)$$

This is not dissimilar to the non-relativistic case where the magnetic energy is simply proportional to the magnetic field.

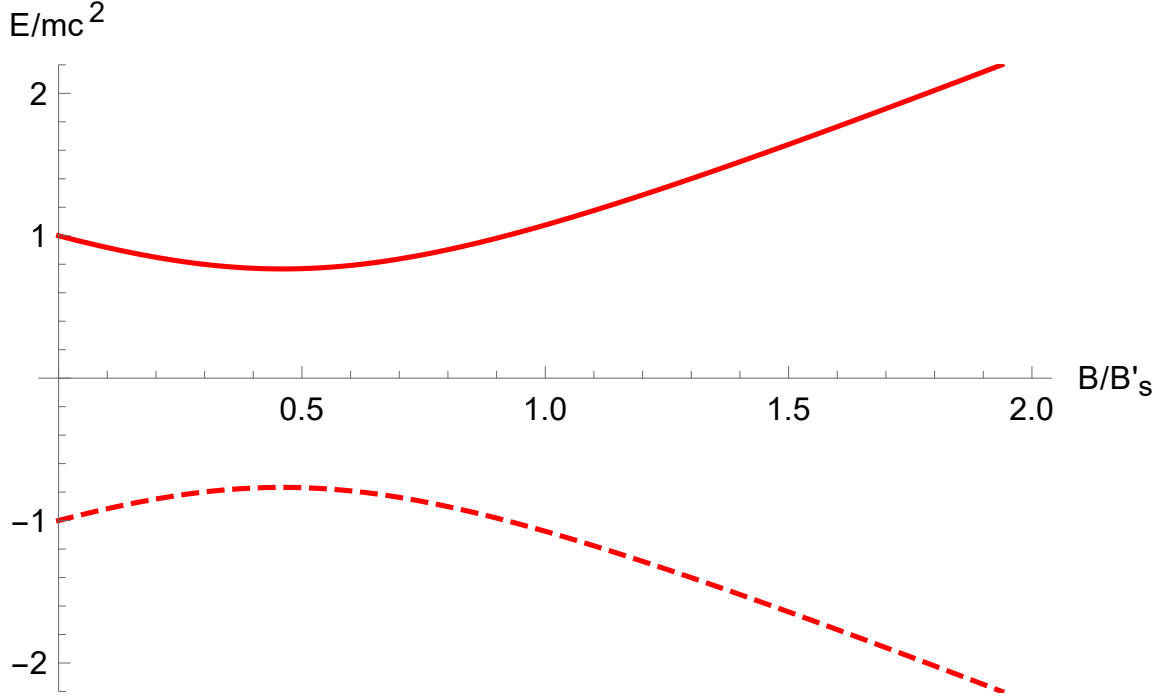


Figure 2.8: The $n = 0, s = 1/2$ ground state for a IKGP proton given by Eq. (2.68) with $g = 5.58$ in a homogeneous magnetic field. The magnetic minimum is well visible for particles with larger anomalous moment such as proton. We consider the particle with no z -direction momentum. The particle state (solid red) and antiparticle (dashed red) are presented. The magnetic field scale is $B'_S = (m_p^2/m_e^2)B_S$.

The most striking feature is that the ground state remains physical for all values of magnetic field when an anomalous moment is included. The self-adjointness of the system is not lost for some critical magnetic field strength. It can be then thought that the magnetic field provides a stabilizing influence on the system. Rather, there exists a “magnetic minimum” located for $n = 0, s = 1/2$ at

$$B_{\min} = \frac{4mc^2}{g^2\mu_B}a, \quad (2.70)$$

which for the electron is

$$B_{\min}^e = \frac{8a_e}{g_e^2} B_S = 1.02126 \times 10^{11} \text{ G} . \quad (2.71)$$

The minimum for a proton is in comparison

$$B_{\min}^p = \frac{8a_p}{g_p^2} \frac{m_p^2}{m_e^2} B_S = 6.841 \times 10^{19} \text{ G} , \quad (2.72)$$

which can be seen in Figure 2.8. Here it is understood that for the calculation of the proton's magnetic minimum, the nuclear mass and magneton was used rather than the electron Bohr magneton. For large enough g-factor, excited states also contain a minimum, but for any nonzero anomalous moment the ground state always does.

2.5 Classical relativistic spin dynamics

We turn away from quantum mechanical approaches to inspect the classical analogue of spin dynamics. Considering the Poincaré group of space-time symmetry transformations (Weinberg, 2005; Greiner and Müller, 2012), it was established by Wigner that elementary particles are group representations and can be characterized by eigenvalues of the Poincaré group's two Casimir operators:

$$C_1 \equiv p_\mu p^\mu = p^2 = m^2 c^2 , \quad (2.73)$$

$$C_2 \equiv w_\mu w^\mu = w^2 , \quad w_\alpha = \frac{1}{2} \varepsilon_{\alpha\beta\mu\nu} M^{\beta\mu} p^\nu , \quad (2.74)$$

where w^α is the Pauli-Lubanski pseudo-vector. Here $M^{\alpha\beta}$ is the relativistic tensor expression for the angular momentum defined via

$$M^{\alpha\beta} = x^\alpha p^\beta - x^\beta p^\alpha + S^{\alpha\beta} \quad (2.75)$$

where $S^{\alpha\beta}$ is the spin angular momentum tensor. The spin tensor $S^{\alpha\beta}$ can be understood via the classical (Cl.) four-spin in the rest frame (RF) as

$$s^\alpha|_{\text{RF}} = (0, \mathbf{s}_{\text{Cl.}}), \quad s_\alpha s^\alpha = -\mathbf{s}_{\text{Cl.}}^2, \quad s_\alpha = \frac{1}{2mc} \varepsilon_{\alpha\beta\mu\nu} S^{\beta\mu} p^\nu, \quad (2.76)$$

where $\mathbf{s}_{\text{Cl.}}$ is the classical Euclidean three-spin (not to be confused with the quantum operator \mathbf{s}). We also note that to make the units correct, the Pauli-Lubanski pseudo-vector and the four-spin are proportional by a factor of $\sqrt{C_1} = mc$. Quantum mechanically (Ohlsson, 2012) $S^{\alpha\beta}$ appears as $\sim \sigma^{\alpha\beta}$ which we've already identified as the spin tensor in Dirac theory defined via the γ^α matrices.

2.5.1 Covariant magnetic potential and modified Lorentz force

We are interested in elementary particles with electric charge e , and elementary magnetic dipole charge $d = \mu/|\mathbf{s}_{\text{Cl.}}|$. Therefore the covariant dynamics must be extended beyond the Lorentz force to incorporate the Stern–Gerlach (SG) force. To achieve a suitable generalization we introduce (Rafelski et al., 2018) the covariant magnetic potential

$$B_\alpha(x, s) \equiv F_{\alpha\beta}^* s^\beta \quad (2.77)$$

As s_α is a pseudo-vector; the product in Eq. (2.77) results in a polar 4-vector B_α . We note that the magnetic dipole potential B_α by construction in terms of the antisymmetric field pseudo-vector $F_{\alpha\beta}^*$ satisfies

$$\partial_\alpha B^\alpha = 0, \quad s \cdot B = 0 \rightarrow B \cdot \frac{ds}{d\tau} + s \cdot \frac{dB}{d\tau}, \quad (2.78)$$

where τ is the proper time.

The zeroth component of the covariant potential in the rest frame Eq. (2.77) reproduces the classical magnetic dipole energy given by

$$U_{\text{Mag.}} = dB^0 = dF^{0\beta} s_\beta = -\boldsymbol{\mu}_{\text{Cl.}} \cdot \mathbf{B}, \quad \boldsymbol{\mu}_{\text{Cl.}} = \mu \frac{\mathbf{s}_{\text{Cl.}}}{|\mathbf{s}_{\text{Cl.}}|}. \quad (2.79)$$

We can then define a covariant magnetic field tensor from the potential Eq. (2.77) which generalizes the covariant Lorentz force F_L^α as

$$G^{\alpha\beta} = \partial^\alpha B^\beta - \partial^\beta B^\alpha = G^{\alpha\beta} = \partial^\alpha F^{*\beta\gamma} s_\gamma - \partial^\beta F^{*\alpha\gamma} s_\gamma, \quad (2.80)$$

$$F_L^\alpha \equiv \frac{dp^\alpha}{d\tau} = e F^{\alpha\beta} u_\beta + d G^{\alpha\beta} u_\beta, \quad (2.81)$$

where u_α is the four-velocity and as previously stated, e and d are the electric and dipole charges. While the first term in Eq. (2.81) is the standard Lorentz force, the second term is a covariant formulation of the SG force.

Because the spin precession is sensitive to the force on a particle, the presence of a SG force will induce precession terms which are second order in spin. The torque on the magnetic moment of the particle can be determined via the properties of the four-spin. Namely s^α is orthogonal (Schwinger, 1974) to the four-velocity yielding

$$u \cdot \frac{ds}{d\tau} + \frac{du}{d\tau} \cdot s \quad (2.82)$$

The spin torque equations can be obtained (Bargmann et al., 1959) by inserting the Lorentz force (in our case the modified Lorentz force) that corresponds to Eq. (2.81) yielding

$$\begin{aligned} \frac{ds^\mu}{d\tau} &= (1 + \tilde{a}) \frac{e}{m} F^{\mu\nu} s_\nu - \tilde{a} \frac{e}{m} u^\mu (u_\alpha F^{\alpha\beta} s_\beta) / c^2 \\ &\quad + (1 + \tilde{b}) \frac{d}{m} G^{\mu\nu} s_\nu - \tilde{b} \frac{d}{m} u^\mu (u_\alpha G^{\alpha\beta} s_\beta) / c^2. \end{aligned} \quad (2.83)$$

The constants \tilde{a} and \tilde{b} are arbitrary allowing for extra terms not forbidden by special relativity. With $d = 0$, Eq. (2.83) are known as the Thomas-Bargmann-Michel-Telegdi (TMBT) equations. In the standard derivation of relativistic spin precession, in the TMBT equation, the \tilde{a} constant is associated with the anomalous magnetic moment.

In allowing for spin precession sourced by a Stern-Gerlach dipole force, an additional constant \tilde{b} must be introduced. The terms in Eq. (2.80) involving the G tensor are spin precession directly originating from dipole forces. In homogeneous

electromagnetic fields, Eq. (2.80) reduces to the standard TBMT equation. These dynamical torque equations have found use in describing neutral and charged systems classically (Formanek et al., 2021b, 2019) and inspired further efforts to improve covariant dynamics (Formanek, 2020).

2.5.2 Equivalency of Gilbertian and Ampèrian Stern-Gerlach forces

We can identify the covariant formulation described in Eq. (2.81) with the SG force in two different ways which define different interpretations of the magnetic dipole. Explicitly magnetic forces in the non-relativistic limit manifest in two variants:

$$\mathbf{F}_G = (\boldsymbol{\mu} \cdot \nabla) \mathbf{B} : \text{Gilbert dipole}, \quad (2.84)$$

$$\mathbf{F}_A = \nabla(\boldsymbol{\mu} \cdot \mathbf{B}) : \text{Ampère dipole}. \quad (2.85)$$

The Gilbert model describes the dipole moment of two magnetic monopole charges; and the Ampère dipole is generated by a loop of electric current. They differ in the directionality of the Euclidean three-force: The Gilbertian dipole force is in the direction of magnetic field while the Ampèrian force is in the direction of gradient. The two forces are related via

$$\nabla(\boldsymbol{\mu} \cdot \mathbf{B}) = (\boldsymbol{\mu} \cdot \nabla) \mathbf{B} + \boldsymbol{\mu} \times (\nabla \times \mathbf{B}), \quad (2.86)$$

with the assumption that the dipole is spatially independent. The second term in the above equation can be rewritten using Ampère's law

$$\boldsymbol{\mu} \times (\nabla \times \mathbf{B}) = \boldsymbol{\mu} \times \left(\mu_0 \mathbf{J} + \frac{1}{c^2} \frac{\partial \mathbf{E}}{\partial t} \right) \quad (2.87)$$

where μ_0 is understood to be the vacuum permeability. The important takeaway is that the Ampèrian (gradient direction) and Gilbertian (field direction) forces are related via a term ultimately sensitive to the external current \mathbf{J} of the system.

Before we show how this manifests in the covariant formulation, we recall the orthogonality of four-velocity and four-spin given in Eq. (2.82). This property allows

us to write the covariant Lorentz force in Eq. (2.81) in two equivalent forms which we will call the Ampèrian $F_{\text{L,A}}^\alpha$ and Gilbertian $F_{\text{L,G}}^\alpha$ covariant expressions for reasons that will become obvious soon

$$F_{\text{L,A}}^\alpha = eF^{\alpha\beta}u_\beta + ds_\gamma u_\beta(\partial^\alpha F^{*\beta\gamma} - \partial^\beta F^{*\alpha\gamma}), \quad (2.88)$$

$$F_{\text{L,G}}^\alpha = eF^{\alpha\beta}u_\beta - d(s_\gamma\partial^\gamma)F^{*\alpha\beta}u_\beta + ds_\gamma T^{\gamma\alpha\beta}u_\beta. \quad (2.89)$$

The tensor $T^{\alpha\mu\nu}$ is the completely antisymmetric

$$T^{\alpha\mu\nu} = \partial^\alpha F^{*\mu\nu} + \partial^\mu F^{*\nu\alpha} + \partial^\nu F^{*\alpha\mu}, \quad (2.90)$$

dual tensor to electric four-current.

We will now show that the expression $F_{\text{L,A}}^\alpha$ depends on an Ampèrian dipole and the proper time derivative of the fields. Recognizing that $d/d\tau = u \cdot \partial$, Eq. (2.88) can be rewritten as

$$F_{\text{L,A}}^\alpha = eF^{\alpha\beta}u_\beta + ds_\gamma \left(\partial^\alpha F^{*\beta\gamma}u_\beta - \frac{d}{d\tau}F^{*\alpha\gamma} \right). \quad (2.91)$$

We evaluate the four-force in the instantaneous rest frame (RF) of the particle such that $u^\alpha = (c, 0)$, $d/d\tau = \partial/\partial t$ and $s^\alpha = (0, \mathbf{s}_{\text{Cl}})$. Noting that $\boldsymbol{\mu} = dc\mathbf{s}_{\text{Cl}}$ this yields

$$F_{\text{L,A}}^0|_{\text{RF}} = -\frac{1}{c}\boldsymbol{\mu} \cdot \left(\frac{\partial \mathbf{B}}{\partial t} - \frac{\partial \mathbf{B}}{\partial t} \right) = 0, \quad (2.92)$$

$$\mathbf{F}_{\text{L,A}}|_{\text{RF}} = e\mathbf{E} + \nabla(\boldsymbol{\mu} \cdot \mathbf{B}) - \frac{1}{c^2}\boldsymbol{\mu} \times \frac{\partial \mathbf{E}}{\partial t}. \quad (2.93)$$

As we see in Eq. (2.93), the second term corresponds to the Ampèrian SG force written in Eq. (2.85).

We can accomplish the same procedure for $F_{\text{L,G}}^\alpha$ which explicitly depends on a

covariant Gilbertian dipole and spin coupling to current. The four-force yields

$$F_{L,G}^0|_{RF} = 0 \quad (2.94)$$

$$\mathbf{F}_{L,G}|_{RF} = e\mathbf{E} + (\boldsymbol{\mu} \cdot \boldsymbol{\nabla})\mathbf{B} + \left(\boldsymbol{\nabla}(\boldsymbol{\mu} \cdot \mathbf{B}) - (\boldsymbol{\mu} \cdot \boldsymbol{\nabla})\mathbf{B} - \frac{1}{c^2}\boldsymbol{\mu} \times \frac{\partial \mathbf{E}}{\partial t} \right) \quad (2.95)$$

If we cancel out the second and forth terms in Eq. (2.95), we re-obtain the Ampèrean three-force written in Eq. (2.93).

However, making use of the expressions in Eq. (2.86) and Ampère's circuital law Eq. (2.87), we can rewrite the above terms yielding

$$\mathbf{F}_{L,G}|_{RF} = e\mathbf{E} + (\boldsymbol{\mu} \cdot \boldsymbol{\nabla})\mathbf{B} + \boldsymbol{\mu} \times \mu_0 \mathbf{J} \quad (2.96)$$

which is the Gilbertian expression for the SG force as given in Eq. (2.84). Our covariant formulation then requires that

$$\mathbf{F}_{L,A}|_{RF} \equiv \mathbf{F}_{L,G}|_{RF} \quad (2.97)$$

Thus we find an equivalence between the Gilbertian and Ampèrean dipoles from the covariant introduction of intrinsic magnetic dipole in our covariant dynamics.

CHAPTER 3

Dynamic neutrino flavor mixing through transition moments

We proposed in Rafelski et al. (2023c) that neutrino flavors are remixed when exposed to strong EM fields travelling as a superposition distinct from the vacuum propagation of free neutrinos. Neutrino mixing is an important topic for studying BSM physics as flavor mixing only occurs in the presence of massive neutrinos allowing for the misalignment between the flavor basis which participates in left-chiral $SU(2)_L$ weak interactions and the mass basis which are the propagating neutrino states.

We discuss the neutrino anomalous magnetic moment (AMM) in Section 3.1. We narrow our analysis for Majorana neutrinos which are allowed only transition magnetic moments which couple different flavors electromagnetically, but do not violate CPT symmetry. Transition moments however notably break lepton number conservation. We discuss the standard flavor mixing program in Section 3.2 and the effective Lagrangian density in Section 3.2.1 containing both Majorana mass and transition moments. In Section 3.2.2 we discuss the chirality of the relativistic Pauli dipole.

The two-flavor neutrino model is evaluated explicitly in Section 3.3 and the remixed electromagnetic-mass eigenstates are obtained in Section 3.3.1. We obtain in Section 3.3.2 an EM-mass basis, distinct from flavor and free-particle mass basis, which mixes flavors as a function of EM fields. The case of two nearly degenerate neutrinos is studied in detail in Section 3.4. Moreover we show solutions relating to full EM field tensor which result in covariant expressions allowing for both magnetic and electrical fields.

3.1 Electromagnetic characteristics of neutrinos

We study the connection between Majorana neutrino transition magnetic dipole moments (Fujikawa and Shrock, 1980; Shrock, 1980, 1982) and neutrino flavor oscillation.

Neutrino electromagnetic (EM) properties have been considered before (Schechter and Valle, 1981; Giunti and Studenikin, 2015; Popov and Studenikin, 2019; Dvornikov, 2019; Chukhnova and Lobanov, 2020) including the effect of oscillation in magnetic fields (Lim and Marciano, 1988; Akhmedov, 1988; Pal, 1992; Elizalde et al., 2004; Akhmedov and Martínez-Miravé, 2022). The influence of transition magnetic moments on solar neutrinos is expected (Martínez-Miravé, 2023), but difficult to measure due to the lack of knowledge of solar magnetism near the core.

The case of transition moments has the mathematical characteristics of an off-diagonal mass which is distinct from normal direct dipole moment behavior. EM field effects are also distinct from weak interaction remixing within matter, *i.e.* the Mikheyev-Smirnov-Wolfenstein effect (Wolfenstein, 1978; Mikheyev and Smirnov, 1985; Mikheev and Smirnov, 1986; Smirnov, 2003).

The size of the neutrino magnetic dipole moment can be constrained as follows: The lower bound is found by higher order standard model interactions with the minimal extension of neutrino mass m_ν included (Fujikawa and Shrock, 1980; Shrock, 1980, 1982). The upper bound is derived from reactor, solar and astrophysical experimental observations (Giunti et al., 2016; Canas et al., 2016; Studenikin, 2016; Aristizabal Sierra et al., 2022). The bounds are expressed in terms of the electron Bohr magneton μ_B as

$$\frac{e\hbar G_F m_\nu c^2}{8\pi^2 \sqrt{2}} \sim 10^{-20} \mu_B < \mu_\nu^{\text{eff}} < 10^{-10} \mu_B, \quad \mu_B = \frac{e\hbar}{2m_e} \quad (3.1)$$

where G_F is the Fermi constant and μ_ν^{eff} is the effective and characteristic size of the neutrino magnetic moment. In Eq. (3.1), the lower bound was estimated using a characteristic mass of $m_\nu \sim 0.1$ eV. From cosmological studies, the sum of neutrino masses is estimated (Aghanim et al., 2020) to be $\sum_i m_i < 0.12$ eV; the effective electron (anti)neutrino mass is bounded (Aker et al., 2022) by $m_e^\nu < 0.8$ eV.

3.2 Neutrino flavor mixing and electromagnetic fields

Oscillation of neutrino flavors observed in experiment is in general interpreted as being due to a difference in neutrino mass and flavor eigenstates. This misalignment between the two representations is described as rotation of the neutrino flavor N -vector where $N = 3$ is the observed number of generations. The unitary mixing matrix $V_{\ell k}$ allows for the change of basis between mass (k) and flavor (ℓ) eigenstates via the transform

$$\nu_\ell = V_{\ell k} \nu_k \rightarrow \begin{pmatrix} \nu_e \\ \nu_\mu \\ \nu_\tau \end{pmatrix} = \begin{pmatrix} V_{e1} & V_{e2} & V_{e3} \\ V_{\mu 1} & V_{\mu 2} & V_{\mu 3} \\ V_{\tau 1} & V_{\tau 2} & V_{\tau 3} \end{pmatrix} \begin{pmatrix} \nu_1 \\ \nu_2 \\ \nu_3 \end{pmatrix}, \quad (3.2)$$

where ν_ℓ is the neutrino four-spinor written in the flavor basis while in the mass basis we use ν_k with $k \in 1, 2, 3$.

The parameterization of the components of the mixing matrix depends on the Dirac or Majorana-nature of the neutrinos. First we recall the Dirac neutrino mixing matrix $U_{\ell k}$ in the standard parameterization (Xing, 2014; Schwartz, 2014)

$$U_{\ell k} = \begin{pmatrix} c_{12}c_{13} & s_{12}c_{13} & s_{13}e^{-i\delta} \\ -s_{12}c_{23} - c_{12}s_{13}s_{23}e^{i\delta} & c_{12}c_{23} - s_{12}s_{13}s_{23}e^{i\delta} & c_{13}s_{23} \\ s_{12}s_{23} - c_{12}s_{13}c_{23}e^{i\delta} & -c_{12}s_{23} - s_{12}s_{13}c_{23}e^{i\delta} & c_{13}c_{23} \end{pmatrix}, \quad (3.3)$$

where $c_{ij} = \cos(\theta_{ij})$ and $s_{ij} = \sin(\theta_{ij})$. In this convention, the three mixing angles $(\theta_{12}, \theta_{13}, \theta_{23})$ are understood to be the Euler angles for generalized rotations and δ is the CP-violating complex phase.

For the Majorana case we must allow a greater number of complex phases: Majorana neutrinos allow up to two additional complex phases ρ and σ which along with δ participate in CP-violation. A parameterization is achieved by introducing an

additional phase matrix $P_{kk'}$

$$V_{\ell k} = U_{\ell k'} P_{k' k}, \quad (3.4)$$

$$P_{kk'} = \text{diag}(e^{i\rho}, e^{i\sigma}, 1). \quad (3.5)$$

The mixing matrix $V_{\ell k}$ defined in Eq. (3.4) can then be used to transform the symmetric mass matrix $M_{\ell\ell'}$ from the flavor basis into the diagonal mass basis

$$M_{\ell\ell'} = \begin{pmatrix} m_{ee}^\nu & m_{e\mu}^\nu & m_{e\tau}^\nu \\ m_{e\mu}^\nu & m_{\mu\mu}^\nu & m_{\mu\tau}^\nu \\ m_{e\tau}^\nu & m_{\mu\tau}^\nu & m_{\tau\tau}^\nu \end{pmatrix}, \quad M_{\ell\ell'}^T = M_{\ell\ell'}, \quad (3.6)$$

$$V_{\ell k}^T M_{\ell\ell'} V_{\ell' k'} = M_{kk'} = m_k \delta_{kk'} = \text{diag}(m_1, m_2, m_3). \quad (3.7)$$

We note the Majorana mass matrix is symmetric due to the anticommuting nature of the neutrino fields $\bar{\nu}\nu = -\nu^T \bar{\nu}^T$ and is in general complex (Adhikary et al., 2013; Giunti and Kim, 2007) though it will be taken to be fully real in this work. There are many interesting models for mass matrices which were pioneered by Fritzsch and Xing (1996, 1998, 2000); Xing (2001) in the leptonic sector. The masses m_k are taken to be real and positive labelling the free propagating states of the three neutrinos.

3.2.1 Effective Majorana neutrino Lagrangian

Given the mass matrix defined in Eq. (3.6), the Majorana mass term in the Lagrangian can be written in the flavor basis as

$$-\mathcal{L}_{\text{mass}}^{\text{Maj.}} = \frac{1}{2} \bar{\nu}_\ell M_{\ell\ell'} \nu_{\ell'} = -\frac{1}{2} \nu_{L,\ell}^T C^\dagger M_{\ell\ell'} \nu_{L,\ell'} + \text{h.c.}, \quad (3.8)$$

where the Majorana fields are written as $\nu = \nu_L + C(\bar{\nu}_L)^T$. The field ν_L refers to left-handed Weyl four-component spinors. Charged conjugated fields are written as $\nu^c = C(\bar{\nu})^T$. The charge conjugation operator C is defined in the usual way in Itzykson and Zuber (1980); p.692.

Given these conventions, we can extend our consideration to include the electro-

magnetic interaction of neutrinos which is possible if neutrinos are equipped with a magnetic moment matrix $\mu_{\ell\ell'}$. We allow for a fixed *external* electromagnetic field tensor $F_{\text{ext}}^{\alpha\beta}(x^\mu)$ which imparts a force on the neutrino fields. We emphasize that $F_{\text{ext}}^{\alpha\beta}$ is not dynamical in our formulation and consists of real functions over four-position and not field operators.

We generalize the AMM Pauli Lagrangian in Eq. (1.31) to account for the Majorana fields in the flavor basis as

$$-\mathcal{L}_{\text{AMM}}^{\text{Maj.}} = \frac{1}{2}\bar{\nu}_\ell \left(\mu_{\ell\ell'} \frac{1}{2} \sigma_{\alpha\beta} F_{\text{ext}}^{\alpha\beta} \right) \nu_{\ell'} = -\frac{1}{2} \nu_{L,\ell}^T C^\dagger \left(\mu_{\ell\ell'} \frac{1}{2} \sigma_{\alpha\beta} F_{\text{ext}}^{\alpha\beta} \right) \nu_{L,\ell'} + \text{h.c.} \quad (3.9)$$

The operator $\sigma_{\alpha\beta}$ is the 4×4 spin tensor defined in Eq. (1.26). We would like to point out some interesting features of the Pauli term most notably that the spin tensor itself is not Hermitian with

$$\sigma_{\alpha\beta}^\dagger = \gamma_0 \sigma_{\alpha\beta} \gamma_0. \quad (3.10)$$

However, the conjugate of the Lagrangian term in Eq. (3.9)

$$\left(\nu^\dagger \gamma_0 \sigma_{\alpha\beta} F_{\text{ext}}^{\alpha\beta} \nu \right)^\dagger = \nu^\dagger \sigma_{\alpha\beta}^\dagger F_{\text{ext}}^{\alpha\beta} \gamma_0 \nu = \nu^\dagger \gamma_0 \sigma_{\alpha\beta} F_{\text{ext}}^{\alpha\beta} \nu, \quad (3.11)$$

is Hermitian. More about the spin tensor's properties will be elaborated on in Section 3.1.

The Majorana magnetic moment matrix acts in flavor space. It satisfies the following constraints (Giunti and Studenikin, 2015) for CPT symmetry reasons and the anticommuting nature of fermions

$$\mu_{\ell\ell'}^\dagger = \mu_{\ell\ell'}, \quad \mu_{\ell\ell'}^T = -\mu_{\ell\ell'}, \quad (3.12)$$

i.e. the AMM matrix $\mu_{\ell\ell'}$ is Hermitian and fully anti-symmetric. This requires that the transition magnetic moment elements are purely imaginary while all diagonal

AMM matrix elements vanish

$$\mu_{\ell\ell'} = \begin{pmatrix} \mu_{ee} & \mu_{e\mu} & \mu_{e\tau} \\ \mu_{\mu e} & \mu_{\mu\mu} & \mu_{\mu\tau} \\ \mu_{\tau e} & \mu_{\tau\mu} & \mu_{\tau\tau} \end{pmatrix} \xrightarrow{\text{Majorana}} \mu_{\ell\ell'} = \begin{pmatrix} 0 & i\mu_{e\mu} & -i\mu_{e\tau} \\ -i\mu_{e\mu} & 0 & i\mu_{\mu\tau} \\ i\mu_{e\tau} & -i\mu_{\mu\tau} & 0 \end{pmatrix}. \quad (3.13)$$

We can combine the mass term in Eq. (3.8) and AMM contribution in Eq. (3.9) into a single effective Lagrangian

$$\mathcal{L}_{\text{eff}}^{\text{Maj.}} = \mathcal{L}_{\text{kinetic}}^{\text{Maj.}} + \mathcal{L}_{\text{mass}}^{\text{Maj.}} + \mathcal{L}_{\text{AMM}}^{\text{Maj.}}, \quad (3.14)$$

$$\mathcal{L}_{\text{eff}}^{\text{Maj.}} = \mathcal{L}_{\text{kinetic}}^{\text{Maj.}} - \frac{1}{2}\bar{\nu}_\ell \left(M_{\ell\ell'} + \mu_{\ell\ell'} \frac{1}{2}\sigma_{\alpha\beta}F_{\text{ext}}^{\alpha\beta} \right) \nu_{\ell'}. \quad (3.15)$$

Eq. (3.15) is our working Lagrangian. For later convenience we define the generalized mass-dipole matrix $\mathcal{M}_{\ell\ell'}$ present in Eq. (3.15) as

$$\mathcal{M}_{\ell\ell'}(\mathbf{E}, \mathbf{B}) \equiv M_{\ell\ell'} + \mu_{\ell\ell'} \frac{1}{2}\sigma_{\alpha\beta}F_{\text{ext}}^{\alpha\beta}, \quad \mathcal{M}_{\ell\ell'}^\dagger = \gamma_0 \mathcal{M}_{\ell\ell'} \gamma_0. \quad (3.16)$$

As neutrinos must propagate as energy eigenstates, our objective is to find the eigenvalues of Eq. (3.15) rather than Eq. (3.7). As the mass eigenvalues are modified by the presence the EM interactions $m \rightarrow \tilde{m}(\mathbf{E}, \mathbf{B})$ so will the mixing matrix, leading to modifications of Eq. (3.4). These electromagnetic components then facilitate time-dependant oscillation among the free-particle mass eigenstates ([Giunti and Studenikin, 2015](#)).

Additionally we may consider matter effects via the weak interaction. Electron (anti)neutrinos passing through matter preferentially interact via weak charge-current (via the W^\pm boson) with electrons which make up the bulk of charged leptons in most matter. The neutral-current (via the Z_0 boson) however affects all flavors and couples to the neutrons within the medium as the electron and proton contributions cancel in charge neutral matter. This can be represented, MSW effect aside, as the weak charge-current V_{CC} and neutral-current V_{NC} effective potentials ([Pal, 1992](#); [Greiner](#)

and Müller, 2009) which contribute to the action as

$$\mathcal{L}_{\text{matter}}^{\text{Maj.}} = \bar{\nu}_\ell(\gamma_0 V_{\ell\ell'})\nu_{\ell'} , \quad V_{\ell\ell'} = \begin{pmatrix} V_{CC} + V_{NC} & 0 & 0 \\ 0 & V_{NC} & 0 \\ 0 & 0 & V_{NC} \end{pmatrix} , \quad (3.17)$$

$$V_{CC} = \sqrt{2}G_F\hbar^2c^2n_e , \quad V_{NC} = -\frac{1}{2}\sqrt{2}G_F\hbar^2c^2n_n . \quad (3.18)$$

The coefficient G_F is the Fermi constant, n_e is the number density of electron matter and n_n is the number density of neutrons within the medium. We note that $V_{\ell\ell'}\gamma_0$ behaves like the zeroth component of a vector-potential. As written, Eq. (3.17) is approximately true for non-relativistic matter.

3.2.2 Chiral properties of the relativistic Pauli dipole

While the Pauli dipole was introduced and discussed in Section 1.1.2, we will further elaborate on details directly relevant to neutrinos. The electromagnetic dipole behavior of the neutrino depends on mathematical properties of the tensor product $\sigma_{\alpha\beta}F_{\text{ext}}^{\alpha\beta}$. We prefer to work in the Weyl (chiral) spinor representation where the EM contribution is diagonal in spin space. Therefore we evaluate the product $\sigma_{\alpha\beta}F_{\text{ext}}^{\alpha\beta}$ in the Weyl representation following Feynman and Gell-Mann (1958) yielding

$$-\frac{1}{2}\sigma_{\alpha\beta}F_{\text{ext}}^{\alpha\beta} = \begin{pmatrix} \boldsymbol{\sigma} \cdot (\mathbf{B} + i\mathbf{E}/c) & 0 \\ 0 & \boldsymbol{\sigma} \cdot (\mathbf{B} - i\mathbf{E}/c) \end{pmatrix} \equiv \begin{pmatrix} \boldsymbol{\sigma} \cdot \mathbf{f}_+ & 0 \\ 0 & \boldsymbol{\sigma} \cdot \mathbf{f}_- \end{pmatrix} , \quad (3.19)$$

where we introduced the complex electromagnetic field form $\mathbf{f}_\pm = \mathbf{B} \pm i\mathbf{E}/c$ showing sensitivity to both magnetic and electric fields. The eigenvalues of Eq. (3.19) were also discussed in Section 2.4. As this expression is diagonal in the Weyl representation, it does not exchange handedness when acting upon a state. This is explicitly understood by the fact that Eq. (3.19) commutes with γ^5 . Since left and right-handed neutrinos are not remixed by magnetic moments, sterile right-handed neutrinos do not need to be introduced. We can also see explicitly in Eq. (3.19) its non-Hermitian character, see Eq. (3.15), of the EM spin-field coupling. Specifically this is mirrored in the

complex field's \mathbf{f}_\pm relation to its complex conjugate $(\mathbf{f}_\pm)^* = \mathbf{f}_\mp$. The complex EM fields have a Hermitian (\mathbf{B}) and anti-Hermitian ($i\mathbf{E}$) part.

Taking the product of \mathbf{f}_\pm with its complex conjugate we find

$$\frac{1}{2} (\boldsymbol{\sigma} \cdot \mathbf{f}_\pm) (\boldsymbol{\sigma} \cdot \mathbf{f}_\mp) = T_{\text{ext}}^{00} \mp \sigma_i T_{\text{ext}}^{0i}, \quad (3.20)$$

where we recognize the stress-energy tensor $T_{\text{ext}}^{\alpha\beta}$ component T_{ext}^{00} for field energy density and T_{ext}^{0i} momentum density respectively

$$T_{\text{ext}}^{00} = \frac{1}{2} (B^2 + E^2/c^2), \quad T_{\text{ext}}^{0i} = \frac{1}{c} \varepsilon_{ijk} E_j B_k. \quad (3.21)$$

As we will see in Section 3.3, Eq. (3.20) will appear in the EM-mass eigenvalues of our effective Lagrangian Eq. (3.14). Using the identity in Eq. (3.19) and Eq. (3.20) we also find the interesting relationship

$$\frac{1}{2} \left(\frac{1}{2} \sigma_{\alpha\beta} F_{\text{ext}}^{\alpha\beta} \right) \left(\frac{1}{2} \sigma_{\alpha\beta} F_{\text{ext}}^{\alpha\beta} \right)^\dagger = \gamma_0 (T_{\text{ext}}^{00} \gamma_0 + T_{\text{ext}}^{0i} \gamma_i). \quad (3.22)$$

Now that we have elaborated on the relevant EM field identities, we turn back to the magnetic dipole and flavor rotation problem.

3.3 Electromagnetic-flavor mixing for two generations

Considering experimental data on neutrino oscillations, it is understood that either the two lighter (normal hierarchy) or the two heavier (inverted hierarchy) neutrino states are close together in mass. If the electromagnetic properties of the neutrino do indeed lead to flavor mixing effects, then it is likely the closer pair of neutrino mass states that are most sensitive to the phenomenon we explore. In the spirit of [Bethe \(1986\)](#), we therefore explore the $N = 2$ two generation (ν_e, ν_μ) toy model.

Following the properties established in Eq. (3.12) and Eq. (3.16) we write down

the two generation mass and dipole matrices as

$$M_{\ell\ell'} = \begin{pmatrix} m_e^\nu & \delta m \\ \delta m & m_\mu^\nu \end{pmatrix}, \quad \mu_{\ell\ell'} = \begin{pmatrix} 0 & i\delta\mu \\ -i\delta\mu & 0 \end{pmatrix}. \quad (3.23)$$

The AMM coupling $\delta\mu$ is taken to be real with a pure imaginary coefficient. While the mass elements $(m_e^\nu, m_\mu^\nu, \delta m)$ are generally complex, we choose in our toy model for them to be fully real

$$m_e^\nu = (m_e^\nu)^*, \quad m_\mu^\nu = (m_\mu^\nu)^*, \quad \delta m = \delta m^*, \quad (3.24)$$

making the mass matrix $M_{\ell\ell'}$ Hermitian. This allows us to more easily evaluate and emphasize the EM contributions to mixing rather than complications arising from the mass matrix.

Using Eq. (3.23) and Eq. (3.24), we write the mass-dipole matrix in Eq. (3.16) in terms of 2×2 flavor components as

$$\mathcal{M}_{\ell\ell'} = \begin{pmatrix} m_e^\nu & \delta m + i\delta\mu\sigma_{\alpha\beta}F_{\text{ext}}^{\alpha\beta}/2 \\ \delta m - i\delta\mu\sigma_{\alpha\beta}F_{\text{ext}}^{\alpha\beta}/2 & m_\mu^\nu \end{pmatrix}, \quad \mathcal{M}_{\ell\ell'}^\dagger = \gamma_0 \mathcal{M}_{\ell\ell'} \gamma_0. \quad (3.25)$$

As noted before, this matrix is not Hermitian due to the inclusion of the spin tensor, therefore it is not guaranteed to satisfy an algebraic eigenvalue equation in its present form which is a requirement for well behaved masses.

This can be remedied by recalling that any arbitrary complex matrix can be diagonalized into its real eigenvalues λ_j by the biunitary transform

$$W_{\ell j}^\dagger \mathcal{M}_{\ell\ell'} Y_{\ell' j'} = \lambda_j \delta_{jj'}, \quad (3.26)$$

where $Y_{\ell j}$ and $W_{\ell j}$ are both unitary matrices. Taking the complex conjugate of

Eq. (3.26), we arrive at

$$(W_{\ell j}^\dagger \mathcal{M}_{\ell\ell'} Y_{\ell'j'})^\dagger = Y_{\ell'j'}^\dagger \gamma_0 \mathcal{M}_{\ell\ell'} \gamma_0 W_{\ell j} = \lambda_j \delta_{jj'}, \quad (3.27)$$

$$Y_{\ell j} = \gamma_0 W_{\ell j} \rightarrow W_{\ell j}^\dagger \mathcal{M}_{\ell\ell'} \gamma_0 W_{\ell'j'} = \lambda_j \delta_{jj'}. \quad (3.28)$$

As $Y_{\ell j}$ and $W_{\ell j}$ are related by a factor of γ_0 based on the conjugation properties of Eq. (3.25), this lets us eliminate $Y_{\ell j}$ and diagonalize using a single unitary matrix $W_{\ell j}$. The related matrix $\mathcal{M}_{\ell\ell'} \gamma_0$ is Hermitian

$$(\mathcal{M}_{\ell\ell'} \gamma_0)^\dagger = \mathcal{M}_{\ell\ell'} \gamma_0, \quad (3.29)$$

and also equivalent to the root of the Hermitian product of Eq. (3.25)

$$(\mathcal{M}\mathcal{M}^\dagger)_{\ell\ell'} = ((\mathcal{M}\gamma_0)(\mathcal{M}\gamma_0))_{\ell\ell'}. \quad (3.30)$$

Therefore a suitable unitary transformation $W_{\ell j}$ rotates flavor ℓ -states into magnetized mass j -states. The eigenvalues λ_j^2 of $(\mathcal{M}\mathcal{M}^\dagger)_{\ell\ell'}$ are the squares of both signs of the eigenvalues of $\mathcal{M}_{\ell\ell'} \gamma_0$. We write this property (with flavor indices suppressed) as

$$W^\dagger (\mathcal{M}\mathcal{M}^\dagger) W = W^\dagger (\mathcal{M}\gamma_0) W W^\dagger (\mathcal{M}\gamma_0) W = \text{diag}(\lambda_1^2, \lambda_2^2). \quad (3.31)$$

We associate $\lambda_j = \tilde{m}_j(\mathbf{E}, \mathbf{B})$ with $j \in 1, 2$ as the effective EM-mass states which are field dependant in this basis.

3.3.1 Separating electromagnetic-mass mixing into two rotations

The matrix $W_{\ell j}$ mixes flavor states into a new basis distinct from the free-particle case however this rotation must smoothly connect with the free-particle case in the limit that the electromagnetic fields go to zero. We proceed to evaluate $W_{\ell j}$ breaking the rotation into two separate unitary transformations:

- (a) Rotation matrix $V_{\ell k}^\dagger(\ell \rightarrow k)$ converting from flavor to free-particle mass
- (b) Rotation matrix $Z_{kj}^{\text{ext}\dagger}(k \rightarrow j)$ converting from free-particle mass to EM-mass

Guided by Eq. (3.2) we write

$$\nu_j = W_{\ell j}^\dagger \nu_\ell = Z_{kj}^{\text{ext}\dagger} V_{\ell k}^\dagger \nu_\ell . \quad (3.32)$$

In the limit that the EM fields go to zero, the electromagnetic rotation becomes unity $Z_{kj}^{\text{ext}} \rightarrow \delta_{kj}$ thereby ensuring the EM-mass basis and free-particle mass basis become equivalent. The rotation Z_{kj}^{ext} can then be interpreted as the external field forced rotation. While our argument above is done explicitly for the two generation case, it can be generalized to accommodate three generations of neutrinos as well.

According to Eq. (3.7), the mass matrix in Eq. (3.23) can be diagonalized in the two generation case by a one parameter unitary mixing matrix $V_{\ell k}$ given by

$$V_{\ell k}(\theta) = \begin{pmatrix} \cos \theta & \sin \theta \\ -\sin \theta & \cos \theta \end{pmatrix} . \quad (3.33)$$

For a real Hermitian 2×2 mass matrix, the rotation matrix $V_{\ell k}$ is real and only depends on the angle θ . The explicit form of the EM-field related rotation Z_{kj}^{ext} introduced in Eq. (3.32) is

$$Z_{kj}^{\text{ext}}(\omega, \phi) = \begin{pmatrix} \cos \omega & e^{i\phi} \sin \omega \\ -e^{-i\phi} \sin \omega & \cos \omega \end{pmatrix} , \quad W_{\ell j}(\theta, \omega, \phi) = V_{\ell k}(\theta) Z_{kj}^{\text{ext}}(\omega, \phi) , \quad (3.34)$$

where Z_{kj}^{ext} depends on the real angle ω and complex phase ϕ . The full rotation $W_{\ell j}$ therefore depends on three parameters when broken into free-particle rotation and EM rotation.

The eigenvalues of the original Hermitian mass matrix in Eq. (3.23) are given by

$$m_{1,2} = \frac{1}{2} \left(m_e^\nu + m_\mu^\nu \mp \sqrt{|\Delta m_0|^2 + 4\delta m^2} \right) , \quad |\Delta m_0| = |m_\mu^\nu - m_\mu^e| . \quad (3.35)$$

We assign m_1 to the lower mass (−) root and m_2 with the larger mass (+) additive

root. The rotation angle θ in Eq. (3.33) is then given by

$$\sin 2\theta = \sqrt{\frac{4\delta m^2}{|\Delta m_0|^2 + 4\delta m^2}}, \quad \cos 2\theta = \sqrt{\frac{|\Delta m_0|^2}{|\Delta m_0|^2 + 4\delta m^2}}. \quad (3.36)$$

In our toy model, the off-diagonal imaginary transition magnetic moment $\mu_{\ell\ell'}$ commutes with the real valued mixing matrix $V_{\ell k}$ and the following relations hold

$$V_{\ell k}^\dagger \mu_{\ell\ell'} V_{\ell' k'} = (V^\dagger V)_{k\ell'} \mu_{\ell' k'} = \mu_{kk'} = \begin{pmatrix} 0 & i\delta\mu \\ -i\delta\mu & 0 \end{pmatrix}. \quad (3.37)$$

We see that the Majorana transition dipoles in our model are off-diagonal in both flavor and mass basis. Therefore the real parameter unitary matrix in Eq. (3.37) cannot rotate a pure imaginary matrix at least in the two generation case. We apply the rotation in Eq. (3.33) to Eq. (3.29) yielding

$$V_{\ell k}^\dagger (\mathcal{M}_{\ell\ell'} \gamma_0) V_{\ell' k'} = V_{\ell k}^\dagger M_{\ell\ell'} \gamma_0 V_{\ell' k'} + V_{\ell k}^\dagger (\mu_{\ell\ell'} \sigma_{\alpha\beta} \gamma_0 F_{\text{ext}}^{\alpha\beta}/2) V_{\ell' k'}, \quad (3.38)$$

$$V_{\ell k}^\dagger (\mathcal{M}_{\ell\ell'} \gamma_0) V_{\ell' k'} = \begin{pmatrix} m_1 \gamma_0 & i\delta\mu \sigma_{\alpha\beta} \gamma_0 F_{\text{ext}}^{\alpha\beta}/2 \\ -i\delta\mu \sigma_{\alpha\beta} \gamma_0 F_{\text{ext}}^{\alpha\beta}/2 & m_2 \gamma_0 \end{pmatrix} \equiv \begin{pmatrix} \mathcal{A} & i\mathcal{C} \\ -i\mathcal{C} & \mathcal{B} \end{pmatrix}, \quad (3.39)$$

where we have defined implicitly the Hermitian elements $(\mathcal{A}, \mathcal{B}, \mathcal{C})$. Applying now both rotations to Eq. (3.29) yields

$$W_{\ell j}^\dagger (\mathcal{M}_{\ell\ell'} \gamma_0) W_{\ell' j'} = Z^{\text{ext}\dagger} \begin{pmatrix} \mathcal{A} & i\mathcal{C} \\ -i\mathcal{C} & \mathcal{B} \end{pmatrix} Z^{\text{ext}} = \lambda_j \delta_{jj'}. \quad (3.40)$$

Eq. (3.40) is therefore the working matrix equation which needs to be solved to identify the EM rotation parameters. As discussed before, this means that the rotation angle ω and phase ϕ are in general functions of electromagnetic fields.

3.3.2 Effective electromagnetic-mass eigenvalues

We will now solve for the rotation parameters necessary to define the EM-mass basis which acts as a distinct propagating basis for neutrinos in external fields. Considering that the j -columns vectors $\mathbf{v}^{(j)}$ of $Z_{k,j}^{\text{ext}}$ as eigenvectors for each eigenvalue λ_j

$$Z_{k,j}^{\text{ext}} = v_k^{(j)} = \begin{pmatrix} \mathbf{v}^1 & \mathbf{v}^2 \end{pmatrix}, \quad (3.41)$$

Eq. (3.40) has the meaning of an eigenvalue equation

$$\begin{pmatrix} \mathcal{A} & i\mathcal{C} \\ -i\mathcal{C} & \mathcal{B} \end{pmatrix} Z^{\text{ext}} = Z^{\text{ext}} \begin{pmatrix} \lambda_1 & 0 \\ 0 & \lambda_2 \end{pmatrix} \rightarrow \begin{pmatrix} \mathcal{A} & i\mathcal{C} \\ -i\mathcal{C} & \mathcal{B} \end{pmatrix} \mathbf{v}^{(j)} = \lambda_j \mathbf{v}^{(j)}. \quad (3.42)$$

Given the eigenvalue equation defined in Eq. (3.42), the effective EM-masses are then solutions to the characteristic polynomial

$$(\mathcal{A} - \lambda_j \gamma_0)(\mathcal{B} - \lambda_j \gamma_0) - \mathcal{C}^2 = 0, \quad (3.43)$$

which we obtained by taking the determinant of Eq. (3.42) over flavor but not spin space. It is useful to define the following identities for the off-diagonal element

$$\mathcal{C}^2 = \delta\mu^2 \left(\frac{1}{2} \sigma_{\alpha\beta} F_{\text{ext}}^{\alpha\beta} \right) \left(\frac{1}{2} \sigma_{\alpha\beta} F_{\text{ext}}^{\alpha\beta} \right)^\dagger = 2\delta\mu^2 \gamma_0 (T_{\text{ext}}^{00} \gamma_0 + T_{\text{ext}}^{0i} \gamma_i), \quad (3.44)$$

and for the diagonal elements

$$(\mathcal{B} - \mathcal{A})^2 = |m_2 - m_1|^2 = |\Delta m|^2, \quad (\mathcal{A} + \mathcal{B})\gamma_0 = m_1 + m_2. \quad (3.45)$$

Eq. (3.44) was obtained using the expression in Eq. (3.22). Because of the spinor behavior of each element, the eigenvalues are obtained with γ_0 coefficients. Eq. (3.43)

therefore has the roots $\lambda_{1,2} = \tilde{m}_{1,2}(\mathbf{E}, \mathbf{B})$

$$\tilde{m}_{1,2}(\mathbf{E}, \mathbf{B}) = \frac{1}{2} \left(m_1 + m_2 \mp \sqrt{|\Delta m|^2 + 8\delta\mu^2\gamma_0 (T_{\text{ext}}^{00}\gamma_0 + T_{\text{ext}}^{0i}\gamma_i)} \right), \quad (3.46)$$

$$\tilde{m}_{1,2}(\mathbf{E}, \mathbf{B}) = \frac{m_1 + m_2}{2} \mp \frac{1}{2} \sqrt{|\Delta m|^2 + 8\delta\mu^2\gamma_0 \left(\gamma_0 \frac{1}{2} \left(B^2 + \frac{E^2}{c^2} \right) + \boldsymbol{\gamma} \cdot \left(\frac{\mathbf{E}}{c} \times \mathbf{B} \right) \right)}$$

$$(3.47)$$

The EM-mass eigenstates $\tilde{m}(\mathbf{E}, \mathbf{B})$ depends on the energy density T_{ext}^{00} of the EM field and the spin projection along the EM momentum density T_{ext}^{0i} . However the coefficient $\delta\mu^2$ is presumed to be very small, therefore the EM contribution only manifests in strong EM fields or where the free-particle case has very nearly or exactly degenerate masses, $\Delta m \rightarrow 0$. When the the electromagnetic fields go to zero, the EM-masses in Eq. (3.47) reduce as expected to the free-particle result.

The complex phase in Eq. (3.34) has the value $\phi = \pi(n - 1/2)$ with $n \in 0, \pm 1, \pm 2, \dots$ making the complex exponential in Eq. (3.34) pure imaginary. Curiously, the phase is not field dependant, but tied to the fact that the Majorana moments are pure imaginary quantities. Complex phases in mixing matrices are generally associated with CP violation such as the Dirac phase δ in Eq. (3.3) which suggests that CP violation in the neutrino sector can be induced in the presence of external EM fields. Some implications of CP violation from transition moments are discussed in [Nieves \(1982\)](#). Analysis of the three generation case is required to show this explicitly, but we postulate that the constant valued complex phases would be replaced with field dependant quantities $\delta \rightarrow \delta(\mathbf{E}, \mathbf{B})$.

We note that the solution in Eq. (3.47) actually contain four distinct EM-mass eigenstates $\tilde{m}_j^s(\mathbf{E}, \mathbf{B})$ with the lower ($j = 1$) and upper ($j = 2$) masses and the additional spin splitting from the alignment ($s = +1$) or anti-alignment ($s = -1$) of the neutrino spin with the momentum density of the external EM field. Spin splitting vanishes for the pure electric or magnetic field cases. For good spin eigenstates $s \in \pm 1$,

we can rewrite Eq. (3.44) with EM fields explicitly as

$$\mathcal{C}_s^2(\mathbf{E}, \mathbf{B}) = 2\delta\mu^2 \left(\frac{1}{2}(B^2 + E^2/c^2) + s|\mathbf{E}/c \times \mathbf{B}| \right). \quad (3.48)$$

The above expression within the square is positive definite, therefore Eq. (3.48) is always real. Spin splitting requires that we consider separate rotations for each spin state as the rotation angle ω_s depends on the spin quantum number

$$\sin 2\omega_s = \sqrt{\frac{4\mathcal{C}_s^2}{|\Delta m|^2 + 4\mathcal{C}_s^2}}, \quad \cos 2\omega_s = \sqrt{\frac{|\Delta m|^2}{|\Delta m|^2 + 4\mathcal{C}_s^2}}. \quad (3.49)$$

The expressions in Eq. (3.49) are mathematically similar to that of the free-particle case written in Eq. (3.36) in the two flavor generation model with the off-diagonal mass being replaced with the EM dependant quantity \mathcal{C}_s .

3.4 Strong field (degenerate mass) and weak field limits

The rotation angles in Eq. (3.49) reveal two distinct limits where EM-masses are dominated by either:

- (a) Intrinsic mass splitting $\mathcal{C}_s \ll |\Delta m|^2$ with $\omega_s \rightarrow 0$
- (b) EM mass splitting $\mathcal{C}_s \gg |\Delta m|^2$ with $\omega_s \rightarrow \pi/4$

For the first case where the masses are not degenerate or the fields are weak, we obtain the expansion

$$\lim_{\mathcal{C}_s \ll |\Delta m|^2} \tilde{m}_{1,2}^s(E, B) = \frac{1}{2} \left(m_1 + m_2 \mp |\Delta m| \left(1 + \frac{2\mathcal{C}_s^2}{|\Delta m|^2} + \dots \right) \right), \quad (3.50)$$

which as stated before reduces to the free-particle case at lowest order.

In the opposite limit, where the masses are very nearly degenerate or fields are strong, the EM-mass eigenvalues in Eq. (3.47) can be approximated by the series

$$\lim_{\mathcal{C}_s \gg |\Delta m|^2} \tilde{m}_{1,2}^s(E, B) = \frac{1}{2} \left(m_1 + m_2 \mp 2\mathcal{C}_s \left(1 + \frac{|\Delta m|^2}{8\mathcal{C}_s^2} + \dots \right) \right) \quad (3.51)$$

For fully degenerate free-particle masses $m_1 = m_2$, this reduces to

$$\lim_{|\Delta m|^2 \rightarrow 0} \tilde{m}_{1,2}^s(E, B) = m_1 \mp \mathcal{C}_s. \quad (3.52)$$

Eq. (3.52) indicates that for degenerate free-particle masses, the effective splitting $|\Delta m_{\text{EM}}| \equiv \mathcal{C}_s$ between masses arises purely from the electromagnetic interaction of the neutrinos. We return to this interesting insight in our final comments.

Because of the bounds in Eq. (3.1) on the effective neutrino magnetic moment, we can estimate the field strength required for an external magnetic field to generate an electromagnetic mass splitting of $|\Delta m_{\text{EM}}| = 10^{-3}$ eV which is a reasonable comparison to intrinsic splitting based on the experimental limits on neutrino masses. Using the upper limit for the neutrino effective moment of $\mu_\nu^{\text{eff}} \sim 10^{-10} \mu_B$ we obtain

$$\left. \frac{\mathcal{C}_s}{\mu_\nu^{\text{eff}}} \right|_{\vec{E}=0} = \frac{10^{-3} \text{ eV}}{10^{-10} \mu_B} \approx 1.7 \times 10^{11} \text{ T}. \quad (3.53)$$

This is near the upper bound of the magnetic field strength of magnetars (Kaspi and Beloborodov, 2017) which are of the order 10^{11} Tesla. In this situation, the EM contribution to the mass splitting rivals the estimated inherent splitting (Workman et al., 2022) of the two closer in mass neutrinos. Primordial magnetic fields (Grasso and Rubinstein, 2001) in the Early Universe may also present an environment for significant EM neutrino flavor mixing as both the external field strength and density of neutrinos would be very large (Rafelski et al., 2023a). The magnetic properties of neutrinos may also have contributed alongside the charged leptons in magnetization in the Early Universe (Steinmetz et al., 2023) prior to recombination.

While the above estimate was done with astrophysical systems in mind, we note that strong electrical fields should also produce EM-mass splitting. Therefore environments near to high Z -nuclei is also of interest (Bouchiat and Bouchiat, 1974, 1997; Safronova et al., 2018) as weak interactions violate parity. Should neutrinos have abnormally large transition magnetic dipole moments, then they should exhibit mass splitting from the neutrino's electromagnetic dipole interaction which may compete with the intrinsic mass differences of the free-particles.

CHAPTER 4

Matter-antimatter origin of cosmic magnetism

We investigate the hypothesis that the observed intergalactic magnetic fields (IGMF) are primordial in nature, predating the recombination epoch. Specifically, we explore the role of the extremely large electron-positron (e^+e^-) pair abundance in the temperature range of $2000 \text{ keV} > T > 20 \text{ keV}$ which only disappeared after Big Bang nucleosynthesis (BBN). We review the status of cosmic magnetism in Section 4.1 which motivates our study. Section 4.2 discusses the extreme electron-positron abundance during this epoch. The statistical and thermodynamic theory of the electron-positron gas is described in Section 4.3. Section 4.4 describes the relativistic paramagnetism of the electron-positron gas. We propose in Section 4.5 a model of self-magnetization caused by spin polarization within the individual species in the gas.

This chapter serves primarily as a review of our work in Steinmetz et al. (2023) and portions of Rafelski et al. (2023a) where we propose that the early universe electron-positron plasma was a highly magnetized environment. We will use natural units ($c = \hbar = k_B = 1$) unless otherwise noted.

NOTE: The letter μ within this chapter will refer exclusively to charged chemical potential and *not* magnetic moment as before.

4.1 Short survey of magnetism in the universe

Macroscopic domains of magnetic fields have been found in all astrophysical environments from compact objects (stars, planets, etc.); interstellar and intergalactic space; and surprisingly in deep extra-galactic void spaces. Considering the ubiquity of magnetic fields in the universe (Giovannini, 2018, 2004; Kronberg, 1994), we search for a common primordial mechanism initiate the diversity of magnetism observed today. In this chapter, IGMF will refer to experimentally observed intergalactic fields of any

origin while primordial magnetic fields (PMF) refers to fields generated via early universe processes possibly as far back as inflation. The conventional elaboration of the origins for cosmic PMFs are detailed in (Gaensler et al., 2004; Durrer and Neronov, 2013; Batista and Saveliev, 2021).

IGMF are notably difficult to measure and difficult to explain. The bounds for IGMF at a length scale of 1 Mpc are today (Neronov and Vovk, 2010; Taylor et al., 2011; Pshirkov et al., 2016; Jedamzik and Saveliev, 2019; Vernstrom et al., 2021)

$$10^{-8} \text{ G} > B_{\text{IGMF}} > 10^{-16} \text{ G}. \quad (4.1)$$

We note that generating PMFs with such large coherent length scales is nontrivial (Giovannini, 2023) though currently the length scale for PMFs are not well constrained (Batista and Saveliev, 2021). Faraday rotation from distant radio active galaxy nuclei (AGN) (Pomakov et al., 2022) suggest that neither dynamo nor astrophysical processes would sufficiently account for the presence of magnetic fields in the universe today if the IGMF strength was around the upper bound of $B_{\text{IGMF}} \simeq 30 - 60$ nG as found in Vernstrom et al. (2021). Such strong magnetic fields would then require that at least some portion of the IGMF arise from primordial sources that predate the formation of stars.

Magnetized baryon inhomogeneities which in turn would produce anisotropies in the cosmic microwave background (CMB) (Jedamzik and Abel, 2013; Abdalla et al., 2022). Jedamzik and Pogosian (2020) propose further that the presence of a magnetic field of $B_{\text{PMF}} \simeq 0.1$ nG could be sufficient to explain the Hubble tension.

Our motivating hypothesis is outlined qualitatively in Figure 4.1 where PMF evolution is plotted over the temperature history of the universe. The descending blue band indicates the range of possible PMF strengths. The different epochs of the universe according to Λ CDM are delineated by temperature. The horizontal lines mark two important scales: (a) the Schwinger critical field strength given by

$$B_C = \frac{m_e^2}{e} \simeq 4.41 \times 10^{13} \text{ G}. \quad (4.2)$$

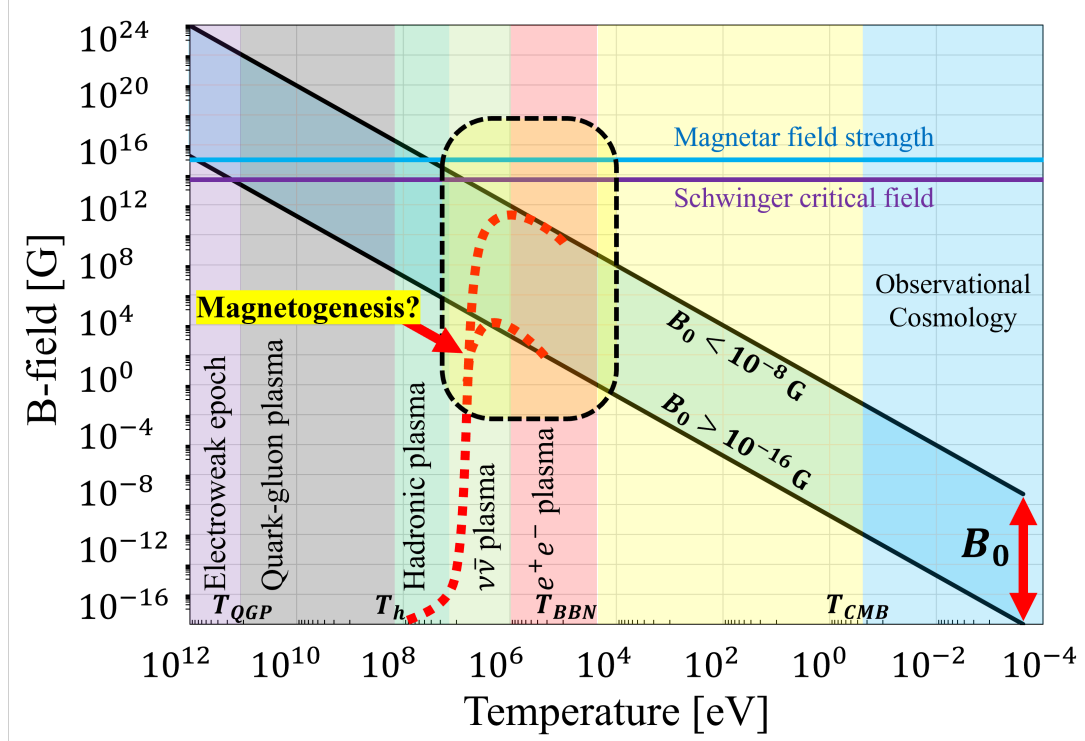


Figure 4.1: Qualitative plot of the primordial magnetic field strength over cosmic time. All figures are printed in temporal sequence in the expanding universe beginning with high temperatures (and early times) on the left and lower temperatures (and later times) on the right.

where electrodynamics is expected to display nonlinear characteristics and (b) the upper field strength seen in magnetars of $\sim 10^{15}$ G. A schematic of magnetogenesis is drawn with the dashed red lines indicating spontaneous formation of the PMF within the early universe plasma itself. The e^+e^- era is notably the final epoch where antimatter exists in large quantities in the cosmos (Rafelski et al., 2023a).

4.2 Electron-positron abundance

As the universe cooled below temperature $T = m_e$ (the electron mass), the thermal electron and positron comoving density depleted by over eight orders of magnitude. At $T_{\text{split}} = 20.3$ keV, the charged lepton asymmetry (mirrored by baryon asymmetry and enforced by charge neutrality) became evident as the surviving excess electrons

persisted while positrons vanished entirely from the particle inventory of the universe due to annihilation.

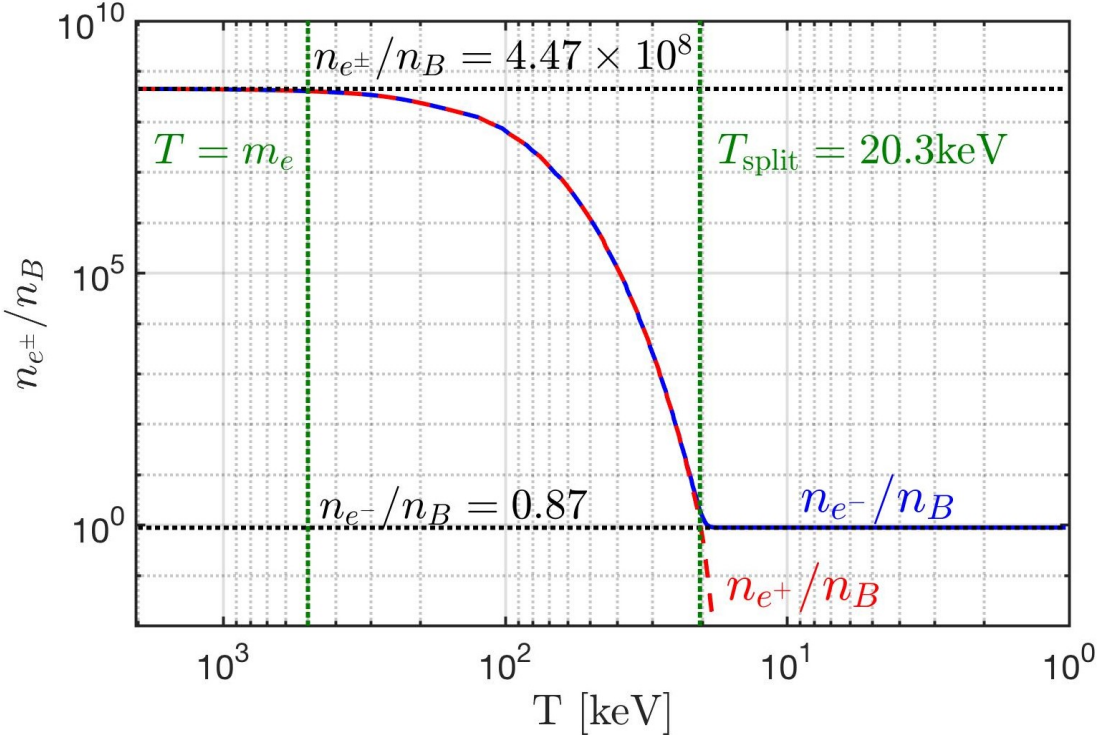


Figure 4.2: Number density of electron e^- and positron e^+ to baryon ratio n_{e^\pm}/n_B as a function of photon temperature in the universe. See text for further details. In this work we measure temperature in units of energy (keV) thus we set the Boltzmann constant to $k_B = 1$. Figure courtesy of Cheng Tao Yang.

The electron-to-baryon density ratio n_{e^-}/n_B is shown in Figure 4.2 as the solid blue line while the positron-to-baryon ratio n_{e^+}/n_B is represented by the dashed red line. These two lines overlap until the temperature drops below $T_{\text{split}} = 20.3$ keV as positrons vanish from the universe marking the end of the e^+e^- plasma and the dominance of the electron-proton (e^-p) plasma. The two vertical dashed green lines denote temperatures $T = m_e \simeq 511$ keV and $T_{\text{split}} = 20.3$ keV. These results were obtained using charge neutrality and the baryon-to-photon content (entropy) of the universe; see details in Rafelski et al. (2023a). The two horizontal black dashed lines denote the relativistic $T \gg m_e$ abundance of $n_{e^\pm}/n_B = 4.47 \times 10^8$ and post-annihilation abundance of $n_{e^-}/n_B = 0.87$. Above temperature $T \simeq 85$ keV, the

e^+e^- primordial plasma density exceeded that of the Sun's core density $n_e \simeq 6 \times 10^{26} \text{ cm}^{-3}$ (Bahcall et al., 2001).

Conversion of the dense e^+e^- pair plasma into photons reheated the photon background (Birrell et al., 2014) separating the photon and neutrino temperatures. The e^+e^- annihilation and photon reheating period lasted no longer than an afternoon lunch break. Because of charge neutrality, the post-annihilation comoving ratio $n_{e^-}/n_B = 0.87$ (Rafelski et al., 2023a) is slightly offset from unity in Figure 4.2 by the presence of bound neutrons in α particles and other neutron containing light elements produced during BBN epoch.

The abundance of baryons is itself fixed by the known abundance relative to photons (Workman et al., 2022) and we employed the contemporary recommended value $n_B/n_\gamma = 6.09 \times 10^{-10}$. The resulting chemical potential needs to be evaluated carefully to obtain the behavior near to $T_{\text{split}} = 20.3 \text{ keV}$ where the relatively small value of chemical potential μ rises rapidly so that positrons vanish from the particle inventory of the universe while nearly one electron per baryon remains. The detailed solution of this problem is found in Fromerth et al. (2012); Rafelski et al. (2023a) leading to the results shown in Figure 4.2.

4.3 Theory of thermal matter-antimatter plasmas

To evaluate magnetic properties of the thermal e^+e^- pair plasma we take inspiration from Ch. 9 of Melrose's treatise on magnetized plasmas (Melrose, 2013). We focus on the bulk properties of thermalized plasmas in (near) equilibrium.

We consider a homogeneous magnetic field domain defined along the z -axis as

$$\mathbf{B} = (0, 0, B), \quad (4.3)$$

with magnetic field magnitude $|\mathbf{B}| = B$. Following Chapter 2, we reprint the microscopic energy (Eq. (2.16) in different notation) of the charged relativistic fermion

within a homogeneous magnetic field given by

$$E_{\sigma,s}^n(p_z, B) = \sqrt{m_e^2 + p_z^2 + eB \left(2n + 1 + \frac{g}{2}\sigma s \right)}, \quad (4.4)$$

where $n \in 0, 1, 2, \dots$ is the Landau orbital quantum number, p_z is the momentum parallel to the field axis and the electric charge is $e \equiv q_{e^+} = -q_{e^-}$. The index σ in Eq. (4.4) differentiates electron (e^- ; $\sigma = +1$) and positron (e^+ ; $\sigma = -1$) states. The index s refers to the spin along the field axis: parallel (\uparrow ; $s = +1$) or anti-parallel (\downarrow ; $s = -1$) for both particle and antiparticle species.

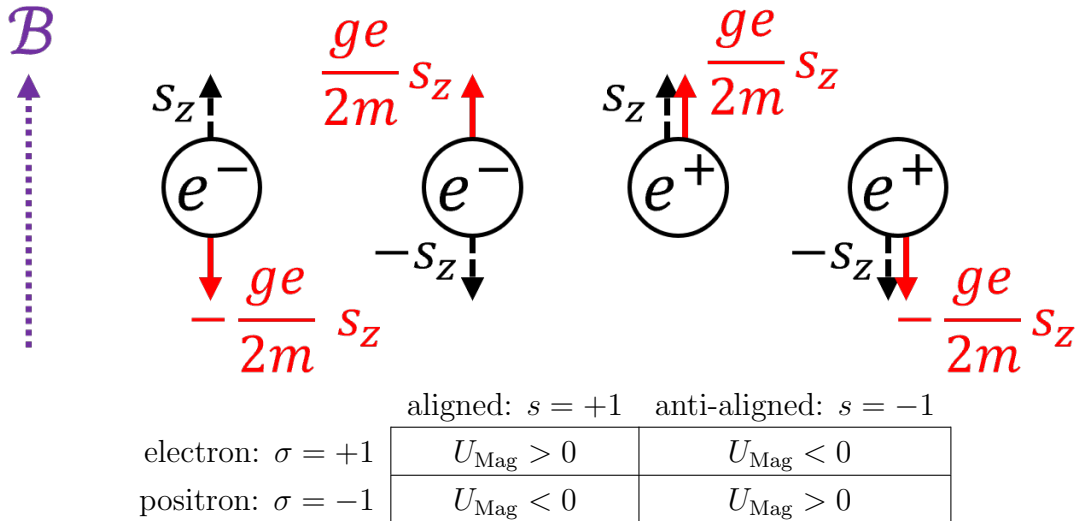


Figure 4.3: Organizational schematic of matter-antimatter (σ) and polarization (s) states with respect to the sign of the non-relativistic magnetic dipole energy U_{Mag} obtainable from Eq. (4.4).

The reason Eq. (4.4) distinguishes between electrons and positrons is to ensure the correct non-relativistic limit for the magnetic dipole energy is reached. Following the conventions found in Tiesinga et al. (2021), we set the gyro-magnetic factor $g \equiv g_{e^+} = -g_{e^-} > 0$ such that electrons and positrons have opposite g -factors and opposite magnetic moments relative to their spin; see Figure 4.3.

We recall the conventions established in Section 1.3. Conservation of magnetic flux requires that the magnetic field through a comoving surface L_0^2 remain unchanged. The magnetic field strength under expansion (Durrer and Neronov, 2013) starting at

some initial time t_0 is then given by

$$B(t) = B_0 \frac{a_0^2}{a^2(t)} \rightarrow B(z) = B_0 (1+z)^2 , \quad (4.5)$$

where B_0 is the comoving value obtained from the contemporary value of the magnetic field today. Magnetic fields in the cosmos generated through mechanisms such as dynamo or astrophysical sources do not follow this scaling (Pomakov et al., 2022). It is only in deep intergalactic space where matter density is low are magnetic fields preserved (and thus uncontaminated) over cosmic time.

From Eq. (1.60) and Eq. (4.5) there emerges a natural ratio of interest which is conserved over cosmic expansion

$b \equiv \frac{eB(t)}{T^2(t)} = \frac{eB_0}{T_0^2} \equiv b_0 = \text{ const.}$

(4.6)

$$10^{-3} > b_0 > 10^{-11} , \quad (4.7)$$

given in natural units ($c = \hbar = k_B = 1$). We computed the bounds for this cosmic magnetic scale ratio by using the present day IGMF observations given by Eq. (4.1) and the present CMB temperature $T_0 = 2.7 \text{ K} \simeq 2.3 \times 10^{-4} \text{ eV}$ (Aghanim et al., 2020).

4.3.1 Eigenstates of magnetic moment in cosmology

As statistical properties depend on the characteristic Boltzmann factor E/T , another interpretation of Eq. (4.6) in the context of energy eigenvalues (such as those given in Eq. (4.4)) is the preservation of magnetic moment energy relative to momentum under adiabatic cosmic expansion. The Boltzmann statistical factor is given by

$$x \equiv \frac{E}{T} . \quad (4.8)$$

We can explore this relationship for the magnetized system explicitly by writing out Eq. (4.8) using the KGP energy eigenvalues written in Eq. (4.4) as

$$x_{\sigma,s}^n = \frac{E_{\sigma,s}^n}{T} = \sqrt{\frac{m_e^2}{T^2} + \frac{p_z^2}{T^2} + \frac{eB}{T^2} \left(2n + 1 + \frac{g}{2}\sigma s\right)}. \quad (4.9)$$

Introducing the expansion scale factor $a(t)$ via Eq. (1.60), Eq. (4.5) and Eq. (4.6). The Boltzmann factor can then be written as

$$x_{\sigma,s}^n(a(t)) = \sqrt{\frac{m_e^2}{T^2(t_0)} \frac{a(t)^2}{a_0^2} + \frac{p_{z,0}^2}{T_0^2} + \frac{eB_0}{T_0^2} \left(2n + 1 + \frac{g}{2}\sigma s\right)}. \quad (4.10)$$

This reveals that only the mass contribution is dynamic over cosmological time. The constant of motion b_0 defined in Eq. (4.6) is seen as the coefficient to the Landau and spin portion of the energy. For any given eigenstate, the mass term drives the state into the non-relativistic limit while the momenta and magnetic contributions are frozen by initial conditions.

In comparison, the Boltzmann factor for the DP energy eigenvalues are given by

$$x_{\sigma,s}^n|_{\text{DP}} = \sqrt{\left(\sqrt{\frac{m_e^2}{T^2} + \frac{eB}{T^2} (2n + 1 + \sigma s)} + \frac{eB}{2m_e T} \left(\frac{g}{2} - 1\right) \sigma s\right)^2 + \frac{p_z^2}{T^2}}, \quad (4.11)$$

which scales during FLRW expansion as

$$x_{\sigma,s}^n(a(t))|_{\text{DP}} = \sqrt{\left(\sqrt{\frac{m_e^2 a(t)^2}{T_0^2} + \frac{eB_0}{T_0^2} (2n + 1 + \sigma s)} + \frac{eB_0}{2m_e T_0} \frac{a_0}{a(t)} \left(\frac{g}{2} - 1\right) \sigma s\right)^2 + \frac{p_{z,0}^2}{T_0^2}}. \quad (4.12)$$

While the above expression is rather complicated, we note that the KGP Eq. (4.10) and DP Eq. (4.11) Boltzmann factors both reduce to the Schrödinger-Pauli limit as $a(t) \rightarrow \infty$ thereby demonstrating that the total magnetic moment is protected under the adiabatic expansion of the universe.

As noted in Section 2.4 and Section 3.3.2, higher order non-minimal magnetic

contributions can be introduced to the Boltzmann factor such as $\sim (e/m)^2 B^2/T^2$. The reasoning above suggests that these terms are suppressed over cosmological time driving the system into minimal electromagnetic coupling with the exception of the anomalous magnetic moment. It is interesting to note that cosmological expansion then serves to ‘smooth out’ the characteristics of more complex electrodynamics erasing them from a statistical perspective in favor of minimal-like dynamics.

4.3.2 Magnetized fermion partition function

To obtain a quantitative description of the above evolution, we study the bulk properties of the relativistic charged/magnetic gasses in a nearly homogeneous and isotropic primordial universe via the thermal Fermi-Dirac or Bose distributions.

The grand partition function for the relativistic Fermi-Dirac ensemble is given by the standard definition

$$\ln \mathcal{Z}_{\text{total}} = \sum_{\alpha} \ln \left(1 + \Upsilon_{\alpha_1 \dots \alpha_m} \exp \left(-\frac{E_{\alpha}}{T} \right) \right), \quad \Upsilon_{\alpha_1 \dots \alpha_m} = \lambda_{\alpha_1} \lambda_{\alpha_2} \dots \lambda_{\alpha_m} \quad (4.13)$$

where we are summing over the set all relevant quantum numbers $\alpha = (\alpha_1, \alpha_2, \dots, \alpha_m)$. We note here the generalized the fugacity $\Upsilon_{\alpha_1 \dots \alpha_m}$ allowing for any possible deformation caused by pressures effecting the distribution of any quantum numbers.

In the case of the Landau problem, there is an additional summation over \tilde{G} which represents the occupancy of Landau states (Greiner et al., 2012b) which are matched to the available phase space within $\Delta p_x \Delta p_y$. If we consider the orbital Landau quantum number n to represent the transverse momentum $p_T^2 = p_x^2 + p_y^2$ of the system, then the relationship that defines \tilde{G} is given by

$$\frac{L^2}{(2\pi)^2} \Delta p_x \Delta p_y = \frac{eBL^2}{2\pi} \Delta n, \quad \tilde{G} = \frac{eBL^2}{2\pi}. \quad (4.14)$$

The summation over the continuous p_z is replaced with an integration and the double

summation over p_x and p_y is replaced by a single sum over Landau orbits

$$\sum_{p_z} \rightarrow \frac{L}{2\pi} \int_{-\infty}^{+\infty} dp_z, \quad \sum_{p_x} \sum_{p_y} \rightarrow \frac{eBL^2}{2\pi} \sum_n, \quad (4.15)$$

where L defines the boundary length of our considered volume $V = L^3$.

The partition function of the e^+e^- plasma can be understood as the sum of four gaseous species

$$\ln \mathcal{Z}_{e^+e^-} = \ln \mathcal{Z}_{e^+}^\uparrow + \ln \mathcal{Z}_{e^+}^\downarrow + \ln \mathcal{Z}_{e^-}^\uparrow + \ln \mathcal{Z}_{e^-}^\downarrow, \quad (4.16)$$

of electrons and positrons of both polarizations ($\uparrow\downarrow$). The change in phase space written in Eq. (4.15) modify the magnetized e^+e^- plasma partition function from Eq. (4.13) into

$$\ln \mathcal{Z}_{e^+e^-} = \frac{eBV}{(2\pi)^2} \sum_{\sigma}^{\pm 1} \sum_s^{\pm 1} \sum_{n=0}^{\infty} \int_{-\infty}^{\infty} dp_z \left[\ln \left(1 + \lambda_{\sigma} \xi_{\sigma,s} \exp \left(-\frac{E_{\sigma,s}^n}{T} \right) \right) \right] \quad (4.17)$$

$$\Upsilon_{\sigma,s} = \lambda_{\sigma} \xi_{\sigma,s} = \exp \frac{\mu_{\sigma} + \eta_{\sigma,s}}{T}, \quad (4.18)$$

where the energy eigenvalues $E_{\sigma,s}^n$ are given in Eq. (4.4). The index σ in Eq. (4.17) is a sum over electron and positron states while s is a sum over polarizations. The index s refers to the spin along the field axis: parallel (\uparrow ; $s = +1$) or anti-parallel (\downarrow ; $s = -1$) for both particle and antiparticle species.

We are explicitly interested in small asymmetries such as baryon excess over antibaryons, or one polarization over another. These are described by Eq. (4.18) as the following two fugacities:

- (a) Chemical fugacity λ_{σ}
- (b) Polarization fugacity $\xi_{\sigma,s}$

For matter (e^- ; $\sigma = +1$) and antimatter (e^+ ; $\sigma = -1$) particles, a nonzero relativistic chemical potential $\mu_{\sigma} = \sigma \mu$ is caused by an imbalance of matter and antimatter. While the primordial electron-positron plasma era was overall charge neutral, there was a small asymmetry in the charged leptons (namely electrons) from baryon asym-

metry (Fromerth et al., 2012; Canetti et al., 2012) in the universe. Reactions such as $e^+e^- \leftrightarrow \gamma\gamma$ constrains the chemical potential of electrons and positrons (Elze et al., 1980) as

$$\mu \equiv \mu_{e^-} = -\mu_{e^+}, \quad \lambda \equiv \lambda_{e^-} = \lambda_{e^+}^{-1} = \exp \frac{\mu}{T}, \quad (4.19)$$

where λ is the chemical fugacity of the system.

We can then parameterize the chemical potential of the e^+e^- plasma as a function of temperature $\mu \rightarrow \mu(T)$ via the charge neutrality of the universe which implies

$$n_p = n_{e^-} - n_{e^+} = \frac{1}{V} \lambda \frac{\partial}{\partial \lambda} \ln \mathcal{Z}_{e^+e^-}. \quad (4.20)$$

In Eq. (4.20), n_p is the observed total number density of protons in all baryon species. The chemical potential defined in Eq. (4.19) is obtained from the requirement that the positive charge of baryons (protons, α particles, light nuclei produced after BBN) is exactly and locally compensated by a tiny net excess of electrons over positrons.

We then introduce a novel polarization fugacity $\xi_{\sigma,s}$ and polarization potential $\eta_{\sigma,s} = \sigma s \eta$. We propose the polarization potential follows analogous expressions as seen in Eq. (4.19) obeying

$$\eta \equiv \eta_{+,+} = \eta_{-,-}, \quad \eta = -\eta_{\pm,\mp}, \quad \xi_{\sigma,s} \equiv \exp \frac{\eta_{\sigma,s}}{T}. \quad (4.21)$$

An imbalance in polarization within a region of volume V results in a nonzero polarization potential $\eta \neq 0$. Conveniently since antiparticles have opposite signs of charge and magnetic moment, the same magnetic moment is associated with opposite spin orientations. A completely particle-antiparticle symmetric magnetized plasma will have therefore zero total angular momentum.

Euler-Maclaurin integration

Before we proceed with the Boltzmann distribution approximation which makes up the bulk of our analysis, we will comment on the full Fermi-Dirac distribution anal-

ysis. The Euler-Maclaurin formula (Abramowitz et al., 1988) is used to convert the summation over Landau levels n into an integration given by

$$\begin{aligned} \sum_{n=a}^b f(n) - \int_a^b f(x)dx &= \frac{1}{2} (f(b) + f(a)) \\ &\quad + \sum_{i=1}^j \frac{b_{2i}}{(2i)!} (f^{(2i-1)}(b) - f^{(2i-1)}(a)) + R(j), \end{aligned} \quad (4.22)$$

where b_{2i} are the Bernoulli numbers and $R(j)$ is the error remainder defined by integrals over Bernoulli polynomials. The integer j is chosen for the level of approximation that is desired. Euler-Maclaurin integration is rarely convergent, and in this case serves only as an approximation within the domain where the error remainder is small and bounded; see Greiner et al. (2012b) for the non-relativistic case. In this analysis, we keep the zeroth and first order terms in the Euler-Maclaurin formula. We note that regularization of the excess terms in Eq. (4.22) is done in the context of strong field QED (Greiner and Reinhardt, 2008) though that is outside our scope.

Using Eq. (4.22) allows us to convert the sum over n quantum numbers in Eq. (4.17) into an integral. Defining

$$f_{\sigma,s}^n = \ln \left(1 + \Upsilon_{\sigma,s} \exp \left(-\frac{E_{\sigma,s}^n}{T} \right) \right), \quad (4.23)$$

Eq. (4.17) for $j = 1$ becomes

$$\begin{aligned} \ln \mathcal{Z}_{e^+e^-} &= \frac{eBV}{(2\pi)^2} \sum_{\sigma,s}^{\pm 1} \int_{-\infty}^{+\infty} dp_z \\ &\quad \left(\int_0^{+\infty} dn f_{\sigma,s}^n + \frac{1}{2} f_{\sigma,s}^0 + \frac{1}{12} \frac{\partial f_{\sigma,s}^n}{\partial n} \Big|_{n=0} + R(1) \right) \end{aligned} \quad (4.24)$$

It will be useful to rearrange Eq. (4.4) by pulling the spin dependency and the ground

state Landau orbital into the mass writing

$$E_{\sigma,s}^n = \tilde{m}_{\sigma,s} \sqrt{1 + \frac{p_z^2}{\tilde{m}_{\sigma,s}^2} + \frac{2eBn}{\tilde{m}_{\sigma,s}^2}}, \quad (4.25)$$

$$\varepsilon_{\sigma,s}^n(p_z, B) = \frac{E_{\sigma,s}^n}{\tilde{m}_{\sigma,s}}, \quad \tilde{m}_{\sigma,s}^2 = m_e^2 + eB \left(1 + \frac{g}{2}\sigma s\right), \quad (4.26)$$

where we introduced the dimensionless energy $\varepsilon_{\sigma,s}^n$ and effective polarized mass $\tilde{m}_{\sigma,s}$ which is distinct for each spin alignment and is a function of magnetic field strength B . The effective polarized mass $\tilde{m}_{\sigma,s}$ allows us to describe the e^+e^- plasma with the spin effects almost wholly separated from the Landau characteristics of the gas when considering the plasma's thermodynamic properties.

With the energies written in this fashion, we recognize the first term in Eq. (4.24) as mathematically equivalent to the free particle fermion partition function with a re-scaled mass $m_{\sigma,s}$. The phase-space relationship between transverse momentum and Landau orbits in Eq. (4.14) and Eq. (4.15) can be succinctly described by

$$p_T^2 \sim 2eBn, \quad 2p_T dp_T \sim 2eBdn, \quad d\mathbf{p}^3 = 2\pi p_T dp_T dp_z \quad (4.27)$$

$$\frac{eBV}{(2\pi)^2} \int_{-\infty}^{+\infty} dp_z \int_0^{+\infty} dn \rightarrow \frac{V}{(2\pi)^3} \int d\mathbf{p}^3 \quad (4.28)$$

which recasts the first term in Eq. (4.24) as

$$\ln \mathcal{Z}_{e^+e^-} = \frac{V}{(2\pi)^3} \sum_{\sigma,s}^{\pm 1} \int d\mathbf{p}^3 \ln \left(1 + \Upsilon_{\sigma,s} \exp \left(-\frac{m_{\sigma,s} \sqrt{1 + p^2/m_{\sigma,s}^2}}{T} \right) \right) + \dots \quad (4.29)$$

As we will see in the proceeding section, this separation of the ‘free-like’ partition function can be reproduced in the Boltzmann distribution limit as well. This marks the end of the analytic analysis without approximations.

4.3.3 Boltzmann approach to electron-positron plasma

Since we address the temperature interval $200 \text{ keV} > T > 20 \text{ keV}$ where the effects of quantum Fermi statistics on the e^+e^- pair plasma are relatively small, but the gas

is still considered relativistic, we will employ the Boltzmann approximation to the partition function in Eq. (4.17). However, we extrapolate our results for presentation completeness up to $T \simeq 4m_e$.

	aligned: $s = +1$	anti-aligned: $s = -1$
electron: $\sigma = +1$	$+ \mu + \eta$	$+ \mu - \eta$
positron: $\sigma = -1$	$- \mu - \eta$	$- \mu + \eta$

Table 4.1: Organizational schematic of matter-antimatter (σ) and polarization (s) states with respect to the chemical μ and polarization η potentials as seen in Eq. (4.32). Companion to Table 4.3.

The partition function shown in equation Eq. (4.17) can be rewritten removing the logarithm as

$$\ln \mathcal{Z}_{e^+ e^-} = \frac{eBV}{(2\pi)^2} \sum_{\sigma,s}^{\pm 1} \sum_{n=0}^{\infty} \sum_{k=1}^{\infty} \int_{-\infty}^{+\infty} dp_z \frac{(-1)^{k+1}}{k} \exp \left(k \frac{\sigma\mu + \sigma s \eta - \tilde{m}_{\sigma,s} \varepsilon_{\sigma,s}^n}{T} \right), \quad (4.30)$$

$$\sigma\mu + \sigma s \eta - \tilde{m}_{\sigma,s} \varepsilon_{\sigma,s}^n < 0, \quad (4.31)$$

which is well behaved as long as the factor in Eq. (4.31) remains negative. We evaluate the sums over σ and s as

$$\begin{aligned} \ln \mathcal{Z}_{e^+ e^-} = & \frac{eBV}{(2\pi)^2} \sum_{n=0}^{\infty} \sum_{k=1}^{\infty} \int_{-\infty}^{+\infty} dp_z \frac{(-1)^{k+1}}{k} \times \\ & \left(\exp \left(k \frac{+ \mu + \eta}{T} \right) \exp \left(-k \frac{\tilde{m}_{+,+} \varepsilon_{+,+}^n}{T} \right) + \exp \left(k \frac{+ \mu - \eta}{T} \right) \exp \left(-k \frac{\tilde{m}_{+,-} \varepsilon_{+,-}^n}{T} \right) \right. \\ & \left. + \exp \left(k \frac{- \mu - \eta}{T} \right) \exp \left(-k \frac{\tilde{m}_{-,+} \varepsilon_{-,+}^n}{T} \right) + \exp \left(k \frac{- \mu + \eta}{T} \right) \exp \left(-k \frac{\tilde{m}_{-,-} \varepsilon_{-,-}^n}{T} \right) \right) \end{aligned} \quad (4.32)$$

We note from Figure 4.3 that the first and forth terms and the second and third terms share the same energies via

$$\varepsilon_{+,+}^n = \varepsilon_{-,-}^n, \quad \varepsilon_{+,-}^n = \varepsilon_{-,+}^n. \quad \varepsilon_{+,-}^n < \varepsilon_{+,+}^n, \quad (4.33)$$

Eq. (4.33) allows us to reorganize the partition function with a new magnetization quantum number s' which characterizes paramagnetic flux increasing states ($s' = +1$) and diamagnetic flux decreasing states ($s' = -1$). This recasts Eq. (4.32) as

$$\ln \mathcal{Z}_{e^+e^-} = \frac{eBV}{(2\pi)^2} \sum_{s'}^{\pm 1} \sum_{n=0}^{\infty} \sum_{k=1}^{\infty} \int_{-\infty}^{+\infty} dp_z \frac{(-1)^{k+1}}{k} \left[2\xi_{s'} \cosh \frac{k\mu}{T} \right] \exp \left(-k \frac{\tilde{m}_{s'} \varepsilon_{s'}^n}{T} \right) \quad (4.34)$$

with dimensionless energy $\varepsilon_{s'}^n$, polarization mass $\tilde{m}_{s'}$, and polarization $\eta_{s'}$ redefined in terms of the moment orientation quantum number s'

$$\tilde{m}_{s'}^2 = m_e^2 + eB \left(1 - \frac{g}{2} s' \right), \quad (4.35)$$

$$\eta \equiv \eta_+ = -\eta_- \quad \xi \equiv \xi_+ = \xi_-^{-1}, \quad \xi_{s'} = \xi^{\pm 1} = \exp \left(\pm \frac{\eta}{T} \right). \quad (4.36)$$

We introduce the modified Bessel function K_ν (see Ch. 10 of [Letessier and Rafelski \(2023\)](#)) of the second kind

$$K_\nu \left(\frac{m}{T} \right) = \frac{\sqrt{\pi}}{\Gamma(\nu - 1/2)} \frac{1}{m} \left(\frac{1}{2mT} \right)^{\nu-1} \int_0^\infty dp p^{2\nu-2} \exp \left(-\frac{m\varepsilon}{T} \right), \quad (4.37)$$

$$\nu > 1/2, \quad \varepsilon = \sqrt{1 + p^2/m^2}, \quad (4.38)$$

allowing us to rewrite the integral over momentum in Eq. (4.34) as

$$\frac{1}{T} \int_0^\infty dp_z \exp \left(-\frac{k\tilde{m}_{s'} \varepsilon_{s'}^n}{T} \right) = W_1 \left(\frac{k\tilde{m}_{s'} \varepsilon_{s'}^n(0, B)}{T} \right). \quad (4.39)$$

The function W_ν serves as an auxiliary function of the form $W_\nu(x) = x K_\nu(x)$. The notation $\varepsilon(0, B)$ in Eq. (4.39) refers to the definition of dimensionless energy found in Eq. (4.26) with $p_z = 0$. The standard Boltzmann distribution is obtained by summing only $k = 1$ and neglecting the higher order terms.

We take advantage again of Euler-Maclaurin integration Eq. (4.22) and integrate the partition function. After truncation of the series and error remainder, the parti-

tion function Eq. (4.30) can then be written in terms of modified Bessel K_ν functions of the second kind and cosmic magnetic scale b_0 , yielding

$$\boxed{\ln \mathcal{Z}_{e^+e^-} \simeq \frac{T^3 V}{\pi^2} \sum_{s'}^{\pm 1} \left[\xi_{s'} \cosh \frac{\mu}{T} \right] \left(x_{s'}^2 K_2(x_{s'}) + \frac{b_0}{2} x_{s'} K_1(x_{s'}) + \frac{b_0^2}{12} K_0(x_{s'}) \right)}, \quad (4.40)$$

$$x_{s'} = \frac{\tilde{m}_{s'}}{T} = \sqrt{\frac{m_e^2}{T^2} + b_0 \left(1 - \frac{g}{2} s' \right)}. \quad (4.41)$$

The latter two terms in Eq. (4.40) proportional to $b_0 K_1$ and $b_0^2 K_0$ are the uniquely magnetic terms present in powers of magnetic scale Eq. (4.6) containing both spin and Landau orbital influences in the partition function. The K_2 term is analogous to the free Fermi gas (Greiner et al., 2012b) being modified only by spin effects.

This ‘separation of concerns’ can be rewritten as

$$\ln \mathcal{Z}_S = \frac{T^3 V}{\pi^2} \sum_{s'}^{\pm 1} \left[\xi_{s'} \cosh \frac{\mu}{T} \right] (x_{s'}^2 K_2(x_{s'})), \quad (4.42)$$

$$\ln \mathcal{Z}_{SO} = \frac{T^3 V}{\pi^2} \sum_{s'}^{\pm} \left[\xi_{s'} \cosh \frac{\mu}{T} \right] \left(\frac{b_0}{2} x_{s'} K_1(x_{s'}) + \frac{b_0^2}{12} K_0(x_{s'}) \right), \quad (4.43)$$

where the spin (S) and spin-orbit (SO) partition functions can be considered independently. When the magnetic scale b_0 is small, the spin-orbit term Eq. (4.43) becomes negligible leaving only paramagnetic effects in Eq. (4.42) due to spin. In the non-relativistic limit, Eq. (4.42) reproduces a quantum gas whose Hamiltonian is defined as the free particle (FP) Hamiltonian plus the magnetic dipole (MD) Hamiltonian which span two independent Hilbert spaces $\mathcal{H}_{FP} \otimes \mathcal{H}_{MD}$. The non-relativistic limit is further discussed in Section 4.3.4.

Writing the partition function as Eq. (4.40) instead of Eq. (4.30) has the additional benefit that the partition function remains finite in the free gas ($B \rightarrow 0$) limit. This is because the free Fermi gas and Eq. (4.42) are mathematically analogous to one another. As the Bessel K_ν functions are evaluated as functions of x_\pm in Eq. (4.41), the ‘free’ part of the partition K_2 is still subject to spin magnetization effects. In

the limit where $B \rightarrow 0$, the free Fermi gas is recovered in both the Boltzmann approximation $k = 1$ and the general case $\sum_{k=1}^{\infty}$.

4.3.4 Non-relativistic limit of the magnetized partition function

While we label the first term in Eq. (4.29) as the ‘free’ partition function, this is not strictly true as the partition function dependant on the magnetic-mass we defined in Eq. (4.26). When determining the magnetization of the quantum Fermi gas, derivatives of the magnetic field B will not fully vanish on this first term which will resulting in an intrinsic magnetization which is distinct from the Landau levels.

This represents magnetization that arises from the spin magnetic energy rather than orbital contributions. To demonstrate this, we will briefly consider the weak field limit for $g = 2$. The effective polarized mass for electrons is then

$$\tilde{m}_+^2 = m_e^2, \quad (4.44)$$

$$\tilde{m}_-^2 = m_e^2 + 2eB, \quad (4.45)$$

with energy eigenvalues

$$E_n^+ = \sqrt{p_z^2 + m_e^2 + 2eBn}, \quad (4.46)$$

$$E_n^- = \sqrt{(E_n^+)^2 + 2eB}. \quad (4.47)$$

The spin anti-aligned states in the non-relativistic (NR) limit reduce to

$$E_n^-|_{\text{NR}} \approx E_n^+|_{\text{NR}} + \frac{eB}{m_e}. \quad (4.48)$$

This shift in energies is otherwise not influenced by summation over Landau quantum number n , therefore we can interpret this energy shift as a shift in the polarization potential from Eq. (4.21). The polarization potential is then

$$\eta_e^{\pm} = \eta_e \pm \frac{eB}{2m_e}, \quad (4.49)$$

allowing us to rewrite the partition function in Eq. (4.30) as

$$\ln \mathcal{Z}_{e^-}|_{NR} = \frac{eBV}{(2\pi)^2} \sum_{s'}^{\pm} \sum_{n=0}^{\infty} \sum_{k=1}^{\infty} \int_{-\infty}^{+\infty} dp_z \frac{(-1)^{k+1}}{k} 2 \cosh(k\beta\eta_e^{s'}) \lambda^k \exp(-k\epsilon_n/T), \quad (4.50)$$

$$\epsilon_n = m_e + \frac{p_z^2}{2m_e} + \frac{eB}{2m_e} (n+1). \quad (4.51)$$

Eq. (4.50) is then the traditional NR quantum harmonic oscillator partition function with a spin dependant potential shift differentiating the aligned and anti-aligned states. We note that in this formulation, the spin contribution is entirely excised from the orbital contribution. Under Euler-Maclaurin integration, the now spin-independant Boltzmann factor can be further separated into ‘free’ and Landau quantum parts as was done in Eq. (4.29) for the relativistic case. We note however that the inclusion of anomalous magnetic moment spoils this clean separation.

4.3.5 Electron-positron chemical potential

In presence of a magnetic field in the Boltzmann approximation, the charge neutrality condition Eq. (4.20) becomes

$$\sinh \frac{\mu}{T} = n_p \frac{\pi^2}{T^3} \left[\sum_{s'}^{\pm 1} \xi_{s'} \left(x_{s'}^2 K_2(x_{s'}) + \frac{b_0}{2} x_{s'} K_1(x_{s'}) + \frac{b_0^2}{12} K_0(x_{s'}) \right) \right]^{-1}. \quad (4.52)$$

Eq. (4.52) is fully determined by the right-hand-side expression if the spin fugacity is set to unity $\eta = 0$ implying no external bias to the number of polarizations except as a consequence of the difference in energy eigenvalues. In practice, the latter two terms in Eq. (4.52) are negligible to chemical potential in the bounds of the primordial e^+e^- plasma considered and only becomes relevant for extreme (see Figure 4.4) magnetic field strengths well outside our scope.

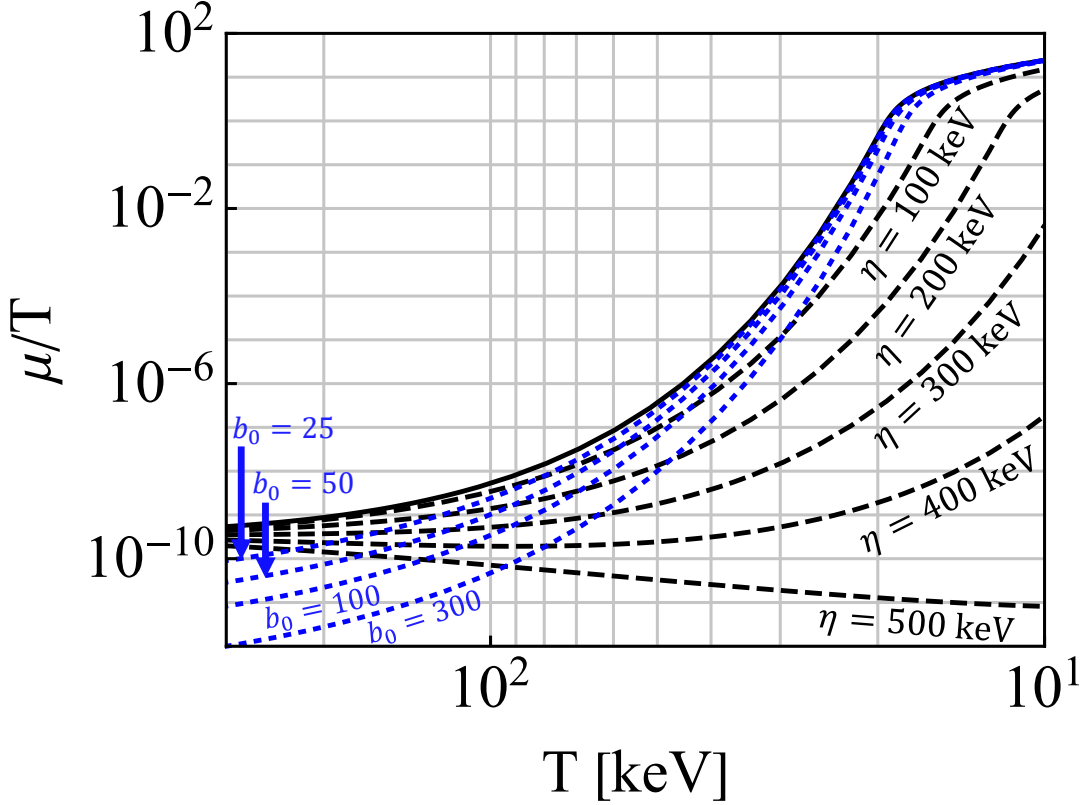


Figure 4.4: The chemical potential over temperature μ/T is plotted as a function of temperature with differing values of spin potential η and magnetic scale b_0 .

Eq. (4.52) simplifies if there is no external magnetic field $b_0 = 0$ into

$$\sinh \frac{\mu}{T} = n_p \frac{\pi^2}{T^3} \left[2 \cosh \frac{\eta}{T} \left(\frac{m_e}{T} \right)^2 K_2 \left(\frac{m_e}{T} \right) \right]^{-1}. \quad (4.53)$$

In Figure 4.4 we plot the chemical potential μ/T in Eq. (4.52) and Eq. (4.53) which characterizes the importance of the charged lepton asymmetry as a function of temperature. Since the baryon (and thus charged lepton) asymmetry remains fixed, the suppression of μ/T at high temperatures indicates a large pair density which is seen explicitly in Figure 4.2. The black line corresponds to the $b_0 = 0$ and $\eta = 0$ case.

The para-diamagnetic contribution from Eq. (4.43) does not appreciably influence μ/T until the magnetic scales involved become incredibly large well outside the observational bounds defined in Eq. (4.1) and Eq. (4.6) as seen by the dotted blue

curves of various large values $b_0 = \{25, 50, 100, 300\}$. The chemical potential is also insensitive to forcing by the spin potential until η reaches a significant fraction of the electron mass m_e in size. The chemical potential for large values of spin potential $\eta = \{100, 200, 300, 400, 500\}$ keV are also plotted as dashed black lines with $b_0 = 0$.

It is interesting to note that there are crossing points where a given chemical potential can be described as either an imbalance in spin-polarization or presence of external magnetic field. While spin potential suppresses the chemical potential at low temperatures, external magnetic fields only suppress the chemical potential at high temperatures.

The profound insensitivity of the chemical potential to these parameters justifies the use of the free particle chemical potential (black line) in the ranges of magnetic field strength considered for cosmology. Mathematically this can be understood as ξ and b_0 act as small corrections in the denominator of Eq. (4.52) if expanded in powers of these two parameters.

4.4 Relativistic paramagnetism of electron-positron gas

The total magnetic flux within a region of space can be written as the sum of external fields and the magnetization of the medium via

$$B_{\text{total}} = B + \mathcal{M}. \quad (4.54)$$

For the simplest mediums without ferromagnetic or hysteresis considerations, the relationship can be parameterized by the susceptibility χ of the medium as

$$B_{\text{total}} = (1 + \chi)B, \quad \mathcal{M} = \chi B, \quad \chi \equiv \frac{\partial \mathcal{M}}{\partial B}, \quad (4.55)$$

with the possibility of both paramagnetic materials ($\chi > 1$) and diamagnetic materials ($\chi < 1$). The e^+e^- plasma however does not so neatly fit in either category as given by Eq. (4.42) and Eq. (4.43). In general, the susceptibility of the gas will itself be a field dependant quantity.

In our analysis, the external magnetic field always appears within the context of the magnetic scale b_0 , therefore we can introduce the change of variables

$$\frac{\partial b_0}{\partial B} = \frac{e}{T^2}. \quad (4.56)$$

The magnetization of the e^+e^- plasma described by the partition function in Eq. (4.40) can then be written as

$$\mathcal{M} \equiv \frac{T}{V} \frac{\partial}{\partial B} \ln \mathcal{Z}_{e^+e^-} = \frac{T}{V} \left(\frac{\partial b_0}{\partial B} \right) \frac{\partial}{\partial b_0} \ln \mathcal{Z}_{e^+e^-}, \quad (4.57)$$

Magnetization arising from other components in the cosmic gas (protons, neutrinos, etc.) could in principle also be included. Localized inhomogeneities of matter evolution are often non-trivial and generally be solved numerically using magneto-hydrodynamics (MHD) (Melrose, 2013; Vazza et al., 2017; Vachaspati, 2021) or with a suitable Boltzmann-Vlasov transport equation. An extension of our work would be to embed magnetization into transport theory (Formanek et al., 2021a). In the context of MHD, primordial magnetogenesis from fluid flows in the electron-positron epoch was considered in Gopal and Sethi (2005); Perrone et al. (2021).

We introduce dimensionless units for magnetization \mathfrak{M} by defining the critical field strength

$$B_C \equiv \frac{m_e^2}{e}, \quad \mathfrak{M} \equiv \frac{\mathcal{M}}{B_C}. \quad (4.58)$$

The scale B_C is where electromagnetism is expected to become subject to non-linear effects, though luckily in our regime of interest, electrodynamics should be linear. We note however that the upper bounds of IGMFs in Eq. (4.1) (with $b_0 = 10^{-3}$; see Eq. (4.6)) brings us to within 1% of that limit for the external field strength in the temperature range considered.

The total magnetization \mathfrak{M} can be broken into the sum of magnetic moment

parallel \mathfrak{M}_+ and magnetic moment anti-parallel \mathfrak{M}_- contributions

$$\mathfrak{M} = \mathfrak{M}_+ + \mathfrak{M}_-. \quad (4.59)$$

We note that the expression for the magnetization simplifies significantly for $g = 2$ which is the ‘natural’ gyro-magnetic factor (Evans and Rafelski, 2022; Rafelski et al., 2023b) for Dirac particles. For illustration, the $g = 2$ magnetization from Eq. (4.57) is then

$$\mathfrak{M}_+ = \frac{e^2}{\pi^2} \frac{T^2}{m_e^2} \xi \cosh \frac{\mu}{T} \left[\frac{1}{2} x_+ K_1(x_+) + \frac{b_0}{6} K_0(x_+) \right], \quad (4.60)$$

$$-\mathfrak{M}_- = \frac{e^2}{\pi^2} \frac{T^2}{m_e^2} \xi^{-1} \cosh \frac{\mu}{T} \left[\left(\frac{1}{2} + \frac{b_0^2}{12x_-^2} \right) x_- K_1(x_-) + \frac{b_0}{3} K_0(x_-) \right], \quad (4.61)$$

$$x_+ = \frac{m_e}{T}, \quad x_- = \sqrt{\frac{m_e^2}{T^2} + 2b_0}. \quad (4.62)$$

As the g -factor of the electron is only slightly above two at $g \simeq 2.00232$ (Tiesinga et al., 2021), the above two expressions for \mathfrak{M}_+ and \mathfrak{M}_- are only modified by a small amount because of anomalous magnetic moment (AMM) and would be otherwise invisible on our figures.

4.4.1 Evolution of electron-positron magnetization

In Figure 4.5, we plot the magnetization as given by Eq. (4.60) and Eq. (4.61) with the spin potential set to unity $\xi = 1$. The lower (solid red) and upper (solid blue) bounds for cosmic magnetic scale b_0 are included. The external magnetic field strength B/B_C is also plotted for lower (dotted red) and upper (dotted blue) bounds. Since the derivative of the partition function governing magnetization may manifest differences between Fermi-Dirac and the here used Boltzmann limit more acutely, out of abundance of caution, we indicate extrapolation outside the domain of validity of the Boltzmann limit with dashes.

We see in Figure 4.5 that the e^+e^- plasma is overall paramagnetic and yields a positive overall magnetization which is contrary to the traditional assumption that

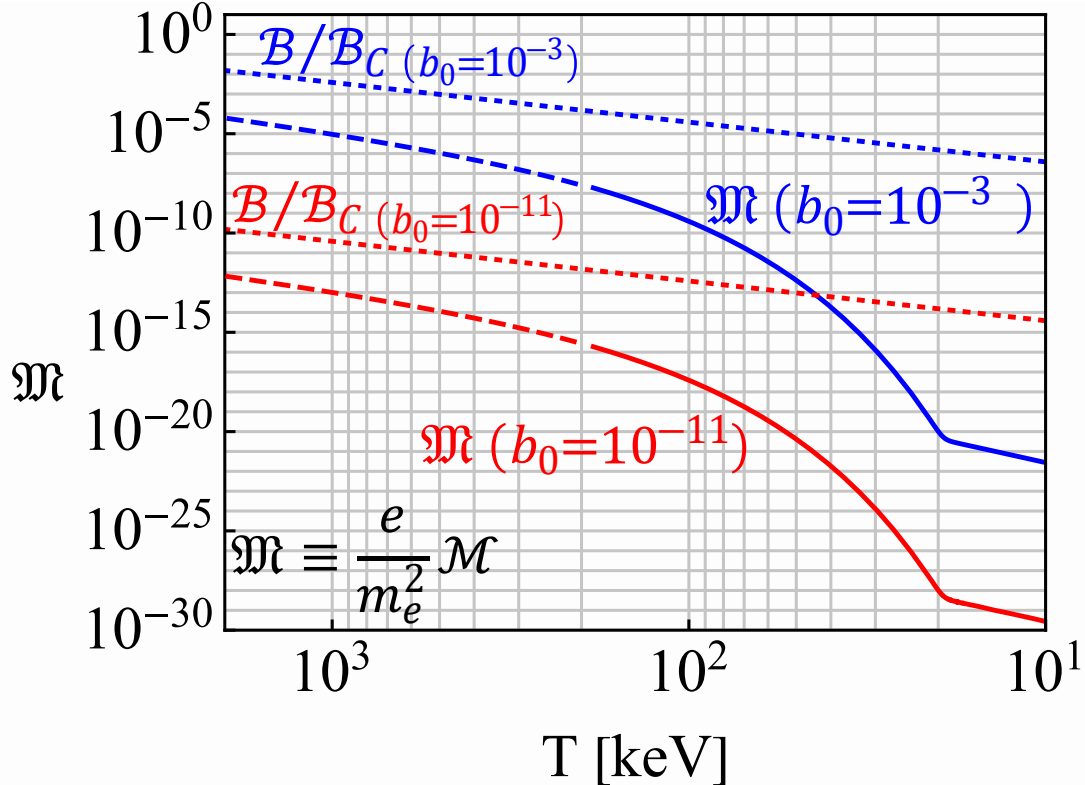


Figure 4.5: The magnetization \mathfrak{M} , with $g = 2$, of the primordial e^+e^- plasma is plotted as a function of temperature. Figure made in collaboration with Cheng Tao Yang.

matter-antimatter plasma lack significant magnetic responses of their own in the bulk. With that said, the magnetization never exceeds the external field under the parameters considered which shows a lack of ferromagnetic behavior.

The large abundance of pairs causes the smallness of the chemical potential seen in Figure 4.4 at high temperatures. As the universe expands and temperature decreases, there is a rapid decrease of the density n_{e^\pm} of e^+e^- pairs. This is the primary cause of the rapid paramagnetic decrease seen in Figure 4.5 above $T = 21$ keV. At lower temperatures $T < 21$ keV there remains a small electron excess (see Figure 4.2) needed to neutralize proton charge. These excess electrons then govern the residual magnetization and dilutes with cosmic expansion.

An interesting feature of Figure 4.5 is that the magnetization in the full temperature range increases as a function of temperature. This is contrary to Curie's

law (Greiner et al., 2012b) which stipulates that paramagnetic susceptibility of a laboratory material is inversely proportional to temperature. However, Curie's law applies to systems with fixed number of particles which is not true in our situation; see Section 4.4.3.

A further consideration is possible hysteresis as the e^+e^- density drops with temperature. It is not immediately obvious the gas's magnetization should simply ‘de-gauss’ so rapidly without further consequence. If the very large paramagnetic susceptibility present for $T \simeq m_e$ is the origin of an overall magnetization of the plasma, the conservation of magnetic flux through the comoving surface ensures that the initial residual magnetization is preserved at a lower temperature by Faraday induced kinetic flow processes however our model presented here cannot account for such effects.

Early universe conditions may also apply to some extreme stellar objects with rapid change in n_{e^\pm} with temperatures above $T = 21$ keV. Production and annihilation of e^+e^- plasmas is also predicted around compact stellar objects (Ruffini et al., 2010; Ruffini and Vereshchagin, 2013) potentially as a source of gamma-ray bursts.

4.4.2 Dependency on g-factor

As discussed at the end of Section 4.4, the AMM of e^+e^- is not relevant in the present model. However out of academic interest, it is valuable to consider how magnetization is effected by changing the g -factor significantly.

The influence of AMM would be more relevant for the magnetization of baryon gasses since the g -factor for protons ($g \approx 5.6$) and neutrons ($g \approx 3.8$) are substantially different from $g=2$. The influence of AMM on the magnetization of thermal systems with large baryon content (neutron stars, magnetars, hypothetical bose stars, etc.) is therefore also of interest (Ferrer and Hackebill, 2019, 2023).

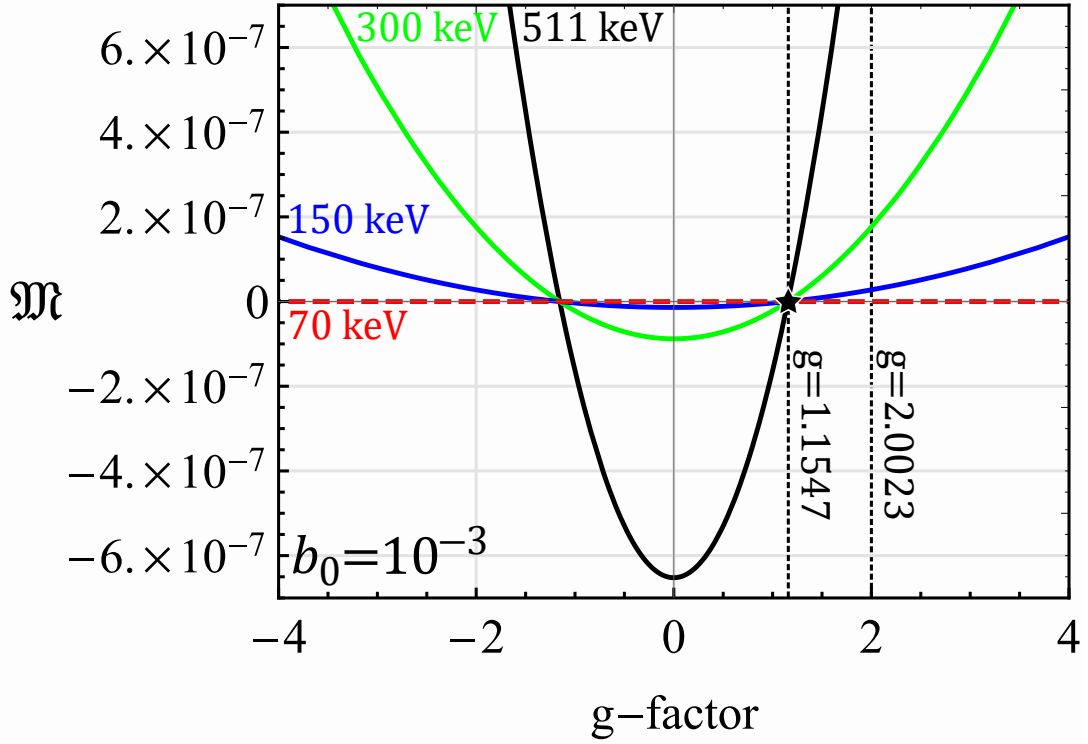


Figure 4.6: The magnetization \mathfrak{M} as a function of g -factor plotted for several temperatures with magnetic scale $b_0 = 10^{-3}$ and polarization fugacity $\xi = 1$.

Eq. (4.60) and Eq. (4.61) with arbitrary g reintroduced is given by

$$\mathfrak{M} = \frac{e^2}{\pi^2} \frac{T^2}{m_e^2} \sum_{s'}^{\pm 1} \xi_{s'} \cosh \frac{\mu}{T} [C_{s'}^1(x_{s'}) K_1(x_{s'}) + C_{s'}^0 K_0(x_{s'})] , \quad (4.63)$$

$$C_{s'}^1(x_{\pm}) = \left[\frac{1}{2} - \left(\frac{1}{2} - \frac{g}{4} s' \right) \left(1 + \frac{b_0^2}{12x_{s'}^2} \right) \right] x_{s'} , \quad C_{s'}^0 = \left[\frac{1}{6} - \left(\frac{1}{4} - \frac{g}{8} s' \right) \right] b_0 , \quad (4.64)$$

where $x_{s'}$ was previously defined in Eq. (4.41).

In Figure 4.6, we plot the magnetization as a function of g -factor between $4 > g > -4$ for temperatures $T = \{511, 300, 150, 70\}$ keV. We find that the magnetization is sensitive to the value of AMM revealing a transition point between paramagnetic ($\mathfrak{M} > 0$) and diamagnetic gasses ($\mathfrak{M} < 0$). Curiously, the transition point was numerically determined to be around $g \simeq 1.1547$ in the limit $b_0 \rightarrow 0$. The exact

position of this transition point however was found to be both temperature and b_0 sensitive, though it moved little in the ranges considered.

It is not surprising for there to be a transition between diamagnetism and paramagnetism given that the partition function (see Eq. (4.42) and Eq. (4.43)) contained elements of both. With that said, the transition point presented at $g \approx 1.15$ should not be taken as exact because of the approximations used to obtain the above results.

It is likely that the exact transition point has been altered by our taking of the Boltzmann approximation and Euler-Maclaurin integration steps. It is known that the Klein-Gordon-Pauli solutions to the Landau problem in Eq. (4.4) have periodic behavior (Steinmetz et al., 2019; Evans and Rafelski, 2022; Rafelski et al., 2023b) for $|g| = k/2$ (where $k \in 1, 2, 3 \dots$).

These integer and half-integer points represent when the two Landau towers of orbital levels match up exactly. Therefore, we propose a more natural transition between the spinless diamagnetic gas of $g = 0$ and a paramagnetic gas is $g = 1$. A more careful analysis is required to confirm this, but that our numerical value is close to unity is suggestive.

4.4.3 Magnetization per lepton

Despite the relatively large magnetization seen in Figure 4.5, the average contribution per lepton is only a small fraction of its overall magnetic moment indicating the magnetization is only loosely organized. Specifically, the magnetization regime we are in is described by

$$\mathcal{M} \ll \mu_B \frac{N_{e^+} + N_{e^-}}{V}, \quad \mu_B \equiv \frac{e}{2m_e}, \quad (4.65)$$

where μ_B is the Bohr magneton and $N = nV$ is the total particle number in the proper volume V . To better demonstrate that the plasma is only weakly magnetized, we define the average magnetic moment per lepton given by along the field (z -direction)

axis as

$$|\vec{m}|_z \equiv \frac{\mathcal{M}}{n_{e^-} + n_{e^+}}, \quad |\vec{m}|_x = |\vec{m}|_y = 0. \quad (4.66)$$

Statistically, we expect the transverse expectation values to be zero. We emphasize here that despite $|\vec{m}|_z$ being nonzero, this doesn't indicate a nonzero spin angular momentum as our plasma is nearly matter-antimatter symmetric. The quantity defined in Eq. (4.66) gives us an insight into the microscopic response of the plasma.

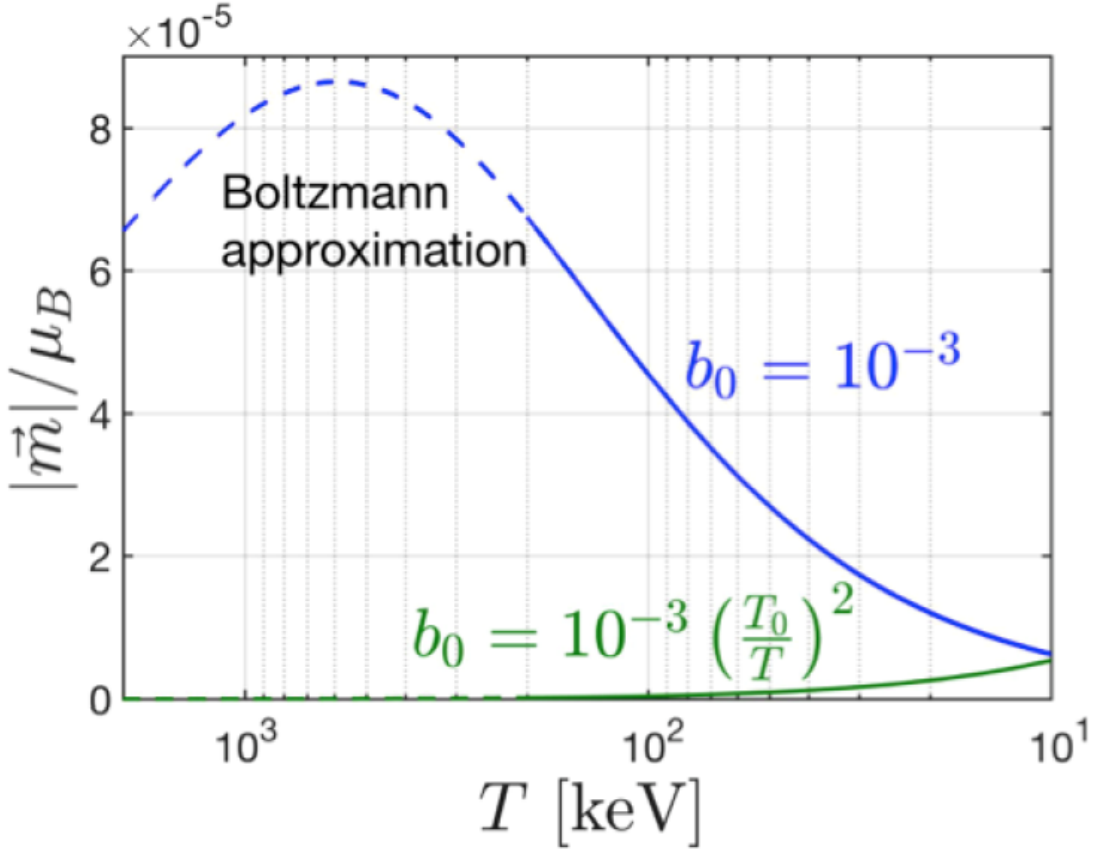


Figure 4.7: The magnetic moment per lepton $|\vec{m}|_z$ along the field axis as a function of temperature. Figure made in collaboration with Cheng Tao Yang.

The average magnetic moment $|\vec{m}|_z$ defined in Eq. (4.66) is plotted in Figure 4.7 which displays how essential the external field is on the ‘per lepton’ magnetization. The $b_0 = 10^{-3}$ case (blue curve) is plotted in the Boltzmann approximation. The dashed lines indicate where this approximation is only qualitatively correct. For

illustration, a constant magnetic field case (solid green line) with a comoving reference value chosen at temperature $T_0 = 10$ keV is also plotted.

If the field strength is held constant, then the average magnetic moment per lepton is suppressed at higher temperatures as expected for magnetization satisfying Curie's law. The difference in Figure 4.7 between the non-constant (blue solid curve) case and the constant field (solid green curve) case demonstrates the importance of the conservation of primordial magnetic flux in the plasma, required by Eq. (4.5). While not shown, if Figure 4.7 was extended to lower temperatures, the magnetization per lepton of the constant field case would be greater than the non-constant case which agrees with our intuition that magnetization is easier to achieve at lower temperatures. This feature again highlights the importance of flux conservation in the system and the uniqueness of the primordial cosmic environment.

4.5 Polarization potential and ferromagnetism

Up to this point, we have neglected the impact that a nonzero spin potential $\eta \neq 0$ (and thus $\xi \neq 1$) would have on the primordial e^+e^- plasma magnetization. In the limit that $(m_e/T)^2 \gg b_0$ the magnetization given in Eq. (4.63) and Eq. (4.64) is entirely controlled by the spin fugacity ξ asymmetry generated by the spin potential η yielding up to first order $\mathcal{O}(b_0)$ in magnetic scale

$$\lim_{m_e^2/T^2 \gg b_0} \mathfrak{M} = \frac{g}{2} \frac{e^2}{\pi^2} \frac{T^2}{m_e^2} \sinh \frac{\eta}{T} \cosh \frac{\mu}{T} \left[\frac{m_e}{T} K_1 \left(\frac{m_e}{T} \right) \right] + b_0 \left(g^2 - \frac{4}{3} \right) \frac{e^2}{8\pi^2} \frac{T^2}{m_e^2} \cosh \frac{\eta}{T} \cosh \frac{\mu}{T} K_0 \left(\frac{m_e}{T} \right) + \mathcal{O}(b_0^2) \quad (4.67)$$

Given Eq. (4.67), we can understand the spin potential as a kind of ‘ferromagnetic’ influence on the primordial gas which allows for magnetization even in the absence of external magnetic fields. This interpretation is reinforced by the fact the leading coefficient is $g/2$.

We suggest that a variety of physics could produce a small nonzero η within a domain of the gas. Such asymmetries could also originate statistically as while the

expectation value of free gas polarization is zero, the variance is likely not.

As $\sinh \eta/T$ is an odd function, the sign of η also controls the alignment of the magnetization. In the high temperature limit Eq. (4.67) with strictly $b_0 = 0$ assumes a form of to lowest order for brevity

$$\lim_{m_e/T \rightarrow 0} \mathfrak{M}|_{b_0=0} = \frac{g}{2} \frac{e^2}{\pi^2} \frac{T^2}{m_e^2} \frac{\eta}{T}, \quad (4.68)$$

While the limit in Eq. (4.68) was calculated in only the Boltzmann limit, it is noteworthy that the high temperature (and $m \rightarrow 0$) limit of Fermi-Dirac distributions only differs from the Boltzmann result by a proportionality factor.

The natural scale of the e^+e^- magnetization with only a small spin fugacity ($\eta < 1$ eV) fits easily within the bounds of the predicted magnetization during this era if the IGMF measured today was of primordial origin. The reason for this is that the magnetization seen in Eq. (4.60), Eq. (4.61) and Eq. (4.67) are scaled by αB_C where α is the fine structure constant.

4.5.1 Hypothesis of ferromagnetic self-magnetization

One exploratory model we propose is to fix the spin polarization asymmetry, described in Eq. (4.21), to generate a homogeneous magnetic field which dissipates as the universe cools down. In this model, there is no external primordial magnetic field ($B_{\text{PMF}} = 0$) generated by some unrelated physics, but rather the e^+e^- plasma itself is responsible for the field by virtue of spin polarization.

This would obey the following assumption of

$$\mathfrak{M}(b_0) = \frac{\mathcal{M}(b_0)}{B_C} \longleftrightarrow \frac{B}{B_C} = b_0 \frac{T^2}{m_e^2}, \quad (4.69)$$

which sets the total magnetization as a function of itself. The spin polarization described by $\eta \rightarrow \eta(b_0, T)$ then becomes a fixed function of the temperature and magnetic scale. The underlying assumption would be the preservation of the homogeneous field would be maintained by scattering within the gas (as it is still in thermal equilibrium) modulating the polarization to conserve total magnetic flux.

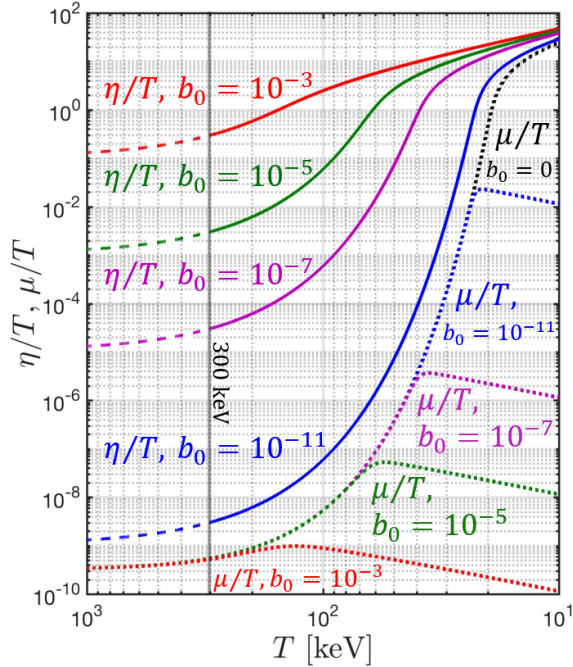


Figure 4.8: The spin potential η and chemical potential μ are plotted under the assumption of self-magnetization through a nonzero spin polarization in bulk of the plasma. Figure made in collaboration with Cheng Tao Yang.

The result of the self-magnetization assumption in Eq. (4.69) for the potentials is plotted in Figure 4.8. The solid lines indicate the curves for η/T for differing values of $b_0 = \{10^{-11}, 10^{-7}, 10^{-5}, 10^{-3}\}$ which become dashed above $T = 300$ keV to indicate that the Boltzmann approximation is no longer appropriate though the general trend should remain unchanged.

The dotted lines are the curves for the chemical potential μ/T . At high temperatures we see that a relatively small η/T is needed to produce magnetization owing to the large densities present. Figure 4.8 also shows that the chemical potential does not deviate from the free particle case until the spin polarization becomes sufficiently high which indicates that this form of self-magnetization would require the annihilation of positrons to be incomplete even at lower temperatures.

This is seen explicitly in Figure 4.9 where we plot the numerical density of particles as a function of temperature for spin aligned ($+\eta$) and spin anti-aligned ($-\eta$) species for both positrons ($-\mu$) and electrons ($+\mu$). Various self-magnetization strengths are

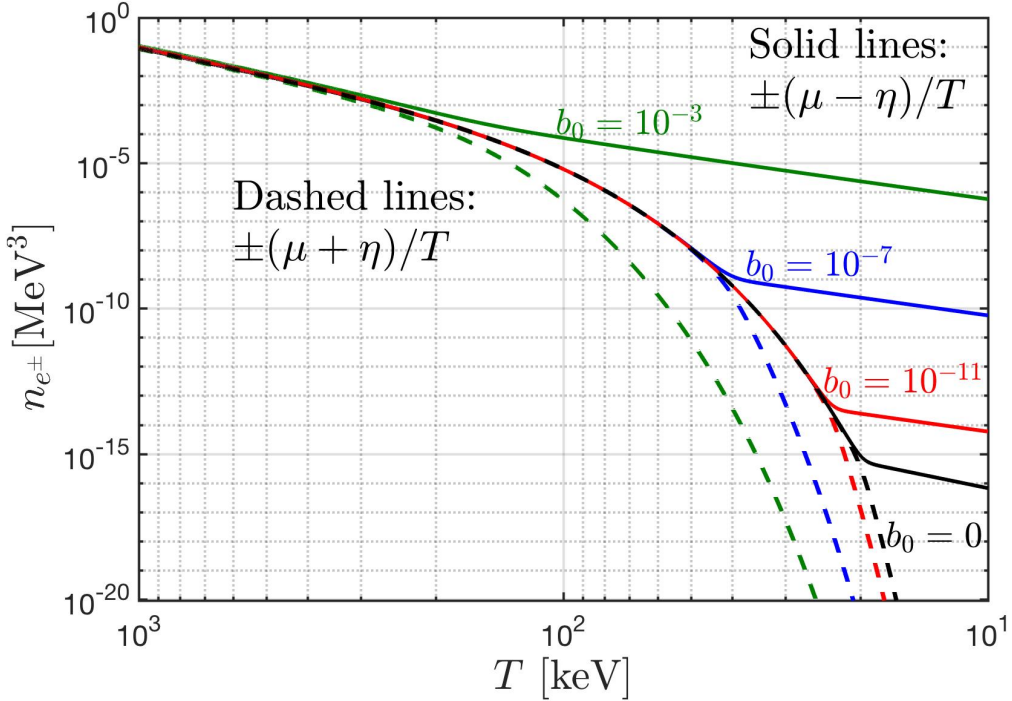


Figure 4.9: The number density n_{e^\pm} of polarized electrons and positrons under the self-magnetization model for differing values of b_0 . Figure courtesy of Cheng Tao Yang.

also plotted to match those seen in Figure 4.8. The nature of T_{split} changes under this model since antimatter and polarization states can be extinguished separately. Positrons persist where there is insufficient electron density to maintain the magnetic flux. Polarization asymmetry therefore appears physical only in the domain where there is a large number of matter-antimatter pairs.

4.5.2 Matter inhomogeneities in the cosmic plasma

In general, an additional physical constraint is required to fully determine μ and η simultaneously as both potentials have mutual dependency (see Section 4.5). We note that spin polarizations are not required to be in balanced within a single species to preserve angular momentum.

The CMB (Aghanim et al., 2020) indicates that the early universe was home to domains of slightly higher and lower baryon densities which resulted in the presence

of galactic super-clusters, cosmic filaments, and great voids seen today. However, the CMB, as measured today, is blind to the localized inhomogeneities required for gravity to begin galaxy and supermassive black hole formation.

Such acute inhomogeneities distributed like a dust (Grayson et al., 2023) in the plasma would make the proton density sharply and spatially dependant $n_p \rightarrow n_p(x)$ which would directly affect the potentials $\mu(x)$ and $\eta(x)$ and thus the density of electrons and positrons locally. This suggests that e^+e^- may play a role in the initial seeding of gravitational collapse. If the plasma were home to such localized magnetic domains, the nonzero local angular momentum within these domains would provide a natural mechanism for the formation of rotating galaxies today.

Recent measurements by the James Webb Space Telescope (JWST) (Yan et al., 2023; Adams et al., 2023; Haro et al., 2023) indicate that galaxy formation began surprisingly early at large redshift values of $z \gtrsim 10$ within the first 500 million years of the universe requiring gravitational collapse to begin in a hotter environment than expected. The observation of supermassive black holes already present (Larson et al., 2023) in this same high redshift period (with millions of solar masses) indicates the need for local high density regions in the early universe whose generation is not yet explained and likely need to exist long before the recombination epoch.

CHAPTER 5

Outlook and key results

Chapter 2: Dynamics of charged particles with arbitrary magnetic moment

We highlighted the comparison of magnetic moment dynamics of DP and KGP formulation of relativistic quantum mechanics. The DP equation breaks up the magnetic moment into an underlying spinor structure part inherent to the Dirac equation, and a dedicated anomalous part. In contrast, for the KGP, the entire effect of magnetic moment is contained in a single Pauli term irrespective of the magnetic moment's size. We find that the two models disagree in their predicted energy levels for the homogeneous magnetic field and the Coulomb field.

For the KGP-Landau levels, Eq. (2.16), we have a simple dependence on the full magnetic moment g -factor and have the correct non-relativistic reduction at lowest order. This simplicity allows, for the KGP equation, the straightforward analysis of physical systems and elegant expressions for their solutions. Thus Dirac's beauty principle favors heavily the KGP considering the Landau levels.

In the case of the Coulomb field there are weak fields differences in both the Lamb shift and fine structure; the contribution to the Lamb shift and fine structure splitting are proportional in KGP to: $g^2/8 - 1/2$, Eq. (2.41) and $g^2/8$, Eq. (2.49) respectively, rather than: DP $g/2 - 1$ Eq. (2.43)) and $g/2 - 1/2$, Eq. (2.51)) respectively.

For strong fields, both DP and KGP share the behavior of a shrinking particle/antiparticle gap for the ground state when $|g| > 2$, though the expressions differ from each other. The models are extremely different in both their predicted energy values and the ultimate fate of the states as B increases. For the KGP equation, the gap vanishes in very strong magnetic fields Eq. (2.56a). KGP also shows state-merging behavior for states of the same total angular momentum.

Chapter 3: Dynamic neutrino flavor mixing through transition moments

We have incorporated electromagnetic effects in the Majorana neutrino mixing matrix by introducing an anomalous transition magnetic dipole moment. We have described the formalism for three generations of neutrinos and explicitly explored the two generation case as a toy model.

In the two generation case, we determined the effect of electric and magnetic fields on flavor rotation in Eq. (3.34) by introducing an electromagnetic flavor unitary rotation Z_{kj}^{ext} . We presented remixed mass eigenstates $\tilde{m}(E, B)$ in Eq. (3.47) which are the propagating mass-states in a background electromagnetic field $F_{\text{ext}}^{\alpha\beta}(x^\mu)$. These EM-mass eigenstates were also further split by spin aligned and anti-aligned states relative to the external field momentum density. There is much left to do to explore further the nascent connection between the spin and the flavor via transition magnetic moments.

The transition dipole moments are the origin of dynamical flavor mixing. While our focus was on Majorana neutrinos, Dirac-type fermions (neutrinos included) may also have non-zero transition dipole moments. These could remix flavor in the presence of strong external background fields. Here quarks are of special interest because they are not only electrically charged, but have color charge as well. This means quarks could in principle possess one, or both, EM and color-charge transition dipole moments, leading to dynamical effects in the CKM mixing matrix within hadrons as well as in quark-gluon plasma.

More speculatively, as transition dipoles act as a mechanism to generate mass by virtue of EM energy density T_{ext}^{00} as seen in Eq. (3.47), an analogous consequence of our work could arise in the presence of a dark vector field in the Universe coupled to neutrinos, resulting in off-diagonal masses in flavor. Massless neutrinos could then obtain dynamical non-zero masses in the Universe by virtue of their interactions originating in dark transition moments.

Chapter 4: Matter-antimatter origin of cosmic magnetism

We characterized the primordial magnetic properties of the early universe before recombination. We studied the temperature range of 2000 keV to 20 keV where all of space was filled with a hot dense electron-positron plasma (to the tune of 450 million pairs per baryon) which occurred within the first few minutes after the Big Bang. We note that our chosen period also includes the era of Big Bang Nucleosynthesis.

We found that subject to a primordial magnetic field, the early universe electron-positron plasma has a significant paramagnetic response due to magnetic moment polarization. We considered the interplay of charge chemical potential, baryon asymmetry, anomalous magnetic moment, and magnetic dipole polarization on the nearly homogeneous medium.

This novel approach to high temperature magnetization shows that the e^+e^- -plasma paramagnetic response (see Eq. (4.60) and Eq. (4.61)) is dominated by the varying abundance of electron-positron pairs, decreasing with decreasing T for $T < m_e c^2$. This is unlike conventional laboratory cases where the number of magnetic particles is constant.

We find that electron-positron magnetization rapidly vanishes as the number of pairs depletes as the universe cools. This therefore presents an opportunity for induced currents to facilitate inhomogeneities in the early universe. We also presented a simple model of self-magnetization of the primordial electron-positron plasma which indicates that only a small polarization asymmetry is required to generate significant magnetic flux when the universe was very hot and dense.

CHAPTER 6

Future research efforts

This chapter contains unpublished work and is exploratory; though we hope to complete this research in the near future. Section 6.1 extends the KGP wave equation to also include chromomagnetic dipole moments necessary for quarks in quantum chromodynamics (QCD). We show explicitly that the dipoles are linear in field tensors and do not mix spin degrees of freedom.

In Section 6.2, we explore CP violation in the neutrino sector in terms of the Jarlskog invariant and modifications to the mass matrix. The CP symmetry of the electric dipole is discussed. This section follows the conventions found in Chapter 3.

The final Section 6.3 is a short description of a personal passion project to integrate spin dynamics into the five dimensional theory of Kaluza-Klein which unifies electromagnetism and gravitation classically. While I have written much on the topic, it remains unfinished and will only occupy a small section of this dissertation.

6.1 Klein-Gordon-Pauli extensions to non-Abelian fields

The KGP approach to wave equations is robust and is useful not only for electromagnetic interactions: This is a first look at adding the strong interaction into KGP inspired in part by [Labun and Rafelski \(2012\)](#). Quarks participate in the strong color interaction of quantum chromodynamics (QCD); therefore they should present a g -factor for both their electromagnetic dipole g_{EM} as well as their QCD chromomagnetic dipole g_{QCD} .

Since color charges follows a more complex $SU(3)$ group structure unlike the more straight forward $U(1)$ of electromagnetism, the “color magnetism” of QCD requires more than just the analogous Pauli term to describe color dipole moments owing due to the fact that QCD has non-Abelian (non-commuting) gluon gauge fields \mathcal{A}^α .

The quarks (like all particles) should obey the quantum mechanical analogue of the energy-momentum relation seen in Eq. (1.50) with the only theoretical difference being a modified covariant derivative. The covariant derivative, written in terms of kinetic momentum, should appear as

$$\text{EM + QCD : } i\hbar\tilde{\nabla} = \pi^\alpha = p^\alpha - q_{\text{EM}}A^\alpha - q_{\text{QCD}}\mathcal{A}^\alpha, \quad (6.1)$$

where q_{EM} is the electric charge of the quarks $q_{\text{EM}}/e \in \pm 1/3, \pm 2/3$ and q_{QCD} is the color charge coupling strength. In many texts the symbol g_s is used for the color coupling strength, but we circumvent that notation using q_{QCD} to avoid confusion with g -factor.

We follow the conventions in Greiner et al. (2006). The eight 3×3 Gell-Mann matrices λ^a are embedded into each independent field as

$$\mathcal{A}^\alpha \equiv \frac{1}{2}\lambda^a\mathcal{A}_a^\alpha, \quad a \in 1 \dots 8, \quad [\lambda^a, \lambda^b] = \frac{i}{2}f^{abc}\lambda^c, \quad (6.2)$$

where \mathcal{A}_a^α are the individual fields for each gluon species in a given representation and f^{abc} is the $SU(3)$ antisymmetric structure function. The non-commuting behavior of the Gell-Mann matrices captures the non-Abelian structure of the gauge fields. The gluon field strength tensor $\mathcal{G}^{\alpha\beta}$ is then

$$\mathcal{G}^{\alpha\beta} = \partial^\alpha\mathcal{A}^\beta - \partial^\beta\mathcal{A}^\alpha + \frac{i}{\hbar}q_{\text{QCD}}[\mathcal{A}^\alpha, \mathcal{A}^\beta], \quad (6.3)$$

$$[\mathcal{A}^\alpha, \mathcal{A}^\beta] = \frac{1}{4}\mathcal{A}_a^\alpha\mathcal{A}_b^\beta[\lambda^a, \lambda^b] = \frac{i}{8}\mathcal{A}_a^\alpha\mathcal{A}_b^\beta f^{abc}\lambda_c. \quad (6.4)$$

Following the same procedure in Section 1.2.2, we can generalize the energy-momentum relation and obtain the EM+QCD variant of the KGP equation for quarks. We find that the resulting quark-KGP equation is

$$\gamma_\alpha\gamma_\beta\pi^\alpha\pi^\beta = \eta_{\alpha\beta}\pi^\alpha\pi^\beta - \frac{q_{\text{EM}}\hbar}{2}\sigma_{\alpha\beta}F^{\alpha\beta} - \frac{q_{\text{QCD}}\hbar}{2}\sigma_{\alpha\beta}\mathcal{G}^{\alpha\beta}, \quad (6.5)$$

$$\left(\eta_{\alpha\beta}\pi^\alpha\pi^\beta - \frac{q_{\text{EM}}\hbar}{2}\sigma_{\alpha\beta}F^{\alpha\beta} - \frac{q_{\text{QCD}}\hbar}{2}\sigma_{\alpha\beta}\mathcal{G}^{\alpha\beta}\right)\Psi = m_q^2c^2\Psi_q, \quad (6.6)$$

which mirrors the electromagnetic case except for the extension of a chromomagnetic Pauli term. We note that m_q is the quark mass and that the field Ψ_q is a color triplet of spinors for: red, green, blue:

$$\Psi_q = \begin{pmatrix} \Psi_r \\ \Psi_g \\ \Psi_b \end{pmatrix}. \quad (6.7)$$

As only the non-commuting portion of Eq. (6.6) (written explicitly in Eq. (6.4)) is off-diagonal in color, this means that the additional non-commuting chromomagnetic term acts as a transition matrix between different quark colors.

This method (based on the commutator of the kinetic momentum) suggests that the color and electromagnetic g -factors both have a natural value of $g_{\text{EM}} = g_{\text{QCD}} = 2$. We can generalize Eq. (6.5) to allow for arbitrary EM and QCD dipole moments g_{EM} and g_{QCD} respectively as

$$\boxed{\left(\eta_{\alpha\beta}\pi^\alpha\pi^\beta - \frac{g_{\text{EM}}}{2} \frac{q_{\text{EM}}\hbar}{2} \sigma_{\alpha\beta}F^{\alpha\beta} - \frac{g_{\text{QCD}}}{2} \frac{q_{\text{QCD}}\hbar}{2} \sigma_{\alpha\beta}\mathcal{G}^{\alpha\beta} \right) \Psi = m_q^2 c^2 \Psi}. \quad (6.8)$$

While in electromagnetism, DP and KGP approaches only differ in the presence of strong EM fields and are otherwise identical in the weak field limit, this cannot be equally said in QCD. The perturbative limit which justifies the DP approach for leptons in QED is possible due to the small value of the fine structure constant which is not true in QCD. Only for high momentum interactions (such as those present in quark-gluon-plasma (QGP) or in energetic collisions) is the perturbative approach applicable (Choudhury and Lahiri, 2015). We emphasize however that the DP approach is only valid where the dipole moment is obtainable via perturbative expansion which may not hold if the g -factor results from non-perturbative physics.

The dipole characteristics (both electromagnetic and chromomagnetic) of the top-quark is of particular interest (Labun and Rafelski, 2013; Vryonidou and Zhang, 2018) because of top-quark's strong coupling to the Higgs and potential BSM physics. We note that current studies focus on a DP approach to chromomagnetism (Zhang and

Willenbrock, 2011; Zhang, 2012; Buarque Franzosi and Zhang, 2015). There is also the added complexity of both the chromomagnetic and magnetic g -factors differing from the natural value independently of one another $g_{\text{EM}} \neq g_{\text{QCD}} \neq 2$. Further study of the KGP approach to chromomagnetism should be pursued. To our knowledge, there is no formulation of Eq. (6.8) as an effective field theory in the manner of Fleming et al. (2001); Bauer et al. (2001) for quarks or for electromagnetically charged fermions as was discussed in Section 1.2.1.

6.2 Electromagnetic forced neutrino CP violation

Electromagnetic processes in the neutrino sector may yield measurable effects in two aspects of neutrino physics:

- (a) Neutrino oscillation which is evidence of the non-zero mass eigenstates
- (b) Charge-parity (CP) violation in the neutrino sector which occurs due to the presence of at least three generations of neutrinos or additional CP violating interactions

Our motivation is to explore the effect of strong electromagnetic fields on neutrino CP violation by analysis of the electromagnetic dipole interaction and determining its influence on the Jarlskog invariant J (Jarlskog, 1985b,a, 2005) which controls the size of CP violation.

One important aspect of neutrino physics is the size of the CP violation (Xing, 2001; Giunti and Kim, 2007; Huber et al., 2022) which can yield insights not only in fundamental physics but cosmology as well. One of the goals of modern neutrino experiments such as DUNE Abi et al. (2020) is to better characterize such effects in astrophysical contexts such as supernova (Abi et al., 2021; Sajjad Athar et al., 2022), solar neutrinos (Akhmedov and Martínez-Miravé, 2022) and magnetars (Lichkunov et al., 2020). Additionally, there may be a connection (Pehlivan et al., 2014; Balaji et al., 2020a,b) between CP violation in the neutrino sector and the anomalous magnetic moment (AMM) of the neutrino.

Amplified CP violation is already expected in matter (Harrison and Scott, 2000) such as when travelling through the Earth’s crust due to the abundance of electrons and the lack of muons and taus which preferentially affect the electron neutrinos via the weak interaction. This effect may also play a role in the primordial universe where neutrinos would propagate through incredibly matter dense gasses such as during the electron-positron epoch (Rafelski et al., 2023a). Matter modifies CP violation because it changes the effective Hamiltonian of the propagating neutrinos, therefore we should look to other possible sources for modification of the Hamiltonian for CP violation amplification or suppression.

The source of direct CP violation in the neutrinos is ultimately attributable to the mismatch between the mass matrices of the charged flavors (e, μ, τ) and the neutral flavors (ν_e, ν_μ, ν_τ). The situation is analogous to the quark sector, where instead the relation is between the upper (u, c, t) and lower quark (d, s, b) flavors.

Therefore mass matrix for charged leptons does not commute with the mass matrix of the neutral leptons and cannot be simultaneously diagonalized except for special cases or degeneracy among the mass eigenstates. We can characterize CP violation by introducing the mixing matrices $V_{\ell k}$ (following the notation in Chapter 3) which diagonalize the individual mass-matrices $M_{\ell\ell'}$ as follows

$$V_{\ell l}^\dagger (M^\nu M^{\nu\dagger})_{\ell\ell'} V_{\ell' k'} = D_{\ell\ell'}^\nu = \text{diag}(m_1^2, m_2^2, m_3^2), \quad (6.9)$$

$$D_{\ell\ell'} = \text{diag}(m_e, m_\mu, m_\tau), \quad (6.10)$$

We have specifically defined the charged leptons flavor states as being simultaneously mass eigenstates without a loss of generality. We will not consider oscillation among the charged leptons, though that may be an avenue of further study Akhmedov (2007).

6.2.1 Jarlskog invariant

The intrinsic CP violation inherent to these mass matrices can be described using the Jarlskog invariant J . We first define the commutator of the charged and neutral

lepton mass matrices as

$$[M^\nu M^{\nu\dagger}, D^2]_{\ell\ell'} = C_{\ell\ell'} . \quad (6.11)$$

As the elements of the neutrino mixing matrix $V_{\ell k}$ can be experimentally determined, the size of the commutator can be expressed using Eq. (6.9) and Eq. (6.10) in terms of the mass eigenstates of the neutrino mass matrix

$$[V(D^\nu)^2 V^\dagger, D^2]_{\ell\ell'} = C_{\ell\ell'} . \quad (6.12)$$

The matrix $C_{\ell\ell'}$ can be unwieldy, so following the procedure by (Jarlskog, 1985b,a, 2005), we take the determinant of $C_{\ell\ell'}$ in Eq. (6.12) which extracts the invariant quantity associated with the size of the CP violation present. Specifically we are interested in the imaginary portion given by

$$\text{Im} [\det(C_{\ell\ell'})] = 2 (\Delta_{12} \Delta_{23} \Delta_{13}) (\Delta_{e\mu} \Delta_{\mu\tau} \Delta_{e\tau}) J , \quad (6.13)$$

where J is the invariant quantity of interest. We define Δ_{ij} via the eigenstates of the mass matrices as

$$\Delta_{ij} \equiv m_i^2 - m_j^2 . \quad (6.14)$$

We can also define the real portion of the determinant and define two quantities R and J together. These two scalars are written in terms of the components of the mixing matrix $V_{\ell k}$ as

$$\mathcal{J}_{ikjl} = \text{Im} [V_{ij} V_{kl} V_{il}^* V_{kj}^*] = J \sum_{m,n} \epsilon_{ikm} \epsilon_{jln} , \quad (6.15)$$

$$\mathcal{R}_{ikjl} = \text{Re} [V_{ij} V_{kl} V_{il}^* V_{kj}^*] = R \sum_{m,n} \epsilon_{ikm} \epsilon_{jln} . \quad (6.16)$$

The benefit of J is it captures the ‘size’ of CP violation in a single value and is identically zero for systems which preserve charge-parity symmetry. From Eq. (6.13)

we can see that CP violation vanishes if the commutator of the mass matrices is purely real, and thus the mixing matrix is also purely real, or if there is degeneracy among the mass eigenstates which absorbs a degree of freedom.

While generally CP violation comes exclusively from the presence of three flavor generations in the Standard Model, we would like to expand the usage of the J -invariant to encompass a family of effects via modification of the mass matrix as was done in Chapter 3. This would encompass CP violation from the number of flavor generations, physical systems (matter, strong fields, etc...) which effectively break CP, or in CP violating terms in the Lagrangian.

6.2.2 Toy model: CP violation amplification

While the specific change to neutrino mixing and CP violation depends on the model of the neutrino dipole moment, a demonstrative model would be to assume that the magnetic moment matrix was simply proportional to the natural mass matrix of the neutrino at low order. Therefore we substitute

$$M_{\ell\ell'}^\nu \rightarrow (M_{\ell\ell'}^\nu)' = M_{\ell\ell'}^\nu (1 + \kappa \sigma_{\alpha\beta} F^{\alpha\beta}) . \quad (6.17)$$

If the same mechanism which produced neutrino masses also produced their dipoles through some BSM physics, this would not be an unreasonable assumption.

As the modified mass matrix commutes entirely with the original mass matrix, the mathematical structure of the commutator in Eq. (6.11) is unchanged

$$[(M^\nu)', M^\nu] = 0 \rightarrow \text{Im}[\det(C_{\ell\ell'})] = \text{Im}[\det(C'_{\ell\ell'})] . \quad (6.18)$$

The determinant calculation is then identical between the two mass matrices. While the overall determinant is fixed, the individual elements which make up the determi-

nant are modified. This yields

$$\text{Im} [\det(C_{\ell\ell'})] = (\Delta_{12}\Delta_{23}\Delta_{13})(\Delta_{e\mu}\Delta_{\mu\tau}\Delta_{e\tau}) J, \quad (6.19)$$

$$\text{Im} [\det(C'_{\ell\ell'})] = (\Delta'_{12}\Delta'_{23}\Delta'_{13})(\Delta_{e\mu}\Delta_{\mu\tau}\Delta_{e\tau}) J', \quad (6.20)$$

where we have added primes to denote new values due to remixing. A similar result occurs in matter in [Harrison and Scott \(2000\)](#). The ratio of modified J' to J is the amplification (or suppression) of CP violation given by

$$\mathcal{R} = \frac{J'}{J} = \frac{(\Delta_{12}\Delta_{23}\Delta_{13})}{(\Delta'_{12}\Delta'_{23}\Delta'_{13})}. \quad (6.21)$$

In our simple proportionality model, this simplifies to

$$\mathcal{R} = \frac{1}{(1 + \kappa\sigma_{\alpha\beta}F^{\alpha\beta})^6}. \quad (6.22)$$

To first order, and evaluating $\sigma_{\alpha\beta}F^{\alpha\beta}$ for homogeneous magnetic fields, Eq. (6.22) can be expressed as

$$\mathcal{R} = 1 \pm 12\kappa B + \mathcal{O}(B^2). \quad (6.23)$$

where we allow for aligned and anti-aligned spin states.

6.2.3 Electric dipole moments and CP symmetry

Here we state the standard picture of CP violation through an electric dipole. The structure of the Pauli term in Eq. (1.31) informs us how to construct the relativistic electric dipole moment (EDM); see [Knecht \(2004\)](#); [Jegerlehner \(2017\)](#). The generalization to include the electric dipole is

$$\delta\mu \rightarrow \delta\tilde{\mu} \equiv \delta\mu + i\epsilon\gamma^5, \quad (6.24)$$

where ϵ is the EDM of the particle. As the natural electric dipole within the Dirac equation is zero, the presence of ϵ is always considered anomalous. The EDM Pauli Lagrangian term is

$$\mathcal{L}_{\text{EDM}} = -\bar{\psi} \left(i\epsilon\gamma^5 \frac{1}{2}\sigma_{\alpha\beta} F^{\alpha\beta} \right) \psi, \quad (6.25)$$

which is of interest because of the inclusion of γ^5 . Taking advantage of the properties of γ^5 , we can write the EDM in Eq. (6.25) as

$$\gamma^5 \sigma_{\mu\nu} = \frac{i}{2} \varepsilon_{\mu\nu\alpha\beta} \sigma^{\alpha\beta} \rightarrow \mathcal{L}_{\text{EDM}} = +\bar{\psi} \left(\epsilon \frac{1}{2} \sigma^{\alpha\beta} F_{\alpha\beta}^* \right) \psi. \quad (6.26)$$

which is more closely analogous to the structure of the AMM in Eq. (1.31) making use of the dual form of the electromagnetic field tensor shown in Eq. (1.29).

Following a procedure similar to the one found in Section 1.1, Eq. (6.26) reduces in the non-relativistic limit to the Hamiltonian density EDM interaction

$$\mathcal{H}_{\text{EDM}} \approx \epsilon \chi^\dagger \boldsymbol{\sigma} \cdot \mathbf{E} \chi. \quad (6.27)$$

The electric dipole is important because the presence of one would signify charge-parity (CP) violation in the theory which provides a method to distinguish between matter and antimatter. We discuss briefly using the parity (P) and time (T) symmetries of the relevant spin \mathbf{s} and field vectors (\mathbf{E}, \mathbf{B}) and their inner products. The even and odd symmetries of each are printed in Table 6.1.

	\mathbf{E}	\mathbf{B}	\mathbf{s}	$\mathbf{s} \cdot \mathbf{E}$	$\mathbf{s} \cdot \mathbf{B}$
T symmetry ($t \rightarrow -t$)	even	odd	odd	odd	even
P symmetry ($\mathbf{x} \rightarrow -\mathbf{x}$)	odd	even	even	odd	even
PT symmetry ($x^\alpha \rightarrow -x^\alpha$)	odd	odd	odd	even	even

Table 6.1: Time (T), parity (P) and PT symmetries of electric \mathbf{E} , magnetic \mathbf{B} , spin \mathbf{s} three-vectors and the inner products which describe the dipole Hamiltonian terms.

The EDM term Eq. (6.27) is overall T-odd and P-odd while the magnetic dipole is T-even and P-even. While EDM dipoles are common in molecular systems, no electric dipole has ever been measured for an elementary particle nor composite particles like the proton or neutron despite extensive searching. As a point of comparison, the EDM of the electron is excluded (Andreev et al., 2018; Roussy et al., 2023) by a bound of $|\epsilon_e/c| < 4.1 \times 10^{-30} e\text{ cm}$.

For CPT symmetry to hold, Table 6.1 implies that both the electric and magnetic dipoles must be C-even. C-symmetry is a more complicated concept to discuss as it is only well-defined relativistically where particle and antiparticle states are simultaneously described by the theory. The Dirac spinor charge conjugates as

$$C : \psi \rightarrow \psi_c = \eta_c C(\bar{\psi})^T = \eta_c C \gamma_0^T \psi^*, \quad (6.28)$$

where C is the charge conjugation matrix satisfying the conjugation relation

$$-C \gamma_\alpha^T C^{-1} = \gamma_\alpha, \quad (6.29)$$

and η_c is an arbitrary complex phase. The exact matrix expression of C depends on the representational basis used (Dirac, Weyl, Majorana, etc...). We're specifically interesting in the following conjugations

$$C : \bar{\psi} \gamma_\alpha \psi \rightarrow -\bar{\psi} \gamma_\alpha \psi, \quad C : \bar{\psi} \sigma_{\alpha\beta} \psi \rightarrow -\bar{\psi} \sigma_{\alpha\beta} \psi, \quad C : A^\alpha \rightarrow -A^\alpha. \quad (6.30)$$

As the spin density $\bar{\psi} \sigma_{\alpha\beta} \psi$ and vector potential A^α (and thus $F^{\alpha\beta}$) are both odd under charge conjugation, the combination present in the AMM Lagrangian Eq. (1.31) is C-even under charge conjugation. The same is true of the EDM Lagrangian Eq. (6.26) which is more easily seen when cast in terms of the dual tensor.

We note that the fields ψ , $\bar{\psi}$ and A^α are considered dynamical *operators* within a quantum field theory. C-symmetry is therefore broken when considering an externally fixed background field such as $A_{\text{ext}}^\alpha(x)$ as $C : A_{\text{ext}}^\alpha(x) \rightarrow A_{\text{ext}}^\alpha(x)$. This distinction bears some importance when discussing the neutrino flavor rotation in Chapter 3. There is

also interest in EDM behavior in the background of curved spacetime (Filho et al., 2023).

6.3 Spin in 5D Kaluza-Klein theory

The ‘miracle’ of Kaluza-Klein (Kaluza, 1921; Klein, 1926) is that both 4D gravitation and electromagnetism emerge from a higher dimension 5D gravitational theory. While the specific importance of Kaluza’s result to the physical world (if there is one) has yet to be revealed, the ideas of Kaluza-Klein have been extensively used to showcase the emergence of unified physics from higher dimensional geometries (Ortin, 2015).

In the modern context, we understand that Kaluza-Klein in its original form cannot strictly be correct as we are operating purely in the classical regime and we are missing the incorporation of the weak and strong interactions as well. With all that said, there is still value in exploring the implications of Kaluza-Klein in that Kaluza’s miracle might very well not be an accident, but a natural result from a fuller more complete implementation of these ideas (Overduin and Wesson, 1997).

The main goal of this research effort is to obtain the spin dynamics of a test particle in the context of a 5D Kaluza-Klein style theory in the same spirit as was accomplished for the general relativistic torque equations

$$\frac{Dp^\mu}{D\tau} + \frac{1}{2} u^\nu s^{\rho\sigma} R^\mu_{\nu\rho\sigma} = 0, \quad \frac{Ds^{\mu\nu}}{D\tau} + 2u^{[\mu} p^{\nu]} = 0, \quad (6.31)$$

which couples spin and precession to a curved spacetime. An additional term is also required to accommodate spin in the kinematic equation. Eq. (6.31) is known as the Mathisson-Papapetrou-Dixon (MPD) equations (Mathisson, 1937; Papapetrou, 1951; Dixon, 1970). The rank-four tensor $R^\mu_{\nu\rho\sigma}$ is the Riemann curvature defined by

$$R^\mu_{\nu\rho\sigma} V^\nu = 2\nabla_{[\rho}\nabla_{\sigma]} V^\mu, \quad (6.32)$$

where V^μ is any arbitrary vector and the notation $[\rho, \sigma]$ indicates a commutator of indices. The significance of Eq. (6.31) is that particle motion will deviate away from

traditional geodesic motion due to a coupling of the curvature to the spin.

To promote the above equations into the Kaluza-Klein framework, we consider Lorentz five-vectors \hat{P}^A which are dressed with a hat and capital Latin letters indices $A \in (0 - 3, 5)$. The position five-vector is then denoted by $\hat{x}^A = (x^\mu, x_5)$ where x_5 is the fifth coordinate position. The 5D Einstein-Hilbert action is

$$\mathcal{S}[\hat{g}_{AB}] = \frac{c^4}{16\pi\hat{G}} \int d\hat{x}^5 \sqrt{-\hat{g}} \hat{R}. \quad (6.33)$$

The variable \hat{G} is the 5D gravitational constant and \hat{R} is the Ricci scalar in the 5D space-time. Kaluza-Klein theories are usually expressed as Ricci-flat theories with the scalar curvature $\hat{R} = 0$, but in general nothing prevents us from including matter or other fields in the five-dimensional bulk by adding terms to the above action.

In a 5D spacetime under Klein's cylindrical condition, a particle under free-fall motion manifests as accelerated motion analogous to Eq. (6.31) caused by the electromagnetic force and an additional scalar force in the four-dimensional sector. Because particles with spin deviate from geodesics in free-fall, there should ultimately be spin precession generated by electromagnetism, the scalar field, and gravitation.

Therefore we propose a classical spin five-vector

$$\hat{s}^A = (s^\alpha, s_5), \quad (6.34)$$

which relates the classical four-spin Eq. (2.76) discussed in Section 2.5 to a new fifth component of spin s_5 . We note that analogously the fifth component of five-momentum is related to the mass of the particle; it is our suggestion that the fifth component of spin is related to the invariant spin magnitude. It is the study of this object that will be left to future publications.

REFERENCES

- Abdalla, E., G. F. Abellán, A. Aboubrahim, A. Agnello, Ö. Akarsu, Y. Akrami, G. Alestas, D. Aloni, L. Amendola, L. A. Anchordoqui, et al. (2022). Cosmology intertwined: A review of the particle physics, astrophysics, and cosmology associated with the cosmological tensions and anomalies. *Journal of High Energy Astrophysics*, **34**, pp. 49–211. doi:[10.1016/j.jheap.2022.04.002](https://doi.org/10.1016/j.jheap.2022.04.002).
- Abi, B. et al. (2020). Long-baseline neutrino oscillation physics potential of the DUNE experiment. *Eur. Phys. J. C*, **80**(10), p. 978. doi:[10.1140/epjc/s10052-020-08456-z](https://doi.org/10.1140/epjc/s10052-020-08456-z).
- Abi, B. et al. (2021). Supernova neutrino burst detection with the Deep Underground Neutrino Experiment. *Eur. Phys. J. C*, **81**(5), p. 423. doi:[10.1140/epjc/s10052-021-09166-w](https://doi.org/10.1140/epjc/s10052-021-09166-w).
- Abramowitz, M., I. A. Stegun, and R. H. Romer (1988). *Handbook of mathematical functions with formulas, graphs, and mathematical tables*. American Association of Physics Teachers.
- Adams, N. J., C. J. Conselice, L. Ferreira, et al. (2023). Discovery and properties of ultra-high redshift galaxies ($9 \leq z \leq 12$) in the JWST ERO SMACS 0723 Field. *Monthly Notices of the Royal Astronomical Society*, **518**(3), pp. 4755–4766. doi:[10.1093/mnras/stac3347](https://doi.org/10.1093/mnras/stac3347).
- Adhikary, B., M. Chakraborty, and A. Ghosal (2013). Masses, mixing angles and phases of general Majorana neutrino mass matrix. *JHEP*, **10**, p. 043. doi:[10.1007/JHEP10\(2013\)043](https://doi.org/10.1007/JHEP10(2013)043). [Erratum: JHEP 09, 180 (2014)].
- Aghanim, N. et al. (2020). Planck 2018 results. VI. Cosmological parameters. *Astron. Astrophys.*, **641**, p. A6. doi:[10.1051/0004-6361/201833910](https://doi.org/10.1051/0004-6361/201833910). [Erratum: Astron. Astrophys. 652, C4 (2021)].
- Aguillard, D. P. et al. (2023). Measurement of the Positive Muon Anomalous Magnetic Moment to 0.20 ppm. *arXiv preprint*. doi:[10.48550/arXiv.2308.06230](https://doi.org/10.48550/arXiv.2308.06230).
- Aker, M. et al. (2022). Direct neutrino-mass measurement with sub-electronvolt sensitivity. *Nature Phys.*, **18**(2), pp. 160–166. doi:[10.1038/s41567-021-01463-1](https://doi.org/10.1038/s41567-021-01463-1).
- Akhmedov, E. (1988). Resonant Amplification of Neutrino Spin Rotation in Matter and the Solar Neutrino Problem. *Phys. Lett. B*, **213**, pp. 64–68. doi:[10.1016/0370-2693\(88\)91048-9](https://doi.org/10.1016/0370-2693(88)91048-9).

- Akhmedov, E. and P. Martínez-Miravé (2022). Solar $\bar{\nu}_e$ flux: revisiting bounds on neutrino magnetic moments and solar magnetic field. *JHEP*, **10**, p. 144. doi:[10.1007/JHEP10\(2022\)144](https://doi.org/10.1007/JHEP10(2022)144).
- Akhmedov, E. K. (2007). Do charged leptons oscillate? *JHEP*, **09**, p. 116. doi:[10.1088/1126-6708/2007/09/116](https://doi.org/10.1088/1126-6708/2007/09/116).
- Andreev, V. et al. (2018). Improved limit on the electric dipole moment of the electron. *Nature*, **562**(7727), pp. 355–360. doi:[10.1038/s41586-018-0599-8](https://doi.org/10.1038/s41586-018-0599-8).
- Angeles-Martinez, R. and M. Napsuciale (2012). Renormalization of the QED of second order spin 1/2 fermions. *Phys. Rev. D*, **85**, p. 076004. doi:[10.1103/PhysRevD.85.076004](https://doi.org/10.1103/PhysRevD.85.076004).
- Aoyama, T. et al. (2020). The anomalous magnetic moment of the muon in the Standard Model. *Phys. Rept.*, **887**, pp. 1–166. doi:[10.1016/j.physrep.2020.07.006](https://doi.org/10.1016/j.physrep.2020.07.006).
- Aristizabal Sierra, D., O. G. Miranda, D. K. Papoulias, and G. S. Garcia (2022). Neutrino magnetic and electric dipole moments: From measurements to parameter space. *Phys. Rev. D*, **105**(3), p. 035027. doi:[10.1103/PhysRevD.105.035027](https://doi.org/10.1103/PhysRevD.105.035027).
- Bahcall, J. N., M. H. Pinsonneault, and S. Basu (2001). Solar Models: Current Epoch and Time Dependences, Neutrinos, and Helioseismological Properties. *The Astrophysical Journal*, **555**(2), p. 990. doi:[10.1086/321493](https://doi.org/10.1086/321493).
- Balaji, S., M. Ramirez-Quezada, and Y.-L. Zhou (2020a). CP violation and circular polarisation in neutrino radiative decay. *JHEP*, **04**, p. 178. doi:[10.1007/JHEP04\(2020\)178](https://doi.org/10.1007/JHEP04(2020)178).
- Balaji, S., M. Ramirez-Quezada, and Y. L. Zhou (2020b). CP violation in neutral lepton transition dipole moment. *JHEP*, **12**, p. 090. doi:[10.1007/JHEP12\(2020\)090](https://doi.org/10.1007/JHEP12(2020)090).
- Bargmann, V., L. Michel, and V. L. Telegdi (1959). Precession of the polarization of particles moving in a homogeneous electromagnetic field. *Phys. Rev. Lett.*, **2**, pp. 435–436. doi:[10.1103/PhysRevLett.2.435](https://doi.org/10.1103/PhysRevLett.2.435).
- Barut, A. O. and J. Kraus (1975). Resonances in e+ e- System Due to Anomalous Magnetic Moment Interactions. *Phys. Lett. B*, **59**, pp. 175–178. doi:[10.1016/0370-2693\(75\)90696-6](https://doi.org/10.1016/0370-2693(75)90696-6).
- Barut, A. O. and J. Kraus (1976). Solution of the Dirac Equation with Coulomb and Magnetic Moment Interactions. *J. Math. Phys.*, **17**, pp. 506–508. doi:[10.1063/1.522932](https://doi.org/10.1063/1.522932).
- Batista, R. A. and A. Saveliev (2021). The Gamma-ray Window to Intergalactic Magnetism. *Universe*, **7**(7). ISSN 2218-1997. doi:[10.3390/universe7070223](https://doi.org/10.3390/universe7070223).

- Bauer, C. W., S. Fleming, D. Pirjol, and I. W. S. (2001). An Effective field theory for collinear and soft gluons: Heavy to light decays. *Phys. Rev. D*, **63**, p. 114020. doi:[10.1103/PhysRevD.63.114020](https://doi.org/10.1103/PhysRevD.63.114020).
- Bethe, H. A. (1986). A Possible Explanation of the Solar Neutrino Puzzle. *Phys. Rev. Lett.*, **56**, p. 1305. doi:[10.1103/PhysRevLett.56.1305](https://doi.org/10.1103/PhysRevLett.56.1305).
- Birrell, J., C. T. Yang, and J. Rafelski (2014). Relic Neutrino Freeze-out: Dependence on Natural Constants. *Nucl. Phys. B*, **890**, pp. 481–517. doi:[10.1016/j.nuclphysb.2014.11.020](https://doi.org/10.1016/j.nuclphysb.2014.11.020).
- Bouchiat, M. A. and C. C. Bouchiat (1974). Weak Neutral Currents in Atomic Physics. *Phys. Lett. B*, **48**, pp. 111–114. doi:[10.1016/0370-2693\(74\)90656-X](https://doi.org/10.1016/0370-2693(74)90656-X).
- Bouchiat, M. A. and C. C. Bouchiat (1997). Parity violation in atoms. *Rept. Prog. Phys.*, **60**, pp. 1351–1396. doi:[10.1088/0034-4885/60/11/004](https://doi.org/10.1088/0034-4885/60/11/004).
- Broderick, A., M. Prakash, and J. M. Lattimer (2000). The Equation of state of neutron star matter in strong magnetic fields. *Astrophys. J.*, **537**, p. 351. doi:[10.1086/309010](https://doi.org/10.1086/309010).
- Bruce, S. A. (2021a). Model of electromagnetic interactions with spin-1/2 neutral particles. *Mod. Phys. Lett. A*, **36**(33), p. 2150236. doi:[10.1142/S0217732321502369](https://doi.org/10.1142/S0217732321502369).
- Bruce, S. A. (2021b). Neutron interactions with electromagnetic fields and single-neutron solitons. *Int. J. Mod. Phys. A*, **36**(26), p. 2150185. doi:[10.1142/S0217751X21501852](https://doi.org/10.1142/S0217751X21501852).
- Bruce, S. A. and J. F. Diaz-Valdes (2020). Relativistic neutron interaction with electric fields revisited. *Eur. Phys. J. A*, **56**(7), p. 191. doi:[10.1140/epja/s10050-020-00196-8](https://doi.org/10.1140/epja/s10050-020-00196-8).
- Buarque Franzosi, D. and C. Zhang (2015). Probing the top-quark chromomagnetic dipole moment at next-to-leading order in QCD. *Phys. Rev. D*, **91**(11), p. 114010. doi:[10.1103/PhysRevD.91.114010](https://doi.org/10.1103/PhysRevD.91.114010).
- Canas, B. C., O. G. Miranda, A. Parada, M. Tortola, and J. W. F. Valle (2016). Updating neutrino magnetic moment constraints. *Phys. Lett. B*, **753**, pp. 191–198. doi:[10.1016/j.physletb.2015.12.011](https://doi.org/10.1016/j.physletb.2015.12.011). [Addendum: Phys.Lett.B 757, 568–568 (2016)].
- Canetti, L., M. Drewes, and M. Shaposhnikov (2012). Matter and Antimatter in the Universe. *New J. Phys.*, **14**, p. 095012. doi:[10.1088/1367-2630/14/9/095012](https://doi.org/10.1088/1367-2630/14/9/095012).
- Carter, B. (1968). Global structure of the Kerr family of gravitational fields. *Phys. Rev.*, **174**, pp. 1559–1571. doi:[10.1103/PhysRev.174.1559](https://doi.org/10.1103/PhysRev.174.1559).

- Chang, E., W. Detmold, K. Orginos, A. Parreno, M. J. Savage, B. C. Tiburzi, and S. R. Beane (2015). Magnetic structure of light nuclei from lattice QCD. *Phys. Rev. D*, **92**(11), p. 114502. doi:[10.1103/PhysRevD.92.114502](https://doi.org/10.1103/PhysRevD.92.114502).
- Choudhury, I. D. and A. Lahiri (2015). Anomalous chromomagnetic moment of quarks. *Mod. Phys. Lett. A*, **30**(23), p. 1550113. doi:[10.1142/S0217732315501138](https://doi.org/10.1142/S0217732315501138).
- Chukhnova, A. V. and A. E. Lobanov (2020). Neutrino flavor oscillations and spin rotation in matter and electromagnetic field. *Phys. Rev. D*, **101**(1), p. 013003. doi:[10.1103/PhysRevD.101.013003](https://doi.org/10.1103/PhysRevD.101.013003).
- Davis, T. M. and C. H. Lineweaver (2004). Expanding confusion: common misconceptions of cosmological horizons and the superluminal expansion of the universe. *Publ. Astron. Soc. Austral.*, **21**, p. 97. doi:[10.1071/AS03040](https://doi.org/10.1071/AS03040).
- Delgado-Acosta, E. G., M. Napsuciale, and S. Rodriguez (2011). Second order formalism for spin 1/2 fermions and Compton scattering. *Phys. Rev. D*, **83**, p. 073001. doi:[10.1103/PhysRevD.83.073001](https://doi.org/10.1103/PhysRevD.83.073001).
- Detmold, W., R. G. Edwards, J. J. Dudek, M. Engelhardt, H. W. Lin, S. Meinel, K. Orginos, and P. Shanahan (2019). Hadrons and Nuclei. *Eur. Phys. J. A*, **55**(11), p. 193. doi:[10.1140/epja/i2019-12902-4](https://doi.org/10.1140/epja/i2019-12902-4).
- Dixon, W. G. (1970). Dynamics of extended bodies in general relativity. I. Momentum and angular momentum. *Proc. Roy. Soc. Lond. A*, **314**, pp. 499–527. doi:[10.1098/rspa.1970.0020](https://doi.org/10.1098/rspa.1970.0020).
- Dunne, G. V. (2014). Extreme quantum field theory and particle physics with IZEST. *Eur. Phys. J. ST*, **223**(6), pp. 1055–1061. doi:[10.1140/epjst/e2014-02156-4](https://doi.org/10.1140/epjst/e2014-02156-4).
- Durrer, R. and A. Neronov (2013). Cosmological magnetic fields: their generation, evolution and observation. *The Astronomy and Astrophysics Review*, **21**, pp. 1–109. doi:[10.1007/s00159-013-0062-7](https://doi.org/10.1007/s00159-013-0062-7).
- Dvornikov, M. (2019). Neutrino spin oscillations in external fields in curved spacetime. *Phys. Rev. D*, **99**(11), p. 116021. doi:[10.1103/PhysRevD.99.116021](https://doi.org/10.1103/PhysRevD.99.116021).
- Ehrenfest, P. (1927). Bemerkung über die angenäherte Gültigkeit der klassischen Mechanik innerhalb der Quantenmechanik. *Z. Phys.*, **45**(7-8), pp. 455–457. doi:[10.1007/BF01329203](https://doi.org/10.1007/BF01329203).
- Eides, M. I., H. Grotch, and V. A. Shelyuto (2001). Theory of light hydrogen - like atoms. *Phys. Rept.*, **342**, pp. 63–261. doi:[10.1016/S0370-1573\(00\)00077-6](https://doi.org/10.1016/S0370-1573(00)00077-6).
- Elizalde, E., E. J. Ferrer, and V. de la Incera (2004). Neutrino propagation in a strongly magnetized medium. *Phys. Rev. D*, **70**, p. 043012. doi:[10.1103/PhysRevD.70.043012](https://doi.org/10.1103/PhysRevD.70.043012).

- Elze, H. T., W. Greiner, and J. Rafelski (1980). The relativistic Fermi gas revisited. *J. Phys. G*, **6**, pp. L149–L153. doi:[10.1088/0305-4616/6/9/003](https://doi.org/10.1088/0305-4616/6/9/003).
- Evans, S. (2022). *Nonperturbative Aspects in the QED Vacuum Related to Anomalous Magnetic Moment*. Ph.D. thesis, Arizona U. URN/HDL: [10150/665648](https://hdl.handle.net/10150/665648).
- Evans, S. and J. Rafelski (2018). Vacuum stabilized by anomalous magnetic moment. *Phys. Rev. D*, **98**(1), p. 016006. doi:[10.1103/PhysRevD.98.016006](https://doi.org/10.1103/PhysRevD.98.016006).
- Evans, S. and J. Rafelski (2022). Emergence of periodic in magnetic moment effective QED action. *Phys. Lett. B*, **831**, p. 137190. doi:[10.1016/j.physletb.2022.137190](https://doi.org/10.1016/j.physletb.2022.137190).
- Fedotov, A., A. Ilderton, F. Karbstein, B. King, D. Seipt, H. Taya, and G. Torgrimsen (2023). Advances in QED with intense background fields. *Phys. Rept.*, **1010**, pp. 1–138. doi:[10.1016/j.physrep.2023.01.003](https://doi.org/10.1016/j.physrep.2023.01.003).
- Ferrara, S., M. Poratti, and V. L. Telegdi (1992). $g = 2$ as the natural value of the tree-level gyromagnetic ratio of elementary particles. *Phys. Rev. D*, **46**, pp. 3529–3537. doi:[10.1103/PhysRevD.46.3529](https://doi.org/10.1103/PhysRevD.46.3529).
- Ferrer, E. J., V. de la Incera, D. Manreza Paret, A. Pérez Martínez, and A. Sanchez (2015). Insignificance of the anomalous magnetic moment of charged fermions for the equation of state of a magnetized and dense medium. *Phys. Rev. D*, **91**(8), p. 085041. doi:[10.1103/PhysRevD.91.085041](https://doi.org/10.1103/PhysRevD.91.085041).
- Ferrer, E. J. and A. Hackebill (2019). Thermodynamics of Neutrons in a Magnetic Field and its Implications for Neutron Stars. *Phys. Rev. C*, **99**(6), p. 065803. doi:[10.1103/PhysRevC.99.065803](https://doi.org/10.1103/PhysRevC.99.065803).
- Ferrer, E. J. and A. Hackebill (2023). The Importance of the Pressure Anisotropy Induced by Strong Magnetic Fields on Neutron Star Physics. *J. Phys. Conf. Ser.*, **2536**(1), p. 012007. doi:[10.1088/1742-6596/2536/1/012007](https://doi.org/10.1088/1742-6596/2536/1/012007).
- Feynman, R. P. (1951). An Operator calculus having applications in quantum electrodynamics. *Phys. Rev.*, **84**, pp. 108–128. doi:[10.1103/PhysRev.84.108](https://doi.org/10.1103/PhysRev.84.108).
- Feynman, R. P. and M. Gell-Mann (1958). Theory of Fermi interaction. *Phys. Rev.*, **109**, pp. 193–198. doi:[10.1103/PhysRev.109.193](https://doi.org/10.1103/PhysRev.109.193).
- Filho, A. A. A., H. Hassanabadi, J. A. A. S. Reis, and L. Lisboa-Santos (2023). Fermions with Electric Dipole Moment in curved spacetime. *arXiv preprint. arXiv:2306.10897*.
- Fleming, S., I. Z. Rothstein, and A. K. Leibovich (2001). Power counting and effective field theory for charmonium. *Phys. Rev. D*, **64**, p. 036002. doi:[10.1103/PhysRevD.64.036002](https://doi.org/10.1103/PhysRevD.64.036002).

- Fock, V. (1937). Proper time in classical and quantum mechanics. *Phys. Z. Sowjetunion*, **12**, pp. 404–425. URL: http://www.neo-classical-physics.info/uploads/3/4/3/6/34363841/fock_-_wkb_and_dirac.pdf.
- Foldy, L. L. (1952). The Electromagnetic Properties of Dirac Particles. *Phys. Rev.*, **87**, pp. 688–693. doi:[10.1103/PhysRev.87.688](https://doi.org/10.1103/PhysRev.87.688).
- Foldy, L. L. and S. A. Wouthuysen (1950). On the Dirac theory of spin 1/2 particle and its nonrelativistic limit. *Phys. Rev.*, **78**, pp. 29–36. doi:[10.1103/PhysRev.78.29](https://doi.org/10.1103/PhysRev.78.29).
- Formanek, M. (2020). *Revisiting Covariant Particle Dynamics*. Ph.D. thesis, Arizona U. URN/HDL: [10150/650804](https://hdl.handle.net/10150/650804).
- Formanek, M., S. Evans, J. Rafelski, A. Steinmetz, and C. T. Yang (2018). Strong fields and neutral particle magnetic moment dynamics. *Plasma Phys. Control. Fusion*, **60**, p. 074006. doi:[10.1088/1361-6587/aac06a](https://doi.org/10.1088/1361-6587/aac06a).
- Formanek, M., C. Grayson, J. Rafelski, and B. Müller (2021a). Current-conserving relativistic linear response for collisional plasmas. *Annals Phys.*, **434**, p. 168605. doi:[10.1016/j.aop.2021.168605](https://doi.org/10.1016/j.aop.2021.168605).
- Formanek, M., A. Steinmetz, and J. Rafelski (2019). Classical neutral point particle in linearly polarized EM plane wave field. *Plasma Phys. Control. Fusion*, **61**(8), p. 084006. doi:[10.1088/1361-6587/ab242e](https://doi.org/10.1088/1361-6587/ab242e).
- Formanek, M., A. Steinmetz, and J. Rafelski (2020). Radiation reaction friction: Resistive material medium. *Phys. Rev. D*, **102**(5), p. 056015. doi:[10.1103/PhysRevD.102.056015](https://doi.org/10.1103/PhysRevD.102.056015).
- Formanek, M., A. Steinmetz, and J. Rafelski (2021b). Motion of classical charged particles with magnetic moment in external plane-wave electromagnetic fields. *Phys. Rev. A*, **103**(5), p. 052218. doi:[10.1103/PhysRevA.103.052218](https://doi.org/10.1103/PhysRevA.103.052218).
- Frenkel, J. (1926). Die Elektrodynamik des rotierenden Elektrons. *Z. Phys.*, **37**, pp. 243–262. doi:[10.1007/BF01397099](https://doi.org/10.1007/BF01397099).
- Fritzsch, H. and Z. Z. Xing (1996). Lepton mass hierarchy and neutrino oscillations. *Phys. Lett. B*, **372**, pp. 265–270. doi:[10.1016/0370-2693\(96\)00107-4](https://doi.org/10.1016/0370-2693(96)00107-4).
- Fritzsch, H. and Z. Z. Xing (1998). Large leptonic flavor mixing and the mass spectrum of leptons. *Phys. Lett. B*, **440**, pp. 313–318. doi:[10.1016/S0370-2693\(98\)01106-X](https://doi.org/10.1016/S0370-2693(98)01106-X).
- Fritzsch, H. and Z. Z. Xing (2000). Mass and flavor mixing schemes of quarks and leptons. *Prog. Part. Nucl. Phys.*, **45**, pp. 1–81. doi:[10.1016/S0146-6410\(00\)00102-2](https://doi.org/10.1016/S0146-6410(00)00102-2).

- Fromerth, M. J., I. Kuznetsova, L. Labun, J. Letessier, and J. Rafelski (2012). From Quark-Gluon Universe to Neutrino Decoupling: $200 < T < 2\text{MeV}$. *Acta Phys. Polon. B*, **43**(12), pp. 2261–2284. doi:[10.5506/APhysPolB.43.2261](https://doi.org/10.5506/APhysPolB.43.2261).
- Fujikawa, K. and R. E. Shrock (1980). The Magnetic Moment of a Massive Neutrino and Neutrino Spin Rotation. *Phys. Rev. Lett.*, **45**, p. 963. doi:[10.1103/PhysRevLett.45.963](https://doi.org/10.1103/PhysRevLett.45.963).
- Gaensler, B. M., R. Beck, and L. Feretti (2004). The origin and evolution of cosmic magnetism. *New Astronomy Reviews*, **48**(11-12), pp. 1003–1012. doi:[10.1016/j.newar.2004.09.003](https://doi.org/10.1016/j.newar.2004.09.003).
- Gerlach, W. and O. Stern (1922). The Magnetic Moment of Silver Atoms. *Z. Phys.*, **9**, pp. 353–355. doi:[10.1007/BF01326984](https://doi.org/10.1007/BF01326984).
- Gesztesy, F., B. Simon, and B. Thaller (1985). On the selfadjointness of Dirac operators with anomalous magnetic moment. *Proceedings of the American Mathematical Society*, **94**(1), pp. 115–118. doi:[10.2307/2044962](https://doi.org/10.2307/2044962).
- Giovannini, M. (2004). The Magnetized universe. *Int. J. Mod. Phys. D*, **13**, pp. 391–502. doi:[10.1142/S0218271804004530](https://doi.org/10.1142/S0218271804004530).
- Giovannini, M. (2018). Probing large-scale magnetism with the Cosmic Microwave Background. *Class. Quant. Grav.*, **35**(8), p. 084003. doi:[10.1088/1361-6382/aab17d](https://doi.org/10.1088/1361-6382/aab17d).
- Giovannini, M. (2023). The scaling of primordial gauge fields. *Physics Letters B*, **842**, p. 137967. ISSN 0370-2693. doi:[10.1016/j.physletb.2023.137967](https://doi.org/10.1016/j.physletb.2023.137967).
- Giunti, C. and C. W. Kim (2007). *Fundamentals of neutrino physics and astrophysics*. Oxford university press. doi:[10.1093/acprof:oso/9780198508717.001.0001](https://doi.org/10.1093/acprof:oso/9780198508717.001.0001).
- Giunti, C., K. A. Kouzakov, Y. F. Li, A. V. Lokhov, A. Studenikin, and S. Zhou (2016). Electromagnetic neutrinos in laboratory experiments and astrophysics. *Annalen Phys.*, **528**, pp. 198–215. doi:[10.1002/andp.201500211](https://doi.org/10.1002/andp.201500211).
- Giunti, C. and A. Studenikin (2015). Neutrino electromagnetic interactions: a window to new physics. *Rev. Mod. Phys.*, **87**, p. 531. doi:[10.1103/RevModPhys.87.531](https://doi.org/10.1103/RevModPhys.87.531).
- Gonoskov, A., T. G. Blackburn, M. Marklund, and S. S. Bulanov (2022). Charged particle motion and radiation in strong electromagnetic fields. *Rev. Mod. Phys.*, **94**(4), p. 045001. doi:[10.1103/RevModPhys.94.045001](https://doi.org/10.1103/RevModPhys.94.045001).
- Gopal, R. and S. Sethi (2005). Generation of magnetic field in the pre-recombination era. *Mon. Not. Roy. Astron. Soc.*, **363**, pp. 521–528. doi:[10.1111/j.1365-2966.2005.09442.x](https://doi.org/10.1111/j.1365-2966.2005.09442.x).

- Grasso, D. and H. R. Rubinstein (2001). Magnetic fields in the early universe. *Phys. Rept.*, **348**, pp. 163–266. doi:[10.1016/S0370-1573\(00\)00110-1](https://doi.org/10.1016/S0370-1573(00)00110-1).
- Grayson, C., M. Formanek, J. Rafelski, and B. Mueller (2022). Dynamic magnetic response of the quark-gluon plasma to electromagnetic fields. *Phys. Rev. D*, **106**(1), p. 014011. doi:[10.1103/PhysRevD.106.014011](https://doi.org/10.1103/PhysRevD.106.014011).
- Grayson, C., C. T. Yang, M. Formanek, and J. Rafelski (2023). Electron–positron plasma in BBN: Damped-dynamic screening. *Annals Phys.*, **458**, p. 169453. doi:[10.1016/j.aop.2023.169453](https://doi.org/10.1016/j.aop.2023.169453).
- Green, J., S. Meinel, M. Engelhardt, S. Krieg, J. Laeuchli, J. Negele, K. Orginos, A. Pochinsky, and S. Syritsyn (2015). High-precision calculation of the strange nucleon electromagnetic form factors. *Phys. Rev. D*, **92**(3), p. 031501. doi:[10.1103/PhysRevD.92.031501](https://doi.org/10.1103/PhysRevD.92.031501).
- Greiner, W. and B. Müller (2009). *Gauge theory of weak interactions*. Springer. doi:[10.1007/978-3-540-87843-8](https://doi.org/10.1007/978-3-540-87843-8).
- Greiner, W. and B. Müller (2012). *Quantum mechanics: symmetries*. Springer Science & Business Media. doi:[10.1007/978-3-642-57976-9](https://doi.org/10.1007/978-3-642-57976-9). [orig. pub. 1984].
- Greiner, W., B. Muller, and J. Rafelski (2012a). *Quantum electrodynamics of strong fields*. Springer Berlin, Heidelberg. doi:[10.1007/978-3-642-82272-8](https://doi.org/10.1007/978-3-642-82272-8). [orig. pub. 1985].
- Greiner, W., L. Neise, and H. Stöcker (2012b). *Thermodynamics and statistical mechanics*. Springer Science & Business Media. doi:[10.1007/978-1-4612-0827-3](https://doi.org/10.1007/978-1-4612-0827-3). [orig. pub. 1995].
- Greiner, W. and J. Reinhardt (2008). *Quantum electrodynamics*. Springer Science & Business Media. doi:[10.1007/978-3-540-87561-1](https://doi.org/10.1007/978-3-540-87561-1).
- Greiner, W., S. Schramm, and E. Stein (2006). *Quantum chromodynamics*. Springer Berlin, Heidelberg. doi:[10.1007/978-3-540-48535-3](https://doi.org/10.1007/978-3-540-48535-3). [orig. pub. 1989].
- Hackebill, A. A. (2022). *Magnetic Field Effects on the Physics of Neutron Stars*. Ph.D. thesis, CUNY, Academic Works. URL: https://academicworks.cuny.edu/gc_etds/5030.
- Haro, P. A., M. Dickinson, S. L. Finkelstein, et al. (2023). Confirmation and refutation of very luminous galaxies in the early universe. *Nature*. doi:[10.1038/s41586-023-06521-7](https://doi.org/10.1038/s41586-023-06521-7).
- Harrison, P. F. and W. G. Scott (2000). CP and T violation in neutrino oscillations and invariance of Jarlskog's determinant to matter effects. *Phys. Lett. B*, **476**, pp. 349–355. doi:[10.1016/S0370-2693\(00\)00153-2](https://doi.org/10.1016/S0370-2693(00)00153-2).

- Hegelich, B. M., G. Mourou, and J. Rafelski (2014). Probing the quantum vacuum with ultra intense laser pulses. *Eur. Phys. J. ST*, **223**(6), pp. 1093–1104. doi:[10.1140/epjst/e2014-02160-8](https://doi.org/10.1140/epjst/e2014-02160-8).
- Hewett, J. L. et al. (2012). Fundamental Physics at the Intensity Frontier. In *Workshop on Fundamental Physics at the Intensity Frontier*. doi:[10.2172/1042577](https://doi.org/10.2172/1042577).
- Holstein, B. R. and S. Scherer (2014). Hadron Polarizabilities. *Ann. Rev. Nucl. Part. Sci.*, **64**, pp. 51–81. doi:[10.1146/annurev-nucl-102313-025555](https://doi.org/10.1146/annurev-nucl-102313-025555).
- Huber, P. et al. (2022). Snowmass Neutrino Frontier Report. In *Snowmass 2021*. arXiv:[2211.08641](https://arxiv.org/abs/2211.08641).
- Itzykson, C. and J. B. Zuber (1980). *Quantum Field Theory*. International Series In Pure and Applied Physics. McGraw-Hill, New York. ISBN 978-0-486-44568-7.
- Jancovici, B. (1969). Radiative correction to the ground-state energy of an electron in an intense magnetic field. *Phys. Rev.*, **187**, pp. 2275–2276. doi:[10.1103/PhysRev.187.2275](https://doi.org/10.1103/PhysRev.187.2275).
- Jarlskog, C. (1985a). A Basis Independent Formulation of the Connection Between Quark Mass Matrices, CP Violation and Experiment. *Z. Phys. C*, **29**, pp. 491–497. doi:[10.1007/BF01565198](https://doi.org/10.1007/BF01565198).
- Jarlskog, C. (1985b). Commutator of the Quark Mass Matrices in the Standard Electroweak Model and a Measure of Maximal *CP* Nonconservation. *Phys. Rev. Lett.*, **55**, p. 1039. doi:[10.1103/PhysRevLett.55.1039](https://doi.org/10.1103/PhysRevLett.55.1039).
- Jarlskog, C. (2005). Invariants of lepton mass matrices and CP and T violation in neutrino oscillations. *Phys. Lett. B*, **609**, pp. 323–329. doi:[10.1016/j.physletb.2005.01.057](https://doi.org/10.1016/j.physletb.2005.01.057).
- Jedamzik, K. and T. Abel (2013). Small-scale primordial magnetic fields and anisotropies in the cosmic microwave background radiation. *JCAP*, **10**, p. 050. doi:[10.1088/1475-7516/2013/10/050](https://doi.org/10.1088/1475-7516/2013/10/050).
- Jedamzik, K. and L. Pogosian (2020). Relieving the Hubble tension with primordial magnetic fields. *Physical Review Letters*, **125**(18), p. 181302. doi:[10.1103/PhysRevLett.125.181302](https://doi.org/10.1103/PhysRevLett.125.181302).
- Jedamzik, K. and A. Saveliev (2019). Stringent limit on primordial magnetic fields from the cosmic microwave background radiation. *Physical review letters*, **123**(2), p. 021301. doi:[10.1103/PhysRevLett.123.021301](https://doi.org/10.1103/PhysRevLett.123.021301).
- Jegerlehner, F. (2017). *The Anomalous Magnetic Moment of the Muon*, volume 274. Springer, Cham. doi:[10.1007/978-3-319-63577-4](https://doi.org/10.1007/978-3-319-63577-4).

- Jentschura, U. and K. Pachucki (1996). Higher-order binding corrections to the Lamb shift of P-2 states. *Phys. Rev. A*, **54**, pp. 1853–1861. doi:[10.1103/PhysRevA.54.1853](https://doi.org/10.1103/PhysRevA.54.1853).
- Kaluza, T. (1921). Zum Unitätsproblem der Physik. *Sitzungsber. Preuss. Akad. Wiss. Berlin (Math. Phys.)*, **1921**, pp. 966–972. doi:[10.1142/S0218271818700017](https://doi.org/10.1142/S0218271818700017).
- Kaspi, V. M. and A. Beloborodov (2017). Magnetars. *Ann. Rev. Astron. Astrophys.*, **55**, pp. 261–301. doi:[10.1146/annurev-astro-081915-023329](https://doi.org/10.1146/annurev-astro-081915-023329).
- Klein, O. (1926). Quantum Theory and Five-Dimensional Theory of Relativity. (In German and English). *Z. Phys.*, **37**, pp. 895–906. doi:[10.1007/BF01397481](https://doi.org/10.1007/BF01397481).
- Knecht, M. (2004). The Anomalous magnetic moment of the muon: A Theoretical introduction. *Lect. Notes Phys.*, **629**, pp. 37–84. doi:[10.1007/978-3-540-44457-2_2](https://doi.org/10.1007/978-3-540-44457-2_2).
- Kronberg, P. P. (1994). Extragalactic magnetic fields. *Reports on Progress in Physics*, **57**(4), p. 325. doi:[10.1088/0034-4885/57/4/001](https://doi.org/10.1088/0034-4885/57/4/001).
- Labun, L. and J. Rafelski (2009). Vacuum Decay Time in Strong External Fields. *Phys. Rev. D*, **79**, p. 057901. doi:[10.1103/PhysRevD.79.057901](https://doi.org/10.1103/PhysRevD.79.057901).
- Labun, L. and J. Rafelski (2012). Higgs two-gluon decay and the top-quark chromomagnetic moment. *arXiv preprint*. doi:[10.48550/arXiv.1210.3150](https://doi.org/10.48550/arXiv.1210.3150).
- Labun, L. and J. Rafelski (2013). Top anomalous magnetic moment and the two photon decay of Higgs boson. *Phys. Rev. D*, **88**, p. 071301. doi:[10.1103/PhysRevD.88.071301](https://doi.org/10.1103/PhysRevD.88.071301).
- Larson, R. L., S. L. Finkelstein, D. D. Kocevski, T. A. Hutchison, J. R. Trump, P. A. Haro, V. Bromm, N. J. Cleri, M. Dickinson, S. Fujimoto, et al. (2023). A CEERS Discovery of an Accreting Supermassive Black Hole 570 Myr after the Big Bang: Identifying a Progenitor of Massive $z > 6$ Quasars. *arXiv preprint*. doi:[10.48550/arXiv.2303.08918](https://doi.org/10.48550/arXiv.2303.08918). [submitted to ApJ].
- Letessier, J. and J. Rafelski (2023). *Hadrons and Quark–Gluon Plasma*. Cambridge Monographs on Particle Physics, Nuclear Physics and Cosmology. Cambridge University Press. doi:[10.1017/9781009290753](https://doi.org/10.1017/9781009290753). Open access. [orig. pub. 2002].
- Lichkunov, A., A. Popov, and A. Studenikin (2020). Neutrino eigenstates and flavour, spin and spin-flavour oscillations in a constant magnetic field. In *2019 European Physical Society Conference on High Energy Physics*. arXiv:[2012.06880](https://arxiv.org/abs/2012.06880).
- Lim, C. S. and W. J. Marciano (1988). Resonant Spin - Flavor Precession of Solar and Supernova Neutrinos. *Phys. Rev. D*, **37**, pp. 1368–1373. doi:[10.1103/PhysRevD.37.1368](https://doi.org/10.1103/PhysRevD.37.1368).

- Martin, P. C. and R. J. Glauber (1958). Relativistic Theory of Radiative Orbital Electron Capture. *Phys. Rev.*, **109**, pp. 1307–1325. doi:[10.1103/PhysRev.109.1307](https://doi.org/10.1103/PhysRev.109.1307).
- Martínez-Miravé, P. (2023). *Neutrino properties from the laboratory and the cosmos*. Ph.D. thesis, Valencia U. doi:[10.48550/arXiv.2309.15446](https://doi.org/10.48550/arXiv.2309.15446). URN/HDL: [10550/89441](https://hdl.handle.net/10550/89441).
- Mathisson, M. (1937). Neue mechanik materieller systeme. *Acta Physica Polonica*, **6**, pp. 163–209.
- Melrose, D. (2013). *Quantum plasmadynamics: Magnetized plasmas*. Springer. doi:[10.1007/978-1-4614-4045-1](https://doi.org/10.1007/978-1-4614-4045-1).
- Mikheev, S. P. and A. Y. Smirnov (1986). Resonant amplification of neutrino oscillations in matter and solar neutrino spectroscopy. *Nuovo Cim. C*, **9**, pp. 17–26. doi:[10.1007/BF02508049](https://doi.org/10.1007/BF02508049).
- Mikheyev, S. P. and A. Y. Smirnov (1985). Resonance Amplification of Oscillations in Matter and Spectroscopy of Solar Neutrinos. *Sov. J. Nucl. Phys.*, **42**, pp. 913–917.
- Neronov, A. and I. Vovk (2010). Evidence for strong extragalactic magnetic fields from Fermi observations of TeV blazars. *Science*, **328**(5974), pp. 73–75. doi:[10.1126/science.1184192](https://doi.org/10.1126/science.1184192).
- Niederle, J. and A. G. Nikitin (2006). Relativistic Coulomb problem for particles with arbitrary half-integer spin. *J. Phys. A*, **39**, pp. 10931–10944. doi:[10.1088/0305-4470/39/34/023](https://doi.org/10.1088/0305-4470/39/34/023).
- Nieves, J. F. (1982). Electromagnetic Properties of Majorana Neutrinos. *Phys. Rev. D*, **26**, p. 3152. doi:[10.1103/PhysRevD.26.3152](https://doi.org/10.1103/PhysRevD.26.3152).
- Ohanian, H. C. (1986). What is spin? *American Journal of Physics*, **54**(6), pp. 500–505. doi:[10.1119/1.14580](https://doi.org/10.1119/1.14580).
- Ohlsson, T. (2012). *Relativistic quantum physics: From advanced quantum mechanics to introductory quantum field theory*. Cambridge University Press. ISBN 978-1-139-21072-0, 978-0-521-76726-2. doi:[10.1017/CBO9781139032681](https://doi.org/10.1017/CBO9781139032681).
- Ortin, T. (2015). *Gravity and Strings*. Cambridge Monographs on Mathematical Physics. Cambridge University Press, 2nd ed. edition. ISBN 978-0-521-76813-9, 978-0-521-76813-9, 978-1-316-23579-9. doi:[10.1017/CBO9781139019750](https://doi.org/10.1017/CBO9781139019750).
- Overduin, J. M. and P. S. Wesson (1997). Kaluza-Klein gravity. *Phys. Rept.*, **283**, pp. 303–380. doi:[10.1016/S0370-1573\(96\)00046-4](https://doi.org/10.1016/S0370-1573(96)00046-4).

- Pacetti, S., R. Baldini Ferroli, and E. Tomasi-Gustafsson (2015). Proton electromagnetic form factors: Basic notions, present achievements and future perspectives. *Phys. Rept.*, **550-551**, pp. 1–103. doi:[10.1016/j.physrep.2014.09.005](https://doi.org/10.1016/j.physrep.2014.09.005).
- Pal, P. B. (1992). Particle physics confronts the solar neutrino problem. *Int. J. Mod. Phys. A*, **7**, pp. 5387–5460. doi:[10.1142/S0217751X92002465](https://doi.org/10.1142/S0217751X92002465).
- Papapetrou, A. (1951). Spinning test particles in general relativity. 1. *Proc. Roy. Soc. Lond. A*, **209**, pp. 248–258. doi:[10.1098/rspa.1951.0200](https://doi.org/10.1098/rspa.1951.0200).
- Pehlivan, Y., A. B. Balantekin, and T. Kajino (2014). Neutrino Magnetic Moment, CP Violation and Flavor Oscillations in Matter. *Phys. Rev. D*, **90**(6), p. 065011. doi:[10.1103/PhysRevD.90.065011](https://doi.org/10.1103/PhysRevD.90.065011).
- Perrone, L. M., G. Gregori, B. Reville, L. O. Silva, and R. Bingham (2021). Neutrino-electron magnetohydrodynamics in an expanding universe. *Phys. Rev. D*, **104**(12), p. 123013. doi:[10.1103/PhysRevD.104.123013](https://doi.org/10.1103/PhysRevD.104.123013).
- Pomakov, V. P., S. P. O’Sullivan, M. Brüggen, F. Vazza, E. Carretti, G. H. Heald, C. Horellou, T. Shimwell, A. Shulevski, and T. Vernstrom (2022). The redshift evolution of extragalactic magnetic fields. *Monthly Notices of the Royal Astronomical Society*, **515**(1), pp. 256–270. doi:[10.1093/mnras/stac1805](https://doi.org/10.1093/mnras/stac1805).
- Popov, A. and A. Studenikin (2019). Neutrino eigenstates and flavour, spin and spin-flavour oscillations in a constant magnetic field. *Eur. Phys. J. C*, **79**(2), p. 144. doi:[10.1140/epjc/s10052-019-6657-z](https://doi.org/10.1140/epjc/s10052-019-6657-z).
- Pshirkov, M. S., P. G. Tinyakov, and F. R. Urban (2016). New limits on extragalactic magnetic fields from rotation measures. *Phys. Rev. Lett.*, **116**(19), p. 191302. doi:[10.1103/PhysRevLett.116.191302](https://doi.org/10.1103/PhysRevLett.116.191302).
- Rafelski, J. and J. Birrell (2014). Traveling Through the Universe: Back in Time to the Quark-Gluon Plasma Era. *J. Phys. Conf. Ser.*, **509**, p. 012014. doi:[10.1088/1742-6596/509/1/012014](https://doi.org/10.1088/1742-6596/509/1/012014).
- Rafelski, J., J. Birrell, A. Steinmetz, and C. T. Yang (2023a). A Short Survey of Matter-Antimatter Evolution in the Primordial Universe. *Universe*, **9**(7), p. 309. doi:[10.3390/universe9070309](https://doi.org/10.3390/universe9070309).
- Rafelski, J., S. Evans, and L. Labun (2023b). Study of QED singular properties for variable gyromagnetic ratio $g \simeq 2$. *Phys. Rev. D*, **107**. doi:[10.1103/PhysRevD.107.076002](https://doi.org/10.1103/PhysRevD.107.076002).
- Rafelski, J., M. Formanek, and A. Steinmetz (2018). Relativistic Dynamics of Point Magnetic Moment. *Eur. Phys. J. C*, **78**(1), p. 6. doi:[10.1140/epjc/s10052-017-5493-2](https://doi.org/10.1140/epjc/s10052-017-5493-2).

- Rafelski, J., L. P. Fulcher, and A. Klein (1978). Fermions and Bosons Interacting with Arbitrarily Strong External Fields. *Phys. Rept.*, **38**, pp. 227–361. doi:[10.1016/0370-1573\(78\)90116-3](https://doi.org/10.1016/0370-1573(78)90116-3).
- Rafelski, J., J. Kirsch, B. Müller, J. Reinhardt, and W. Greiner (2017). Probing QED Vacuum with Heavy Ions. *FIAS Interdisc. Sci. Ser.*, pp. 211–251. doi:[10.1007/978-3-319-44165-8_17](https://doi.org/10.1007/978-3-319-44165-8_17).
- Rafelski, J., A. Steinmetz, and C. T. Yang (2023c). Dynamic fermion flavor mixing through transition dipole moments. *arXiv preprint*. doi:[10.48550/arXiv.2309.15797](https://doi.org/10.48550/arXiv.2309.15797). [submitted to Int. Journal of Mod. Phys. A].
- Roussy, T. S. et al. (2023). An improved bound on the electron's electric dipole moment. *Science*, **381**(6653), p. adg4084. doi:[10.1126/science.adg4084](https://doi.org/10.1126/science.adg4084).
- Ruffini, R. and G. Vereshchagin (2013). Electron-positron plasma in GRBs and in cosmology. *Nuovo Cim. C*, **036**(s01), pp. 255–266. doi:[10.1393/ncc/i2013-11500-0](https://doi.org/10.1393/ncc/i2013-11500-0).
- Ruffini, R., G. Vereshchagin, and S. S. Xue (2010). Electron-positron pairs in physics and astrophysics: from heavy nuclei to black holes. *Phys. Rept.*, **487**, pp. 1–140. doi:[10.1016/j.physrep.2009.10.004](https://doi.org/10.1016/j.physrep.2009.10.004).
- Safronova, M. S., D. Budker, D. DeMille, D. F. J. Kimball, A. Derevianko, and C. W. Clark (2018). Search for New Physics with Atoms and Molecules. *Rev. Mod. Phys.*, **90**(2), p. 025008. doi:[10.1103/RevModPhys.90.025008](https://doi.org/10.1103/RevModPhys.90.025008).
- Sajjad Athar, M. et al. (2022). Status and perspectives of neutrino physics. *Prog. Part. Nucl. Phys.*, **124**, p. 103947. doi:[10.1016/j.ppnp.2022.103947](https://doi.org/10.1016/j.ppnp.2022.103947).
- Sakurai, J. J. (1967). *Advanced quantum mechanics*. Pearson Education India.
- Schechter, J. and J. W. F. Valle (1981). Majorana Neutrinos and Magnetic Fields. *Phys. Rev. D*, **24**, pp. 1883–1889. doi:[10.1103/PhysRevD.25.283](https://doi.org/10.1103/PhysRevD.25.283). [Erratum: Phys.Rev.D 25, 283 (1982)].
- Schwartz, M. D. (2014). *Quantum Field Theory and the Standard Model*. Cambridge University Press. doi:[10.1017/9781139540940](https://doi.org/10.1017/9781139540940).
- Schwinger, J. (1974). Spin precession—a dynamical discussion. *American Journal of Physics*, **42**(6), pp. 510–513. doi:[10.1119/1.1987764](https://doi.org/10.1119/1.1987764).
- Schwinger, J. S. (1951). On gauge invariance and vacuum polarization. *Phys. Rev.*, **82**, pp. 664–679. doi:[10.1103/PhysRev.82.664](https://doi.org/10.1103/PhysRev.82.664).
- Shrock, R. E. (1980). New Tests For, and Bounds On, Neutrino Masses and Lepton Mixing. *Phys. Lett. B*, **96**, pp. 159–164. doi:[10.1016/0370-2693\(80\)90235-X](https://doi.org/10.1016/0370-2693(80)90235-X).

- Shrock, R. E. (1982). Electromagnetic Properties and Decays of Dirac and Majorana Neutrinos in a General Class of Gauge Theories. *Nucl. Phys. B*, **206**, pp. 359–379. doi:[10.1016/0550-3213\(82\)90273-5](https://doi.org/10.1016/0550-3213(82)90273-5).
- Smirnov, A. Y. (2003). The MSW effect and solar neutrinos. In *10th International Workshop on Neutrino Telescopes*, pp. 23–43. doi:[10.48550/arXiv.hep-ph/0305106](https://arxiv.org/abs/hep-ph/0305106).
- Steinmetz, A., M. Formanek, and J. Rafelski (2019). Magnetic Dipole Moment in Relativistic Quantum Mechanics. *Eur. Phys. J. A*, **55**(3), p. 40. doi:[10.1140/epja/i2019-12715-5](https://doi.org/10.1140/epja/i2019-12715-5).
- Steinmetz, A., C. T. Yang, and J. Rafelski (2023). Matter-antimatter origin of cosmic magnetism. doi:[10.48550/arXiv.2308.14818](https://arxiv.org/abs/2308.14818). [Submitted to Phys. Rev. D].
- Studenikin, A. (2016). Status and perspectives of neutrino magnetic moments. *J. Phys. Conf. Ser.*, **718**(6), p. 062076. doi:[10.1088/1742-6596/718/6/062076](https://doi.org/10.1088/1742-6596/718/6/062076).
- Taylor, A. M., I. Vovk, and A. Neronov (2011). Extragalactic magnetic fields constraints from simultaneous GeV–TeV observations of blazars. *Astronomy & Astrophysics*, **529**, p. A144. doi:[10.1051/0004-6361/201116441](https://doi.org/10.1051/0004-6361/201116441).
- Thaller, B. (2013). *The Dirac equation*. Springer Science & Business Media. ISBN 978-3-662-02753-0. doi:[10.1007/978-3-662-02753-0](https://doi.org/10.1007/978-3-662-02753-0). [orig. pub. 1992].
- Tiesinga, E., P. J. Mohr, D. B. Newell, and B. N. Taylor (2021). CODATA recommended values of the fundamental physical constants: 2018. *Rev. Mod. Phys.*, **93**(2), p. 025010. doi:[10.1103/RevModPhys.93.025010](https://doi.org/10.1103/RevModPhys.93.025010).
- Tsai, W. Y. and A. Yildiz (1971). Motion of charged particles in a homogeneous magnetic field. *Phys. Rev. D*, **4**, pp. 3643–3648. doi:[10.1103/PhysRevD.4.3643](https://doi.org/10.1103/PhysRevD.4.3643).
- Vachaspati, T. (2021). Progress on cosmological magnetic fields. *Rept. Prog. Phys.*, **84**(7), p. 074901. doi:[10.1088/1361-6633/ac03a9](https://doi.org/10.1088/1361-6633/ac03a9).
- Vaquera-Araujo, C. A., M. Napsuciale, and R. Angeles-Martinez (2013). Renormalization of the QED of Self-Interacting Second Order Spin 1/2 Fermions. *JHEP*, **01**, p. 011. doi:[10.1007/JHEP01\(2013\)011](https://doi.org/10.1007/JHEP01(2013)011).
- Vazza, F., M. Brüggen, C. Gheller, S. Hackstein, D. Wittor, and P. M. Hinz (2017). Simulations of extragalactic magnetic fields and of their observables. *Class. Quant. Grav.*, **34**(23), p. 234001. doi:[10.1088/1361-6382/aa8e60](https://doi.org/10.1088/1361-6382/aa8e60).
- Veltman, M. J. G. (1998). Two component theory and electron magnetic moment. *Acta Phys. Polon. B*, **29**, pp. 783–798. doi:[10.48550/arXiv.hep-th/9712216](https://arxiv.org/abs/hep-th/9712216). URL: <https://www.actaphys.uj.edu.pl/R/29/3/783/pdf>.

- Vernstrom, T., G. Heald, F. Vazza, T. J. Galvin, J. L. West, N. Locatelli, N. Fornengo, and E. Pinetti (2021). Discovery of magnetic fields along stacked cosmic filaments as revealed by radio and X-ray emission. *Monthly Notices of the Royal Astronomical Society*, **505**(3), pp. 4178–4196. doi:[10.1093/mnras/stab1301](https://doi.org/10.1093/mnras/stab1301).
- Vryonidou, E. and C. Zhang (2018). Dimension-six electroweak top-loop effects in Higgs production and decay. *JHEP*, **08**, p. 036. doi:[10.1007/JHEP08\(2018\)036](https://doi.org/10.1007/JHEP08(2018)036).
- Weinberg, S. (1972). *Gravitation and cosmology: principles and applications of the general theory of relativity*. John Wiley & Sons.
- Weinberg, S. (2005). *The Quantum theory of fields. Vol. 1: Foundations*. Cambridge University Press. ISBN 978-0-521-67053-1, 978-0-511-25204-4. doi:[10.1017/CBO9781139644167](https://doi.org/10.1017/CBO9781139644167).
- Weisskopf, V. (1936). *The electrodynamics of the vacuum based on the quantum theory of the electron*, p. 206–226. Cambridge University Press. doi:[10.1017/CBO9780511608223.018](https://doi.org/10.1017/CBO9780511608223.018). [translated and reprinted in 1994].
- Wolfenstein, L. (1978). Neutrino Oscillations in Matter. *Phys. Rev. D*, **17**, pp. 2369–2374. doi:[10.1103/PhysRevD.17.2369](https://doi.org/10.1103/PhysRevD.17.2369).
- Workman, R. L. et al. (2022). Review of Particle Physics. *PTEP*, **2022**, p. 083C01. doi:[10.1093/ptep/ptac097](https://doi.org/10.1093/ptep/ptac097).
- Xing, Z. Z. (2001). Commutators of lepton mass matrices, CP violation, and matter effects in-medium baseline neutrino experiments. *Phys. Rev. D*, **63**, p. 073012. doi:[10.1103/PhysRevD.63.073012](https://doi.org/10.1103/PhysRevD.63.073012).
- Xing, Z. Z. (2014). Neutrino Physics. In *1st Asia-Europe-Pacific School of High-Energy Physics*, pp. 177–217. doi:[10.5170/CERN-2014-001.177](https://doi.org/10.5170/CERN-2014-001.177).
- Yan, H., Z. Ma, C. Ling, C. Cheng, and J. Huang (2023). First Batch of $z \approx 11\text{--}20$ Candidate Objects Revealed by the James Webb Space Telescope Early Release Observations on SMACS 0723-73. *Astrophys. J. Lett.*, **942**(1), p. L9. doi:[10.3847/2041-8213/aca80c](https://doi.org/10.3847/2041-8213/aca80c).
- Yang, C. T., M. Formanek, A. Steinmetz, and J. Rafelski (2023). Decomposition of Fermi gas into zero and finite temperature distributions with examples. *In preparation*. [submitted to Int. Journal of Theor. Phys.].
- Zhang, C. (2012). *Effective field theory for top quark physics*. Ph.D. thesis, Illinois U., Urbana. URN/HDL: [2142/29627](https://hdl.handle.net/2142/29627).
- Zhang, C. and S. Willenbrock (2011). Effective-Field-Theory Approach to Top-Quark Production and Decay. *Phys. Rev. D*, **83**, p. 034006. doi:[10.1103/PhysRevD.83.034006](https://doi.org/10.1103/PhysRevD.83.034006).

APPENDIX A

Magnetic dipole moment in relativistic quantum mechanics

Steinmetz, A., Formanek, M. & Rafelski, J. Magnetic dipole moment in relativistic quantum mechanics. European Physical Journal A **55**, 40 (2019). [10.1140/epja/i2019-12715-5](https://doi.org/10.1140/epja/i2019-12715-5)

Copyright (2019) by Springer Nature. Reprinted with kind permission of The European Physical Journal (EPJ). Reprint permission for this thesis granted under License Agreement 5600921273203
License date: August 2nd, 2023.

Magnetic dipole moment in relativistic quantum mechanics

Andrew Steinmetz^a, Martin Formanek^b, and Johann Rafelski^c

Department of Physics, The University of Arizona, Tucson, AZ, 85721, USA

Received: 4 December 2018 / Revised: 27 January 2019

Published online: 26 March 2019

© Società Italiana di Fisica / Springer-Verlag GmbH Germany, part of Springer Nature, 2019

Communicated by T. Biro

Abstract. We investigate relativistic quantum mechanics (RQM) for particles with arbitrary magnetic moment. We compare two well known RQM models: a) Dirac equation supplemented with an incremental Pauli term (DP); b) Klein-Gordon equations with full Pauli EM dipole moment term (KGP). We compare exact solutions to the external field cases in the limit of weak and strong (critical) fields for: i) homogeneous magnetic field, and ii) the Coulomb $1/r$ -potential. For i) we consider the Landau energies and the Landau states as a function of the gyromagnetic factor (g -factor). For ii) we investigate contribution to the Lamb shift and the fine structure splitting. For both we address the limit of strong binding and show that these two formulations grossly disagree. We discuss possible experiments capable of distinguishing between KGP and DP models in laboratory. We describe the impact of our considerations in the astrophysical context (magnetars). We introduce novel RQM models of magnetic moments which can be further explored.

1 Introduction

1.1 Magnetic moment in QM

We have recently recognized [1] that an additional physical principle or guiding assumption is required to uniquely characterize relativistic *classical* particle dynamics with magnetic moment. In the current work we address the *quantum dynamics* non-uniqueness [2,3].

In the following we study relativistic Fermi particles with “anomalous” $a \neq 0$ gyromagnetic ratio g *i.e.* anomalous magnetic moment (AMM)

$$\mu = g \frac{e\hbar}{2mc} \frac{\sigma}{2} \equiv -g\mu_B \frac{\sigma}{2}, \quad a \equiv \frac{g}{2} - 1, \quad (1)$$

where μ_B is the Bohr magneton¹.

We address two different models of introducing anomalous magnetic moment in QM:

- a) the Dirac-Pauli (DP) first order equation which is the Dirac equation where g -factor is precisely fixed to the $g = 2$, with the addition of an incremental Pauli term; and
- b) the Klein-Gordon-Pauli (KGP) second order equation which “squares” the Dirac equation and thereafter allows the magnetic moment μ to vary independently of charge and mass, unlike Dirac theory.

These two approaches coincide when the anomaly a vanishes. However, all particles that have magnetic moments differ from the Dirac value $g = 2$, either due to their composite nature, or, for point particles, due to the quantum vacuum fluctuation effect.

We find that even a small magnetic anomaly has a large effect in the limit of strong fields generated by massive magnetar stars [4]. Therefore it is not clear that the tacit assumption of $g = 2$ in the case of strong fields [5–7] is allowed [8]. This argument is especially strong considering tightly bound composite particles such as protons and neutrons where the large anomalous magnetic moment can be taken as an external prescribed parameter unrelated to the elementary quantum vacuum fluctuations, and it is of particular interest to study the dynamical behavior of these particles in fields of magnetar strength. This interest carries over to the environment of strong fields created in focus of ultra-intense laser pulses and the associated particle production processes [9,10]. We consider also precision spectroscopic experiments and recognize consequences even in the weak coupling limit. We evaluate contributions for precision hydrogen muonic atom Lamb shift experiments [11].

All the above provides motivation for a closer analysis of how different methods of introducing anomalous magnetic moment to RQM lead to different physical predictions, which allows model elimination by comparison with experiment. While we will discuss consequences of the previously explored DP equation, the majority of the novel material in this paper will deal with the KGP equation which has received less attention in prior literature

and thus, for purpose of this work, most of the results need to be newly derived, except where noted otherwise.

One of the important outcomes of this work is the recognition of additional selection criteria for effective field theory (EFT) approaches offered by the presence of strong fields. In the weak field environment, both methods, KGP and DP, are suitable as EFT methods of dealing with magnetic moment. Our results show vital differences in the physical outcomes in presence of strong fields. We will argue that the DP version is not favored and that the KGP-EFT approach may need a further improvement. In our work we address solely point particles, thus challenges of Zemach moments [12] do not enter the present discussion.

The advantage of the KGP dynamics is that it incorporates both possible signs of the magnetic moment, irrespective of the sign of the electric charge, a choice that is lost in the DP single particle model. The magnetic moment sign choice is tacitly made when writing for the Dirac operator $\gamma \cdot p \pm m$; choosing minus sign in the mass term we choose the conventional magnetic moment sign, the other sign leads to opposite magnetic moment sign. The incorporation of both magnetic moment signs in fundamental equation for relativistic fermion dynamics doubles the number of degrees of freedom from usual 4 in the Dirac case to $2 \times 4 = 8$ in the KGP case.

Some may ask why the behavior of effective single particle model theories in the presence of strong external fields warrants our interest. A foundational motivation to offer the present study is that we believe it has never been settled which quantum theory description should be the basis for the development of the quantum field theory of matter and fields: for example Schwinger in the study of Euler-Heisenberg-Schwinger effective EM action [13] computes the vacuum fluctuations adopting as basis the KGP dynamics, followed by factor 1/2 to remove the magnetic moment sign degeneracy as both particles with positive and negative magnetic moment were allowed to fluctuate in the vacuum.

1.2 Outline

We introduce in quantitative fashion relativistic quantum equations with anomalous magnetic moment in sect. 2, presenting both DP (sect. 2.1) and KGP (sect. 2.2) equations. Relativistic covariance of both KGP and DP equations is addressed in sect. 2.3. In sect. 2.4 we discuss currents and the physical degrees of freedom inherent to the higher order formulation in sect. 2.5. This also allows us to comment on the procedure of canonical 2nd quantization, but the full treatment is beyond the scope of the present work.

We then turn in sect. 3 to study the case of a homogeneous magnetic field. We solve the KGP equation in sect. 3.1 and analyze the Landau levels using the ladder operator method in sect. 3.2. We show in sect. 3.3 that, like the nonrelativistic case, the Landau levels lose their degeneracy in the presence of an anomalous magnetic moment, but that this degeneracy is restored for certain values of the g -factor. We compare these results to the DP case in

sect. 3.4, relying on solutions available in literature [14]. We argue that DP solutions, which do not depend only on the magnetic moment of a particle but in an incoherent way also on anomaly, lack the required physical simplicity we see in the KGP case.

In sect. 4 we solve the KGP-Coulomb problem and report the exact energy levels along with the perturbative expansion showing the influence of the (anomalous) magnetic moment on the fine structure and Lamb shift which differ from the expressions obtained in Dirac ($g = 2$) or DP formulations. We evaluate the hydrogen and certain exotic atom effects, searching for an opportunity for further experimental insight in modern spectroscopic experiments.

Section 5 deals with the consequences of strong binding exhibited in critical high strength fields. The appropriateness of using the DP and KGP equations as effective theories is discussed in sect. 5.1. The case of extreme magnetic fields, such as those found in magnetars, is considered in sect. 5.2. Section 5.3 suggests an improved version of the KGP equation, which produces better strong field behavior. For critical binding of high- Z nuclei we compare in sect. 5.4 the analytic solutions of the KGP equation to the numerical solutions of DP presented by Thaller [15], and review another analysis done by Barut and Kraus [16,17]. Our findings are summarized in sect. 6 where we also discuss future research directions.

2 Relativistic equation with anomalous magnetic moment

2.1 Dirac-Pauli equation

The DP formulation is given by the Dirac equation with an additional Pauli term that is responsible for the anomalous moment

$$\left(\gamma^\mu (i\hbar c\partial_\mu - eA_\mu) - mc^2 - a \frac{e\hbar}{4mc} \sigma_{\mu\nu} F^{\mu\nu} \right) \psi = 0, \quad (2)$$

where

$$\sigma_{\mu\nu} = \frac{i}{2} [\gamma_\mu, \gamma_\nu], \quad (3)$$

is the spin tensor that is proportional to the commutator of the gamma matrices and $F^{\mu\nu}$ is the standard EM field tensor. Unless otherwise stated, all gamma matrices will be evaluated in the Dirac representation.

The last term in eq. (2), known as the Pauli term, represents a coupling of magnetic moment to electric and magnetic fields and evaluates to

$$\frac{1}{2} \sigma_{\mu\nu} F^{\mu\nu} = i\alpha \cdot \mathbf{E} - \boldsymbol{\Sigma} \cdot \mathbf{B}, \quad (4)$$

where we use the conventions

$$\boldsymbol{\alpha} = \gamma^0 \boldsymbol{\gamma}, \quad \boldsymbol{\Sigma} = \gamma^5 \boldsymbol{\alpha}, \quad \gamma_5 = i\gamma_0 \gamma_1 \gamma_2 \gamma_3, \quad \gamma_5^2 = 1. \quad (5)$$

Equation (2) in the non-relativistic limit incorporates the Hamiltonian term

$$\hat{H}_{\text{AMM}} = -a \frac{e\hbar}{2mc} \boldsymbol{\sigma} \cdot \mathbf{B}, \quad (6)$$

^a e-mail: ajsteinmetz@email.arizona.edu

^b e-mail: martinformanek@email.arizona.edu

^c e-mail: rafelski@physics.arizona.edu

¹ We will use the conventions of negative electric charge $e = -|e|$ and Gaussian units throughout.

which is the energy due to an anomalous magnetic moment. One refers here to the Shrödinger-Pauli (SP) equation.

The popularity of eq. (2) is due to its close connection to the Dirac equation. Moreover, DP allows for small anomalous moments perturbative exploration of any problem which has known Dirac equation solutions. The disadvantages are also known:

- 1) The total magnetic moment is obscured having been split into an explicit anomalous contribution; and the implicit contribution buried in the spinor structure of the DP equation. This is not surprising given the *ad-hoc* nature of introducing anomalous magnetic moment in this way.
- 2) This formulation is barred from being the basis for a well behaved quantum field perturbative treatment; the interaction Lagrangian, which produces the anomalous moment,

$$\mathcal{L}_{AMM} = -a \frac{e\hbar}{4mc} \bar{\psi} \sigma_{\mu\nu} \psi F^{\mu\nu}, \quad (7)$$

is non renormalizable [18] as the coupling coefficient has natural units of length.

2.2 Klein-Gordon-Pauli equation

The KGP equation, unlike the Dirac or its DP extension, is second order in derivatives

$$\left((ihc\partial_\mu - eA_\mu)^2 - m^2 c^4 - \frac{g}{2} \frac{e\hbar c}{2} \sigma^{\mu\nu} F_{\mu\nu} \right) \Psi = 0. \quad (8)$$

For $g = 2$ one finds eq. (8) by first considering the Dirac equation

$$\mathfrak{D}_+ \psi = (\gamma^\mu (ihc\partial_\mu - eA_\mu) - mc^2) \psi = 0. \quad (9)$$

The operator \mathfrak{D}_+ is considered to be the “positive mass” operator which vanishes on a wave function with positive mass eigenstate. We can then “square” eq. (9) by introducing the substitution

$$\psi \rightarrow \mathfrak{D}_- \Psi, \quad (10)$$

$$\mathfrak{D}_- = (\gamma^\mu (ihc\partial_\mu - eA_\mu) + mc^2), \quad (11)$$

into eq. (9), yielding

$$\mathfrak{D}_+ \mathfrak{D}_- \Psi = 0, \quad (12)$$

where \mathfrak{D}_- is the corresponding negative mass operator. This operator is related to the traditional positive mass operator via chiral operator γ^5 conjugation

$$\mathfrak{D}_- = -\gamma^5 \mathfrak{D}_+ \gamma^5, \quad [\mathfrak{D}_+, \mathfrak{D}_-] = 0. \quad (13)$$

We should point out that the substitution eq. (10) requires some coefficient of proportionality to preserve the required units, which will be discussed further in sect. 2.4

when normalizing states of Ψ . Making use of the commutation and anti-commutation relations of the gamma matrices, it is easy to verify that eq. (12) is the KGP eq. (8) for $g = 2$.

The KGP formulation was introduced by Fock [19] (however, with $g = 2$) and subsequently studied by Feynman and Gell-Mann [20], Brown [2], in the context of weak interactions. This interest is motivated by the observation that all operators in the wave equation eq. (8) commute with γ^5 therefore all eigenfunctions are good chiral eigenstates.

On first sight parity seems to be violated by the Pauli term, since it does not commute with γ^0 . However, the parity of EM fields is opposite, and this behavior assures that actual solutions are also parity eigenfunctions. This is seen more explicitly by writing eq. (4) in the format

$$\frac{1}{2} \sigma^{\mu\nu} F_{\mu\nu} = \boldsymbol{\sigma} \cdot (i\gamma^5 \mathbf{E} - \mathbf{B}). \quad (14)$$

The presence in eq. (8) of a single (Pauli) term which contains the entire spin and thus magnetic moment behavior of the particle makes the separation of charge and magnetic dipole moment more natural. By allowing the g -factor to vary to any value we are able to introduce the anomalous magnetic moment in the context of a second order equation.

The price we pay in the KGP case is losing the connection to the first order Dirac equation and the simple conjugation properties of eq. (13). In other words, it is no longer obvious how to convert back to a first order equation without considering some other line of thought. Equation (8) takes on the form of an inhomogeneous Klein-Gordon equation acting on a four-spinor field.

We can show that eq. (8) is mathematically distinct from eq. (2) by attempting to “square” eq. (2), which produces cross terms between momentum and the Pauli term which are absent in eq. (8). Efforts have also been made exploring KGP as the basis of a quantum field theory and its renormalization [21,22]. KGP has also found use as an effective field theory providing a description of the Compton scattering of low energy protons [23].

It is of relevance to always remember that the KGP equation remains a 4-spinor equation. We can introduce two 2-spinors which will be of immediate use when we normalize the KGP solutions we will study. Specifically, the stationary wave function $\Psi_E(\mathbf{x})$ can be cast into the format

$$\Psi_E = \begin{pmatrix} \chi_E^s \\ \phi_E^s \end{pmatrix}. \quad (15)$$

Here both χ_E^s and ϕ_E^s are two-component spinors. For completeness let us restate the stationary form of KGP equation in this notation

$$\begin{pmatrix} K_{KG} + s_g \cdot \mathbf{B} & -is_g \cdot \mathbf{E} \\ -is_g \cdot \mathbf{E} & K_{KG} + s_g \cdot \mathbf{B} \end{pmatrix} \begin{pmatrix} \chi_E^s \\ \phi_E^s \end{pmatrix} = 0, \quad (16)$$

where we introduced

$$K_{KG} \equiv (E - eV)^2 - (ihc\nabla - e\mathbf{A})^2 - m^2 c^4, \quad (17)$$

$$s_g \equiv gec \frac{\hbar\sigma}{2}. \quad (18)$$

This form, eq. (16), shows explicitly that the Coulomb problem involves the full 4-spinor dynamics, while the magnetic field problem naturally separates into upper and lower components.

It is possible to prediagonalize and separate the 4-spinor format into two 2-spinor equations, which is Feynman's preferred form [20]. First we break Ψ into upper and lower components as seen in eq. (16) allowing the rewriting of the KGP equation as a set of two coupled equations for χ_E^s, ϕ_E^s . Then we add and subtract the two equations yielding

$$0 = \left((ihc\partial_\mu - eA_\mu)^2 - m^2 c^4 + s_g \cdot \mathbf{F}_\pm \right) (\chi_E^s \mp \phi_E^s), \quad (19)$$

with

$$\mathbf{F}_\pm = \mathbf{B} \pm i\mathbf{E}. \quad (20)$$

The above procedure is equivalent to expressing the KGP equation in the Weyl or chiral representation. This turns out to complicate the understanding of what particle (and antiparticle) solutions are and we will not use this further in our work.

2.3 Relativistic covariance

A well studied ingredient to relativistic quantum mechanics is the symmetry of the equations under Lorentz transformation for boosts and rotations (Poincaré symmetry) by including translations and discrete transformations. More specifically we require that wave equations are a) equivalent when written in another reference frame and b) there exists a prescription of how to relate the equations between the two frames RF and RF' . For the Dirac equation this procedure is well-known and will be repeated for completeness. The Dirac equation in the primed frame RF' is

$$(\gamma^\mu (ihc\partial'_\mu - eA'_\mu) - mc^2) \psi' = 0. \quad (21)$$

We note that the gamma matrices will be unchanged during transformation and that four-vectors transform as

$$\gamma'^\mu = \gamma^\mu, \quad A'^\mu = a^\mu_\nu A^\nu, \quad (22)$$

where a^μ_ν are the set of matrices which facilitate the transformations. The primed wave function ψ' must be related to ψ linearly through some matrix S

$$\psi' = S\psi, \quad (23)$$

which is determined by the structure of Lorentz transformations. For eq. (21) to be equivalent to eq. (9), the matrix S must satisfy

$$S^{-1} \gamma^\mu S = a^\mu_\nu \gamma^\nu. \quad (24)$$

Using the method of infinitesimal transformations

$$a_\mu^\nu = \delta_\mu^\nu + \epsilon_\mu^\nu, \quad \epsilon_{\mu\nu} = -\epsilon_{\nu\mu}, \quad S = 1 + S_{inf.}, \quad (25)$$

for arbitrary boosts or rotations S has the form

$$S = \exp \left(-\frac{i}{4} \sigma^{\mu\nu} \epsilon_{\mu\nu} \right). \quad (26)$$

For the KGP equation, the procedure is similar. We will rewrite eq. (8) as

$$(\hbar^2 c^2 h_{\mu\nu} \nabla_A^\mu \nabla_A^\nu + m^2 c^4) \Psi = 0, \quad (27a)$$

$$h_{\mu\nu} = g_{\mu\nu} - i \frac{g}{2} \sigma_{\mu\nu}, \quad \nabla_A^\mu = \partial^\mu + \frac{ie}{\hbar c} A^\mu, \quad (27b)$$

where ∇_A^μ is the gauge covariant derivative. The tensor $h_{\mu\nu}$ can be interpreted as an extended metric tensor. In the frame RF' , eq. (27a) is

$$(\hbar^2 c^2 h'_{\mu\nu} \nabla_A^\mu \nabla_A^\nu + m^2 c^4) \Psi' = 0. \quad (28)$$

As the tensor $h_{\mu\nu}$ is made up of commutators and anti-commutators of γ^μ , it is unchanged. If we again require that the wave function Ψ transforms linearly then

$$h'_{\mu\nu} = h_{\mu\nu}, \quad \Psi' = M\Psi. \quad (29)$$

For the KGP equation to be relativistically covariant then the matrix M must satisfy

$$M^{-1} h_{\mu\nu} M = a_\mu^\alpha a_\nu^\beta h_{\alpha\beta}. \quad (30)$$

Since the metric tensor is unchanged by this transformation, the above equation reduces to

$$M^{-1} \sigma_{\mu\nu} M = a_\mu^\alpha a_\nu^\beta \sigma_{\alpha\beta}. \quad (31)$$

The g -factor which appears in the tensor $h_{\mu\nu}$ vanishes in eq. (31) which means that g -factor does not effect the Lorentz (or Poincaré) covariance of the KGP equation. Therefore magnetic moment does not modify Poincaré symmetry. Without difficulty we can also rewrite eq. (31) using products of eq. (24), which means that

$$S = M. \quad (32)$$

Alternatively this result can be obtained by considering the infinitesimal transformations and making use of the commutator $[\sigma^{\mu\nu}, \sigma^{\alpha\beta}]$. The DP equation also is covariant due to eq. (32).

2.4 Conserved currents

Before continuing to the Coulomb 1/r-potential problem which is one of the cases studied in this work we consider how solutions to the KGP equation are to be normalized, asking if the spin structure interferes in some manner. An appropriate Lagrangian that describes the equation of motion in eq. (8) is given by [23]

$$\mathcal{L} = \hbar^2 c^2 \left(\nabla_A^\mu \bar{\Psi} \right) h_{\mu\nu} \left(\nabla_A^\nu \Psi \right) - m^2 c^4 \bar{\Psi} \Psi. \quad (33)$$

We note that the field Ψ must have units [length]⁻¹, which differs from the Dirac or DP ψ fields, which have units of [length]^{-3/2}.

The conserved current can then be expressed as

$$\begin{aligned} \mathcal{J}^\mu &= -\frac{\partial \mathcal{L}}{\partial c\hbar c_A \mu} \equiv \mathcal{J}_{\text{Conv}}^\mu + \mathcal{J}_{\text{Mag}}^\mu \\ &= i\bar{\Psi}(\nabla_A^\mu\Psi) - i\left(\nabla_A^{\mu\dagger}\bar{\Psi}\right)\Psi \\ &\quad + \frac{g}{2}\bar{\Psi}\sigma^\mu\left(\nabla_A^\beta\Psi\right) - \frac{g}{2}\left(\nabla_A^{\beta\dagger}\bar{\Psi}\right)\sigma_\beta^\mu\Psi. \end{aligned} \quad (34)$$

The conserved current eq. (34) can be interpreted as the sum of a convection current $\mathcal{J}_{\text{Conv}}$ and magnetization current \mathcal{J}_{Mag} . This is nearly identical to the familiar Gordon Decomposition of the Dirac current, with the exception that the magnetization current is proportional to the g -factor; the only other difference being that the Ψ and ψ fields have different units and therefore differ in constants in front of the current terms.

$$\mathcal{J}_{\text{Conv}}^\mu = i\bar{\Psi}(\nabla_A^\mu\Psi) - i\left(\nabla_A^{\mu\dagger}\bar{\Psi}\right)\Psi, \quad (35a)$$

$$\mathcal{J}_{\text{Mag}}^\mu = -\frac{g}{2}\partial_\beta\left(\bar{\Psi}\sigma^\beta\Psi\right). \quad (35b)$$

The magnetic current eq. (35b) is given by the divergence of the spin density, and by antisymmetry of $\sigma^{\beta\mu}$ it is conserved. Since the total current \mathcal{J}^μ eq. (34) is conserved, $\mathcal{J}_{\text{Conv}}^\mu$ eq. (35a) is also conserved.

2.5 Physical degrees of freedom

The case $g = 2$ arises from the product of two covariant Dirac equations differing in sign of m , see eq. (12). Thus in the set of KGP solutions we obtain contains not four but eight types of basis solutions. Aside of spin ($2x$) and charge (= particle-antiparticle) ($2x$), we now also have magnetic moment sign ($2x$). This is so since in the non-relativistic reduction the sign of m in the Dirac equation is found in the magnetic moment $\mu \propto g/(\pm m)$. Using the techniques pioneered by Feshbach and Villars [24], the KGP equation can be explicitly separated into an 8-component equation [25, 26] (these authors restrict themselves to $g = 2$) showing the large space the KGP equation occupies when compared to the Dirac equation.

This feature of the KGP equation is desirable since it allows us to pick the opposite sign of magnetic moment for particles doublets such as proton and neutron without inventing a new dynamical equation. We do not see a reason why this interpretation of the doubling of the number of degrees of freedom cannot be maintained for $g \neq 2$.

Like in the Dirac and similarly the KG equations, one must wisely choose the basic states that now belong to a relatively large eight degrees of freedom. We take the convective current as the base for the normalization of eigenstates that in the non-relativistic limit become the solutions of the Pauli equation. The normalization reduces therefore to

$$N = 2 \int d\mathbf{x}^3 \bar{\Psi}_E(E - eV)\Psi_E. \quad (36)$$

In the KGP case we have second non-positivity originating in the spinor character of the wave function Ψ_E . Inserting eq. (15) into eq. (36)

$$N = 2 \int d\mathbf{x}^3 \left(\chi_E^{+s}(E - eV)\chi_E^s - \phi_E^{+s}(E - eV)\phi_E^s \right). \quad (37)$$

Unlike the case of the KG equation we are dealing with a spinor equation and we need to set up the meaning of eq. (36) so that particle interpretation is possible. Here we note that KGP normalization combines challenges seen in both Dirac and Klein-Gordon cousins.

The norm eq. (37) is not positive definite since:

- Like in KG equation the coefficient $E - eV$ in eq. (36) can be positive and negative, for the plane wave solutions the norm follows the sign of E , and there are both positive and negative energy solutions. In the KG-Boson case one associates this sign with the charge of the Bose-(anti)particle considered.
- In reduction of the spinor eq. (36) to componentwise eq. (37) we recognize the additional sign depending on which component dominates; this is reminiscent of the Dirac equation solution.

- A third minus sign arises considering the choice of creation of particles and antiparticles sets in the quantum Fermi field operator

$$\hat{\Psi} = \sum_{+} \hat{b}_+\psi_+ + \sum_{-} \hat{d}_-^\dagger\psi_-, \quad E_+ > 0, \quad E_- < 0, \quad (38)$$

where like in the Dirac case we assign the negative energy solutions (for weak fields) to be the antiparticle states associated with a creation operator. The sign arises since in bilinear forms we need to commute

$$d_j d_i^\dagger = -d_i^\dagger d_j + \delta_{ij}, \quad (39)$$

so that $d_j|0\rangle = 0$ in matrix elements.

All together we have $2^3 = 8$ different cases corresponding to 8 degrees of freedom of the KGP equation as we noted earlier.

A complete discussion of this matter reaches beyond our objective for a comparative study of solutions of DP and KGP. However, we do want to remark that in order to compensate the additional sign of E in the norm not present in the Dirac equation, we must assign the antiparticle character to the lower two components of the KGP spinor; that is, to the ϕ_E^s in eq. (37). The canonical quantization procedure is now implemented as follows: the conjugate momentum Π_Ψ to the KGP field Ψ from

$$\Pi_\Psi \equiv \frac{\delta I}{\delta \dot{\Psi}} = \hbar^2 c \nabla_A^{\dagger 0} \bar{\Psi} - \hbar^2 c \frac{g}{2} \nabla_A^\dagger \bar{\Psi} \cdot \boldsymbol{\alpha}, \quad (40)$$

where I is the action and we demand

$$\{\Pi_\Psi(\mathbf{x}', t), \Psi(\mathbf{x}, t)\} = i\hbar \delta^3(\mathbf{x} - \mathbf{x}'), \quad (41)$$

which requires a full set of all 8 different (real) solutions of KGP equations to form a completeness relation implicit in eq. (41). The charge operator

$$Q = -\frac{ie}{2\hbar} [\Pi_\Psi(\mathbf{x}', t), \Psi(\mathbf{x}, t)] \quad (42)$$

is organized to count antiparticle states with opposite sign of charge compared to particles.

3 Homogeneous magnetic fields

The simplest situation involving magnetism is the behavior of a particle under the influence of a homogeneous magnetic field

$$\mathbf{B} = B\hat{z}, \quad (43)$$

where the magnetic field is chosen to point in the z -direction. Therefore, it is an excellent probe of magnetic moment dynamics. The energy levels of charged particles in such fields are known as Landau levels. In nonrelativistic quantum mechanics with magnetic moment the energy levels are given by

$$E^{NR} = \frac{p_z^2}{2m} + \frac{e\hbar B}{mc} \left(n + \frac{1}{2} - \frac{g}{2}s \right), \quad (44)$$

where the principle quantum number has the values $n = 0, 1, 2, \dots$ and $s = \pm 1/2$ describes whether the magnetic moment is aligned or anti-aligned with the magnetic field. For the case of $g = 2$, it is common to define the Landau level quantum number

$$\lambda_L = n + \frac{1}{2} - s, \quad (45)$$

which has values $\lambda_L = 0, 1, 2, \dots$. As long as there is no anomalous moment, all the Landau levels except the ground state $\lambda_L = 0$ are double degenerate as there are two combinations of principle quantum number and spin orientation which can produce any given Landau level.

This degeneracy is broken by the introduction of an anomalous $g \neq 2$ moment

$$E^{NR} = \frac{p_z^2}{2m'} + \frac{e\hbar B}{mc} (\lambda_L - as). \quad (46)$$

This breaking of degeneracy is shared in the relativistic DP and KGP formulations of this problem, but how that breaking occurs differs between them and will be explored in sect. 3.5.

3.1 The KGP-Landau problem

We see in eq. (16) that the problem separates into 2-spinor dynamics. To solve for the homogeneous magnetic fields in the KGP case we must choose an appropriate gauge. The two most common are the Landau and symmetric gauges,

$$\mathbf{A}_L = B(0, x, 0)^T, \quad \mathbf{A}_S = \frac{B}{2}(-y, x, 0)^T, \quad (47)$$

respectively. We will choose the symmetric gauge which benefits from preserving rotational symmetry.

Solving for χ the KGP, eq. (8) for homogeneous magnetic fields then becomes

$$\left(\left(i\hbar \frac{\partial}{\partial t} \right)^2 - \left(i\hbar c \frac{\partial}{\partial x} - e \frac{B}{2} y \right)^2 - \left(i\hbar c \frac{\partial}{\partial y} + e \frac{B}{2} x \right)^2 \right.$$

$$\left. - \left(i\hbar c \frac{\partial}{\partial z} \right)^2 - m^2 c^4 + \frac{g}{2} e \hbar c \boldsymbol{\sigma} \cdot \mathbf{B} \right) \chi = 0. \quad (48)$$

Considering only energy eigenstates and recognizing that $\mathbf{p} = -i\hbar \nabla$ is the momentum operator and $L_z = xp_y - yp_x$ is the z -component of angular momentum, eq. (48) reduces to

$$\begin{aligned} &\left(E^2 - m^2 c^4 - p^2 c^2 + e L_z c B \right. \\ &\quad \left. - \frac{1}{4} e^2 B^2 (x^2 + y^2) + \frac{g}{2} e \hbar c \boldsymbol{\sigma} \cdot \mathbf{B} \right) \chi = 0. \end{aligned} \quad (49)$$

Using the substitutions

$$E \rightarrow m'c^2, \quad \frac{E^2 - m^2 c^4}{2E} \rightarrow E', \quad (50)$$

we arrive at the Schrödinger-style Hamiltonian equation

$$E' \chi = \left(\frac{p_z^2}{2m'} + \frac{e^2 B^2}{8m' c^2} (x^2 + y^2) - \frac{e}{2m' c} (\mathbf{L} + g\mathbf{S}) \cdot B \hat{z} \right) \chi, \quad (51)$$

with the spin operator defined as $\mathbf{S} = \frac{\hbar}{2}\boldsymbol{\sigma}$. The Hamiltonian in eq. (51) consists of three separate systems whose operators mutually commute

$$H_{\text{Total}} = H_{\text{HO}} + H_{\text{free}} + H_{\text{Mag}}. \quad (52)$$

We introduce the cyclotron frequency

$$\omega_c = eB/m'c. \quad (53)$$

The three terms are:

- the harmonic oscillator (HO) with characteristic angular frequency $\omega_c = 2\omega$

$$H_{\text{HO}} = \frac{p_x^2}{2m'} + \frac{p_y^2}{2m'} + \frac{1}{2}m'\omega^2(x^2 + y^2), \quad (54a)$$

- the free particle Hamiltonian in the z -direction

$$H_{\text{free}} = \frac{p_z^2}{2m'}, \quad (54b)$$

- and the magnetic interaction

$$H_{\text{Mag.}} = -\frac{e}{2m'c} (\mathbf{L} + g\mathbf{S}) \cdot B \hat{z}. \quad (54c)$$

The magnetic interaction eq. (54c) is of a familiar form that describes Zeeman splitting including its dependence on the g -factor. Because any operator in one Hamiltonian mutually commutes will all operators of the other two Hamiltonians in eqs. (54a), (54b), (54c), e.g. $[H, L_z] = 0$, their energy eigenvalues simply add together.

3.2 Ladder operators

The Cartesian basis in eq. (54a) is undesirable because the z -direction angular momentum quantum number ℓ_z is dependent on the n_x and n_y HO quantum numbers. It is not too troublesome to disentangle the HO quantum numbers when rewriting the Hamiltonian eq. (54a) in terms of ladder operators.

First, however, we move into an auxiliary basis by introducing complex position and momentum variables

$$\begin{aligned} w &= \frac{1}{\sqrt{2}}(x - iy), & w^\dagger &= \frac{1}{\sqrt{2}}(x + iy), \\ p_w &= \frac{1}{\sqrt{2}}(p_x + ip_y), & p_w^\dagger &= \frac{1}{\sqrt{2}}(p_x - ip_y), \end{aligned} \quad (55)$$

which have the nonzero commutation properties

$$[w, p_w] = i\hbar. \quad (56)$$

Using the above, the HO Hamiltonian eq. (54a) now can be written

$$H_{\text{HO}} = \frac{p_w^\dagger p_w}{m'} + m' \omega^2 w^\dagger w. \quad (57)$$

We then introduce the ladder operators

$$\begin{aligned} a &= \frac{1}{\sqrt{2}}(\beta w + ip_w^\dagger/\beta\hbar), & b &= \frac{1}{\sqrt{2}}(\beta w^\dagger + ip_w/\beta\hbar), \\ a^\dagger &= \frac{1}{\sqrt{2}}(\beta w^\dagger - ip_w/\beta\hbar), & b^\dagger &= \frac{1}{\sqrt{2}}(\beta w - ip_w^\dagger/\beta\hbar), \\ \beta &= \sqrt{m'\omega/\hbar}, \end{aligned} \quad (58)$$

with nonzero commutation properties

$$[a, a^\dagger] = [b, b^\dagger] = 1. \quad (59)$$

This converts eq. (57) into

$$H_{\text{HO}} = \hbar\omega(a^\dagger a + b^\dagger b + 1). \quad (60)$$

The benefit of all this labor is that L_z can be expressed in terms of these ladder operators

$$L_z = \hbar(a^\dagger a - b^\dagger b), \quad (61)$$

which transforms the HO eq. (54a) and magnetic eq. (54c) Hamiltonians into

$$\begin{aligned} H_{\text{HO}} + H_{\text{Mag}} &= \hbar\omega(a^\dagger a + b^\dagger b + 1) \\ -\hbar\omega(a^\dagger a - b^\dagger b) - g\omega S_z &= \hbar\omega(2b^\dagger b + 1) - g\omega S_z. \end{aligned} \quad (62)$$

This formulation depends only on one pair of ladder operators as determined by the right or left handed nature of the mutually orthogonal \hat{x} , \hat{y} , and \hat{B} unit vectors; in this case we have chosen the right handed convention. The energy eigenvalues of eq. (62) are

$$\begin{aligned} E_{\text{HO}} + E_{\text{Mag}} &= \hbar\omega(2n + 1 - gs) \\ &= \hbar\omega_c \left(n + \frac{1}{2} - \frac{g}{2}s \right). \end{aligned} \quad (63)$$

The Hamiltonian eq. (54a) can be used to determine the operator equations of motion via $d\mathcal{O}/dt = i[H, \mathcal{O}]/\hbar$ yielding the relevant quantities

$$m' \frac{dw}{dt} = i\sqrt{2}\hbar\beta b^\dagger = \pi_w, \quad (64a)$$

$$\frac{d\pi_w}{dt} = -2\omega\sqrt{2}\hbar\beta b^\dagger = 2i\omega\pi_w, \quad (64b)$$

where π_w is understood to be the kinetic momentum in the complex auxiliary variables. The above two equations combined yield the constant of motion

$$w_0 = w - \pi_w/2im'\omega = x_0 - iy_0. \quad (65)$$

This constant of motion corresponds to the center of the particle's orbit and represents an infinite degeneracy of the system in the xy -plane [27].

The wave function χ is then a two spinor X_s of the form

$$\chi = X_s \frac{1}{\sqrt{n!}}(a^\dagger)^n \chi_0, \quad S_z X_s = s\hbar X_s,$$

$$\chi_0 = (\beta/\pi)^{1/4} f(w) \exp \left[ip_z z/\hbar - \frac{1}{2}\beta^2 w^\dagger w \right], \quad (66)$$

where the ground state wave function χ_0 was arrived at by solving $b\chi_0 = 0$ and $f(w)$ is an arbitrary function that depends on the states χ being an eigenstate of some combination of eq. (65). The normalization of eq. (66) depends on the form of $|f(w)|^2$, eq. (37), and the sign of the energy. Now we can finally return to the full Hamiltonian eq. (52); its eigenvalues rewritten using the ladder operator basis eq. (58) are

$$E' = \frac{p_z^2}{2m'} + \frac{e\hbar B}{m'c} \left(n + \frac{1}{2} - \frac{g}{2}s \right), \quad (67)$$

which depends on the principle quantum number with values $n = 0, 1, 2, \dots$ and the already defined spin orientation numbers. The physical relativistic energies can be obtained by undoing the substitutions in eq. (50) yielding from eq. (67)

$$E^2 = m^2 c^4 + p_z^2 c^2 + 2e\hbar c B \left(n + \frac{1}{2} - \frac{g}{2}s \right), \quad (68a)$$

$$E = \pm \sqrt{m^2 c^4 + p_z^2 c^2 + 2e\hbar c B \left(n + \frac{1}{2} - \frac{g}{2}s \right)}. \quad (68b)$$

This expression for the relativistic Landau levels is the same [27, 28] as found for the Landau levels for the Dirac equation setting $g = 2$ in eq. (68b).

3.3 Nonrelativistic energies

Restricting ourselves to the positive energy spectrum, the nonrelativistic reduction of eq. (68b) can be carried out in

the large mass limit yielding

$$\begin{aligned} E &= mc^2 + \frac{p_z^2}{2m} + 2\mu_B B(\lambda_L - as) - \frac{p_z^4}{8m^3 c^2} \\ &\quad - \frac{p_z^2}{2m} \frac{2\mu_B B}{mc^2}(\lambda_L - as) - \frac{2\mu_B^2 B^2}{mc^2}(\lambda_L - as)^2 + \mathcal{O}(1/m^5), \end{aligned} \quad (69)$$

which contains the expected terms such as the nonrelativistic kinetic energy in the z -direction, the first relativistic correction to kinetic energy, the Landau energies, and cross terms that behave like modifications to the mass of the particle.

3.4 The DP Landau problem

The Landau levels for the DP equation are known [14]. They are given by

$$E_{DP}^2 = \left(\sqrt{m^2 c^4 + 2e\hbar c B \lambda_L} - \frac{eB\hbar}{2mc}(g-2)s \right)^2 + p_z^2 c^2, \quad (70a)$$

$$E_{DP} = \pm \sqrt{\left(\sqrt{m^2 c^4 + 2e\hbar c B \lambda_L} - \frac{eB\hbar}{2mc}(g-2)s \right)^2 + p_z^2 c^2}, \quad (70b)$$

which in our opinion fails Dirac's principle of mathematical beauty when compared to the KGP result eq. (68b). While both eqs. (68b) and (70b) have the correct nonrelativistic reduction at the lowest order to eq. (44), the latter obscures the physical interpretation. The most egregious issue with the DP-Landau levels is that, in a perturbative expansion, it includes cross terms between the $g = 2$ magnetic moment and anomalous terms in $a = (g-2)/2$; thus the result does not depend on the particle magnetic moment alone; there is a functional dependence on the magnetic anomaly a . The presence of these cross terms implies that above first order the results cannot be given in terms of the full magnetic moment alone. In contrast, for the KGP-Landau levels, eq. (70b), the entire effect of magnetic moment is contained in a single term. Thus Dirac's beauty principle favors heavily the KGP.

3.5 State degeneracy

The KGP-Landau and DP-Landau levels above the ground state lose their (accidental) degeneracy for $g \neq 2$ as we reported below eq. (46). This is shown schematically in fig. 1. The anomaly also causes the ground state to be pushed downward, such that $E^2 < m^2$; if the anomaly and the magnetic field are large enough, states above the ground state are also pushed below the rest mass energy of the particle.

However, in the KGP eq. (68b) we recognize a periodicity considering the energy as a function of g . We recall that in eq. (68b) $n = 0, 1, 2, \dots$ As g varies, each time $gs/2$

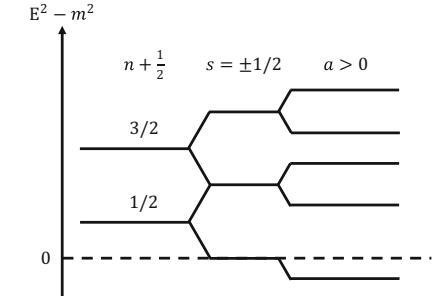


Fig. 1. Diagram of KGP-Landau levels for particles with zero z -component momentum.

crosses an integer value, for a different value of n the energy eigenvalue E repeat as a function of changing g . All possible values of energy E are reached (at fixed m and p_z^2) for $-2 \leq g \leq 2$. Moreover, while for almost all $g \neq 2$ the degeneracy is completely broken, this periodicity implies that energy degeneracy is restored for values [29]

$$g_k/2 = 1 + k, \quad \lambda'_L = \lambda_L - ks, \quad (71)$$

where $k = 0, \pm 1, \pm 2, \dots$ The Landau levels eq. (68a) contain an infinite number of degenerate levels bounded from below. Certain states change the sign of the magnetic energy and their total energies become unphysical in the limit that $g_k B$ becomes large; for even k there are $k/2$ such states and for odd k there are $(k+1)/2$.

4 Hydrogen-like atoms

The hydrogen-like atom provides us a spectroscopic standard candle and one generally explores novel and interesting behavior by comparing against the known Hydrogen-like Dirac spectrum. The Dirac Coulomb solutions are found in many textbooks. The DP case has been discussed extensively by Thaller in ref. [15] and we compare with these results. What is missing in literature is a solution of the KGP equation, which we accomplish analytically for the Coulomb potential

$$V_C \equiv eA^0 = \frac{Z\alpha\hbar c}{r}, \quad \mathbf{A} = \mathbf{0}. \quad (72)$$

Here α , when not a vector, denotes the fine structure constant and Z is the integer-charge (in units of $|e|$) of the nucleus.

4.1 The KGP-Coulomb problem

We consider stationary energy states $\Psi = e^{-iEt/\hbar}\Psi_E$ and express the derivatives in eq. (8) in spherical coordinates

yielding the differential equation

$$\left(\frac{E^2 - m^2 c^4}{\hbar^2 c^2} + \frac{Z^2 \alpha^2}{r^2} + \frac{2E Z \alpha}{\hbar c r} + \frac{1}{r} \frac{\partial^2}{\partial r^2} r - \frac{L^2 / \hbar^2}{r^2} - \frac{g}{2} \frac{e}{2 \hbar c} \sigma_{\mu\nu} F^{\mu\nu} \right) \Psi_E = 0. \quad (73)$$

Here we used

$$(-ih\nabla)^2 \Psi = -\frac{\hbar^2}{r} \frac{\partial^2}{\partial r^2} (r\Psi) + \frac{L^2}{r^2} \Psi, \quad (74)$$

where L^2 is the orbital angular momentum (squared) operator.

In the laboratory frame the Coulomb field is a pure electrical field without an accompanying magnetic field; therefore the Pauli term only depends on electric field and reduces to

$$-\frac{g}{2} \frac{e}{2 \hbar c} \sigma_{\mu\nu} F^{\mu\nu} = -\frac{g}{2} Z \alpha \frac{i\alpha \cdot \hat{r}}{r^2}. \quad (75)$$

It is helpful to introduce Dirac's spin alignment operator

$$\mathcal{K} = \gamma^0 \left(1 + \boldsymbol{\Sigma} \cdot \frac{\mathbf{L}}{\hbar} \right), \quad (76)$$

which determines if the spin and orbital angular momentum are aligned or anti-aligned and allows us to write the angular momentum squared operator as

$$L^2/\hbar^2 = \mathcal{K} (\mathcal{K} - \gamma^0). \quad (77)$$

The operator \mathcal{K} commutes with $\alpha \cdot \hat{r}$ and its eigenvalues are given as either positive or negative integers $\kappa = \pm(j+1/2) = \pm 1, \pm 2, \dots$, where j is the total angular momentum quantum number. Following the convention of Rose [30] the operator \mathcal{K} (which shares eigenstates with J^2) is written as

$$\mathcal{K}|j, \kappa\rangle = -\kappa|j, \kappa\rangle, \quad (78)$$

where $\kappa < 0$ are parallel states of $j = \ell + 1/2$ while $\kappa > 0$ are anti-parallel states of $j = \ell - 1/2$ with $\ell \geq 1$.

Equation (73) can then be written as

$$0 = \left(\frac{E^2 - m^2 c^4}{\hbar^2 c^2} + \frac{2E Z \alpha}{\hbar c r} + \frac{1}{r} \frac{\partial^2}{\partial r^2} r - \frac{\mathcal{K}(\mathcal{K} - \gamma^0) - Z^2 \alpha^2 - \frac{g}{2} Z \alpha (i\alpha \cdot \hat{r})}{r^2} \right) \Psi_E. \quad (79)$$

As expected, in relativistic quantum mechanics, the angular momentum eigenvalues must take on non-integer values which in the limit of classical mechanics corresponds to orbits which do not close [31]. This "effective" angular momentum depends explicitly on g -factor. The difficulty of this equation is that the effective angular momentum operator is non-diagonal in spinor space due to the presence of $\alpha \cdot \hat{r}$ which mixes upper and lower components.

Following the procedure of Martin and Glauber [32], and Biedenharn [33] we introduce the operator

$$\mathfrak{L} = -\gamma^0 \mathcal{K} - \frac{g}{2} Z \alpha (i\alpha \cdot \hat{r}), \quad (80)$$

but with the novel modification that g -factor directly appears in the second term. This operator commutes with the spin-alignment operator \mathcal{K} and has eigenvalues

$$A = \pm \sqrt{\kappa^2 - \frac{g^2}{4} Z^2 \alpha^2}, \quad (81)$$

where the absolute values are denoted as $\lambda = |A|$. The numerator of the last term in eq. (79) can be then replaced by

$$\mathcal{K}(\mathcal{K} - \gamma^0) - Z^2 \alpha^2 - \frac{g}{2} Z \alpha (i\alpha \cdot \hat{r}) = \mathfrak{L}(\mathfrak{L} + 1) + \left(\frac{g^2}{4} - 1 \right) Z^2 \alpha^2. \quad (82)$$

If the g -factor is taken to be $g = 2$, then the differential eq. (79) reverts to the one discussed in Martin and Glauber's work [32]. The coefficient $g^2/4 - 1$ will be commonly seen to precede new more complicated terms, which conveniently vanish for $|g| = 2$ demonstrating that as function of g there is a "cusp" [29] for $|g| = 2$. This will become especially evident when we discuss strongly bound systems in sect. 5, which behave very differently for $|g| < 2$ versus $|g| > 2$.

Eigenstates of both \mathfrak{L} and E then satisfy

$$\left(\frac{E^2 - m^2 c^4}{\hbar^2 c^2} + \frac{2E Z \alpha}{\hbar c r} + \frac{1}{r} \frac{\partial^2}{\partial r^2} r - \frac{\lambda(\lambda \pm 1) + (g^2/4 - 1) Z^2 \alpha^2}{r^2} \right) \Psi_E^{\pm\lambda} = 0, \quad (83)$$

which is diagonal having removed the odd matrix operator in eq. (79) but at a cost of doubling the number of solutions introducing both $\pm\lambda$ spectra.

It is helpful to introduce dimensionless radial variable ρ and associated quantities

$$\rho = Ar, \quad A = 2 \frac{\sqrt{m^2 c^4 - E^2}}{\hbar c}, \quad B = \frac{2Z\alpha E}{\hbar c A}. \quad (84)$$

The wave function Ψ is separable into a product of radial and angular functions. We will return to the angular wave functions in sect. 4.2. The radial wave function can be substituted with $\Psi \propto U/r$ allowing us to rewrite eq. (83) as

$$\left(\frac{\partial^2}{\partial \rho^2} - \frac{1}{4} + \frac{B}{\rho} - \frac{\lambda(\lambda \pm 1) + (g^2/4 - 1) Z^2 \alpha^2}{\rho^2} \right) U_E^{\pm\lambda} = 0. \quad (85)$$

The radial wave function, obtained by taking both the $\rho \rightarrow 0$ and $\rho \rightarrow \infty$ limits of eq. (85), is given by

$$U_E^{\pm\lambda} = N' \rho^{1/2+\nu} \exp[-\rho/2] F(\rho), \quad (86a)$$

$$\nu = \sqrt{(\lambda \pm 1/2)^2 + \left(\frac{g^2}{4} - 1 \right) Z^2 \alpha^2}. \quad (86b)$$

While the general mathematical solution allows both positive and negative ν , only positive values will reproduce the KG-Coulomb or Dirac-Coulomb spectrum for appropriate values of g -factor, therefore at this time we will only assume positive values. The other solutions are too singular and cannot be normalized. The radial normalization is then

$$1 = 2 \int_0^\infty (E - V_C) |U_E^{\pm\lambda}|^2 d\rho. \quad (87)$$

The orthogonality of the angular components of matrix elements are considered separately.

The series $F(\rho)$ is the confluent hypergeometric function

$$F(\rho) = 1 + \frac{a}{c} \rho + \frac{a(a+1)}{c(c+1)} \frac{\rho^2}{2} + \dots, \quad a = \nu + 1/2 - B, \quad c = 2\nu + 1, \quad (88)$$

truncated at the term $a+n_r=0$ to satisfy eq. (85), where n_r is the node quantum number which takes on the values $n_r = 0, 1, 2, \dots$. The energy levels of the KGP-Coulomb equation are then

$$E_{\pm\lambda}^{n_r, j} = \frac{mc^2}{\sqrt{1 + \frac{Z^2 \alpha^2}{(n_r+1/2+\nu)^2}}}, \quad (89a)$$

$$\nu = \sqrt{(\lambda \pm 1/2)^2 + \left(\frac{g^2}{4} - 1 \right) Z^2 \alpha^2}, \quad (89b)$$

$$\lambda = \sqrt{(j+1/2)^2 - \frac{g^2}{4} Z^2 \alpha^2}. \quad (89c)$$

Equation (89a) is the same "Sommerfeld-style" expression for energy that we can obtain from the Dirac or KG equations. The difference between them arises from the expression of the relativistic angular momentum which depends on g -factor for the KGP equation. The KGP eigenvalues eq. (89a) were also obtained by Niederle and Nikitin [34] using a tensor-spinorial approach for arbitrary half-integer spin particles.

4.2 Angular functions

The spherical part of the wave function is given by $\Omega_{\mathfrak{L}}^{\mathcal{K}, J_z}$, which are orthonormal spherical eigenspinors of the operators \mathfrak{L} , \mathcal{K} , J^2 , and J_z . More detailed information for the angular solutions can be found in Martin and Glauber [32]. To define the angular part it is first useful to define angular eigenstates of good parity (eigenstates of γ^0), being also eigenstates of \mathcal{K} , J^2 , and J_z operators

$$\gamma^0 \Omega_{\pm}^{\kappa, j_z} = \pm \Omega_{\pm}^{\kappa, j_z}, \quad (90)$$

which can be written as a

$$\Omega_{\pm}^{\kappa, j_z} = \sqrt{\frac{j+z}{2j}} Y_{j-1/2}^{\pm 1/2} X_{\pm}^+ + \sqrt{\frac{j-z}{2j}} Y_{j-1/2}^{\pm 1/2} X_{\pm}^-, \quad (91)$$

for states where parity and spin orientation eigenvalues have opposite signs $\text{sgn}(\langle \gamma^0 \rangle) = -\text{sgn}(\langle \mathcal{K} \rangle)$ and

$$\Omega_{\pm}^{\kappa, j_z} = \sqrt{\frac{j-z+1}{2j+2}} Y_{j+1/2}^{j_z-1/2} X_{\pm}^+ - \sqrt{\frac{j+z+1}{2j+2}} Y_{j+1/2}^{j_z+1/2} X_{\pm}^-, \quad (92)$$

for states where parity and spin orientation have the same sign $\text{sgn}(\langle \gamma^0 \rangle) = \text{sgn}(\langle \mathcal{K} \rangle)$.

The Y_{ℓ}^m are the traditional orthonormal spherical harmonics and X_{\pm}^{\pm} are eigenspinors of Σ_z and γ^0 with

$$\Sigma_z X_{\pm}^{\pm} = \pm X_{\pm}^{\pm}, \quad \gamma^0 X_{\pm}^{\pm} = \pm X_{\pm}. \quad (93)$$

Because γ^0 and the parity operator γ^0 do not commute, the states $\Omega_{\pm}^{\mathcal{K}, J_z}$ are then linear combinations of eq. (91) and eq. (92) given by projecting the good parity states onto states of good \mathcal{K} via

$$\Omega_{\pm\lambda}^{\kappa < 0, j_z} = \frac{\lambda \pm \mathfrak{L}}{2\lambda} \Omega_{\mp}^{\kappa < 0, j_z}, \quad \Omega_{\pm\lambda}^{\kappa > 0, j_z} = \frac{\lambda \pm \mathfrak{L}}{2\lambda} \Omega_{\pm}^{\kappa > 0, j_z}. \quad (94)$$

The overall wave function including the radial part eq. (86a) is then

$$\Psi = N'_{n_r, \pm\lambda} \rho^{\nu-1/2} \exp[-\rho/2] F(\rho) \Omega_{\pm\lambda}^{\kappa, j_z}. \quad (95)$$

4.3 Dirac and Klein-Gordon spectrum

Because we are treating g -factor as an unbounded parameter we need to verify that the Dirac and Klein-Gordon energy spectra, which can be found in most texts, see for example Baym [31] and Itzykson and Zuber [35], emerges from the appropriate limit of g -factor. In the limit $g \rightarrow 2$ for the Dirac case the expressions for λ and ν reduce to

$$\lim_{g \rightarrow 2} \lambda = \sqrt{(j+1/2)^2 - Z^2 \alpha^2}, \quad (96a)$$

$$\lim_{g \rightarrow 2} \nu_{\pm\lambda} = \lambda \pm 1/2. \quad (96b)$$

This procedure requires taking the root of perfect squares; therefore, the sign information is lost in eq. (96a). As long as $Z^2 \alpha^2 < 3/4$ we can drop the absolute value notation as ν is always positive. The energy is then given by

$$E_{\pm\lambda}^{n_r, j} = \frac{mc^2}{\sqrt{1 + \frac{Z^2 \alpha^2}{(n_r+1/2+\nu)^2}}}. \quad (97)$$

The \pm notation is read as the upper value corresponding to the $+\lambda$ states and the lower value corresponding to the $-\lambda$ states.

The ground state energy (with: $n_r = 0$, $\Lambda < 0$, $j = 1/2$) is therefore

$$E_{-\lambda(j=1/2)}^{0,1/2} = mc^2 \sqrt{1 - Z^2 \alpha^2}, \quad (98)$$

as expected for the Dirac-Coulomb ground state. Equation (97) reproduces the Dirac-Coulomb energies and also

contains a degeneracy between states of opposite λ sign, same j quantum number and node quantum numbers offset by one

$$E_{-\lambda}^{n_r+1,j} = E_{+\lambda}^{n_r,j}, \quad (99)$$

which will see in sect. 4.4 corresponds to the degeneracy between $2S_{1/2}$ and $2P_{1/2}$ states. There is no degeneracy for the $E_{-\lambda}^{0,j}$ states.

In the limit that $g \rightarrow 0$, which is the KG case, the expressions are given by

$$\lim_{g \rightarrow 0} \lambda = j + 1/2, \quad (100a)$$

$$\lim_{g \rightarrow 0} \nu_{\pm\lambda} = \sqrt{(j+1)^2 - Z^2\alpha^2}, \quad (100b)$$

which reproduces the correct expressions for the energy levels for the Klein-Gordon case

$$E_{\pm\lambda}^{n_r,j} = \frac{mc^2}{\sqrt{1 + \frac{Z^2\alpha^2}{(n_r+1/2 + \sqrt{(j+1)^2 - Z^2\alpha^2})^2}}}, \quad (101)$$

except that in this limit we are still considering the total angular momentum quantum number j rather than orbital momentum quantum number ℓ . It is interesting to note that the KG-Coulomb problem's energy formula contains $\ell + 1/2$, which matches identically to our half-integer j values; therefore, this artifact of spin, untethered and invisible by the lack of magnetic moment, does not alter the energies of the states. The degeneracy in energy levels are given by

$$E_{-\lambda}^{n_r,j+1} = E_{+\lambda}^{n_r,j}, \quad (102)$$

with levels of opposite λ sign, same node quantum number and shifted j values by one. In a similar fashion to the Dirac case, here we have no degeneracy for $E_{-\lambda}^{n_r,1/2}$ states. In sect. 4.4 we will convert from n_r , j and $\pm\lambda$ to the familiar quantum numbers of n , j and ℓ allowing for easy comparison with the hydrogen spectrum in standard notation.

4.4 Nonrelativistic limit for energies

The first regime of interest to understand the effect of variable g in the KGP-Coulomb problem is the nonrelativistic limit characterized by the weak binding of low-Z atoms. This will allow us to compare directly with the Schrödinger hydrogen-like atom energies. We start by expanding eq. (89a) in powers of $Z\alpha$ to compare to the known hydrogen spectrum.

To order $\mathcal{O}(Z^4\alpha^4)$ the energy levels are given by

$$\begin{aligned} \frac{E_{\pm\lambda}^{n_r,j}}{mc^2} &= 1 - \frac{1}{2} \frac{Z^2\alpha^2}{(n_r + 1/2 + (\nu_{\pm\lambda})|_{Z=0})^2} \\ &+ \frac{(\nu_{\pm\lambda})'|_{Z=0} Z^3\alpha^3}{(n_r + 1/2 + (\nu_{\pm\lambda})|_{Z=0})^3} \\ &+ \frac{1}{2} \frac{(3/4 - 3(\nu_{\pm\lambda})|_{Z=0}^2) Z^4\alpha^4}{(n_r + 1/2 + (\nu_{\pm\lambda})|_{Z=0})^4} \\ &+ \frac{1}{2} \frac{(\nu_{\pm\lambda})''|_{Z=0} Z^4\alpha^4}{(n_r + 1/2 + (\nu_{\pm\lambda})|_{Z=0})^3} + \mathcal{O}(Z^6\alpha^6), \end{aligned} \quad (103)$$

where primed $\nu_{\pm\lambda}$ indicate derivatives with respect to $Z\alpha$. These derivatives evaluate to

$$\begin{aligned} (\nu_{\pm\lambda})|_{Z=0} &= j + 1/2 \pm 1/2, \\ (\nu_{\pm\lambda})'|_{Z=0} &= 0, \\ (\nu_{\pm\lambda})''|_{Z=0} &= \frac{(g^2/4 - 1)}{j + 1/2 \pm 1/2} - \frac{g^2/4}{j + 1/2}. \end{aligned} \quad (104)$$

Equation (103) then simplifies to

$$\begin{aligned} \frac{E_{\pm\lambda}^{n_r,j}}{mc^2} &= 1 - \frac{1}{2} \frac{Z^2\alpha^2}{(n_r + j + 3/2)^2} \\ &+ \frac{3}{8} \frac{Z^4\alpha^4}{(n_r + j + 3/2)^4} \\ &+ \frac{1}{2} \left(\frac{(g^2/4 - 1)}{j + 1/2} - \frac{g^2/4}{j + 1/2} \right) \frac{Z^4\alpha^4}{(n_r + j + 3/2)^3} \\ &+ \mathcal{O}(Z^6\alpha^6). \end{aligned} \quad (105)$$

In the non relativistic limit, the node quantum number corresponds to the principle quantum number via $n_r = n' - j - 1/2$ with $n' = 1, 2, 3, \dots$. Using eqs. (105) and (80) we see that in the non relativistic limit $+\lambda$ corresponds to $\kappa > 0$ or anti-aligned spin-angular momentum with $j = \ell - 1/2$ and $\ell \geq 1$. Conversely $-\lambda$ corresponds to $\kappa < 0$ or aligned spin-angular momentum with $j = \ell + 1/2$.

With all this input we arrive at

$$\begin{aligned} \frac{E_{\kappa<0}^{n_r,j}}{mc^2} &= 1 - \frac{1}{2} \frac{Z^2\alpha^2}{(n'+1)^2} + \frac{3}{8} \frac{Z^4\alpha^4}{(n'+1)^4} \\ &+ \frac{1}{2} \frac{(g^2/4 - 1)}{j+1} \frac{Z^4\alpha^4}{(n'+1)^3} \\ &- \frac{1}{2} \frac{g^2/4}{j+1/2} \frac{Z^4\alpha^4}{(n'+1)^3} + \mathcal{O}(Z^6\alpha^6). \end{aligned} \quad (106)$$

Lastly we recast, for the $\kappa > 0$ states, the principle quantum number as $n' + 1 \rightarrow n$ with $n \geq 2$ and we simply relabel $n' \rightarrow n$ for $\kappa < 0$ states. This allows eq. (106) to

be completely written in terms of n , j , and ℓ as

$$\begin{aligned} \frac{E_{\ell}^{n,j}}{mc^2} &= 1 - \frac{1}{2} \frac{Z^2\alpha^2}{n^2} + \frac{3}{8} \frac{Z^4\alpha^4}{n^4} \\ &+ \frac{1}{2} \frac{(g^2/4 - 1)}{\ell + 1/2} \frac{Z^4\alpha^4}{n^3} \\ &- \frac{1}{2} \frac{g^2/4}{j + 1/2} \frac{Z^4\alpha^4}{n^3} + \mathcal{O}(Z^6\alpha^6), \end{aligned} \quad (107)$$

where it is understood that $n - \ell \geq 1$, this condition allows us to write what was previously described in eq. (106) as two distinct spectra now as a single energy spectra. In the limit $g \rightarrow 2$ or $g \rightarrow 0$ the correct expansion to order $Z^4\alpha^4$ of the Dirac or KG energies are obtained. In the following we explore some consequences of our principal nonrelativistic result, eq. (107).

4.5 Lamb shift

The breaking of degeneracy in eq. (107) between states of differing ℓ orbital quantum number, but the same total angular momentum j and principle quantum number n is responsible for the Lamb shift due to anomalous magnetic moment. The only term in eq. (107) (up to order $Z^4\alpha^4$) that breaks the degeneracy between the $E_{\ell=j+1/2}^{n,j}$ and $E_{\ell=j-1/2}^{n,j}$ states for $n \geq 2$ is the fourth term. This is unsurprising as it depends exclusively on quantum number ℓ and n . The lowest order Lamb shift due to anomalous magnetic moment is then

$$\begin{aligned} \frac{\Delta E_{\text{gLamb}}^{2S_{1/2}-2P_{1/2}}}{mc^2} &= E_{\ell=j-1/2}^{n,j} - E_{\ell=j+1/2}^{n,j} \\ &= (g^2/8 - 1/2) \left(\frac{1}{j} - \frac{1}{j+1} \right) \frac{Z^4\alpha^4}{n^3}. \end{aligned} \quad (108)$$

For the $2S_{1/2}$ and $2P_{1/2}$ states eq. (108) reduces to

$$\begin{aligned} \frac{\Delta E_{\text{gLamb}}^{2S_{1/2}-2P_{1/2}}}{mc^2} &= (g^2/8 - 1/2) \frac{Z^4\alpha^4}{6} \\ &= (a + a^2/2) \frac{Z^4\alpha^4}{6}. \end{aligned} \quad (109)$$

Our result in eqs. (108) and (109) is sensitive to $g^2/8 - 1/2 = a + a^2/2$. Traditionally the Lamb shift due to an anomalous lepton magnetic moment is obtained perturbatively [35] by considering the DP equation which is sensitive to $g/2 - 1 = a$ the shift takes on the expression at lowest order

$$\begin{aligned} \frac{\Delta E_{\text{gLamb,DP}}^{2S_{1/2}-2P_{1/2}}}{mc^2} &= \left(\frac{g-2}{2} \right) \frac{Z^4\alpha^4}{6} \\ &= a \frac{Z^4\alpha^4}{6}. \end{aligned} \quad (110)$$

It is of experimental interest to resolve this discrepancy between the first order DP equation and the second order

fermion formulation KGP. We recall the present day values

$$a_e = 1159.65218091(26) \times 10^{-6} \simeq \frac{\alpha}{2\pi}, \quad (111a)$$

$$a_\mu - a_e = 6.2687(6) \times 10^{-6}. \quad (111b)$$

The largest contribution to the anomalous moment for charged leptons is, as indicated the lowest order QED Schwinger result $a = \alpha/2\pi$. For the KGP approach, the anomalous g -factor mixes contributions of different powers of fine structure α . Precision values for the fundamental constants are taken from [36]. For the $2S_{1/2}-2P_{1/2}$ states, the shift is

$$\frac{\Delta E_{\text{gLamb}}^{2S_{1/2}-2P_{1/2}}}{mc^2} = \frac{Z^4\alpha^5}{12\pi} + \frac{Z^4\alpha^6}{48\pi^2}. \quad (112)$$

The scale of the discrepancy between KGP and DP for the hydrogen atom is then

$$\begin{aligned} \Delta E_{\text{gLamb,KGP}}^{2S_{1/2}-2P_{1/2}} - \Delta E_{\text{gLamb,DP}}^{2S_{1/2}-2P_{1/2}} &= \frac{\alpha^6 mc^2}{48\pi^2} \\ &= 1.62881214 \times 10^{-10} \text{ eV} = 39.3845030 \text{ kHz}, \end{aligned} \quad (113)$$

without taking into account the standard corrections such as reduced mass, recoil, radiative, or finite nuclear size; for more information on those corrections please refer to [36–39]. It is to be understood that the corrections presented here are illustrative of the effect magnetic moment has on the spectroscopic levels, but that further work is required to compare these to experiment: for example we look here on behavior of point particles only.

While the discrepancy is small for the hydrogen system, it is ≈ 40 kHz and will be visible in this or next generation's spectroscopic experiments. The discrepancy is also non-negligible for hydrogen-like exotics such as proton-antiproton because the proton g -factor is much larger

$$g_p = 5.585694702(17), \quad a_p = 1.792847351(9). \quad (114)$$

The discrepancy for the proton-antiproton system is

$$\Delta E_{\text{gLamb,KGP}}^{2S_{1/2}-2P_{1/2}} - \Delta E_{\text{gLamb,DP}}^{2S_{1/2}-2P_{1/2}} = 0.71268151 \text{ eV}. \quad (115)$$

The Lamb shift is of interest to the muonic-hydrogen system as is used to measure the proton charge radius $R_p^{\mu\text{LS}}$. Experimentally, the exotic atom study yields [11]

$$R_p^{\mu\text{LS}} = 0.84087(39) \text{ fm}, \quad (116)$$

which is 4% off the CODATA value for the proton charge radius R_p^{COD}

$$R_p^{\text{COD}} = 0.8775(51) \text{ fm}, \quad (117)$$

a discrepancy of 7 sigma. In terms of the Lamb shift, assuming the CODATA value, this corresponds to an unexplained additional shift of approximately 0.31 meV. The modification to the μP Lamb shift due to the KGP equation for muonic-hydrogen, the KGP-DP discrepancy is

$$\Delta E_{\text{gLamb,KGP}}^{2S_{1/2}-2P_{1/2}} - \Delta E_{\text{gLamb,DP}}^{2S_{1/2}-2P_{1/2}} = 3.394064 \times 10^{-8} \text{ eV}, \quad (118)$$

which is too small to explain the result of Pohl *et al.* [11].

However, this does not disqualify the possible magnetic moment involvement in this discrepancy: the magnetic moment coupling via KGP equation should be considered in the study of scattering cross section of electrons on protons which is a decisive input into the CODATA proton radius value. Moreover, we see effects related to other relativistic forms of magnetic moment interaction which can modify the muonic Lamb shift. We return to these questions at the end of this work.

4.6 Fine structure

The fifth term in eq. (107), which depends on j and n , will shift the levels due to an anomalous moment, but does not contribute to the Lamb shift. Rather this expression, which contains the spin-orbit $\mathbf{L} \cdot \mathbf{S}$ coupling, is responsible for the fine structure splittings. From eq. (107) the fine structure splitting is given by

$$\frac{\Delta E_{\text{gFS}}^{n,\ell}}{mc^2} = E_\ell^{n,j=\ell+1/2} - E_\ell^{n,j=\ell-1/2} = (g^2/8) \left(\frac{1}{\ell} - \frac{1}{\ell+1} \right) \frac{Z^4 \alpha^4}{n^3}. \quad (119)$$

The splitting between the $2P_{3/2}$ and $2P_{1/2}$ states is therefore

$$\frac{\Delta E_{\text{gFS}}^{2P_{3/2}-2P_{1/2}}}{mc^2} = (g^2/8) \frac{Z^4 \alpha^4}{16} = (1/2 + a + a^2/2) \frac{Z^4 \alpha^4}{16}. \quad (120)$$

In comparison the fine structure dependence on g -factor in the DP equation is given as

$$\frac{\Delta E_{\text{gFS,DP}}^{2P_{3/2}-2P_{1/2}}}{mc^2} = \left(\frac{g-1}{2} \right) \frac{Z^4 \alpha^4}{16} = (1/2 + a) \frac{Z^4 \alpha^4}{16}. \quad (121)$$

Just as in the case of the Lamb shift, we find that the KGP and DP equations disagree for fine structure splitting. For the hydrogen atom this discrepancy is

$$\Delta E_{\text{gFS,KGP}}^{2P_{3/2}-2P_{1/2}} - \Delta E_{\text{gFS,DP}}^{2P_{3/2}-2P_{1/2}} = \frac{\alpha^6 mc^2}{128\pi^2} = 6.10804553 \times 10^{-11} \text{ eV} = 14.7691885 \text{ kHz}, \quad (122)$$

and for proton-antiproton, the fine structure splitting discrepancy is

$$\Delta E_{\text{gFS,KGP}}^{2P_{3/2}-2P_{1/2}} - \Delta E_{\text{gFS,DP}}^{2P_{3/2}-2P_{1/2}} = 0.26725557 \text{ eV}. \quad (123)$$

For fine structure of the muonic-hydrogen system, the KGP-DP discrepancy is

$$\Delta E_{\text{gFS,KGP}}^{2S_{1/2}-2P_{1/2}} - \Delta E_{\text{gFS,DP}}^{2S_{1/2}-2P_{1/2}} = 1.272774 \times 10^{-8} \text{ eV}. \quad (124)$$

We can make a general observation that non minimal magnetic coupling, such as we have studied in the DP and KGP cases, enlarge energy level splittings. The above shows that these discrepancies will remain when calculating within more realistic finite nuclear size context.

5 Critical binding

5.1 Applicability of DP or KGP to critical fields

Care must be taken when interpreting the results presented in sect. 3. For physical electrons the AMM interaction is the result of vacuum fluctuations whose strength also depends on the strength of the field. For example in the large magnetic field limit a QED computation shows that the ground state is instead of eq. (70b) given by [40]

$$E_0 \approx mc^2 + \frac{\alpha}{4\pi} mc^2 \ln^2 \left(\frac{2ehB}{m^2 c^3} \right) \quad (125)$$

which even for enormous magnetic fields does not deviate significantly from the rest mass-energy of the electron. Further the AMM radiative corrections approach zero for higher Landau levels [41]. Therefore the AMM in the case of electrons does not have a significant effect in highly magnetized environments such as those found in astrophysics (magnetars).

The situation is different for composite particles such as the proton, neutron and light nuclei whose anomalous magnetic moments are dominated by their internal structure and not by vacuum fluctuations. In this situation we expect that the AMM interaction in high magnetic fields remains significant. Therefore, asking whether the DP or KGP equations better describes the dynamics of composite hadrons and atomic nuclei in presence of magnetar strength fields is a relevant question despite the standard choice in literature being the DP equation [42]. The same question can be asked for certain exotic hydrogen-like atoms where the constituent particles have anomalous moments which can be characterized as an external parameter.

5.2 Homogeneous magnetic fields

As noted in sect. 3.2 the magnetic moment anomaly can flip the sign of the magnetic energy for the least excited states causing the gap between particle and antiparticle states to decrease with magnetic field strength. Setting $p_z = 0$ in eq. (68a), we show in fig. 2 that the energy of the lowest KGP Landau eigenstate $n = 0, s = 1/2$ reaches zero where the gap between particle and antiparticle states vanishes for the field

$$B_{\text{crit}}^e = \frac{B_S^e}{a_e} = 861 B_S^e = 3.8006 \times 10^{16} \text{ G}, \quad (126a)$$

$$B_{\text{crit}}^p = \frac{B_S^p}{a_p} = \frac{1}{1.79} B_S^p = 8.3138 \times 10^{19} \text{ G}, \quad (126b)$$

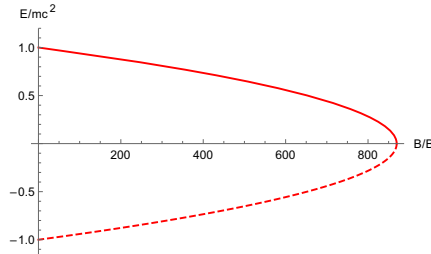


Fig. 2. The $n = 0, s = 1/2$ ground state for a KGP electron given by eq. (68b) with $g/2 - 1 = \alpha/2\pi$ in a homogeneous magnetic field. We consider the particle with no z -direction momentum. The particle state (solid red) and antiparticle (dashed red) are presented.

where B_S is the so-called Schwinger critical field [13].

$$B_S^e \equiv \frac{m_e^2 c^3}{e\hbar} = \frac{m_e c^2}{2\mu_B} = 4.4141 \times 10^{13} \text{ G}, \quad (127a)$$

$$B_S^p \equiv \frac{m_p^2 c^3}{e\hbar} = \frac{m_p c^2}{2\mu_N} = 1.4882 \times 10^{20} \text{ G}. \quad (127b)$$

The numerical results are evaluated for the anomalous moment of the electron and proton, given by eqs. (111a) and (114). At the critical field strength B_{crit} the Hamiltonian loses self-adjointness and the KGP loses its predictive properties. The Schwinger critical field eq. (127a) denotes the boundary when electrodynamics is expected to behave in an intrinsically nonlinear fashion, and the equivalent electric field configurations become unstable [43]. However, it is also possible that the vacuum is stabilized by such strong magnetic fields [8].

The critical magnetic fields as shown in eq. (126a) appear in discussion of magnetars [4]. The magnetar field is expected to be more than 100-fold that of the Schwinger critical magnetic field which is on the same order of magnitude as B_{crit} for an electron. While the critical field for a proton exceeds that of a magnetar, the dynamics of protons (and neutrons) in such fields is nevertheless significantly modified. A correct description of magnetic moment therefore has relevant consequences to astrophysics.

Figure 3 shows analogous reduction in particle/antiparticle energy gap for the DP equation. In this case the vanishing point happens at a larger magnetic field strength. This time the solutions continue past this point, but require allowing the states to cross into the opposite continua which we consider unphysical. We are not satisfied with either model's behavior though the KGP description is preferable for reasons stated earlier in sect. 3. However, it is undesirable that both KGP and DP solutions loose physical meaning and vacuum stability in strong magnetic fields.

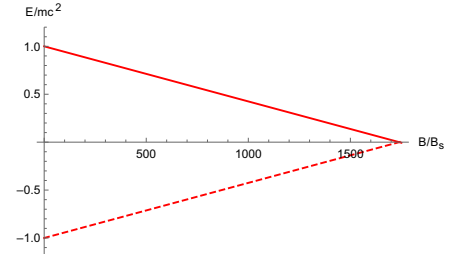


Fig. 3. The $n = 0, s = 1/2$ ground state for a DP electron given by eq. (70b) with $g/2 - 1 = \alpha/2\pi$ in a homogeneous magnetic field. We consider the particle with no z -direction momentum. The particle state (solid red) and antiparticle (dashed red) are presented.

5.3 Extension to the KGP equation

We have seen that at a sufficiently strong magnetic field an unexpected instability can occur in the presence of magnetic field alone. Of interest is a further extension capable of restoring the stability of the system. We show that such an improvement of the KGP equation is possible. This opens a new research direction which is beyond the scope of this work. However, it is so easy to show how this works that we cannot resist the temptation. The approach is based on noting a self-evident relationship between magnetic moment and mass.

The constituent equation, which we will refer to as the Improved-KGP or IKGP, takes the form

$$\left(ihc\partial_\mu - eA_\mu \right)^2 - \left(mc^2 + \frac{g}{4}\mu_B \sigma^{\mu\nu} F_{\mu\nu} \right)^2 \Psi = 0. \quad (128)$$

We introduce

$$\tilde{m} = m + \frac{g}{4} \frac{\mu_B}{c^2} \sigma^{\mu\nu} F_{\mu\nu}, \quad (129)$$

as an effective magnetic mass which is off-diagonal in spinor-space in the Dirac representation. IKGP differs from the KGP by the presence of the additional interaction term

$$\delta V \equiv \left(\frac{g}{2} \mu_B \right)^2 \left(\frac{1}{2} \sigma^{\mu\nu} F_{\mu\nu} \right)^2, \quad (130)$$

which is proportional to the square of the magnetic moment

$$\left(\frac{1}{2} \sigma^{\mu\nu} F_{\mu\nu} \right)^2 = 2(\mathcal{S} + \gamma^5 \mathcal{P}), \quad (131)$$

where the invariants of the EM field are defined as

$$\mathcal{S} = \frac{1}{2}(B^2 - E^2), \quad \mathcal{P} = \mathbf{E} \cdot \mathbf{B}. \quad (132)$$

This modification can be thought of as “completing the square” of KGP.

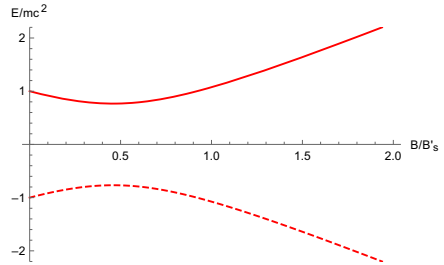


Fig. 4. The $n = 0$, $s = 1/2$ ground state for a KGP proton given by eq. (133) with $g = 5.58$ in a homogeneous magnetic field. The magnetic minimum is well visible for particles with larger anomalous moment such as proton. We consider the particle with no z -direction momentum. The particle state (solid red) and antiparticle (dashed red) are presented. The magnetic field scale is $B'_S = (m_p^2/m_e^2)B_S$.

For the homogeneous magnetic field the IKGP equation can be solved in much the same way as the KGP equation in sect. 3. One obtains eigenvalues noting a simple shift that occurs in view of eq. (130) which predicts a shift of m^2 quadratic in the magnetic field. The resulting energy levels are

$$E = \pm \sqrt{m^2 c^4 + \left(\frac{g}{2} \mu_B\right)^2 B^2 + 2e\hbar c B \left(n + \frac{1}{2} - \frac{g}{2}s\right)}. \quad (133)$$

An interesting feature is that in the ultra-high magnetic fields ($B \gg B_S$), eq. (133) approximates

$$E \approx \frac{g}{2} \mu_B B, \quad (134)$$

which is not dissimilar to the non-relativistic case where the magnetic energy is simply proportional to the magnetic field.

The most striking feature is that the ground state remains physical for all values of magnetic field when an anomalous moment is included and the self-adjointness of the system is not lost for some critical magnetic field strength. It can be then thought that the magnetic field provides a stabilizing influence on the system. Rather, there exists a “magnetic minimum” located for $n = 0$, $s = 1/2$ at

$$B_{\min} = \frac{4mc^2}{g^2 \mu_B}, \quad (135)$$

which for an electron is

$$B_{\min}^e = \frac{8a_e}{g_e^2} B_S = 1.02126 \times 10^{11} \text{ G}. \quad (136)$$

We are in particular interested in the environment of the magnetar stars. We thus evaluate using eq. (114) the minimum for a proton

$$B_{\min}^p = \frac{8a_p}{g_p^2} \frac{m_p^2}{m_e^2} B_S = 6.841 \times 10^{19} \text{ G}, \quad (137)$$

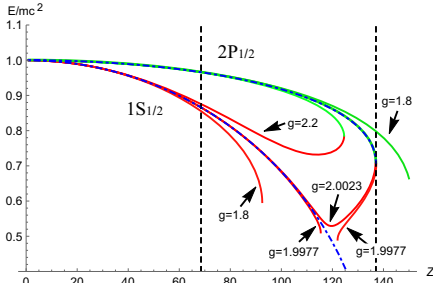


Fig. 5. The KGP $1S_{1/2}$ (lower red curves) and $2P_{1/2}$ (upper green curves) energy levels for g -factor values $g = \{1.8, 1.9977, 2.0023, 2.2\}$ are shown for large Z hydrogen-like atoms. The curves for the Dirac $g = 2$ case for (lower dashed blue) $1S_{1/2}$ and (upper dashed blue) $2P_{1/2}$ are also presented.

which can be seen in fig. 4. Here it is understood that for the calculation of the proton's magnetic minimum, the nuclear mass and magneton was used rather than the electron Bohr magneton. For large enough g -factor, excited states may also contain a minimum, but for any nonzero anomalous moment the ground state always does.

5.4 The Coulomb problem

For the case of $g = 2$ hydrogen-like systems with large Z nuclei, there is extensive background related to the long study of the solutions of the Dirac equation [5–7]. For $g \neq 2$ and $1/r$ singular potential we refer back to the exact expression for the energy levels in eq. (89a). In the situation of critical electric fields, states lose self-adjointness for large Z . For $|g| < 2$, just as in the Dirac energy levels for $1/r$ singular potential, but if $|g| > 2$ there is merging of particle to particle states (and antiparticle to antiparticle) for states of the same total angular momentum quantum number j , but opposite spin orientations.

This behavior can be seen in fig. 5, which shows the meeting of the $1S_{1/2}$ and $2P_{1/2}$ states. For $|g| < 2$ there is no state merging, but for small anomalies the solution is discontinuous in the sense that even for $1S_{1/2}$ we see in fig. 5 a maximum allowed value of Z at a finite energy. This behavior is reminiscent of the behavior we are familiar with for $1/r$ potential for the $2P_{1/2}$ (seen in fig. 5) and many other $g = 2$ eigenstates. We know from study of numerical solutions of the Dirac equation that the regularization of the Coulomb potential by a finite nuclear size removes this singular behavior. It remains to be seen how this exactly works in the context of the KGP equation allowing for the magnetic anomaly.

The Dirac $g = 2$ case acts as unique “cusp” point because even for very small anomalies, as emphasized in fig. 1, the behavior of the states is strongly modified for the situation of high intensity Coulomb fields which are present in large Z hydrogen-like nuclei.

Thaller [15] presented numerically computed DP equation energy levels for large Z hydrogen like atoms. These numerical solutions involve crossings in energy levels between states with the same total angular quantum number j , but differing spin orientations such as $1S_{1/2}$ and $2P_{1/2}$; these states also have the behavior of diving into the antiparticle lower continuum even for $1/r$ -potential. These features are not present for the KGP-Coulomb solution. However, there is a similarity between the numerical solutions of the DP equation and our analytical KGP solutions, because for $|g| > 2$ the merging states as described above correspond to the crossing states in the DP solution.

The DP equation also allows for the so-called superposition states as described by Barut and Kraus [16, 17]. Such states represent resonances due to the magnetic interaction that reside incredibly close to the center of the atom i.e. $\sqrt{\langle r^2 \rangle} \approx a\hbar/mc$, but this feature is absent from the KGP formation of the Coulomb problem as all KGP-Coulomb wave functions which can be normalized can be successfully matched to their Dirac ($g = 2$) companions.

Because analytical solutions of DP equation, unlike our results for KGP, are not available it is hard to pinpoint precisely the origin of the diverse unpalatable behavior. However, we can hypothesize that the problems arise due to the pathological structure of DP equation where the magnetic anomaly rather than full magnetic moment appears. In any case we see that the Thaller solutions present pathologies quite akin to those we already described in our study of Landau energies. On the other hand KGP framework for large Z shows some exciting and nice analytical behavior.

6 Conclusions

As we discussed in this work, there have been two natural extensions of the relativistic quantum mechanics to include anomalous magnetic moments; we also proposed a third one in sect. 5.3. Our study shows that description of magnetic moment in the context of relativistic quantum physics is today an unfinished subject. In view of the results presented we recognize that inherent to DP is a division of magnetic moment, a conserved quantity, into two different mathematical components. Readers who think that anything, but DP, is an invalid framework have to be at peace with this while rejecting a more natural unified description within the KGP dynamics.

Looking back at our results we highlight the comparison of magnetic moment dynamics of DP and KGP formulation of relativistic quantum mechanics. The DP equation breaks up the magnetic moment into an underlying spinor structure part inherent to the Dirac equation, and a dedicated anomalous part. In contrast, for the KGP, the entire effect of magnetic moment is contained in a single Pauli term irrespective of the magnetic moment's size. We find that the two models disagree in their predicted energy levels for the homogeneous magnetic field and the Coulomb field.

For Landau levels both eqs. (68b) and (70b) have the correct non-relativistic reduction at lowest order to

eq. (44), the latter is much more unwieldy and obscures the physical interpretation. Moreover, in the relativistic limit the DP-Landau level energies eqs. (44) and (70b) is that they include cross terms between the $g = 2$ magnetic moment and anomalous terms in $a = (g - 2)/2$, thus the result does not depend on the particle magnetic moment alone, there is a functional dependence on the magnetic anomaly a as well. This is in our opinion not acceptable. On the contrary, for the KGP-Landau levels, eq. (68b), we have a simple dependence on the full magnetic moment g -factor. This simplicity allows, for the KGP equation, the straightforward analysis of physical systems and elegant expressions for their solutions. Thus Dirac's beauty principle favors heavily the KGP considering the Landau levels.

In the case of the Coulomb field there are even for weak fields measurable differences in both the Lamb shift and fine structure; the contribution to the Lamb shift and fine structure splitting are proportional to: KGP $g^2/8 - 1/2$, eq. (108) and $g^2/8$, eq. (119) respectively, rather than: DP $g/2 - 1$ eq. (110) and $g/2 - 1/2$, eq. (121) respectively.

- For strong fields, both DP and KGP share the behavior of a shrinking particle/antiparticle gap for the ground state when $|g| > 2$, though the expressions differ from each other, see sect. 5.2. The models are extremely different in both their predicted energy values and the ultimate fate of the states as B increases. For the KGP equation, the gap vanishes for in very strong magnetic fields eq. (126a), and for DP the fields have to be even stronger. In both cases this behavior is unphysical and this issue can be resolved by the modification introduced as the IKGP equation eq. (128) for homogeneous magnetic fields in sect. 5.3. The IKGP equation produces new phenomena which we hope to address separately in near future.
- For strong fields with large Z hydrogen-like atoms, in the KGP model, there is a difficult to interpret merging of states that share the same total angular momentum, but differ in orbital angular momentum; the states lose physical meaning at the merging point (see fig. 5). These are the same states that are problematic in the DP equation in that they cross, rather than merge. Either case indicates interesting physics involving these states.

This shows that both formulations of magnetic moment, DP and KGP, cannot be simultaneously correct and it is likely that one of these descriptions more closely describes nature. The quantum level splitting differences, which are on the order of tens of kHz for the hydrogen atom, are either already within reach or will soon be in reach of modern spectroscopic experiments. These differences, however, are not sufficient to explain mysteries such as the proton radius puzzle of Pohl *et al.* [11]. However, we did not study the relativistic scattering in KGP context which provides the other “end” of the puzzle. We also see further opportunity since there can be still better ef

fective approaches characterizing point magnetic moment dynamics in the realm of RQM (sect. 5.3).

Because for the time being the magnetic moment interaction cannot be uniquely defined in quantum mechanics as discussed here, a behavior we also found in the classical dynamics, [1], there is a strong motivation to continue the study of different models of this phenomenon until a convincing formulation emerges, or the experiment can settle which of the models better reflects reality. While the benefit of such study to atomic and nuclear systems is immediately obvious, there are ramifications relevant to stellar astrophysics as discussed in sects. 5.2 and 5.3 and cosmology through the study of (Dirac) neutrinos which are predicted [44] to have a small, but yet undetected, magnetic moment.

One of us (JR) thanks his colleagues Tobias Fischer and Ludwik Turko at the University of Wroclaw for fruitful discussions, and acknowledges support of his visits in Wroclaw by the Polish National Science Center under contract No. UMO-2016/23/B/ST2/00720.

Data Availability Statement This manuscript has no associated data or the data will not be deposited. [Authors' comment: This theoretical manuscript has no associated data.]

Publisher's Note The EPJ Publishers remain neutral with regard to jurisdictional claims in published maps and institutional affiliations.

References

1. J. Rafelski, M. Formanek, A. Steinmetz, Eur. Phys. J. C **78**, 6 (2018) arXiv:1712.01825 [physics.class-ph].
2. L.M. Brown, Phys. Rev. **111**, 957 (1958).
3. M.J.G. Veltman, Acta Phys. Pol. B **29**, 783 (1998) arXiv:hep-th/9712216.
4. V.M. Kaspi, A. Beloborodov, Annu. Rev. Astron. Astrophys. **55**, 261 (2017) arXiv:1703.00068 [astro-ph.HE].
5. J. Rafelski, L.P. Fulcher, A. Klein, Phys. Rep. **38**, 227 (1978).
6. W. Greiner, B. Müller, J. Rafelski, *Quantum Electrodynamics of Strong Fields* (Springer-Verlag Berlin Heidelberg, 1985).
7. J. Rafelski, J. Kirsch, B. Müller, J. Reinhardt, W. Greiner, *Probing QED vacuum with heavy ions*, in *New horizons in fundamental physics*, FIAS Interdisc. Sci. Ser. (Springer, 2017) pp. 211–251 arXiv:1604.08690 [nucl-th].
8. S. Evans, J. Rafelski, Phys. Rev. D **98**, 016006 (2018) arXiv:1805.03622 [hep-ph].
9. G.V. Dunne, Eur. Phys. J. ST **223**, 1055 (2014).
10. E.M. Hegelich, G. Mourou, J. Rafelski, Eur. Phys. J. ST **223**, 1093 (2014) arXiv:1412.8234 [physics.optics].
11. R. Pohl, R. Gilman, G.A. Miller, K. Pachucki, Annu. Rev. Nucl. Part. Sci. **63**, 175 (2013) arXiv:1301.0905 [physics.atom-ph].
12. A.C. Zemach, Phys. Rev. **104**, 1771 (1956).
13. J.S. Schwinger, Phys. Rev. **82**, 664 (1951).
14. W.Y. Tsai, A. Yildiz, Phys. Rev. D **4**, 3643 (1971).
15. B. Thaller, *The Dirac Equation* (Springer, 1992).
16. A.O. Barut, J. Kraus, Phys. Lett. B **59**, 175 (1975).
17. A.O. Barut, J. Kraus, J. Math. Phys. **17**, 506 (1976).
18. M. Knecht, *The Anomalous Magnetic Moment of the Muon: A Theoretical Introduction*, in *Lect. Notes Phys.*, Vol. **629** (Springer, 2004) pp. 37–84, arXiv:hep-ph/0307239.
19. V. Fock, Phys. Z. Sowjetunion **12**, 404 (1937).
20. R.P. Feynman, M. Gell-Mann, Phys. Rev. **109**, 193 (1958).
21. J.L. Cortes, J. Gamboa, L. Velazquez, Phys. Lett. B **313**, 108 (1993) arXiv:hep-th/9301071.
22. R. Angeles-Martinez, M. Napsuciale, Phys. Rev. D **85**, 076004 (2012) arXiv:1112.1134 [hep-ph].
23. E.G. Delgado-Acosta, M. Napsuciale, S. Rodriguez, Phys. Rev. D **83**, 073001 (2011) arXiv:1012.4130 [hep-ph].
24. H. Feshbach, F. Villars, Rev. Mod. Phys. **30**, 24 (1958).
25. B.A. Robson, D.S. Staudte, J. Phys. A: Math. Gen. **29**, 157 (1996).
26. D.S. Staudte, J. Phys. A: Math. Gen. **29**, 169 (1996).
27. M.H. Johnson, B.A. Lippmann, Phys. Rev. **77**, 702 (1950).
28. E.J. Ferrer, V. de la Incera, Nucl. Phys. B **824**, 217 (2010) arXiv:0905.1733 [hep-ph].
29. J. Rafelski, L. Labun, *A Cusp in QED at $g = 2$* , arXiv:1205.1835 [hep-ph] (2012).
30. M.E. Rose, *Relativistic Electron Theory* (John Wiley & Sons, 1961) p. 51.
31. G.A. Baym, *Lectures on Quantum Mechanics* (Westview Press, 1969) p. 526.
32. P.C. Martin, R.J. Glauber, Phys. Rev. **109**, 1307 (1958).
33. L.C. Biedenharn, Phys. Rev. **126**, 845 (1962).
34. J. Niederle, A.G. Nikitin, J. Phys. A **39**, 10931 (2006) arXiv:hep-th/0412214.
35. C. Itzykson, J.-B. Zuber, *Quantum Field Theory* (McGraw-Hill, 1980) p. 360.
36. P.J. Mohr, B.N. Taylor, D.B. Newell, Rev. Mod. Phys. **84**, 1527 (2012) arXiv:1203.5425 [physics.atom-ph].
37. J.R. Sapirstein, D.R. Yennie, in *Quantum Electrodynamics*, edited by T. Kinoshita (World Scientific, 1990) Chapt. 12, pp. 560–672.
38. U. Jentschura, K. Pachucki, Phys. Rev. A **54**, 1853 (1996).
39. M.I. Eides, H. Grotch, V.A. Shelyuto, Phys. Rep. **342**, 63 (2001) arXiv:hep-ph/0002158.
40. B. Jancovici, Phys. Rev. **187**, 2275 (1969).
41. E.J. Ferrer, V. de la Incera, D. Manreza Paret, A. Pérez Martínez, A. Sanchez, Phys. Rev. D **91**, 085041 (2015) arXiv:1501.06616 [hep-ph].
42. A. Broderick, M. Prakash, J.M. Lattimer, Astrophys. J. **537**, 351 (2000) astro-ph/0001537.
43. L. Labun, J. Rafelski, Phys. Rev. D **79**, 057901 (2009) arXiv:0808.0874 [hep-ph].
44. K. Fujikawa, R. Shrock, Phys. Rev. Lett. **45**, 963 (1980).

APPENDIX B

Strong fields and neutral particle magnetic moment dynamics

Formanek, M., Stefan, E., Rafelski, J., Steinmetz, A., Yang, C. T. Strong fields and neutral particle magnetic moment dynamics. *Plasma Physics and Controlled Fusion* 60, 7 (2018):

074006. [10.1088/1361-6587/aac06a](https://doi.org/10.1088/1361-6587/aac06a)

Copyright (2018) by IOP Publishing. All rights reserved. Reproduced with permission under License Agreement 1384591-1 License date: August 9th, 2023. This is the Accepted Manuscript version of an article accepted for publication in Plasma Physics and Controlled Fusion. IOP Publishing Ltd is not responsible for any errors or omissions in this version of the manuscript or any version derived from it. The Version of Record is available online at [10.1088/1361-6587/aac06a](https://doi.org/10.1088/1361-6587/aac06a).

Strong fields and neutral particle magnetic moment dynamics

Martin Formanek, Stefan Evans, Johann Rafelski,
Andrew Steinmetz, and Cheng-Tao Yang,

Department of Physics, The University of Arizona, Tucson, AZ 85721, USA

Abstract. Interaction of magnetic moment of point particles with external electromagnetic fields experiences unresolved theoretical and experimental discrepancies. In this work we point out several issues within the relativistic quantum mechanics and the QED and we describe effects related to a new covariant classical model of magnetic moment dynamics. Using this framework we explore the invariant acceleration experienced by neutral particles coupled to an external plane wave field through the magnetic moment: we study the case of ultra-relativistic Dirac neutrinos with magnetic moments in the range of 10^{-11} to $10^{-20} \mu_B$; and we address the case of slowly moving neutrons. We explore how critical accelerations for neutrinos can be experimentally achieved in laser-pulse interactions. The radiation of accelerated neutrinos can serve as an important test distinguishing between Majorana and Dirac nature of neutrinos.

PACS numbers: 13.40.Em, 06.30.Ka, 41.75.Jv

Keywords: magnetic moment, laser-driven acceleration, neutrino, neutron

Submitted to: *Plasma Phys. Control. Fusion*

Accepted April 26, 2018

1. Introduction

The general consensus in theoretical physics is that the final word on classical Electrodynamics has not yet been said. More than a hundred and fifty years have passed since its original inception by Faraday, Maxwell and many others in the 19th century, and we still face unsolved conceptual problems of a fundamental nature. One of the most prominent issues of classical Electrodynamics is the problem of radiation reaction [1, 2, 3].

Of comparable relevance is the incomplete understanding of the magnetic (Stern-Gerlach type) force, i.e. the interaction of the magnetic moment of a point particle with an external electro-magnetic (EM) field in both classical and quantum mechanics [4, 5]. A related experimental discrepancy exists: as of July 2017 there is a 3.5 standard deviations difference between the calculated magnetic moment of the muon based on Standard Model QFT corrections and experimental measurements [6].

We report on the recent progress in understanding the magnetic moment dynamics [7]. Here we are interested in the dynamics of a neutral particle with non-zero magnetic moment placed in an external EM field. Any new magnetic moment physics is in this situation a first order effect. As an application of these considerations we describe how Dirac neutrinos could be studied experimentally, by exploiting their interaction with intense laser fields. We note another effort to improve understanding of particle interaction with strong laser fields [8]. Our work can also contribute to the study of plasma behavior influenced by external non-homogeneous fields.

Before addressing the primary contents of this report we will first consider briefly the quantum physics of the magnetic moment in section 2, clarifying how the classical and quantum physics relate. We summarize the insights of Ref. [7] in section 3, and we obtain the invariant acceleration acting on any particle in the plane wave field in section 4, before describing the physics of ultrarelativistic neutrinos in interaction with the plane wave field in section 5.

2. Relativistic Quantum Mechanics

2.1. Dynamical equations

Every quantum particle should be described using three free parameters: its mass, its electric charge and its magnetic moment. However, the Dirac equation reduces the number of parameters to two, by predicting the magnetic moment $\mu = geh/2m$ with the gyromagnetic ratio $g = 2$. In reality, the effective g -factor is never exactly equal to two and in our effort to understand the dynamics of realistic particles

we need to generalize our expressions to account for an anomalous magnetic moment with $a = g/2 - 1$. The deviancy can be small, such as in electrons and muons due to quantum electrodynamics effects, or large, such as in protons and neutrons due to their internal structures.

The primary method of treating the anomalous magnetic dipole moment is by modification of the Dirac equation to include what is known as the Pauli term, containing the anomaly deviation $a \neq 0$ in the format

$$(\gamma_\mu(i\hbar\partial^\mu - eA^\mu) - mc)\psi = a \frac{e\hbar}{4mc}\sigma_{\mu\nu}F^{\mu\nu}\psi. \quad (1)$$

The main problem with this approach is that the modified Dirac equation cannot be used to compute virtual processes, since the additional so called Pauli term diverges and requires counter terms.

An alternative theoretical description of magnetic moment first “squares” the Dirac equation, resulting in a second order formulation similar to the Klein-Gordon (KG) equation for spin 0 particles supplemented with the Pauli term

$$\left((i\hbar\partial_\mu - eA_\mu)^2 - \frac{ge\hbar}{4}\sigma^{\mu\nu}F_{\mu\nu} - m^2c^2 \right) \psi = 0, \quad (2)$$

where $\sigma^{\mu\nu} = \frac{i}{2}[\gamma^\mu, \gamma^\nu]$. A solution of the Dirac equation is also a solution of this KG-Pauli Eq. (2) once $g = 2$ is chosen. The problem with KG-Pauli is that one must carefully analyze and understand the set of solutions of the higher order equation.

The advantage of KG-Pauli Eq. (2), compared to Dirac-Pauli Eq. (1) is that we can choose an arbitrary value of the gyromagnetic factor g ; if value $g = 2$ ‘works’ so will an arbitrary value. We emphasize that these two quantum equations, the Dirac-Pauli Eq. (1) and the KG-Pauli Eq. (2), are not equivalent and result in different physical behavior. Thus experiment will determine which form corresponds to the quantum physics of e.g. bound states in hydrogen-like Coulomb potential. We will return to this matter under separate cover.

2.2. Magnetic moment in QED

In principle quantum electrodynamics is formulated around a Dirac particle with $g = 2$ with modifications arising in the context of a perturbative expansion leading to the evaluation of the actual magnetic moment, i.e. $g \neq 2$ of the electron in perturbative series that today requires in precision study also the consideration of strong interactions and vacuum structure. This approach masks the opportunity to use the actual particle magnetic moment for particles responsible for the vacuum properties such as in vacuum polarization.

The study of the vacuum response to external fields has a long and distinguished history that spans

over 80 years, starting with computation of the lowest order effect by Uehling [9] in 1935 and the development of the nonperturbative Euler-Heisenberg (EH) effective action characterizing all the physical phenomena present in constant fields, including the decay of the field into electron positron pairs [10]. These studies introduce counter terms which served as predecessors to the full quantum field theoretical charge renormalization scheme. This effective action was revisited in a field theoretical context by Schwinger, which extended these considerations to include a demonstration of transparency of the vacuum to single electromagnetic plane wave [11]. However, all these considerations required particles to have the Dirac value of magnetic moment $g = 2$.

When $g \neq 2$ is introduced, a modification of the analytical form of the effective EH action is discovered [12, 13] and further non-trivial modifications in the vacuum structure arise [14, 15]. A solution to the previously divergent result for effective action with $|g| > 2$ was obtained [13]. Similarly the modification of the vacuum polarization was found [14]

$$\pi(q^2) = -\frac{e^2}{12\pi^2} \left(\frac{3}{8}g^2 - \frac{1}{2} \left(1 - \frac{4m^2}{q^2} \right) \right) \times \left[\frac{1}{3} + \int_0^1 dx \ln \left(1 - \frac{q^2}{m^2} x(1-x) \right) \right]. \quad (3)$$

The coefficient in Eq.(3) shows explicitly all three parameters of a particle: its magnetic moment in form of g , its charge e and its mass m . One can easily recombine terms to show dependence on the magnetic anomaly $a = g/2 - 1$. This form demonstrates that in perturbative QED expansion, the magnetic moment dependence arises from the higher order QED vacuum polarization tensor (the photon line crossing the loop) contributing. This format hides the appearance of the actual particle magnetic moment in the vacuum polarization as is seen in Eq.(3). We will return to the question how magnetic moment is renormalized under separate cover.

Once we recognize the dependence of vacuum polarization on magnetic moment and the dependence of EH effective action on magnetic moment one must further revisit Schwinger's proof of vacuum transparency to a single plane wave for $g \neq 2$.

3. Magnetic moment in classical theory

There are two models which describe the magnetic moment of a point particle. The 'Amperian' Model approximates the particle magnetic moment by a current loop which leads to a force

$$F_{ASG} = \nabla(\boldsymbol{\mu} \cdot \mathcal{B}), \quad (4)$$

where $\boldsymbol{\mu}$ is the magnetic moment of the particle and \mathcal{B} is magnetic field. On the other hand the 'Gilbertian'

Model creates a magnetic dipole, consisting of two hypothetical monopoles, and leads to a different expression

$$\mathcal{F}_{GSG} = (\boldsymbol{\mu} \cdot \nabla) \mathcal{B}. \quad (5)$$

We expect that there should be a way to reconcile these classical models and to create a covariant description of the dynamics for both particle 4-velocity u^μ and spin s^μ , which would unite these two approaches. There have been efforts to do so - the first covariant model was created by Frenkel [4, 16]. This model is based on classical arguments starting with the principle of least action and couples back the spin motion of the particle with the particle motion.

Another method of approach begins with relativistic quantum Dirac theory which naturally incorporates description of the spin behavior (although $g = 2$ strictly) and finding an appropriate classical limit should yield a full classical description of the particle behavior. The most important example of such an approach is the Foldy-Wouthuysen transformation [5]

Both of these approaches predict different behavior in the external EM field and can be distinguished experimentally as was explored in the article [8]. We learn from this work that ultra-intense laser pulses are especially suitable for investigating the viability of such models.

As presented in the work [7], the spin of a particle should not be its quantum property but rather a classical characteristic similar to the particle's mass. Both of these are eigenvalues of Casimir operators of the Poincaré group of space-time symmetry transformations, whose values describe a representation of this group for a given particle. This insight allowed us to create a new covariant description of the spin dynamics of particles [7] which has the form

$$\dot{u}^\mu = \frac{1}{m} (qF^{\mu\nu} - s \cdot \partial F^{*\mu\nu} d) u_\nu, \quad (6)$$

$$\dot{s}^\mu = \frac{1+\tilde{a}}{m} \left(qF^{\mu\nu} - \frac{1+\tilde{b}}{1+\tilde{a}} s \cdot \partial F^{*\mu\nu} d \right) s_\nu - \tilde{a} \frac{u^\mu}{mc^2} \left(u \cdot \left(qF - \frac{\tilde{b}}{\tilde{a}} s \cdot \partial F^* d \right) \cdot s \right), \quad (7)$$

where \tilde{a} and \tilde{b} are arbitrary constants. We explicitly distinguish between particle charge q and elementary magnetic dipole charge d , which is used to convert the spin of a particle s to the magnetic moment $\boldsymbol{\mu}$ as $c|s|d \equiv |\boldsymbol{\mu}|$. Finally, the dual EM tensor reads $F^{*\mu\nu} = \epsilon_{\mu\nu\alpha\beta} F^{\alpha\beta}/2$, with the fully antisymmetric tensor defined as $\epsilon_{0123} \equiv +1$ (beware of a sign if contravariant indices are used).

We see that the equation of motion Eq.(14) of the particle depends explicitly on the spin dynamics Eq.(7) through the spin 4-vector $s^\mu(\tau)$, thus generating

covariant generalization of the Lorentz force to include Stern-Gerlach force. For particles with zero magnetic moment $d = 0$ these dynamical equations reduce to Thomas-Bargmann-Michel-Telegdi (TBMT) equations [17, 18] with $\tilde{a} = a$. TBMT equations are widely used to model particle dynamics in external fields and yet these do not contain coupling of the spin to the particle motion.

On the other hand, we can also explore the other limit: the dynamics of neutral particles $q = 0$ with magnetic moment $d \neq 0$ in external fields. Equations (14), (7) become only functions of parameter \tilde{b} , which we will further explore in section 5.

To conclude this short overview of the results obtained in Ref. [7] we note that the two forms of the force, the Amperian and the Gilbertian, were shown to be equivalent. Thus a consistent theoretical framework now exists for exploring the dynamics of a magnetic moment in external fields.

4. Dynamics of particles in a plane wave field

4.1. Invariant acceleration

The generalized Lorentz force equation reads [7], see Eq.(14)

$$\dot{u}^\mu = \frac{1}{m} \tilde{F}^{\mu\nu} u_\nu, \quad \tilde{F}^{\mu\nu} \equiv qF^{\mu\nu} - s \cdot \partial F^{*\mu\nu} d. \quad (8)$$

Imagine a point particle with both electric charge and magnetic moment in the plane wave field given by expression

$$A^\mu(\xi) = A_0 \varepsilon^\mu f(\xi), \quad \xi = k \cdot x, \quad k \cdot \varepsilon = 0, \quad k^2 = 0, \quad (9)$$

where k^μ is a wave vector of the plane wave; ε^μ its polarization; ξ phase; and A_0 amplitude. $f(\xi)$ is a function characterizing the laser pulse. Just the formula for the dynamics of the 4-velocity Eq.(8) alone is sufficient to obtain an expression for invariant acceleration in the plane wave field. In this case the generalized EM tensor reads

$$\begin{aligned} \tilde{F}^{\mu\nu} = A_0 q(k^\mu \varepsilon^\nu - k^\nu \varepsilon^\mu) f'(\xi) \\ - A_0 f''(\xi) (k \cdot s) \epsilon^{\mu\nu\alpha\beta} k_\alpha \varepsilon_\beta d, \end{aligned} \quad (10)$$

where primes denote derivatives of the pulse function $f(\xi)$ with respect to its phase. If we multiply this expression with k^μ we get zero because of the identities in Eq.(9). Then Eq.(8) implies that

$$k \cdot \dot{u} = 0, \quad \Rightarrow \quad k \cdot u = k \cdot u(0), \quad (11)$$

is an integral of motion. We can obtain the invariant acceleration by squaring the expression Eq.(8), which can be evaluated using Eq.(9), antisymmetric properties of ϵ , our integral of motion Eq.(11), and contraction identity

$$\epsilon^{\mu\nu\alpha\beta} \epsilon_{\mu\rho\gamma\delta} = -\delta^{\nu\alpha\beta}_{\rho\gamma\delta}, \quad (12)$$

which is a generalized Kronecker delta. The final result is

$$\dot{u}^2 = -\frac{A_0^2}{m^2} [q^2 f'(\xi)^2 + (k \cdot s)^2 f''(\xi)^2 d^2] (k \cdot u(0))^2. \quad (13)$$

The cross term vanishes because the force due to particle electric charge and magnetic moment are orthogonal for a plane wave field. The only unknown in this expression is the product $(k \cdot s(\tau))$, which is still a function of proper time.

4.2. Neutral particle dynamics

As explained in the reference [7] the torque Eq. (7) is constructed to be compatible with the force Eq.(8). For neutral particles we require in addition as did Ref.[19] that torque involves full magnetic moment; that is, for the particle at rest in the laboratory frame we have the torque $\propto \boldsymbol{\mu} \times \mathcal{B}$. Restating the force equation for neutral particles the two dynamical equations thus are

$$\dot{u}^\mu = -s \cdot \partial F^{*\mu\nu} u_\nu \frac{d}{m}, \quad (14)$$

$$\dot{s}^\mu = cd \left(F^{\mu\nu} s_\nu - \frac{u^\mu}{c^2} (u \cdot F \cdot s) \right) - s \cdot \partial F^{*\mu\nu} s_\nu \frac{d}{m}. \quad (15)$$

The full analytical solution of these equations are in preparation for publication under separate cover. Here of importance is the solution for the projection of spin on the wave vector of the laser

$$k \cdot s(\tau) = k \cdot s(0) \cos[A_0 d(f(\xi(\tau)) - f(\xi_0))] - \frac{W}{c} \sin[A_0 d(f(\xi(\tau)) - f(\xi_0))], \quad (16)$$

where W is determined by initial conditions

$$W \equiv [(k \cdot u(0))(\varepsilon \cdot s(0)) - (\varepsilon \cdot u(0))(k \cdot s(0))]. \quad (17)$$

It is very important to know $k \cdot s(\tau)$ because the invariant acceleration of the particle, obtained by squaring Eq.(14), is

$$\dot{u}^2(\tau) = -(k \cdot s(\tau))^2 (k \cdot u(0))^2 f''(\xi)^2 \frac{A_0^2 d^2}{m^2}. \quad (18)$$

The invariant acceleration therefore depends on the products $(k \cdot u(0))$ and $(k \cdot s(\tau))$. The first one is a Doppler shifted laser frequency as seen by the particle being hit by the laser pulse. In the laboratory frame with

$$u^\mu(0) = \gamma_0 c(1, \boldsymbol{\beta}_0), \quad k^\mu = \omega(1, \hat{\mathbf{k}})/c, \quad \epsilon^\mu = (0, \hat{\boldsymbol{\epsilon}}), \quad (19)$$

we can write

$$k \cdot u(0) = \gamma_0 (1 - \hat{\mathbf{k}} \cdot \boldsymbol{\beta}_0) \omega. \quad (20)$$

To evaluate Eq.(18) we further need $(k \cdot s(0))$, denoting the initial alignment of the particle spin and the wave vector. Since $u \cdot s = 0$, the initial spin 4-vector in the laboratory frame reads

$$s_L^\mu(0) = (\boldsymbol{\beta}_0 \cdot \mathbf{s}_{0L}, \mathbf{s}_{0L}), \quad (21)$$

$$\mathbf{s}_{0L} = \mathbf{s}_0 + \frac{\gamma_0 - 1}{\beta_0^2} (\beta_0 \cdot \mathbf{s}_0) \beta_0, \quad (22)$$

where \mathbf{s}_{0L} is the Lorentz transform of the initial spin of the particle \mathbf{s}_0 given in its rest frame. Therefore

$$\frac{c}{\omega} \mathbf{k} \cdot \mathbf{s}(0) = \gamma_0 (\beta_0 \cdot \mathbf{s}_0) - (\gamma_0 - 1) (\beta_0 \cdot \mathbf{s}_0) (\beta_0 \cdot \hat{\mathbf{k}}) - \hat{\mathbf{k}} \cdot \mathbf{s}_0. \quad (23)$$

For the particle beam pointing against the laser pulse $\beta_0 \cdot \hat{\mathbf{k}} = -1$, we pick up a factor of γ_0

$$\frac{c}{\omega} \mathbf{k} \cdot \mathbf{s}(0) = \gamma_0 (\beta_0 + 1) (\beta_0 \cdot \mathbf{s}_0) - (\beta_0 \cdot \mathbf{s}_0) - \hat{\mathbf{k}} \cdot \mathbf{s}_0. \quad (24)$$

$k \cdot s(0)$ factor plays an important role in the ultrarelativistic interactions discussed in the following section.

Finally, the combination of the initial conditions Eq. (17) evaluated in the laboratory frame reads

$$\frac{W}{c} = \gamma_0 \frac{\omega}{c} \left[-\hat{\mathbf{e}} \cdot \mathbf{s}_0 + \left(1 - \frac{1}{\gamma_0} \right) (\beta_0 \cdot \mathbf{s}_0) (\beta_0 \cdot \hat{\mathbf{e}}) + (\hat{\mathbf{k}} \cdot \beta_0) (\hat{\mathbf{e}} \cdot \mathbf{s}_0) - (\beta_0 \cdot \hat{\mathbf{e}}) (\hat{\mathbf{k}} \cdot \mathbf{s}_0) \right], \quad (25)$$

which is also proportional to only one (in general highly relativistic) γ_0 factor.

5. Neutrino acceleration (ultrarelativistic limit)

As discussed in preceding sections we are especially interested in the case of charge neutral particles in the external EM fields. The most prominent examples of such particles are neutrons and neutrinos. In the absence of the classical Lorentz force the particle dynamics is governed by spin effects and can directly be used to measure the related properties of particles.

The interaction of neutrinos with a laser field was studied previously [20] as a higher order scattering effect, but in the framework we developed [7] neutrinos couple with external fields via magnetic moment directly.

We recall that by symmetry arguments only the Dirac neutrino can have a magnetic moment: in essence this is because the Majorana neutrino is the antiparticle of itself and thus under EM interactions must be neutral in both charge and magnetic moment. A very significant effort is underway to discover the double beta-decay [21] that could demonstrate that the neutrino is of the Majorana type. However, one can question if a nil result would mean that the neutrino is a Dirac neutrino [22]. We believe that the measurement of neutrino interactions with an external field via its magnetic moment would demonstrate that the neutrino is of the Dirac type. Our objective in the following is to show that we not only can expect observable effects when relativistic neutrinos interact with an intense EM plane wave pulse, but that a measurement of the magnetic moment of the neutrino should be possible.

5.1. Magnetic moment of the neutrino

The dipole magnetic moment is a well studied electromagnetic property of the Dirac neutrino. A minimal extension of the Standard Model with non-zero Dirac neutrino masses places a lower bound on the magnetic moment of the neutrino mass eigenstate ν_i proportional to its mass m_i and reads [23]

$$\mu_i = \frac{3 G_F m_e m_i}{4 \sqrt{2} \pi^2} \mu_B = 3.2 \times 10^{-19} \left(\frac{m_i}{\text{eV}} \right) \mu_B, \quad (26)$$

where $\mu_B = e\hbar/2m_e$ is the Bohr magneton. This value is several orders of magnitude smaller than the present experimental upper bound [24]

$$\mu_\nu < 2.9 \times 10^{-11} \mu_B. \quad (27)$$

5.2. Neutrino acceleration in the external field

We consider a beam of neutrinos with $E_\nu \simeq 20$ GeV. This energy of neutrinos is currently accessible, for example the OPERA experiment used 17 GeV neutrinos produced at CERN [25]. For the rest mass of neutrinos we take $m_\nu = 0.2$ eV and laser source with photon energy $E_\gamma = 1$ eV. The de Broglie wavelength for such neutrinos compared to the wavelength of the laser light is

$$\lambda_\nu = \frac{E_\gamma}{E_\nu(kin)} \approx \frac{E_\gamma}{E_\nu} \approx 5 \times 10^{-11}, \quad (28)$$

where we neglected the mass of the neutrinos compared to their energy. This justifies the classical treatment because the wavelength of the 1 eV laser light is 11 orders of magnitude larger than the wavelength of the 20 GeV neutrinos, therefore the quantum wave character of neutrinos will be invisible. The amplitude A_0 of the laser field vector potential can be expressed in terms of the dimensionless normalized amplitude a_0 as

$$A_0 = \frac{m_e c}{e} a_0. \quad (29)$$

The current state of the art for laser systems is $a_0 \sim 10^2$. The elementary dipole charge of the neutrino can be rewritten using the neutrino magnetic moment in units of Bohr magneton as

$$d = \frac{e}{m_e c} \mu [\mu_B]. \quad (30)$$

This makes the relevant product

$$A_0 d = a_0 \mu_\nu [\mu_B] \approx 10^{-9} - 10^{-11} \quad (31)$$

for state of the art laser systems and possible range of values for neutrino magnetic moment Eqs. (26, 27). From the Eq.(25) we get ultrarelativistic limit for W/c term and using (Eq. (24)) ultrarelativistic limit for product $k \cdot s(0)$

$$\frac{W}{c} \sim \frac{\gamma_0 \hbar \omega}{c}, \quad k \cdot s(0) \sim \frac{\gamma_0 \hbar \omega}{c}. \quad (32)$$

This means that for our extremely small $A_0 d$ (Eq. (31)) we can see from Eq. (16) that there is no (neutrino) spin precession and

$$k \cdot s(\tau) \approx k \cdot s(0), \quad (33)$$

with a very high precision.

Equation (18) allows us to evaluate the invariant acceleration which the 20 GeV neutrino experiences in the external plane wave field

$$\sqrt{\dot{u}^2} \approx \left| (k \cdot s(0)) (k \cdot u(0)) f''(\xi) \frac{A_0 d}{m_\nu} \right|. \quad (34)$$

We turn now to estimate individual terms:

i) The Doppler shifted frequency ($k \cdot u(0)$) is given in the laboratory frame by the formula (20) and for the ultra relativistic neutrinos with velocity β_0 oriented against the laser beam propagation direction $\hat{\mathbf{k}}$ we can write

$$k \cdot u(0) = \gamma_0 (1 - \hat{\mathbf{k}} \cdot \beta_0) \omega \approx 2 \gamma_0 \omega \approx 2 \frac{E_\nu E_\gamma}{m_\nu c^2 \hbar}. \quad (35)$$

ii) The product $k \cdot s(0)$ (Eq. (24)) is in the ultrarelativistic case proportional to

$$k \cdot s(0) \approx \frac{\gamma_0 \hbar \omega}{c} \approx \frac{E_\nu}{m_\nu c^2} \frac{E_\gamma}{c}. \quad (36)$$

iii) Finally, we want to write the result in the units of critical acceleration for the neutrino which is

$$a_c = \frac{m_\nu c^3}{\hbar}. \quad (37)$$

Substituting all terms in equations (29-37) into (34) yields an expression for the acceleration

$$\sqrt{\dot{u}^2} [a_c] \approx a_0 f''(\xi) \frac{(E_\nu [\text{eV}]^2 (E_\gamma [\text{eV}]^2)^2)}{(m_\nu [\text{eV}]^4)} \mu_\nu [\mu_B]. \quad (38)$$

For our 20 GeV neutrinos we see that the critical acceleration can be achieved in the whole range of magnetic moment that Dirac neutrinos could have $\mu_\nu \in (10^{-11} - 10^{-20}) \mu_B$ for corresponding laser pulse parameters in the range

$$a_0 f''(\xi) \in (10^{-13} - 10^{-4}). \quad (39)$$

The state of the art laser systems have dimensionless normalized amplitude a_0 , Eq. (29) on the order of 10^2 . Even the second derivative of the laser pulse function can be high, because typically we get $f(\xi)$ as a product of oscillating function $\sin(\xi)$ and envelope $g(\xi)$ which has a second derivative

$$f''(\xi) = (\sin(\xi) g(\xi))'' = -\sin(\xi) g(\xi) + 2 \cos(\xi) g'(\xi) + \sin(\xi) g''(\xi). \quad (40)$$

The dominant term that we can exploit is the first derivative of the envelope function which can be very high on the front of the pulses with high contrast ratio. For example if the intensity of the light drops by 99% from the maximum on the distance of half wavelength (therefore field amplitude drops by 90% on

the same distance) we get $g'(\xi) = 0.9/\pi \sim 10^{-1}$. Thus we believe that critical neutrino acceleration can be achieved for the whole range of permissible neutrino magnetic moment with accessible laser systems.

Relativistic high intensity neutrino beams are available, and continue to be developed, at particle accelerators (CERN, Fermilab) for neutrino oscillation experiments and related ‘intensity frontier’ research. The typical energy of a high intensity $\nu, \bar{\nu}$ -beam is at 10-20 GeV level, but a beam-dump sourced beam at CERN-LHC would produce neutrinos with 100 times higher energy. This high-energy beam of neutrinos responds by a factor γ_0^2 in our favor. In comparison to accelerator sourced neutrinos, the highest natural ν -flux on Earth is at 0.6–1 MeV from $p\bar{p}$ -solar fusion chains. Interactions with the laser light at this energy would be suppressed by a factor 10^8 compared to the 10 GeV neutrino beam, but the solar source ‘shines’ with 100% duty cycle tracking sky location of the Sun also across the Earth. This shows that before an experiment can be realized, prioritization and optimization between the intensity of the laser light, the accessible energy of neutrinos, and the luminosity of the neutrino flux have to be studied in order to select an optimal experimental environment

5.3. Neutrino radiation

There are multiple ways how an accelerated neutrino can radiate. It certainly produces magnetic dipole electromagnetic radiation as discussed in Refs.[19, 27].

At 20 GeV energy it is even possible that the neutrino will emit (virtual) electro-weak bosons W^\pm and Z^0 , which will decay into relatively high 10-GeV energy scale, and thus more easily observable, either dilepton pairs, and/or hadronic showers (hadronic decay of Z^0, W^\pm). Thus with some probability shooting a laser pulse onto an incoming 20 GeV neutrino beam may catalyze GeV scale particle production, a process that would be hard to interpret otherwise.

While experiments seeking double- β -decay of Majorana neutrinos are underway, an experiment seeking evidence for Dirac neutrino has not been available before. The possible ultra-intense laser pulse catalysis of radiation by an ultra-relativistic neutrino provides this opportunity for the first time. Therefore these processes will be subject to future study. Aside demonstrating possible Dirac nature of the neutrino, such experiments would provide vital information about the neutrino magnetic moment and mass.

6. Neutrons

6.1. Neutron acceleration

Given that a neutron is about 5×10^9 heavier compared to a neutrino one cannot expect a Lorentz-factor $\gamma_0 = E_n/m_nc^2$ that is anywhere near to the value 10^{11} that makes neutrino magnetic interactions with the external field strong. Even so, we note that iThemba LABS can produce neutrons with kinetic energy of 200 MeV [26], which corresponds to $E_n \approx 960$ MeV. This still places their dynamics into a classical regime, since $\lambda_n/\lambda_\gamma \approx 5 \times 10^{-9}$ for 1 eV laser photons.

Even though the magnitude of the magnetic moment for the neutron is several orders of magnitude larger $|\mu_n| = 1 \times 10^{-3} \mu_B$ the neutrons are 10^9 times heavier and in conclusion we would require the product $a_0 f''(\xi)$ to be as high as 10^{23} in order to achieve critical accelerations which is definitely not currently accessible. On the other hand the neutron-external magnetic field interaction is appreciable and has been used to keep a neutron beam in a storage ring [28]. The EM plane wave interaction with neutrons introduces a novel method of neutron motion and spin motion control.

6.2. Polarization of non-relativistic neutrons

We need the neutrons to move slowly enough so that we can consider the non-relativistic limit, but not so slowly that we have to take into account quantum mechanical effects. For example, slow neutrons at 10 eV have $\beta_0 \sim 10^{-4}$ and $\lambda_n/\lambda_\gamma \sim 10^{-6}$ for a 1 eV laser source, which still puts them well into the classical region.

This time the product $A_0 d$ which governs the spin precession is for the state of the art laser appreciable $A_0 d \approx 10^{-1}$ which makes both terms in the spin precession Eq. (16) relevant and spin of neutron indeed rotates in the external laser field.

The estimate of the $k \cdot s(0)$ term (Eq. (24)) in the zeroth order of β_0 is

$$k \cdot s(0) \approx -\frac{\omega}{c} \hat{k} \cdot s_0, \quad (41)$$

and the term W/c (Eq. (25)) in the zeroth order of β_0 reads

$$\frac{W}{c} \approx -\frac{\omega}{c} \hat{\epsilon} \cdot s_0. \quad (42)$$

This means that the spin precession equation, Eq. (16), reduces to

$$\hat{k} \cdot s(t) \approx \hat{k} \cdot s_0 \cos[A_0 d(f(\xi(t)) - f(\xi_0))] - \hat{\epsilon} \cdot s_0 \sin[A_0 d(f(\xi(t)) - f(\xi_0))]. \quad (43)$$

We see in Eq. (43) that just as in the relativistic result Eq. (16), in the non-relativistic limit the spin precesses with $A_0 d f(\xi(t))$. However, unlike for neutrinos, given the large magnetic moment of

neutrons, the spin precession can be significant. The spin projection oscillates between initial alignments with direction of plane wave propagation and against the polarization vector (and vice-versa). This is in agreement with the expectation based on non-relativistic torque action, which we will further discuss elsewhere.

6.3. Neutron lifespan

Closing the discussion of neutron dynamics we draw attention to the recent recognition that neutron decay anomaly, i.e. the lifespan inconsistency between ‘in bottle’, and ‘in flight’ measurements, could be related to an unknown dark matter decay of the neutron [29]. We have explored the question if this inconsistency could be due to the neutron lifespan being affected by the strong field environment accompanying the ‘in flight’ type measurement experiments [30]. We were considering the modification of the proper time by the strong field. Since it is hard to accelerate neutrons using their magnetic moment we did not identify an effect. However, this lifespan discrepancy and associated presence of strong fields remains a topic deserving further theoretical and, in the context of laser strong fields, novel experimental investigation employing i.g. neutrons kept in a storage ring [28] accompanied by a EM plane wave.

7. Conclusions

The novel domain of EM magnetic moment interactions in external fields which has been recently formulated also holds promise to enhance the understanding of physics of plasmas. In this paper we focused on the dynamics on neutral particles, namely neutrinos and neutrons. The purpose of this paper was to introduce new particle physics opportunities present in the ultra intense laser physics frontier. Among results we have obtained is for example that (ultra-relativistic) neutrinos embedded in ultra-strong high contrast laser pulses are not subjected to any appreciable spin precession unlike neutrons for which spin dynamics becomes important.

The relevant Eq. (16) and, respectively, Eq. (43) depend alone on the behavior related to TBMT torque dynamics, section 3. However, a prior study of covariant neutron (spin) dynamics in the presence of a EM plane wave is not known to us and we believe that these results are presented here for the first time.

We have proposed exploration of laser pulse interaction with ultrarelativistic neutrinos. As our discussion shows the ultra large neutrino Lorentz- γ_0 factor enhances the interaction strength with the external field opening opportunity to revolutionize the study of physical properties of the Dirac neutrinos as

both the mass and the magnetic moment could be studied through the magnetic moment EM radiation and/or W/Z radiation decay channels.

Here it is important to realize that only a positive outcome of the double- β decay experiment proves that neutrino is a Majorana particle; in the absence of a result a complementary experiment aiming to recognize Dirac neutrino magnetic moment would serve as an important test which could resolve the question whether the neutrino is a Dirac or a Majorana particle.

References

- [1] Y. Hadad, L. Labun, J. Rafelski, N. Elkina, C. Klier and H. Ruhl, “Effects of Radiation-Reaction in Relativistic Laser Acceleration,” Phys. Rev. D **82**, 096012 (2010) doi:10.1103/PhysRevD.82.096012 [arXiv:1005.3980 [hep-ph]].
- [2] S. E. Gralla, A. I. Harte and R. M. Wald, “A Rigorous Derivation of Electromagnetic Self-force,” Phys. Rev. D **80**, 024031 (2009) doi:10.1103/PhysRevD.80.024031 [arXiv:0905.2391 [gr-qc]].
- [3] H. Spohn, “Dynamics of charged particles and their radiation field,” Cambridge University press (2004), ISBN 9780521037075.
- [4] J. Frenkel, “Die Elektrodynamik des rotierenden Elektrons,” Z. Phys. **37**, 243 (1926). doi:10.1007/BF01397099
- [5] L. L. Foldy and S. A. Wouthuysen, “On the Dirac theory of spin 1/2 particle and its nonrelativistic limit,” Phys. Rev. **78**, 29 (1950). doi:10.1103/PhysRev.78.29
- [6] D. Giusti, V. Lubicez, G. Martinelli, F. Sanfilippo and S. Simula, “Strange and charm HVP contributions to the muon ($g - 2$) including QED corrections with twisted-mass fermions,” JHEP **1710**, 157 (2017) doi:10.1007/JHEP10(2017)157 [arXiv:1707.03019 [hep-lat]].
- [7] J. Rafelski, M. Formanek and A. Steinmetz, “Relativistic Dynamics of Point Magnetic Moment,” Eur. Phys. J. C **78**, no. 1, 6 (2018) doi:10.1140/epjc/s10052-017-5493-2 [arXiv:1712.01825 [physics.class-ph]].
- [8] M. Wen, C. H. Keitel and H. Bauke, “Spin-one-half particles in strong electromagnetic fields: Spin effects and radiation reaction,” Phys. Rev. A **95**, no. 4, 042102 (2017) doi:10.1103/PhysRevA.95.042102 [arXiv:1610.08951 [physics.plasm-ph]].
- [9] E. A. Uehling, “Polarization effects in the positron theory,” Phys. Rev. **48** (1935) 55, doi:10.1103/PhysRev.48.55
- [10] W. Heisenberg and H. Euler, “Consequences of Dirac’s theory of positrons,” Z. Phys. **98**, 714 (1936) doi:10.1007/BF01343663 [physics/0605038].
- [11] J. S. Schwinger, “On gauge invariance and vacuum polarization,” Phys. Rev. **82**, 664 (1951). doi:10.1103/PhysRev.82.664
- [12] L. Labun and J. Rafelski, “Acceleration and Vacuum Temperature,” Phys. Rev. D **86**, 041701 (2012) doi:10.1103/PhysRevD.86.041701 [arXiv:1203.6148 [hep-ph]].
- [13] J. Rafelski and L. Labun, “A Cusp in QED at $g=2$,” [arXiv:1205.1835 [hep-ph]].
- [14] R. Angeles-Martinez and M. Napsuciale, “Renormalization of the QED of second order spin 1/2 fermions,” Phys. Rev. D **85**, 076004 (2012) doi:10.1103/PhysRevD.85.076004 [arXiv:1112.1134 [hep-ph]].
- [15] C. A. Vaquera-Araujo, M. Napsuciale and R. Angeles-Martinez, “Renormalization of the QED of Self-Interacting Second Order Spin 1/2 Fermions,” JHEP **1301**, 011 (2013) doi:10.1007/JHEP01(2013)011 [arXiv:1205.1557 [hep-ph]].
- [16] J. Frenkel, “Spinning electrons,” Nature **117**, 2949 (1926).
- [17] L. H. Thomas, “The motion of a spinning electron,” Nature **117**, 514 (1926). doi:10.1038/117514a0
- [18] V. Bargmann, L. Michel and V. L. Telegdi, “Precession of the polarization of particles moving in a homogeneous electromagnetic field,” Phys. Rev. Lett. **2**, 435 (1959). doi:10.1103/PhysRevLett.2.435
- [19] P. D. Morley and D. J. Buetner, “Instantaneous Power Radiated from Magnetic Dipole Moments,” Astropart. Phys. **62**, 7 (2015) doi:10.1016/j.astropartphys.2014.07.005 [arXiv:1407.1274 [astro-ph.HE]].
- [20] S. Meuren, C. H. Keitel and A. Di Piazza, “Nonlinear neutrino-photon interactions inside strong laser pulses,” JHEP **1506**, 127 (2015) doi:10.1007/JHEP06(2015)127 [arXiv:1504.02722 [hep-ph]].
- [21] C. Alduino *et al.* [CUORE Collaboration], “First Results from CUORE: A Search for Lepton Number Violation via $\bar{\nu}_e \beta \beta$ Decay of ^{130}Te ,” Phys. Rev. Lett. **120**, no. 13, 132501 (2018) doi:10.1103/PhysRevLett.120.132501 [arXiv:1710.07988 [nucl-ex]].
- [22] M. Hirsch, R. Srivastava and J. W. F. Valle, “Can one ever prove that neutrinos are Dirac particles?,” Phys. Lett. B **781**, 302 (2018) doi:10.1016/j.physletb.2018.03.073 [arXiv:1711.06181 [hep-ph]].
- [23] K. Fujikawa and R. Shrock, “The Magnetic Moment of a Massive Neutrino and Neutrino Spin Rotation,” Phys. Rev. Lett. **45**, 963 (1980). doi:10.1103/PhysRevLett.45.963
- [24] C. Patrignani *et al.* [Particle Data Group], “Review of Particle Physics,” Chin. Phys. C **40**, no. 10, 100001 (2016). doi:10.1088/1674-1137/40/10/100001
- [25] D. Duchesneau [OPERA Collaboration], “Latest results from the OPERA experiment,” J. Phys. Conf. Ser. **888**, no. 1, 012004 (2017). doi:10.1088/1742-6596/888/1/012004
- [26] M. Mosconi, E. Musonza, A. Buffler, R. Nolte, S. Röttger, and F. D. Smit, “Characterisation of the high-energy neutron beam at iThemba LABS,” Radiation Measurements **45**, no. 10, 1342 (2010).
- [27] J.D. Jackson, “Classical Electrodynamics”, 2nd Edition, Wiley, (1975).
- [28] W. Paul, F. Anton, W. Mampe, L. Paul and S. Paul, “Measurement of the Neutron Lifetime in a Magnetic Storage Ring,” Z. Phys. C **45**, 25 (1989). doi:10.1007/BF01556667
- [29] B. Fornal and B. Grinstein, “Dark Matter Interpretation of the Neutron Decay Anomaly,” arXiv:1801.01124 [hep-ph].
- [30] J. S. Nico *et al.*, “Measurement of the neutron lifetime by counting trapped protons in a cold neutron beam,” Phys. Rev. C **71**, 055502 (2005) doi:10.1103/PhysRevC.71.055502 [nucl-ex/0411041].

APPENDIX C

Relativistic dynamics of point magnetic moment

Rafelski, J., Formanek, M., Steinmetz, A. Relativistic dynamics of point magnetic moment. *Eur. Phys. J. C* **78**, 6 (2018). [10.1140/epjc/s10052-017-5493-2](https://doi.org/10.1140/epjc/s10052-017-5493-2)

Copyright (2018) by Springer Nature. Reprinted with kind permission of The European Physical Journal (EPJ). This article is an open access article distributed under the terms and conditions of the Creative Commons Attribution ([CC BY 4.0](#)) license.



Relativistic dynamics of point magnetic moment

Johann Rafelski^a, Martin Formanek, Andrew Steinmetz

Department of Physics, The University of Arizona, Tucson, AZ 85721, USA

Received: 1 December 2017 / Accepted: 19 December 2017 / Published online: 3 January 2018
© The Author(s) 2018. This article is an open access publication

Abstract The covariant motion of a classical point particle with magnetic moment in the presence of (external) electromagnetic fields is revisited. We are interested in understanding extensions to the Lorentz force involving point particle magnetic moment (Stern–Gerlach force) and how the spin precession dynamics is modified for consistency. We introduce spin as a classical particle property inherent to Poincaré symmetry of space-time. We propose a covariant formulation of the magnetic force based on a ‘magnetic’ 4-potential and show how the point particle magnetic moment relates to the Amperian (current loop) and Gilbertian (magnetic monopole) descriptions. We show that covariant spin precession lacks a unique form and discuss the connection to $g = 2$ anomaly. We consider the variational action principle and find that a consistent extension of the Lorentz force to include magnetic spin force is not straightforward. We look at non-covariant particle dynamics, and present a short introduction to the dynamics of (neutral) particles hit by a laser pulse of arbitrary shape.

1 Introduction

The (relativistic) dynamics of the particle magnetic moment μ , i.e. the proper time dynamics of spin $s^\mu(\tau)$, has not been fully described before. Our interest in this topic originates in a multitude of current research topics:

- the ongoing effort to understand the magnetic moment anomaly of the muon [1,2];
- questions regarding how elementary magnetic dipoles (e.g. neutrons) interact with external fields [3,4];
- particle dynamics in ultra strong magnetic fields created in relativistic heavy ion collisions [5,6];
- magnetars, stellar objects with extreme $\mathcal{O}(10^{11})$ T magnetic fields [7,8];

^ae-mail: jrafelski@yahoo.com

- the exploration of particle dynamics in laser generated strong fields [9];
- neutron beam guidance and neutron storage rings [10];
- and
- the finding of unusual quantum spin dynamics when gyromagnetic ratio $g \neq 2$ [11,12].

The results we present will further improve the understanding of plasma physics in the presence of inhomogeneous magnetic fields, and improve formulation of radiation reaction forces, and topics not further discussed in this presentation.

In the context of the electromagnetic (EM) Maxwell–Lorentz theory we learn in the classroom that:

1. The magnetic moment μ has an interaction energy with a magnetic field \mathcal{B}

$$E_m = -\mu \cdot \mathcal{B}. \quad (1)$$

The corresponding Stern–Gerlach force \mathcal{F}_{SG} has been written in two formats

$$\mathcal{F}_{SG} \equiv \begin{cases} \nabla(\mu \cdot \mathcal{B}), & \text{Amperian Model}, \\ (\mu \cdot \nabla) \mathcal{B}, & \text{Gilbertian Model}. \end{cases} \quad (2)$$

The name ‘Amperian’ relates to the loop current generating the force. The ‘Gilbertian’ model invokes a magnetic dipole made of two magnetic monopoles. These two forces written here in the rest frame of a particle are related [3,4]. We will show that an internal spin based magnetic dipole appears naturally; it does not need to be made of magnetic monopoles or current loops. We find that both force expressions in Eq. (2) are equivalent; this equivalence arises from covariant dynamics we develop and requires additional terms in the particle rest frame complementing those shown in Eq. (2).

2. The torque \mathcal{T} that a magnetic field \mathcal{B} exercises on a magnetic dipole μ tends to align the dipole with the direction of a magnetic field \mathcal{B}

$$\mathcal{T} \equiv \frac{ds}{dt} = \mu \times \mathcal{B} = g\mu_B \frac{s}{\hbar/2} \times \mathcal{B}, \quad \mu_B \equiv \frac{e\hbar}{2m}. \quad (3)$$

The magnetic moment is defined in general in terms of the product of Bohr magneton μ_B with the gyromagnetic ratio g , $|\mu| \equiv g\mu_B$. In Eq. (3) we used $|s| = \hbar/2$ for a spin-1/2 particle; a more general expression will be introduced in Sect. 3.1.1.

We used the same coefficient μ to characterize both the Stern–Gerlach force Eq. (2) and spin precession force Eq. (3). However, there is no compelling argument to do so and we will generalize this hypothesis – it is well known that Dirac quantum dynamics of spin-1/2 particles predicts both the magnitude $g = 2$ and identity of magnetic moments entering Eqs. (2) and (3).

While the conservation of electrical charge is rooted in gauge invariance symmetry, the magnitude of electrical charge has remained a riddle. The situation is similar for the case of the magnetic moment μ : spin properties are rooted in the Poincaré symmetry of space-time, however, the strength of spin interaction with magnetic field, Eqs. (1) and (3), is arbitrary but unique for each type of (classical) particle. Introducing the gyromagnetic ratio g we in fact create an additional conserved particle quality. This becomes clearer when we realize that the appearance of ‘ e ’ does not mean that particles we study need to be electrically charged.

First principle considerations of point particle relativistic dynamics experience some difficulties in generating Eqs. (2) and (3), as a rich literature on the subject shows – we will cite only work that is directly relevant to our approach; for further 70+ references see the recent numerical study of spin effects and radiation reaction in a strong electromagnetic field [9].

For what follows it is important to know that the spin precession Eq. (3) is a result of spatial rotational invariance which leads to angular and spin coupling, and thus spin dynamics can be found without a new dynamical principle as has been argued e.g. by Van Dam and Ruijgrok [13] and Schwinger [14]. Similar physics content is seen in the work of Skagerstam and Stern [15,16], who considered the context of fiber bundle structure focusing on Thomas precession.

Covariant generalization of the spin precession Eq. (3) is often attributed to the 1959 work by Bergmann–Michel–Telegdi [17]. However we are reminded [18–20] that this result was discovered already 33 years earlier by Thomas [21,22] at the time when the story of the electron gyromagnetic ratio $g = 2$ was unfolding. Following Jackson [18] we call the corresponding equation TBMT. Frenkel, who published [23,24] at the same time with L.H. Thomas explored the covariant form of the Stern–Gerlach force, a task we complete in this work.

There have been numerous attempts to improve the understanding of how spin motion back-reacts into the Lorentz force, generating the Stern–Gerlach force. In the 1962 review Nyborg [25] summarized efforts to formulate the covariant theory of electromagnetic forces including particle intrinsic magnetic moment. In 1972 Itzykson and Voros [26] proposed a covariant variational action principle formulation introducing the inertia of spin I , seeking a consistent variational principle but they found that no new dynamical insight resulted in this formulation.

Our study relates most to the work of Van Dam and Ruijgrok [13]. This work relies on an action principle and hence there are in the Lorentz force inconsistent terms that violate the constraint that the speed of light is constant, see e.g. their Eq. 3.11 and remarks: ‘The last two terms are $\mathcal{O}(e^2)$ and will be omitted in what follows.’ Other authors have proposed mass modifications to compensate for terms, a step which is equally unacceptable. For this reason our approach is intuitive, without insisting on ‘in principle there is an action’. Once we have secured a consistent, unique covariant extension of the Lorentz force, we explore the natural variational principle action. We find it is not consistent and we identify the origin of the variational principle difficulties.

We develop the concept of the classical point particle spin vector in the following Sect. 2. Our discussion relates to Casimir invariants rooted in space-time symmetry transformations. Using Poincaré group generators and Casimir eigenvalues we construct the particle momentum p^μ and particle space-like spin pseudo-vector s^μ . In Sect. 3 we present a consistent picture of the Stern–Gerlach force (Sect. 3.1) and generalize the TBMT precession equation (Sect. 3.2) to be linear in both, the EM field and EM field derivatives. We connect the Amperian form of SG force (3.1.1) with the Gilbertian force (3.1.2). We discuss non-uniqueness of spin dynamics (3.2.3) with consideration of the impact on muon $g - 2$ experiments. We show in Sect. 4 that the natural choice of action for the considered dynamical system does not lead to a consistent set of equations; in this finding we align with all prior studies of Stern–Gerlach extension to the Lorentz force.

In the final part of this work, Sect. 5, we show some of the physical consequences of this theoretical framework. In Sect. 5.1 we present a more detailed discussion of dynamical equations for the case of a particle in motion with a given $\beta = v/c$ and \mathcal{E} , \mathcal{B} in the laboratory. In Sect. 5.2 we study the solution of the dynamical equations for the case of an EM light wave pulse hitting a neutral particle. We have obtained exact solutions of this problem, details will follow under separate cover [27]. The concluding Sect. 6 is a brief summary of our findings.

1.1 Notation

For most of our notation, see Ref. [28]. Here we note that we use the SI unit system and the metric:

$$\text{diag } g_{\mu\nu} = \{1, -1, -1, -1\}, \quad p_\mu p^\mu = g_{\mu\nu} p^\mu p^\nu = \frac{E^2}{c^2} - \mathbf{p}^2,$$

We further recognize the totally antisymmetric covariant pseudo-tensor ϵ :

$$\epsilon_{\mu\nu\alpha\beta} = \sqrt{-g} \begin{cases} (-1)^{\text{perm}} & \text{if all indices are distinct} \\ 0 & \text{otherwise,} \end{cases}$$

where ‘perm’ is the signature of the permutation. It is important to remember when transiting to non-covariant notation in the laboratory frame of reference that the analog contravariant pseudo-tensor due to the odd number of space-like dimensions is negative for even permutations and positive for odd permutations. The Appendix B of Ref. [29] presents an introduction to ϵ .

We will introduce an elementary magnetic dipole charge d – the limitations of the alphabet force us to adopt the letter d otherwise used to describe the electric dipole to be the elementary magnetic dipole charge. The magnetic dipole charge of a particle we call d converts the spin vector s to magnetic dipole vector μ ,

$$sd\mathbf{c} = \boldsymbol{\mu}, \quad d \equiv \frac{|\boldsymbol{\mu}|}{c|s|}. \quad (4)$$

The factor c is needed in SI units since in the EM-tensor $F^{\mu\nu}$ has as elements \mathcal{E}/c and \mathcal{B} . It seems natural to introduce also $s^\mu d = \mu^\mu$, but this object can be confusing therefore we will stick to the product $s^\mu d$, however we always replace $sd \rightarrow \mu/c$. Note that we place d to the right of pertinent quantities to avoid confusion such as dx .

We cannot avoid the appearance in the same equation of both magnetic moment $\boldsymbol{\mu}$ and vacuum permeability μ_0 .

2 Spin vector

A classical intrinsic covariant spin has not been clearly defined or even identified in prior work. In some work addressing covariant dynamics of particles with intrinsic spin and magnetic moment, particle spin is by implication solely a quantum phenomenon. Therefore we describe the precise origin of classical spin conceptually and introduce it in explicit terms in the following.

Considering the Poincaré group of space-time symmetry transformations [30,31], it has been established that elementary particles have to be in a representation that is characterized by eigenvalues of two Casimir operators (a ‘bar’ marks operators)

$$\bar{C}_1 \equiv \bar{p}_\mu \bar{p}^\mu = \bar{p}^2 \equiv m^2 c^2, \quad \bar{C}_2 \equiv \bar{w}_\alpha \bar{w}^\alpha. \quad (5)$$

All physical point ‘particles’ have fixed eigenvalues of C_1, C_2 . The quantities (with a bar) \bar{p}^μ and \bar{w}^α are differ-

ential operators constructed from generators of the symmetry transformations of space-time; that is 10 generators of the Poincaré group of symmetry transformations of 4-space-time: \bar{p}^μ for translations, \bar{J} for rotations and \bar{K} for boosts. Once we construct suitable operator valued quantities we will transition to the physics of ‘c-number’ valued (without bar) variables as used in classical dynamics where all quantities will be normal numbers and rely on the eigenvalues of Casimir operators C_1, C_2 for each type of particle.

In Eq. (5) the first of the space-time operators based on generators of the four space-time translations p^μ guarantees that a point particle has a conserved inertial mass m (with a value specific for any particle type). The second Casimir operator C_2 is obtained from the square of the Pauli–Lubanski pseudo-4-vector

$$\bar{w}_\alpha = \bar{M}_{\alpha\beta}^* \bar{p}^\beta, \quad \bar{M}_{\alpha\beta}^* \equiv \frac{1}{2} \epsilon_{\alpha\beta\mu\nu} \bar{M}^{\mu\nu}. \quad (6)$$

Here $\bar{M}^{\mu\nu}$ is the antisymmetric tensor (operator) created from three Lorentz-boost generators \bar{K} and three space rotation generators \bar{J} such that

$$\frac{1}{2} \bar{M}_{\mu\nu} \bar{M}^{\nu\mu} = \bar{K}^2 - \bar{J}^2, \quad \frac{1}{4} \bar{M}_{\mu\nu}^* M^{\mu\nu} = \bar{J} \cdot \bar{K}. \quad (7)$$

These relations help us see that

$$F^{\mu\nu}(\mathbf{e}/c \rightarrow \bar{K}, \mathcal{B} \rightarrow \bar{J}) = \bar{M}^{\mu\nu}.$$

The generators \bar{J} , \bar{K} of space-time transformations are recognized by their commutation relations. They are used in a well known way to construct representations of the Lorentz group.

In terms of the generator tensor $\bar{M}^{\nu\mu}$ the covariant definition of the particle spin (operator) vector is

$$\bar{s}_\mu \equiv \frac{\bar{w}_\mu}{\sqrt{C_1}} = \bar{M}_{\mu\nu}^* \frac{\bar{u}^\nu}{c}, \quad \bar{u}^\mu \equiv \frac{c \bar{p}^\mu}{\sqrt{C_1}} = \frac{\bar{p}^\mu}{m}. \quad (8)$$

According to Eq. (8), spin \bar{s}_μ is a pseudo-vector, as required for angular dynamics. The dimension of \bar{s}^μ is the same as the dimension of the generator of space rotations \bar{J} . We further find that \bar{s}^μ is orthogonal to the 4-velocity (operator) \bar{u}^μ

$$c\bar{s} \cdot \bar{u} = \bar{u}^\nu \bar{M}_{\nu\mu}^* \bar{u}^\mu = 0, \quad (9)$$

by virtue of the antisymmetry of \bar{M}^* evident in the definition Eq. (6). The definition of the particle spin (operator) is unique: no other space-like (space-like given the orthogonality $s \cdot \bar{u} = 0$) pseudo-vector associated with the Poincaré group describing space-time symmetry transformations can be constructed.

We now transition to c-numbered quantities (dropping the bar): an observer ‘(0)’ co-moving with a particle measures

the 4-momentum and 4-spin s^μ

$$p_{(0)}^\mu \equiv \{\sqrt{C_1}, 0, 0, 0\}, \quad s_{(0)}^\mu \equiv \{0, 0, 0, \sqrt{|C_2|/C_1}\} \quad (10)$$

where according to convention the \hat{z} -axis of the coordinate system points in the direction of the intrinsic spin vector s . In the particle rest frame we see that

$$0 = p_{(0)}^\mu s_{(0)\mu}^{(0)} = p^\mu s_\mu|_{(0)} = m(u^\mu s_\mu)|_{\text{any frame}}, \quad (11)$$

is consistent with the operator equation Eq. (9); more generally, any space-like vector is normal to the time-like 4-velocity vector. For the magnitude of the spin vector we obtain

$$-s^2 \equiv s_{(0)}^\mu s_{(0)\mu}^{(0)} \equiv s^\mu s_\mu|_{(0)} = s^2|_{\text{any frame}} = \frac{-|C_2|}{C_1}. \quad (12)$$

We keep in mind that s^2 must always be a constant of motion in any frame of reference. Its value $s \cdot s = -s^2$ is always negative, appropriate for a space-like vector. Similarly

$$p_{(0)}^\mu p_\mu^{(0)} = p^2|_{\text{any frame}} = C_1 \equiv m^2 c^2, \quad (13)$$

must be a constant of motion in any frame of reference and the value p^2 is positive, appropriate for a time-like vector.

As long as forces are small in the sense discussed in Ref. [28] we can act as if the rules of relativity apply to both inertial and (weakly) accelerated frames of reference. This allows us to explore the action of forces on particles in their rest frame where Eq. (10) defines the state of a particle. By writing the force laws in covariant fashion we can solve for the dynamical evolution of $p^\mu(\tau)$, $s^\mu(\tau)$ as classical numbered variables.

3 Covariant dynamics

3.1 Generalized Lorentz force

3.1.1 Magnetic dipole potential and Amperian force

We have gone to great lengths in Sect. 2 to argue for the existence of particle intrinsic spin. For all massive particles this implies the existence of a particle intrinsic magnetic dipole moment, without need for magnetic monopoles to exist or current loops. Spin naturally arises in the context of symmetries of Minkowski space-time, it is not a quantum property.

In view of the above it is appropriate to study classical dynamics of particles that have both, an elementary electric charge e , and an elementary magnetic dipole charge d . The covariant dynamics beyond the Lorentz force needs to incorporate the Stern–Gerlach force. Thus the extension has to

contain the elementary magnetic moment of a particle contributing to this force. To achieve a suitable generalization we introduce the magnetic potential

$$B_\mu(x, s) d \equiv F_{\mu\nu}^*(x) s^\nu d, \quad F_{\mu\nu}^* = \frac{1}{2} \epsilon_{\mu\nu\alpha\beta} F^{\alpha\beta}. \quad (14)$$

We use the dual pseudo-tensor since s_μ is a pseudo-vector; the product in Eq. (14) results in a polar 4-vector B_μ . We note that the magnetic dipole potential B_μ by construction in terms of the antisymmetric field pseudo-vector $F_{\mu\nu}^*$, satisfies

$$\partial_\mu B^\mu = 0, \quad s \cdot B = 0, \rightarrow \quad B \cdot \frac{ds}{d\tau} = -s \cdot \frac{dB}{d\tau}. \quad (15)$$

The additional potential energy of a particle at rest placed in this magnetic dipole potential is

$$U_{(0)} \equiv B^0 c d = c F_{0\nu}^*(x) s^\nu d = -|\mu| \mathcal{B} \cdot \frac{s}{|s|} \equiv -\mu \cdot \mathcal{B}. \quad (16)$$

This shows Eq. (14) describes the energy content seen in Eq. (1); all factors are appropriate.

The explicit format of this new force is obtained when we use Eq. (14) to define a new antisymmetric tensor

$$G^{\mu\nu} = \partial^\mu B^\nu - \partial^\nu B^\mu = s_\alpha [\partial^\mu F^{*\nu\alpha} - \partial^\nu F^{*\mu\alpha}]. \quad (17)$$

Equation (17) allows us to add to the Lorentz force

$$m\dot{u}^\mu = H^{\mu\nu} u_\nu, \quad H^{\mu\nu} = e F^{\mu\nu} + G^{\mu\nu} d. \quad (18)$$

In the G -tensor we note the appearance in the force of the derivative of EM fields which is required if we are to see the Amperian model variant of the Stern–Gerlach force Eq. (2) as a part of generalized Lorentz force.

The Amperian–Stern–Gerlach (ASG) force 4-vector is obtained by multiplying $u_\nu d$ with the G -tensor Eq. (17). Thus the total 4-force a particle of charge e and magnetic dipole charge d experiences is

$$F_{\text{ASG}}^\mu = e F^{\mu\nu} u_\nu - u \cdot \partial F^{*\mu\nu} s_\nu d + \partial^\mu (u \cdot F^* \cdot s d). \quad (19)$$

In the particle rest frame we have

$$u^\nu|_{\text{RF}} = \{c, \mathbf{0}\}, \quad c s^\nu d|_{\text{RF}} = \{0, \boldsymbol{\mu}\}. \quad (20)$$

We can use Eq. (20) to read-off from Eq. (18) the particle rest frame force to be

$$F_{\text{ASG}}^\mu|_{\text{RF}} = \left\{ 0, e \mathcal{E} - \frac{1}{c^2} \boldsymbol{\mu} \times \frac{\partial \mathcal{E}}{\partial t} + \nabla(\boldsymbol{\mu} \cdot \mathcal{B}) \right\}, \quad (21)$$

where two contributions $\partial(\boldsymbol{\mu} \cdot \mathcal{B})/\partial t$ to F^0 cancel. Each of the three terms originates in one of the covariant terms in the sequence shown. The result is what one calls the Amperian model originating in dipoles created by current loops. This is however, not the last word in regard to the form of the force.

3.1.2 Gilbertian model Stern–Gerlach force

We restate the Stern–Gerlach–Lorentz force Eq. (18), showing the derivative terms explicitly,

$$\dot{m}u^\mu = eF^{\mu\nu}u_\nu + (\partial^\mu(u \cdot F^* \cdot s) - s_\alpha u \cdot \partial F^{*\mu\alpha})d. \quad (22)$$

Multiplying with s^μ the last term vanishes due to antisymmetry of F^* and we obtain

$$s \cdot \dot{u} = \frac{1}{m}s \cdot (eF - s \cdot \partial F^* d) \cdot u. \quad (23)$$

This equation suggests that we explore

$$eF^{\mu\nu} \rightarrow [\tilde{F}^{\mu\nu} \equiv eF^{\mu\nu} - s \cdot \partial F^{*\mu\nu} d], \quad (24)$$

as the generalized Lorentz force replacing the usual field tensor eF by \tilde{F} in a somewhat simpler way compared to the original $H^{\mu\nu}$ Eq. (18) modification.

We demonstrate now that the field modification seen in Eq. (24) leads to a different and fully equivalent format of the force. We replace in the first term in Eq. (22) $F \rightarrow \tilde{F}$ and add the extra term from Eq. (24) to the two remainder terms. Changing the index naming we can write symmetrically

$$\begin{aligned} \dot{m}u^\mu &= \tilde{F}^{\mu\nu}u_\nu \\ &+ s_\alpha(\partial^\alpha F^{*\mu\beta} + \partial^\mu F^{*\beta\alpha} + \partial^\beta F^{*\alpha\mu})u_\beta d. \end{aligned} \quad (25)$$

The tensor appearing in the parentheses in the 2nd line of Eq. (25) is antisymmetric under any of the three exchanges of the indices. It is therefore proportional to the totally antisymmetric tensor $\epsilon^{\alpha\mu\beta\gamma}$ which must be contracted with some 4-vector V_γ containing a gradient of the EM dual field tensor, there are two such available 4-vectors $\partial^\kappa F_{\kappa\gamma}^*$ which vanishes by virtue of Maxwell equations, and

$$V_\gamma = \frac{1}{2}\epsilon_{\gamma\kappa\eta\xi}\partial^\kappa F^{*\eta\xi} = \partial^\kappa F_{\kappa\gamma} = \mu_0 j_\gamma.$$

Thus we introduce the Gilbertian form of the 4-force

$$F_{\text{GSG}}^\mu = \tilde{F}^{\mu\nu}u_\nu - \mu_0 j^\gamma\epsilon_{\gamma\alpha\beta\nu}u^\alpha s^\beta g^{\nu\mu}d. \quad (26)$$

Note that in our formulation the Amperian and the Gilbertian 4-forces are identical

$$F_{\text{ASG}}^\mu = F_{\text{GSG}}^\mu, \quad (27)$$

they are just written differently.

In the rest frame of a particle, see Eq. (20) the Gilbertian force Eq. (27) is

$$F_{\text{GSG}}^\mu|_{\text{RF}} = \{0, e\mathcal{E} + (\boldsymbol{\mu} \cdot \nabla)\mathcal{B} + \mu_0\boldsymbol{\mu} \times \mathbf{j}\}. \quad (28)$$

It is interesting to see the mechanism by which the two formats of the forces are equal to each other in the particle rest frame. With

$$\nabla(\boldsymbol{\mu} \cdot \mathcal{B}) - (\boldsymbol{\mu} \cdot \nabla)\mathcal{B} = \boldsymbol{\mu} \times (\nabla \times \mathcal{B}),$$

we show that the difference between Eqs. (21) and (28) vanishes

$$[\mathbf{F}_{\text{ASG}} - \mathbf{F}_{\text{GSG}}]_{\text{RF}} = \boldsymbol{\mu} \times \left(-\frac{1}{c^2} \frac{\partial \mathcal{E}}{\partial t} + \nabla \times \mathcal{B} - \mu_0 \mathbf{j} \right) = 0. \quad (29)$$

The terms in parentheses cancel according to Maxwell equations confirming that both the Amperian and the Gilbertian forces are equal taking as an example the instantaneous rest frame. From now on we will use Gilbertian form of the force and in later examples we will focus on particle motion in vacuum, $j^\mu = 0$.

In this discussion of forces we kept the electrical charge e and the elementary magnetic moment ‘charge’ d Eq. (4) as independent qualities of a point particle. As noted in the introduction it is common to set $|\boldsymbol{\mu}| \equiv g\mu_B$, see above Eq. (3). Hence we can have both, charged particles without magnetic moment, or neutral particles with magnetic moment, aside from particles that have both charge and magnetic moment. For particles with both charge and magnetic moment we can write, using Gilbertian format of force

$$m\dot{u}^\mu = \tilde{F}^{\mu\nu}u_\nu = e \left(F^{\mu\nu} - (1+a)\lambda \frac{s \cdot \partial}{|s|} F^{*\mu\nu} \right) u_\nu, \quad (30)$$

where $a = (g-2)/2$ is the gyromagnetic ratio anomaly. The Compton wavelength $\lambda = \hbar/mc$ defines the scale at which the spatial field inhomogeneity is relevant; note that inhomogeneities of the field are boosted in size for a particle in motion, a situation which will become more explicit in Sect. 5.1.3.

3.2 Spin motion

3.2.1 Conventional TBMT

For particles with $m \neq 0$ differentiating Eq. (11) with respect to proper time we find

$$\dot{u} \cdot s + u \cdot \dot{s} = 0, \quad (31)$$

where we introduced proper time derivative $\dot{s}^\mu = ds^\mu/d\tau$. Schwinger observed [14] that given Eq. (31) one can use the covariant form of the dynamical Lorentz force equations for $du^\mu/d\tau$ to obtain

$$u_\mu \left(\frac{ds^\mu}{d\tau} - \frac{e}{m} F^{\mu\nu} s_\nu \right) = 0. \quad (32)$$

Here $F^{\mu\nu}$ is the usual EM field tensor. Equation (32) has the general TBMT solution

$$\frac{ds^\mu}{d\tau} = \frac{e}{m} F^{\mu\nu} s_\nu + \frac{\tilde{a}e}{m} \left(F^{\mu\nu} s_\nu - \frac{u^\mu}{c^2} (u \cdot F \cdot s) \right), \quad (33)$$

where we used the notation $u \cdot F \cdot s \equiv u_\mu F^{\mu\nu} s_\nu$.

In Eq. (33) \tilde{a} is an arbitrary constant considering that the additional term multiplied with u^μ vanishes. On the other hand we can read off the magnetic moment entering Eq. (3): the last term is higher order in $1/c^2$. Hence in the rest frame of the particle we see that $2(1+\tilde{a}) = g$ i.e. Eq. (33) reproduces Eq. (3) with the magnetic moment coefficient when $\tilde{a} = a$. Therefore, as introduced, $\tilde{a} = a$ is the $g \neq 2$ anomaly. However, in Eq. (33) we could for example use $\tilde{a} = (g^2 - 4)/8 = a + a^2/2$, which classical limit of quantum dynamics in certain specific conditions implies [12]. In this case $\tilde{a} \rightarrow a$ up to higher order corrections. This means that measurement of \tilde{a} as performed in experiments [1,2] depends on derivation of the relation of \tilde{a} with a obtained from quantum theory. These remarks apply even before we study gradient in field corrections.

3.2.2 Gradient corrections to TBMT

The arguments by Schwinger, see Eqs. (31)–(33), are ideally positioned to obtain in a consistent way generalization of the TBMT equations including the gradient of fields terms required for consistency. We use Eq. (24) in Eq. (33) to obtain

$$\begin{aligned} \frac{ds^\mu}{d\tau} &= \frac{1+\tilde{a}}{m} (eF^{\mu\nu} - s \cdot \partial F^{*\mu\nu} d) s_\nu \\ &+ \frac{\tilde{a}}{mc^2} (s \cdot eF \cdot u - s \cdot \partial s \cdot F^* u d) u^\mu. \end{aligned} \quad (34)$$

The dominant gradient of field correction arises for an elementary particle from the 2nd term in the first line in Eq. (34), considering the coefficient of the second line $a = \alpha_2/2\pi + \dots = 1.2 \times 10^{-3}$. One should remember that given the precision of the measurement [1,2] of \tilde{a} , which is driven by the first term in the second line in Eq. (34), we cannot in general neglect the new 2nd term in first line in Eq. (34), even if the characteristic length defining the gradient magnitude is the Compton wavelength λ , see Eq. (30).

3.2.3 Non-uniqueness of gradient corrections to TBMT

It is not self-evident that the form Eq. (34) is unique. To see that a family of possible extensions TBMT arises we recall the tensor Eq. (18) $H^{\mu\nu}$ made of the two potentials A^μ and B^μ . We now consider the spin dynamics in terms of the two field tensors, F and G replacing the usual EM-tensor $F^{\mu\nu}$ in the Schwinger solution, Eq. (33). In other words, we explore the dynamics according to

$$\begin{aligned} \frac{ds^\mu}{d\tau} &= \frac{1}{m} eF^{\mu\nu} s_\nu + \frac{\tilde{a}e}{m} \left(F^{\mu\nu} s_\nu - \frac{u^\mu}{c^2} (u \cdot F \cdot s) \right) \\ &+ G^{\mu\nu} s_\nu \frac{d}{m} + \left(G^{\mu\nu} s_\nu - \frac{u^\mu}{c^2} (u \cdot G \cdot s) \right) \frac{\tilde{b}d}{m}. \end{aligned} \quad (35)$$

Two different constants \tilde{a} and \tilde{b} are introduced now since the two terms shown involving F and G tensors could be included in Schwinger solution independently with different constants. Intuition demands that $\tilde{a} = \tilde{b}$. However, aside from algebraic simplicity we do not find any compelling argument for this assumption.

We return now to the definition of the G tensor Eq. (17) to obtain

$$\begin{aligned} G^{\mu\nu} s_\nu &= (s_\nu s_\alpha \partial^\mu F^{*\nu\alpha} - s \cdot \partial F^{*\mu\alpha} s_\nu) \\ &= -s \cdot \partial F^{*\mu\nu} s_\nu. \end{aligned} \quad (36)$$

The first term in the first line vanishes by antisymmetry of F^* tensor. We also have

$$u \cdot G \cdot s = -s \cdot \partial u \cdot F^* \cdot s. \quad (37)$$

Using Eqs. (36) and (37) we can combine in Eq. (35) the first two terms in both lines, and the last terms in both lines to obtain

$$\begin{aligned} \frac{ds^\mu}{d\tau} &= \frac{1+\tilde{a}}{m} \left(eF^{\mu\nu} - \frac{1+\tilde{b}}{1+\tilde{a}} s \cdot \partial F^{*\mu\nu} d \right) s_\nu \\ &- \tilde{a} \frac{u^\mu}{mc^2} \left(u \cdot \left(eF - \frac{\tilde{b}}{\tilde{a}} s \cdot \partial F^* d \right) \cdot s \right). \end{aligned} \quad (38)$$

This equation agrees with Eq. (34) only when $\tilde{a} = \tilde{b}$. However, this requirement is neither mathematically nor physically necessary. For example using Eq. (26) we easily check $s \cdot \dot{u} + u \cdot \dot{s} = 0$ without any assumptions about \tilde{a}, \tilde{b} .

As Eq. (35) shows the physical difference between factors \tilde{a} and \tilde{b} is related to the nature of the interaction: the ‘magnetic’ tensor G is related to \tilde{b} only. Thus for a neutral particle $e \rightarrow 0$ we see in Eq. (38) that the torque depends only on \tilde{b} . Conversely, when the effect of magnetic potential is negligible Eq. (38) becomes the textbook spin dynamics that depends on \tilde{a} alone.

To make further contact with textbook physics we note that the coefficient of the first term in Eq. (38)

$$\frac{1+\tilde{a}}{m}e = 2(1+\tilde{a})\frac{e\hbar}{2m}\frac{1}{\hbar} = \tilde{g}\mu_B\frac{1}{\hbar}, \quad \tilde{g} = 2(1+\tilde{a}), \quad (39)$$

should reproduce in leading order the torque coefficient in Eq. (3) as is expected from study of quantum correspondence. However, quantum correspondence could mean $\tilde{a} = a + a^2/2$, which follows comparing exact solutions of the Dirac equation with spin precession for the case we explored [12] and which is not exactly the motion of a muon in a storage ring. However, this means that in order to compare the measurement of magnetic moment of the muon carried out on macroscopic scale [1,2] with quantum computations requires a further step, the establishment of quantum correspondence at the level of precision at which the anomaly is measured.

4 Search for variational principle action

At the beginning of earlier discussions of a covariant extension to the Lorentz force describing the Stern–Gerlach force was always a well invented covariant action. However, the Lorentz force itself is not a consistent complement of the Maxwell equations. The existence of radiation means that an accelerated particle experiences radiation friction. The radiation-reaction force has not been incorporated into a variational principle [28,32]. Thus we should not expect that the Stern–Gerlach force must originate in a simple action.

We seek a path $x^\mu(\tau)$ in space-time that a particle will take considering an action that is a functional of the 4-velocity $u^\mu(\tau) = dx^\mu/d\tau$ and spin $s^\mu(\tau)$. Variational principle requires an action $I(u, x; s)$. When I respects space-time symmetries, the magnitudes of particle mass and spin are preserved in the presence of electromagnetic (EM) fields. We also need to assure that $u^2 = c^2$ which constrains the form of force and thus I that is allowed. Moreover, we want to preserve gauge invariance of the resultant dynamics.

The component in the action that produced the LHS (inertia part) of the Lorentz force remains in discussion. To generate the Lorentz force one choice of action is

$$I_{Lz}(u, x) = - \int d\tau mc\sqrt{u^2} - e \int d\tau u(\tau) \cdot A(x(\tau)). \quad (40)$$

We note that reparametrization of $\tau \rightarrow k\tau$ considering $u = dx/d\tau$ has no effect on the value of I_{Lz} .

Variation with respect to path leads to

$$\frac{d}{d\tau} mc \frac{u^\mu}{\sqrt{u^2}} = L_z^\mu = u_\nu \partial^\mu e A^\nu - \frac{d e A^\mu}{d\tau}, \quad (41)$$

where the RHS produces upon differentiation of $e A^\mu(x(\tau))$ the usual Lorentz force

$$L_{Lz}^\mu = e(\partial^\mu A^\nu - \partial^\nu A^\mu) u_\nu = e F^{\mu\nu} u_\nu. \quad (42)$$

Multiplying Eq. (41) with $m c u_\mu / \sqrt{u^2}$ we establish by anti-symmetry of the tensor $F^{\mu\nu}$ Eq. (42) that the product with the LHS in Eq. (41) also vanishes. This means that $(mc u_\nu / \sqrt{u^2})^2 = m^2 c^2 \equiv p^2 = \text{Const}$. Henceforth

$$p^\mu \equiv mc \frac{u^\mu}{\sqrt{u^2}}. \quad (43)$$

There is a problem when we supplement in Eq. (40) the usual action I_{Lz} by a term I_m based on our prior consideration of $A^\mu \rightarrow A^\mu + B^\mu$, see Sect. 3.1.1. The problem one encounters is that the quantity B^μ contains additional dependence on $s^\mu(\tau)$ which adds another term to the force. Let us look at the situation explicitly

$$I(u, x; s) = I_{Lz} + I_m, \quad I_m \equiv - \int d\tau u \cdot B(u, x; s) d. \quad (44)$$

Here the dependence on $s^\mu(\tau)$ is akin to a parameter dependence; some additional consideration defines the behavior, in our case this is the TBMT equations.

Varying with respect to the path the modified action Eq. (44) we find the modified covariant force

$$\frac{dp^\mu}{d\tau} = L_z^\mu + L_{S1}^\mu + L_{S2}^\mu, \quad (45)$$

with two new contributions

$$L_{S1}^\mu = (\partial^\mu B^\nu - \partial^\nu B^\mu) u_\nu = G^{\mu\nu} u_\nu, \quad (46)$$

$$L_{S2}^\mu = -F^{*\mu\nu} \frac{ds_\nu}{d\tau} d. \quad (47)$$

We applied here with $A \rightarrow B$ the result seen in Eq. (41), and the additional term L_{S2}^μ follows by remembering to take proper time derivative of s^μ . The first term Eq. (46) is as we identified previously in Eq. (18). We note that another additional term arises if and when an additional power of $\sqrt{u^2}$ accompanies $u \cdot B$ as was done in [13]. In either case, an unsolved problem is created by the torque-like term, Eq. (47).

If we replace in our thoughts $ds_\nu/d\tau$ in Eq. (47) by the TBMT equation Eq. (33) or as would be more appropriate by its extended version Eq. (35), we see that the force L_{S2}^μ would be quadratic in the fields containing also field derivatives. However, by assumption we modified the action limiting the new term in Eq. (44) to be linear in the fields and derivatives. Finding non linear terms we learn that this assumption was not justified. However, if we add the quadratic in fields term to the action we find following the chain of arguments just

presented that a cubic term is also required and so on; with derivatives of fields appearing at each iteration.

We have searched for some time for a form that avoids this circular conundrum, but akin to previous authors we did not find one. Clearly a ‘more’ first principle approach would be needed to create a consistent variational principle based equation system. On the other hand we have presented a formulation of spin dynamics which does not require a variational principle in the study of particle dynamics: as is we have obtained a dynamical equation system empirically. Our failing in the search for an underlying action is not critical. A precedent situation comes to mind here: the radiation emitted by accelerated charges introduces a ‘radiation friction’ which must be studied [28,32] without an available action, which is also based on empirical knowledge about the energy loss arising for accelerated charges.

5 Experimental consequences

5.1 Non covariant form of dynamical equations

5.1.1 Laboratory frame

In most physical cases we create a particle guiding field which is at rest in the laboratory. Particle motion occurs with respect to this prescribed field and thus in nearly all situations it is practical to study particle position $z^\mu(\tau)$ in the laboratory frame of reference. Employing the Lorentz-coordinate transformations from the particle rest frame to the laboratory frame we obtain

$$\frac{dz^\mu}{d\tau} \equiv u^\mu|_L = c\gamma(1, \beta), \quad \beta \equiv \frac{d\mathbf{z}}{dct} = \frac{\mathbf{v}}{c}, \quad (48)$$

$$s^\mu|_L = \left\{ \gamma\beta \cdot s, \left(\frac{\gamma}{\gamma+1} \gamma \beta \cdot s \right) \beta + s \right\}, \quad (49)$$

where as usual $\gamma = 1/\sqrt{1-\beta^2}$ and where one often sees the spin term written as $\gamma^2/(\gamma+1) = (\gamma-1)/\beta^2$.

One easily checks that Eqs. (48) and (49) also satisfy Eq. (11): $u_\mu s^\mu = 0$. A classic result of TBMT reported in textbooks is that the longitudinal polarization $\hat{\beta} \cdot s$ for $g \simeq 2$ and $\beta \rightarrow 1$ is a constant of motion. This shows that for a relativistic particle the magnitude of both time-like and space-like components of the spin 4-vector Eq. (49) can be arbitrarily large, even if the magnitude of the 4-vector is bounded $s_\mu s^\mu = -s^2$. This behavior parallels the behavior of 4-velocity $u^\mu u_\mu = c^2$.

We remind that to obtain in the laboratory frame the usual Lorentz force we use the 4-velocity with respect to the Laboratory frame Eq. (48), with laboratory defined tensor F , i.e. with laboratory given \mathcal{E} , \mathcal{B} EM-fields

$$\frac{d(mu^\mu|_L)}{d\tau} = (e F^{\mu\nu} u_\nu)|_L = e F^{\mu\nu}|_L u_\nu|_L. \quad (50)$$

Sometimes it is of advantage to transform Eq. (50) to the particle rest frame. Such a transformation L with $Lu|_{\text{rest}} = u_L$ when used on the left hand side in Eq. (50) produces proper time differentiation of the transformation operator, see also [33]. Such transformation into a co-rotating frame of reference originates the Thomas precession term in particle rest frame for the torque equation. This term is naturally present in the covariant formulation when we work in the laboratory reference frame.

For the full force Eq. (26) we thus have

$$\frac{d(mu^\mu|_L)}{d\tau} = e F^{\mu\nu}|_L u_\nu|_L \quad (51)$$

$$- d s_\alpha|_L (\partial^\alpha F^{*\mu\nu})|_L u_\nu|_L. \quad (52)$$

We see that in the laboratory frame of reference a covariant gradient of the fields is prescribed, i.e. that some apparatus prescribes the magnitude

$$Q^{\alpha\mu\nu}|_L \equiv \partial^\alpha F^{*\mu\nu}|_L, \quad (53)$$

which allows for a moving particle with $u^\mu|_L$ Eq. (48) and $s^\mu|_L$ Eq. (49) to experience the Stern–Gerlach force F_{SG}^μ

$$F_{SG}^\mu|_L \equiv -d s_\alpha|_L Q^{\alpha\mu\nu}|_L u_\nu|_L. \quad (54)$$

We have gone to extraordinary length in arguing Eq. (54) to make sure that the forthcoming finding of the Lorentz boost of field inhomogeneity is not questioned.

5.1.2 Magnetic potential in the laboratory frame

We evaluate in the laboratory frame the form of Eq. (14). The computation is particularly simple once we first recall the laboratory format of the Lorentz force F_L^μ

$$F_L^\mu|_L = F^{\mu\nu}(x) u_\nu|_L = c\gamma \{ \beta \cdot \mathcal{E}/c, \mathcal{E}/c + \beta \times \mathcal{B} \} \quad (55)$$

The magnetic part of the action will be evaluated (see second line below) in analogy to above. We now consider

$$\begin{aligned} B \cdot u|_L &= u \cdot F^* \cdot s|_L = -s^\mu|_L (F_{\mu\nu}^* u^\nu)|_L \\ &= -s^\nu|_L c\gamma \{ -\beta \cdot \mathcal{B}, \mathcal{B} - \beta \times \mathcal{E}/c \} \\ &= c\gamma \left(\beta \cdot s \beta \cdot \mathcal{B} \frac{\gamma}{\gamma+1} - s \cdot (\mathcal{B} - \beta \times \mathcal{E}/c) \right) \end{aligned} \quad (56)$$

where we used in 2nd line (i) $F_{\mu\nu}^*$ follows from the usual $F^{\mu\nu}$ upon exchange of $\mathcal{E}/c \leftrightarrow \mathcal{B}$ and (ii) flip $\beta \rightarrow -\beta$ to account for contravariant and not covariant 4-velocity. In the 3rd line we used $\gamma(\gamma/(\gamma+1)-1) = -\gamma/(\gamma+1)$. Notable

in Eq. (56) is the absence of the highest power γ^2 as all terms cancel, the result is linear in (large) γ .

For the magnetic potential energy of a particle in the laboratory frame we obtain

$$U \equiv B \cdot u|_L d = \gamma \left(K \hat{\beta} \cdot \mu \hat{\beta} \cdot \mathcal{B} - \mu \cdot (\mathcal{B} - \beta \times \mathcal{E}/c) \right), \quad (57)$$

$$K = \beta^2 \frac{\gamma}{\gamma + 1} = 1 - \sqrt{1 - \beta^2} = \begin{cases} \frac{1}{2}\beta^2, & \text{for } \beta \rightarrow 0, \\ 1, & \text{for } \beta \rightarrow 1. \end{cases}$$

Equation (57) extends the rest frame $\beta = 0$ Eq. (16) and represents a covariant generalization of Eq. (1). In ultrarelativistic limit all terms in Eq. (57) have the same magnitude.

5.1.3 Field to particle energy transfer

We now consider the energy gain by a particle per unit of laboratory time, that is we study the zeroth component of Eq. (26)

$$\frac{dE}{dt} = c \frac{d\tau}{dt} \frac{d(mu^0|_L)}{d\tau} = c\gamma^{-1} \tilde{F}^{0v} u_v|_L = e\mathcal{E} \cdot v + cd s^\alpha|_L (\partial_\alpha \mathcal{B})|_L \cdot v, \quad (58)$$

$$\frac{dE}{dt} = (e\mathcal{E} + (\mu \cdot \nabla) \mathcal{B}) \cdot v$$

$$+ \gamma \beta \cdot \mu \left(\frac{\partial \mathcal{B}}{\partial dt} + \frac{\gamma}{\gamma + 1} (\beta \cdot \nabla) \mathcal{B} \right) \cdot v, \quad (59)$$

A further simplification is achieved considering

$$\frac{\partial \mathcal{B}}{\partial dt} + (\beta \cdot \nabla) \mathcal{B} = \frac{\partial \mathcal{B}}{\partial dt} + \sum_{i=1}^3 \frac{dx_i}{cdt} \frac{\partial \mathcal{B}}{\partial x_i} = \frac{d\mathcal{B}}{cdt}, \quad (60)$$

where the total derivative with respect to time accounts for both, the change in time of the laboratory given field \mathcal{B} , and the change due to change of position in the field by the moving particle. We thus find two parts

$$\frac{dE}{dt} = v \cdot (e\mathcal{E} + (\mu \cdot \nabla) \mathcal{B} - K\hat{\beta} \cdot \mu (\hat{\beta} \cdot \nabla) \mathcal{B}) + \beta \cdot \frac{d\mathcal{B}}{dt} \gamma \beta \cdot \mu, \quad (61)$$

where the 2nd line is of particular interest as it is proportional to γ . Focusing our attention on this last term: we can use $\beta = cp/E$ and $\gamma\beta = p/mc$. Upon multiplication with E and remembering that $c^2 pdp = EdE$ we obtain

$$p \cdot \left(\frac{dp}{dt} - \frac{d\mathcal{B}}{dt} \frac{\mu \cdot p}{mc^2} \right) = 0, \quad (62)$$

which in qualitative terms implies an exponential response of particle momentum as it crosses a magnetic field

$$|p| \simeq mc e^{\pm(|\mathcal{B}| - |\mathcal{B}_0|)|p|/mc^2}.$$

However, even a magnetar magnetic field of up 10^{11} T will not suffice to impact electron momentum decisively in view of the smallness of the electron magnetic moment 5.810^{-11} MeV/T. However, in ultrarelativistic heavy ion collisions at the LHC 10,000 times stronger very non-homogeneous \mathcal{B} -fields arise.

5.2 Neutral particle hit by a light pulse

5.2.1 Properties of equations

The dynamical equations developed here have a considerably more complex form compared to the Lorentz force and TBMT spin precession in constant fields [33]. We need field gradients in the Stern-Gerlach force, and in the related correction in the TBMT equations. Since the new physics appears only in the presence of a particle magnetic moment, we simplify by considering neutral particles. We now show that the external field described by a light wave (pulse) lends itself to an analytical solution effort. This context could be of practical relevance in the study of laser interaction with magnetic atoms, molecules, the neutron and maybe neutrinos.

For $e = 0$ our Eqs. (26) and (38) read

$$\dot{u}^\mu = -s \cdot \partial F^{*\mu\nu} u_\nu \frac{d}{m}, \quad (64)$$

$$\dot{s}^\mu = -s \cdot \partial F^{*\mu\nu} s_\nu \frac{1 + \tilde{b}}{m} d + u^\mu u \cdot (s \cdot \partial) F^* \cdot s \frac{\tilde{b} d}{mc^2}. \quad (65)$$

The external light wave field is a pulse with

$$A^\mu = e^\mu f(\xi), \quad \xi = k \cdot x, \quad k \cdot \varepsilon = 0. \quad (66)$$

The derivative of the dual EM tensor for linear fixed in space pulse polarization ε^μ is

$$(s \cdot \partial) F^{*\mu\nu} = (k \cdot s) \epsilon^{\mu\nu\alpha\beta} k_\alpha \varepsilon_\beta f''(\xi), \quad (67)$$

where prime ‘‘ $'$ ’ indicates a derivative with respect to the phase ξ .

Notice that if we contract Eq. (67) with k_μ or ε_μ we get zero because the Levi-Civita tensor $\epsilon^{\mu\nu\alpha\beta}$ is totally antisymmetric. Therefore contracting Eq. (64) with either k_μ or ε_μ we find

$$0 = k \cdot \dot{u} \rightarrow k \cdot u = k \cdot u(0), \quad u^\mu(0) = u^\mu(\tau_0) \quad (68)$$

$$0 = \varepsilon \cdot \dot{u} \rightarrow \varepsilon \cdot u = \varepsilon \cdot u(0). \quad (69)$$

We further note that the argument of the light pulse Eq. (66) satisfies

$$\xi = k \cdot x \rightarrow \dot{\xi} = k \cdot \dot{x} = k \cdot u = k \cdot u(0), \quad (70)$$

where we used Eq. (68). Thus we conclude that the particle follows the pulse such that

$$\xi = k \cdot x = \tau k \cdot u(0) + \xi_0, \quad \xi_0 = k \cdot x(0). \quad (71)$$

The two conservation laws Eqs. (68) and (69) along with Eq. (70) make the light pulse an interesting example amenable to an analytical solution.

We now evaluate several invariants in the laboratory frame seeking understanding of their relevance. A particle moving in the laboratory frame in consideration of Eq. (48) experiences in its rest frame a plane wave with the Doppler shifted frequency

$$k \cdot u(0) = \gamma_0(1 - \mathbf{n} \cdot \boldsymbol{\beta}_0)\omega, \quad (72)$$

which is unbounded as it grows with particle laboratory Lorentz- γ_0 . However, $k \cdot s$, the projection of spin onto plane wave 4-momentum k^μ , is bounded. To see this we recall the constraint Eq. (11), which in the laboratory frame reads

$$S_L^0 - \boldsymbol{\beta} \cdot S_L = 0. \quad (73)$$

We thus obtain

$$k \cdot s(\tau) = k \cdot s(\tau)|_L = |\mathbf{k}| (S_L^0 - \mathbf{n} \cdot S_L) = |\mathbf{k}| (\boldsymbol{\beta} - \mathbf{n}) \cdot S_L, \quad (74)$$

where we used Eq. (73) in the last equality. Since $\boldsymbol{\beta}$ and $\mathbf{n} = \mathbf{k}/|\mathbf{k}|$ are unit-magnitude vectors we find

$$(k \cdot s(\tau))^2 \leq 4k^2 S_L^2. \quad (75)$$

The magnitude of the spin vector in the lab frame is constrained by Eq. (12)

$$-s^2 = S_L^{02} - S_L^2 = (\boldsymbol{\beta} \cdot S_L)^2 - S_L^2. \quad (76)$$

where we again used Eq. (73). Combining Eqs. (75) and (76) we see that except when the particle is moving exactly in the direction of S_L , the magnitude of $(k \cdot s(\tau))^2$ is bounded.

5.2.2 Invariant acceleration and spin precession

Even without knowing the explicit form for $u^\mu(\tau)$, $s^\mu(\tau)$ we were able to obtain [27] the invariant acceleration

$$\dot{u}^2(\tau) = - \left(\frac{d}{m} f''(\xi(\tau)) k \cdot s(\tau) k \cdot u(0) \right)^2. \quad (77)$$

This result can be directly obtained by evaluating the square of Eq. (64).

We see in Eq. (77) that the magnitude of the 4-force created by a light pulse and acting on an ultrarelativistic particle is dependent on the square of the product of the 2nd derivative of the pulse function with respect to ξ , $f''(\xi)$, with the Doppler shifted frequency Eq. (72). The value Eq. (77) is negative since acceleration is a space-like vector.

As we discussed below Eq. (76) the spin precession factor $k \cdot s$ seen in Eq. (77) is bounded. We were able to obtain a soluble formulation of the spin precession dynamics described by the dimensionless variable

$$y = k \cdot s(\tau) \frac{\tilde{b} d}{mc C_1}, \quad (78)$$

which satisfies the differential equation

$$\left(\frac{dy(s)}{ds} \right)^2 = y^2(1 - y^2) \quad s = (f'(\xi(\tau)) - f'(\xi_0)) C_1 \quad (79)$$

obtained performing suitable manipulations of dynamical equations prior to solving for $u^\mu(\tau)$, $s^\mu(\tau)$. We are seeking bounded periodic solutions of the nonlinear Eq. (79) no matter how large the constant C_1 becomes, which is determined by the initial conditions

$$C_1 \equiv \frac{\tilde{b} d}{mc} k \cdot s(0) C_2, \quad C_2 \geq 1, \quad (80)$$

$$C_2 \equiv \sqrt{\frac{|(k \cdot u)^2| s^2 - [(k \cdot u)(\varepsilon \cdot s) - (\varepsilon \cdot u)(k \cdot s)]^2}{c^2 (k \cdot s)^2}} \Big|_{\tau=0}. \quad (81)$$

C_2 contains the initial particle Lorentz- γ factor. One can see several possible solutions of interest of Eq. (79); for example $y = \sin(\phi(s))$ satisfies all constraints. It leads to the pendulum type differential equation and we recognize that high intensity light pulses can flip particle spin. However, there are other relevant solutions, e.g. $y \propto 1/\cosh z$.

Upon solution of Eq. (79) $k \cdot s(\tau)$ is known. Given Eq. (71) we also know the dependence of Eq. (67) on proper time τ . Hence Eq. (64) can be solved for u^μ and Eq. (65) can be solved for s^μ resulting in an analytical solution of the dynamics of a neutral magnetic dipole moment in the field of a light pulse of arbitrary shape. The full description of the dynamics exceeds in length this presentation and will follow [27].

6 Conclusions

The Stern–Gerlach covariant extension of the Lorentz force has seen considerable interest as there are many immediate applications listed in first paragraph. Here we have:

- introduced in Eq. (10) the covariant classical 4-spin vector s^μ in a way expected in the context of Poincaré symmetry of space-time;
- presented a unique linear in fields form of the covariant magnetic moment potential, Eq. (14), which leads to a natural generalization of the Lorentz force;
- shown that the resultant Amerrian, Eq. (19), and Gilbertian, Eq. (26), forms of the magnetic moment force are equivalent;
- extended the TBMT torque dynamics, Eq. (35), making these consistent with the modifications of the Lorentz force;
- demonstrated the need to connect the magnetic moment magnitude entering the Stern–Gerlach force with the one seen in the context of torque dynamics, Sect. 3.2.3;
- shown that variational principle based dynamics has systematic failings when both position and spin are addressed within present day conceptual framework, see Sect. 4;
- reduced the covariant dynamical equations to laboratory frame of reference uncovering important features governing the coupled dynamics, see Sect. 5.1;
- obtained work done by variations of magnetic field in space-time on a particle, Eq. (61);
- shown salient features of solutions of neutral particles with non-zero magnetic moment hit by a laser pulse, see Sect. 5.2.

Open Access This article is distributed under the terms of the Creative Commons Attribution 4.0 International License (<http://creativecommons.org/licenses/by/4.0/>), which permits unrestricted use, distribution, and reproduction in any medium, provided you give appropriate credit to the original author(s) and the source, provide a link to the Creative Commons license, and indicate if changes were made.

Funded by SCOAP³.

References

- J. Grange et al. [Muon g-2 Collaboration], Muon (g-2) technical design report. FERMILAB-FN-0992-E. [arXiv:1501.06858](https://arxiv.org/abs/1501.06858) [physics.ins-det]
- G.W. Bennett et al. [Muon g-2 Collaboration], Final report of the muon E821 anomalous magnetic moment measurement at BNL. Phys. Rev. D **73**, 072003 (2006). <https://doi.org/10.1103/PhysRevD.73.072003>
- K.T. McDonald, *Forces on Magnetic Dipoles* (Joseph Henry Laboratories, Princeton University, Princeton). <http://www.physics.princeton.edu/~mcdonald/examples/neutron.pdf>. Retrieved November 2017; document dated October 26, 2014; updated February 17, 2017
- F. Mezei, La nouvelle vague in polarized neutron scattering. Physica B+C **137**, 295 (1986). [https://doi.org/10.1016/0378-4363\(86\)90335-9](https://doi.org/10.1016/0378-4363(86)90335-9)
- X.G. Huang, Electromagnetic fields and anomalous transports in heavy-ion collisions—a pedagogical review. Rep. Prog. Phys. **79**(7), 076302 (2016). <https://doi.org/10.1088/0034-4885/79/7/076302>; [arXiv:1509.04073](https://arxiv.org/abs/1509.04073) [nucl-th]
- M. Greif, C. Greiner, Z. Xu, Magnetic field influence on the early dynamics of heavy-ion collisions. Phys. Rev. C **96**, 014903 (2017). <https://doi.org/10.1103/PhysRevC.96.014903>; [arXiv:1704.06505](https://arxiv.org/abs/1704.06505) [hep-ph]
- R. Turolla, S. Zane, A. Watts, Magnetars: the physics behind observations. A review. Rep. Prog. Phys. **78**(11), 116901 (2015). <https://doi.org/10.1088/0034-4885/78/11/116901>; [arXiv:1507.02924](https://arxiv.org/abs/1507.02924) [astro-ph.HE]
- A. Sedrakian, X.G. Huang, M. Sinha, J.W. Clark, From microphysics to dynamics of magnetars. J. Phys. Conf. Ser. **861**(1), 012025 (2017). <https://doi.org/10.1088/1742-6596/861/1/012025>; [arXiv:1701.00895](https://arxiv.org/abs/1701.00895) [astro-ph.HE]
- M. Wen, C.H. Keitel, H. Bauke, Spin-one-half particles in strong electromagnetic fields: spin effects and radiation reaction. Phys. Rev. A **95**, 042102 (2017). <https://doi.org/10.1103/PhysRevA.95.042102>; [arXiv:1610.08951](https://arxiv.org/abs/1610.08951) [physics.plasm-ph]
- K.J. Kugler, W. Paul, U. Trinks, A magnetic storage ring for neutrons. Phys. Lett. **72B**, 422 (1978). [https://doi.org/10.1016/0370-2693\(78\)90154-5](https://doi.org/10.1016/0370-2693(78)90154-5)
- J. Rafelski, L. Labun, A cusp in QED at $g = 2$. [arXiv:1205.1835](https://arxiv.org/abs/1205.1835) [hep-ph]
- A. Steinmetz et al., in preparation
- H. Van Dam, T.W. Ruijgrok, Classical relativistic equations for particles with spin moving in external fields. Physica A **104**, 281 (1980). [https://doi.org/10.1016/0378-4371\(80\)90088-6](https://doi.org/10.1016/0378-4371(80)90088-6)
- J.S. Schwinger, Spin precession—a dynamical discussion. Am. J. Phys. **42**, 510 (1974). <https://doi.org/10.1119/1.1987764>
- B.-S. Skagerstam, A. Stern, Lagrangian descriptions of classical charged particles with spin. Phys. Scr. **24**, 493 (1981). <https://doi.org/10.1088/0031-8949/24/3/002>
- A.P. Balachandran, G. Marmo, B.-S. Skagerstam, A. Stern, Gauge theories and fibre bundles—applications to particle dynamics. Lect. Notes Phys. **188**, 1 (1983). https://doi.org/10.1007/3-540-12724-0_1, 2nd. Edition: [arXiv:1702.08910](https://arxiv.org/abs/1702.08910) [quant-ph]
- V. Bargmann, L. Michel, V.L. Telegdi, Precession of the polarization of particles moving in a homogeneous electromagnetic field. Phys. Rev. Lett. **2**, 435 (1959). <https://doi.org/10.1103/PhysRevLett.2.435>
- J.D. Jackson, Examples of the zeroth theorem of the history of science. Am. J. Phys. **76**, 704 (2008). <https://doi.org/10.1119/1.2904468> (see case VI)
- V. Hushwater, On the discovery of the classical equations for spin motion in electromagnetic field. Am. J. Phys. **82**, 6 (2014). <https://doi.org/10.1119/1.4821347>
- J.D. Jackson, Jackson responds. Am. J. Phys. **82**, 7 (2014)
- L.H. Thomas, The motion of a spinning electron. Nature **117**, 514 (1926). <https://doi.org/10.1038/117514a0> (Issue of April 10, discussion of spin precession for $g = 2$)
- L.H. Thomas, The kinematics of an electron with an axis. Philos. Mag. Ser. **7**(3), 1 (1927). <https://doi.org/10.1080/14786440108564170>
- J. Frenkel, (no title letter to editors). Nature **117**, 653 (1926) (Issue of 8 May)
- J. Frenkel, Die Elektrodynamik des rotierenden Elektrons, (translated: The dynamics of spinning electron). Z. Phys. **37**, 243 (1926). <https://doi.org/10.1007/BF01397099>
- P. Nyborg, On classical theories of spinning particles. II. Nuovo Cimento **23**, 47 (1962). <https://doi.org/10.1007/BF02733541>
- C. Itzykson, A. Voros, Classical electrodynamics of point particles. Phys. Rev. D **5**, 2939 (1972). <https://doi.org/10.1103/PhysRevD.5.2939>
- M. Formanek, S. Evans, J. Rafelski, A. Steinmetz, C.T. Yang, Strong fields and neutrino magnetic moment dynamics. [arXiv:1712.07698](https://arxiv.org/abs/1712.07698) [hep-ph]
- J. Rafelski, *Relativity Matters: From Einstein's EMC2 to Laser Particle Acceleration and Quark-Gluon Plasma* (Springer, Heidelberg, 2017). [https://doi.org/10.1007/978-3-319-51230-3](https://doi.org/10.1007/978-3-319-51231-0)
- R.M. Wald, *General Relativity* (Chicago University Press, Chicago, 1984). <https://doi.org/10.7208/chicago/9780226870373.001.0001>, ISBN:0-226-87033-2
- W. Greiner, J. Rafelski, *Spezielle Relativitätstheorie: Ein Lehr- und Übungsbuch für Anfangssemester* (translated: Special Theory of Relativity: A Text and exercise book for undergraduates); appeared as Volume 3a of Walter Greiner Series in Theoretical Physics; H. Deutsch (Frankfurt 1984, 1989, 1992). ISBN:3-87144-711-0; 1989; ISBN:3-97171-1063-4; and 1992: ISBN:3-8171-1205-X
- Y. Hadad, L. Labun, J. Rafelski, N. Elkina, C. Klier, H. Ruhl, Effects of radiation-reaction in relativistic laser acceleration. Phys. Rev. D **82**, 096012 (2010). <https://doi.org/10.1103/PhysRevD.82.096012>
- A.E. Lobanov, O.S. Pavlova, Solutions of the classical equation of motion for a spin in an electromagnetic field. Theor. Math. Phys. **121**, 1691 (1999). <https://doi.org/10.1007/BF02557213>. Translated from Russian: **121**, 509 (1999)

APPENDIX D

Dynamic fermion flavor mixing through transition dipole moments

Rafelski, J., Steinmetz, A., Yang, C.T. Dynamic fermion flavor mixing through transition dipole moments. *arXiv preprint.* 2023. [arXiv:2309.15797 \[hep-ph\]](https://arxiv.org/abs/2309.15797)

Copyright (2023) by the authors. Contribution to the book edited by Gerhard Buchalla, Dieter Lüst and Zhi-Zhong Xing dedicated to memory of Harald Fritzsch. Submitted an a separate article to International Journal of Modern Physics A.

Dynamic fermion flavor mixing through transition dipole moments

Johann Rafelski^{DOI}, Andrew Steinmetz^{DOI}, and Cheng Tao Yang^{DOI}

Department of Physics, The University of Arizona, Tucson, AZ 85721, USA

Received 27 September 2023

We show that Majorana neutrino flavor mixing can be driven by transition dipole moments in the presence of external electromagnetic fields. We demonstrate the sensitivity of the rotation mixing matrix to strong fields obtaining dynamical mass eigenstates in the two-flavor model. The three-flavor case, and extensions to the quark sector, are introduced.

Keywords: Majorana neutrinos; transition magnetic dipoles; electromagnetic fields.

PACS numbers: 14.60.Lm, 14.60.Pq, 13.15.+g, 13.40.Em

1. Introduction

Advancement of the understanding of neutrino physical properties attracts much interest today. Neutrinos are very abundant in the Universe; they were a dominant form of energy density in the Universe for much of its history, and they influence stellar and supernova evolution. As neutrinos are naturally massless in the standard model, the observed flavor oscillation signal non-vanishing neutrino mass. This suggests that neutrinos could provide a window to explore Beyond Standard Model (BSM) physics. This also motivates intense efforts to determine whether they are Dirac-type or Majorana-type fermions, with the latter serving as their own antiparticle.

We study the connection between Majorana neutrino transition magnetic dipole moments^{1–3} and neutrino flavor oscillation. Neutrino electromagnetic (EM) properties have been considered before,^{4–7} including the effect of oscillation^{8–12} in magnetic fields. The case of transition moments has the mathematical characteristics of an off-diagonal mass, which is distinct from normal direct dipole moment behavior. EM field effects are also distinct from weak interaction remixing within matter, *i.e.* the Mikheyev-Smirnov-Wolfenstein effect.^{13–15}

For the case of two nearly degenerate neutrinos with transition moments, we determine in an explicit manner their eigenstates in the presence of EM fields. We obtain an EM-mass basis, distinct from flavor and free-particle mass basis, which mixes flavors as a function of EM fields. Moreover, we show solutions relating to full EM field tensor, which result in covariant expressions allowing for both magnetic and electrical fields we have not seen considered before. As neutrinos are electrically

neutral, they have no intrinsic magnetic moment due to their spin; therefore any nonzero dipole moment is anomalous.

An anomalous magnetic moment (AMM) can be introduced into the neutrino Lagrangian via a Pauli term.^{16–18} Noteworthy for Majorana neutrinos, they can only possess transition magnetic moments which couple different flavors electromagnetically and do not violate CPT symmetry. Transition moments break lepton number conservation, therefore neutrino flavors could be remixed when exposed to strong EM fields.

The size of the neutrino magnetic dipole moment can be constrained as follows: The lower bound is found by higher order standard model interactions with the minimal extension of neutrino mass m_ν included.^{1–3} The upper bound is derived from reactor, solar, and astrophysical experimental observations.^{19–22} The bounds are expressed in terms of the electron Bohr magneton μ_B as

$$\frac{e\hbar G_F m_\nu c^2}{8\pi^2 \sqrt{2}} \sim 10^{-20} \mu_B < \mu_\nu^{\text{eff}} < 10^{-10} \mu_B, \quad \mu_B = \frac{e\hbar}{2m_e}, \quad (1)$$

where G_F is the Fermi constant and μ_ν^{eff} is the characteristic size of the neutrino magnetic moment. In Eq. (1), the lower bound was estimated using a characteristic mass of $m_\nu \sim 0.1$ eV. From cosmological studies, the sum of neutrino masses is estimated²³ to be $\sum_i m_i < 0.12$ eV; the electron (anti)neutrino mass is bounded²⁴ by $m_e^\nu < 0.8$ eV.

We discuss the standard flavor mixing method and explore the Lagrangian density containing both Majorana mass and transition dipole moments in Sec. 2. In Sec. 2.3 we discuss the properties of the relativistic Pauli dipole. The two-flavor neutrino model is evaluated explicitly in Sec. 3 where the remixed electromagnetic-mass eigenstates are obtained. The strong field (degenerate mass) and weak field limits are explored. While we focus our analysis on Majorana neutrinos, we note that the techniques in this work can be extended to apply to Dirac fermions in general; therefore they may be of interest also in the quark and charged lepton sector. Our results and future research outlook are described in Sec. 4.

2. Neutrino flavor mixing and electromagnetic fields

2.1. Standard flavor mixing method

Oscillation of neutrino flavors observed in experiment is in general interpreted as being due to a difference in neutrino mass and flavor eigenstates. This misalignment between the two representations is described as rotation of the neutrino flavor N -vector where $N = 3$ is the observed number of generations. The unitary mixing matrix $V_{\ell k}$ allows for the change of basis between mass (k) and flavor (ℓ) eigenstates via the transform

$$\nu_\ell = \sum_{k=1}^3 V_{\ell k} \nu_k \rightarrow \begin{pmatrix} \nu_e \\ \nu_\mu \\ \nu_\tau \end{pmatrix} = \begin{pmatrix} V_{e1} & V_{e2} & V_{e3} \\ V_{\mu 1} & V_{\mu 2} & V_{\mu 3} \\ V_{\tau 1} & V_{\tau 2} & V_{\tau 3} \end{pmatrix} \begin{pmatrix} \nu_1 \\ \nu_2 \\ \nu_3 \end{pmatrix}, \quad (2)$$

where ν_ℓ is the neutrino state four-spinor written in the flavor basis, while in the mass basis we use ν_k with $k \in 1, 2, 3$. Hereafter we will use implied summation over repeated flavor indices. Spinor indices will be suppressed.

The parameterization of the components of the mixing matrix depends on the Dirac or Majorana nature of the neutrinos. First we recall the Dirac neutrino mixing matrix $U_{\ell k}$ in the standard parameterization¹⁸

$$U_{\ell k} = \begin{pmatrix} c_{12}c_{13} & s_{12}c_{13} & s_{13}e^{-i\delta} \\ -s_{12}c_{23} - c_{12}s_{13}s_{23}e^{i\delta} & c_{12}c_{23} - s_{12}s_{13}s_{23}e^{i\delta} & c_{13}s_{23} \\ s_{12}s_{23} - c_{12}s_{13}c_{23}e^{i\delta} & -c_{12}s_{23} - s_{12}s_{13}c_{23}e^{i\delta} & c_{13}c_{23} \end{pmatrix}, \quad (3)$$

where $c_{ij} = \cos(\theta_{ij})$ and $s_{ij} = \sin(\theta_{ij})$. In this convention, the three mixing angles $(\theta_{12}, \theta_{13}, \theta_{23})$ are understood to be the Euler angles for generalized rotations and δ is the CP-violating complex phase.

For the Majorana case we must allow a greater number of complex phases: Majorana neutrinos allow up to two additional complex phases ρ and σ , which along with δ , participate in CP-violation. A parameterization is achieved by introducing an additional phase matrix $P_{kk'}$

$$V_{\ell k} = U_{\ell k'} P_{k'k}, \quad (4)$$

$$P_{k'k} = \text{diag}(e^{i\rho}, e^{i\sigma}, 1). \quad (5)$$

The mixing matrix $V_{\ell k}$ defined in Eq. (4) can then be used to transform the symmetric mass matrix $M_{\ell\ell'}$ from the flavor basis into the diagonal mass basis

$$V_{\ell k}^T M_{\ell\ell'} V_{\ell' k'} = M_{kk'} = m_k \delta_{kk'} = \text{diag}(m_1, m_2, m_3). \quad (6)$$

We note that there are many interesting models for mass matrices which were pioneered by Fritzsch and Xing^{25–28} in the leptonic sector. The masses m_k are taken to be real and positive labelling the free propagating states of the three neutrinos.

2.2. Majorana neutrino with dipole transition moment

Turning now to the action, the Majorana mass term in the Lagrangian can be written in the flavor basis as

$$-\mathcal{L}_{\text{mass}}^{\text{Maj.}} = \frac{1}{2} \bar{\nu}_\ell M_{\ell\ell'} \nu_{\ell'}, \quad M_{\ell\ell'}^T = M_{\ell\ell'}, \quad (7)$$

where the Majorana fields are written as $\nu = \nu_L + C(\bar{\nu}_L)^T$ and $\bar{\nu} = \nu^\dagger \gamma_0$ is the Dirac adjoint. The field ν_L refers to left-handed chiral four-component spinors. The charge conjugation matrix C is defined in the usual way in Ref. 17, p.692. Charged conjugated fields are written as $\nu^c = C(\bar{\nu})^T$. The Majorana mass matrix is symmetric, due to the anticommuting nature of the neutrino fields $\bar{\nu}\nu = -\nu^T \bar{\nu}^T$. It is in general complex,^{29,30} though it will be taken to be fully real in this work. This is also why we have not shown the Hermitian conjugate in Eq. (7).

Given these conventions, we can extend our consideration to include the electromagnetic interaction of neutrinos, which is possible if neutrinos are equipped

with a magnetic moment matrix $\mu_{\ell\ell'}$. We allow for a fixed *external* electromagnetic field tensor $F_{\text{ext}}^{\alpha\beta}(x^\mu)$, which imparts a force on the neutrino fields. We emphasize that $F_{\text{ext}}^{\alpha\beta}$ is not dynamical in our formulation; it consists of real functions over four-position and does not contain field operators.

We generalize the AMM Pauli spin-field Lagrangian to account for the Majorana fields in the flavor basis following the approach of Ref. 31

$$-\mathcal{L}_{\text{AMM}}^{\text{Maj.}} = \frac{1}{2} \bar{\nu}_\ell \left(\mu_{\ell\ell'} \frac{1}{2} \sigma_{\alpha\beta} F_{\text{ext}}^{\alpha\beta} \right) \nu_{\ell'}. \quad (8)$$

The operator $\sigma_{\alpha\beta}$ is the 4×4 spin tensor defined by the commutator of the gamma matrices. We would like to point out some interesting features of the Pauli term most notably that the spin tensor itself is not Hermitian with

$$\sigma_{\alpha\beta}^\dagger = \gamma_0 \sigma_{\alpha\beta} \gamma_0. \quad (9)$$

However, the conjugate of the Lagrangian term in Eq. (8),

$$\left(\nu^\dagger \gamma_0 \sigma_{\alpha\beta} F_{\text{ext}}^{\alpha\beta} \nu \right)^\dagger = \nu^\dagger \sigma_{\alpha\beta}^\dagger F_{\text{ext}}^{\alpha\beta} \gamma_0 \nu = \nu^\dagger \gamma_0 \sigma_{\alpha\beta} F_{\text{ext}}^{\alpha\beta} \nu, \quad (10)$$

is Hermitian. More about the spin tensor's properties will be elaborated on in Sec. 2.3.

The Majorana magnetic moment matrix acts in flavor space. It satisfies the following constraints⁵ for CPT symmetry reasons and the anticommuting nature of fermions

$$\mu_{\ell\ell'}^\dagger = \mu_{\ell\ell'}, \quad \mu_{\ell\ell'}^T = -\mu_{\ell\ell'}, \quad (11)$$

i.e. the AMM matrix $\mu_{\ell\ell'}$ is Hermitian and fully anti-symmetric. This requires that the transition magnetic moment elements are purely imaginary while all diagonal AMM matrix elements vanish

$$\mu_{\ell\ell'} = \begin{pmatrix} \mu_{ee} & \mu_{e\mu} & \mu_{e\tau} \\ \mu_{\mu e} & \mu_{\mu\mu} & \mu_{\mu\tau} \\ \mu_{\tau e} & \mu_{\tau\mu} & \mu_{\tau\tau} \end{pmatrix} \xrightarrow{\text{Majorana}} \mu_{\ell\ell'} = \begin{pmatrix} 0 & i\mu_{e\mu} & -i\mu_{e\tau} \\ -i\mu_{e\mu} & 0 & i\mu_{\mu\tau} \\ i\mu_{e\tau} & -i\mu_{\mu\tau} & 0 \end{pmatrix}. \quad (12)$$

We can combine the mass term in Eq. (7) and AMM contribution in Eq. (8) into a single effective Lagrangian

$$\mathcal{L}_{\text{eff}}^{\text{Maj.}} = \mathcal{L}_{\text{kinetic}}^{\text{Maj.}} + \mathcal{L}_{\text{mass}}^{\text{Maj.}} + \mathcal{L}_{\text{AMM}}^{\text{Maj.}}, \quad (13)$$

$$\mathcal{L}_{\text{eff}}^{\text{Maj.}} = \mathcal{L}_{\text{kinetic}}^{\text{Maj.}} - \frac{1}{2} \bar{\nu}_\ell \left(M_{\ell\ell'} + \mu_{\ell\ell'} \frac{1}{2} \sigma_{\alpha\beta} F_{\text{ext}}^{\alpha\beta} \right) \nu_{\ell'}. \quad (14)$$

Eq. (14) is our working Lagrangian. We define the generalized mass-dipole matrix $\mathcal{M}_{\ell\ell'}$ present in Eq. (14) as

$$\mathcal{M}_{\ell\ell'}(E, B) \equiv M_{\ell\ell'} + \mu_{\ell\ell'} \frac{1}{2} \sigma_{\alpha\beta} F_{\text{ext}}^{\alpha\beta}, \quad \mathcal{M}_{\ell\ell'}^\dagger = \gamma_0 \mathcal{M}_{\ell\ell'} \gamma_0. \quad (15)$$

The presence the EM interaction generated by the transition dipole moment is now understood to create an effective mass $m \rightarrow \tilde{m}(E, B)$ inducing new EM dependence

of the mixing matrix, leading to modifications seen in Eq.(4). As neutrinos propagate as energy eigenstates, our objective is to recognize and understand the effect of mass modification due to electromagnetic field; thus we consider the eigenvalues of Eq.(15) rather than those seen in Eq.(6). The electromagnetic effect then contributes to the time-dependant oscillation among the free-particle mass eigenstates.⁵

2.3. Chiral properties of the relativistic Pauli dipole

The electromagnetic dipole behavior of the neutrino depends on the mathematical properties of the tensor product $\sigma_{\alpha\beta}F_{\text{ext}}^{\alpha\beta}$. We prefer to work in the Weyl (chiral) spinor representation where the EM contribution is diagonal in spin space. Therefore, we evaluate the product $\sigma_{\alpha\beta}F_{\text{ext}}^{\alpha\beta}$ in the Weyl representation following Feynman and Gell-mann,³² yielding

$$-\frac{1}{2}\sigma_{\alpha\beta}F_{\text{ext}}^{\alpha\beta} = \begin{pmatrix} \vec{\sigma} \cdot (\vec{B} + i\vec{E}/c) & 0 \\ 0 & \vec{\sigma} \cdot (\vec{B} - i\vec{E}/c) \end{pmatrix} \equiv \begin{pmatrix} \vec{\sigma} \cdot \vec{f}_+ & 0 \\ 0 & \vec{\sigma} \cdot \vec{f}_- \end{pmatrix}, \quad (16)$$

where we introduced the complex electromagnetic field form $\vec{f}_{\pm} = \vec{B} \pm i\vec{E}/c$ showing sensitivity to both magnetic and electric fields. As this expression is diagonal in the Weyl representation, it does not exchange handedness when acting upon a state. Since left and right-handed neutrinos are not remixed by transition magnetic moments, sterile right-handed neutrinos do not need to be introduced. We can also see explicitly in Eq.(16) its non-Hermitian character, see Eq.(14), of the EM spin-field coupling. Specifically this is mirrored in the complex field's \vec{f}_{\pm} relation to its complex conjugate $(\vec{f}_{\pm})^* = \vec{f}_{\mp}$. The complex EM fields have a Hermitian (\vec{B}) and anti-Hermitian ($i\vec{E}$) part.

For later convenience, we note how the EM invariants \mathcal{S} and \mathcal{P} help explain the AMM term

$$\frac{1}{2}\left(\frac{1}{2}\sigma_{\alpha\beta}F_{\text{ext}}^{\alpha\beta}\right)^2 = \begin{pmatrix} \mathcal{S} + i\mathcal{P} & 0 \\ 0 & \mathcal{S} - i\mathcal{P} \end{pmatrix} = \mathcal{S} - i\gamma_5\mathcal{P}, \quad (17)$$

$$\mathcal{S} \equiv \frac{1}{2}(B^2 - E^2/c^2), \quad \mathcal{P} \equiv \vec{B} \cdot \vec{E}/c, \quad \frac{1}{2}\vec{f}_{\pm} \cdot \vec{f}_{\pm} = \mathcal{S} \pm i\mathcal{P}. \quad (18)$$

The combination of these invariants make up the eigenvalues of the Pauli term. Moreover, taking the product of \vec{f}_{\pm} with its complex conjugate we find

$$\frac{1}{2}\left(\vec{\sigma} \cdot \vec{f}_{\pm}\right)\left(\vec{\sigma} \cdot \vec{f}_{\mp}\right) = T_{\text{ext}}^{00} \mp \sigma_i T_{\text{ext}}^{0i}, \quad (19)$$

where we recognize the stress-energy tensor $T_{\text{ext}}^{\alpha\beta}$ component T_{ext}^{00} for field energy density, and T_{ext}^{0i} momentum density, respectively

$$T_{\text{ext}}^{00} = \frac{1}{2}(B^2 + E^2/c^2), \quad T_{\text{ext}}^{0i} = \frac{1}{c}\varepsilon_{ijk}E_jB_k. \quad (20)$$

As we will see in Sec.3, Eq.(19) will appear in the EM-mass eigenvalues of our effective Lagrangian Eq.(13). Using the identity in Eq.(16) and Eq.(19) we also find the interesting relationship

$$\frac{1}{2}\left(\frac{1}{2}\sigma_{\alpha\beta}F_{\text{ext}}^{\alpha\beta}\right)\left(\frac{1}{2}\sigma_{\alpha\beta}F_{\text{ext}}^{\alpha\beta}\right)^{\dagger} = \gamma_0(T_{\text{ext}}^{00}\gamma_0 + T_{\text{ext}}^{0i}\gamma_i). \quad (21)$$

Now that we have elaborated on the relevant EM field identities, we turn back to the magnetic dipole and flavor rotation problem.

3. Two-flavor toy model of electromagnetic-mass mixing

3.1. Fundamentals of electromagnetic mixing method

Considering experimental data on neutrino oscillations, it is understood that either the two lighter (normal hierarchy) or the two heavier (inverted hierarchy) neutrino states are close together in mass. If the electromagnetic properties of the neutrino do indeed lead to flavor mixing effects, then it is likely the closer pair of neutrino mass states that are most sensitive to the phenomenon we explore. In the spirit of Bethe,³³ we therefore explore the $N = 2$ two generation (ν_e, ν_μ) toy model.

Following the properties established in Eq.(11) and Eq.(15) we write down the two generation mass and dipole matrices as

$$M_{\ell\ell'} = \begin{pmatrix} m_e^\nu & \delta m \\ \delta m & m_\mu^\nu \end{pmatrix}, \quad \mu_{\ell\ell'} = \begin{pmatrix} 0 & i\delta\mu \\ -i\delta\mu & 0 \end{pmatrix}. \quad (22)$$

The AMM coupling $\delta\mu$ is taken to be real with a pure imaginary coefficient. While the mass elements $(m_e^\nu, m_\mu^\nu, \delta m)$ are generally complex, we choose in our toy model for them to be fully real

$$m_e^\nu = (m_e^\nu)^*, \quad m_{\nu_\mu} = (m_\mu^\nu)^*, \quad \delta m = \delta m^*, \quad (23)$$

making the mass matrix $M_{\ell\ell'}$ Hermitian. This allows us to more easily evaluate the EM contributions to mixing, avoiding the complications arising from the mass matrix.

Using Eq.(22) and Eq.(23), we write the mass-dipole matrix in Eq.(15) in terms of 2×2 flavor components as

$$\mathcal{M}_{\ell\ell'} = \begin{pmatrix} m_e^\nu & \delta m + i\delta\mu\sigma_{\alpha\beta}F_{\text{ext}}^{\alpha\beta}/2 \\ \delta m - i\delta\mu\sigma_{\alpha\beta}F_{\text{ext}}^{\alpha\beta}/2 & m_\mu^\nu \end{pmatrix}, \quad \mathcal{M}_{\ell\ell'}^\dagger = \gamma_0\mathcal{M}_{\ell\ell'}\gamma_0. \quad (24)$$

As noted before, this matrix is not Hermitian due to the inclusion of the spin tensor. However, any arbitrary complex matrix can be diagonalized into its real eigenvalues λ_j by the biunitary transform

$$W_{\ell j}^\dagger \mathcal{M}_{\ell\ell'} Y_{\ell'j'} = \lambda_j \delta_{jj'}, \quad (25)$$

where $Y_{\ell j}$ and $W_{\ell j}$ are both unitary matrices. Taking the complex conjugate of Eq.(25), we arrive at

$$(W_{\ell j}^\dagger \mathcal{M}_{\ell\ell'} Y_{\ell'j'})^\dagger = Y_{\ell j'}^\dagger \gamma_0 \mathcal{M}_{\ell\ell'} \gamma_0 W_{\ell'j} = \lambda_j \delta_{jj'}, \quad (26)$$

Dynamic fermion flavor mixing through transition dipole moments 7

$$Y_{\ell j} = \gamma_0 W_{\ell j} \rightarrow W_{\ell j}^\dagger \mathcal{M}_{\ell\ell'} \gamma_0 W_{\ell'j'} = \lambda_j \delta_{jj'} . \quad (27)$$

As $Y_{\ell j}$ and $W_{\ell j}$ are related by a factor of γ_0 based on the conjugation properties of Eq. (24), this lets us eliminate $Y_{\ell j}$ and diagonalize using a single unitary matrix $W_{\ell j}$. The related matrix $\mathcal{M}_{\ell\ell'} \gamma_0$ is Hermitian

$$(\mathcal{M}_{\ell\ell'} \gamma_0)^\dagger = \mathcal{M}_{\ell\ell'} \gamma_0 , \quad (28)$$

and also equivalent to the root of the Hermitian product of Eq. (24)

$$(\mathcal{M}\mathcal{M}^\dagger)_{\ell\ell'} = ((\mathcal{M}\gamma_0)(\mathcal{M}\gamma_0))_{\ell\ell'} . \quad (29)$$

Therefore a suitable unitary transformation $W_{\ell j}$ rotates flavor ℓ -states into magnetized mass j -states. The eigenvalues λ_j^2 of $(\mathcal{M}\mathcal{M}^\dagger)_{\ell\ell'}$ are the squares of both signs of the eigenvalues of $\mathcal{M}_{\ell\ell'} \gamma_0$. We write this property (with flavor indices suppressed) as

$$W^\dagger (\mathcal{M}\mathcal{M}^\dagger) W = W^\dagger (\mathcal{M}\gamma_0) W W^\dagger (\mathcal{M}\gamma_0) W = \text{diag}(\lambda_1^2, \lambda_2^2) . \quad (30)$$

We recognize $\lambda_j = \tilde{m}_j(E, B)$ with $j \in 1, 2$ as the effective mass states which are EM-field dependant in this basis.

3.2. Separating electromagnetic-mass mixing

The matrix $W_{\ell j}$ mixes flavor states into a new basis distinct from the free-particle case however this rotation must smoothly connect with the free-particle case in the limit that the electromagnetic fields go to zero. We proceed to evaluate $W_{\ell j}$, breaking the rotation into two separate unitary transformations: a) rotation $V_{\ell k}^\dagger (\ell \rightarrow k)$ to free-particle mass; and b) rotation $Z_{kj}^{\text{ext}} (k \rightarrow j)$ to the EM-mass basis. Guided by Eq. (2) we write

$$\nu_j = W_{\ell j}^\dagger \nu_\ell = Z_{kj}^{\text{ext}} V_{\ell k}^\dagger \nu_\ell . \quad (31)$$

In the limit that the EM fields go to zero, the electromagnetic rotation becomes unity $Z_{kj}^{\text{ext}} \rightarrow \delta_{kj}$, thereby ensuring the EM-mass basis and the free-particle mass basis become equivalent. The rotation Z_{kj}^{ext} can then be interpreted as the external field forced rotation. While our argument above is done explicitly for the two generation case, it can be generalized to accommodate three generations of neutrinos as well.

According to Eq. (6), the mass matrix in Eq. (22) can be diagonalized in the two generation case by a one parameter unitary mixing matrix $V_{\ell k}$ given by

$$V_{\ell k}(\theta) = \begin{pmatrix} \cos \theta & \sin \theta \\ -\sin \theta & \cos \theta \end{pmatrix} . \quad (32)$$

For a real Hermitian 2×2 mass matrix, the rotation matrix $V_{\ell k}$ is real and only depends on the rotation angle θ . The explicit form of the EM-field related rotation Z_{kj}^{ext} introduced in Eq. (31) is

$$Z_{kj}^{\text{ext}}(\omega, \phi) = \begin{pmatrix} \cos \omega & e^{i\phi} \sin \omega \\ -e^{-i\phi} \sin \omega & \cos \omega \end{pmatrix} , \quad W_{\ell j}(\theta, \omega, \phi) = V_{\ell k}(\theta) Z_{kj}^{\text{ext}}(\omega, \phi) , \quad (33)$$

8 *J. Rafelski, A. Steinmetz, and C. T. Yang*

where Z_{kj}^{ext} depends on the real angle ω and the complex phase ϕ . The full rotation $W_{\ell j}$ therefore depends on three parameters when broken into the free-particle rotation and the EM rotation.

The eigenvalues of the original Hermitian mass matrix in Eq. (22) are given by

$$m_{1,2} = \frac{1}{2} \left(m_{\nu_e} + m_{\nu_\mu} \mp \sqrt{|\Delta m_0|^2 + 4\delta m^2} \right) , \quad |\Delta m_0| = |m_{\nu_\mu} - m_{\nu_e}| . \quad (34)$$

We assign m_1 to the lower mass ($-$) root and m_2 with the larger mass ($+$) additive root. The rotation θ in Eq. (32) is then given by

$$\sin 2\theta = \sqrt{\frac{4\delta m^2}{|\Delta m_0|^2 + 4\delta m^2}} , \quad \cos 2\theta = \sqrt{\frac{|\Delta m_0|^2}{|\Delta m_0|^2 + 4\delta m^2}} . \quad (35)$$

In our toy model, the off-diagonal imaginary transition magnetic moment $\mu_{\ell\ell'}$ commutes with the real valued mixing matrix $V_{\ell k}$ and the following relations hold

$$V_{\ell k}^\dagger \mu_{\ell\ell'} V_{\ell'k'} = (V^\dagger V)_{k\ell'} \mu_{\ell\ell'} = \mu_{kk'} = \begin{pmatrix} 0 & i\delta\mu \\ -i\delta\mu & 0 \end{pmatrix} . \quad (36)$$

We see that the Majorana transition dipoles in our model are off-diagonal in both flavor and mass basis. Therefore the real parameter unitary matrix in Eq. (36) cannot rotate a pure imaginary matrix at least in the two flavor case. We apply the rotation in Eq. (32) to Eq. (28) yielding

$$V_{\ell k}^\dagger (\mathcal{M}_{\ell\ell'} \gamma_0) V_{\ell'k'} = V_{\ell k}^\dagger M_{\ell\ell'} \gamma_0 V_{\ell'k'} + V_{\ell k}^\dagger (\mu_{\ell\ell'} \sigma_{\alpha\beta} \gamma_0 F_{\text{ext}}^{\alpha\beta}/2) V_{\ell'k'} , \quad (37)$$

$$V_{\ell k}^\dagger (\mathcal{M}_{\ell\ell'} \gamma_0) V_{\ell'k'} = \begin{pmatrix} m_1 \gamma_0 & i\delta\mu \sigma_{\alpha\beta} \gamma_0 F_{\text{ext}}^{\alpha\beta}/2 \\ -i\delta\mu \sigma_{\alpha\beta} \gamma_0 F_{\text{ext}}^{\alpha\beta}/2 & m_2 \gamma_0 \end{pmatrix} \equiv \begin{pmatrix} \mathcal{A} & i\mathcal{C} \\ -i\mathcal{C} & \mathcal{B} \end{pmatrix} , \quad (38)$$

where we have defined implicitly the Hermitian elements $(\mathcal{A}, \mathcal{B}, \mathcal{C})$. Applying now both rotations to Eq. (28) yields

$$W_{\ell j}^\dagger (\mathcal{M}_{\ell\ell'} \gamma_0) W_{\ell'j'} = Z_{kj}^{\text{ext}} \begin{pmatrix} \mathcal{A} & i\mathcal{C} \\ -i\mathcal{C} & \mathcal{B} \end{pmatrix} Z^{\text{ext}} = \lambda_j \delta_{jj'} . \quad (39)$$

Eq. (39) is therefore the working matrix equation which needs to be solved to identify the EM rotation parameters. As discussed before, this means that the rotation angle ω and the phase ϕ are in general functions of electromagnetic fields.

3.3. Dynamic electromagnetic-mass eigenvalue results

We will now solve for the rotation parameters necessary to define the EM-mass basis which acts as a distinct propagating basis for neutrinos in external fields. Considering that the j -columns vectors $v_k^{(j)}$ of Z_{kj}^{ext} are eigenvectors for each λ_j

$$Z_{kj}^{\text{ext}} = v_k^{(j)} = (v^1 \ v^2) , \quad (40)$$

Eq. (39) has the meaning of an eigenvalue equation

$$\begin{pmatrix} \mathcal{A} & i\mathcal{C} \\ -i\mathcal{C} & \mathcal{B} \end{pmatrix} Z^{\text{ext}} = Z^{\text{ext}} \begin{pmatrix} \lambda_1 & 0 \\ 0 & \lambda_2 \end{pmatrix} \rightarrow \begin{pmatrix} \mathcal{A} & i\mathcal{C} \\ -i\mathcal{C} & \mathcal{B} \end{pmatrix} v^{(j)} = \lambda_j v^{(j)}. \quad (41)$$

Given the eigenvalue equation defined in Eq. (41), we obtain the effective EM-masses as solutions to the characteristic polynomial

$$(\mathcal{A} - \lambda_j \gamma_0)(\mathcal{B} - \lambda_j \gamma_0) - \mathcal{C}^2 = 0, \quad (42)$$

which we obtained by taking the determinant of Eq. (41) over flavor but not spin space. It is useful to define the following identities for the off-diagonal element

$$\mathcal{C}^2 = \delta\mu^2 \left(\frac{1}{2} \sigma_{\alpha\beta} F_{\text{ext}}^{\alpha\beta} \right) \left(\frac{1}{2} \sigma_{\alpha\beta} F_{\text{ext}}^{\alpha\beta} \right)^{\dagger} = 2\delta\mu^2 \gamma_0 (T_{\text{ext}}^{00} \gamma_0 + T_{\text{ext}}^{0i} \gamma_i), \quad (43)$$

and for the diagonal elements

$$(\mathcal{B} - \mathcal{A})^2 = |m_2 - m_1|^2 = |\Delta m|^2, \quad (\mathcal{A} + \mathcal{B})\gamma_0 = m_1 + m_2. \quad (44)$$

Eq. (43) was obtained using the expression in Eq. (21). Because of the spinor behavior of each element, the eigenvalues are obtained with γ_0 coefficients. Eq. (42) therefore has the roots $\lambda_{1,2} = \tilde{m}_{1,2}(E, B)$

$$\tilde{m}_{1,2}(E, B) = \frac{1}{2} \left(m_1 + m_2 \mp \sqrt{|\Delta m|^2 + 8\delta\mu^2 \gamma_0 (T_{\text{ext}}^{00} \gamma_0 + T_{\text{ext}}^{0i} \gamma_i)} \right), \quad (45)$$

$$\tilde{m}_{1,2}(E, B) = \frac{1}{2} \left(m_1 + m_2 \mp \sqrt{|\Delta m|^2 + 8\delta\mu^2 \gamma_0 \left(\gamma_0 \frac{1}{2} \left(B^2 + \frac{E^2}{c^2} \right) + \vec{\gamma} \cdot \left(\frac{\vec{E}}{c} \times \vec{B} \right) \right)} \right). \quad (46)$$

The EM-mass eigenstates $\tilde{m}(E, B)$ depends on the energy density T_{ext}^{00} of the EM field and the spin projection along the EM momentum density T_{ext}^{0i} . However the coefficient $\delta\mu^2$ is presumed to be very small, therefore the EM contribution only manifests in strong EM fields or where the free-particle case has very nearly or exactly degenerate masses, $\Delta m \rightarrow 0$. When the electromagnetic fields go to zero, the EM-masses in Eq. (46) reduce as expected to the free-particle result.

The complex phase in Eq. (33) has the value $\phi = \pi(n - 1/2)$ with $n \in 0, \pm 1, \pm 2, \dots$ making the complex exponential in Eq. (33) pure imaginary. Curiously, the phase is not field dependant, but tied to the fact that the Majorana momenta are pure imaginary quantities. Complex phases in mixing matrices are generally associated with CP violation such as the Dirac phase δ in Eq. (3) which suggests that CP violation in the neutrino sector can be induced in the presence of external EM fields. Further analysis of the three generation case is left to future work.

We note that the solution in Eq. (46) actually contain four distinct EM-mass eigenstates $\tilde{m}_j(E, B)$ with the lower ($j = 1$) and the upper ($j = 2$) masses, and the additional spin splitting from the alignment ($s = +1$), or anti-alignment ($s = -1$), of the neutrino spin with the momentum density of the external EM field. Spin splitting

vanishes for the pure electric or magnetic field cases. For good spin eigenstates $s \in \pm 1$, we can rewrite Eq. (43) with EM fields explicitly as

$$\mathcal{C}_s^2(E, B) = 2\delta\mu^2 \left(\frac{1}{2} (B^2 + E^2/c^2) + s|\vec{E}/c \times \vec{B}| \right). \quad (47)$$

The above expression within the square is positive definite; therefore Eq. (47) is always real. Spin splitting requires that we consider separate rotations for each spin state as the rotation angle ω_s depends on the spin quantum number

$$\sin 2\omega_s = \sqrt{\frac{4\mathcal{C}_s^2}{|\Delta m|^2 + 4\mathcal{C}_s^2}}, \quad \cos 2\omega_s = \sqrt{\frac{|\Delta m|^2}{|\Delta m|^2 + 4\mathcal{C}_s^2}}. \quad (48)$$

The expressions in Eq. (48) are mathematically similar to that of the free-particle case written in Eq. (35) in the two flavor generation model with the off-diagonal mass being replaced with the EM dependant quantity \mathcal{C}_s .

3.4. Strong field (degenerate mass) and weak field limits

The rotation angles in Eq. (48) reveal two distinct limits where EM-masses are dominated by either: a) the intrinsic mass splitting $\mathcal{C}_s \ll |\Delta m|^2$ with $\omega_s \rightarrow 0$ or b) the EM contribution $\mathcal{C}_s \gg |\Delta m|^2$ where $\omega_s \rightarrow \pi/4$. For the first case where the masses are not degenerate or the fields are weak, we obtain the expansion

$$\lim_{\mathcal{C}_s \ll |\Delta m|^2} \tilde{m}_{1,2}^s(E, B) = \frac{1}{2} \left(m_1 + m_2 \mp |\Delta m| \left(1 + \frac{2\mathcal{C}_s^2}{|\Delta m|^2} + \dots \right) \right), \quad (49)$$

which as stated before reduces to the free-particle case at lowest order.

In the opposite limit, where the masses are very nearly degenerate or fields are strong, the EM-mass eigenvalues in Eq. (46) can be approximated by the series

$$\lim_{\mathcal{C}_s \gg |\Delta m|^2} \tilde{m}_{1,2}^s(E, B) = \frac{1}{2} \left(m_1 + m_2 \mp 2\mathcal{C}_s \left(1 + \frac{|\Delta m|^2}{8\mathcal{C}_s^2} + \dots \right) \right) \quad (50)$$

For fully degenerate free-particle masses $m_1 = m_2$, this reduces to

$$\lim_{|\Delta m|^2 \rightarrow 0} \tilde{m}_{1,2}^s(E, B) = m_1 \mp \mathcal{C}_s. \quad (51)$$

Equation (51) indicates that for degenerate free-particle masses, the splitting $|\Delta m_{\text{EM}}| \equiv \mathcal{C}_s$ between effective EM-masses arises purely from the electromagnetic interaction of the neutrinos. We return to this interesting insight in our final comments.

Because of the bounds in Eq. (1) on the neutrino magnetic moment, we can estimate the field strength required for an external magnetic field to generate an electromagnetic mass splitting of $|\Delta m_{\text{EM}}| = 10^{-3}$ eV which is a reasonable comparison to intrinsic splitting of the two similar massive neutrinos based on the

experimental limits on neutrino masses.³⁴ Using the upper limit for the neutrino magnetic moment of $\mu_\nu^{\text{eff}} \sim 10^{-10} \mu_B$ we obtain

$$\frac{C_s}{\mu_\nu^{\text{eff}}} \Big|_{E=0} = \frac{10^{-3} \text{ eV}}{10^{-10} \mu_B} \approx 1.7 \times 10^{11} \text{ T}. \quad (52)$$

This is near the upper bound of the magnetic field strength of magnetars³⁵ which are of the order 10^{11} Tesla. In this situation, the EM contribution to the mass splitting rivals the estimated inherent splitting³⁴ of the two closer in mass neutrinos. Primordial magnetic fields³⁶ in the Early Universe may also present an environment for significant EM neutrino flavor mixing as both the external field strength and the density of neutrinos would be very large.³⁷ The magnetic properties of neutrinos may also have contributed alongside the charged leptons in magnetization in the Early Universe³⁸ prior to recombination.

While the above estimate was done with astrophysical systems in mind, we note that strong electrical fields should also produce EM-mass splitting. Therefore environments near to high Z -nuclei also of interest,^{39–41} as weak interactions violate parity. Should neutrinos have abnormally large transition magnetic dipole moments, then they should exhibit mass splitting from the neutrino's electromagnetic dipole interaction which may compete with the intrinsic mass differences of the free-particles.

4. Conclusions

We have incorporated electromagnetic effects in the Majorana neutrino mixing matrix by introducing an anomalous transition magnetic dipole moment. We have described the formalism for three generations of neutrinos and explicitly explored the two generation case as a toy model.

In the two generation case, we determined the effect of electric and magnetic fields on flavor rotation in Eq. (33) by introducing an electromagnetic flavor unitary rotation Z_{kj}^{ext} . We presented remixed mass eigenstates $\tilde{m}(E, B)$ in Eq. (46) which are the propagating mass-states in a background electromagnetic field $F_{\text{ext}}^{\alpha\beta}(x^\mu)$. These EM-mass eigenstates were also further split by spin aligned and anti-aligned states relative to the external field momentum density. There is much left to do to explore further the nascent connection between the spin and the flavor via transition magnetic moments.

Of particular interest is the case of nearly degenerate free-particle mass eigenstates where the EM effects are most manifest. For nearly degenerate masses compared to EM fields described by $C_s(E, B) \gg |\Delta m|^2$ in Eq. (47), the mass splitting is dominated by the electromagnetic contribution. This effect could be most relevant in the strong magnetic field environments, such as around magnetars or primordial magnetic fields in the Early Universe, where it could be capable of competing with the mass splitting seen in the two closer neutrino mass states. We also emphasize that dense matter environments may also be relevant where the electrical

field energy density is large. A natural extension of this work would be to include the in matter weak interaction remixing as an additional term in the effective Lagrangian Eq. (14).

The transition dipole moments are the origin of dynamical flavor mixing. While our focus was on Majorana neutrinos, Dirac-type fermions (neutrinos included) may also have non-zero transition dipole moments. These could remix flavor in the presence of strong external background fields. Here quarks are of special interest because they are not only electrically charged, but have color charge as well. This means quarks could in principle possess one, or both, EM and color-charge transition dipole moments, leading to dynamical effects in the CKM mixing matrix within hadrons as well as in quark-gluon plasma.

More speculatively, as transition dipoles act as a mechanism to generate mass by virtue of EM energy density T_{ext}^{00} as seen in Eq. (46), an analogous consequence of our work could arise in the presence of a dark vector field in the Universe coupled to neutrinos, resulting in off-diagonal masses in flavor. Massless neutrinos could then obtain dynamical non-zero masses in the Universe by virtue of their interactions originating in dark transition moments.

Acknowledgements

This article is dedicated to the memory of Harald Fritzsch. A version of this article with extended personal remarks appears in the book dedicated to the memory of Harald Fritzsch edited by Gerhard Buchalla, Dieter Lüst and Zhi-Zhong Xing. With Harald's passing we lost a friend and, equally importantly, a colleague whose quick mind, willingness to listen, and clarity of thought, helped in some of our research challenges. We had very much wished to hear Harald's opinion on this work.

References

1. K. Fujikawa and R. E. Shrock. The Magnetic Moment of a Massive Neutrino and Neutrino Spin Rotation. *Phys. Rev. Lett.*, 45:963, 1980. doi:10.1103/PhysRevLett.45.963.
2. R. E. Shrock. New Tests For, and Bounds On, Neutrino Masses and Lepton Mixing. *Phys. Lett. B*, 96:159–164, 1980. doi:10.1016/0370-2693(80)90235-X.
3. R. E. Shrock. Electromagnetic Properties and Decays of Dirac and Majorana Neutrinos in a General Class of Gauge Theories. *Nucl. Phys. B*, 206:359–379, 1982. doi:10.1016/0550-3213(82)90273-5.
4. J. Schechter and J. W. F. Valle. Majorana Neutrinos and Magnetic Fields. *Phys. Rev. D*, 24:1883–1889, 1981. [Erratum: Phys.Rev.D 25, 283 (1982)]. doi:10.1103/PhysRevD.25.283.
5. C. Giunti and A. Studenikin. Neutrino electromagnetic interactions: a window to new physics. *Rev. Mod. Phys.*, 87:531, 2015. arXiv:1403.6344, doi:10.1103/RevModPhys.87.531.
6. A. Popov and A. Studenikin. Neutrino eigenstates and flavour, spin and spin-flavour oscillations in a constant magnetic field. *Eur. Phys. J. C*, 79(2):144, 2019. arXiv:1902.08195, doi:10.1140/epjc/s10052-019-6657-z.

7. A. V. Chukhnova and A. E. Lobanov. Neutrino flavor oscillations and spin rotation in matter and electromagnetic field. *Phys. Rev. D*, 101(1):013003, 2020. [arXiv:1906.09351](#), doi:10.1103/PhysRevD.101.013003.
8. C. S. Lim and W. J. Marciano. Resonant Spin - Flavor Precession of Solar and Supernova Neutrinos. *Phys. Rev. D*, 37:1368–1373, 1988. doi:10.1103/PhysRevD.37.1368.
9. E. Akhmedov. Resonant Amplification of Neutrino Spin Rotation in Matter and the Solar Neutrino Problem. *Phys. Lett. B*, 213:64–68, 1988. doi:10.1016/0370-2693(88)91048-9.
10. P. B. Pal. Particle physics confronts the solar neutrino problem. *Int. J. Mod. Phys. A*, 7:5387–5460, 1992. doi:10.1142/S0217751X92002465.
11. E. Elizalde, E. J. Ferrer, and V. de la Incera. Neutrino propagation in a strongly magnetized medium. *Phys. Rev. D*, 70:043012, 2004. [arXiv:hep-ph/0404234](#), doi:10.1103/PhysRevD.70.043012.
12. E. Akhmedov and P. Martínez-Miravé. Solar $\bar{\nu}_e$ flux: revisiting bounds on neutrino magnetic moments and solar magnetic field. *JHEP*, 10:144, 2022. [arXiv:2207.04516](#), doi:10.1007/JHEP10(2022)144.
13. L. Wolfenstein. Neutrino Oscillations in Matter. *Phys. Rev. D*, 17:2369–2374, 1978. doi:10.1103/PhysRevD.17.2369.
14. S. P. Mikheyev and A. Yu. Smirnov. Resonance Amplification of Oscillations in Matter and Spectroscopy of Solar Neutrinos. *Sov. J. Nucl. Phys.*, 42:913–917, 1985.
15. A. Yu. Smirnov. The MSW effect and solar neutrinos. In *10th International Workshop on Neutrino Telescopes*, pages 23–43, 5 2003. [arXiv:hep-ph/0305106](#), doi:10.48550/arXiv.hep-ph/0305106.
16. A. Steinmetz, M. Formanek, and J. Rafelski. Magnetic Dipole Moment in Relativistic Quantum Mechanics. *Eur. Phys. J. A*, 55(3):40, 2019. [arXiv:1811.06233](#), doi:10.1140/epja/i2019-12715-5.
17. C. Itzykson and J. B. Zuber. *Quantum Field Theory*. McGraw-Hill, New York, 1980.
18. M. D. Schwartz. *Quantum Field Theory and the Standard Model*. Cambridge University Press, 2014. doi:10.1017/9781139540940.
19. C. Giunti, K. A. Kouzakov, Y. F. Li, A. V. Lokhov, A. Studenikin, and S. Zhou. Electromagnetic neutrinos in laboratory experiments and astrophysics. *Annalen Phys.*, 528:198–215, 2016. [arXiv:1506.05387](#), doi:10.1002/andp.201500211.
20. B. C. Canas, O. G. Miranda, A. Parada, M. Tortola, and J. W. F. Valle. Updating neutrino magnetic moment constraints. *Phys. Lett. B*, 753:191–198, 2016. [Addendum: *Phys.Lett.B* 757, 568–568 (2016)]. [arXiv:1510.01684](#), doi:10.1016/j.physletb.2015.12.011.
21. A. Studenikin. Status and perspectives of neutrino magnetic moments. *J. Phys. Conf. Ser.*, 718(6):062076, 2016. [arXiv:1603.00337](#), doi:10.1088/1742-6596/718/6/062076.
22. D. Aristizabal Sierra, O. G. Miranda, D. K. Papoulias, and G. S. Garcia. Neutrino magnetic and electric dipole moments: From measurements to parameter space. *Phys. Rev. D*, 105(3):035027, 2022. [arXiv:2112.12817](#), doi:10.1103/PhysRevD.105.035027.
23. N. Aghanim et al. Planck 2018 results. VI. Cosmological parameters. *Astron. Astrophys.*, 641:A6, 2020. [Erratum: *Astron.Astrophys.* 652, C4 (2021)]. [arXiv:1807.06209](#), doi:10.1051/0004-6361/201833910.
24. M. Aker et al. Direct neutrino-mass measurement with sub-electronvolt sensitivity. *Nature Phys.*, 18(2):160–166, 2022. [arXiv:2105.08533](#), doi:10.1038/s41567-021-01463-1.
25. H. Fritzsch and Z. Z. Xing. Lepton mass hierarchy and neutrino oscillations. *Phys. Lett. B*, 372:265–270, 1996. [arXiv:hep-ph/9509389](#), doi:10.1016/0370-2693(96)00107-4.
26. H. Fritzsch and Z. Z. Xing. Large leptonic flavor mixing and the mass spectrum of leptons. *Phys. Lett. B*, 440:313–318, 1998. [arXiv:hep-ph/9808272](#), doi:10.1016/S0370-2693(98)01106-X.
27. H. Fritzsch and Z. Z. Xing. Mass and flavor mixing schemes of quarks and leptons. *Prog. Part. Nucl. Phys.*, 45:1–81, 2000. [arXiv:hep-ph/9912358](#), doi:10.1016/S0146-6410(00)00102-2.
28. Z. Z. Xing. Commutators of lepton mass matrices, CP violation, and matter effects in medium baseline neutrino experiments. *Phys. Rev. D*, 63:073012, 2001. [arXiv:hep-ph/0009294](#), doi:10.1103/PhysRevD.63.073012.
29. B. Adhikary, M. Chakraborty, and A. Ghosal. Masses, mixing angles and phases of general Majorana neutrino mass matrix. *JHEP*, 10:043, 2013. [Erratum: *JHEP* 09, 180 (2014)]. [arXiv:1307.0988](#), doi:10.1007/JHEP10(2013)043.
30. C. Giunti and C. W. Kim. *Fundamentals of neutrino physics and astrophysics*. Oxford university press, 2007. doi:10.1093/acprof:oso/9780198508717.001.0001.
31. M. J. G. Veltman. Two component theory and electron magnetic moment. *Acta Phys. Polon. B*, 29:783–798, 1998. URL: <https://www.actaphys.uj.edu.pl/R/29/3/783/pdf>, arXiv:hep-th/9712216.
32. R. P. Feynman and M. Gell-Mann. Theory of Fermi interaction. *Phys. Rev.*, 109:193–198, 1958. doi:10.1103/PhysRev.109.193.
33. H. A. Bethe. A Possible Explanation of the Solar Neutrino Puzzle. *Phys. Rev. Lett.*, 56:1305, 1986. doi:10.1103/PhysRevLett.56.1305.
34. R. L. Workman et al. Review of Particle Physics. *PTEP*, 2022:083C01, 2022. doi:10.1093/ptep/ptac097.
35. V. M. Kaspi and A. Beloborodov. Magnetars. *Ann. Rev. Astron. Astrophys.*, 55:261–301, 2017. [arXiv:1703.00068](#), doi:10.1146/annurev-astro-081915-023329.
36. D. Grasso and H. R. Rubinstei. Magnetic fields in the early universe. *Phys. Rept.*, 348:163–266, 2001. [arXiv:astro-ph/0009061](#), doi:10.1016/S0370-1573(00)00110-1.
37. J. Rafelski, J. Birrell, A. Steinmetz, and C. T. Yang. A Short Survey of Matter-Antimatter Evolution in the Primordial Universe. *Universe*, 9(7):309, 2023. [arXiv:2305.09055](#), doi:10.3390/universe9070309.
38. A. Steinmetz, C. T. Yang, and J. Rafelski. Matter-antimatter origin of cosmic magnetism. [Submitted to PRD], 2023. [arXiv:2308.14818](#), doi:10.48550/arXiv.2308.14818.
39. M. A. Bouchiat and C. C. Bouchiat. Weak Neutral Currents in Atomic Physics. *Phys. Lett. B*, 48:111–114, 1974. doi:10.1016/0370-2693(74)90656-X.
40. M. A. Bouchiat and C. C. Bouchiat. Parity violation in atoms. *Rept. Prog. Phys.*, 60:1351–1396, 1997. doi:10.1088/0034-4885/60/11/004.
41. M. S. Safronova, D. Budker, D. DeMille, D. F. J. Kimball, A. Derevianko, and C. W. Clark. Search for New Physics with Atoms and Molecules. *Rev. Mod. Phys.*, 90(2):025008, 2018. [arXiv:1710.01833](#), doi:10.1103/RevModPhys.90.025008.

APPENDIX E

A Short Survey of Matter-Antimatter Evolution in the Primordial Universe

Rafelski, J., Birrell, J., Steinmetz, A., Yang, C.T. A Short Survey of Matter-Antimatter Evolution in the Primordial Universe. *Universe* 2023, 9, 309. [10.3390/universe9070309](https://doi.org/10.3390/universe9070309)

Copyright (2023) by the authors. Licensee MDPI, Basel, Switzerland. This article is an open access article distributed under the terms and conditions of the Creative Commons Attribution (CC BY 4.0) license.

Review

A Short Survey of Matter-Antimatter Evolution in the Primordial Universe

Johann Rafelski * , Jeremiah Birrell , Andrew Steinmetz  and Cheng Tao Yang 

Department of Physics, The University of Arizona, Tucson, AZ 85721, USA

* Correspondence: johann@arizona.edu

Abstract: We offer a survey of the matter-antimatter evolution within the primordial Universe. While the origin of the tiny matter-antimatter asymmetry has remained one of the big questions in modern cosmology, antimatter itself has played a large role for much of the Universe’s early history. In our study of the evolution of the Universe we adopt the position of the standard model Lambda-CDM Universe implementing the known baryonic asymmetry. We present the composition of the Universe across its temperature history while emphasizing the epochs where antimatter content is essential to our understanding. Special topics we address include the heavy quarks in quark-gluon plasma (QGP), the creation of matter from QGP, the free-streaming of the neutrinos, the vanishing of the muons, the magnetism in the electron-positron cosmos, and a better understanding of the environment of the Big Bang Nucleosynthesis (BBN) producing the light elements. We suggest but do not explore further that the methods used in exploring the early Universe may also provide new insights in the study of exotic stellar cores, magnetars, as well as gamma-ray burst (GRB) events. We describe future investigations required in pushing known physics to its extremes in the unique laboratory of the matter-antimatter early Universe.

Keywords: particles; plasmas and electromagnetic fields in cosmology; quarks to cosmos



Citation: Rafelski, J.; Birrell, J.; Steinmetz, A.; Yang, C.T. A Short Survey of Matter-Antimatter Evolution in the Primordial Universe. *Universe* **2023**, *9*, 309. <https://doi.org/10.3390/universe9070309>

Academic Editor: Stefano Profumo

Received: 28 April 2023

Revised: 16 June 2023

Accepted: 19 June 2023

Published: 27 June 2023



Copyright: © 2023 by the authors. Licensee MDPI, Basel, Switzerland. This article is an open access article distributed under the terms and conditions of the Creative Commons Attribution (CC BY) license (<https://creativecommons.org/licenses/by/4.0/>).

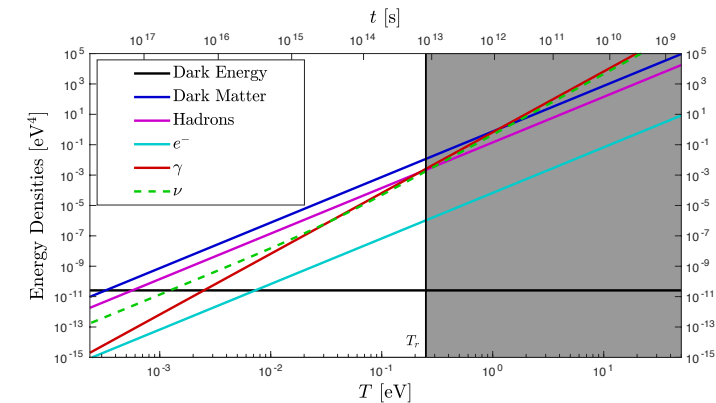


Figure 1. Contemporary and recent Universe composition: In this example we assumed present day composition to be 69% dark energy, 26% dark matter, 5% baryons, <1% photons and neutrinos. The dashed line shows how introduction of 2×0.1 eV mass in two of the three neutrinos impacts the energy density evolution (Neutrino mass choice is just for illustration. Other values are possible). The recombination temperature $T_r \approx 0.25$ eV delimits the era when the Universe was opaque shown as the shaded region.

After the general overview, we take the opportunity to enlarge in some detail our more recent work in special topics. In Section 2, we describe the chemical potentials of the QGP plasma species leading up to hadronization, Hubble expansion of the QGP plasma, and the abundances of heavy quarks. In Section 3 we discuss the formation of matter during hadronization, the role of strangeness, and the unique circumstances which led to pions remaining abundant well after all other hadrons were diluted or decayed. We review the roles of muons and neutrinos in the leptonic epoch in Section 4. The e^\pm plasma epoch is described in Section 5 which is the final stage of the Universe where antimatter played an important role. Here we introduce the statistical physics description of electrons and positron gasses, their relation to the baryon density, and the magnetization of the e^\pm plasma prior to the disappearance of the positrons shortly after Big Bang Nucleosynthesis (BBN). A more careful look at the effect of the dense e^\pm plasma on BBN is underway. One interesting feature of having an abundant e^\pm plasma is the possibility of magnetization in the early Universe which we consider in Section 5.2. We introduce in this work the spin magnetic moment polarization for the first time in the context of cosmology. We address this using spin-magnetization and mean-field theory where all the spins respond to the collective bulk magnetism self generated by the plasma. We stop our survey at a temperature of $T = 20$ keV with the disappearance of the positrons signifying the end of antimatter dynamics at cosmological scales.

This primordial Universe is a plasma physics laboratory with unique properties not found in terrestrial laboratories or stellar environments due to the high amount of antimatter present. We suggest in Section 6 areas requiring further exploration including astrophysical systems where positron content is considerable and the possibility for novel compact objects with persistent positron content is discussed. While the disappearance of baryonic matter is well described in the literature, it has not always been appreciated how long the leptonic ($\bar{\mu} = \mu^+$ and $\bar{e} = e^+$) antimatter remains a significant presence in the Universe’s evolutionary history. We show that the e^\pm epoch is a prime candidate to resolve several related cosmic mysteries such as early Universe matter in-homogeneity and the origin of cosmic magnetic fields. While the plasma epochs of the early Universe

in our long gone past, plasmas which share features with the primordial Universe might possibly exist in the contemporary Universe today. Such extraordinary stellar objects could possess properties dynamics relevant to gamma-ray burst (GRB) [4–7], black holes [8–10] and neutron stars (magnetars) [11,12].

1.2. The Five Plasma Epochs

At an early time in the standard cosmological model, the Universe began as a fireball, filling all space, with extremely high temperature and energy density [13]. Our domain of the present day Universe originated from an ultra-relativistic plasma which contained almost a perfect symmetry between matter and antimatter except for a small discrepancy of one part in 10^9 which remains a mystery today. There are two general solutions of this problem both of which suppose that the Universe's initial conditions were baryon-antibaryon number symmetric in order to avoid 'fine-tuning' to a specific value:

- A Case of baryonic number (charge) conservation: In order to separate space domains in which either matter or antimatter is albeit very slightly dominant we need a 'force' capable of dynamically creating this matter-antimatter separation. This requires that two of the three Sakharov [14,15] conditions be fulfilled:

1. Violation of CP-invariance allowing to distinguish matter from antimatter
2. Non-stationary conditions in absence of local thermodynamic equilibrium

Other than very distant antimatter domains [16] the missing antimatter could be perhaps 'stored' in a compact structure [17–19].

- B There is no known cause for baryon charge conservation. Therefore it is possible to consider the full Sakharov model with

3. Absence of baryonic charge conservation

Allowing the dynamical formation of the uniform matter-antimatter asymmetry typically occurring prior to the epoch governed by physics confirmed by current experiment to which environs we restrict this short survey. A well studied example is the Affleck-Dine mechanism [20].

Very early formation of baryon asymmetry is further supported by the finding that the known CP-violation in the Standard Model's weak sector is insufficient to explain in quantitative terms the baryon asymmetry [21]. However, baryon asymmetry could develop at a later stage in Universe evolution. We show in this review that this remains a topic deserving further investigation. In this work we take a homogeneous prescribed baryon asymmetry obtained from observed baryon to photon ratio in the Universe. Additional comments on the situation in the context of non-equilibria processes are made in Section 2.2, at the end of Section 4.2, and in Section 6.

The primordial hot Universe fireball underwent several practically adiabatic phase changes which dramatically evolved its bulk properties as it expanded and cooled. We present an overview Figure 2 of particle families across all epochs in the Universe, as a function of temperature and thus time. The cosmic plasma, after the electroweak symmetry breaking epoch and presumably inflation, occurred in the early Universe in the following sequence:

1. **Primordial quark-gluon plasma:** At early times when the temperature was between $130 \text{ GeV} > T > 150 \text{ MeV}$ we have the building blocks of the Universe as we know them today, including the leptons, vector bosons, and all three families of deconfined quarks and gluons which propagated freely. As all hadrons are dissolved into their constituents during this time, strongly interacting particles u, d, s, t, b, c, g controlled the fate of the Universe. Here we will only look at the late-stage evolution at around 150 MeV.
2. **Hadronic epoch:** Around the hadronization temperature $T_h \approx 150 \text{ MeV}$, a phase transformation occurred forcing the strongly interacting particles such as quarks and gluons to condense into confined states [22]. It is here where matter as we know it today forms and the Universe becomes hadronic-matter dominated. In

the temperature range $150 \text{ MeV} > T > 20 \text{ MeV}$ the Universe is rich in physics phenomena involving strange mesons and (anti)baryons including (anti)hyperon abundances [23,24].

3. **Lepton-photon epoch:** For temperature $10 \text{ MeV} > T > 2 \text{ MeV}$, the Universe contained relativistic electrons, positrons, photons, and three species of (anti)neutrinos. Muons vanish partway through this temperature scale. In this range, neutrinos were still coupled to the charged leptons via the weak interaction [25,26]. During this time the expansion of the Universe is controlled by leptons and photons almost on equal footing.
4. **Final antimatter epoch:** After neutrinos decoupled and become free-streaming, referred to as neutrino freeze-out, from the cosmic plasma at $T = 2 \text{ MeV}$, the cosmic plasma was dominated by electrons, positrons, and photons. We have shown in [27] that this plasma existed until $T \approx 0.02 \text{ MeV}$ such that BBN occurred within a rich electron-positron plasma. This is the last time the Universe will contain a significant fraction of its content in antimatter.
5. **Moving towards a matter dominated Universe:** The final major plasma stage in the Universe began after the annihilation of the majority of e^\pm pairs leaving behind a residual amount of electrons determined by the baryon asymmetry in the Universe and charge conservation. The Universe was still opaque to photons at this point and remained so until the recombination period at $T \approx 0.25 \text{ eV}$ starting the era of observational cosmology with the CMB. This final epoch of the primordial Universe will not be described in detail here, but is well covered in [28].

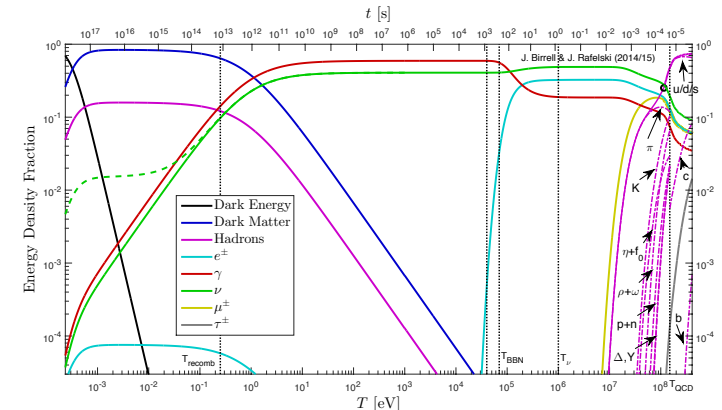


Figure 2. Normalized Universe constituent matter and radiation components Ω_i are evolved over cosmological timescales (top scale, bottom scale is temperature T) from contemporary observational cosmology to the QGP epoch of the Universe. Vertical lines denote transitions between distinct epochs. Solid neutrino (green) line shows contribution of massless neutrinos, while the dashed line shows 1 massless and $2 \times 0.1 \text{ eV}$ neutrinos (Neutrino mass choice is just for illustration. Other values are possible).

Each plasma outlined above contributes to the thermal behavior of the Universe over time. This is illustrated in Figure 3 where the fractional drop in temperature during each plasma transformation is plotted. Each subsequent plasma lowers the available degrees of freedom (as the particle inventory is whittled away) as the Universe cools [29,30]. Each drop in degrees of freedom represents entropy being pumped into the photons as entropy is conserved (up until local gravitational processes become relevant) in an expanding

Universe. As there are no longer degrees of freedom to consume, thereby reheating the photon field further, the fractional temperature remains constant today.

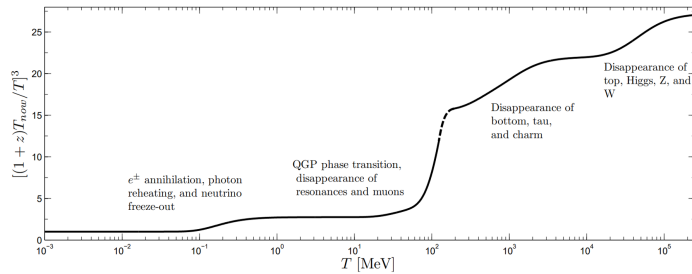


Figure 3. The evolution of the photon reheating (black line) process in terms of fractional temperature change in the Universe. Figure adapted from [29]. The dashed portion is a qualitative description subject to the exact model of QGP hadronization.

In Figure 2 we begin on the right at the end of the QGP era. The first dotted vertical line shows the QGP phase transition and hadronization, near $T = 150$ MeV. The hadron era proceeds with the disappearance of muons, pions, and heavier hadrons. This constitutes a reheating period, with energy and entropy from these particles being transferred to the remaining e^\pm , photon, neutrino plasma. The black circle near $T = 115$ MeV denotes our change from 2 + 1-flavor lattice QCD [31–33] data for the hadron energy density, taken from Borsanyi et al. [34,35], to an ideal gas model [36] at lower temperature. We note that the hadron ideal gas energy density matches the lattice results to less than a percent at $T = 115$ MeV [37].

To the right of the QGP transition region, the solid hadron line shows the total energy density of quarks and gluons. From top to bottom, the dot-dashed hadron lines to the right of the transition show the energy density fractions of 2 + 1-flavor (u,d,s) lattice QCD matter (almost indistinguishable from the total energy density), charm, and bottom (both in the ideal gas approximation). To the left of the transition the dot-dashed lines show the pion, kaon, $\eta + f_0$, $\rho + \omega$, nucleon, Δ , and Υ contributions to the energy fraction.

Continuing to the second vertical line at $T = \mathcal{O}(1)$ MeV, we come to the annihilation of e^\pm and the photon reheating period. Notice that only the photon energy density fraction increases, as we assume that neutrinos are already decoupled at this time and hence do not share in the reheating process, leading to a difference in photon and neutrino temperatures. This is not strictly correct but it is a reasonable simplifying assumption for the current purpose; see [25,38–40]. We next pass through a long period, from $T = \mathcal{O}(1$ MeV) until $T = \mathcal{O}(1$ eV), where the energy density is dominated by photons and free-streaming neutrinos. BBN occurs in the approximate range $T = 40\text{--}70$ keV and is indicated by the next two vertical lines in Figure 2. It is interesting to note that, while the hadron fraction is insignificant at this time, there is still a substantial background of e^\pm pairs during BBN (see Section 5.1).

We then come to the beginning of the matter dominated regime, where the energy density is dominated by the combination of dark matter and baryonic matter. This transition is the result of the redshifting of the photon and neutrino energy, $\rho \propto a^{-4} \propto T^4$, whereas for non-relativistic matter $\rho \propto a^{-3} \propto T^3$. Recombination and photon decoupling occurs near the transition to the matter dominated regime, denoted by the (Figure 2) vertical line at $T = 0.25$ eV.

Finally, as we move towards the present day CMB temperature of $T_{\gamma,0} = 0.235$ meV on the left hand side, we have entered the dark energy dominated regime. For the present day values, we have used the energy densities proscribed by the Planck parameters [41]

using Equation (14) and zero Universe spatial curvature. The photon energy density is fixed by the CMB temperature $T_{\gamma,0}$ and the neutrino energy density is fixed by $T_{\gamma,0}$ along with the photon to neutrino temperature ratio and neutrino masses. Both constitute $<1\%$ of the current energy budget.

The Universe evolution and total energy densities were computed using massless neutrinos, but for comparison we show the energy density of massive neutrinos in the dashed green line. For the dashed line we used two neutrino flavors with masses $m_\nu = 0.1$ eV and one massless flavor. Note that the inclusion of neutrino mass causes the leveling out of the neutrino energy density fraction during the matter dominated period, as compared to the continued redshifting of the photon energy.

1.3. The Lambda- Λ CDM Universe

Here we provide background on the standard Λ CDM cosmological (FLRW-Universe) model that is used in the computation of the composition of the Universe over time. We use the spacetime metric with metric signature $(+1, -1, -1, -1)$ in spherical coordinates

$$ds^2 = c^2 dt^2 - a^2(t) \left[\frac{dr^2}{1 - kr^2} + r^2(d\theta^2 + \sin^2(\theta)d\phi^2) \right] \quad (1)$$

characterized by the scale parameter $a(t)$ of a spatially homogeneous Universe. The geometric parameter k identifies the Gaussian geometry of the spacial hyper-surfaces defined by co-moving observers. Space is a Euclidean flat-sheet for the observationally preferred value $k = 0$ [28,41,42]. In this case it can be more convenient to write the metric in rectangular coordinates

$$ds^2 = c^2 dt^2 - a^2(t) [dx^2 + dy^2 + dz^2]. \quad (2)$$

We will work in units where $\hbar = 1$, $c = 1$.

The global Universe dynamics can be characterized by two quantities: the Hubble parameter H , a strongly time dependent quantity on cosmological time scales, and the deceleration parameter q :

$$H(t)^2 \equiv \left(\frac{\dot{a}}{a} \right)^2 = \frac{8\pi G_N}{3} \rho_{tot}, \quad (3)$$

$$\frac{\ddot{a}}{a} = -qH^2, \quad q \equiv -\frac{a\ddot{a}}{\dot{a}^2}, \quad \dot{H} = -H^2(1+q), \quad (4)$$

where G_N is the Newtonian gravitational constant and ρ_{tot} is the energy density of the Universe and composed of the various energy densities in the Universe. The deceleration parameter q is defined in terms of the second derivative of the scale parameter.

In Figure 4 Left we illustrate the late stage evolution of the parameters H and q given in Equations (3) and (4) compared to temperature. This illustrates how the Universe evolves according to the Friedmann Equations (3) and (4) above. The deceleration begins radiation dominated with $q = 1$ and then transitions to matter dominated $q = 1/2$. Within the Λ CDM model the contemporary Universe is undergoing a transition from matter dominated to dark energy dominated, where the deceleration would settle on the asymptotic value of $q = -1$ [29]. However, several alternate models: phantom energy [43], Chaplygin gas [44], or more generally dynamic (spatially and/or time dependent) dark energy [45] cannot be excluded in absence of strong evidence for the constancy of dark energy.

Within the Λ CDM model only usual forms of energy are relevant before recombination epoch, see Figure 2. Any alternate model can be thus constrained by understanding precisely the evolution of the Universe prior to this epoch. Part of the program of this survey is to connect the late stage evolution to the very early Universe during and prior to BBN accounting for the unexpectedly considerable antimatter content.

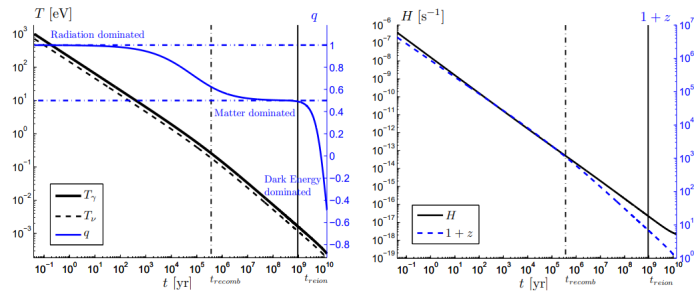


Figure 4. **Left:** The numerically solved later $t > 10^{-1}$ yr evolution of photon and neutrino background temperatures T_γ , T_ν (black and black dashed lines) and the deceleration parameter q (thin blue line) over the lifespan of the Universe. **Right:** The evolution of the Hubble parameter $1/H$ (black line) and redshift z (blue dashed line) which is related to the scale parameter $a(t)$. Figure adapted from [29].

The current tension in Hubble parameter measurements [46–48] might benefit from closer inspection of these earlier denser periods should these contribute to modification of the conventional model of Universe expansion. We further note that the JWST has recently discovered that galaxy formation began earlier than predicted which requires reevaluation of early Universe matter inhomogeneities [49]. Figure 4 Right shows the close relationship between the redshift z and the Hubble parameter. Deviations separating the two occur from the transitions which changed the deceleration value.

The Einstein equations with a cosmological constant Λ corresponding to dark energy are:

$$G^{\mu\nu} = R^{\mu\nu} - \left(\frac{R}{2} + \Lambda\right)g^{\mu\nu} = 8\pi G_N T^{\mu\nu}, \quad R = g_{\mu\nu} R^{\mu\nu}. \quad (5)$$

The homogeneous and isotropic symmetry considerations imply that the stress energy tensor is determined by an energy density and an isotropic pressure

$$T_v^\mu = \text{diag}(\rho, -P, -P, -P). \quad (6)$$

It is common to absorb the Einstein cosmological constant Λ into the energy and pressure

$$\rho_\Lambda = \frac{\Lambda}{8\pi G_N}, \quad P_\Lambda = -\frac{\Lambda}{8\pi G_N} \quad (7)$$

and we implicitly consider this done from now on.

Two dynamically independent Friedmann equations [50] arise using the metric Equation (1) in Equation (5):

$$\frac{8\pi G_N}{3}\rho = \frac{\dot{a}^2 + k}{a^2} = H^2 \left(1 + \frac{k}{a^2}\right), \quad \frac{4\pi G_N}{3}(\rho + 3P) = -\frac{\ddot{a}}{a} = qH^2. \quad (8)$$

We can eliminate the strength of the interaction, G_N , solving both these equations for $8\pi G_N/3$, and equating the result to find a relatively simple constraint for the deceleration parameter:

$$q = \frac{1}{2} \left(1 + 3\frac{P}{\rho}\right) \left(1 + \frac{k}{a^2}\right). \quad (9)$$

For a spatially flat Universe, $k = 0$, note that in a matter-dominated era where $P/\rho < 1$ we have $q \simeq 1/2$; for a radiative Universe where $3P = \rho$ we find $q = 1$; and in a

dark energy Universe in which $P = -\rho$ we find $q = -1$. Spatial flatness is equivalent to the assertion that the energy density of the Universe equals the critical density

$$\rho = \rho_{\text{crit}} \equiv \frac{3H^2}{8\pi G_N}. \quad (10)$$

The CMB power spectrum is sensitive to the deceleration parameter and the presence of spatial curvature modifies q . The Planck results [28,41,42] constrain the effective curvature energy density fraction,

$$\Omega_K \equiv 1 - \rho/\rho_{\text{crit}}, \quad (11)$$

to

$$|\Omega_K| < 0.005. \quad (12)$$

This indicates a nearly flat Universe which is spatially Euclidean. We will work within an exactly spatially flat cosmological model, $k = 0$. As must be the case for any solution of Einstein's equations, Equation (8) implies that the energy momentum tensor of matter is divergence free:

$$T^{\mu\nu}_{;\nu} = 0 \Rightarrow -\frac{\dot{\rho}}{\rho + P} = 3\frac{\dot{a}}{a} = 3H. \quad (13)$$

A dynamical evolution equation for $\rho(t)$ arises once we combine Equation (13) with Equation (8), eliminating H . Given an equation of state $P(\rho)$, solutions of this equation describes the dynamical evolution of matter in the Universe. In practice, we evolve the system in both directions in time. On one side, we start in the present era with the energy density fractions fit by the central values found in Planck data [41]

$$H_0 = 67.4 \text{ km/s/Mpc}, \quad \Omega_b = 0.05, \quad \Omega_c = 0.26, \quad \Omega_\Lambda = 0.69, \quad (14)$$

and integrate backward in time. On the other hand, we start in the QGP era with an equation of state determined by an ideal gas of SM particles, combined with a perturbative QCD equation of state for quarks and gluons [35], and integrate forward in time. As the Universe continues to dilute from dark energy in the future, the cosmic equation of state will become well approximated by the de Sitter inflationary metric which is a special case of FLRW.

2. QGP Epoch

2.1. Conservation Laws in QGP

During the first $\Delta t \approx 30 \mu\text{s}$ after the Big Bang, the early Universe is a hot soup that containing the elementary primordial building blocks of matter and antimatter [13]. In particular it contained the light quarks which are now hidden in protons and neutrons. Beyond this there were also electrons, photons, neutrinos, and massive strange and charm quarks. These interacting particle species were kept in chemical and thermal equilibrium with one another. Gluons which mediated the color interaction are very abundant as well. This primordial phase lasted as long as the temperature of the Universe was more than 110,000 times than the expected temperature $T_\odot = 1.36 \text{ keV}$ ($1.58 \times 10^7 \text{ K}$) at the center of the Sun [51].

The conditions in the early Universe and those created in relativistic collisions of heavy atomic nuclei differ somewhat: whereas the primordial quark-gluon plasma survives for about 25 μs in the Big Bang, the comparable extreme conditions created in ultra-relativistic nuclear collisions are extremely short-lived [52] on order of 10^{-23} s . As a consequence of the short lifespan of laboratory QGP in heavy-ion collisions [53,54], they are not subject to the same weak interaction dynamics [55] as the characteristic times for weak processes are too lengthy [56]. Therefore our ability to recreate the conditions of the primordial QGP are limited due to the relativistic explosive disintegration of the extremely hot dense relativistic ‘fireballs’ created in modern accelerators. This disparity is seen in Figure 5, where



the chemical potential of QGP $\mu_q = \mu_B/3$ [57] for various values of entropy-per-baryon s/b relevant to relativistic particle accelerators are plotted alongside the evolution of the cosmic hadronic plasma chemical potential. The confinement transition boundary (red line in Figure 5) was calculated using a parameters obtained from [58] in agreement with lattice results [59]. The QGP precipitates hadrons in the cosmic fluid at a far higher entropy ratio than those accessible by terrestrial means and the two manifestations of QGP live far away from each other on the QCD phase diagram [60].

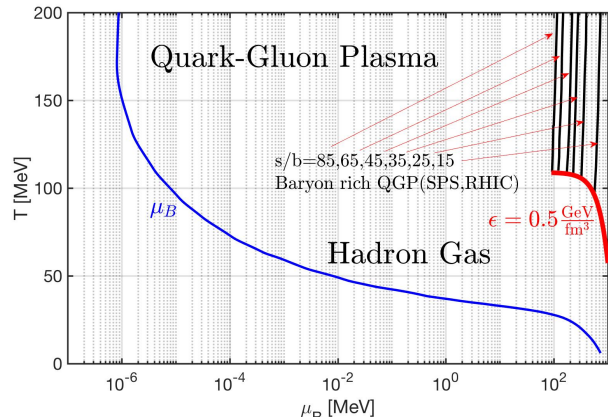


Figure 5. The evolution of the cosmic baryon chemical potential μ_B after hadronization (blue line). Curves for QGP (thin black line) created in terrestrial accelerators for differing entropy-per-baryon s/b values are included [57]. The boundary (red line) where QGP condenses into hadrons is illustrated at an energy density of $0.5 \text{ GeV}/\text{fm}^3$ as determined through lattice computation [59].

The work of Fromerth et al. [23] allows us to parameterize the chemical potentials μ_d , μ_e , and μ_ν during this epoch as they are the lightest particles in each main thermal category: quarks, charged leptons, and neutral leptons. The quark chemical potential is determined by the following three constraints [23]:

1. Electric charge neutrality $Q = 0$, given by

$$\frac{Q}{V} = n_Q \equiv \sum_f Q_f n_f(\mu_f, T) = 0 \quad (15)$$

where Q_f is the charge and n_f is the numerical density of each species f . Q is a conserved quantity in the Standard Model under global $U(1)_{EM}$ symmetry. This is summed over all particles present in the QGP epoch.

2. Baryon number and lepton number neutrality $B - L = 0$, given by

$$\frac{B - L}{V} = n_B - n_L \equiv \sum_f (B_f - L_f) n_f(\mu_f, T) = 0 \quad (16)$$

where L_f and B_f are the lepton and baryon number for the given species f . This condition is phenomenologically motivated by baryogenesis and is exactly conserved in the Standard Model under global $U(1)_{B-L}$ symmetry. We note many Beyond-Standard-Model (BSM) models also retain this as an exact symmetry though Majorana neutrinos do not.

3. The entropy-per-baryon density ratio s/n_B is a constant and can be written as

$$\frac{s}{B} = \frac{s}{n_B} = \frac{\sum_f s_f(\mu_f, T)}{\sum_f B_f n_f(\mu_f, T)} = \text{const} \quad (17)$$

where s_f is the entropy density of given species f . As the expanding Universe remains in thermal equilibrium, the entropy is conserved within a co-moving volume. The baryon number within a co-moving volume is also conserved. As both quantities dilute with $1/a(t)^3$ within a normal volume, the ratio of the two is constant. This constraint does not become broken until spatial inhomogeneities from gravitational attraction becomes significant, leading to increases in local entropy.

At each temperature T , the above three conditions form a system of three coupled, nonlinear equations of the three chosen unknowns (here we have μ_d , μ_e , and μ_ν). In Figure 6 we present numerical solutions to the conditions Equations (15)–(17) and plot the chemical potentials as a function of time. As seen in the figure, the three potentials are in alignment during the QGP phase until the hadronization epoch where the down quark chemical potential diverges from the leptonic chemical potentials before reaching an asymptotic value at late times. This asymptotic value is given as approximately $\mu_q \approx m_N/3$ the mass of the nucleons and represents the confinement of the quarks into the protons and neutrons at the end of hadronization.

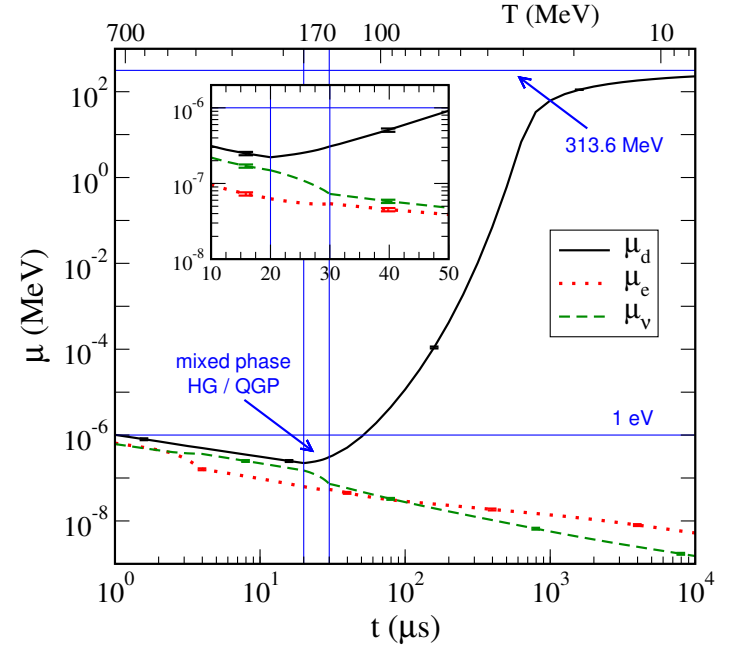


Figure 6. Plot of the down quark chemical potential (black), electron chemical potential (dotted red) and neutrino chemical potential (dashed green) as a function of time. These are 2003 unpublished results of Fromerth & Rafelski [61]; also presented in Ref. [62].

This asymptotic limit is also shown in Figure 7 where we present the down quark chemical potential for different values of the entropy-to-baryon ratio. While the s/n_B ratio has large consequences for the plasma at high temperatures, the chemical potential is insensitive to this parameter at low temperatures the degrees of freedom are dominated by the remaining baryon number rather than the thermal degrees of freedom of the individual quarks. Therefore the entropy to baryon value today greatly controls the quark content when the Universe was very hot. We note that the distribution of quarks in the QGP plasma does not remain fixed to the Fermi-Dirac distribution for thermal and entropic equilibrium. The quark partition function is instead

$$\ln Z_{\text{quarks}} = \sum_q \ln \left(1 + Y_q(t) e^{-\beta E_q} \right), \quad Y_q(t) = \gamma_q(t) \lambda_q \quad q = u, d, c, s, t, b, \quad (18)$$

which is summed over all quarks and their quantum numbers. In Equation (18), λ_q is the quark fugacity while $\gamma_q(t)$ is the temporal inhomogeneity of the population distribution [62]. The product of the two $Y_q(t) = \gamma_q(t) \lambda_q$ is then defined as the generalized fugacity for the species. Because of nuclear reactions, these distributions populate and depopulate over time which pulls the gas off entropic equilibrium while retaining temperature T with the rest of the Universe [58]. When $\gamma \neq 1$, the entropy of the quarks is no longer minimized. As entropy in the cosmic expansion is conserved overall, this means the entropy gain or loss is then related to the entropy moving between the quarks or its products.

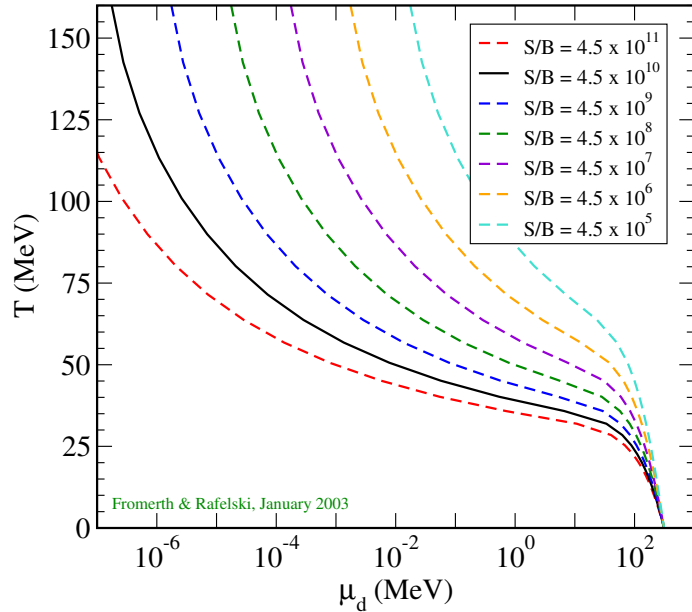


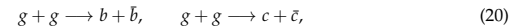
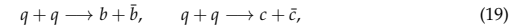
Figure 7. Plot of the down quark chemical potential μ_d as a function of temperature for differing values of entropy-per-baryon S/B ratios (2003 unpublished, Fromerth & Rafelski [62]).

In practice, the generalized fugacity is $Y = 1$ during the QGP epoch as the quarks in early Universe remained in both thermal and entropic equilibrium. This is because the Universe's expansion was many orders of magnitude slower than the process reaction

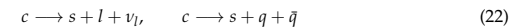
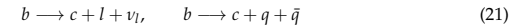
and decay timescales [58]. However near the hadronization temperature, heavy quarks abundance and deviations from chemical equilibrium have not yet been studied in great detail. We show in Section 2.2 and [63] that the bottom quarks can deviate from chemical equilibrium $\gamma \neq 1$ by breaking the detailed balance between reactions of the quarks.

2.2. Heavy Flavor: Bottom and Charm in QGP

In the QGP epoch, up and down (u, d) (anti)quarks are effectively massless and remain in equilibrium via quark-gluon fusion. Strange (s) (anti)quarks are in equilibrium via weak, electromagnetic, and strong interactions until $T \sim 12$ MeV [24]. In this section, we focus on the heavier charm and bottom (c, b) (anti)quarks. In primordial QGP, the bottom and charm quarks can be produced from strong interactions via quark-gluon pair fusion processes and disappear via weak interaction decays. For production, we have the following processes



for bottom and charm and



for their decay. A detailed calculation of production and decay rate can be found in [63].

In the early Universe within the temperature range $130 \text{ GeV} > T > 150 \text{ MeV}$ we have the following particles: photons, 8_c -gluons, W^\pm, Z^0 , three generations of 3_c -quarks and leptons in the primordial QGP. The Hubble parameter can be written as the sum of particle energy densities ρ_i for each species

$$H^2 = \frac{8\pi G_N}{3} (\rho_\gamma + \rho_{\text{lepton}} + \rho_{\text{quark}} + \rho_{g, W^\pm, Z^0}), \quad (23)$$

where G_N is Newton's constant of gravitation. Ultra-relativistic particles (which are effectively massless) and radiation dominate the speed of expansion.

The Universe's characteristic expansion time constant $1/H$ is seen in Figure 8 (both Top and Bottom figures). The (top) figure plots the relaxation time for the production and decay of charm quarks as a function of temperature. For the entire duration of QGP, the Hubble time is larger than the decay lifespan and production times of the charm quark. Therefore, the heavy charm quark remains in equilibrium as its processes occur faster than the expansion of the Universe. Additionally, the charm quark production time is faster than the charm quark decay. The faster quark-gluon pair fusion keeps the charm in chemical equilibrium up until hadronization. After hadronization, charm quarks form heavy mesons that decay into multi-particles quickly. Charm content then disappears from the Universe's particle inventory.

In Figure 8 Bottom we plot the relaxation time for production and decay of the bottom quark with different masses as a function of temperature. It shows that both production and decay are faster than the Hubble time $1/H$ for the duration of QGP. Unlike charm quarks however, the relaxation time for bottom quark production intersects with bottom quark decay at a temperatures dependant on the mass of the bottom. This means that the bottom quark decouples from the primordial plasma before hadronization as the production process slows down at low temperatures. The speed of weak interaction decays then dilutes bottom quark content of the QGP plasma pulling the distribution off equilibrium with $Y \neq 1$ (see Equation (18)) in the temperature domain below the crossing point, but before hadronization. All of this occurs with rates faster than Hubble expansion and thus as the Universe expands, the system departs from a detailed chemical balance rather than thermal freezeout.

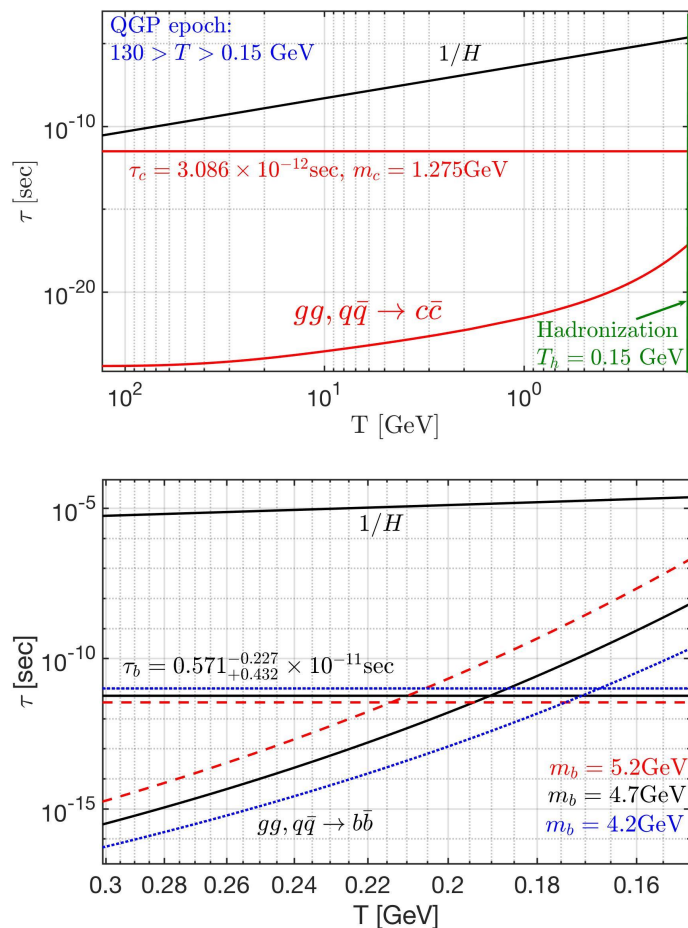


Figure 8. Comparison of Hubble time $1/H$, quark lifespan τ_q , and characteristic time for production via quark-gluon pair fusion for (Top figure) charm and (Bottom figure) bottom quarks as a function of temperature. Both figures end at approximately the hadronization temperature of $T_h \approx 150 \text{ MeV}$. Three different masses $m_b = 4.2 \text{ GeV}$ (blue short dashes), 4.7 GeV , (solid black), 5.2 GeV (red long dashes) for bottom quarks are plotted to account for its decay width.

Let us describe the dynamical non-equilibrium of bottom quark abundance in QGP in more detail. The competition between decay and production reaction rates for bottom quarks in the early Universe can be written as

$$\frac{1}{V} \frac{dN_b}{dt} = (1 - Y_b^2) R_b^{\text{Source}} - Y_b R_b^{\text{Decay}}, \quad (24)$$

where N_b is the bottom quark abundance, Y_b is the general fugacity of bottom quarks, and R_b^{Source} and R_b^{Decay} are the thermal reaction rates per volume of production and decay of bottom quark, respectively [63]. The bottom source rate is controlled by quark-gluon pair fusion rate which vanishes upon hadronization. The decay rate depends on whether the bottom quarks are unconfined and free or bound within B -mesons which is controlled by the plasma temperature. Under the adiabatic approximation, we solve for the generalized bottom fugacity Y_b in Equation (24) yielding

$$Y_b = \frac{R_b^{\text{Decay}}}{2R_b^{\text{Source}}} \left[\sqrt{1 + (2R_b^{\text{Source}}/R_b^{\text{Decay}})^2} - 1 \right]. \quad (25)$$

In Figure 9 we show the fugacity of the bottom quarks as a function of temperature $T = 0.3 \sim 0.15 \text{ GeV}$ for different masses of bottom quarks. In all cases, we have prolonged non-equilibrium $Y_b \neq 1$ because the decay and production rates of bottom quarks are of comparable temporal size to one another. The bottom content of QGP is exhausted as $Y_b \rightarrow 0$ as the Universe cools in temperature. For smaller masses, some bottom quark content is preserved up until hadronization as the strong interaction formation rate slows the depletion from weak decay near the QGP to HG phase transformation.

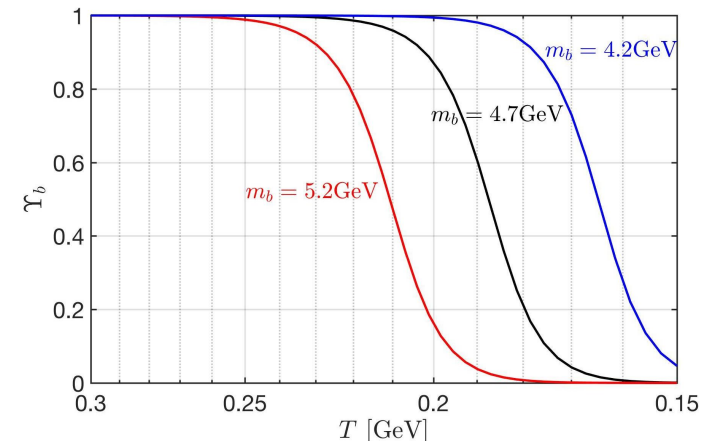


Figure 9. The generalized fugacity Y_b of free unconfined bottom quark as a function of temperature in QGP up to the hadronization temperature of $T_h \approx 150 \text{ MeV}$ for three different bottom masses $m_b = 4.2 \text{ GeV}$ (solid blue), 4.7 GeV , (solid black), 5.2 GeV (solid red).

As demonstrated above, the bottom quark flavor is capable to imprint arrow in time on physical processes being out of chemical equilibrium during the epoch $T = 0.3 \sim 0.15 \text{ GeV}$. This is one of the required Sakharov condition (see Section 1.2) for baryogenesis. Our results provide a strong motivation to explore the physics of baryon non-conservation involving the bottom quarks and bound $b\bar{b}$ bottomonium states in a thermal environment. Given that the non-equilibrium of bottom flavor arises at a relatively low QGP temperature allows for the baryogenesis to occur across primordial QGP hadronization epoch [63]. This result establishes the temperature era for the non-equilibrium abundance of bottom quarks.

3. Hadronic Epoch

3.1. The Formation of Matter

It is in this epoch that the matter of the Universe, including all the baryons which make up visible matter today, was created [61,62]. Unlike the fundamental particles, such as the quarks or W and Z , the mass of these hadrons is not due to the Higgs mechanism, but rather from the condensation of the QCD vacuum [13,64,65]. The quarks from which protons and neutrons are made have a mass more than 100 times smaller than these nucleons. The dominant matter mass-giving mechanism arises from quark confinement [66]. Light quarks are compressed by the quantum vacuum structure into a small space domain a hundred times smaller than their natural ‘size’. A heuristic argument can be made by considering the variance in valence quark momentum Δp required by the Heisenberg uncertainty principle by confining them to a space of order $\Delta x \approx 1$ fm and the energy density of the attractive gluon field required to balance that outward pressure. That energy cost then manifests as the majority of the nucleon mass. The remaining few percent of mass is then due to the fact that quarks also have inertial mass provided by the Higgs mechanism as well as the electromagnetic mass for particles with charge.

The QGP-hadronization transformation is not instantaneous and involves a transitory period containing both hadrons and QGP [62]. Therefore the conservation laws outlined in Equations (15)–(17) can be violated in one phase as long as it is equally compensated in the other phase. This means the partition function during hadronization, and thus the formation of matter, should be parameterized between the hadron gas (HG) component and QGP component as

$$\ln \mathcal{Z}_{tot} = f_{HG}(T) \ln \mathcal{Z}_{HG} + [1 - f_{HG}(T)] \ln \mathcal{Z}_{QGP}, \quad (26)$$

where $f_{HG}(T)$ is the proportion of the phase space occupied by the hadron gas with values between $0 < f_{HG} < 1$. The charge neutrality condition Equation (15) is then modified to be

$$n_{Q,HG+QGP} = f_{HG}(T)n_{HG,Q} + [1 - f_{HG}(T)]n_{QGP,Q} = 0. \quad (27)$$

At a temperature of $T_h \approx 150$ MeV, the quarks and gluons become confined and condense into hadrons (both baryons and mesons). During this period, the number of baryon-antibaryon pairs is sufficiently high that the asymmetry (of ~ 1 in 10^9) would be essentially invisible until a temperature of between 40–50 MeV. We note that CPT symmetry is protected by the lack of asymmetry in normal Standard Model reactions to some large factor by the accumulation of scattering events through the majority of the Universe’s evolution. CPT-violation is similarly restricted by possible mass difference in the Kaons [67] via the hypothetical difference in strange-antistrange quark masses which are expected to be small if not identically zero.

In Figure 10, we present the fraction of visible radiation and matter split between the baryons, mesons, and photons and leptons. For a brief early Universe period after QGP hadronization when the large amount of antimatter found in antiquarks converted into the dense gas of hadrons, their contribution to the energy density of the Universe competed with that of radiation and leptons [62]. Mass of matter will not emerge again until the late Universe after recombination though by that point dark matter would become the dominant form of matter in the cosmos.

The chemical potential of baryons after hadronization can be determined by the conserved baryon-per-entropy ratio under adiabatic expansion. Considering the net baryon density in the early Universe with temperature range $150\text{ MeV} > T > 5\text{ MeV}$ [24] we write

$$\begin{aligned} \frac{(n_B - n_{\bar{B}})}{s} &= \frac{1}{s} [(n_p - n_{\bar{p}}) + (n_n - n_{\bar{n}}) + (n_Y - n_{\bar{Y}})] \\ &= \frac{45}{2\pi^4 g_*^s} \sinh\left[\frac{\mu_B}{T}\right] F_N \left[1 + \frac{F_Y}{F_N} \sqrt{\frac{1 + e^{-\mu_B/T}}{1 + e^{\mu_B/T}} \frac{F_Y/F_K}{F_Y/F_K}} \right]. \end{aligned} \quad (28)$$

where μ_B is the baryon chemical potential, g_*^s represents the effective entropic degrees of freedom, and we employ phase-space functions F_i for the set of nucleon N , kaon K , and hyperon Y particles. These functions are defined in Section 11.4 of [58] and given by

$$F_N = \sum_{N_i} g_{N_i} W(m_{N_i}/T), \quad N_i = n, p, \Delta(1232), \quad (29)$$

$$F_K = \sum_{K_i} g_{K_i} W(m_{K_i}/T), \quad K_i = K^0, \bar{K}^0, K^\pm, K^*(892), \quad (30)$$

$$F_Y = \sum_{Y_i} g_{Y_i} W(m_{Y_i}/T), \quad Y_i = \Lambda, \Sigma^0, \Sigma^\pm, \Sigma(1385), \quad (31)$$

where g_{N_i, K_i, Y_i} is the degeneracy of each baryonic species. We define the function $W(x) = x^2 K_2^B(x)$ where K_2^B is the modified Bessel function of integer order “2”.

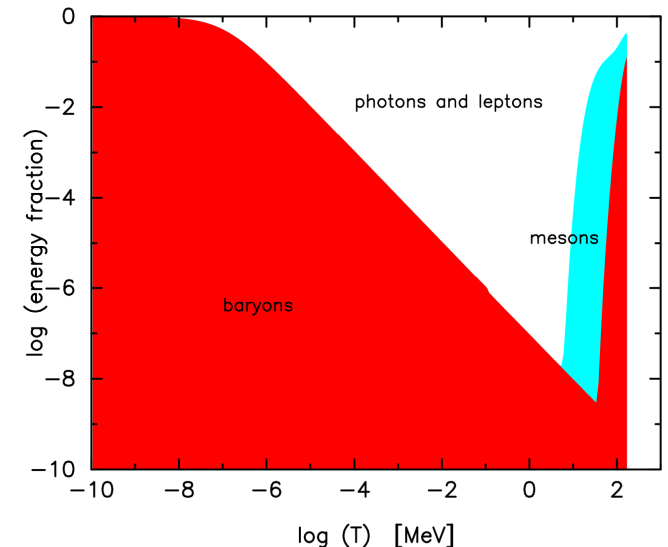


Figure 10. The fractional energy density of the luminous Universe (photons and leptons (white), mesons (blue), and hadrons (red)) as a function of the temperature of the Universe from hadronization to the contemporary era. This figure is a companion figure to Figure 2 (2003 unpublished, Fromerth & Rafelski [62]).

The net baryon-per-entropy-ratio can be obtained from the present-day measurement of the net baryon-per-photon ratio $(n_B - n_{\bar{B}})/n_\gamma$, where n_γ is the contemporary photon number density from the CMB [24]. This value is determined to be

$$\frac{n_B - n_{\bar{B}}}{s} = \frac{n_B - n_{\bar{B}}}{s} \Big|_{t_0} = (0.865 \pm 0.008) \times 10^{-10}. \quad (32)$$

We arrive at this ratio from considering the observed baryon-per-photon ratio [68] of

$$\frac{n_B - n_{\bar{B}}}{n_\gamma} = (0.609 \pm 0.006) \times 10^{-9}, \quad (33)$$

as well as the entropy-per-particle [23] for massless bosons and fermions

$$s/n|_{\text{boson}} \approx 3.60, \quad s/n|_{\text{fermion}} \approx 4.20. \quad (34)$$

Considering the inventory of strange mesons and baryons in the cosmos after hadronization, we evaluated the temperature of the net baryon disappearance in Figure 11. In solving Equation (28) numerically, we plot the baryon and antibaryon number density as a function of temperature in the range $150 \text{ MeV} > T > 5 \text{ MeV}$. The temperature where antibaryons disappear from the Universe inventory can be defined when the ratio $n_{\bar{B}}/(n_B - n_{\bar{B}}) = 1$. This condition was reached at temperature $T = 38.2 \text{ MeV}$ which is in agreement with the qualitative result in Kolb and Turner [69]. After this temperature, the net baryon density dilutes with a residual co-moving conserved quantity determined by the baryon asymmetry.

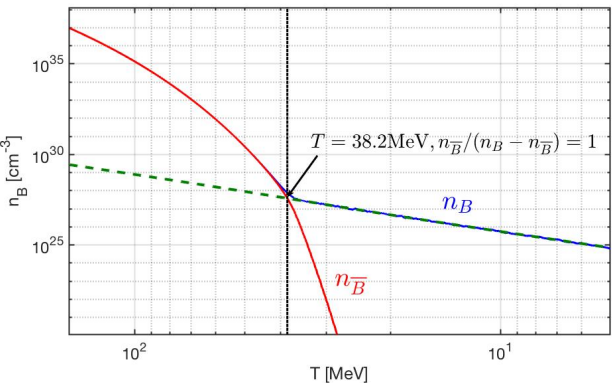


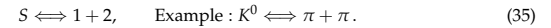
Figure 11. The baryon (blue solid line) and antibaryon (red solid line) number density as a function of temperature in the range $150 \text{ MeV} > T > 5 \text{ MeV}$. The green dashed line is the extrapolated value for baryon density. The temperature $T = 38.2 \text{ MeV}$ (black dashed vertical line) is denoted when the ratio $n_{\bar{B}}/(n_B - n_{\bar{B}}) = 1$ which define the condition where antibaryons disappear from the Universe.

The antibaryon disappearance temperature does not depend on baryon and lepton number neutrality $L = B$. Rather, it depends only on the baryon-per-entropy ratio which is assumed to be constant during the Universe's evolution, a condition which is maintained well after the plasmas discussed here vanish. The assumption of co-moving baryon number conservation is justified by the wealth of particle physics experiments, and the co-moving entropy conservation in an adiabatic evolving Universe is a common assumption.

3.2. Strangeness Abundance

As the energy contained in QGP is used up to create mesons, that is massive particles containing matter and antimatter, the high abundance of (anti)strange (s, \bar{s}) quark pairs present in the plasma is preserved. A smaller abundance of (anti)charm (c, \bar{c}) can combine with abundant strange quarks to form 'exotic' heavy mesons. With time, charmness and later strangeness decay away as these flavors are heavier than the light (u, d) quarks and antiquarks. Unlike charm, which disappears from the particle inventory relatively quickly, strangeness can still persist [24] in the Universe until $T \approx \mathcal{O}(10 \text{ MeV})$. As already noted, the meson sector is of particular interest in our work since mesons carry antimatter in form of their antiquark component. After the loss of antibaryons at $T = 38.2 \text{ MeV}$, Figure 11, the remaining light mesons then act as a proxy for the hadronic antimatter evolution.

We illustrate this by considering an unstable strange particle S decaying into two particles 1 and 2 which themselves have no strangeness content. In a dense and high-temperature plasma with particles 1 and 2 in thermal equilibrium, the inverse reaction populates the system with particle S . This is written schematically as



The natural decay of the daughter particles provides the intrinsic strength of the inverse strangeness production reaction rate. As long as both decay and production reactions are possible, particle S abundance remains in thermal equilibrium. This balance between production and decay rates is called a detailed balance. The thermal reaction rate per time and volume for two-to-one particle reactions $1 + 2 \rightarrow 3$ has been presented before [70,71]. In full kinetic and chemical equilibrium, the reaction rate per time per volume is given by [71]:

$$R_{12 \rightarrow 3} = \frac{g_3}{(2\pi)^2} \frac{m_3}{\tau_3^0} \int_0^\infty \frac{p_3^2 dp_3}{E_3} \frac{e^{E_3/T}}{e^{E_3/T} \pm 1} \Phi(p_3), \quad (36)$$

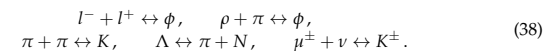
where τ_3^0 is the vacuum lifetime of particle 3. The positive sign "+" is for the case when particle 3 is a boson, while it is negative "-" for fermions. The function $\Phi(p_3)$ in the non-relativistic limit $m_3 \gg p_3, T$ can be written as

$$\Phi(p_3 \rightarrow 0) = 2 \frac{1}{(e^{E_1/T} \pm 1)(e^{E_2/T} \pm 1)}. \quad (37)$$

When back-reactions are faster than the Universe expansion, a condition we characterize in the following, we can explore the Universe composition assuming both kinetic and particle abundance equilibrium (chemical equilibrium). In Figure 12 we numerically solve for the chemical potential of strangeness and show the chemical equilibrium particle abundance ratios [24] for various mesons, the baryons, and their antiparticles. In the temperature range $150 \text{ MeV} > T > 40 \text{ MeV}$ the Universe is rich in physical phenomena involving strange mesons and (anti)baryons including (anti)hyperon abundances. While antibaryons vanish after temperature $T \approx 40 \text{ MeV}$, kaons persist compared to baryons until $T = 20 \text{ MeV}$. For temperatures $T < 20 \text{ MeV}$, the Universe becomes light-quark baryons dominant. Pions $\pi(q\bar{q})$ persist the longest of the mesons (a feature explored in Section 3.3) until $T = 5.6 \text{ MeV}$. Pions are the most abundant hadrons in this period because of their low mass and the inverse decay reaction $\gamma + \gamma \rightarrow \pi^0$ which assures chemical equilibrium [70].

Below $T = 5.6 \text{ MeV}$, we have $n_\pi/n_B < 1$ and the number density of pion become sub-dominant compared to the remaining baryons. It is important to realize that hadrons always are a part of the evolving Universe, a point we wish to see emphasized more in literature. For temperatures $150 \text{ MeV} > T > 20 \text{ MeV}$ the Universe is meson-dominant with (anti)strangeness well represented in the meson sector with $s = \bar{s}$. Below temperature $T < 13 \text{ MeV}$, strangeness inventory is mostly found in the hyperons as we have $(s - \bar{s}) \neq 0$. We note that hyperons never exceed baryon content throughout the hadron epoch. This period of meson physics ends the stage of the Universe where antimatter was dominant in the quark sector.

In Figure 13 we schematically show important source reactions for strange quark abundance in baryons and mesons considering both open and hidden strangeness ($s\bar{s}$ -content). The important strangeness processes (involving both the quark and lepton sectors) are



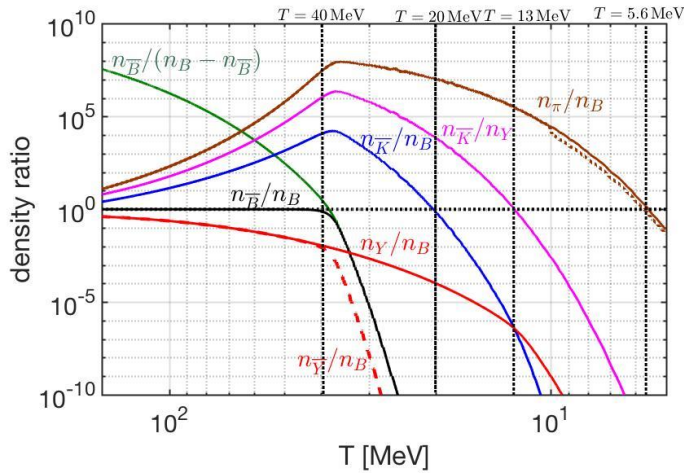


Figure 12. Ratios of hadronic particle number densities as a function of temperature $150 \text{ MeV} > T > 5 \text{ MeV}$ in the early Universe with baryon B yields: Pions $\pi(q\bar{q})$ (brown line), kaons $K(q\bar{s})$ (blue line), antibaryon \bar{B} (black line), hyperon Y (red line) and antihyperons \bar{Y} (dashed red line). Also shown is the \bar{K}/Y ratio (purple line) and the \bar{B} to asymmetry $B - \bar{B}$ ratio (green line). Temperature crossings are included (as vertical dashed black lines) at $T = 40 \text{ MeV}, 20 \text{ MeV}, 13 \text{ MeV}, 5.6 \text{ MeV}$ as different abundances become sub-dominant compared to other species. The dashed brown line represents the drop in overall pion π abundance when the vanishing of the charged pions π^\pm from the particle inventory is taken into account.

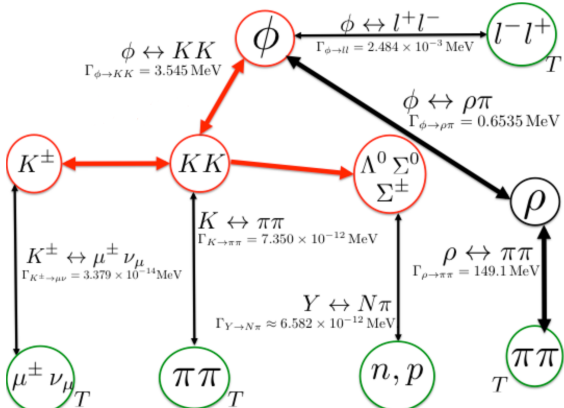


Figure 13. The strangeness abundance changing reactions in the primordial Universe. Red circles show strangeness carrying hadronic particles and thick red lines denote effectively instantaneous reactions. Thick black lines show relatively strong hadronic reactions.

Muons and pions are coupled through electromagnetic reactions

$$\mu^+ + \mu^- \leftrightarrow \gamma + \gamma, \quad \pi^0 \leftrightarrow \gamma + \gamma, \quad (39)$$

to the photon background and retain their chemical equilibrium respectively [70,72]. The large $\phi \leftrightarrow K + K$ rate assures ϕ and K are in relative chemical equilibrium.

Once the primordial Universe expansion rate (given as the inverse of the Hubble parameter $1/H$) overwhelms the strongly temperature-dependent back-reaction, the decay $S \rightarrow 1 + 2$ occurs out of balance and particle S disappears from the Universe. In order to determine where exactly strangeness disappears from the Universe inventory we explore the magnitudes of a relatively large number of different rates of production and decay processes and compare these with the Hubble time constant [24]. Strangeness then primarily resides in two domains:

- Strangeness in the mesons
- Strangeness in the (anti)hyperons

In the meson domain, the relevant interaction rates competing with Hubble time are the reactions

$$\begin{aligned} \pi + \pi &\leftrightarrow K, & \mu^\pm + \nu \leftrightarrow K^\pm, \\ l^+ + l^- &\leftrightarrow \phi, & \rho + \pi \leftrightarrow \phi, & \pi + \pi \leftrightarrow \rho. \end{aligned} \quad (40)$$

The relaxation times τ_i for these processes are compared with Hubble time in Figure 14. The criteria for a detailed reaction balance is broken once a process crosses above the Hubble time $1/H$ and thus can no longer be considered as subject to adiabatic evolution. As the Universe cools, these various processes freeze out as they cross this threshold. In Table 1 we show the characteristic strangeness reactions and their freeze-out temperatures in the hadronic epoch.

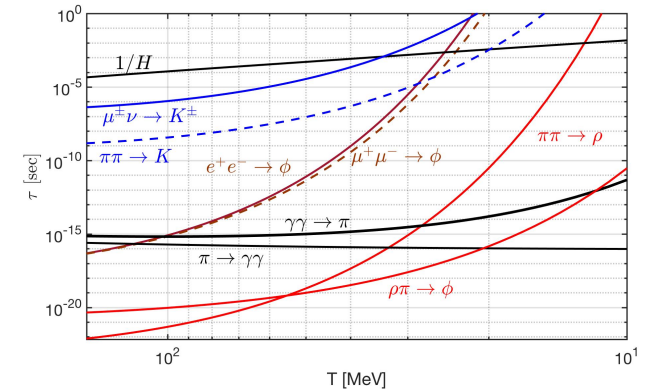


Figure 14. The hadronic reaction relaxation times τ_i in the meson sector as a function of temperature compared to Hubble time $1/H$ (black solid line). The following processes are presented: The leptonic (solid blue line) and strong (dashed blue line) kaon K processes, the electronic (solid dark red line) and muonic (dashed dark red line) phi meson ϕ processes, the forward and backward (thick black lines) electromagnetic pion π processes, and the strong (red lines) rho meson ρ processes.

Table 1. The characteristic strangeness reaction, their freeze-out temperature, and temperature width in the hadronic epoch.

Reactions	Freeze-Out Temperature (MeV)	ΔT_f (MeV)
$\mu^\pm \nu \rightarrow K^\pm$	$T_f = 33.8$ MeV	3.5 MeV
$e^+ e^- \rightarrow \phi$	$T_f = 24.9$ MeV	0.6 MeV
$\mu^+ \mu^- \rightarrow \phi$	$T_f = 23.5$ MeV	0.6 MeV
$\pi\pi \rightarrow K$	$T_f = 19.8$ MeV	1.2 MeV
$\pi\pi \rightarrow \rho$	$T_f = 12.3$ MeV	0.2 MeV

Once freeze-out occurs and the corresponding detailed balance is broken, the inverse decay reactions act like a “hole” in the strangeness abundance siphoning strangeness out of the Universe’s particle inventory. The first freeze-out reaction is the weak interaction kaon production process

$$\mu^\pm + \nu_\mu \rightarrow K^\pm, \quad T_f^{K^\pm} = 33.8 \text{ MeV}, \quad (41)$$

which is followed by the electromagnetic ϕ meson production process

$$l^- + l^+ \rightarrow \phi, \quad T_f^\phi = 23 \sim 25 \text{ MeV}. \quad (42)$$

Hadronic kaon production via pions follows next in the freeze-out process

$$\pi + \pi \rightarrow K, \quad T_f^K = 19.8 \text{ MeV}. \quad (43)$$

as it becomes slower than the Hubble expansion. The reactions

$$\gamma + \gamma \leftrightarrow \pi, \quad \rho + \pi \leftrightarrow \phi \quad (44)$$

remain faster compared to $1/H$ for the duration of the hadronic plasma epoch. Most ρ meson decays are faster [68] than ϕ meson producing processes and cannot contribute to the strangeness creation in the meson sector. Below the temperature $T < 20$ MeV, all the detail balances in the strange meson sector are broken by freeze-out and the strangeness inventory in meson sector disappears rapidly.

Were it not for the small number of baryons present, strangeness would entirely vanish with the loss of the mesons. In order to understand strangeness in hyperons in the baryonic domain, we evaluated the reactions

$$\pi + N \leftrightarrow K + \Lambda, \quad \bar{K} + N \leftrightarrow \Lambda + \pi, \quad \Lambda \leftrightarrow N + \pi, \quad (45)$$

for strangeness production, exchange, and decay respectively in detail. The general form for thermal reaction rate per volume is discussed in Ch. 17 of [58]. In Figure 15 we show that for $T < 20$ MeV, the reactions for the hyperon Λ production is dominated by $\bar{K} + N \leftrightarrow \Lambda + \pi$. Both strangeness and antistrangeness disappear from the Universe via the reactions

$$\Lambda \rightarrow N + \pi, \quad K \rightarrow \pi + \pi, \quad (46)$$

which conserves $s = \bar{s}$. Beginning with $T = 12.9$ MeV, the dominant reaction is $\Lambda \leftrightarrow N + \pi$, which shows that at lower temperatures strangeness content resides in the Λ baryon. This behavior is seen explicitly in Figure 12 where the hyperon abundance (of which the Λ baryon is a member) exceeds the rapidly diminishing kaon abundance as the Universe cools. While hyperons never form a dominant component of the hadronic content of the Universe, it is an important life-boat for strangeness persisting after the more transitory mesons. In this case, the strangeness abundance becomes asymmetric and we have $s \gg \bar{s}$ at temperatures $T < 12.9$ MeV. Hence, strange hyperons and antihyperons

could enter into dynamic non-equilibrium condition including $\langle s - \bar{s} \rangle \neq 0$. The primary conclusion of the study of strangeness production and content in the early Universe, following on QGP hadronization, is that the relevant temperature domains indicate a complex interplay between baryon and meson (strange and non-strange) abundances and non-trivial decoupling from equilibrium for strange and non-strange mesons.

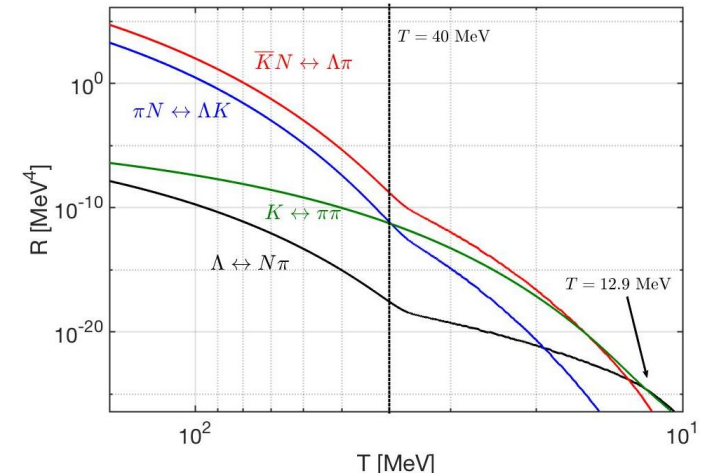


Figure 15. Thermal reaction rate R per volume and time for important hadronic strangeness production, exchange and decay processes as a function of temperature $150 \text{ MeV} > T > 10 \text{ MeV}$. The following processes are presented: $\Lambda \leftrightarrow N\pi$ (solid black line), $K \leftrightarrow \pi\pi$ (solid green line), $\pi N \leftrightarrow \Lambda K$ (solid blue line), $\bar{K}N \leftrightarrow \Lambda\pi$ (solid red line). Two temperature crossings are denoted at $T = 40 \text{ MeV}$, 12.9 MeV .

3.3. Pion Abundance

Pions ($q\bar{q}, q \in u, d$), the lightest hadrons, are the dominant hadrons in the hadronic era and the most abundant hadron family well into the leptonic epoch (see Section 4). The neutral pion π^0 vacuum lifespan of $\tau_{\pi^0}^0 = (8.52 \pm 0.18) \times 10^{-17} \text{ s}$ [68] is far shorter compared to the Hubble expansion time of $1/H = (10^{-3} \sim 10^{-4}) \text{ s}$ within this epoch as depicted in Figure 14.

At seeing such a large discrepancy in characteristic times, one is tempted to presume that the decay process dominates and that π^0 disappears quickly in the hadronic gas. However, in the high temperature $T = \mathcal{O}(100 \text{ MeV}) \sim \mathcal{O}(10 \text{ MeV})$ thermal bath of this era, the inverse decay reaction forms neutral pions π^0 at rate corresponding to the decay process maintaining the abundance of the species (see Figure 12). In general, π^0 is produced in the QED plasma predominantly by thermal two-photon fusion:

$$\gamma + \gamma \rightarrow \pi^0. \quad (47)$$

This formation process is simply the inverse of the dominant decay process. While we do not address it in detail here, the π^\pm charged pions are also in thermal equilibrium with the other pions species via hadronic and electromagnetic reactions

$$\pi^0 + \pi^0 \leftrightarrow \pi^+ + \pi^-, \quad l^+ + l^- \leftrightarrow \pi^+ + \pi^-, \quad \gamma + \gamma \leftrightarrow \pi^+ + \pi^-. \quad (48)$$

Of these, the hadronic interaction is the fastest and controls the charged pion abundance most directly [23,73] such that the condition

$$\rho_{\pi^0} \sim \rho_{\pi^\pm}, \quad (49)$$

where ρ is the energy density of the species and is maintained for most of the hadronic era. We point out that in the late (colder) hadronic era, the charged pions will scatter off the remaining baryons with asymmetric reactions due to the lack of antibaryons. The smallness of the electronic e^+e^- formation of π^0 is characterized by its small branching ratio in π^0 decay $B = \Gamma_{ee}/\Gamma_{\gamma\gamma} = 6.2 \pm 0.5 \times 10^{-8}$ [68] which can be neglected compared to photon fusion. The general form for invariant production rates and relaxation time is discussed in [70] where we have for the photon fusion process

$$R_{\gamma\gamma \rightarrow \pi^0} = \int \frac{d^3 p_\pi}{(2\pi)^3 2E_\pi} \int \frac{d^3 p_{2\gamma}}{(2\pi)^3 2E_{2\gamma}} \int \frac{d^3 p_{1\gamma}}{(2\pi)^3 2E_{1\gamma}} (2\pi)^4 \delta^4(p_{1\gamma} + p_{2\gamma} - p_\pi) \times \sum_{\text{spin}} |\langle p_{1\gamma} p_{2\gamma} | M | p_\pi \rangle|^2 f_\pi(p_\pi) f_\gamma(p_{1\gamma}) f_\gamma(p_{2\gamma}) Y_\gamma^{-2} Y_{\pi^0}^{-1} e^{u \cdot p_\pi/T}, \quad (50)$$

where Y_i is the fugacity and f_i is the Bose-Einstein distribution of particle i , and M is the matrix element for the process. Since the $\gamma + \gamma \rightarrow \pi^0$ is the dominant mechanism of pion production, we can omit all sub-dominant processes, and the dynamic equation of π^0 abundance can be written as [23]:

$$\frac{d}{dt} Y_{\pi^0} = \frac{1}{\tau_T} Y_{\pi^0} + \frac{1}{\tau_S} Y_{\pi^0} + \frac{1}{\tau_{\pi^0}} (Y_\gamma^2 - Y_{\pi^0}), \quad (51)$$

where τ_T and τ_S are the kinematic relaxation times for temperature and entropy evolution and τ_{π^0} is the chemical relaxation time for π^0 . We have

$$\begin{aligned} \frac{1}{\tau_T} &\equiv -T^3 g^* \frac{d(n_\pi/(Y_3 g^* T^3))/dT}{dn_\pi/dY_3} \dot{T}, \\ \frac{1}{\tau_S} &\equiv -\frac{n_\pi/Y_3}{dn_\pi/dY_3} \frac{d \ln(g^* V T^3)}{dT} \dot{T}, \\ \tau_{\pi^0} &= \frac{dn_{\pi^0}/dY_{\pi^0}}{R_{\pi^0}}, \end{aligned} \quad (52)$$

where n_{π^0} is the number density of pions. A minus sign is introduced in the above expressions to maintain $\tau_T, \tau_S > 0$. Since entropy is conserved within the radiation-dominated epoch, we have $T^3 V = \text{constant}$ thus $d(T^3 V(T))/dT = 0$. This implies the entropic relaxation time is infinite yielding $1/\tau_S = 0$. The effect of Universe expansion and dilution of number density is described by $1/\tau_T$. Comparing τ_T to the chemical relaxation time τ_{π^0} can provide the quantitative condition for freeze-out from chemical equilibrium. In the case of pion mass being much larger than the temperature, $m_\pi \gg T$, we have [73]

$$\tau_T \approx \frac{T}{m_\pi H}. \quad (53)$$

In Figure 14 we compare the relaxation time of τ_{π^0} to the Hubble time $1/H$ which shows that $\tau_{\pi^0} \ll 1/H$. In such a case, the yield of π^0 is expected to remain in chemical equilibrium (even as its thermal number density gradually decreases) with no freeze-out temperature occurring. This makes pions distinct from all other meson species. This phenomenon can be attributed to the high population of photons as in such an environment, it remains sufficiently probable to find high-energy photons to fuse back into neutral pions π^0 [23] for the duration of large pion abundance. As shown in Figure 12, pions remained as proxy for hadronic matter and antimatter down to $T = 5.6$ MeV.

4. Leptonic Epoch

4.1. Thermal Degrees of Freedom

The leptonic epoch, dominated by photons and both charged and neutral leptons, is notable for being the last time where neutrinos played an active role in the Universe's thermal dynamics before decoupling and becoming free-streaming. In the early stage of this plasma after the hadronization era ended $T \approx \mathcal{O}(10 \text{ MeV})$, neutrinos represented the highest energy density followed by the light charged leptons and then finally the photons. The differing relativistic limit energy densities can be related by

$$\rho_{e^\pm} \approx \left(2 \times \frac{7}{8}\right) \rho_\gamma, \quad \rho_\nu \approx \left(3 \times \frac{7}{8}\right) \rho_\gamma. \quad (54)$$

The reason for this hierarchy is because of the degrees of freedom [29,58] available in each species in thermal equilibrium; the factor $7/8$ arises from the difference in pressure contribution between bosons and fermions.

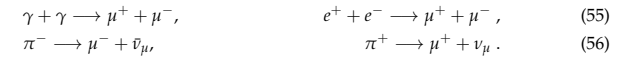
While photons only exhibit two polarization degrees of freedom, the charged light leptons could manifest as both matter (electrons), antimatter (positrons) and as well as two polarizations yielding $2 \times 2 = 4$. The neutral leptons made up of the neutrinos however had three thermally active species $3 \times 2 = 6$ boosting their energy density in that period to more than any other contribution. The muon-antimuon energy density was also controlled by its degrees of freedom matching that of e^\pm until $T \approx \mathcal{O}(100 \text{ MeV})$, still well within the hadronic epoch, when the heavier lepton no longer satisfied the ultra-relativistic (and thus massless) limit. This separation of the two lighter charge lepton dynamics is seen in Figure 2 after hadronization.

The known cosmic degrees of freedom require that if and when neutrinos are Dirac-like and have chiral right-handed (matter) components, then these right handed components must not drive the neutrino effective degrees of freedom N_{eff}^ν away from three. In a more general context the non-interacting sterile neutrinos could also inflate N_{eff}^ν during this epoch for the same reasoning [74–78] or have a connection to dark matter [79,80]. The neutrino degrees of freedom will be more fully discussed in Section 4.5.

4.2. Muon Abundance

As seen in Section 3.2, muon abundance and their associated reactions are integral to the understanding of the strangeness and antistrangeness content of the primordial Universe [24]. Therefore we determine to what extent and temperature (anti)muons remained in chemical abundance equilibrium. Without a clear boundary separating the hadronic epoch from the leptonic epoch, there is complete overlap in the hadronic and leptonic species dynamics in the period $T = \mathcal{O}(10 \text{ MeV}) \sim \mathcal{O}(1 \text{ MeV})$.

In the cosmic plasma, muons can be produced by predominately electromagnetic and weak interaction processes



Provided that all particles shown on the left-hand side of each reaction (namely the photons, electrons (positrons) and charged pions) exist in chemical equilibrium, the back-reaction for each of the above processes occurs in detailed balance.

The scattering angle averaged thermal reaction rate per volume for the reaction $a\bar{a} \rightarrow b\bar{b}$ in Boltzmann approximation is given by [58]

$$R_{a\bar{a} \rightarrow b\bar{b}} = \frac{g_a g_{\bar{a}}}{1 + I} \frac{T}{32\pi^4} \int_{s_{th}}^{\infty} ds \frac{s(s - 4m_a^2)}{\sqrt{s}} \sigma_{a\bar{a} \rightarrow b\bar{b}} K_1(\sqrt{s}/T), \quad (57)$$

where s_{th} is the threshold energy for the reaction, $\sigma_{a\bar{a} \rightarrow b\bar{b}}$ is the cross section for the given reaction. We introduce the factor $1/(1+I)$ to avoid the double counting of indistinguishable pairs of particles where $I = 1$ for an identical pair and $I = 0$ for a distinguishable pair.

The muon weak decay processes are

$$\mu^- \rightarrow \nu_\mu + e^- + \bar{\nu}_e, \quad \mu^+ \rightarrow \bar{\nu}_\mu + e^+ + \nu_e, \quad (58)$$

with the vacuum life time $\tau_\mu = 2.197 \times 10^{-6}$ s producing (anti)neutrino pairs of differing flavor and electrons(positrons). We recall the considerable shorter vacuum lifetime of pions $\tau_{\pi^\pm} = 2.6033 \times 10^{-8}$ s. The thermal decay rate per volume in the Boltzmann limit is [70]

$$R_i = \frac{g_i}{2\pi^2} \left(\frac{T^3}{\tau_i} \right) \left(\frac{m_i}{T} \right)^2 K_1(m_i/T) \quad (59)$$

where τ_i is the vacuum lifespan of a given particle i .

These production and decay rates for muonic processes are evaluated in [72]. From this, we can determine the temperature when muons rather suddenly disappear from the particle inventory of the Universe which occurs when their decay rate exceeds their production rate. In Figure 16 we show the invariant thermal reaction rates per volume and time for the relevant muon reactions. As the temperature decreases in the expanding Universe, the initially dominant production rates become rapidly smaller due to the mass threshold effect. This is allowing the production and decay rates to become equal. The characteristic times are much faster than the Hubble time (not shown in Figure 16). Muon abundance therefore disappears just when the decay rate overwhelms production at the temperature $T_{dis} = 4.20$ MeV.

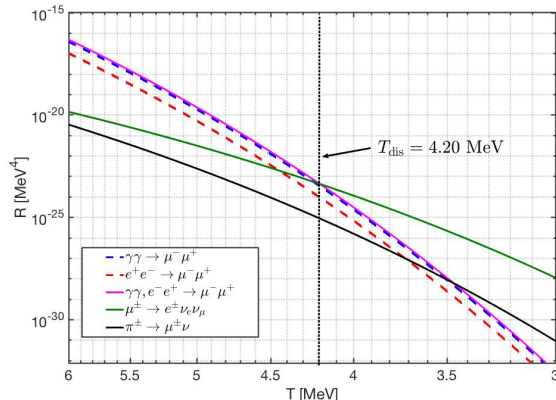


Figure 16. The thermal reaction rate per volume for muon related reactions as a function of temperature adapted from [72]. The dominant reaction rates for μ^\pm production are: The $\gamma\gamma$ channel (blue dashed line), $e^\pm e^-$ (red dashed line), these two combined as the total electromagnetic rate (pink solid line), and the charged pion decay feed channel (black solid line). The muon decay rate is also shown (green solid line). The crossing point between the electromagnetic production processes and the muonic decay rate is seen as the dashed vertical black line at $T_{dis} = 4.2$ MeV.

In Figure 17 we show that the number density ratio of muons to baryons n_{μ^\pm}/n_B at the muon disappearance temperature $T_{dis} = 4.20$ MeV is $n_{\mu^\pm}/n_B \approx 0.91$ [24]. Interestingly, this means that the muon abundance may still be able to influence baryon evolution up to this point because their number density is comparable to that of baryons (there are

no antibaryons). This coincidence of abundance offers a novel and tantalizing model-building opportunity for both baryon-antibaryon separation models and/or strangelet formation models.

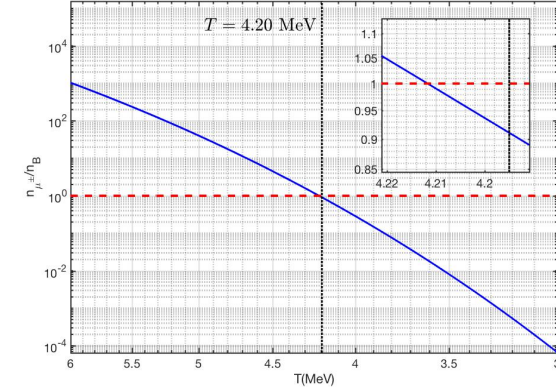


Figure 17. The density ratio between μ^\pm and baryons n_{μ^\pm}/n_B (blue solid line) is plotted as a function of temperature. The red dashed line indicates a density ratio value of $n_{\mu^\pm}/n_B = 1$. The density ratio at the muon disappearance temperature (vertical black dashed line) is about $n_{\mu^\pm}/n_B(T_{dis}) \approx 0.911$.

4.3. Neutrino Masses and Oscillation

Neutrinos are believed to have a small, but nonzero mass due to the phenomenon of flavor oscillation [81–83]. This is seen in the flux of neutrinos from the Sun, and also in terrestrial reactor experiments. In the Standard Model neutrinos are produced via weak charged current (mediated by the W boson) as flavor eigenstates. If the neutrino was truly massless, then whatever flavor was produced would be immutable as the propagating state. However, if neutrinos have mass, then they propagate through space as their mass-momentum eigenstates. Neutrino masses can be written in terms of an effective theory where the mass term contains various couplings between neutrino states determined by some BSM theory. The exact form of such a BSM theory is outside the scope of this work, we refer the reader to some standard references [84–87].

Within the Standard Model keeping two degrees of freedom for each neutrino flavor the Majorana fermion mass term is given by

$$\mathcal{L}_m^{Maj.} = -\frac{1}{2} \bar{\nu}_L^\alpha M_{\alpha\beta}^\alpha (\nu_L^\beta)^c + h.c., \quad (60)$$

where $\nu^c = \hat{C}(\bar{\nu})^T$ is the charge conjugate of the neutrino field. The operator $\hat{C} = i\gamma^2\gamma^0$ is the charge conjugation operator. An interesting consequence of neutrinos being Majorana particles is that they would be their own antiparticles like photons allowing for violations of total lepton number. Neutrinoless double beta decay is an important, yet undetected, evidence for Majorana nature of neutrinos [88]. Majorana neutrinos with small masses can be generated from some high scale via the See-Saw mechanism [89–91] which ensures that the degrees of freedom separate into heavy neutrinos and light nearly massless Majorana neutrinos. The See-Saw mechanism then provides an explanation for the smallness of the neutrino masses as has been experimentally observed.

A flavor eigenstate ν^α can be described as a superposition of mass eigenstates ν^k with coefficients given by the Pontecorvo-Maki-Nakagawa-Sakata (PMNS) mixing matrix [92,93] which are both in general complex and unitary. This is given by

$$\nu^\alpha = \sum_k U_{\alpha k}^* \nu^k, \quad \alpha = e, \mu, \tau, \quad k = 1, 2, 3, \dots, n \quad (61)$$

where U is the PMNS mixing matrix. The PMNS matrix is the lepton equivalent to the CKM mixing matrix which describes the misalignment between the quark flavors and their masses. For Majorana neutrinos, there can be up to three complex phases (δ, ρ, γ) which are CP-violating [94] which are present when the number of generations is $n \geq 3$. For Dirac-like neutrinos, only the δ complex phase is required. In principle, the number of mass eigenstates can exceed three, but is restricted to three generations in most models. By standard convention [95] found in the literature we parameterize the rotation matrix U as

$$U = \begin{pmatrix} c_{12}c_{13} & s_{12}c_{13} & s_{13}e^{-i\delta} \\ -s_{12}c_{23} - c_{12}s_{13}s_{23}e^{i\delta} & c_{12}c_{23} - s_{12}s_{13}s_{23}e^{i\delta} & c_{13}s_{23} \\ s_{12}s_{23} - c_{12}s_{13}c_{23}e^{i\delta} & -c_{12}s_{23} - s_{12}s_{13}c_{23}e^{i\delta} & c_{13}c_{23} \end{pmatrix} \times \begin{pmatrix} 1 & & \\ e^{i\rho} & & \\ & e^{i\gamma} & \end{pmatrix}, \quad (62)$$

where $c_{ij} = \cos(\theta_{ij})$ and $s_{ij} = \sin(\theta_{ij})$. In this convention, the three mixing angles $(\theta_{12}, \theta_{13}, \theta_{23})$, are understood to be the Euler angles for generalized rotations.

The neutrino proper masses are generally considered to be small with values no more than 0.1 eV. Because of this, neutrinos produced during fusion within the Sun or radioactive fission in terrestrial reactors on Earth propagate relativistically. Evaluating freely propagating plane waves in the relativistic limit yields the vacuum oscillation probability between flavors ν_α and ν_β written as [96]

$$\begin{aligned} P_{\alpha \rightarrow \beta} = & \delta_{\alpha\beta} - 4 \sum_{i < j}^n \operatorname{Re} \left[U_{\alpha i} U_{\beta i}^* U_{\alpha j}^* U_{\beta j} \right] \sin^2 \left(\frac{\Delta m_{ij}^2 L}{4E} \right) \\ & + 2 \sum_{i < j}^n \operatorname{Im} \left[U_{\alpha i} U_{\beta i}^* U_{\alpha j}^* U_{\beta j} \right] \sin \left(\frac{\Delta m_{ij}^2 L}{2E} \right), \quad \Delta m_{ij}^2 \equiv m_i^2 - m_j^2 \end{aligned} \quad (63)$$

where L is the distance traveled by the neutrino between production and detection. The square mass difference Δm_{ij}^2 has been experimentally measured [96]. As oscillation only restricts the differences in mass squares, the precise values of the masses cannot be determined from oscillation experiments alone. It is also unknown under what hierarchical scheme (normal or inverted) [97,98] the masses are organized as two of the three neutrino proper masses are close together in value.

It is important to point out that oscillation does not represent any physical interaction (except when neutrinos must travel through matter which modulates the ν_e flavor [99,100]) or change in the neutrino during propagation. Rather, for a given production energy, the superposition of mass eigenstates each have unique momentum and thus unique group velocities. This mismatch in the wave propagation leads to the oscillatory probability of flavor detection as a function of distance.

We further note that non-interacting BSM so called sterile neutrinos of any mass have not yet been observed despite extensive searching. The existence of such neutrinos, if they were ever thermally active in the early cosmos would leave fingerprints on the Cosmic Neutrino Background (CNB) spectrum [78]. The presence of an abnormally large anomalous magnetic moment [84,101–106] for the neutrino would also possibly leave traces in the evolution of the early Universe.

4.4. Neutrino Freeze-Out

The relic neutrino background (or CNB) is believed to be a well-preserved probe of a Universe only a second old which at some future time may become experimentally accessible. The properties of the neutrino background are influenced by the details of the freeze-out or decoupling process at a temperature $T = \mathcal{O}$ (2 MeV). The freeze-out process, whereby a particle species stops interacting and decouples from the photon background, involves several steps that lead to the species being described by the free-streaming momentum distribution. We outline freeze-out properties, including what distinguishes it from the equilibrium distributions [25].

Chemical freeze-out of a particle species occurs at the temperature, T_{ch} , when particle number changing processes slow down and the particle abundance can no longer be maintained at an equilibrium level. Prior to the chemical freeze-out temperature, number changing processes are significant and keep the particle in chemical (and thermal) equilibrium, implying that the distribution function has the Fermi-Dirac form, obtained by maximizing entropy at fixed energy (parameter $1/T$) and particle number (parameter λ)

$$f_c(t, E) = \frac{1}{\lambda \exp(E/T) + 1}, \text{ for } T(t) > T_{ch}. \quad (64)$$

Kinetic freeze-out occurs at the temperature, T_f , when momentum exchanging interactions no longer occur rapidly enough to maintain an equilibrium momentum distribution. When $T_f < T(t) < T_{ch}$, the number-changing process no longer occurs rapidly enough to keep the distribution in chemical equilibrium but there is still sufficient momentum exchange to keep the distribution in thermal equilibrium. The distribution function is therefore obtained by maximizing entropy, with fixed energy, particle number, and antiparticle number separately. This implies that the distribution function has the form

$$f_k(t, E) = \frac{1}{Y^{-1} \exp(E/T) + 1}, \text{ for } T_f < T(t) < T_{ch}. \quad (65)$$

The time dependent generalized fugacity $Y(t)$ controls the occupancy of phase space and is necessary once $T(t) < T_{ch}$ in order to conserve particle number.

For $T(t) < T_f$ there are no longer any significant interactions that couple the particle species of interest and so they begin to free-stream through the Universe, i.e., travel on geodesics without scattering. The Einstein-Vlasov equation can be solved, see [107], to yield the free-streaming momentum distribution

$$f(t, E) = \frac{1}{Y^{-1} e^{\sqrt{p^2/T^2+m^2/T_f^2}} + 1} \quad (66)$$

where the free-streaming effective temperature

$$T(t) = \frac{T_f a(t_k)}{a(t)} \quad (67)$$

is obtained by redshifting the temperature at kinetic freeze-out. The corresponding free-streaming energy density, pressure, and number densities are given by

$$\rho = \frac{d}{2\pi^2} \int_0^\infty \frac{(m^2 + p^2)^{1/2} p^2 dp}{Y^{-1} e^{\sqrt{p^2/T^2+m^2/T_f^2}} + 1}, \quad (68)$$

$$P = \frac{d}{6\pi^2} \int_0^\infty \frac{(m^2 + p^2)^{-1/2} p^4 dp}{Y^{-1} e^{\sqrt{p^2/T^2+m^2/T_f^2}} + 1}, \quad (69)$$

$$n = \frac{d}{2\pi^2} \int_0^\infty \frac{p^2 dp}{Y^{-1} e^{\sqrt{p^2/T^2+m^2/T_f^2}} + 1}, \quad (70)$$

where d is the degeneracy of the particle species. These differ from the corresponding expressions for an equilibrium distribution in Minkowski space by the replacement $m \rightarrow mT(t)/T_f$ only in the exponential.

The separation of the freeze-out process into these three regimes is of course only an approximation. In principle, there is a smooth transition between them. However, it is a very useful approximation in cosmology. See [38,108] for methods capable of resolving these smooth transitions.

To estimate the freeze-out temperature we need to solve the Boltzmann equation with different types of collision terms. In [109] we detail a new method for analytically simplifying the collision integrals and show that the neutrino freeze-out temperature is controlled by standard model (SM) parameters. The freeze-out temperature depends only on the magnitude of the Weinberg angle in the form $\sin^2 \theta_W$, and a dimensionless relative interaction strength parameter η ,

$$\eta \equiv M_p m_e^3 G_F^2, \quad M_p^2 \equiv \frac{1}{8\pi G_N}, \quad (71)$$

a combination of the electron mass m_e , Newton constant G_N (expressed above in terms of Planck mass M_p), and the Fermi constant G_F . The dimensionless interaction strength parameter η in the present-day vacuum has the value

$$\eta_0 \equiv M_p m_e^3 G_F^2 \Big|_0 = 0.04421. \quad (72)$$

The magnitude of $\sin^2 \theta_W$ is not fixed within the SM and could be subject to variation as a function of time or temperature. In Figure 18 we show the dependence of neutrino freeze-out temperatures for ν_e and $\nu_{\mu,\tau}$ on SM model parameters $\sin^2 \theta_W$ and η in detail. The impact of SM parameter values on neutrino freeze-out and the discussion of the implications and connections of this work to other areas of physics, namely Big Bang Nucleosynthesis and dark radiation can be found in detail in [109–112].

After neutrinos freeze-out, the neutrino co-moving entropy is independently conserved. However, the presence of electron-positron rich plasma until $T = 20$ keV provides the reaction $\gamma\gamma \rightarrow e^-e^+ \rightarrow \nu\bar{\nu}$ to occur even after neutrinos decouple from the cosmic plasma. This suggests the small amount of e^\pm entropy can still transfer to neutrinos until temperature $T = 20$ keV and can modify free streaming distribution and the effective number of neutrinos.

We expect that incorporating oscillations into the freeze-out calculation would yield a smaller freeze-out temperature difference between neutrino flavors as oscillation provides a mechanism in which the heavier flavors remain thermally active despite their direct production becoming suppressed. In work by Mangano et al. [38], neutrino freeze-out including flavor oscillations is shown to be a negligible effect.

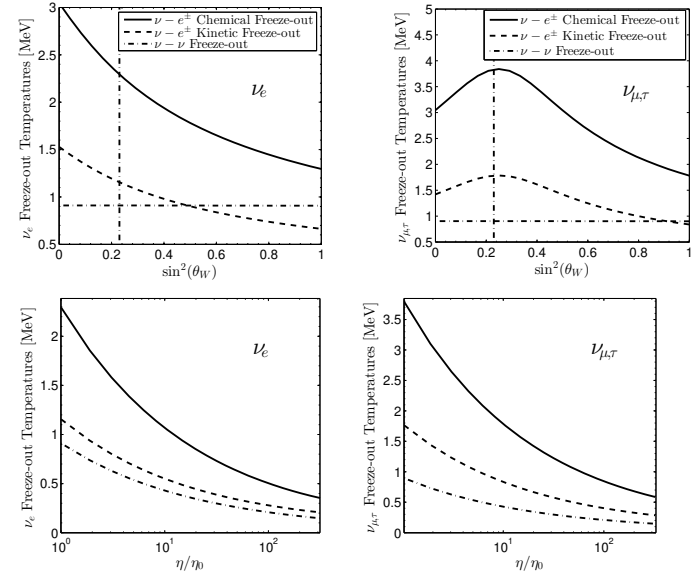


Figure 18. Freeze-out temperatures for electron neutrinos (left) and μ, τ neutrinos (right) for the three types of freeze-out processes adapted from paper [109]. Top panels print temperature curves as a function of $\sin^2 \theta_W$ for $\eta = \eta_0$, the vertical dashed line is $\sin^2 \theta_W = 0.23$; bottom panels are printed as a function of relative change in interaction strength η/η_0 obtained for $\sin^2 \theta_W = 0.23$.

4.5. Effective Number of Neutrinos

The population of each flavor of neutrino is not a fixed quantity throughout the evolution of the Universe. In the earlier hot Universe, the population of neutrinos is controlled thermally and to maximize entropy, each flavor is equally filled. As the expansion factor $a(t)$ is radiation dominated for much of this period (see Figure 2), the CMB is ultimately sensitive to the total energy density within the neutrino sector (which is sometimes referred to as the dark radiation contribution). This is described by the effective number of neutrinos N_ν^{eff} which captures the number of relativistic degrees of freedom for neutrinos as well as any reheating that occurred in the sector after freeze-out. This quantity is related to the total energy density in the neutrino sector as well as the photon background temperature of the Universe via

$$N_\nu^{\text{eff}} \equiv \frac{\rho_\nu^{\text{tot}}}{\frac{7\pi^2}{120} \left(\frac{4}{11}\right)^{4/3} T_\gamma^4}, \quad (73)$$

where ρ_ν^{tot} is the total energy density in neutrinos and T_γ is the photon temperature.

N_ν^{eff} is defined such that three neutrino flavors with zero participation of neutrinos in reheating during e^\pm annihilation results in $N_\nu^{\text{eff}} = 3$. The factor of $(4/11)^{4/3}$ relates the photon temperature to the (effective) temperature of the free-streaming neutrinos after e^\pm annihilation, under the assumption of zero neutrino reheating. Strictly speaking, the number of true degrees of freedom is exactly determined by the number of neutrino families and available quantum numbers, therefore deviations of $N_\nu^{\text{eff}} > 3$ are to be understood as reheating which goes into the neutrino energy density ρ_ν^{tot} .

Experimentally, N_{ν}^{eff} has been determined from CMB data by the Planck collaboration [28] in their 2018 analysis yielding $N_{\nu,\text{exp}}^{\text{eff}} = 2.99 \pm 0.17$ though this value has evolved substantially since their 2013 and 2015 analyses [41,42]. Precise study of neutrino decoupling (as outlined in Section 4.4) and thus freeze-out can improve the predictions for the value of N_{ν}^{eff} . Many studies focus on improving the calculation of decoupling through various means such as

1. Determining the dependence of freeze-out on the natural constants found in the Standard Model of particle physics [26,109].
2. The entropy transfer from electron-positron annihilation and finite temperature correction at neutrino decoupling [39,113,114].
3. Neutrino decoupling with flavor oscillations [38,40]. Nonstandard neutrino interactions have been investigated, including neutrino electromagnetic [101–105,115] and nonstandard neutrino electron coupling [115].

As N_{ν}^{eff} is only a measure of the relativistic energy density leading up to photon decoupling, a natural alternative mechanism for obtaining $N_{\nu}^{\text{eff}} > 3$ is the introduction of additional, presently not discovered, weakly interacting massless particles [80,116–119]. Alternatively, theories outside conventional freeze-out considerations have been proposed to explain the tension in N_{ν}^{eff} including: QGP as the possible source of N_{ν}^{eff} or connection between lepton asymmetry L and N_{ν}^{eff} .

The natural consistency of the reported CMB range of N_{ν}^{eff} with the range of QGP hadronization temperatures, motivates the exploration of a connection between N_{ν}^{eff} and the decoupling of sterile particles at and below the QGP phase transition [120]. This demonstrates that that $N_{\nu}^{\text{eff}} > 3.05$ can be associated with the appearance of several light particles at QGP hadronization in the early Universe that either are weakly interacting in the entire space or is only allowed to interact within the deconfined domain, in which case their coupling would be strong. Such particles could leave a clear dark radiation experimental signature in relativistic heavy-ion experiments that produce the deconfined QGP phase.

In standard Λ CDM, the asymmetry between leptons and antileptons $L \equiv [N_L - N_{\gamma}]/N_{\gamma}$ (normalized with the photon number) is generally assumed to be small (nanoscale) such that the net normalized lepton number equals the net baryon number $L = B$ where $B = [N_B - N_B]/N_{\gamma}$. Barenboim, Kinney, and Park [121,122] note that the lepton asymmetry of the Universe is one of the most weakly constrained parameters in cosmology and they propose that models with leptogenesis are able to accommodate a large lepton number asymmetry surviving up to today.

If lepton number is grossly broken, this could provide a connection between cosmic neutrino properties and the baryon-antibaryon asymmetry present in the Universe today [122]. We quantify in [123] the impact of large lepton asymmetry on Universe expansion and show that there is another ‘natural’ choice $L \simeq 1$, making the net lepton number and net photon number in the Universe similar. Thus because N_{ν}^{eff} can be understood as a characterization of the relativistic dark radiation energy content in the early Universe, independent of its source, there still remains ambiguity in regard to measurements of N_{ν}^{eff} .

5. Electron-Positron Epoch

5.1. The Last Bastion of Antimatter

The electron-positron epoch of the early Universe was home to Big Bang Nucleosynthesis (BBN), the annihilation of most electrons and positrons reheating both the photon and neutrino fields, as well as setting the stage for the eventual recombination period which would generate the cosmic microwave background (CMB). The properties of the electron-positron e^{\pm} plasma in the early Universe has not received appropriate attention in an era of precision BBN studies [124]. The presence of e^{\pm} pairs before and during BBN has been acknowledged by Wang, Bertulani and Balantekin [125,126] over a decade ago. This however was before necessary tools were developed to explore the connection between electron and neutrino plasmas [25,38,109].

During the late stages of the e^{\pm} epoch where BBN occurred, the matter content of the Universe was still mostly dominated by the light charged leptons by many orders of magnitude even though the Hubble parameter was still mostly governed by the radiation behavior of the neutrinos and photons. In Figure 19 we show that the dense e^{\pm} plasma in the early Universe under the hypothesis charge neutrality and entropy conservation as a function of temperature $2 \text{ MeV} > T > 10 \text{ keV}$ [27]. The plasma is electron-positron rich, i.e., $n_{e^{\pm}} \gg n_B$ in the early Universe until leptonic annihilation at $T_{\text{split}} = 20.36 \text{ keV}$. For $T < T_{\text{split}}$ the positron density n_{e^+} quickly vanishes because of annihilation leaving only a residual electron density as required by charge conservation.

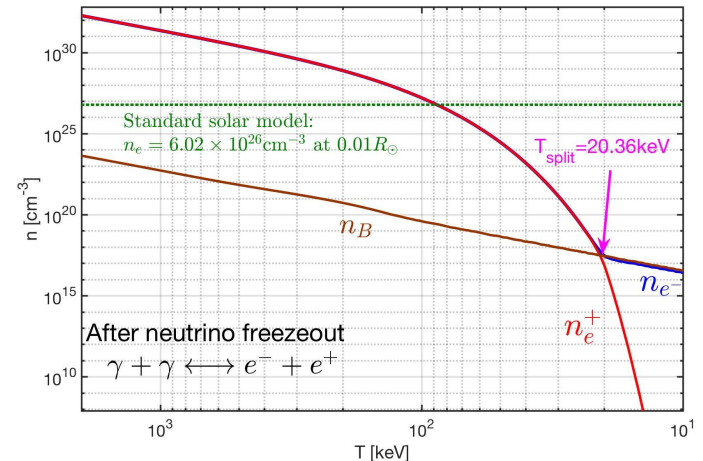


Figure 19. The e^{\pm} number densities as a function of temperature in the range $2 \text{ MeV} > T > 10 \text{ keV}$. The blue solid line is the electron density n_{e^-} , the red solid line is the positron density n_{e^+} , and the brown solid line is the baryon density n_B . For comparison, we also show the green dotted line as the solar electron density within the solar core [127].

The temperatures during this epoch were also cool enough that the electrons and positrons could be described as partially non-relativistic to fairly good approximation while also still being as energy dense as the Solar core making it a relatively unique plasma environment not present elsewhere in cosmology. Considering the energy density between non-relativistic e^{\pm} and baryons, we can write the ratio of energy densities as

$$\chi \equiv \frac{\rho_e + \rho_{e^+}}{\rho_B + \rho_n} = \frac{m_e(n_e + n_{e^+})}{n_B(m_p X_p + m_n X_n)} = \left(\frac{n_e + n_{e^+}}{n_B} \right) \left(\frac{m_e}{m_p X_p + m_n X_n / 2} \right), \quad (74)$$

where we consider all neutrons as bound in 4H_e after BBN. Species ratios $X_p = n_p/n_B$ and $X_n = n_n/n_B$ are given by the PDG [96] as

$$X_p = 0.878, \quad X_n = 0.245, \quad (75)$$

with masses

$$m_e = 0.511 \text{ MeV}, \quad m_p = 938.272 \text{ MeV}, \quad m_n = 939.565 \text{ MeV}. \quad (76)$$

In Figure 20 we plot the energy density ratio Equation (74) as a function of temperature $10\text{ keV} < T < 200\text{ keV}$. This figure shows that the energy density of electron and positron is dominant until $T = 28.2\text{ keV}$, i.e., at higher temperatures we have $\rho_e \gg \rho_B$. Until around $T \approx 85\text{ keV}$, the e^\pm number density remained higher than that of the solar core, though notably at a much higher temperature than the Sun's core of $T_\odot = 1.36\text{ keV}$ [51]. After $T = 28.2\text{ keV}$, where $\rho_e \ll \rho_B$, the ratio becomes constant around $T = 20\text{ keV}$ because of positron annihilation and charge neutrality.

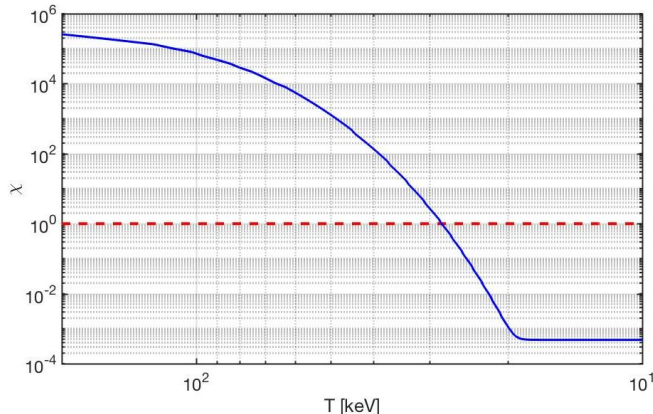


Figure 20. The energy density ratio χ (solid blue line) between e^\pm and baryons as a function of temperature from $10\text{ keV} < T < 200\text{ keV}$. The dashed red line crossing point represents where the baryon density exceeds that of the electron-positron pairs.

5.2. Cosmic Magnetism

The Universe today filled with magnetic fields [128] at various scales and strengths both within galaxies and in deep extra-galactic space far and away from matter sources. Extra-galactic magnetic fields (EGMF) are not well constrained today, but are required by observation to be non-zero [129,130] with a magnitude between $10^{-12}\text{ T} > B_{\text{EGMF}} > 10^{-20}\text{ T}$ over Mpc coherent length scales. The upper bound is constrained from the characteristics of the CMB while the lower bound is constrained by non-observation of ultra-energetic photons from blazars [131]. There are generally considered two possible origins [132,133] for extra-galactic magnetic fields: (a) matter-induced dynamo processes involving Amperian currents and (b) primordial (or relic) seed magnetic fields whose origins may go as far back as the Big Bang itself. It is currently unknown which origin accounts for extra-galactic magnetic fields today or if it some combination of the two models. Even if magnetic fields in the Universe today are primarily driven via amplification through Amperian matter currents, such models could still benefit from the presence of primordial fields to act as catalyst. The purpose of this section is then to consider the magnetization properties of the e^\pm plasma period due to spin which has not yet been considered.

While matter (and thus electrons) are relatively dilute today, the early Universe plasmas contained relatively large quantity of both matter (e^-) and antimatter (e^+). We explore here the spin response of the electron-positron plasma to external and self-magnetization fields thus developing methods for future detailed study.

As magnetic flux is conserved over co-moving surfaces, we see in Figure 21 that the primordial relic field is expected to dilute as $B \propto 1/a(t)^2$. This means the contemporary small bounded values of $5 \times 10^{-12}\text{ T} > B_{\text{relic}} > 10^{-20}\text{ T}$ (coherent over $\mathcal{O}(1\text{ Mpc})$ distances) may have once represented large magnetic fields in the early Universe. Therefore,

correctly describing the dynamics of this e^\pm plasma is of interest when considering modern cosmic mysteries such as the origin of extra-galactic magnetic fields [129,131]. While most approaches tackle magnetized plasmas from the perspective of classical or semi-classical magneto-hydrodynamics (MHD) [134–137], our perspective is to demonstrate that fundamental quantum statistical analysis can lead to further insights on the behavior of magnetized plasmas.

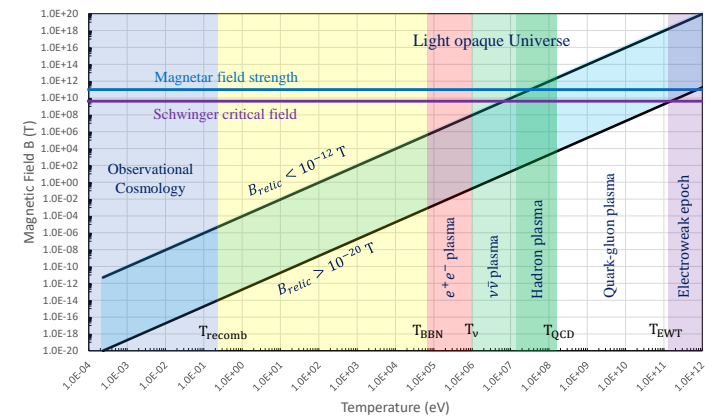


Figure 21. Qualitative value of the primordial magnetic field over the evolutionary lifespan of the Universe. The upper and lower black lines represent extrapolation of the EGMF bounds into the past. The major phases of the Universe are indicated with shaded regions. The values of the Schwarzschild critical field (purple line) and the upper bound of surface magnetar field strength (blue line) are included for scale.

As a starting point, we consider the energy eigenvalues of charged fermions within a homogeneous magnetic field. Here, we have several choices: We could assume the typical Dirac energy eigenvalues with gyro-magnetic g-factor set to $g = 2$. But as electrons, positrons and most plasma species have anomalous magnetic moments (AMM), we require a more complete model. Particle dynamics of classical particles with AMM are explored in [138–141]. Another option would be to modify the Dirac equation with a Pauli term [142], often called the Dirac-Pauli (DP) approach, via

$$\hat{H}_{\text{AMM}} = -a \frac{e}{2m_e} \frac{\sigma_{\mu\nu} F^{\mu\nu}}{2}, \quad (77)$$

where $\sigma_{\mu\nu}$ is the spin tensor proportional to the commutator of the gamma matrices and $F^{\mu\nu}$ is the EM field tensor. For the duration of this section, we will remain in natural units ($\hbar = c = k_B = 1$) unless explicitly stated otherwise. The AMM is defined via g-factor as

$$\frac{g}{2} = 1 + a. \quad (78)$$

This approach, while straightforward, would complicate the energies making analytic understanding and clarity difficult without a clear benefit. Modifying the Dirac equation with Equation (77) yields the following eigen-energies

$$E_n^s|_{DP} = \sqrt{\left(\sqrt{m_e^2 + 2eB\left(n + \frac{1}{2} - s\right)} - \frac{eB}{2m}(g-2)s \right)^2 + p_z^2} \quad (79)$$

This model for the electron-positron plasma of the early Universe has been used in work such as Strickland et al. [143]. Our work in this section is then in part a companion piece which compares and contrasts the DP model of fermions to our preferred model for the AMM via the Klein-Gordon-Pauli (KGP) equation given by

$$\left((i\partial_\mu - eA_\mu)^2 - m_e^2 - e\frac{g}{2}\frac{\sigma_{\mu\nu}F^{\mu\nu}}{2} \right)\Psi = 0. \quad (80)$$

We wish to emphasize, that each of the three above models (Dirac, DP, KGP) are distinct and have differing physical consequences and are not interchangeable which we explored in the context of hydrogen-like atoms in [144]. Recent work done in [145] discuss the benefits of KGP over other approaches for $g \neq 2$ from a quantum field theory perspective. Exploring the statistical behavior of KGP in a cosmological context can lead to new insights in magnetization which may be distinguished from pure $g = 2$ behavior of the Dirac equation or the *ad hoc* modification imposed by the Pauli term in DP. One major improvement of the KGP approach over the more standard DP approach is that the energies take eigenvalues which are mathematically similar to the Dirac energies. Considering the e^\pm plasma in a uniform magnetic field B pointing along the z -axis, the energy of e^\pm fermions can be written as

$$E_n^s = \sqrt{p_z^2 + \tilde{m}^2 + 2eBn}, \quad \tilde{m}^2 = m_e^2 + eB(1 - gs), \quad s = \pm\frac{1}{2}, \quad n = 0, 1, 2, 3, \dots \quad (81)$$

where n is the principle quantum number for the Landau levels and s is the spin quantum number. Here we introduce a notion of effective mass \tilde{m} which inherits the spin-specific part of the energy adding them to the mass. This convention is also generalizable to further non-minimal electromagnetic models with more exotic energy contributions such that we write a general replacement as

$$m_e^2 \rightarrow \tilde{m}^2(B). \quad (82)$$

This definition also pulls out the ground state Landau energy separating it from the remainder of the Landau tower of states. One restriction is that the effective mass must remain positive definite in our analysis thus we require

$$\tilde{m}^2(B) = m_e^2 + eB(1 - gs) > 0. \quad (83)$$

This condition fails under ultra-strong magnetic fields of order

$$B_{\text{crit}} = \frac{m_e^2}{ea} = \frac{B_S}{a} \approx 3.8 \times 10^{12} \text{ T}, \quad (84)$$

where B_S is the Schwinger critical field strength. For electrons, this field strength is well above the window of magnetic field strengths of interest during the late e^\pm epoch.

5.3. Landau Eigen-Energies in Cosmology

There is another natural scale for the magnetic field besides Equation (84) when considering the consequences of FLRW expansion on the e^\pm gas. As the Universe expands, different terms in the energies and thus partition function evolve as a function of the scale

factor $a(t)$ which arises in the FLRW metric. We can consider the expansion to be an adiabatic process which results in a smooth shifting of the relevant dynamical quantities. From the conservation of magnetic flux through a co-moving surface, the magnetic field under expansion starting at some initial time t_0 is given by

$$B(t) = B(t_0) \frac{a(t_0)^2}{a(t)^2}. \quad (85)$$

As the Universe expands, the temperature also cools as the cosmological redshift reduces the momenta of particles in the Universe lowering their contribution to the energy content of the Universe. This cosmological redshift is written as

$$p_i(t) = p_i(t_0) \frac{a(t_0)}{a(t)}, \quad T(t) = T(t_0) \frac{a(t_0)}{a(t)}. \quad (86)$$

The momenta scale with the same factor as temperature as it is the origin of cosmological redshift. The energy of massive free particles in the Universe scales differently based on their momentum (and thus temperature). When hot and relativistic, particle energy scales with inverse scale factors like radiation. However as particles transition to non-relativistic momenta, their energies scale with the inverse square of the scale factor like magnetic flux.

$$E(t) = E(t_0) \frac{a(t_0)}{a(t)} \xrightarrow{\text{NR}} E(t_0) \frac{a(t_0)^2}{a(t)^2}. \quad (87)$$

This occurs because of the functional dependence of energy on momentum in the relativistic versus non-relativistic cases. The argument in the Boltzmann statistical factor is given by

$$X_n^s \equiv \frac{E_n^s}{T}. \quad (88)$$

We can explore this relationship for the magnetized system explicitly by writing out Equation (88) using the KGP eigen-energies as

$$X_n^s = \sqrt{\frac{m_e^2}{T^2} + \frac{p_z^2}{T^2} + \frac{2eB}{T^2} \left(n + \frac{1}{2} - \frac{gs}{2} \right)}, \quad (89)$$

where we now introduce the expansion scale factor via Equations (85) and (86). The Boltzmann factor can then be written as

$$X_n^s[a(t)] = \sqrt{\frac{m_e^2}{T^2(t_0)} \frac{a(t)^2}{a(t_0)^2} + \frac{p_z^2(t_0)}{T^2(t_0)} + \frac{2eB(t_0)}{T^2(t_0)} \left(n + \frac{1}{2} - \frac{gs}{2} \right)}. \quad (90)$$

This reveals that only the mass contribution is dynamic over cosmological time. For any given eigen-state, the mass term increases driving the state into the non-relativistic limit while the momenta and magnetic contributions are frozen by initial conditions.

Following reasoning outlined in [144,145] we will proceed using the KGP eigen-energies. Motivated by Equation (90), we can introduce a dimensionless cosmic magnetic scale which is frozen in the homogeneous case as

$$b_0 \equiv \frac{eB}{T^2} = \frac{eB\hbar c^2}{(k_B T)^2} (\text{S.I.}), \quad (91)$$

where we've included the expression explicitly in full SI units. We can estimate the value of b_0 from the bounds of the extra-galactic magnetic field strength and the temperature of the Universe today. If the origin of deep space extra-galactic magnetic fields are relic fields

from the early Universe, which today are expected to exist between $5 \times 10^{-12} \text{ T} > B_{\text{relic}} > 10^{-20} \text{ T}$, then at temperature $T = 2.7 \text{ K}$, the value of the cosmic magnetic scale is between

$$5.5 \times 10^{-3} > b_0 > 1.1 \times 10^{-11}. \quad (92)$$

This should remain constant in the Universe at-large up to the last epoch the Universe was sufficiently magnetized to disturb this value. As the electron-proton ($e^- p$) plasma which generated the CMB was relatively dilute over its duration, it was unlikely sufficiently magnetized to significantly alter this value over extra-galactic scales. Rather, the first candidate plasma, going backwards in time, to have been sufficiently magnetized and dense to have set the relic field magnetic scale would have been the electron-positron plasma which existed during the duration of Big Bang Nucleosynthesis (BBN) and beforehand.

Higher order non-minimal magnetic contributions which can be introduced via Equation (82) to the eigen-energies like $\approx \mu_B^2 B^2 / T^2$ are even more suppressed over cosmological time which drives the system into minimal electromagnetic coupling with the exception of the anomalous magnetic moment in the KGP eigenenergies. It is interesting to note that cosmological expansion serves to “smooth out” the characteristics of more complex BSM electrodynamics erasing them from a statistical perspective in favor of the minimal or minimal-like dynamics. As b_0 is a constant of expansion, assuming the electron-proton plasma between the CMB and electron-positron annihilation did not greatly disturbed it, we can calculate the remnant values at the temperature $T = 50 \text{ keV}$ (which takes place in the middle of BBN) with the expression

$$B(T) = \frac{b_0}{e} T^2, \quad (93)$$

yielding a range of field strengths

$$2.3 \times 10^5 \text{ T} > B(T = 50 \text{ keV}) > 4.6 \times 10^{-4} \text{ T}, \quad (94)$$

during which the electron-positron plasma in the Universe had a number density comparable to that of the Solar core [127]. We note that while the density of leptons is comparable to that of the solar core during this period, the temperature is not. The e^\pm plasma during BBN was far hotter than the solar core’s comparatively cool temperature of $T_\odot = 1.37 \text{ keV}$ [51].

5.4. Electron-Positron Statistical Physics

We now turn our attention now to the statistical behavior of the e^\pm system. We can utilize the general fermion partition function given by [146]

$$\ln \mathcal{Z} = \sum_{\alpha} \ln \left(1 + e^{-\beta(E-\eta)} \right), \quad (95)$$

where $\beta = 1/T$, α is the set of all quantum numbers in the system, and η is the generalized chemical potential. The magnetized e^\pm system should be considered a system of four quantum species: Particles and antiparticles, and spin aligned and anti-aligned. Taken together we consider a system where all electrons and positrons are spin aligned or anti-aligned with the magnetic field B and the partition function of the system is written as

$$\ln \mathcal{Z}_{\text{tot}} = \frac{2eBV}{(2\pi)^2} \sum_{\sigma}^{\pm 1} \sum_{s}^{\pm 1/2} \sum_{n=0}^{\infty} \int_0^{\infty} dp_z \left[\ln \left(1 + Y_{\sigma}^s(x) e^{-\beta E_n^s} \right) \right], \quad (96)$$

$$Y_{\sigma}^s(x) = \gamma(x) \lambda_{\sigma}^s, \quad \lambda_{\sigma}^s = e^{(\sigma \eta_e + s \eta_s)/T}, \quad (97)$$

where η_e is the electron chemical potential and η_s is the spin chemical potential for the generalized fugacity λ_{σ}^s . The parameter $\gamma(x)$ is a spatial field which controls the distribution inhomogeneity of the Fermi gas. Inhomogeneities can arise from the influence of other forces on the gas such as gravitational forces. Deviations of $\gamma \neq 1$ represent configurations

of reduced entropy (maximum entropy yields the normal Fermi distribution itself with $\gamma = 1$) without pulling the system off a thermal temperature.

This situation is similar to that of the quarks during QGP, but instead the deviation is spatial rather than in time. This is precisely the kind of behavior that may arise in the e^\pm epoch as the dominant photon thermal bath keeps the Fermi gas in thermal equilibrium while spatial inhomogeneity could spontaneously develop. For the remainder of this work, we will retain $\gamma(x) = 1$. The energy E_n^\pm can be written as

$$E_n^\pm = \sqrt{p_z^2 + \tilde{m}_\pm^2 + 2eBn}, \quad \tilde{m}_\pm^2 = m_e^2 + eB \left(1 \mp \frac{g}{2} \right), \quad (98)$$

where the \pm script refers to spin aligned and anti-aligned eigenvalues. As we are interested in the temperature domain $T = 50 \text{ keV}$, we can consider a semi-relativistic approach obtained by the Boltzmann approximation. Taking the limit $m_e/T \ll 1$, we obtain the first order Boltzmann approximation for semi-relativistic electrons and positrons. The Euler-Maclaurin formula is used to replace the sum over Landau levels with an integration which lets us split the partition function into three segments

$$\ln \mathcal{Z}_{\text{tot}} = \ln \mathcal{Z}_{\text{free}} + \ln \mathcal{Z}_B + \ln \mathcal{Z}_R, \quad (99)$$

where we define

$$\ln \mathcal{Z}_{\text{free}} = \frac{T^3 V}{2\pi^2} \sum_{i=\pm} \left[2 \cosh \left(\frac{\eta_e^i}{T} \right) \right] x_i^2 K_2(x_i), \quad x_i = \frac{\tilde{m}_i}{T} \quad (100)$$

$$\ln \mathcal{Z}_B = \frac{eBT V}{2\pi^2} \sum_{i=\pm} \left[2 \cosh \left(\frac{\eta_e^i}{T} \right) \right] \left[\frac{x_i}{2} K_1(x_i) + \frac{b_0}{12} K_0(x_i) \right], \quad (101)$$

$$\ln \mathcal{Z}_R = \frac{eBT V}{\pi^2} \sum_{i=\pm} \left[2 \cosh \left(\frac{\eta_e^i}{T} \right) \right] R. \quad (102)$$

The parameter R is the error remainder which is defined by integrals over Bernoulli polynomials. The parameter η_e^\pm indicates that the chemical potential may be modified by the spin chemical potential and is in general non-zero as defined in Equation (97).

While this would require further derivation to demonstrate explicitly, the benefit of the Euler-Maclaurin approach is if the error contribution remains finite or bound for the magnetized partition function, then a correspondence between the free Fermi partition function (with noticeably modified effective mass \tilde{m}_\pm) and the magnetized Fermi partition function can be established. The mismatch between the summation and integral in the Euler-Maclaurin formula would then encapsulate the immediate magnetic response and deviation from the free particle phase space.

While we label $\ln \mathcal{Z}_{\text{free}}$ in Equation (100) as the “free” partition function, this is not strictly true as this contribution to the overall partition function is a function of the effective mass we defined earlier in Equation (82). When determining the magnetization of the quantum Fermi gas, derivatives of the magnetic field B will not fully vanish on this first term which will result in an intrinsic magnetization which is distinct from the contribution from the ground state and mismatch between the quantized Landau levels and the continuum of the free momentum. Specifically, this free Fermi contribution represents the magnetization that uniquely arises from the spin magnetic energy rather than orbital contributions.

Assuming the error remainder R is small and can be neglected, we can rewrite Equations (100) and (101) obtaining

$$\ln \mathcal{Z}_{\text{tot}} = \frac{T^3 V}{2\pi^2} \sum_{i=\pm} \left[2 \cosh \left(\frac{\eta_e^i}{T} \right) \right] \left\{ x_i^2 K_2(x_i) + \frac{b_0}{2} x_i K_1(x_i) + \frac{b_0^2}{12} K_0(x_i) \right\}. \quad (103)$$

Equation (103) is a surprisingly compact expression containing only tractable functions and will be our working model for the remainder of the work. Note that the above does not take into consideration density inhomogeneities and is restricted to the domain where the plasma is well described as a Maxwell-Boltzmann distribution. With that said, we have not taken the non-relativistic expansion of the eigen-energies.

5.5. Charge Neutrality and Chemical Potential

We explore the chemical potential of dense magnetized electron-positron plasma in the early Universe under the hypothesis of charge neutrality and entropy conservation. To learn about orders of magnitude we set in the following $\eta_e = \eta_e^+ - \eta_e^-$ and focus on the interval in the post-BBN temperature range $50 \text{ keV} > T > 20 \text{ keV}$. We return to the full problem under separate cover. The charge neutrality condition can be written as

$$(n_e - n_\bar{e}) = n_p = \left(\frac{n_p}{n_B} \right) \left(\frac{n_B}{s_{\gamma,\nu,e}} \right) s_{\gamma,\nu,e} = X_p \left(\frac{n_B}{s_{\gamma,\nu}} \right) s_{\gamma,\nu}, \quad X_p \equiv \frac{n_p}{n_B}, \quad (104)$$

where n_p and n_B is the number density of protons and baryons respectively.

The radiation entropy component is given by $s_{\gamma,\nu}$. The entropy density contribution of e^\pm is negligible compared to the photon and neutrino entropy density at post-BBN temperatures $50 \text{ keV} > T > 20 \text{ keV}$ because the low densities of $n_e \ll n_{\gamma,\nu}$ relative to the photon and neutrino gasses. The entropy density can be written as [69]

$$s = \frac{2\pi^2}{45} g_s T_\gamma^3, \quad g_s = \sum_{i=\text{boson}} g_i \left(\frac{T_i}{T_\gamma} \right)^3 + \frac{7}{8} \sum_{i=\text{fermion}} g_i \left(\frac{T_i}{T_\gamma} \right)^3, \quad (105)$$

where g_s is the effective degree of freedom that contribute from boson and fermion species. The parameters X_p and (n_B/s) (see Equation (32)) can be determined by the observation, yielding $X_p = 0.878 \pm 0.015$ [96]. The net number density of electrons can be obtained by using the partition function of electron-positron plasma in the Boltzmann limit Equation (103) (with $g = 2$) as follows:

$$\begin{aligned} (n_e - n_\bar{e}) &= \frac{T}{V} \frac{\partial}{\partial \eta_e} \ln Z_{tot} \\ &= \frac{T^3}{2\pi^2} [2 \sinh(\eta_e/T)] \sum_{i=\pm} \left[x_i^2 K_2(x_i) + \frac{b_0}{2} x_i K_1(x_i) + \frac{b_0^2}{12} K_0(x_i) \right]. \end{aligned} \quad (106)$$

Substituting Equation (106) into the charge neutrality condition Equation (104) we can solve the chemical potential of electron η_e/T yielding

$$\sinh(\eta_e/T) = \frac{2\pi^2}{2T^3} \frac{X_p(n_B/s_{\gamma,\nu}) s_{\gamma,\nu}}{\sum_{i=\pm} \left[x_i^2 K_2(x_i) + \frac{b_0}{2} x_i K_1(x_i) + \frac{b_0^2}{12} K_0(x_i) \right]}, \quad (107)$$

$$\rightarrow \frac{2\pi^2 n_p}{2T^3} \frac{X_p(n_B/s_{\gamma,\nu}) s_{\gamma,\nu}}{2x^2 K_2(x)}, \quad x = m_e/T, \quad \text{for } b_0 = 0. \quad (108)$$

We see in Equation (108) that for the case $b_0 = 0$, the chemical potential agrees with the free particle result in [27].

5.6. Magnetization of the Electron-Positron Plasma

We consider the electron-positron plasma in the mean field approximation where the external field is representative of the “bulk” internal magnetization of the gas. Each particle is therefore responding to the averaged magnetic flux generated by its neighbors as well as any global external field contribution. Considering the magnetized electron-positron

partition function Equation (103) we introduce dimensionless magnetization in S.I units and the critical field as follows

$$\frac{M}{H_c} = \frac{1}{H_c} \frac{k_B T}{V} \frac{\partial \ln Z_{tot}}{\partial B}, \quad H_c = \frac{B_c}{\mu_0}, \quad B_c = \frac{m_e^2 c^4}{e \hbar c^2}. \quad (109)$$

Applying Equation (109) to Equation (103) we arrive at the expression

$$M_\pm = \frac{eT^2}{2\pi^2} \left[2 \cosh\left(\frac{\eta_e}{T}\right) \right] \{c_1(x_\pm) K_1(x_i) + c_0 K_0(x_\pm)\}, \quad (110)$$

$$c_1(x_\pm) = \left[\frac{1}{2} - \left(\frac{1}{2} \pm \frac{g}{4} \right) \left(1 + \frac{b_0^2}{12x_\pm^2} \right) \right] x_\pm, \quad c_0 = \left[\frac{1}{6} - \left(\frac{1}{4} \pm \frac{g}{8} \right) \right] b_0. \quad (111)$$

Substituting the chemical potential Equation (107) into Equation (110) we can solve the magnetization M numerically. Considering the case $g = 2$ the magnetization can be written as the sum of the aligned and anti-aligned polarizations

$$M = M_+ + M_-, \quad (112)$$

where the functions M_\pm are defined as

- A. The aligned polarized gas is described by $\tilde{m}_+ = m_e$ and $x = \tilde{m}_+/T$. The magnetization of this contribution is therefore

$$M_+ = \frac{eT^2}{\pi^2} \sqrt{1 + \sinh^2(\eta_e/T)} \left(\frac{1}{2} x_+ K_1(x_+) + \frac{b_0}{6} K_0(x_+) \right) \quad (113)$$

- B. The spin anti-aligned gas has effective masses $\tilde{m}_- = \sqrt{m_e^2 + 2eB}$, and $x_- = \tilde{m}_-/T$. This yields a magnetization contribution of

$$M_- = -\frac{eT^2}{\pi^2} \sqrt{1 + \sinh^2(\eta_e/T)} \left[\left(\frac{1}{2} + \frac{b_0^2}{12x_-^2} \right) x_- K_1(x_-) + \frac{b_0}{3} K_0(x_-) \right] \quad (114)$$

Using the cosmic magnetic scale parameter b_0 and chemical potential η_e/T we solve the magnetization numerically. In Figure 22, we present the outcome of this estimate. The solid lines (red for the lower bound of b_0 and blue for the higher bound of b_0) showing that the magnetization depends on the magnetic scale b_0 .

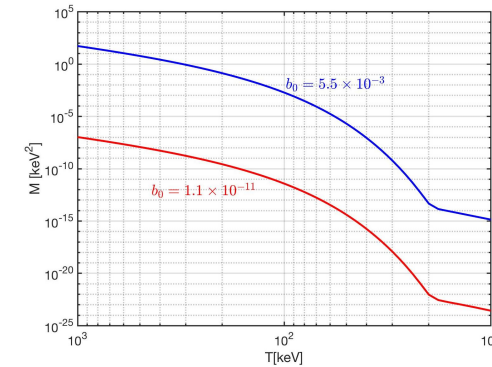


Figure 22. Estimate for the spin magnetization as a function of temperature in the range $10^3 \text{ keV} > T > 10 \text{ keV}$, see text for detail.

6. Looking in the Cosmic Rear-View Mirror

The present day Universe seems devoid of antimatter but the primordial Universe was nearly matter-antimatter symmetric. There was only a fractional nano-scale excess of matter which today makes up the visible matter we see around us. All that remains of the tremendous initial amounts of matter-antimatter from the Big Bang is now seen as background thermal entropy. The origin of this nano-matter excess remains to this day an unresolved puzzle. If matter asymmetry emerged along the path of the Universe's evolution, as most think, the previously discussed Sakharov conditions (see Section 1.2) must be fulfilled.

We explored several major epochs in the Universe evolution where antimatter, in all its diverse forms, played a large role. Emphasis was placed on understanding the thermal and chemical equilibria arising within the context of the Standard Model of particle physics. We highlighted that primordial quark-gluon plasma (QGP, which existed for $\approx 25 \mu\text{s}$) is an important antimatter laboratory with its gargantuan antimatter content. Study of the QGP fireballs created in heavy-ion collisions performed today informs our understanding of the early Universe and vice versa [37,54,147,148], even though the primordial quark-gluon plasma under cosmic expansion explores a location in the phase diagram of QCD inaccessible to relativistic collider experiments considering both net baryon density, see Figure 5, and longevity of the plasma. We described (see Section 2.2) that the QGP epoch near to hadronization condition possessed bottom quarks in a non-equilibrium abundance. This novel QGP-Universe feature may be of interest in consideration of the QGP epoch as possible source for baryon asymmetry [63].

Bottom non-equilibrium is one among a few interesting results presented bridging the temperature gap between QGP hadronization at temperature $T \approx 150 \text{ MeV}$ and neutrino freeze-out. Specifically we shown **perseistence of:**

- Strangeness abundance, present beyond the loss of the antibaryons at $T = 38.2 \text{ MeV}$.
- Pions, which are equilibrated via photon production long after the other hadrons disappear; these lightest hadrons are also dominating the Universe baryon abundance down to $T = 5.6 \text{ MeV}$.
- Muons, disappearing at around $T = 4.2 \text{ MeV}$, the condition when their decay rate outpaces their production rate.

At yet lower temperatures neutrinos make up the largest energy fraction in the Universe driving the radiation dominated cosmic expansion. Partway through this neutrino dominated Universe, in temperature range $T \in 3.5 - 1 \text{ MeV}$ (range spanning differing flavor freeze-out, chemical equilibria, and even variation in standard natural constants; see Figure 18), the neutrinos freeze-out and decouple from the rest of the thermally active matter in the Universe. We consider neutrino decoupling condition as a function of elementary constants: If these constants were not all "constant" or significantly temperature dependent, a noticeable entropy flow of annihilating e^\pm plasma into neutrinos could be present, generating additional so-called neutrino degrees of freedom.

We presented a detailed study of the evolving disappearance of the lightest antimatter, the positrons; we quantify the magnitude of the large positron abundance during and after Big Bang Nucleosynthesis (BBN), see Figure 19. In fact the energy density of electron-positron plasma exceeds greatly that of baryonic matter during and following the BBN period with the last positrons vanishing from the Universe near temperature $T = 20 \text{ keV}$, see Figure 20.

Looking forward, we note that some of the topics we explored deserve a more intense followup work:

- The study of matter baryogenesis in the context of bottom quarks chemical non-equilibrium persistence near to QGP hadronization;
- The impact of relatively dense e^\pm plasma on BBN processes;
- Exploration of spatial inhomogeneities in dense e^\pm plasma and eventual large scale structure formation and related spontaneous self magnetization process.

- Appearance of a significant positron abundance at $T > 25 \text{ keV}$ creates interest in understanding astrophysical object with core temperatures at, and beyond, this super-hot value; the high positron content enables in case of instability a rapid gamma ray formation akin to GRB events.

GRBs are current knowledge frontier: a tremendous amount of matter [6] must be converted into gammas in a short time-span of a few seconds. Ruffini and collaborators [4,7–9,11,149] suggests that strong field production of large amounts of antimatter which can be subsequently annihilated offers the most direct solution. This avoids the problem of excessive photon pressure needing to be balanced in super-hot objects where positron antimatter is already pre-existent. However, GRB events which lack classic after-signature supernova [150,151] could originate from novel super-hot stellar objects with primordial Universe properties which naturally possess, rather than create, larger amounts of positrons capable of rapid catalysis of gamma-rays upon gravitational collapse.

In conclusion: We hope that this work provides to all interested parties a first glimpse at the very interesting epoch of Universe evolution involving in sequence numerous plasma phases made of all particles known today. In this work we provided a background and connection for more specific periods found in the comprehensive literature of observational cosmology [152–156], the recombination period [28,157], BBN [124,158,159], and baryon asymmetry [96,160,161] or the origin of dark matter [30,162,163]. The Universe above temperatures $T > 130 \text{ GeV}$ and the inflation era [164,165] was outside the purview of this work.

Author Contributions: Conceived the article, supervised the development of research results, directed mode of presentation by J.R. equal weight by J.B.; A.S. and C.T.Y. Conceptualization: J.R.; software: J.B., A.S., C.T.Y.; validation: J.R., J.B., A.S., C.T.Y.; formal analysis: J.R., J.B., A.S., C.T.Y.; investigation: J.R., J.B., A.S., C.T.Y.; resources: J.R., J.B., A.S., C.T.Y.; data curation: J.R., J.B., A.S., C.T.Y.; writing—original draft preparation: J.B., A.S., C.T.Y.; writing—review and editing: J.R.; A.S.; visualization: J.R., J.B., A.S., C.T.Y.; supervision: J.R.; project administration: J.R.; All authors have read and agreed to the published version of the manuscript.

Funding: This research received no external funding.

Data Availability Statement: This is a theoretical review, all results were converted into graphic display at creation and were in this format shared with the reader.

Acknowledgments:



Figure 23. ICRANet group at work, Remo Ruffini on right. Photo by Johann Rafelski.



Figure 24. Lizhi Fang (on right), his wife Shuxian Li (center) and Shufang Su (Today: Physics Department Head at the University of Arizona) in April 2004. Photo taken by Johann Rafelski at his home in Tucson.



Figure 25. Remo Ruffini (on left) and Johann Rafelski beneath a sunset in Tucson, AZ on October 7th, 2012. The photo was taken by She Sheng Xue at a celebratory gathering honoring the life of Lizhi Fang.

This work was written in celebration of Professor Remo Ruffini's birthday, his contributions to astrophysics and cosmology and the large number of students and young scientists he mentored (see Figure 23). To close, we also acknowledge our mentor and colleague in the Department of Physics at the University of Arizona, Lizhi Fang [1–3] (see Figure 24) who passed away on April 6, 2012 at his home in Tucson, Arizona. Lizhi introduced Remo Ruffini to us, his career and life is remembered and celebrated (see Figure 25) as we continue to piece together the tapestry of the cosmos.

Conflicts of Interest: The authors declare no conflict of interest.

References

- Fang, L.; Ruffini, R. (Eds.) Cosmology of the Early Universe. In *Advanced Series in Astrophysics and Cosmology*; World Scientific: Singapore, 1984; Volume 1.
- Fang, L.; Ruffini, R. (Eds.) Galaxies, Quasars, and Cosmology. In *Advanced Series in Astrophysics and Cosmology*; World Scientific: Singapore, 1985; Volume 2.
- Fang, L.; Ruffini, R. (Eds.) Quantum cosmology. In *Advanced Series in Astrophysics and Cosmology*; World Scientific: Singapore, 1987; Volume 3.
- Ruffini, R.; Bianco, C.L.; Chardonnet, P.; Fraschetti, F.; Xue, S.S. On the interpretation of the burst structure of grbs. *Astrophys. J. Lett.* **2001**, *555*, L113–L116. [[astro-ph/0106532](#)]. [[CrossRef](#)]
- Aksenov, A.G.; Bianco, C.L.; Ruffini, R.; Vereshchagin, G.V. GRBs and the thermalization process of electron-positron plasmas. *AIP Conf. Proc.* **2008**, *1000*, 309–312. [[arXiv:astro-ph/0804.2807](#)]. [[CrossRef](#)]
- Aksenov, A.G.; Ruffini, R.; Vereshchagin, G.V. Pair plasma relaxation time scales. *Phys. Rev. E* **2010**, *81*, 046401. [[arXiv:astro-ph.HE/1003.5616](#)]. [[CrossRef](#)]
- Ruffini, R.; Vereshchagin, G. Electron-positron plasma in GRBs and in cosmology. *Nuovo Cim. C* **2013**, *036*, 255–266. [[arXiv:astro-ph.CO/1205.3512](#)]. [[CrossRef](#)]
- Ruffini, R.; Vitagliano, L.; Xue, S.S. Electron-positron-photon plasma around a collapsing star. In Proceedings of the 10th Marcel Grossmann Meeting on Recent Developments in Theoretical and Experimental General Relativity, Gravitation and Relativistic Field Theories (MG X MMIII), Rio de Janeiro, Brazil, 20–26 July 2003; pp. 295–302. [[astro-ph/0304306](#)]. [[CrossRef](#)]
- Ruffini, R.; Vereshchagin, G.; Xue, S.S. Electron-positron pairs in physics and astrophysics: From heavy nuclei to black holes. *Phys. Rept.* **2010**, *487*, 1–140. [[arXiv:astro-ph/0910.0974](#)]. [[CrossRef](#)]
- Ruffini, R.; Salmonson, J.D.; Wilson, J.R.; Xue, S.S. On the pair-electromagnetic pulse from an electromagnetic black hole surrounded by a baryonic remnant. *Astron. Astrophys.* **2000**, *359*, 855. [[astro-ph/0004257](#)].
- Han, W.B.; Ruffini, R.; Xue, S.S. Electron and positron pair production of compact stars. *Phys. Rev. D* **2012**, *86*, 84004. [[arXiv:astro-ph.HE/1110.0700](#)]. [[CrossRef](#)]
- Belvedere, R.; Pugliese, D.; Rueda, J.A.; Ruffini, R.; Xue, S.S. Neutron star equilibrium configurations within a fully relativistic theory with strong, weak, electromagnetic, and gravitational interactions. *Nucl. Phys. A* **2012**, *883*, 1–24. [[arXiv:astro-ph.SR/1202.6500](#)]. [[CrossRef](#)]
- Rafelski, J. Melting Hadrons, Boiling Quarks. *Eur. Phys. J. A* **2015**, *51*, 114. [[arXiv:nucl-th/1508.03260](#)]. [[CrossRef](#)]
- Sakharov, A.D. Violation of CP Invariance, C asymmetry, and baryon asymmetry of the universe. *Pisma Zh. Eksp. Teor. Fiz.* **1967**, *5*, 32–35. [[CrossRef](#)]
- Sakharov, A.D. Baryon asymmetry of the universe. *Sov. Phys. Uspekhi* **1991**, *34*, 417–421. [[CrossRef](#)]
- Cohen, A.G.; De Rujula, A.; Glashow, S.L. A Matter-antimatter universe? *Astrophys. J.* **1998**, *495*, 539–549. [[astro-ph/9707087](#)]. [[CrossRef](#)]
- Khlopov, M.Y.; Rubin, S.G.; Sakharov, A.S. Possible origin of antimatter regions in the baryon dominated universe. *Phys. Rev. D* **2000**, *62*, 083505. [[hep-ph/0003285](#)]. [[CrossRef](#)]
- Blinnikov, S.I.; Dolgov, A.D.; Postnov, K.A. Antimatter and antistars in the universe and in the Galaxy. *Phys. Rev. D* **2015**, *92*, 023516. [[arXiv:astro-ph.HE/1409.5736](#)]. [[CrossRef](#)]
- Khlopov, M.Y.; Leclan, O.M. The Formalism of Milky-Way Antimatter-Domains Evolution. *Galaxies* **2023**, *11*, 50. [[CrossRef](#)]
- Affleck, I.; Dine, M. A New Mechanism for Baryogenesis. *Nucl. Phys. B* **1985**, *249*, 361–380. [[CrossRef](#)]
- Rubakov, V.A.; Shaposhnikov, M.E. Electroweak baryon number nonconservation in the early universe and in high-energy collisions. *Usp. Fiz. Nauk* **1996**, *166*, 493–537. [[hep-ph/9603208](#)]. [[CrossRef](#)]
- Letessier, J.; Rafelski, J. Hadron production and phase changes in relativistic heavy ion collisions. *Eur. Phys. J. A* **2008**, *35*, 221–242. [[nucl-th/0504028](#)]. [[CrossRef](#)]
- Fromerth, M.J.; Kuznetsova, I.; Labun, L.; Letessier, J.; Rafelski, J. From Quark-Gluon Universe to Neutrino Decoupling: $200 < T < 2\text{MeV}$. *Acta Phys. Polon. B* **2012**, *43*, 2261–2284. [[arXiv:nucl-th/1211.4297](#)]. [[CrossRef](#)]
- Yang, C.T.; Rafelski, J. Cosmological strangeness abundance. *Phys. Lett. B* **2022**, *827*, 136944. [[arXiv:hep-ph/2108.01752](#)]. [[CrossRef](#)]
- Birrell, J.; Yang, C.T.; Chen, P.; Rafelski, J. Relic neutrinos: Physically consistent treatment of effective number of neutrinos and neutrino mass. *Phys. Rev. D* **2014**, *89*, 23008. [[arXiv:astro-ph.CO/1212.6943](#)]. [[CrossRef](#)]
- Birrell, J. Non-Equilibrium Aspects of Relic Neutrinos: From Freeze-out to the Present Day. Ph.D. Thesis, University of Arizona, Tucson, AZ, USA, 2014. [[arXiv:nucl-th/1409.4500](#)].
- Grayson, C.; Yang, C.T.; Rafelski, J. Electron-Positron Plasma in the BBN epoch. 2023, *in preparation*.
- Aghanim, N.; Akrami, Y.; Ashdown, M.; Aumont, J.; Baccigalupi, C.; Ballardini, M.; Banday, A.J.; Barreiro, R.B.; Bartolo, N.; Basak, S.; et al. Planck 2018 results. VI. Cosmological parameters. *Astron. Astrophys.* **2021**, *641*, A6. [[arXiv:astro-ph.CO/1807.06209](#)]. [[CrossRef](#)]
- Rafelski, J.; Birrell, J. Traveling Through the Universe: Back in Time to the Quark-Gluon Plasma Era. *J. Phys. Conf. Ser.* **2014**, *509*, 012014. [[arXiv:nucl-th/1311.0075](#)]. [[CrossRef](#)]
- Wantz, O.; Shellard, E.P.S. Axion Cosmology Revisited. *Phys. Rev. D* **2010**, *82*, 123508. [[arXiv:astro-ph.CO/0910.1066](#)]. [[CrossRef](#)]
- Kronfeld, A.S. Lattice Gauge Theory and the Origin of Mass. In *100 Years of Subatomic Physics*; World Scientific: Singapore, 2013; pp. 493–518. [[arXiv:physics.hist-ph/1209.3468](#)]. [[CrossRef](#)]
- D'Elia, M.; Mariti, M.; Negro, F. Susceptibility of the QCD vacuum to CP-odd electromagnetic background fields. *Phys. Rev. Lett.* **2013**, *110*, 082002. [[arXiv:hep-lat/1209.0722](#)]. [[CrossRef](#)]
- Bonati, C.; Cossu, G.; D'Elia, M.; Mariti, M.; Negro, F. Effective θ term by CP-odd electromagnetic background fields. *PoS* **2014**, *LATTICE2013*, *360*. [[arXiv:hep-lat/1312.2805](#)]. [[CrossRef](#)]
- Borsanyi, S. Thermodynamics of the QCD transition from lattice. *Nucl. Phys. A* **2013**, *904–905*, 270c–277c. [[arXiv:hep-lat/1210.6901](#)]. [[CrossRef](#)]
- Borsanyi, S.; Fodor, Z.; Hoelbling, C.; Katz, S.D.; Krieg, S.; Szabo, K.K. Full result for the QCD equation of state with 2 + 1 flavors. *Phys. Lett. B* **2014**, *730*, 99–104. [[arXiv:hep-lat/1309.5258](#)]. [[CrossRef](#)]
- Bernstein, J. *Kinetic Theory in the Expanding Universe*; Cambridge Monographs on Mathematical Physics, Cambridge University Press: Cambridge, UK, 1988. [[CrossRef](#)]

37. Philipsen, O. The QCD equation of state from the lattice. *Prog. Part. Nucl. Phys.* **2013**, *70*, 55–107. [[arXiv:hep-lat/1207.5999](#)]. [[CrossRef](#)]
38. Mangano, G.; Miele, G.; Pastor, S.; Pinto, T.; Pisanti, O.; Serpico, P.D. Relic neutrino decoupling including flavor oscillations. *Nucl. Phys. B* **2005**, *729*, 221–234. [[hep-ph/0506164](#)]. [[CrossRef](#)]
39. Fornengo, N.; Kim, C.W.; Song, J. Finite temperature effects on the neutrino decoupling in the early universe. *Phys. Rev. D* **1997**, *56*, 5123–5134. [[hep-ph/9702324](#)]. [[CrossRef](#)]
40. Mangano, G.; Miele, G.; Pastor, S.; Peloso, M. A Precision calculation of the effective number of cosmological neutrinos. *Phys. Lett. B* **2002**, *534*, 8–16. [[astro-ph/0111408](#)]. [[CrossRef](#)]
41. Planck Collaboration. Planck 2013 results. XVI. Cosmological parameters. *Astron. Astrophys.* **2014**, *571*, A16. [[arXiv:astro-ph.CO/1303.5076](#)]. [[CrossRef](#)]
42. Planck Collaboration. Planck 2015 results. XIII. Cosmological parameters. *Astron. Astrophys.* **2016**, *594*, A13. [[arXiv:astro-ph.CO/1502.01589](#)]. [[CrossRef](#)]
43. Caldwell, R.R.; Kamionkowski, M.; Weinberg, N.N. Phantom energy and cosmic doomsday. *Phys. Rev. Lett.* **2003**, *91*, 071301. [[astro-ph/0302506](#)]. [[CrossRef](#)]
44. Bilic, N.; Tupper, G.B.; Viollier, R.D. Unification of dark matter and dark energy: The Inhomogeneous Chaplygin gas. *Phys. Lett. B* **2002**, *535*, 17–21. [[astro-ph/0111325](#)]. [[CrossRef](#)]
45. Benevento, G.; Hu, W.; Raveri, M. Can Late Dark Energy Transitions Raise the Hubble constant? *Phys. Rev. D* **2020**, *101*, 103517. [[arXiv:astro-ph.CO/2002.11707](#)]. [[CrossRef](#)]
46. Perivolaropoulos, L.; Skara, F. Challenges for Λ CDM: An update. *New Astron. Rev.* **2022**, *95*, 101659. [[arXiv:astro-ph.CO/2105.05208](#)]. [[CrossRef](#)]
47. Di Valentino, E.; Mena, O.; Pan, S.; Visinelli, L.; Yang, W.; Melchiorri, A.; Mota, D.F.; Riess, A.G.; Silk, J. In the realm of the Hubble tension—A review of solutions. *Class. Quant. Grav.* **2021**, *38*, 153001. [[arXiv:astro-ph.CO/2103.01183](#)]. [[CrossRef](#)]
48. Aluri, P.K.; Cea, P.; Chingangbam, P.; Chu, M.C.; Clowes, R.G.; Hutsemekers, D.; Kochappan, J.P.; Lopez, A.M.; Liu, L.; et al. Is the observable Universe consistent with the cosmological principle? *Class. Quant. Grav.* **2023**, *40*, 094001. [[arXiv:astro-ph.CO/2207.05765](#)]. [[CrossRef](#)]
49. Yan, H.; Ma, Z.; Ling, C.; Cheng, C.; Huang, J.S. First Batch of $z \approx 11\text{--}20$ Candidate Objects Revealed by the James Webb Space Telescope Early Release Observations on SMACS 0723-73. *Astrophys. J. Lett.* **2023**, *942*, L9. [[arXiv:astro-ph.GA/2207.11558](#)]. [[CrossRef](#)]
50. Weinberg, S. *Gravitation and Cosmology: Principles and Applications of the General Theory of Relativity*; John Wiley and Sons: New York, NY, USA, 1972.
51. Castellani, V.; Degl’Innocenti, S.; Fiorentini, G.; Lissia, M.; Ricci, B. Solar neutrinos: Beyond standard solar models. *Phys. Rept.* **1997**, *281*, 309–398. [[astro-ph/9606180](#)]. [[CrossRef](#)]
52. Rafelski, J.; Letessier, J.; Torrieri, G. Strange hadrons and their resonances: A Diagnostic tool of QGP freezeout dynamics. *Phys. Rev. C* **2002**, *64*, 054907. [[CrossRef](#)]
53. Ollitrault, J.Y. Anisotropy as a signature of transverse collective flow. *Phys. Rev. D* **1992**, *46*, 229–245. [[CrossRef](#)] [[PubMed](#)]
54. Petraki, M.; Letessier, J.; Petráček, V.; Rafelski, J. Hadron production and quark-gluon plasma hadronization in Pb-Pb collisions at $\sqrt{s_{NN}} = 2.76$ TeV. *Phys. Rev. C* **2013**, *88*, 034907. [[arXiv:hep-ph/1303.2098](#)]. [[CrossRef](#)]
55. Ryu, S.; Paquet, J.F.; Shen, C.; Denicol, G.S.; Schenke, B.; Jeon, S.; Gale, C. Importance of the Bulk Viscosity of QCD in Ultrarelatativistic Heavy-Ion Collisions. *Phys. Rev. Lett.* **2015**, *115*, 132301. [[arXiv:nucl-th/1502.01675](#)]. [[CrossRef](#)]
56. Rafelski, J. Formation and Observables of the Quark-Gluon Plasma. *Phys. Rept.* **1982**, *88*, 331.
57. Rafelski, J.; Schnabel, A. Quark-Gluon Plasma in Nuclear Collisions at 200-GeV/A. *Phys. Lett. B* **1988**, *207*, 6–10. [[CrossRef](#)]
58. Letessier, J.; Rafelski, J. *Hadrons and Quark-Gluon Plasma*; Cambridge Monographs on Particle Physics, Nuclear Physics and Cosmology, Cambridge University Press: Cambridge, UK, 2023. [[CrossRef](#)]
59. Bazavov, A.; Bhattacharya, T.; DeTar, C.; Ding, H.-T.; Gottlieb, S.; Gupta, R.; Hegde, P.; Heller, U.; Karsch, F.; Laermann, E.; et al. Equation of state in (2 + 1)-flavor QCD. *Phys. Rev. D* **2014**, *90*, 094503. [[arXiv:hep-lat/1407.6387](#)]. [[CrossRef](#)]
60. Jacak, B.V.; Muller, B. The exploration of hot nuclear matter. *Science* **2012**, *337*, 310–314. [[CrossRef](#)]
61. Fromerth, M.J.; Rafelski, J. *Hadronization of the quark Universe*; University of Arizona: Tucson, AZ, USA, 2005. [[astro-ph/0211346](#)].
62. Rafelski, J. Discovery of Quark-Gluon-Plasma: Strangeness Diaries. *Eur. Phys. J. ST* **2020**, *229*, 1–140. [[arXiv:hep-ph/1911.00831](#)]. [[CrossRef](#)]
63. Yang, C.T.; Rafelski, J. Possibility of bottom-catalyzed matter genesis near to primordial QGP hadronization. *arXiv* **2023**, arXiv:2004.06771. [[arXiv:hep-ph/2004.06771](#)].
64. Roberts, C.D. On Mass and Matter. *AAPPB Bull.* **2021**, *31*, 6. [[arXiv:hep-ph/2101.08340](#)]. [[CrossRef](#)]
65. Roberts, C.D. Origin of the Proton Mass. *EPJ Web Conf.* **2023**, *282*, 01006. [[arXiv:hep-ph/2211.09905](#)]. [[CrossRef](#)]
66. Hagedorn, R. How We Got to QCD Matter from the Hadron Side: 1984. *Lect. Notes Phys.* **1985**, *221*, 53–76. [[CrossRef](#)]
67. Fromerth, M.J.; Rafelski, J. Limit on CPT violating quark anti-quark mass difference from the neutral kaon system. *Acta Phys. Polon. B* **2003**, *34*, 4151–4156. [[hep-ph/0211362](#)].
68. Tanabashi, M. et al. (Particle Data Group). Review of Particle Physics. *Phys. Rev. D* **2018**, *98*, 030001. [[CrossRef](#)]
69. Kolb, E.W.; Turner, M.S. *The Early Universe*; CRC Press: Boca Raton, FL, USA, 1990.

70. Kuznetsova, I.; Habs, D.; Rafelski, J. Pion and muon production in e[−], e⁺, gamma plasma. *Phys. Rev. D* **2008**, *78*, 014027. [[arXiv:hep-ph/0803.1588](#)]. [[CrossRef](#)]
71. Kuznetsova, I.; Rafelski, J. Unstable Hadrons in Hot Hadron Gas in Laboratory and in the Early Universe. *Phys. Rev. C* **2010**, *82*, 035203. [[arXiv:hep-th/1002.0375](#)]. [[CrossRef](#)]
72. Rafelski, J.; Yang, C.T. The muon abundance in the primordial Universe. *Acta Phys. Polon. B* **2021**, *52*, 277. [[arXiv:hep-ph/2103.07812](#)]. [[CrossRef](#)]
73. Kuznetsova, I. Particle Production in Matter at Extreme Conditions. Master’s Thesis, The University of Arizona, Tucson, AZ, USA, 2009. [[arXiv:hep-th/0909.0524](#)].
74. Kopp, J.; Maltoni, M.; Schwetz, T. Are There Sterile Neutrinos at the eV Scale? *Phys. Rev. Lett.* **2011**, *107*, 091801. [[arXiv:hep-ph/1103.4570](#)]. [[CrossRef](#)]
75. Hamann, J.; Hannestad, S.; Raffelt, G.G.; Wong, Y.Y.Y. Sterile neutrinos with eV masses in cosmology: How disfavoured exactly? *J. Cosmol. Astropart. Phys.* **2011**, *9*, 34. [[arXiv:astro-ph.CO/1108.4136](#)]. [[CrossRef](#)]
76. Kopp, J.; Machado, P.A.N.; Maltoni, M.; Schwetz, T. Sterile Neutrino Oscillations: The Global Picture. *J. High Energy Phys.* **2013**, *5*, 50. [[arXiv:hep-ph/1303.3011](#)]. [[CrossRef](#)]
77. Lello, L.; Boyanovsky, D. Cosmological Implications of Light Sterile Neutrinos produced after the QCD Phase Transition. *Phys. Rev. D* **2015**, *91*, 063502. [[arXiv:astro-ph.CO/1411.2690](#)]. [[CrossRef](#)]
78. Birrell, J.; Rafelski, J. Proposal for Resonant Detection of Relic Massive Neutrinos. *Eur. Phys. J. C* **2015**, *75*, 91. [[arXiv:hep-ph/1402.3409](#)]. [[CrossRef](#)]
79. Weinberg, S. Goldstone Bosons as Fractional Cosmic Neutrinos. *Phys. Rev. Lett.* **2013**, *110*, 241301. [[arXiv:astro-ph.CO/1305.1971](#)]. [[CrossRef](#)]
80. Giusarma, E.; Di Valentino, E.; Lattanzi, M.; Melchiorri, A.; Mena, O. Relic Neutrinos, thermal axions and cosmology in early 2014. *Phys. Rev. D* **2014**, *90*, 043507. [[arXiv:astro-ph.CO/1403.4852](#)]. [[CrossRef](#)]
81. Fukuda, Y.; Hayakawa, T.; Ichihara, E.; Inoue, K.; Ishihara, K.; Ishino, H.; Itow, Y.; Kajita, T.; Kameda, J.; Kasuga, S.; et al. Evidence for oscillation of atmospheric neutrinos. *Phys. Rev. Lett.* **1998**, *81*, 1562–1567. [[hep-ex/9807003](#)]. [[CrossRef](#)]
82. Eguchi, K.; Enomoto, S.; Furuno, K.; Goldman, J.; Hanada, H.; Ikeda, H.; Ikeda, K.; Inoue, K.; Ishihara, K.; Itoh, W.; et al. First results from KamLAND: Evidence for reactor antineutrino disappearance. *Phys. Rev. Lett.* **2003**, *90*, 21802. [[hep-ex/0212021](#)]. [[CrossRef](#)] [[PubMed](#)]
83. Fogli, G.L.; Lisi, E.; Marrone, A.; Palazzo, A. Global analysis of three-flavor neutrino masses and mixings. *Prog. Part. Nucl. Phys.* **2006**, *57*, 742–795. [[hep-ph/0506083](#)]. [[CrossRef](#)]
84. Giunti, C.; Studenikin, A. Neutrino electromagnetic interactions: A window to new physics. *Rev. Mod. Phys.* **2015**, *87*, 531. [[arXiv:hep-ph/1403.6344](#)]. [[CrossRef](#)]
85. Fritzsch, H.; Xing, Z.Z. Mass and flavor mixing schemes of quarks and leptons. *Prog. Part. Nucl. Phys.* **2000**, *45*, 1–81. [[hep-ph/9912358](#)]. [[CrossRef](#)]
86. Giunti, C.; Kim, C.W. *Fundamentals of Neutrino Physics and Astrophysics*; Oxford University Press: Oxford, UK, 2007.
87. Fritzsch, H. Neutrino Masses and Flavor Mixing. *Mod. Phys. Lett. A* **2015**, *30*, 1530012. [[arXiv:hep-ph/1503.01857](#)]. [[CrossRef](#)]
88. Dolinski, M.J.; Poon, A.W.P.; Rodejohann, W. Neutrinoless Double-Beta Decay: Status and Prospects. *Ann. Rev. Nucl. Part. Sci.* **2019**, *69*, 219–251. [[arXiv:nucl-ex/1902.04097](#)]. [[CrossRef](#)]
89. Arkani-Hamed, N.; Dimopoulos, S.; Dvali, G.R.; March-Russell, J. Neutrino masses from large extra dimensions. *Phys. Rev. D* **2001**, *65*, 024032. [[hep-ph/9811448](#)]. [[CrossRef](#)]
90. Ellis, J.R.; Lola, S. Can neutrinos be degenerate in mass? *Phys. Lett. B* **1999**, *458*, 310–321. [[hep-ph/9904279](#)]. [[CrossRef](#)]
91. Casas, J.A.; Ibarra, A. Oscillating neutrinos and $\mu \rightarrow e, \gamma$. *Nucl. Phys. B* **2001**, *618*, 171–204. [[hep-ph/0103065](#)]. [[CrossRef](#)]
92. King, S.F.; Luhn, C. Neutrino Mass and Mixing with Discrete Symmetry. *Rept. Prog. Phys.* **2013**, *76*, 56201. [[arXiv:hep-ph/1301.1340](#)]. [[CrossRef](#)]
93. Fernandez-Martinez, E.; Hernandez-Garcia, J.; Lopez-Pavon, J. Global constraints on heavy neutrino mixing. *J. High Energy Phys.* **2016**, *8*, 33. [[arXiv:hep-ph/1605.08774](#)]. [[CrossRef](#)]
94. Pascoli, S.; Petcov, S.T.; Riotto, A. Leptogenesis and Low Energy CP Violation in Neutrino Physics. *Nucl. Phys. B* **2007**, *774*, 1–52. [[hep-ph/0611388](#)]. [[CrossRef](#)]
95. Schwartz, M.D. *Quantum Field Theory and the Standard Model*; Cambridge University Press: Cambridge, UK, 2014.
96. Particle Data Group. Review of Particle Physics. *Prog. Theor. Exp. Phys.* **2022**, *2022*, 083C01. [[CrossRef](#)]
97. Avignone, F.T., III; Elliott, S.R.; Engel, J. Double Beta Decay, Majorana Neutrinos, and Neutrino Mass. *Rev. Mod. Phys.* **2008**, *80*, 481–516. [[arXiv:nucl-ex/0708.1033](#)]. [[CrossRef](#)]
98. Esteban, I.; Gonzalez-Garcia, M.C.; Maltoni, M.; Schwetz, T.; Zhou, A. The fate of hints: Updated global analysis of three-flavor neutrino oscillations. *J. High Energy Phys.* **2020**, *9*, 178. [[arXiv:hep-ph/2007.14792](#)]. [[CrossRef](#)]
99. Alvarez-Ruso, L.; Sajjad Athar, M.; Barbaro, M.B.; Cherdack, D.; Christy, M.E.; Coloma, P.; Donnelly, T.W.; Dytman, S.; de Gouvea, A.; Hill, R.J.; et al. NuSTEC White Paper: Status and challenges of neutrino–nucleus scattering. *Prog. Part. Nucl. Phys.* **2018**, *100*, 1–68. [[arXiv:hep-ph/1706.03621](#)]. [[CrossRef](#)]
100. Abi, B.; Acciarri, R.; Acero, M.A.; Adamov, G.; Adams, D.; Adinolfi, M.; Ahmad, Z.; Ahmed, J.; Alion, T.; Monsalve, S.A.; et al. Deep Underground Neutrino Experiment (DUNE), Far Detector Technical Design Report, Volume II: DUNE Physics. *arXiv* **2002**, arXiv:2002.03005. [[arXiv:hep-ex/2002.03005](#)].

101. Morgan, J.A. Cosmological upper limit to neutrino magnetic moments. *Phys. Lett. B* **1981**, *102*, 247–250. [[CrossRef](#)]
102. Fukugita, M.; Yazaki, S. Reexamination of Astrophysical and Cosmological Constraints on the Magnetic Moment of Neutrinos. *Phys. Rev. D* **1987**, *36*, 3817. [[CrossRef](#)] [[PubMed](#)]
103. Vogel, P.; Engel, J. Neutrino Electromagnetic Form-Factors. *Phys. Rev. D* **1989**, *39*, 3378. [[CrossRef](#)]
104. Elmfors, P.; Enqvist, K.; Raffelt, G.; Sigl, G. Neutrinos with magnetic moment: Depolarization rate in plasma. *Nucl. Phys. B* **1997**, *503*, 3–23. [[hep-ph/9703214](#)]. [[CrossRef](#)]
105. Giunti, C.; Studenikin, A. Neutrino electromagnetic properties. *Phys. Atom. Nucl.* **2009**, *72*, 2089–2125. [[arXiv:hep-ph/0812.3646](#)]. [[CrossRef](#)]
106. Canas, B.C.; Miranda, O.G.; Parada, A.; Tortola, M.; Valle, J.W.F. Updating neutrino magnetic moment constraints. *Phys. Lett. B* **2016**, *753*, 191–198. [[arXiv:hep-ph/1510.01684](#)]. [[CrossRef](#)]
107. Choquet-Bruhat, Y. *General Relativity and the Einstein Equations*; Oxford University Press: Oxford, UK, 2008.
108. Birrell, J.; Wilkening, J.; Rafelski, J. Boltzmann Equation Solver Adapted to Emergent Chemical Non-equilibrium. *J. Comput. Phys.* **2015**, *281*, 896–916. [[arXiv:math.NA/1403.2019](#)]. [[CrossRef](#)]
109. Birrell, J.; Yang, C.T.; Rafelski, J. Relic Neutrino Freeze-out: Dependence on Natural Constants. *Nucl. Phys. B* **2014**, *890*, 481–517. [[arXiv:nucl-th/1406.1759](#)]. [[CrossRef](#)]
110. Dreiner, H.K.; Hanusek, M.; Kim, J.S.; Sarkar, S. Gravitino cosmology with a very light neutralino. *Phys. Rev. D* **2012**, *85*, 65027. [[arXiv:hep-ph/1111.5715](#)]. [[CrossRef](#)]
111. Boehm, C.; Dolan, M.J.; McCabe, C. Increasing Neff with particles in thermal equilibrium with neutrinos. *J. Cosmol. Astropart. Phys.* **2012**, *12*, 27. [[arXiv:astro-ph.CO/1207.0497](#)]. [[CrossRef](#)]
112. Blennow, M.; Fernandez-Martinez, E.; Mena, O.; Redondo, J.; Serra, P. Asymmetric Dark Matter and Dark Radiation. *J. Cosmol. Astropart. Phys.* **2012**, *7*, 22. [[arXiv:hep-ph/1203.5803](#)]. [[CrossRef](#)]
113. Dicus, D.A.; Kolb, E.W.; Gleeson, A.M.; Sudarshan, E.C.G.; Teplitz, V.L.; Turner, M.S. Primordial Nucleosynthesis Including Radiative, Coulomb, and Finite Temperature Corrections to Weak Rates. *Phys. Rev. D* **1982**, *26*, 2694. [[CrossRef](#)]
114. Heckler, A.F. Astrophysical applications of quantum corrections to the equation of state of a plasma. *Phys. Rev. D* **1994**, *49*, 611–617. [[CrossRef](#)]
115. Mangano, G.; Miele, G.; Pastor, S.; Pinto, T.; Pisanti, O.; Serpico, P.D. Effects of non-standard neutrino-electron interactions on relic neutrino decoupling. *Nucl. Phys. B* **2006**, *756*, 100–116. [[hep-ph/0607267](#)]. [[CrossRef](#)]
116. Anchordoqui, L.A.; Goldberg, H. Neutrino cosmology after WMAP 7-Year data and LHC first Z' bounds. *Phys. Rev. Lett.* **2012**, *108*, 81805. [[arXiv:hep-ph/1111.7264](#)]. [[CrossRef](#)]
117. Abazajian, K.N.; Acero, M.A.; Agarwalla, S.K.; Aguilar-Arevalo, A.A.; Albright, C.H.; Antusch, S.; Arguelles, C.A.; Balantekin, A.B.; Barenboim, G.; Barger, V.; et al. Light Sterile Neutrinos: A White Paper. *arXiv* **2012**, arXiv:1204.5379. [[arXiv:hep-ph/1204.5379](#)].
118. Anchordoqui, L.A.; Goldberg, H.; Steigman, G. Right-Handed Neutrinos as the Dark Radiation: Status and Forecasts for the LHC. *Phys. Lett. B* **2013**, *718*, 1162–1165. [[arXiv:hep-ph/1211.0186](#)]. [[CrossRef](#)]
119. Steigman, G. Equivalent Neutrinos, Light WIMPs, and the Chimera of Dark Radiation. *Phys. Rev. D* **2013**, *87*, 103517. [[arXiv:astro-ph.CO/1303.0049](#)]. [[CrossRef](#)]
120. Birrell, J.; Rafelski, J. Quark-gluon plasma as the possible source of cosmological dark radiation. *Phys. Lett. B* **2015**, *741*, 77–81. [[arXiv:nucl-th/1404.6005](#)]. [[CrossRef](#)]
121. Barenboim, G.; Kinney, W.H.; Park, W.I. Resurrection of large lepton number asymmetries from neutrino flavor oscillations. *Phys. Rev. D* **2017**, *95*, 43506. [[arXiv:hep-ph/1609.01584](#)]. [[CrossRef](#)]
122. Barenboim, G.; Park, W.I. A full picture of large lepton number asymmetries of the Universe. *J. Cosmol. Astropart. Phys.* **2017**, *4*, 48. [[arXiv:hep-ph/1703.08258](#)]. [[CrossRef](#)]
123. Yang, C.T.; Birrell, J.; Rafelski, J. Lepton Number and Expansion of the Universe. *arXiv* **2018**, arXiv:1812.05157. [[arXiv:hep-ph/1812.05157](#)]
124. Pitrou, C.; Coc, A.; Uzan, J.P.; Vangioni, E. Precision big bang nucleosynthesis with improved Helium-4 predictions. *Phys. Rept.* **2018**, *754*, 1–66. [[arXiv:astro-ph.CO/1801.08023](#)]. [[CrossRef](#)]
125. Wang, B.; Bertulani, C.A.; Balantekin, A.B. Electron screening and its effects on Big-Bang nucleosynthesis. *Phys. Rev. C* **2011**, *83*, 18801. [[arXiv:astro-ph.CO/1010.1565](#)]. [[CrossRef](#)]
126. Hwang, E.; Jang, D.; Park, K.; Kusakabe, M.; Kajino, T.; Balantekin, A.B.; Maruyama, T.; Ryu, C.M.; Cheoun, M.K. Dynamical screening effects on big bang nucleosynthesis. *J. Cosmol. Astropart. Phys.* **2021**, *11*, 17. [[arXiv:nucl-th/2102.09801](#)]. [[CrossRef](#)]
127. Bahcall, J.N.; Pinsonneault, M.H.; Basu, S. Solar models: Current epoch and time dependences, neutrinos, and helioseismological properties. *Astrophys. J.* **2001**, *555*, 990–1012. [[astro-ph/0010346](#)]. [[CrossRef](#)]
128. Kronberg, P.P. Extragalactic magnetic fields. *Rept. Prog. Phys.* **1994**, *57*, 325–382. [[CrossRef](#)]
129. Anchordoqui, L.A.; Goldberg, H. A Lower bound on the local extragalactic magnetic field. *Phys. Rev. D* **2002**, *65*, 21302. [[hep-ph/0106217](#)]. [[CrossRef](#)]
130. Widrow, L.M. Origin of galactic and extragalactic magnetic fields. *Rev. Mod. Phys.* **2002**, *74*, 775–823. [[astro-ph/0207240](#)]. [[CrossRef](#)]
131. Neronov, A.; Vovk, I. Evidence for strong extragalactic magnetic fields from Fermi observations of TeV blazars. *Science* **2010**, *328*, 73–75. [[arXiv:astro-ph.HE/1006.3504](#)]. [[CrossRef](#)]

132. Widrow, L.M.; Ryu, D.; Schleicher, D.R.G.; Subramanian, K.; Tsagas, C.G.; Treumann, R.A. The First Magnetic Fields. *Space Sci. Rev.* **2012**, *166*, 37–70. [[arXiv:astro-ph.CO/1109.4052](#)]. [[CrossRef](#)]
133. Vazza, F.; Locatelli, N.; Rajpurohit, K.; Banfi, S.; Dominguez-Fernandez, P.; Wittor, D.; Angelinelli, M.; Inchingolo, G.; Brienza, M.; Hackstein, S.; et al. Magnetogenesis and the Cosmic Web: A Joint Challenge for Radio Observations and Numerical Simulations. *Galaxies* **2021**, *9*, 109. [[arXiv:astro-ph.CO/2111.09129](#)]. [[CrossRef](#)]
134. Berezhiani, V.; Tsintsadze, L.; Shukla, P. Influence of electron-positron pairs on the wakefields in plasmas. *Phys. Scr.* **1992**, *46*, 55. [[CrossRef](#)]
135. Berezhiani, V.; Mahajan, S. Large relativistic density pulses in electron-positron-ion plasmas. *Phys. Rev. E* **1995**, *52*, 1968. [[CrossRef](#)]
136. Schlickeiser, R.; Kolberg, U.; Yoon, P.H. Primordial Plasma Fluctuations. I. Magnetization of the Early Universe by Dark Aperiodic Fluctuations in the Past Myon and Prior Electron–Positron Annihilation Epoch. *Astrophys. J.* **2018**, *857*, 29. [[CrossRef](#)]
137. Melrose, D. *Quantum Plasmadynamics: Magnetized Plasmas*; Springer: Berlin/Heidelberg, Germany, 2013. [[CrossRef](#)]
138. Rafelski, J.; Formanek, M.; Steinmetz, A. Relativistic Dynamics of Point Magnetic Moment. *Eur. Phys. J. C* **2018**, *78*, 6. [[arXiv:physics.class-ph/1712.01825](#)]. [[CrossRef](#)]
139. Formanek, M.; Evans, S.; Rafelski, J.; Steinmetz, A.; Yang, C.T. Strong fields and neutral particle magnetic moment dynamics. *Plasma Phys. Control. Fusion* **2018**, *60*, 74006. [[arXiv:hep-ph/1712.07698](#)]. [[CrossRef](#)]
140. Formanek, M.; Steinmetz, A.; Rafelski, J. Radiation reaction friction: Resistive material medium. *Phys. Rev. D* **2020**, *102*, 56015. [[arXiv:hep-ph/2004.09634](#)]. [[CrossRef](#)]
141. Formanek, M.; Steinmetz, A.; Rafelski, J. Motion of classical charged particles with magnetic moment in external plane-wave electromagnetic fields. *Phys. Rev. A* **2021**, *103*, 52218. [[arXiv:physics.class-ph/2103.02594](#)]. [[CrossRef](#)]
142. Thaller, B. *The Dirac Equation*; Springer Science & Business Media: Berlin/Heidelberg, Germany, 2013.
143. Strickland, M.; Dexheimer, V.; Menezes, D.P. Bulk Properties of a Fermi Gas in a Magnetic Field. *Phys. Rev. D* **2012**, *86*, 125032. [[arXiv:nucl-th/1209.3276](#)]. [[CrossRef](#)]
144. Steinmetz, A.; Formanek, M.; Rafelski, J. Magnetic Dipole Moment in Relativistic Quantum Mechanics. *Eur. Phys. J. A* **2019**, *55*, 40. [[arXiv:hep-ph/1811.06233](#)]. [[CrossRef](#)]
145. Rafelski, J.; Evans, S.; Labun, L. Study of QED singular properties for variable gyromagnetic ratio $g \simeq 2$. *Phys. Rev. D* **2023**, *107*, 76002. [[arXiv:hep-th/2212.13165](#)]. [[CrossRef](#)]
146. Elze, H.T.; Greiner, W.; Rafelski, J. The relativistic ideal Fermi gas revisited. *J. Phys. G* **1980**, *6*, L149–L153. [[CrossRef](#)]
147. Borsanyi, S.; Fodor, Z.; Guenther, J.; Kampert, K.-H.; Katz, S.D.; Kawanai, T.; Kovacs, T.G.; Mages, S.W.; Pasztor, A.; Pittler, F.; et al. Calculation of the axion mass based on high-temperature lattice quantum chromodynamics. *Nature* **2016**, *539*, 69–71. [[arXiv:hep-lat/1606.07494](#)]. [[CrossRef](#)]
148. Rafelski, J. Connecting QGP–Heavy Ion Physics to the Early Universe. *Nucl. Phys. B Proc. Suppl.* **2013**, *243–244*, 155–162. [[arXiv:astro-ph.CO/1306.2471](#)]. [[CrossRef](#)]
149. Aksenen, A.G.; Ruffini, R.; Vereshchagin, G.V. Thermalization of electron-positron-photon plasmas with an application to GRB. *AIP Conf. Proc.* **2008**, *966*, 191–196. [[CrossRef](#)]
150. Burns, E.; Svirkin, D.; Fenimore, E.; Kann, D.A.; Fernandez, J.F.A.; Frederiks, D.; Hamburg, R.; Lesage, S.; Temirava, Y.; Tsvetkova, A.; et al. GRB 221009A: The BOAT. *Astrophys. J. Lett.* **2023**, *946*, L31. [[arXiv:astro-ph.HE/2302.14037](#)]. [[CrossRef](#)]
151. Levan, A.J.; Lamb, C.P.; Schneider, B.; Hjorth, J.; Zafar, T.; Postigo, A.D.; Sargent, B.; Mullally, S.E.; Izzo, L.; D’Avanzo, P.; et al. The First JWST Spectrum of a GRB Afterglow: No Bright Supernova in Observations of the Brightest GRB of all Time, GRB 221009A. *Astrophys. J. Lett.* **2023**, *946*, L28. [[arXiv:astro-ph.HE/2302.07761](#)]. [[CrossRef](#)]
152. Davis, M.; Efstathiou, G.; Frenk, C.S.; White, S.D.M. The Evolution of Large Scale Structure in a Universe Dominated by Cold Dark Matter. *Astrophys. J.* **1985**, *292*, 371–394. [[CrossRef](#)]
153. Navarro, J.F.; Frenk, C.S.; White, S.D.M. The Structure of cold dark matter halos. *Astrophys. J.* **1996**, *462*, 563–575. [[astro-ph/9508025](#)]. [[CrossRef](#)]
154. Moore, B.; Ghigna, S.; Governato, F.; Lake, G.; Quinn, T.R.; Stadel, J.; Tozzi, P. Dark matter substructure within galactic halos. *Astrophys. J. Lett.* **1999**, *524*, L19–L22. [[astro-ph/9907411](#)]. [[CrossRef](#)]
155. Springel, V.; White, S.D.M.; Jenkins, A.; Frenk, C.S.; Yoshida, N.; Gao, L.; Navarro, J.; Thacker, R.; Croton, D.; Helly, J.; et al. Simulating the joint evolution of quasars, galaxies and their large-scale distribution. *Nature* **2005**, *435*, 629–636. [[astro-ph/0504097](#)]. [[CrossRef](#)] [[PubMed](#)]
156. Arbey, A.; Mahmoudi, F. Dark matter and the early Universe: A review. *Prog. Part. Nucl. Phys.* **2021**, *119*, 103865. [[arXiv:hep-ph/2104.11488](#)]. [[CrossRef](#)]
157. Planck Collaboration. Planck 2018 results. I. Overview and the cosmological legacy of Planck. *Astron. Astrophys.* **2020**, *641*, A1. [[arXiv:astro-ph.CO/1807.06205](#)]. [[CrossRef](#)]
158. Steigman, G. Primordial Nucleosynthesis in the Precision Cosmology Era. *Ann. Rev. Nucl. Part. Sci.* **2007**, *57*, 463–491. [[arXiv:astro-ph/0712.1100](#)]. [[CrossRef](#)]
159. Cyburt, R.H.; Fields, B.D.; Olive, K.A.; Yeh, T.H. Big Bang Nucleosynthesis: 2015. *Rev. Mod. Phys.* **2016**, *88*, 015004. [[arXiv:astro-ph.CO/1505.01076](#)]. [[CrossRef](#)]
160. Kuzmin, V.A.; Rubakov, V.A.; Shaposhnikov, M.E. On the Anomalous Electroweak Baryon Number Nonconservation in the Early Universe. *Phys. Lett. B* **1985**, *155*, 36. [[CrossRef](#)]

161. Canetti, L.; Drewes, M.; Shaposhnikov, M. Matter and Antimatter in the Universe. *New J. Phys.* **2012**, *14*, 95012. [[arXiv:hep-ph/1204.4186](#)]. [[CrossRef](#)]
162. Bertone, G.; Hooper, D.; Silk, J. Particle dark matter: Evidence, candidates and constraints. *Phys. Rept.* **2005**, *405*, 279–390. [[hep-ph/0404175](#)]. [[CrossRef](#)]
163. Peccei, R.D. The Strong CP problem and axions. *Lect. Notes Phys.* **2008**, *741*, 3–17. [[hep-ph/0607268](#)]. [[CrossRef](#)]
164. Baumann, D. Inflation. In Proceedings of the Theoretical Advanced Study Institute in Elementary Particle Physics: Physics of the Large and the Small, Boulder, CO, USA, 1–26 June 2009; pp. 523–686. [[arXiv:hep-th/0907.5424](#)]. [[CrossRef](#)]
165. Allahverdi, R.; Amin, M.A.; Berlin, A.; Bernal, N.; Byrnes, C.T.; Delos, M.S.; Erickcek, A.L.; Escudero, M.; Figueroa, D.G.; Freese, K.; et al. The First Three Seconds: A Review of Possible Expansion Histories of the Early Universe. *Open J. Astrophys.* **2021**, *4*, 1. [[arXiv:astro-ph.CO/2006.16182](#)]. [[CrossRef](#)]

Disclaimer/Publisher’s Note: The statements, opinions and data contained in all publications are solely those of the individual author(s) and contributor(s) and not of MDPI and/or the editor(s). MDPI and/or the editor(s) disclaim responsibility for any injury to people or property resulting from any ideas, methods, instructions or products referred to in the content.

APPENDIX F

Matter-antimatter origin of cosmic magnetism

Steinmetz, A., Yang, C.T. & Rafelski, J. Matter-antimatter origin of cosmic magnetism. *arXiv preprint*. 2023. [arXiv:2308.14818 \[hep-ph\]](https://arxiv.org/abs/2308.14818)

Copyright (2023) by the authors. Submitted to Physical Review D.

Matter-antimatter origin of cosmic magnetism

Andrew Steinmetz^D, Cheng Tao Yang^D, and Johann Rafelski^D
Department of Physics, The University of Arizona, Tucson, AZ 85721, USA
(Dated: August 22, 2023)

We explore the hypothesis that the abundant presence of relativistic antimatter (positrons) in the primordial universe is the source of the intergalactic magnetic fields we observe in the universe today. We evaluate both Landau diamagnetic and magnetic dipole moment paramagnetic properties of the very dense primordial electron-positron e^+e^- -plasma, and obtain in quantitative terms the relatively small magnitude of the e^+e^- magnetic moment polarization asymmetry required to produce a consistent self-magnetization in the universe.

I. INTRODUCTION

Macroscopic domains of magnetic fields have been found around compact objects (stars, planets, etc.); between stars; within galaxies; between galaxies in clusters; and in deep extra-galactic void spaces. The bounds for intergalactic magnetic fields (IGMF) at a length scale of 1 Mpc are today [1–5]

$$10^{-8} \text{ G} > \mathcal{B}_{\text{IGMF}} > 10^{-16} \text{ G}. \quad (1)$$

Considering the ubiquity of magnetic fields in the universe [6–8], we search for a common cosmic primordial mechanism considering the electron-positron e^+e^- -pair plasma [9, 10]: We investigate the novel hypothesis that the observed IGMF originates in the large scale non-Ampérian (i.e. non-current sourced in the ‘‘Gilbertian’’ sense [11]) primordial magnetic fields (PMF) created in the dense cosmic e^+e^- -pair plasma by magnetic dipole moment paramagnetism competing with Landau’s diamagnetism.

Our study of pre-recombination Gilbertian dipole moment magnetization of the e^+e^- -plasma is also motivated by the difficulty in generating Ampérian PMFs with large coherent length scales implied by the IGMF [12], though currently the length scale for PMFs are not well constrained either [13]. The conventional elaboration of the origins for cosmic PMFs are detailed in [13–15].

Faraday rotation from distant radio active galaxy nuclei (AGN) [16] suggest that neither dynamo nor astrophysical processes would sufficiently account for the presence of magnetic fields in the universe today if the IGMF strength was around the upper bound of $\mathcal{B}_{\text{IGMF}} \simeq 30 - 60 \text{ nG}$ as found in Ref. [5]. The presence of magnetic fields of this magnitude would then require that at least some portion of IGMFs to arise from primordial sources predating the formation of stars. The presence of $\mathcal{B}_{\text{PMF}} \simeq 0.1 \text{ nG}$ according to Ref. [17] could be sufficient to explain the Hubble tension.

In this work our focus is to establish the Gilbertian (non-Ampérian = non-current) magnetic properties of the very dense e^+e^- cosmic matter-antimatter plasma. In this framework, the magnetization of the early universe requires a large density of strong magnetic dipoles. Due to their large magnetic moment ($\propto e/m_e$) electrons and positrons magnetically dominate the universe. The

dense e^+e^- -plasma is characterized in Fig. 1: We show the antimatter (positron) abundance as a ratio to the prevailing baryon density as a function of cosmic photon temperature T . In this work we measure T in units of energy (keV) thus we set the Boltzmann constant to $k_B = 1$. We consider all results in temporal sequence in the expanding universe, thus we begin with high T and early times on the left in Fig. 1 and end at lower T and later times on the right.

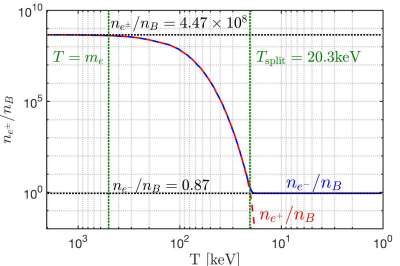


FIG. 1. Number density of electron e^- and positron e^+ to baryon ratio $n_{e\pm}/n_B$ as a function of photon temperature in the universe. See text in Sect. II for further details.

We evaluate the magnetic moment polarization required for PMF magnitude of the spontaneous Gilbertian magnetization. Magnetic flux persistence implies that once the e^+e^- -pair plasma fades out, the ambient large scale Gilbertian magnetic field is maintained by the induced Ampérian (current) sources arising in the residual $e^-p^+e^{++}$ -plasma ultimately leading to the observed large scale structure IGMF.

As we see in Fig. 1 at $T > m_e c^2 = 511 \text{ keV}$ the e^+e^- -pair abundance was nearly 450 million pairs per baryon, dropping to about 100 million pairs per baryon at the pre-BBN temperature of $T = 100 \text{ keV}$. The number of e^+e^- -pairs is large compared to the residual ‘unpaired’ electrons neutralizing the baryon charge locally down to $T_{\text{split}} = 20.3 \text{ keV}$. Since electrons and positrons have opposite magnetic moments, the magnetized dense e^+e^- -plasma entails negligible net local spin density in statisti-

tical average. The residual very small polarization of unpaired electrons complements the magnetic field induced polarization of the proton component.

As shown in Fig. 2 in Ref. [9], following hadronization of the quark-gluon plasma (QGP) and below about $T = 100\,000 \text{ keV}$, in terms of energy density the early universe’s first hour consists of photons, neutrinos and the e^+e^- -pair plasma. Massive dark matter and dark energy are negligible during this era. While we study the magnetic moment polarization of e^+e^- -plasma we do not address here its origin. However, we recall that the pair plasma decouples from the neutrino background near to $T = 2000 \text{ keV}$ [18]. Therefore we consider the magnetic properties of the e^+e^- -pair plasma in the temperature range $2000 \text{ keV} > T > 20 \text{ keV}$ and focus on the range $200 \text{ keV} > T > 20 \text{ keV}$ where the most rapid antimatter abundance changes occurs and where the Boltzmann approximation is valid. This is notably the final epoch where antimatter exists in large quantities in the cosmos [9].

The abundance of antimatter shown in Fig. 1 is obtained and discussed in more detail in Sect. II. Our analysis in Sect. III the four relativistic fermion gases (particle and antiparticle and both polarizations) where the spin and spin-orbit contributions are evaluated in Sect. IIIA. The influence of magnetization on the charge chemical potential is determined in Sect. IIIB. We show in Sect. IV, accounting for the matter-antimatter asymmetry present in the universe, that magnetization is nonzero. Our description of relativistic paramagnetism is covered in Sect. IV A. The balance between paramagnetic and diamagnetic response is evaluated as a function of particle gyromagnetic ratio in Sect. IVB. The per-lepton magnetization is examined in Sect. IVC distinguishing between cosmic and laboratory cases, in the latter case the number of magnetic dipoles is fixed, while in the universe the (comoving) number can vary with T .

Sect. V covers the consequences of forced magnetization via a magnetic moment polarization chemical potential. We find in Sect. VA that magnetization can be spontaneously increased in strength near the IGMF upper limit seen in Eq. (1) given sufficient magnetic moment polarization. A model of self-magnetization is explored in Sect. VB which indicates the need for flux conserving currents at low temperatures. Our findings are summarized in Sect. VI. We also suggest and a wealth of future follow-up projects mostly depending on introduction of transport theory that accounts for spin of particles in presence of a magnetic field.

II. COSMIC ELECTRON-POSITRON PLASMA ABUNDANCE

As the universe cooled below temperature $T = m_e$ (the electron mass), the thermal electron and positron comoving density depleted by over eight orders of magnitude. At $T_{\text{split}} = 20.3 \text{ keV}$, the charged lepton asymmetry (mir-

rored by baryon asymmetry and enforced by charge neutrality) became evident as the surviving excess electrons persisted while positrons vanished entirely from the particle inventory of the universe due to annihilation.

The electron-to-baryon density ratio n_e-/n_B is shown in Fig. 1 as the solid blue line while the positron-to-baryon ratio n_e+/n_B is represented by the dashed red line. These two lines overlap until the temperature drops below $T_{\text{split}} = 20.3 \text{ keV}$ as positrons vanish from the universe marking the end of the e^+e^- -plasma and the dominance of the electron-proton (e^-p)-plasma. The two vertical dashed green lines denote temperatures $T = m_e \simeq 511 \text{ keV}$ and $T_{\text{split}} = 20.3 \text{ keV}$. These results were obtained using charge neutrality and the baryon-to-photon content (entropy) of the universe; see details in [9]. The two horizontal black dashed lines denote the relativistic $T \gg m_e$ abundance of $n_{e\pm}/n_B = 4.47 \times 10^8$ and post-annihilation abundance of $n_e-/n_B = 0.87$. Above temperature $T \simeq 85 \text{ keV}$, the e^+e^- primordial plasma density exceeded that of the Sun’s core density $n_e \simeq 6 \times 10^{26} \text{ cm}^{-3}$ [19].

Conversion of the dense e^+e^- -pair plasma into photons reheated the photon background [18] separating the photon and neutrino temperatures. The e^+e^- annihilation and photon reheating period lasted no longer than an afternoon lunch break. Because of charge neutrality, the post-annihilation comoving ratio $n_e-/n_B = 0.87$ [9] is slightly offset from unity in Fig. 1 by the presence of bound neutrons in α particles and other neutron containing light elements produced during BBN epoch.

To obtain a quantitative description of the above evolution, we study the bulk properties of the relativistic charged/magnetic gasses in a nearly homogeneous and isotropic primordial universe via the thermal Fermi-Dirac or Bose distributions. For matter (e^- ; $\sigma = +1$) and antimatter (e^+ ; $\sigma = -1$) particles, a nonzero relativistic chemical potential $\mu_\sigma = \sigma \mu$ is caused by an imbalance of matter and antimatter. While the primordial electron-positron plasma era was overall charge neutral, there was a small asymmetry in the charged leptons from baryon asymmetry [20, 21] in the universe. Reactions such as $e^+e^- \leftrightarrow \gamma\gamma$ constrains the chemical potential of electrons and positrons [22] as

$$\mu \equiv \mu_{e^-} = -\mu_{e^+}, \quad \lambda \equiv \lambda_{e^-} = \lambda_{e^+}^{-1} = \exp \frac{\mu}{T}, \quad (2)$$

where λ is the fugacity of the system.

During the e^+e^- -plasma epoch, the density changed dramatically over time (see Fig. 1) changing the chemical potential in turn. We can then parameterize the chemical potential of the e^+e^- -plasma as a function of temperature $\mu \rightarrow \mu(T)$ via the charge neutrality of the universe which implies

$$n_p = n_{e^-} - n_{e^+} = \frac{1}{V} \lambda \frac{\partial}{\partial \lambda} \ln Z_{e^+e^-}. \quad (3)$$

In Eq. (3), n_p is the observed total number density of protons in all baryon species. The parameter V relays

the proper volume under consideration and $\ln Z_{e^+e^-}$ is the partition function for the electron-positron gas. The chemical potential defined in Eq. (2) is obtained from the requirement that the positive charge of baryons (protons, α particles, light nuclei produced after BBN) is exactly and locally compensated by a tiny net excess of electrons over positrons.

The abundance of baryons is itself fixed by the known abundance relative to photons [23] and we employed the contemporary recommended value $n_B/n_\gamma = 6.09 \times 10^{-10}$. The resulting chemical potential needs to be evaluated carefully to obtain the behavior near to $T_{\text{split}} = 20.3$ keV where the relatively small value of chemical potential μ rises rapidly so that positrons vanish from the particle inventory of the universe while nearly one electron per baryon remains. The detailed solution of this problem is found in Refs. [9, 20] leading to the results shown in Fig. 1. These results are obtained allowing for Fermi-Dirac and Bose statistics, however it is often numerically sufficient to consider the Boltzmann distribution limit; see Sect. III A.

The partition function of the e^+e^- -plasma can be understood as the sum of four gaseous species

$$\ln Z_{e^+e^-} = \ln Z_{e^+}^\uparrow + \ln Z_{e^+}^\downarrow + \ln Z_{e^-}^\uparrow + \ln Z_{e^-}^\downarrow, \quad (4)$$

of electrons and positrons of both polarizations. In the presence of a magnetic field \mathcal{B} along a primary axis, there is some modification of the usual relativistic fermion partition function which is now given by

$$\ln Z_{e^+e^-} = \frac{e\mathcal{B}V}{(2\pi)^2} \sum_{\sigma}^{\pm 1} \sum_{s}^{\pm 1} \sum_{n=0}^{\infty} \int_{-\infty}^{\infty} dp_z \left[\ln \left(1 + \lambda_{\sigma} \xi_{\sigma,s} \exp \left(-\frac{E}{T} \right) \right) \right], \quad (5)$$

$$\lambda_{\sigma} \xi_{\sigma,s} = \exp \frac{\mu_{\sigma} + \eta_{\sigma,s}}{T}, \quad (6)$$

where p_z is the momentum parallel to the field axis and electric charge is $e \equiv q_{e^+} = -q_{e^-}$. The index σ in Eq. (5) is a sum over electron and positron states while s is a sum over polarizations. The index s refers to the spin along the field axis: parallel (\uparrow ; $s = +1$) or anti-parallel (\downarrow ; $s = -1$) for both particle and antiparticle species.

As the gas is electrically neutral, we will for the time being ignore charge-charge interactions. There is an additional deformation of the distribution from particle creation and destruction correlations; see Ch. 11 of [24] in the context of quark flavors. These will be not included as the considering volume is always large. The quantum numbers of the energy eigenstate E will be elaborated on in Sect. III.

We are explicitly interested in small asymmetries such as baryon excess over antibaryons, or one polarization over another. These are described by Eq. (6) as the following two fugacities:

b. Polarization fugacity $\xi_{\sigma,s}$

The chemical fugacity λ_{σ} (defined in Eq. (2) above) describes deformation of the Fermi-Dirac distribution due to nonzero chemical potential μ . An imbalance in electrons and positrons leads as discussed earlier to a nonzero particle chemical potential $\mu \neq 0$. We then introduce a novel polarization fugacity $\xi_{\sigma,s}$ and polarization potential $\eta_{\sigma,s} = \sigma s \eta$. We propose the polarization potential follows analogous expressions as seen in Eq. (2) obeying

$$\eta \equiv \eta_{+,+} = \eta_{--,--}, \quad \eta = -\eta_{\pm,\mp}, \quad \xi_{\sigma,s} \equiv \exp \frac{\eta_{\sigma,s}}{T}. \quad (7)$$

An imbalance in polarization within a region of volume V results in a nonzero magnetic moment potential $\eta \neq 0$. Conveniently since antiparticles have opposite sign of charge and magnetic moment, the same magnetic moment is associated with opposite spin orientation for particles and antiparticles independent of degree of spin-magnetization. A completely particle-antiparticle symmetric magnetized plasma will have therefore zero total angular momentum. This is of course very different from the situation today of a matter dominated universe.

III. THEORY OF MAGNETIZED MATTER-ANTIMATTER PLASMAS

As the universe undergoes isotropic expansion, the temperature decreases adiabatically [25] and conserves entropy as

$$T(t) = T_0 \frac{a_0}{a(t)} \rightarrow T(z) = T_0(1+z), \quad (8)$$

where $a(t)$ is the scale factor defined by the Friedmann-Lemaître-Robertson-Walker (FLRW) metric [26] and z is the redshift. The comoving temperature T_0 is given by the present day temperature of the CMB, with contemporary scale factor $a_0 = 1$. Within a homogeneous magnetic domain, the magnetic field magnitude varies [15] over cosmic expansion as

$$\mathcal{B}(t) = \mathcal{B}_0 \frac{a_0^2}{a^2(t)} \rightarrow \mathcal{B}(z) = \mathcal{B}_0(1+z)^2, \quad (9)$$

where \mathcal{B}_0 is the comoving value of the magnetic field obtained from the contemporary value today given in Eq. (1). Non-primordial magnetic fields (which are generated through other mechanisms such as dynamo or astrophysical sources) do not follow this scaling [16]. The presence of matter and late universe structure formation also contaminates the primordial field evolution in Eq. (9). It is only in deep intergalactic space where primordial fields remain preserved and comoving over cosmic time.

From Eq. (8) and Eq. (9) emerges a natural ratio of interest here which is conserved over cosmic expansion

$$b \equiv \frac{e\mathcal{B}(t)}{T^2(t)} = \frac{e\mathcal{B}_0}{T_0^2} \equiv b_0 = \text{const.} \quad (10)$$

$$10^{-3} > b_0 > 10^{-11}, \quad (11)$$

given in natural units ($c = \hbar = k_B = 1$). We computed the bounds for this cosmic magnetic scale ratio by using the present day IGMF observations given by Eq. (1) and the present CMB temperature $T_0 = 2.7$ K $\simeq 2.3 \times 10^{-4}$ eV [27].

To evaluate magnetic properties of the thermal e^+e^- -pair plasma we take inspiration from Ch. 9 of Melrose's treatise on magnetized plasmas [28]. We focus on the bulk properties of thermalized plasmas in (near) equilibrium. In considering e^+e^- -pair plasma, we introduce the microscopic energy of the charged relativistic fermion within a homogeneous (z -direction) magnetic field [29]. The energy eigenvalue is given by

$$E_{\sigma,s}^n(p_z, \mathcal{B}) = \sqrt{m_e^2 + p_z^2 + e\mathcal{B} \left(2n + 1 + \frac{g}{2} \sigma s \right)}, \quad (12)$$

where $n = 0, 1, 2, \dots$ is the Landau orbital quantum number. Eq. (12) differentiates between electrons and positrons which is to ensure the correct non-relativistic limit is reached; see Fig. 2. The parameter g is the gyromagnetic (g -factor) of the particle. Following the conventions found in [30], we set $g \equiv g_{e^+} = -g_{e^-} > 0$ such that electrons and positrons have opposite g -factors and opposite magnetic moments which is schematically shown in Fig. 2.

As statistical properties depend on the characteristic Boltzmann factor E/T , another interpretation of Eq. (10) in the context of energy eigenvalues (such as those given in Eq. (12)) is the preservation of magnetic moment energy relative to momentum under adiabatic cosmic expansion.

We rearrange Eq. (12) by pulling the spin dependency and the ground state Landau orbital into the mass writing

$$E_{\sigma,s}^n = \tilde{m}_{\sigma,s} \sqrt{1 + \frac{p_z^2}{\tilde{m}_{\sigma,s}^2} + \frac{2e\mathcal{B}n}{\tilde{m}_{\sigma,s}^2}}, \quad (13)$$

$$\varepsilon_{\sigma,s}^n(p_z, \mathcal{B}) = \frac{E_{\sigma,s}^n}{\tilde{m}_{\sigma,s}}, \quad \tilde{m}_{\sigma,s}^2 = m_e^2 + e\mathcal{B} \left(1 + \frac{g}{2} \sigma s \right), \quad (14)$$

where we introduced the dimensionless energy $\varepsilon_{\sigma,s}^n$ and effective polarized mass $\tilde{m}_{\sigma,s}$ which is distinct for each spin alignment and is a function of magnetic field strength \mathcal{B} . The effective polarized mass $\tilde{m}_{\sigma,s}$ allows us to describe the e^+e^- -plasma with the spin effects almost wholly separated from the Landau characteristics of the gas when considering the plasma's thermodynamic properties.

Since we address the temperature interval $200 \text{ keV} > T > 20 \text{ keV}$ where the effects of quantum Fermi statistics on the e^+e^- -pair plasma are relatively small, but the gas is still considered relativistic, we will employ the Boltzmann approximation to the partition function in Eq. (5). However, we extrapolate our results for presentation completeness up to $T \simeq 4m_e$.

In general, modifications due to quantum statistical phase-space reduction for fermions are expected to suppress results by about 20% in the extrapolated regions.

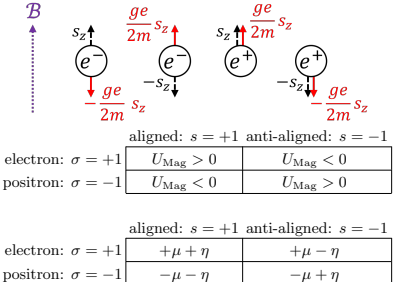


FIG. 2. Organizational schematic of matter-antimatter (σ) and polarization (s) states with respect to the sign of the non-relativistic magnetic dipole energy U_{Mag} (obtainable from Eq. (12)) and the chemical μ and polarization η potentials as seen in Eq. (17).

We will continue to search for semi-analytical solutions for Fermi statistics in relativistic e^+e^- -pair gasses to compliment the Boltzmann solution offered here.

A. Unified treatment of para and diamagnetism

We will proceed in this section with the Boltzmann approximation for the limit where $T \lesssim m_e$. The partition function shown in equation Eq. (5) can be rewritten removing the logarithm as

$$\ln Z_{e^+e^-} = \frac{e\mathcal{B}V}{(2\pi)^2} \sum_{\sigma}^{\pm 1} \sum_{s}^{\pm 1} \sum_{n=0}^{\infty} \int_{-k}^{+\infty} dp_z \left(\frac{(-1)^{k+1}}{k} \exp \left(\frac{k(\sigma\mu + \sigma s\eta - \tilde{m}_{\sigma,s}\varepsilon_{\sigma,s}^n)}{T} \right) \right), \quad (15)$$

$$\sigma\mu + \sigma s\eta - \tilde{m}_{\sigma,s}\varepsilon_{\sigma,s}^n < 0, \quad (16)$$

which is well behaved as long as the factor in Eq. (16) remains negative. We evaluate the sums over σ and s as

$$\begin{aligned} \ln Z_{e^+e^-} = & \frac{e\mathcal{B}V}{(2\pi)^2} \sum_{n=0}^{\infty} \sum_{k=1}^{\infty} \int_{-\infty}^{+\infty} dp_z \frac{(-1)^{k+1}}{k} \\ & \left(\exp \left(k \frac{+\mu + \eta}{T} \right) \exp \left(-k \frac{\tilde{m}_{+,+}\varepsilon_{+,+}^n}{T} \right) \right. \\ & + \exp \left(k \frac{+\mu - \eta}{T} \right) \exp \left(-k \frac{\tilde{m}_{+,-}\varepsilon_{+,-}^n}{T} \right) \\ & + \exp \left(k \frac{-\mu - \eta}{T} \right) \exp \left(-k \frac{\tilde{m}_{-,-}\varepsilon_{-,-}^n}{T} \right) \\ & \left. + \exp \left(k \frac{-\mu + \eta}{T} \right) \exp \left(-k \frac{\tilde{m}_{-,+}\varepsilon_{-,+}^n}{T} \right) \right). \end{aligned} \quad (17)$$

We note from Fig. 2 that the first and forth terms and the second and third terms share the same energies via

$$\varepsilon_{+,+}^n = \varepsilon_{-,-}^n, \quad \varepsilon_{+,-}^n = \varepsilon_{-,+}^n, \quad \varepsilon_{+,-}^n < \varepsilon_{+,+}^n. \quad (18)$$

Eq. (18) allows us to reorganize the partition function with a new magnetization quantum number s' which characterizes paramagnetic flux increasing states ($s' = +1$) and diamagnetic flux decreasing states ($s' = -1$). This recasts Eq. (17) as

$$\ln Z_{e^+e^-} = \frac{eBV}{(2\pi)^2} \sum_{s'}^{\pm 1} \sum_{n=0}^{\infty} \sum_{k=1}^{\infty} \int_{-\infty}^{+\infty} dp_z \frac{(-1)^{k+1}}{k} \left[2\xi_{s'} \cosh \frac{k\mu}{T} \right] \exp \left(-k \frac{\tilde{m}_{s'} \varepsilon_{s'}^n}{T} \right), \quad (19)$$

with dimensionless energy, polarization mass, and polarization redefined in terms of s'

$$\varepsilon_{s'=+1}^n = \varepsilon_{-,-}^n, \quad \varepsilon_{s'=-1}^n = \varepsilon_{+,+}^n, \quad (20)$$

$$\tilde{m}_{s'}^2 = m_e^2 + eB \left(1 - \frac{g}{2} s' \right), \quad (21)$$

$$\eta \equiv \eta_+ = -\eta_- \quad \xi \equiv \xi_+ = \xi_-^{-1}. \quad (22)$$

We introduce the modified Bessel function K_ν (see Ch. 10 of [24]) of the second kind

$$K_\nu \left(\frac{m}{T} \right) = \frac{\sqrt{\pi}}{\Gamma(\nu - 1/2)} \frac{1}{m} \left(\frac{1}{2mT} \right)^{\nu-1} \int_0^\infty dp p^{2\nu-2} \exp \left(-\frac{m\varepsilon}{T} \right), \quad (23)$$

$$\nu > 1/2, \quad \varepsilon = \sqrt{1 + p^2/m^2}, \quad (24)$$

allowing us to rewrite the integral over momentum in Eq. (19) as

$$\frac{1}{T} \int_0^\infty dp_z \exp \left(-\frac{k\tilde{m}_{s'} \varepsilon_{s'}^n}{T} \right) = W_1 \left(\frac{k\tilde{m}_{s'} \varepsilon_{s'}^n (0, \mathcal{B})}{T} \right). \quad (25)$$

The function W_ν serves as an auxiliary function of the form $W_\nu(x) = x K_\nu(x)$. The notation $\varepsilon(0, \mathcal{B})$ in Eq. (25) refers to the definition of dimensionless energy found in Eq. (14) with $p_z = 0$.

The standard Boltzmann distribution is obtained by summing only $k = 1$ and neglecting the higher order terms. The Euler-Maclaurin formula [31] is used to convert the summation over Landau levels into an integration given by

$$\sum_{n=0}^{\infty} W_1(n) = \int_0^\infty dn W_1(n) + \frac{1}{2} [W_1(\infty) + W_1(0)] + \frac{1}{12} \left[\left. \frac{\partial W_1}{\partial n} \right|_\infty - \left. \frac{\partial W_1}{\partial n} \right|_0 \right] + \mathcal{R} \quad (26)$$

where \mathcal{R} is the resulting power series and error remainder of the integration defined in terms of Bernoulli polynomials. Euler-Maclaurin integration is rarely convergent, and in this case serves only as an approximation

within the domain where the error remainder is small and bounded; see Ref. [32] for the non-relativistic case. In this analysis, we keep the zeroth and first order terms in the Euler-Maclaurin formula. We note that regularization of the excess terms in Eq. (26) is done in the context of strong field QED [33] though that is outside our scope.

After truncation of the series and error remainder and combining Eq. (15) through Eq. (26), the partition function can then be written in terms of modified Bessel K_ν functions of the second kind, yielding

$$\begin{aligned} \ln Z_{e^+e^-} &\simeq \frac{T^3 V}{\pi^2} \sum_{s'}^{\pm 1} \left[\xi_{s'} \cosh \frac{\mu}{T} \right. \\ &\quad \left. \left(x_{s'}^2 K_2(x_{s'}) + \frac{b_0}{2} x_{s'} K_1(x_{s'}) + \frac{b_0^2}{12} K_0(x_{s'}) \right) \right], \end{aligned} \quad (27)$$

$$x_{s'} = \frac{\tilde{m}_{s'}}{T} = \sqrt{\frac{m_e^2}{T^2} + b_0 \left(1 - \frac{g}{2} s' \right)}. \quad (28)$$

The latter two terms in Eq. (27) proportional to $b_0 K_1$ and $b_0^2 K_0$ are the uniquely magnetic terms present containing both spin and Landau orbital influences in the partition function. The K_2 term is analogous to the textbook-case of free Fermi gas [32], being modified only by spin effects.

This ‘separation of concerns’ can be rewritten as

$$\ln Z_S = \frac{T^3 V}{\pi^2} \sum_{s'}^{\pm 1} \left[\xi_{s'} \cosh \frac{\mu}{T} \right] (x_{s'}^2 K_2(x_{s'})), \quad (29)$$

$$\begin{aligned} \ln Z_{SO} &= \frac{T^3 V}{\pi^2} \sum_{s'}^{\pm 1} \left[\xi_{s'} \cosh \frac{\mu}{T} \right] \\ &\quad \left(\frac{b_0}{2} x_{s'} K_1(x_{s'}) + \frac{b_0^2}{12} K_0(x_{s'}) \right), \end{aligned} \quad (30)$$

where the spin (S) and spin-orbit (SO) partition functions can be considered independently. When the magnetic scale b_0 is small, the spin-orbit term Eq. (30) becomes negligible leaving only paramagnetic effects in Eq. (29) due to spin. In the non-relativistic limit, Eq. (29) reproduces a quantum gas whose Hamiltonian is defined as the free particle (FP) Hamiltonian plus the magnetic dipole (MD) Hamiltonian which span two independent Hilbert spaces $\mathcal{H}_{FP} \otimes \mathcal{H}_{MD}$.

Writing the partition function as Eq. (27) instead of Eq. (15) has the additional benefit that the partition function remains finite in the free gas ($\mathcal{B} \rightarrow 0$) limit. This is because the free Fermi gas and Eq. (29) are mathematically analogous to one another. As the Bessel K_ν functions are evaluated as functions of x_\pm in Eq. (28), the ‘free’ part of the partition K_2 is still subject to dipole magnetization effects. In the limit where $\mathcal{B} \rightarrow 0$, the free Fermi gas is recovered in both the Boltzmann approximation $k = 1$ and the general case $\sum_{k=1}^{\infty}$.

B. Charge chemical potential response

In presence of a magnetic field in the Boltzmann approximation, the charge neutrality condition Eq. (3) becomes

$$\begin{aligned} \sinh \frac{\mu}{T} &= n_p \frac{\pi^2}{T^3} \\ &\left[\sum_{s'}^{\pm 1} \xi_{s'} \left(x_{s'}^2 K_2(x_{s'}) + \frac{b_0}{2} x_{s'} K_1(x_{s'}) + \frac{b_0^2}{12} K_0(x_{s'}) \right) \right]^{-1}. \end{aligned} \quad (31)$$

Eq. (31) is fully determined by the right-hand-side expression if the magnetic moment fugacity is set to unity $\eta = 0$ implying no external bias to the number of polarizations except as a consequence of the difference in energy eigenvalues. In practice, the latter two terms in Eq. (31) are negligible to chemical potential in the bounds of the primordial e^+e^- -plasma considered and only becomes relevant for extreme (see Fig. 3) magnetic field strengths well outside our scope.

Eq. (31) simplifies if there is no external magnetic field $b_0 = 0$ into

$$\sinh \frac{\mu}{T} = n_p \frac{\pi^2}{T^3} \left[2 \cosh \frac{\eta}{T} \left(\frac{m_e}{T} \right)^2 K_2 \left(\frac{m_e}{T} \right) \right]^{-1}. \quad (32)$$

In Fig. 3 we plot the chemical potential μ/T in Eq. (31) and Eq. (32) which characterizes the importance of the charged lepton asymmetry as a function of temperature. Since the baryon (and thus charged lepton) asymmetry remains fixed, the suppression of μ/T at high temperatures indicates a large pair density which is seen explicitly in Fig. 1. The black line corresponds to the $b_0 = 0$ and $\eta = 0$ case.

The para-diamagnetic contribution from Eq. (30) does not appreciably influence μ/T until the magnetic scales involved become incredibly large well outside the observational bounds defined in Eq. (1) and Eq. (10) as seen by the dotted blue curves of various large values $b_0 = \{25, 50, 100, 300\}$. The chemical potential is also insensitive to forcing by the magnetic moment potential until η reaches a significant fraction of the electron mass m_e in size. The chemical potential for large values of magnetic moment potential $\eta = \{100, 200, 300, 400, 500\}$ keV are also plotted as dashed black lines with $b_0 = 0$.

It is interesting to note that there are crossing points where a given chemical potential can be described as either an imbalance in magnetic moment polarization or presence of external magnetic field. While magnetic moment potential suppresses the chemical potential at low temperatures, external magnetic fields only suppress the chemical potential at high temperatures.

The profound insensitivity of the chemical potential to these parameters justifies the use of the free particle chemical potential (black line) in the ranges of magnetic field strength considered for cosmology. Mathematically this can be understood as ξ and b_0 act as small corrections

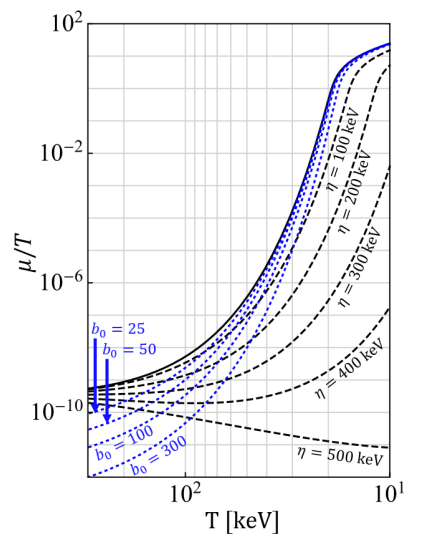


FIG. 3. The chemical potential over temperature μ/T is plotted as a function of temperature with differing values of magnetic moment potential η and magnetic scale b_0 .

in the denominator of Eq. (31) if expanded in powers of these two parameters.

IV. GILBERTIAN MAGNETIZATION OF ELECTRON-POSITRON PLASMA

The total magnetic flux within a region of space can be written as the sum of external fields and the magnetization of the medium via

$$\mathcal{B}_{\text{total}} = \mathcal{B} + \mathcal{M}. \quad (33)$$

For the simplest mediums without ferromagnetic or hysteresis considerations, the relationship can be parameterized by the susceptibility χ of the medium as

$$\mathcal{B}_{\text{total}} = (1 + \chi)\mathcal{B}, \quad \mathcal{M} = \chi\mathcal{B}, \quad (34)$$

with the possibility of both paramagnetic materials ($\chi > 1$) and diamagnetic materials ($\chi < 1$). The e^+e^- -plasma however does not so neatly fit in either category as given by Eq. (29) and Eq. (30). In general, the susceptibility of the gas will itself be a field dependant quantity given by

$$\chi \equiv \frac{\partial \mathcal{M}}{\partial \mathcal{B}}. \quad (35)$$

In our analysis, the external magnetic field always appears within the context of the magnetic scale b_0 , therefore we can introduce the change of variables

$$\frac{\partial b_0}{\partial \mathcal{B}} = \frac{e}{T^2}. \quad (36)$$

The magnetization of the e^+e^- -plasma described by the partition function in Eq. (27) can then be written as

$$\mathcal{M} \equiv \frac{T}{V} \frac{\partial}{\partial \mathcal{B}} \ln Z_{e^+e^-} = \frac{T}{V} \left(\frac{\partial b_0}{\partial \mathcal{B}} \right) \frac{\partial}{\partial b_0} \ln Z_{e^+e^-}, \quad (37)$$

Magnetization arising from other components in the cosmic gas (protons, neutrinos etc.) could in principle also be included. Localized inhomogeneities of matter evolution are often non-trivial and generally be solved numerically using magneto-hydrodynamics (MHD) [28, 34, 35]. In the context of MHD, primordial magnetogenesis from fluid flows in the electron-positron epoch was considered in [36, 37].

We introduce dimensionless units for magnetization \mathfrak{M} by defining the critical field strength

$$\mathcal{B}_C \equiv \frac{m_e^2}{e}, \quad \mathfrak{M} \equiv \frac{\mathcal{M}}{\mathcal{B}_C}. \quad (38)$$

The scale \mathcal{B}_C is where electromagnetism is expected to become subject to non-linear effects, though luckily in our regime of interest, electrodynamics should be linear. We note however that the upper bounds of IGMFs in Eq. (1) (with $b_0 = 10^{-3}$; see Eq. (10)) brings us to within 1% of that limit for the external field strength in the temperature range considered.

The total magnetization \mathfrak{M} can be broken into the sum of magnetic moment parallel \mathfrak{M}_+ and magnetic moment anti-parallel \mathfrak{M}_- contributions

$$\mathfrak{M} = \mathfrak{M}_+ + \mathfrak{M}_-. \quad (39)$$

We note that the expression for the magnetization simplifies significantly for $g = 2$ which is the ‘natural’ gyromagnetic factor [38, 39] for Dirac particles. For illustration, the $g = 2$ magnetization from Eq. (37) is then

$$\mathfrak{M}_+ = \frac{e^2}{\pi^2} \frac{T^2}{m_e^2} \xi \cosh \frac{\mu}{T} \left[\frac{1}{2} x_+ K_1(x_+) + \frac{b_0}{6} K_0(x_+) \right], \quad (40)$$

$$-\mathfrak{M}_- = \frac{e^2}{\pi^2} \frac{T^2}{m_e^2} \xi^{-1} \cosh \frac{\mu}{T} \left[\left(\frac{1}{2} + \frac{b_0}{12x_-^2} \right) x_- K_1(x_-) + \frac{b_0}{3} K_0(x_-) \right], \quad (41)$$

$$x_+ = \frac{m_e}{T}, \quad x_- = \sqrt{\frac{m_e^2}{T^2} + 2b_0}. \quad (42)$$

As the g -factor of the electron is only slightly above two at $g \simeq 2.00232$ [30], the above two expressions for \mathfrak{M}_+ and \mathfrak{M}_- are only modified by a small amount because of anomalous magnetic moment (AMM) and would be otherwise invisible on our figures. We will revisit AMM in Sect. IV B.

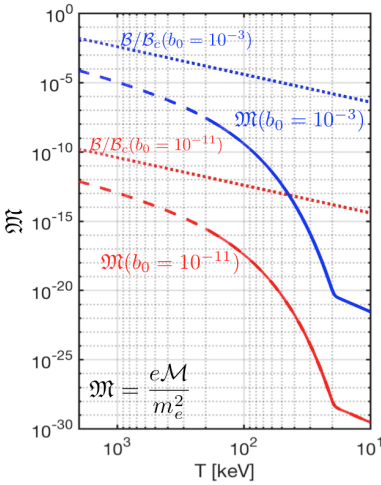


FIG. 4. The magnetization \mathfrak{M} , with $g = 2$, of the primordial e^+e^- -plasma is plotted as a function of temperature.

A. Magnetic response of electron-positron plasma

In Fig. 4, we plot the magnetization as given by Eq. (40) and Eq. (41) with the magnetic moment potential set to unity $\xi = 1$. The lower (solid red) and upper (solid blue) bounds for cosmic magnetic scale b_0 are included. The external magnetic field strength B/B_C is also plotted for lower (dotted red) and upper (dotted blue) bounds. Since the derivative of the partition function governing magnetization may manifest differences between Fermi-Dirac and the here used Boltzmann limit more acutely, out of abundance of caution, we indicate extrapolation outside the domain of validity of the Boltzmann limit with dashes.

We see in Fig. 4 that the e^+e^- -plasma is overall paramagnetic and yields a positive overall magnetization which is contrary to the traditional assumption that matter-antimatter plasma lack significant magnetic responses of their own in the bulk. With that said, the magnetization never exceeds the external field under the parameters considered which shows a lack of ferromagnetic behavior.

The large abundance of pairs causes the smallness of the chemical potential seen in Fig. 3 at high temperatures. As the universe expands and temperature decreases, there is a rapid decrease of the density n_{e^\pm} of e^+e^- -pairs. This is the primary the cause of the rapid paramagnetic decrease seen in Fig. 4 above $T_{\text{split}} = 20.3$ keV. At lower temperatures $T < 20.3$ keV there re-

mains a small electron excess (see Fig. 1) needed to neutralize proton charge. These excess electrons then govern the residual magnetization and dilutes with cosmic expansion.

An interesting feature of Fig. 4 is that the magnetization in the full temperature range increases as a function of temperature. This is contrary to Curie’s law [32] which stipulates that paramagnetic susceptibility of a laboratory material is inversely proportional to temperature. However, Curie’s law applies to systems with fixed number of particles which is not true in our situation; see Sect. IV C.

A further consideration is possible hysteresis as the e^+e^- density drops with temperature. It is not immediately obvious the gas’s magnetization should simply ‘de-gauss’ so rapidly without further consequence. If the very large paramagnetic susceptibility present for $T \simeq m_e$ is the origin of an overall magnetization of the plasma, the conservation of magnetic flux through the comoving surface ensures that the initial residual magnetization is preserved at a lower temperature by Faraday induced kinetic flow processes however our model presented here cannot account for such effects. Some consequences of enforced magnetization are considered in Sect. V.

Early universe conditions may also apply to some extreme stellar objects with rapid change in n_{e^\pm} with temperatures above $T_{\text{split}} = 20.3$ keV. Production and annihilation of e^+e^- -plasmas is also predicted around compact stellar objects [40, 41] potentially as a source of gamma-ray bursts (GRB).

B. g-factor balance between para and diamagnetism

As discussed at the end of Sect. IV, the AMM of e^+e^- is not relevant in the present model. However out of academic interest, it is valuable to consider how magnetization is effected by changing the g -factor significantly.

The influence of AMM would be more relevant for the magnetization of baryon gasses since the g -factor for protons ($g \approx 5.6$) and neutrons ($g \approx 3.8$) are substantially different from $g = 2$. The influence of AMM on the magnetization of thermal systems with large baryon content (neutron stars, magnetars, hypothetical bose stars, etc.) is therefore also of interest [42, 43].

Eq. (40) and Eq. (41) with arbitrary g reintroduced is

$$\mathfrak{M} = \frac{e^2}{\pi^2} \frac{T^2}{m_e^2} \sum_{s'}^{\pm 1} \xi_{s'} \cosh \frac{\mu}{T} \quad (43)$$

$$[C_{s'}^1(x_{s'}) K_1(x_{s'}) + C_{s'}^0 K_0(x_{s'})],$$

$$C_{s'}^1(x_{\pm}) = \left[\frac{1}{2} - \left(\frac{1}{2} - \frac{g}{4s'} \right) \left(1 + \frac{b_0^2}{12x_{s'}^2} \right) \right] x_{s'}, \quad (44)$$

$$C_{s'}^0 = \left[\frac{1}{6} - \left(\frac{1}{4} - \frac{g}{8s'} \right) \right] b_0. \quad (45)$$

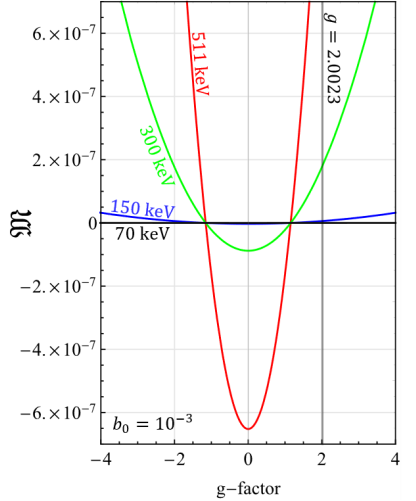


FIG. 5. The magnetization \mathfrak{M} as a function of g -factor plotted for several temperatures with magnetic scale $b_0 = 10^{-3}$ and polarization fugacity $\xi = 1$.

where $x_{s'}$ was previously defined in Eq. (28).

In Fig. 5, we plot the magnetization as a function of g -factor between $4 > g > -4$ for temperatures $T = \{511, 300, 150, 70\}$ keV. We find that the magnetization is sensitive to the value of AMM revealing a transition point between paramagnetic ($\mathfrak{M} > 0$) and diamagnetic gasses ($\mathfrak{M} < 0$).

Curiously, the transition point was numerically determined to be around $g \simeq 1.1547$ in the limit $b_0 \rightarrow 0$. The exact position of this transition point however was found to be both temperature and b_0 sensitive, though it moved little in the ranges considered.

It is not surprising for there to be a transition between diamagnetism and paramagnetism given that the partition function (see Eq. (29) and Eq. (30)) contained elements of both. With that said, the transition point presented at $g \approx 1.15$ should not be taken as exact because of the approximations used to obtain the above results.

It is likely that the exact transition point has been altered by our taking of the Boltzmann approximation and Euler-Maclaurin integration steps. It is known that the Klein-Gordon-Pauli solutions to the Landau problem in Eq. (12) have periodic behavior [29, 38, 39] for $|g| = k/2$ (where $k \in 1, 2, 3, \dots$).

These integer and half-integer points represent when the two Landau towers of orbital levels match up exactly. Therefore, we propose a more natural transition between

the spinless diamagnetic gas of $g = 0$ and a paramagnetic gas is $g = 1$. A more careful analysis is required to confirm this, but that our numerical value is close to unity is suggestive.

C. Laboratory versus the relativistic electron-positron-universe

Despite the relatively large magnetization seen in Fig. 4, the average contribution per lepton is only a small fraction of its overall magnetic moment indicating the magnetization is only loosely organized. Specifically, the magnetization regime we are in is described by

$$\mathcal{M} \ll \mu_B \frac{N_{e^+} + N_{e^-}}{V}, \quad \mu_B \equiv \frac{e}{2m_e}, \quad (46)$$

where μ_B is the Bohr magneton and $N = nV$ is the total particle number in the proper volume V . To better demonstrate that the plasma is only weakly magnetized, we define the average magnetic moment per lepton given by along the field (z -direction) axis as

$$|\vec{m}|_z \equiv \frac{\mathcal{M}}{n_{e^-} + n_{e^+}}, \quad |\vec{m}|_x = |\vec{m}|_y = 0. \quad (47)$$

Statistically, we expect the transverse expectation values to be zero. We emphasize here that despite $|\vec{m}|_z$ being nonzero, this doesn't indicate a nonzero spin angular momentum as our plasma is nearly matter-antimatter symmetric. The quantity defined in Eq. (47) gives us an insight into the microscopic response of the plasma.

The average magnetic moment $|\vec{m}|_z$ defined in Eq. (47) is plotted in Fig. 6 which displays how essential the external field is on the 'per lepton' magnetization. Both the $b_0 = 10^{-11}$ (lower plot, red curve) and $b_0 = 10^{-3}$ (upper plot, blue curve) cosmic magnetic scale bounds are plotted in the Boltzmann approximation. The dashed lines indicate where this approximation is only qualitatively correct. For illustration, a constant magnetic field case (solid green line) with a comoving reference value chosen at temperature $T_0 = 10$ keV is also plotted.

If the field strength is held constant, then the average magnetic moment per lepton is suppressed at higher temperatures as expected for magnetization satisfying Curie's law. The difference in Fig. 6 between the non-constant (red and blue solid curves) case and the constant field (solid green curve) case demonstrates the importance of the conservation of primordial magnetic flux in the plasma, required by Eq. (9).

While not shown, if Fig. 6 was extended to lower temperatures, the magnetization per lepton of the constant field case would be greater than the non-constant case which agrees with our intuition that magnetization is easier to achieve at lower temperatures. This feature again highlights the importance of flux conservation in the system and the uniqueness of the primordial cosmic environment.

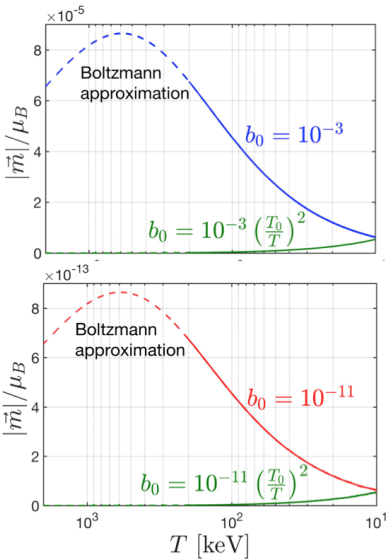


FIG. 6. The magnetic moment per lepton $|\vec{m}|_z$ along the field axis as a function of temperature.

V. MAGNETIC MOMENT POLARIZATION AND FERROMAGNETISM

A. Magnetic moment chemical potential

Up to this point, we have neglected the impact that a nonzero magnetic moment potential $\eta \neq 0$ (and thus $\xi \neq 1$) would have on the primordial e^+e^- -plasma magnetization. In the limit that $(m_e/T)^2 \gg b_0$ the magnetization given in Eq. (43) and Eq. (44) is entirely controlled by the magnetic moment fugacity ξ asymmetry generated by the magnetic moment potential η yielding up to first order $\mathcal{O}(b_0)$ in magnetic scale

$$\begin{aligned} \lim_{m_e^2/T^2 \gg b_0} \mathfrak{M} &= \frac{g e^2}{2 \pi^2 m_e^2} \sinh \frac{\eta}{T} \cosh \frac{\mu}{T} \left[\frac{m_e}{T} K_1 \left(\frac{m_e}{T} \right) \right] \\ &+ b_0 \left(g^2 - \frac{4}{3} \right) \frac{e^2}{8 \pi^2 m_e^2} \cosh \frac{\eta}{T} \cosh \frac{\mu}{T} K_0 \left(\frac{m_e}{T} \right) + \mathcal{O}(b_0^2) \end{aligned} \quad (48)$$

Given Eq. (48), we can understand the magnetic moment potential as a kind of 'ferromagnetic' influence on the primordial gas which allows for magnetization even in the absence of external magnetic fields. This interpretation is reinforced by the fact the leading coefficient is

$g/2$.

We suggest that a variety of physics could produce a small nonzero η within a domain of the gas. Such asymmetries could also originate statistically as while the expectation value of free gas polarization is zero, the variance is likely not.

As $\sinh \eta/T$ is an odd function, the sign of η also controls the alignment of the magnetization. In the high temperature limit Eq. (48) with strictly $b_0 = 0$ assumes a form of to lowest order for brevity

$$\lim_{m_e/T \rightarrow 0} \mathfrak{M}|_{b_0=0} = \frac{g e^2}{2 \pi^2 m_e^2} \frac{T^2}{T} \eta, \quad (49)$$

While the limit in Eq. (49) was calculated in only the Boltzmann limit, it is noteworthy that the high temperature (and $m \rightarrow 0$) limit of Fermi-Dirac distributions only differs from the Boltzmann result by a proportionality factor.

The natural scale of the e^+e^- magnetization with only a small magnetic moment fugacity ($\eta < 1$ eV) fits easily within the bounds of the predicted magnetization during this era if the IGMF measured today was of primordial origin. The reason for this is that the magnetization seen in Eq. (40), Eq. (41) and Eq. (48) are scaled by $\alpha \mathcal{B}_C$ where α is the fine structure constant.

B. Self-magnetization

One exploratory model we propose is to fix the magnetic moment polarization asymmetry, described in Eq. (7), to generate a homogeneous magnetic field which dissipates as the universe cools down. In this model, there is no pre-existing external primordial magnetic field generated by some unrelated physics, but rather the e^+e^- -plasma itself is responsible for the creation of ($\mathcal{B}_{\text{PMF}} \neq 0$) field by virtue of magnetic moment polarization.

This would obey the following assumption of

$$\mathfrak{M}(b_0) = \frac{\mathcal{M}(b_0)}{\mathcal{B}_C} \longleftrightarrow \frac{\mathcal{B}}{\mathcal{B}_C} = b_0 \frac{T^2}{m_e^2}, \quad (50)$$

which sets the total magnetization as a function of itself. The magnetic moment polarization described by $\eta \rightarrow \eta(b_0, T)$ then becomes a fixed function of the temperature and magnetic scale. The underlying assumption would be the preservation of the homogeneous field would be maintained by scattering within the gas (as it is still in thermal equilibrium) modulating the polarization to conserve total magnetic flux.

The result of the self-magnetization assumption in Eq. (50) for the potentials is plotted in Fig. 7. The solid lines indicate the curves for η/T for differing values of $b_0 = \{10^{-11}, 10^{-7}, 10^{-5}, 10^{-3}\}$ which become dashed above $T = 300$ keV to indicate that the Boltzmann approximation is no longer appropriate though the general trend should remain unchanged.

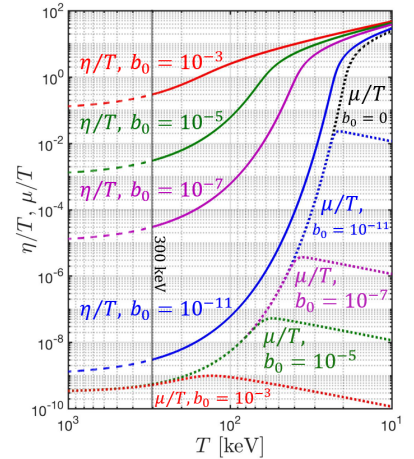


FIG. 7. The magnetic moment potential η and chemical potential μ are plotted under the assumption of self-magnetization through a nonzero magnetic moment polarization in bulk of the plasma.

The dotted lines are the curves for the chemical potential μ/T . At high temperatures we see that a relatively small η/T is needed to produce magnetization owing to the large densities present. Fig. 7 also shows that the chemical potential does not deviate from the free particle case until the magnetic moment polarization becomes sufficiently high which indicates that this form of self-magnetization would require the annihilation of positrons to be incomplete even at lower temperatures.

This is seen explicitly in Fig. 8 where we plot the numerical density of particles as a function of temperature for spin aligned ($+\eta$) and spin anti-aligned ($-\eta$) species for both positrons ($-\mu$) and electrons ($+\mu$). Various self-magnetization strengths are also plotted to match those seen in Fig. 7. The nature of T_{split} changes under this model since antimatter and polarization states can be extinguished separately. Positrons persist where there is insufficient electron density to maintain the magnetic flux. Polarization asymmetry therefore appears physical only in the domain where there is a large number of matter-antimatter pairs.

The low T -behavior of Fig. 8 will need further corroboration after Ampérian currents as a source of magnetic field are incorporated: The Gilbertian sources, here magnetic dipole moment paramagnetism and Landau diamagnetism, may not be dominant magnetic sources when e^+e^- -pairs are of comparable number to the residual electron and proton abundance.

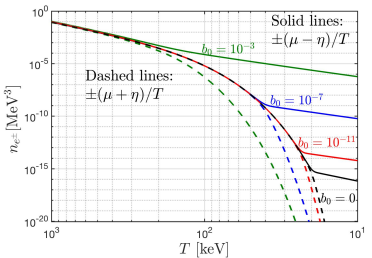


FIG. 8. The number density $n_{e\pm}$ of polarized electrons and positrons under the self-magnetization model for differing values of b_0 .

VI. SUMMARY AND DISCUSSION

This work is an effort to interpret the intergalactic magnetic fields of today as originating in primordial fields generated in the first hour of the universe's existence. In Sect. II have demonstrated that the e^+e^- -pair plasma is an appropriate non-electrical current candidate source for the primordial field: It is (a) very dense, (b) made of particles with highest magnetic moment in nature, (c) and displays a strong paramagnetic response. Therefore expanding on our work in [9], we explored its paramagnetic magnetization in the early universe temperature range between 2000 keV $> T >$ 20 keV.

In Sect. III we define the comoving scale, b_0 , of the magnetic field expressed in dimensionless units estimated between $10^{-3} > b_0 > 10^{-11}$. We believe considering conservation of magnetic flux that b_0 once created is most likely a conserved property of the expanding universe. Antiparticles (e^+) have the opposite sign of charge, and thus magnetic moment, compared to particles (e^-). Therefore in an e^+e^- -pair plasma, net magnetization can be associated with opposite spin orientations for particles and antiparticles without the accompaniment of a net angular momentum in the volume considered. This is of course very different from the matter dominated universe arising below $T \simeq 20$ keV which includes the current epoch.

The e^+e^- -pair plasma environment is well beyond the reach of all present day laboratory and known astrophysical environments. As seen in Fig. 1 the lower temperature limit, where the last e^+e^- -pair disappeared, is 15 times the Sun's core temperature [19] $T_\odot = 1.37$ keV. Laboratory conditions to explore our results depend on presence of e^+e^- -pair abundance which in turn depends on sufficiently stable thermal photon content.

Both Landau diamagnetism and magnetic dipole moment paramagnetism are relevant in the analysis of dense e^+e^- -plasma Gilbertian (non-current) magnetization. The high temperature relevance of paramagnetism

relies on the high abundance of pairs. In the theoretical treatment of Sect. III, this is accounted for by introducing effective polarization mass \tilde{m} in Eq. (14). This allows for the separation of the spin portion of the relativistic partition function from the spin-orbital portion (Landau diamagnetism) in Sect. IIIA. In Sect. IIIB we determined the effect of magnetism on the chemical potential; see Fig. 3.

This novel approach to high temperature magnetization allows using Sect. IV to show that the e^+e^- -plasma paramagnetic response (see Eq. (40) and Eq. (41)) is dominated by the varying abundance of electron-positron pairs, decreasing with decreasing T for $T < m_ec^2$. This is unlike conventional laboratory cases where the number of magnetic particles is constant.

In our domain of interest, we determine in Sect. IVC that cosmic magnetization is not sensitive to the anomalous magnetic moment of the electron. Considering magnetization as a function of g -factor we find a transition seen in Fig. 5 between paramagnetic and diamagnetic gasses. The per-lepton magnetization is shown in Sect. IVC and Fig. 6 indicating the plasma is only weakly organized in its response.

In Sect. V we explored spin asymmetry (defined in Sect. II and Eq. (7)) via the magnetic moment chemical potential. We showed in Sect. V how self-magnetization can be induced by magnetic moment polarization via a novel magnetic moment fugacity. We obtained in Sect. V the required primordial degree of magnetic moment polarization necessary to understand today's IGFM. Our study demonstrates that the early universe required at high temperatures only a minute asymmetry in magnetic moment polarization to produce required spontaneous magnetization.

Our results lead to extensions of present day paradigms but offer many opportunities for improvement. The high temperature domain would require a full inventory of particles including neutrinos and muons before their disappearance or decoupling. The full Fermi-Dirac and Bose-Einstein statistics instead of the Boltzmann approximation would then be employed.

Beyond e^+e^- -plasma, the quark-gluon plasma at $T > 15000$ keV is also of great interest. The up-quark has the largest natural charge-to-mass e/m ratio among elementary particles besides the electron. A connection from the quark-gluon plasma to the e^+e^- -plasma then requires understanding of the impact of the hadronization process on magnetization, and vice-versa, a consideration of hadronization as a magnetization mechanism. We note that the contribution of $\mu^+\mu^-$ -plasma to magnetization is reduced by a factor $\simeq 200$ compared to e^+e^- -plasma due to the $\propto e/m_\mu$ behavior of magnetic moments. We also note that the complex neutrino decoupling process near to $T = 2000$ keV should be explored as a source of magnetization mechanism.

Near to $T = 80$ keV just prior to BBN we have $4.47 \times 10^8 e^+e^-$ -pairs per baryon and a primordial magnetic field in range of $10^0 - 10^1$ Gauss. BBN thus occurs

in an environment as different as can be imagined from the empty space network of nuclear reactions explored. Our work creates the question in what way the presence of a primordial magnetic field could have impacted BBN and vice-versa, if BBN could provide the mechanism for spontaneous magnetization. The e^+e^- -pair impact is already being considered [10].

Below $T_{\text{split}} = 20.3$ keV the universe's particle inventory is dominated by electrons, protons, and α -particles. In order to conserve the magnetic flux originating in the polarized homogeneous e^+e^- -pair plasma a very different model will need to be developed allowing for fragmentation of the homogeneous plasma universe into polarization domains and evolving Ampérian kinetic current curl responses. The effort to connect the bulk magnetization due to discrete dipoles by Ampérian magnetization generated through currents and inhomogeneous flows will require study of transport equations allowing for magnetic moment polarization.

Recent measurements by the James Webb Space Telescope (JWST) [44–46] indicate that maturing galaxies already present at a large redshift value of $z \gtrsim 10$ within the first 500 million years of the universe. This requires gravitational collapse to begin earlier in a hotter environment. Additionally the observation of supermassive (with millions of solar masses) black holes

already present [47] in this same high redshift era indicate the need for exceptionally small-scale high mass density regions in the early universe. There is a natural mechanism present in our work needed to create the above condition: As the universe evolved, the rapid 10^8 drop in e^+e^- abundance within the temperature range 100 keV $> T > 20.3$ keV shown in Fig. 1 could be inducing dynamical currents preserving (comoving) magnetic flux in the emerging $p^+\alpha^+e^-$ -plasma and in turn generate vortex seeds for small scale baryonic matter localization which could support anisotropies in the cosmic microwave background (CMB) [25, 48].

To conclude: This work shows that the paramagnetic and diamagnetic e^+e^- -plasma properties may play a pivotal role in understanding the primordial universe. In particular we have shown that the possible self-magnetization of the cosmic e^+e^- -plasma provides a novel and credible proposal for interpretation and exploration of magnetic fields in the universe.

ACKNOWLEDGMENTS

Johann Rafelski would like to acknowledge the fruitful discussions with Massimo Giovannini at CERN which partly inspired this work.

- [1] A. Neronov and I. Vovk. Evidence for strong extragalactic magnetic fields from fermi observations of tev blazars. *Science*, 328(5974):73–75, 2010. doi: 10.1126/science.1184192.
- [2] A. M. Taylor, I. Vovk, and A. Neronov. Extragalactic magnetic fields constraints from simultaneous gev-tev observations of blazars. *Astronomy & Astrophysics*, 529: A144, 2011. doi: 10.1051/0004-6361/20116441.
- [3] M. S. Pshirkov, P. G. Tinyakov, and F. R. Urban. New limits on extragalactic magnetic fields from rotation measures. *Phys. Rev. Lett.*, 116(19):191302, 2016. doi: 10.1103/PhysRevLett.116.191302.
- [4] K. Jedamzik and A. Saveliev. Stringent limit on primordial magnetic fields from the cosmic microwave background radiation. *Physical review letters*, 123(2):021301, 2019. doi: 10.1103/PhysRevLett.123.021301.
- [5] T. Vernstrom, G. Heald, F. Vazza, T. J. Galvin, J. L. West, N. Locatelli, N. Fornengo, and E. Pinetti. Discovery of magnetic fields along stacked cosmic filaments as revealed by radio and X-ray emission. *Monthly Notices of the Royal Astronomical Society*, 505(3):4178–4196, 05 2021. doi:10.1093/mnras/stab1301.
- [6] M. Giovannini. Probing large-scale magnetism with the Cosmic Microwave Background. *Class. Quant. Grav.*, 35(8):084003, 2018. doi:10.1088/1361-6382/aa17d.
- [7] M. Giovannini. The Magnetized universe. *Int. J. Mod. Phys. D*, 13:391–502, 2004. doi: 10.1142/S0218271804004530.
- [8] P. P. Kronberg. Extragalactic magnetic fields. *Reports on Progress in Physics*, 57(4):325, 1994. doi:10.1088/0034-4885/57/4/001.
- [9] J. Rafelski, J. Birrell, A. Steinmetz, and C. T. Yang. A Short Survey of Matter-Antimatter Evolution in the Primordial Universe. *Universe*, 9(7):309, 2023. doi: 10.3390/universe907309.
- [10] C. Grayson, C. T. Yang, M. Formanek, and J. Rafelski. Electron-positron plasma in BBN: damped-dynamic screening. *arXiv preprint*, 2023. doi: 10.48550/arXiv.2307.11264. [in press in Annals of Physics].
- [11] J. Rafelski, M. Formanek, and A. Steinmetz. Relativistic Dynamics of Point Magnetic Moment. *Eur. Phys. J. C*, 78(1):6, 2018. doi:10.1140/epjc/s10052-017-5493-2.
- [12] M. Giovannini. The scaling of primordial gauge fields. *Physics Letters B*, 842:137967, 2023. ISSN 0370-2693. doi:10.1016/j.physletb.2023.137967.
- [13] R. A. Batista and A. Saveliev. The gamma-ray window to intergalactic magnetism. *Universe*, 7(7), 2021. ISSN 2218-1997. doi:10.3390/universe7070223.
- [14] B. M. Gaensler, R. Beck, and L. Feretti. The origin and evolution of cosmic magnetism. *New Astronomy Reviews*, 48(11–12):1003–1012, 2004. doi: 10.1016/j.newar.2004.09.003.
- [15] R. Durrer and A. Neronov. Cosmological magnetic fields: their generation, evolution and observation. *The Astronomy and Astrophysics Review*, 21:1–109, 2013. doi: 10.1007/s00159-013-0062-7.
- [16] V. P. Pomakov, S. P. O'Sullivan, M. Brüggen, F. Vazza, E. Carretti, G. H. Heald, C. Horellou, T. Shimwell, A. Shulevski, and T. Vernstrom. The redshift evolution of extragalactic magnetic fields. *Monthly Notices of the Royal Astronomical Society*, 515(1):256–270, 2022. doi:

- 10.1093/mnras/stac1805.
- [17] K. Jedamzik and L. Pogosian. Relieving the hubble tension with primordial magnetic fields. *Physical Review Letters*, 125(18):181302, 2020. doi: 10.1103/PhysRevLett.125.181302.
- [18] J. Birrell, C. T. Yang, and J. Rafelski. Relic Neutrino Freeze-out: Dependence on Natural Constants. *Nucl. Phys. B*, 890:481–517, 2014. doi: 10.1016/j.nuclphysb.2014.11.020.
- [19] J. N. Bahcall, M. H. Pinsonneault, and S. Basu. Solar models: Current epoch and time dependences, neutrinos, and helioseismological properties. *The Astrophysical Journal*, 555(2):990, jul 2001. doi:10.1086/321493.
- [20] M. J. Fromerth, I. Kuznetsova, L. Labun, J. Letessier, and J. Rafelski. From Quark-Gluon Universe to Neutrino Decoupling: $200 < T < 2\text{MeV}$. *Acta Phys. Polon. B*, 43(12):2261–2284, 2012. doi:10.5506/APhysPolB.43.2261.
- [21] L. Canetti, M. Drewes, and M. Shaposhnikov. Matter and Antimatter in the Universe. *New J. Phys.*, 14:095012, 2012. doi:10.1088/1367-2630/14/9/095012.
- [22] H. T. Elze, W. Greiner, and J. Rafelski. The relativistic Fermi gas revisited. *J. Phys. G*, 6:L149–L153, 1980. doi: 10.1088/0305-4616/6/9/003.
- [23] R. L. Workman et al. Review of Particle Physics. *PTEP*, 2022:083C01, 2022. doi:10.1093/ptep/ptac097.
- [24] J. Letessier and J. Rafelski. *Hadrons and Quark–Gluon Plasma*. Cambridge Monographs on Particle Physics, Nuclear Physics and Cosmology. Cambridge University Press, 2023. doi:10.1017/9781009290753. Open access. [Orig. pub. year: 2002].
- [25] E. Abdalla, G. F. Abellán, A. Aboubrahim, A. Agnello, O. Akarsu, Y. Akrami, G. Alestas, D. Aloni, L. Amendola, L. A. Anchordoqui, et al. Cosmology intertwined: A review of the particle physics, astrophysics, and cosmology associated with the cosmological tensions and anomalies. *Journal of High Energy Astrophysics*, 34:49–211, 2022. doi:10.1016/j.jheap.2022.04.002.
- [26] S. Weinberg. *Gravitation and cosmology: principles and applications of the general theory of relativity*. John Wiley & Sons, 1972.
- [27] N.ghanim et al. Planck 2018 results. VI. Cosmological parameters. *Astron. Astrophys.*, 641:A6, 2020. doi:10.1051/0004-6361/201833910. [Erratum: *Astron. Astrophys.* 652, C4 (2021)].
- [28] D. Melrose. *Quantum plasmadynamics: Magnetized plasmas*. Springer, 2013. doi:10.1007/978-1-4614-4045-1.
- [29] A. Steinmetz, M. Formanek, and J. Rafelski. Magnetic Dipole Moment in Relativistic Quantum Mechanics. *Eur. Phys. J. A*, 55(3):40, 2019. doi:10.1140/epja/i2019-12715-5.
- [30] Eite Tiesinga, Peter J. Mohr, David B. Newell, and Barry N. Taylor. CODATA recommended values of the fundamental physical constants: 2018. *Rev. Mod. Phys.*, 93(2):025010, 2021. doi: 10.1103/RevModPhys.93.025010.
- [31] M. Abramowitz, I. A. Stegun, and R. H. Romer. *Handbook of mathematical functions with formulas, graphs, and mathematical tables*. American Association of Physics Teachers, 1988.
- [32] W. Greiner, L. Neise, and H. Stöcker. *Thermodynamics and statistical mechanics*. Springer Science & Business Media, 2012. doi:10.1007/978-1-4612-0827-3. [Orig. pub. year: 1995].
- [33] W. Greiner and J. Reinhardt. *Quantum electrodynamics*. Springer Science & Business Media, 2008. doi: 10.1007/978-3-540-87561-1.
- [34] F. Vazza, M. Brüggen, C. Gheller, S. Hackstein, D. Wittor, and P. M. Hinz. Simulations of extragalactic magnetic fields and of their observables. *Class. Quant. Grav.*, 34(23):234001, 2017. doi:10.1088/1361-6382/aa8e60.
- [35] T. Vachaspati. Progress on cosmological magnetic fields. *Rept. Prog. Phys.*, 84(7):074901, 2021. doi:10.1088/1361-6633/ac03a9.
- [36] R. Gopal and S. Sethi. Generation of magnetic field in the pre-recombination era. *Mon. Not. Roy. Astron. Soc.*, 363: 521–528, 2005. doi:10.1111/j.1365-2966.2005.09442.x.
- [37] L. M. Perrone, G. Gregori, B. Reville, L. O. Silva, and R. Bingham. Neutrino-electron magnetohydrodynamics in an expanding universe. *Phys. Rev. D*, 104(12):123013, 2021. doi:10.1103/PhysRevD.104.123013.
- [38] S. Evans and J. Rafelski. Emergence of periodic in magnetic moment effective QED action. *Phys. Lett. B*, 831: 137190, 2022. doi:10.1016/j.physletb.2022.137190.
- [39] J. Rafelski, S. Evans, and L. Labun. Study of QED singular properties for variable gyromagnetic ratio $g \simeq 2$. *Phys. Rev. D*, 107, 2023. doi: 10.1103/PhysRevD.107.076002.
- [40] R. Ruffini, G. Vereshchagin, and S. S. Xue. Electron-positron pairs in physics and astrophysics: from heavy nuclei to black holes. *Phys. Rept.*, 487:1–140, 2010. doi: 10.1016/j.physrep.2009.10.004.
- [41] R. Ruffini and G. Vereshchagin. Electron-positron plasma in GRBs and in cosmology. *Nuovo Cim. C*, 036 (s01):255–266, 2013. doi:10.1393/ncc/i2013-11500-0.
- [42] E. J. Ferrer and A. Hackebill. Thermodynamics of Neutrons in a Magnetic Field and its Implications for Neutron Stars. *Phys. Rev. C*, 99(6):065803, 2019. doi: 10.1103/PhysRevC.99.065803.
- [43] E. J. Ferrer and A. Hackebill. The Importance of the Pressure Anisotropy Induced by Strong Magnetic Fields on Neutron Star Physics. *J. Phys. Conf. Ser.*, 2536(1): 012007, 2023. doi:10.1088/1742-6596/2536/1/012007.
- [44] H. Yan, Z. Ma, C. Ling, C. Cheng, and J. Huang. First Batch of $z \approx 11\text{--}20$ Candidate Objects Revealed by the James Webb Space Telescope Early Release Observations on SMACS 0723-73. *Astrophys. J. Lett.*, 942(1):L9, 2023. doi:10.3847/2041-8213/aca80c.
- [45] N. J. Adams, C. J. Conseilce, L. Ferreira, et al. Discovery and properties of ultra-high redshift galaxies ($9 < z < 12$) in the JWST ERO SMACS 0723 field. *Monthly Notices of the Royal Astronomical Society*, 518(3):4755–4766, 2023. doi:10.1093/mnras/stac3347.
- [46] P. A. Haro, M. Dickinson, S. L. Finkelstein, et al. Confirmation and refutation of very luminous galaxies in the early universe. *Nature*, 2023. doi:10.1038/s41586-023-06521-7.
- [47] R. L. Larson, S. L. Finkelstein, D. D. Kocevski, T. A. Hutchison, J. R. Trump, P. A. Haro, V. Bromm, N. J. Cleri, M. Dickinson, S. Fujimoto, et al. A CEERS discovery of an accreting supermassive black hole 570 myr after the big bang: Identifying a progenitor of massive $z > 6$ quasars. *arXiv preprint*, 2023. doi: 10.48550/arXiv.2303.08918. [submitted to ApJ].
- [48] K. Jedamzik and T. Abel. Small-scale primordial magnetic fields and anisotropies in the cosmic microwave background radiation. *JCAP*, 10:050, 2013. doi: 10.1088/1475-7516/2013/10/050.